UNIVERSITY OF SOUTHAMPTON

FACULTY OF MEDICINE

Cancer Sciences

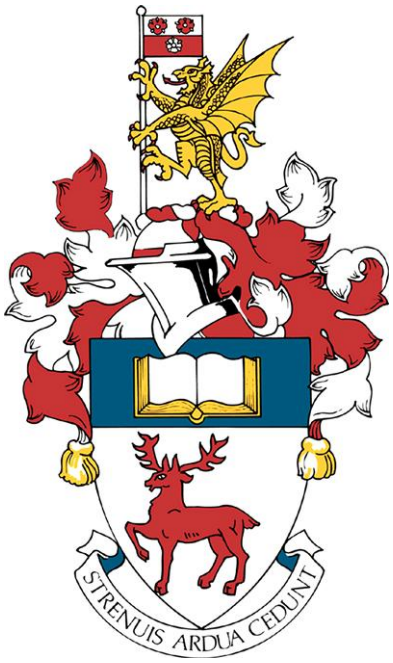

Combination of immunomodulatory cyclophosphamide with anti-PD-1 monoclonal antibody therapy to improve survival in preclinical models of neuroblastoma

by

Emily Rose Webb

PhD Thesis

December 2018

UNIVERSITY OF SOUTHAMPTON

ABSTRACT

FACULTY OF MEDICINE

Cancer Sciences

PhD Thesis

Combination of immunomodulatory cyclophosphamide with anti-PD-1 monoclonal antibody therapy to improve survival in preclinical models of neuroblastoma

Emily Rose Webb

Neuroblastoma (NB) is one of the most common childhood cancers, constituting 8% of paediatric cancers, and 15% of paediatric cancer deaths. The majority of patients have high risk disease, with poor outcome despite intensive treatment regimens. Current therapies, which include chemotherapy and radiotherapy, are highly toxic, with significant treatment related mortality, and there is little scope for further intensification. Alternatives strategies, such as immunotherapy are a priority for improving patient outcomes. A number of different immunotherapies, such as anti-GD2 antibody therapy, have shown promise in NB, but combining these with conventional chemotherapy regimens is challenging. Classically, chemotherapy has been regarded as immunosuppressive but recent work has highlighted that this may not entirely be accurate for certain immunogenic chemotherapies. Furthermore, immunomodulatory antibodies such as checkpoint inhibitors have shown efficacy in adult cancers such as melanoma, with little investigation into their potency in paediatric tumours. Although NB tumours are not particularly inherently immunogenic, the application of an 'immunogenic' chemotherapy may render them susceptible to further immunomodulatory immunotherapy.

Firstly this study aimed to identify the immunomodulating effects of cyclophosphamide (CPM) treatment on immune cells, within murine NB models. To achieve this, CPM's ability to induce 'immunogenic cell death' (ICD) markers both *in vitro* and *in vivo* was investigated. Induction of ecto-CRT, Hsp-70 and HMGB1 expression was observed. Secondly, effects of different doses of CPM on the immune cell infiltrates in the tumour microenvironment were studied *in vivo* using syngeneic murine NB models. It was demonstrated that low dose CPM was able to selectively deplete and possibly reduce the suppressive activity tumour infiltrating Treg cells in both NXS2 and 9464D NB models, alongside maintaining and activating $CD8^+$ and $CD4^+$ T cells. Additionally, using an apoptosis resistant NB cell line and mouse strain, investigation into whether ICD induction or Treg depletion is most critical aspect of CPM immunomodulation was conducted. It was observed that overexpression of BCL-2 either in the tumour cell line *in vitro* or Treg cells *in vivo*, prevented apoptosis and CPM dependent depletion.

Finally, it was assessed whether immunogenic CPM could be efficiently combined with immunomodulatory antibody therapy to slow tumour growth, utilising a combination of syngeneic and spontaneous transgenic NB models. Experiments utilising the three *in vivo* models demonstrated that combination of CPM with anti-PD-1 antibody led to an increase in survival over monotherapies alone, which was further enhanced by a metronomic weekly dosing strategy. Ongoing work is exploring this approach, to refine and establish the most effective chemotherapy and antibody combination in NB preclinical models, along with defining the mechanisms behind combination efficacy.

Table of Contents

Table of Contents ..... **i**

List of Tables ..... **x**

List of Figures ..... **xi**

Acknowledgements ..... **xix**

Definitions and Abbreviations ..... **xxi**

Chapter 1: Introduction **1**

1.1 Cancer **1**

1.1.1 Biology of cancer 1

1.1.2 United Kingdom (UK) cancer statistics 3

1.1.3 Challenges of paediatric cancer 5

1.2 Neuroblastoma **9**

1.2.1 Clinical overview 9

1.2.2 Staging and outcomes 10

1.2.3 Current treatment strategies for high-risk disease 11

1.2.4 Can prognosis be improved? 12

1.3 Immune system and cancer **13**

1.3.1 Innate immune cell subsets 13

1.3.1.1 Myeloid cells 14

1.3.1.2 NK cells and NKT cells 17

1.3.2 Adaptive immune cell subsets 18

1.3.2.1 T cells 18

1.3.2.2 B cells 20

1.3.3 Fc gamma receptors 22

1.3.4 Immune checkpoints 22

1.3.5 Immune response to tumour cells 24

1.3.6 Immunoediting and the suppressive tumour microenvironment 27

1.4 Chemotherapy in cancer therapy **29**

1.4.1 Classical chemotherapy 29

1.4.2 Chemotherapies used in the treatment of NB 30
1.4.3 Apoptosis inducing vs immunogenic cell death inducing chemotherapy 31
1.4.4 Effect of chemotherapy on immune cell subsets 35
1.5 Immunotherapy in cancer treatment 39
1.5.1 Monoclonal antibodies 39
1.5.1.1 Direct targeting - anti-GD2 antibody therapy 44
1.5.2 Monoclonal antibodies – immunomodulatory 46
1.5.2.1 Anti-CTLA-4 antibodies 46
1.5.2.2 Anti-PD-1 antibodies 47
1.5.2.3 Anti-4-1BB antibodies 49
1.5.3 Cellular based immunotherapies 49
1.5.4 Immunotherapy and immune modulation in NB 51
1.5.5 Synergy of chemotherapy and immunotherapy 54
1.6 Hypothesis and aims 57
1.6.1 Hypothesis 57
1.6.2 Aims 57
Chapter 2: Materials and Methods 59
2.1 Animals 59
2.1.1 Ethics 59
2.1.2 AJ and C57BL/6 mice 59
2.1.3 TH-MYCN$^{+/-}$ 59
2.1.3.1 Genotyping 59
2.1.3.2 Tumour monitoring 60
2.1.4 Vav-BCL-2 Transgenic mice 61
2.2 Cell lines 61
2.2.1 NXS2 61
2.2.2 9464D 61
2.3 Antibodies 62

2.3.1 In house produced antibodies 62
2.3.2 Commercially sourced antibodies 62
2.4 Antibody modifications 64
2.4.1 Deglycosylation of EW1.9 64
2.4.2 Sodium Dodecyl Sulphate Polyacrylamide Gel Electrophoresis (SDS-PAGE) analysis to confirm deglycosylation 64
2.5 Syngeneic NXS2 mouse model of neuroblastoma 65
2.5.1 Subcutaneous model 65
2.6 Syngeneic 9464D mouse model of neuroblastoma 65
2.6.1 Subcutaneous (SC) model 65
2.7 Chemotherapy agents 65
2.7.1 *In vitro* use 65
2.7.2 *In vivo* use 66
2.8 Assessment of the effect of chemotherapy and anti-PD-1 treatment on immune cell subsets and T cell markers 66
2.8.1 Tumour inoculation 66
2.8.2 Administration of Chemotherapy 66
2.8.3 Administration of EW1-9 antibodies 66
2.8.4 Tissue collection and processing 66
2.8.5 Serial blood sampling 67
2.9 Flow cytometry 67
2.9.1 Live/dead staining 67
2.9.2 Direct staining 67
2.9.3 Intracellular staining 68
2.9.4 Flow cytometry analysis 68
2.10 *In vitro* assessment of cell death 68
2.10.1 Induction of cell death 68
2.10.2 MTT assay 69
2.11 Analysis of immunogenic cell death (ICD) marker expression *in vitro* 69

2.11.1 Induction of cell death 69

2.11.2 Direct staining for ICD markers 69

2.12 Development of a BCL-2 overexpressing 9464D line 70

2.12.1 Phoenix-eco cells 70

Phoenix-Eco cells were plated into 6 well plates to be cultured in DMEM supplemented with 10% FCS, 2mM glutamine, 1mM sodium pyruvate, 100U/ml streptomycin and 100µg/ml penicillin (all from Gibco). Cells were cultured at 37^{o}C at 10% CO_2, and maintained at a confluency of around 50%. 70

2.12.2 Transfection of Phoenix-Eco cells with GFP vector 70

2.12.3 Spin transduction of 9464D cells 70

2.12.4 Puromycin and hygromycin cell death curves 71

2.12.5 Analysis of human BCL-2 expression by intracellular flow cytometry 71

2.13 Western blots 71

2.13.1 Harvesting cell lysates 71

2.13.2 Bradford assay for assessing protein concentration 72

2.13.3 Sodium Dodecyl Sulphate Polyacrylamide Gel Electrophoresis (SDS-PAGE) 72

2.13.4 Gel transfer to membrane 72

2.13.5 Blocking and primary antibody incubation 72

2.13.6 Secondary antibody incubation and imaging 73

2.14 Analysis of HMGB1 after CPM administration by IHC 73

2.14.1 Tumour collection 73

2.14.2 Cutting of slides and fixation 73

2.14.3 Immunohistochemistry of OCT frozen sections 73

2.14.4 HMGB1 immunohistochemistry of formalin fixed paraffin embedded sections 74

2.14.5 HMGB1 immunofluorescence of 9464D cells 74

2.14.6 Imaging 74

2.15 Assessment of antibody half-life by ELISA 75

2.15.1 Blood sampling and serum collection 75

2.15.2 Enzyme linked immunosorbent assay (ELISA) 75

2.16 Assessment of anti-drug response by ELISA 76

2.16.1 Injection of antibodies 76

2.16.2 Anti-drug response ELISA 76

2.17 Combination treatment of cyclophosphamide and anti-PD-1 mAb in TH-MYCN transgenic mouse model 76

2.17.1 Tumour presentation 76

2.17.2 Administration of treatments 76

2.17.3 Survival analysis 77

2.18 Statistical analysis 77

Chapter 3: Immunophenotyping preclinical models of neuroblastoma 79

3.1 Chapter introduction 79

3.2 Results 81

3.2.1 Establishment of a 9464D sub-cutaneous model 81

3.2.2 Comparison of the immune infiltrate within tumours of *in vivo* models of NB 83

3.2.2.1 Flow cytometry gating strategy for immunophenotyping of murine NB tumours 84

3.2.2.2 Immunophenotyping non-tumour bearing spleens of AJ, C57BL/6 and TH-MYCN$^{+/-}$ mice. 87

3.2.2.3 GD2 and MHC class I expression 89

3.2.2.4 Myeloid cells: neutrophils, monocytes and macrophages 91

3.2.2.5 Fc gamma receptors 92

3.2.2.6 NK cells + B cells 94

3.2.2.7 T cell subsets 96

3.2.3 Establishment of transplant models of TH-MYCN$^{+/-}$ tumours 98

3.2.3.1 Myeloid infiltrates in sub cutaneous and IP passaged TH-MYCN$^{+/-}$ tumours compared to spontaneous TH-MYCN$^{+/-}$ tumours 100

3.2.3.2 NK and B cell infiltrates in TH-MYCN$^{+/-}$ passaged tumours compared to TH-MYCN$^{+/-}$ spontaneous tumours 102

3.2.3.3 Analysis of T cell subsets and ratios within TH-MYCN$^{+/-}$ subcutaneous and intraperitoneal passaged tumours compared to spontaneous TH-MYCN$^{+/-}$ tumours 103

3.3 Chapter discussion 106

Chapter 4: Immunogenic cell death induction and immune cell modulation by cyclophosphamide 113

4.1 Chapter introduction 113

4.2 Results 115

4.2.1 Establishing *in vitro* cytotoxic doses of mafosfamide and doxorubicin on NB murine cell lines 115

4.2.1.1 Determining a standard curve and cell seeding density for NXS2 and 9464D cell lines with a MTT assay 115

4.2.1.2 Assessing metabolic activity after chemotherapy application 116

4.2.2 Induction of immunogenic cell death markers on NB cells after chemotherapy treatment *in vitro* 119

4.2.2.1 Ecto-CRT and Hsp-70 expression on NB cell lines after cytotoxic drug application 119

4.2.2.2 Expression of HMGB1 in 9464D cells *in vitro* after MAF treatment, and *ex vivo* after CPM 121

4.2.3 Immunophenotyping of NXS2 and 9464D tumours *ex vivo* after CPM administration 123

4.2.3.1 Effects of CPM on myeloid infiltration in NXS2 and 9464D spleens and tumours 124

4.2.3.2 Effects of CPM on B cell, NK and NKT cell infiltration in NXS2 and 9464D tumours and spleens 127

4.2.3.3 Effects of CPM on T cell infiltration in NXS2 and 9464D tumours and spleens 130

4.2.3.4 Effects of CPM on Treg infiltration and T cell ratios in NXS2 and 9464D tumours and spleens 133

4.2.4 T cell subset modulation after CPM administration in non-tumour tissues 136
4.2.5 Phenotyping of FcγRs on myeloid subsets in 9464D tumours 140
4.2.6 Modulation of NXS2 TIL numbers and phenotypes at Day 3 post CPM administration 144
4.2.6.1 Effect of CPM on T cell phenotypes in NXS2 tumours after 72 hrs 145
4.2.7 Modulation of T cells at Day 3 and Day 10 post CPM administration in 9464D tumours 148
4.2.7.1 Effect on T cell percentages at Day 3 and Day 10 post CPM administration 150
4.2.7.2 Effect on T cell memory populations at Day 3 and Day 10 post 40mg/kg CPM 152
4.2.7.3 Modulation of T cell subset phenotype at Day 3 and Day 10 post 40mg/kg CPM 154
4.2.8 Investigating the importance of ICD or Treg depletion in CPM induced immunomodulation 159
4.2.8.1 Transfection of phoenix-Eco cells and establishment of selection dose of puromycin and hygromycin in 9464D 159
4.2.8.2 GFP expression of transduced 9464D cells after puromycin selection 161
4.2.8.3 hBCL-2 expression in transduced 9464D cells after hygromycin selection 162
4.2.9 Assessment of chemotherapy cytotoxicity on hBCL-2 transduced 9464D cell lines 165
4.2.10 Assessment of growth of hBCL-2 9464D cell line *in vivo* 168
4.2.11 Modulation of T cell subsets of 9464D SC tumours in vav-BCL2 transgenic mice compared to C57BL/6 mice 171

4.3 Discussion 174

Chapter 5: Combination of low dose CPM with anti-PD-1 antibody therapy increases survival in preclinical models of NB 185

5.1 Chapter introduction 185

5.2 Results 187

5.2.1 Assessment of WT and DG EW1-9 antibody serum levels in AJ and C57BL/6 mice 187

5.2.2 Combining CPM with immunomodulatory antibody therapy 189

5.2.2.1 Anti-4-1BB therapy 189

5.2.2.2 Anti-CTLA-4 therapy 191

5.2.2.3 Anti-PD-1 therapy 193

5.2.3 Combining CPM with anti-PD-1 antibody therapy in smaller NXS2 tumour bearing mice. 195

5.2.4 Combination of CPM and anti-PD-1 antibodies in 9464D subcutaneous tumour model 196

5.2.4.1 Combining CPM and anti-PD-1 antibody therapy in 5x5 mm and palpable 9464D tumour bearing mice 199

5.2.5 Immunophenotyping of peripheral blood mononuclear cells of combination therapy treated mice 204

5.2.6 Analysis of GD2 and PD-L1 expression on NXS2 and 9464D tumours after combination therapy 207

5.2.6.1 Analysis of TIL populations in tumours of combination therapy treated NXS2 and 9464D tumour bearing mice 210

5.2.6.2 Memory populations in TILs of NXS2 and 9464D tumours after combination therapy 216

5.2.7 Tumour infiltrating myeloid percentages in tumours of NXS2 and 9464D combination therapy treated mice 222

5.2.8 Metronomic dosing of CPM and anti-PD-1 antibody in 9464D tumour bearing mice 226

5.2.8.1 Metronomic dosing in 9464D palpable tumour bearing mice 229

5.2.9 Assessment of CPM and anti-PD-1 antibody therapy in TH-MYCN spontaneous NB model 231

5.3 Discussion 233

Chapter 6: Discussion and Future Work 241

6.1 Discussion 241

6.2 Future work.....247

Chapter 7: Appendix.....251

Chapter 8: References 259

List of Tables

Table 1.1 International NB Risk Group (INGR) staging system 10

Table 1.2 INRG pretreatment classification schema 11

Table 1.3 Murine IgG isotypes and their binding affinity 42

Table 1.4 List of currently approved MAbs for cancer immunotherapy 44

Table 2.1 Master mix for TH-MYCN genotyping PCR reaction 60

Table 2.2 PCR cycle for TH-MCYN genotyping 60

Table 2.3 In house produced monoclonal antibodies 62

Table 2.4 Commercially sourced antibodies 64

Table 3.1 Summary table comparing immune infiltrates into tumours of the three murine models of NB 97

Table 4.1 Immunophenotyping panel of T cell markers for flow cytometry of 9464D tumours at Day 3 and Day 10 post CPM administration 148

Table 5.1 Summary of immunophenotyping data from combination therapy of NXS2 tumour bearing mice 225

Table 5.2 Summary of immunophenotyping data from combination therapy of 9464D tumour bearing mice 226

List of Figures

Figure 1.1 UK cancer incidence rates of 20 most common cancers in 2015 4

Figure 1.2 10 year survival rate of selected adult cancers 2010-2011..... 5

Figure 1.3 UK cancer incidence rates of paediatric cancers between 2006-2008 7

Figure 1.4 10 year survival rates for paediatric cancers 2001-2005 8

Figure 1.5 Example of current high-risk NB treatment programme (SIOPEN trial) 12

Figure 1.6 Mechanisms of antigen presentation by professional APCs..... 16

Figure 1.7 Generation of an anti-tumour immune response is dependent on DC activation . 25

Figure 1.8 Immune synapse formation and immune checkpoints..... 26

Figure 1.9 The suppressive tumour microenvironment network 28

Figure 1.10 Chemotherapy driven ICD mechanisms in tumour cells..... 33

Figure 1.11 Basic structure of an IgG antibody molecule..... 41

Figure 1.12 Immunotherapy of NB 54

Figure 3.1 Tumour growth and survival of 9464D passaged tumours in C57BL/6 mice 82

Figure 3.2 Macroscopic images of tumours and spleen from three different NB murine models 84

Figure 3.3 Examples of myeloid flow cytometry gaiting strategies for immunophenotyping tumours of murine neuroblastoma models 85

Figure 3.4 Examples of lymphocyte flow cytometry gaiting strategies for immunophenotyping tumours of murine neuroblastoma models 86

Figure 3.5 Immunophenotyping of spleens from tumour bearing and non-tumour bearing of the three murine neuroblastoma models..... 88

Figure 3.6 GD2 and MHC I expression on tumours NXS2 and TH-MYCN tumours ex vivo..... 90

Figure 3.7 Myeloid populations within NXS2, 9464D and TH-MYCN NB tumours 92

Figure 3.8 FcγR expression on 3 myeloid cell subsets within spleens and NXS2 and TH-MYCN tumours 94

Figure 3.9 Lymphocyte populations within NXS2, NB9464 and TH-MYCN tumours and spleens95

Figure 3.10 Tumour appearance and growth of tumours passaged from spontaneous TH-MYCN 99

Figure 3.11 Analysis of tumour infiltrating and splenic myeloid populations of TH-MYCN sub cutaneous and intraperitoneal re-passaged tumours compared to spontaneous TH-MYCN tumours.....101

Figure 3.12 Analysis of tumour infiltrating and splenic NK and B cell populations of TH-MYCN sub cutaneous and intraperitoneal repassaged tumours compared to spontaneous TH-MYCN tumours 102

Figure 3.13 Analysis of tumour infiltrating and splenic T cell populations of TH-MYCN sub cutaneous and intraperitoneal repassaged tumours compared to spontaneous TH-MYCN tumours.....104

Figure 3.14 Analysis of tumour infiltrating and splenic T cell ratios of TH-MYCN sub cutaneous and intraperitoneal repassaged tumours compared to spontaneous TH-MYCN tumours 105

Figure 4.1 MTT standard curve optimisation with murine cell lines 115

Figure 4.2 Percentage of seeded cells remaining after administration of mafosfamide.....117

Figure 4.3 Percentage of seeded cells remaining after doxorubicin administration 118

Figure 4.4 Expression of ecto-CRT and HSP-70 on NXS2 and 9464D cells after chemotherapy application 120

Figure 4.5 Expression of HMGB1 after MAF application in 9464D cells.....122

Figure 4.6 HMGB1 staining of FFPE 9464D tumours after CPM administration 122

Figure 4.7 Experimental schematic of NXS2 and 9464D Immunophenotyping 123

Figure 4.8 Effect of CPM administration on myeloid infiltrates in NXS2 tumours and spleens125

Figure 4.9 Effect of CPM administration on myeloid infiltrates in 9464D tumours and spleens126

Figure 4.10 Effect of CPM administration on B, NK and NKT cell infiltrates in NXS2 tumours and spleens 128

Figure 4.11 Effect of CPM administration on B, NK and NKT cell infiltrates in 9464D tumours and spleens 129

Figure 4.12 Effect of CPM administration on T cell infiltrates in NXS2 tumours and spleens 131

Figure 4.13 Effect of CPM administration on T cell infiltrates in 9464D tumours and spleens132

Figure 4.14 Effect of CPM administration on Treg cell infiltrates and T cell ratios in NXS2 tumours and spleens 134

Figure 4.15 Effect of CPM administration on Treg cell infiltrates and T cell ratios in 9464D tumours and spleens 135

Figure 4.16 Flow cytometry gating for T cell populations on lymph nodes and PBMCs 136

Figure 4.17 Effects of CPM administration on T cell subsets within LNs 137

Figure 4.18 Effects of CPM administration on T cell subsets within PBMCs 138

Figure 4.19 Heat map of Treg percentages in NXS2 and 9464D tissues after CPM administration 139

Figure 4.20 Percentages of myeloid cell subsets at Day 3 and Day 10 after CPM administration in 9464D tumours 141

Figure 4.21 Modulation of FcγRs in 9464D tumours by CPM administration at Day 3 and Day 10 142

Figure 4.22 Modulation of AI ratios of FcγRs on myeloid populations at Day 3 and Day 10 after CPM administration 143

Figure 4.23 Gating and marker analysis examples for T cell subsets in tumours after CPM administration 144

Figure 4.24 Heat map of T cell percentages and ratios in NXS2 tumours after CPM administration 145

Figure 4.25 Modulation of a selection of markers on TILs in NXS2 tumours after CPM administration 146

Figure 4.26 Heat map of modulation of markers on T cell subsets in NXS2 tumours after CPM administration. 147

Figure 4.27 Gating strategies for T cell populations in tumours..... 149

Figure 4.28 Gating for double positive marker analysis example for T cell subsets in tumours after CPM administration..... 150

Figure 4.29 Modulation of T cell subset percentages and ratios Day 3 and Day 10 post CPM administrations 151

Figure 4.30 Heat map of T cell percentages and subset ratios in 9464D tumours at Day3 and Day 10 post CPM administration..... 152

Figure 4.31 Effect of CPM on T cell memory populations at Day 3 post administration..... 153

Figure 4.32 Effect of CPM on T cell memory populations at Day 10 post administration..... 154

Figure 4.33 Modulation of CD8+ phenotype at Day 3 and Day 10 post 40mg/kg CPM..... 155

Figure 4.34 Modulation of CD4+ phenotype at Day 3 and Day 10 post 40mg/kg CPM..... 156

Figure 4.35 Modulation of Treg phenotype at Day 3 and Day 10 post 40mg/kg CPM 157

Figure 4.36 Heat map of modulation of markers on T cell subsets in 9464D tumours at Day 3 and Day 10 after CPM administration. 158

Figure 4.37 GFP expression of transfected Phoenix-Eco cells 160

Figure 4.38 Development of puromycin and hygromycin kill curve for 9464D cells to determine appropriate selection dose..... 161

Figure 4.39 GFP expression of transduced 9464D cells after puromycin selection..... 162

Figure 4.40 Expression of hBCL-2 in transduced 9464D cells after hygromycin selection..... 164

Figure 4.41 Morphology of transduced 9464D cell lines compared to 9464D parent line 165

Figure 4.42 MTT assays after cytotoxic application using parental, EV and hBCL-2 9464D cell lines 167

Figure 4.43 Western blot analysis of apoptosis activation after MAF treatment in 9464D cell lines 168

Figure 4.44 Tumour growth curves of hBCL-2 transduced 9464D cell line..... 170

Figure 4.45 Tumour growth curves of hBCL-2 transduced 9464D cell line in NOD/SCID mice171

Figure 4.46 Effect of CPM administration on 9464D tumour TILs in both C57BL/6 and vav-BCL-2 mice 172

Figure 4.47 Modulation of PD-1 after CPM administration on 9464D tumour TILs in both C57BL/6 and vav-BCL-2 mice.....173

Figure 5.1 EW1-9(WT) and EW1-9(DG) antibody serum levels in C57BL/6 mice.....188

Figure 5.2 Tumour growth and survival of NXS2 tumour bearing mice after CPM and anti-4-1BB therapy.....190

Figure 5.3 Tumour growth and survival of NXS2 tumour bearing mice after CPM and anti-CTLA-4 therapy.....192

Figure 5.4 Representative example of tumour growth and survival of NXS2 tumour bearing mice after CPM and anti-PD-1 therapy.....194

Figure 5.5 Combined data of survival of NXS2 tumour bearing mice after CPM and anti-PD-1 therapy.....195

Figure 5.6 Tumour growth and survival of NXS2 tumour bearing mice after CPM and anti-PD-1 therapy at 5x5 mm start point.....197

Figure 5.7 Tumour growth and survival of 9464D tumour bearing mice after CPM and anti-PD-1 therapy at 8x8 mm start point.....198

Figure 5.8 Representative example of tumour growth and survival of 9464D tumour bearing mice after CPM and anti-PD-1 therapy at 5x5 mm start point.....200

Figure 5.9 Combined data of survival of 9464D tumour bearing mice after CPM and anti-PD-1 therapy at 5x5 mm tumour start point.....201

Figure 5.10 Representative example of tumour growth and survival of 9464D tumour bearing mice after CPM and anti-PD-1 therapy at palpable start point.....202

Figure 5.11 Combined data of survival of 9464D tumour bearing mice after CPM and anti-PD-1 therapy at palpable tumour start point.....203

Figure 5.12 T cell percentages in blood of NXS2 tumour bearing mice after combination therapy 205

Figure 5.13 T cell percentages in blood of 9464D tumour bearing mice after combination therapy 206

Figure 5.14 GD2 and PD-L1 expression on NXS2 tumours after combination therapy. 208

Figure 5.15 GD2 and PD-L1 expression on 9464D tumours after combination therapy..... 209

Figure 5.16 Immunophenotyping of tumour infiltrating lymphocytes after combination therapy in NXS2 tumour bearing mice 211

Figure 5.17 Immunophenotyping of tumour infiltrating lymphocytes after combination therapy in 9464D tumour bearing mice 212

Figure 5.18 PD-1 expression on TILs after combination therapy in NXS2 tumour bearing mice213

Figure 5.19 PD-1 expression on TILs after combination therapy in 9464D tumour bearing mice 214

Figure 5.20 Ki67 expression on TILs after combination therapy in NXS2 tumour bearing mice215

Figure 5.21 Ki67 expression on TILs after combination therapy in 9464D tumour bearing mice 216

Figure 5.22 Memory populations of TILs in NXS2 tumours after combination therapy..... 218

Figure 5.23 Memory populations of TILs in 9464D tumours after combination therapy 219

Figure 5.24 Memory population ratios of TILs in NXS2 tumours after combination therapy 220

Figure 5.25 Memory population ratios of TILs in 9464D tumours after combination therapy221

Figure 5.26 Immunophenotyping of tumour infiltrating myeloid cells after combination therapy in NXS2 tumour bearing mice. 223

Figure 5.27 Immunophenotyping of tumour infiltrating myeloid cells after combination therapy in 9464D tumour bearing mice. 224

Figure 5.28 Representative example of tumour growth and survival of 9464D tumour bearing mice after metronomic CPM and anti-PD-1 therapy at 5x5 mm start point228

Figure 5.29 Combined data of survival of 9464D tumour bearing mice after CPM and anti-PD-1 therapy at 5x5 mm tumour start point 229

Figure 5.30 Tumour growth and survival of 9464D tumour bearing mice after metronomic CPM and anti-PD-1 therapy at palpable start point 230

Figure 5.31 Survival of TH-MYCN mice treated with combination of CPM + EW1-9(DG) therapy 232

Figure 6.1 Summary of proposed mechanism of action of CPM and anti-PD-1 antibody therapy in NB models.....246

Figure 7.1 MSCV PIG GFP vector map for GFP transduction.....251

Figure 7.2 pMIG vector map for BCL-2 transduction.....252

Figure 7.3 Modulation of T cell percentages in NXS2 tumours after CPM administration 253

Figure 7.4 Immunophenotyping of tumours from BCL-2 transduced 9464D cell lines 254

Figure 7.5 EW1-9(WT) and EW1-9(DG) antibody serum concentrations over time in AJ mice255

Figure 7.6 T cell PD-1 and Ki67 expression in blood of NXS2 tumour bearing mice after combination therapy.....256

Figure 7.7 T cell PD-1 and Ki67 expression in blood of 9464D tumour bearing mice after combination therapy.....257

DECLARATION OF AUTHORSHIP

I, **EMILY ROSE WEBB**

declare that this thesis and the work presented in it are my own and has been generated by me as the result of my own original research.

Combination of immunomodulatory cyclophosphamide with anti-PD-1 monoclonal antibody therapy to improve survival in preclinical models of neuroblastoma

I confirm that:

1. This work was done wholly or mainly while in candidature for a research degree at this University;
2. Where any part of this thesis has previously been submitted for a degree or any other qualification at this University or any other institution, this has been clearly stated;
3. Where I have consulted the published work of others, this is always clearly attributed;
4. Where I have quoted from the work of others, the source is always given. With the exception of such quotations, this thesis is entirely my own work;
5. I have acknowledged all main sources of help;
6. Where the thesis is based on work done by myself jointly with others, I have made clear exactly what was done by others and what I have contributed myself;
7. None of this work has been published before submission:

Signed:

Date:

Acknowledgements

First and foremost I would like to thank my supervisors, Dr Juliet Gray and Prof Stephen Beers for their constant guidance and support throughout the project, and Prof Mark Cragg for his input at lab meetings. A big thank you is reserved for all of the Biomedical Research Facility staff, particularly Vikki English, Sam Martin and Lisa Dunning, for their brilliant training and constant help with all the *in vivo* work. Furthermore, I would like to thank Silvia Lanati, Alistair Easton and Julia Moreno Vicente for being brilliant and helpful colleagues in the Gray group. The antibody production team deserve a special thank you for producing all the in-house antibodies. All members of the Antibody and Vaccine group deserve a big thank you for being fantastic colleagues and people to work with. Importantly, I would like to thank the Neuroblastoma Society and University of Southampton for funding this project.

Personally, I would like to thank Gareth for putting up with me spending my weekends in the lab rather than exploring the south coast in the van together. Most importantly my greatest thank you is reserved for all of my family. Firstly, the constant (friendly) academic competition with my brother Josh, has always driven me to do everything first. Although this isn't so hard being the oldest, but you did publish a paper before me which I will always regret! However, to have you constantly nipping at my heels has always spurred me on, and in my eyes, you are an excellent historian and deserve everything you achieve. Finally, without the constant support from my parents for all these years, I would not be where I am today. This included little things such as encouraging my love of science as a child (although this was mainly dinosaur directed), proofreading my essays, pushing me to always try my best, and supporting me when everything didn't quite go to plan. However, I would like to thank them mostly for being fantastic role models who created a brilliant childhood environment for myself and my equally academically inclined brother, to allow us to both to achieve everything we have today. They are two amazingly hard working and caring people and no one could ask for better parents. Mum and Dad, everything I will ever achieve, is always done for you.

xx

Definitions and Abbreviations

A:I	Activatory: inhibitory ratio
ABCB1	ATP-binding cassette (ABC) transporter ABCB1
ACT	Adoptive cell transfer
ADCC	Antibody dependent cellular cytotoxicity
ADCP	Antibody dependent cellular phagocytosis
APC	Antigen presenting cell
ATP	Adenosine triphosphate
BCL-2	B cell lymphoma 2
BCR	B cell receptor
bMMRD	Biallelic mismatch repair deficiency
Breg	B regulatory cell
BSA	Bovine serum albumin
Ca2+	Calcium ions
CAR	Chimeric antigen receptor
CD	Cluster of differentiation
CDC	Complement dependent cytotoxicity
cDCs	Conventional DCs
CDRs	Complimentary determining regions
CH	Constant heavy chain domain
CIS	Cisplatin
CL	Constant light chain domain
CM	Central memory T cell

CPM	Cyclophosphamide
CRT	Calreticulin
CTL	Cytotoxic T lymphocyte
CTLA4	Cytotoxic T lymphocyte antigen 4
DAMPs	Damage associated molecular patterns
DC	Dendritic cell
DG	Deglycosylated
DMEM	Dulbecco Modified Eagle Medium
DMSO	Dimethyl sulfoxide
DOX	Doxorubicin
ECM	Extracellular matrix
EFS	Event free survival
ELISA	Enzyme-liked immunosorbent assay
EM	Effector memory T cell
EOMES	Eomesodermin
ER	Endoplasmic reticulum
EV	Empty vector
Fab	Fragment antibody binding
Fc	Fragment crystalizable
FCS	Foetal calf serum
FcγR	Fc gamma receptor
FDA	Food and Drug Administration
FoxP3	Forkhead box P3
FSC	Forward scatter

G-CSF	Granulocyte colony stimulating factor
GD2	Disialoganglioside 2
GDSC	Granulocyte derived suppressor cell
GFP	Green fluorescent protein
GITR	Glucocorticoid-induced TNFR-related protein
GM-CSF	Granulocyte macrophage colony stimulating factor
GN	Glutamine and non-essential amino acids
HAMA	Human anti-mouse antibodies
hBCL-2	Human BCL-2
HLA	Human leukocyte antigen
HMGB1	High mobility group box 1
HPV	Human papilloma virus
HRP	Horse radish peroxidase
Hsp	Heat shock protein
ICD	Immunogenic cell death
IDO	Indoleamine 2,3-dioxygenase
IF	Immunofluorescence
IFNγ	Interferon gamma
IgG	Immunoglobulin gamma
IHC	Immunohistochemistry
IL	Interleukin
iNKT	Invariant natural killer T cell
INRG	International Neuroblastoma Risk Group
INRGSS	INRG staging system

IP	Intraperitoneal
iirAEs	Immune related adverse events
ITAM	Immunoreceptor tyrosine based activatory motifs
ITIM	Immunoreceptor tyrosine based inhibitory motifs
ITSM	Immunoreceptor tyrosine switch motif
kDa	Kilodaltons
LA	Lung adenocarcinoma
mAb	Monoclonal antibody
MAF	Mafosfamide
M-CSF	Macrophage colony stimulating factor
MDSC	Myeloid derived suppressor cell
MFI	Mean fluorescence intensity
MHC I	Major histocompatability complex class I
MHC II	Major histocompatability complex class II
MICA/B	MHC I chain related molecules A/B
mIgG	Mouse IgG
MMP9	Matrix metalloproteinase 9
MOPS	3-(N-mopholino) propanesulfonic acid
MTT	3-(4,5-dimethylthiazol-2-yl)-2,5-diphenyltetrazolium bromide
NB	Neuroblastoma
NET	Neutrophil extracellular trap
NK	Natural Killer
NKT	Natural Killer T cell
NLRP3	Nucleotide-binding domain (NOD)-like receptor protein 3

NSCLC	Non-small cell lung cancer
NSSM	Nonsynonymous somatic mutations
OCT	Optimal cutting temperature compound
OS	Overall survival
OXA	Oxaliplatin
PAMPs	Pathogen associated molecular patterns
PBMC	Peripheral blood mononuclear cells
PBS	Phosphate buffered saline
PCR	Polymerase chain reaction
PD-1	Programmed Death
pDCs	Plasmacytoid DCs
PD-L1/2	Programmed death ligand 1/2
PFA	Paraformaldehyde
PGE2	Prostaglandin E2
PI	Propidium iodide
PNGase	Peptide:N-Glycosidase F
RA	13-cis-retinoic acid
ROS	Reactive oxygen species
RPMI	Roswell Park Memorial Institute medium
RT	Room temperature
SC	Subcutaneous
scFV	Single chain variable fragment
SDS	Sodium Dodecyl Sulphate
SDS-PAGE	SDS-Polyacrylamide Gel Electrophoresis

SIOPEN	International Society of Paediatric Oncology Europe Neuroblastoma
siRNA	Small interfering RNA
SSC	Side scatter
TA	Tumour antigen
TAM	Tumour associated macrophages
Tbet	T-box transcription factor TBX21
TCR	T cell receptor
TGF	Transforming growth factor
TGFβ	Tumour growth factor beta
Th	T helper cell
TH-MYCN	Tyrosine hydroxylase-MYCN
TILs	Tumour infiltrating lymphocytes
TLR	Toll-like receptor
TME	Tumour microenvironment
TNFR	Tumour necrosis receptor
TNFα	Tumour necrosis factor - alpha
Treg	T regulatory cell
UK	United Kingdom
ULBP1-3	UL16-binding proteins 1-3
VEGF	Vascular endothelial growth factor
VEGF-A	Vascular endothelial growth factor-A
VH	Variable heavy chain domain
VL	Variable light chain domain
WB	Western blot

WT	Wild type

Chapter 1: Introduction

1.1 Cancer

1.1.1 Biology of cancer

Multicellular organisms are constructed of collections of cells with distinct processes which cooperate to form tissues. Distinct tissues come together to form organs, and organs work together to produce an organism's form and function. The cellular building blocks all contain the same genetic material, however access to the appropriate genes for that particular cell type are highly regulated to ensure correcting functioning and control of these cells. Despite this, these genetic control process can become aberrant, due to cellular aging, environmental factors or predisposing genetic abnormalities. This can lead to uncontrolled proliferation, malignant transformation and eventual metastatic dissemination, properties which denote a cancer cell abnormal phenotype. Therefore, cancer can be viewed as a group of cells which, due to a variety of factors, are the result uncontrolled proliferative growth.

Cancer cells were described as possessing certain 'hallmarks' first defined in 2000 and updated in 2011 by Hanahan and Weinberg [1,2]. These hallmarks represent processes that normal cells can acquire and accumulate which drives them along the pathway to tumorigenesis and malignancy. First proposed were six distinct hallmarks including: sustaining proliferative signalling, resisting cell death, inducing angiogenesis, activating invasion and metastasis, evading growth suppressors, and enabling replicative immortality [2]. A principle hallmark defining a cancer cell is sustaining proliferative signalling, in which cancer cells can dysregulate growth factor pathways to continuously progress through the cell cycle. Cancer cells can produce their own growth factor ligands, stimulate stromal cells in the tumour microenvironment (TME) to produce growth factors and dysregulation of growth receptor expression [3-5]. Another essential hallmark to ensure tumour growth and progression acquired by tumour cells is the ability to resist cell death. For this cancer cells dysregulate molecular mechanisms to escape cell death by apoptosis which would usually be triggered other oncogenic processes. As well as leading to cancer progression acquisition of this hallmark can also lead to resistance to therapy [6]. Notably, tumours are known to have loss of p53 function, a prominent tumour suppression protein which induces apoptosis in response to DNA damage [7]. The induction of blood vessel formation known as angiogenesis is an essential process for tumour progression. Cancer cells can induce the growth of new blood vessels to support their growth, which allow for nutrient delivery and reduction of hypoxia. In adulthood, angiogenesis is only utilised physiologically in processes such as wound healing and therefore is usually transient.

However, in tumours the 'angiogenic switch' always remains activated [8]. To do this, tumours can secrete vascular endothelial growth factor-A (VEGF-A) themselves, or induce stromal support cells to do this. This factor leads to sprouting of new blood vessels, which are often poorly structured and leaky, supporting the TME and promoting further growth. For tumour progression to late stage cancer, invasion and eventual metastasis to distant sites occurs. To achieve this, cancer cells change shape and alter their attachment to cells and the extracellular matrix (ECM). This includes loss of adhesion molecule E-cadherin which is commonly seen in metastasising tumours [9,10].

After the seminal 2000 review, Hanahan and Weinberg updated the hallmarks with an additional 4 'emerging' hallmarks and characteristics, i.e: avoiding immune destruction, deregulating cellular energetic hallmarks, tumour-promoting inflammation and genome instability characteristics [1]. Cancer cells which develop genome instability characteristics are more likely to acquire multiple mutations which lead to the further development of the hallmarks described above. These mutant genotypes can lead to development of aggressive sub-clones of dominant cancer cells. This characteristic led to the hypothesis that tumour progression is a multistep process of sub-clonal expression acquiring new mutant genotypes [11]. Together with genomic instability, tumour promoting inflammation is a characteristic driver of cancer formation and progression. This inflammation relies on the invasion of immune cells, both innate and adaptive, in similar processes as seen in physiological inflammatory conditions [12]. Within the invading immune cells, both tumour eradicating (as discussed below) and tumour promoting cells are present. Immune cells which promote tumour inflammation enhance tumourigenesis and lead to further acquisition of malignant hallmarks, such as promoting angiogenesis. Linked to the characteristic tumour promoting inflammation is the cancer hallmark of evading immune destruction. Cancer cells need to develop evasion strategies against anti-tumour immune cells, in order to progress to increased malignancy. Increases in incidence of viral-induced cancers in immunocompromised patients has shown the importance of immune surveillance in keeping cancers at bay [13]. Many tumours are known to have cluster of differentiation (CD)3+ effector T cell infiltration, however these tumours still grow and progress, suggesting immune evasion strategies evolve in tumours. This can include downregulation of major histocompatibility complex I (MHC I), stimulating inhibition of T cells by utilising checkpoint pathways, secretion of immunosuppressive cytokines and recruitment of regulatory immune cells [14,15]. The balance of tumour promoting and tumour eradicating immune cells will be discussed in later sections in more detail. Finally, a hallmark recently described is the ability to reprogramme energy metabolism within tumour cells. Consequent to the aberrant proliferation, tumours require great amounts of energy to growth which, due to poorly organised vasculature, is normally lacking deep within the TME. To overcome this, tumour cells alter their energy metabolism from oxidative phosphorylation, to glycolysis utilising pyruvate metabolism.

This shift was first described by Warburg as a characteristic of cancer cells [16]. This mechanism allows cancers cells to function and proliferate in low oxygen and nutrient poor conditions as is usually found deep within large tumours.

All of the characteristics and hallmarks discussed above are utilised by cancer cells to ensure growth and progression of the tumours, and drives malignancy of the cells. However, these hallmarks are rarely shared by normal cells in their physiological environments, producing characteristics and pathways that can be exploited for novel cancer treatments. This includes but not limited to, anti-inflammatory drugs, immune activating monoclonal antibodies, glycolysis inhibitors and VEGF inhibitors. Consequently, this highlights the importance of understanding the underlying biology not just of cancer cells, but the environment they reside in, before considering possible pathways to target therapeutically.

1.1.2 United Kingdom (UK) cancer statistics

In the UK there are nearly 360,000 new cases of cancer every year (as of 2015), with around 160,000 deaths attributed to cancer. Of these cases, it is thought that 38% are preventable, attributable to lifestyle and environment (https://www.cancerresearchuk.org/health-professional/cancer-statistics-for-the-uk#heading-Zero). These figures demonstrate the large clinical burden that diagnosis, treatment and management of cancer poses, and therefore investigation into effective treatments alongside early diagnosis techniques is greatly needed. Cancers are defined into categories by a combination of factors including, but not limited to, anatomical location, histology and genetic aberrations. Of the 20 most common cancers in the UK (as of 2015) breast, prostate, lung and bowel cancer account for 53% of all cases (**Figure 1.1**). Despite the high numbers a new cancer cases, 50% of people diagnosed, survive cancer for more than 10 years (2010-2011). However, this varies greatly between different cancer types, as demonstrated in **Figure 1.2**. Survival rates for adult cancers have doubled over the past 40 years, resultant of a drive of early diagnosis, better clinical practice and the development of more precise and effective treatment strategies.

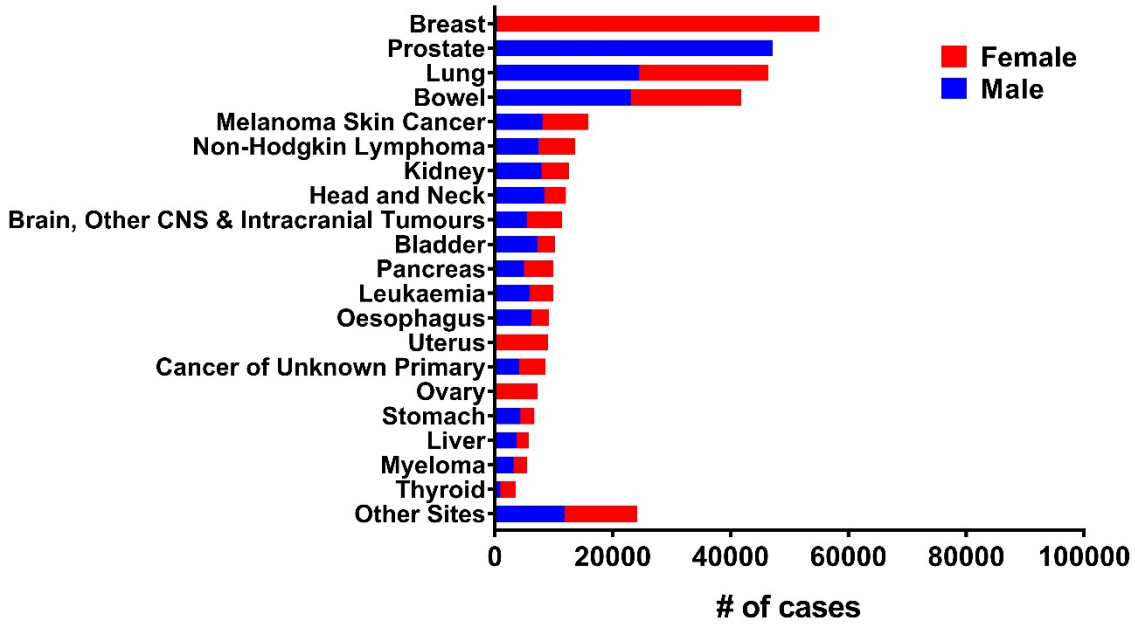

Figure 1.1 UK cancer incidence rates of 20 most common cancers in 2015

Incidence rates of the 20 most common cancers in adults are shown as numbers of cases in 2015. Female cases are shown in red and male in blue. Based on a graphic created by Cancer Research UK, accessed Nov 2018 (https://www.cancerresearchuk.org/health-professional/cancer-statistics/incidence/common-cancers-compared#heading-Zero)

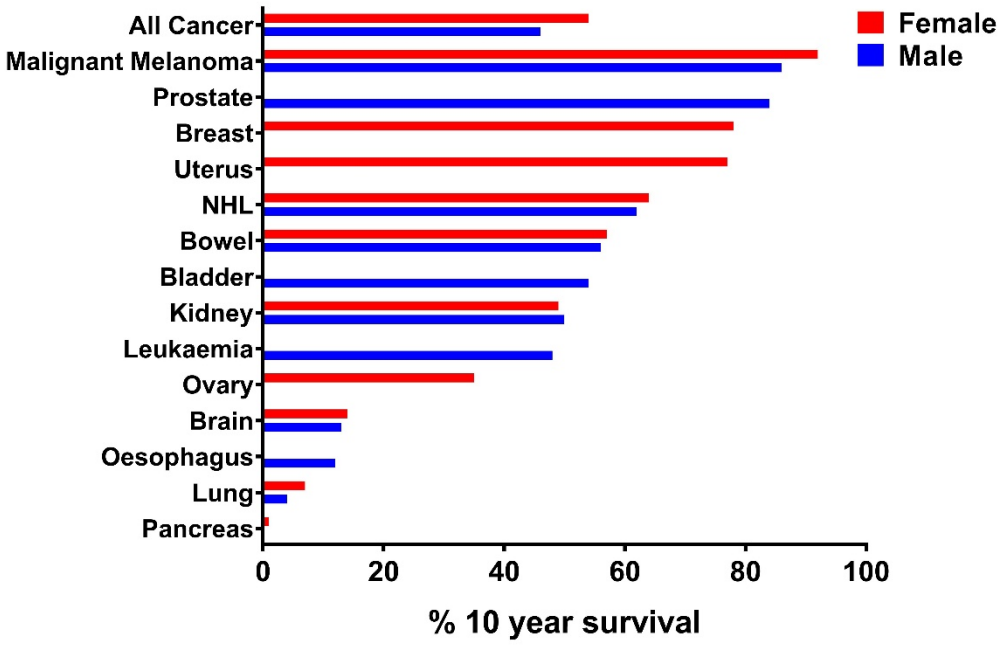

Figure 1.2 10 year survival rate of selected adult cancers 2010-2011

Percentage survival rates at 10 years of 10 selected cancers between 2010 and 2011. Female data is shown in red with male shown in blue. **NHL** = non-Hodgkin lymphoma. Based on graphics created by Cancer Research UK, accessed Nov 2018 (https://www.cancerresearchuk.org/health-professional/cancer-statistics/survival/common-cancers-compared#heading-One)

1.1.3 Challenges of paediatric cancer

In the UK, around 1800 new cases of childhood cancers are reported each year, resulting in 231 deaths (in 2015). Importantly, there has been a 13% increase in childhood cancer incidence since the early 1990's. Despite this, less than 1% of total cancer cases are childhood cancers and therefore these diseases remain extremely rare compared to adult cancers. However, 82% of children with cancer survive for 5 or more years after diagnosis (2006-10 – https://www.cancerresearchuk.org/health-professional/cancer-statistics/childrens-cancers).
These numbers lead to small patient cohorts for clinical trials resulting in the need for trials to be conducted over multiple sites and involving international collaboration. This results in specific challenges for paediatric oncology trials, such as requiring more funding and longer recruitment periods to ensure enough patients are enrolled to deliver accurate data.

When comparing the composition of the most common cancers found in children (**Figure 1.3**) to adult cancer (**Figure 1.1**), great disparity can be observed. For paediatric cases, the most commonly diagnosed cancers are leukaemia, lymphomas and embryonal tumours, without any major environmental drivers. However, in adults solid cancers which have strong environmental and age related drivers such as lung, melanoma and bowel are the most prevalent. Furthermore, it has been demonstrated that paediatric cancers have a reduced 'mutational burden' when compared to most

adult cancers [17]. This could be due to adult cancers, particularly lung and melanoma, being largely driven by aging and exposure to environmental carcinogens such as tobacco and UV radiation. These environmental exposures and aging of cells lead to DNA damage accumulation and therefore drives aberrant mutations within adult cancers, which can determine efficacy of certain immunotherapies [18]. Conversely, in paediatric cancers patients are very young and therefore have not been exposed to many if any environmental drivers of mutation at the time of cancer diagnosis. This demonstrates that childhood cancers arise with minimal mutational burden, and therefore have fewer neoantigens and are less immunogenic. [18,19].

10 year survival rates from paediatric cancers are also different compared to adult cancers as shown in **Figure 1.4** and **Figure 1.2** respectively. Overall, 10 year survival is relatively high at around 65%, and for certain paediatric cancers such as retinoblastoma and lymphomas this is near to 100%. Generally, these rates are higher than in adult cancers which have an average 10 year survival of around 50%. However, certain cancers such as bone sarcoma and sympathetic nervous system tumours, which includes neuroblastoma, have relatively low survival rates compared to other paediatric cancers.

Importantly, the peak age of paediatric cancer development is 0-4 years (2012-2014 - (https://www.cancerresearchuk.org/health-professional/cancer-statistics/childrens-cancers/incidence), meaning patients can be very young at commencement of treatment, adding to the challenges of their care. Furthermore, with regard to immunotherapy, children do not have a mature immune system and have encountered less immune challenges in their short lives, resulting in a more naïve immune system compared to adult patients, but may be more robust than geriatric adults, due to immune system decline [20,21].

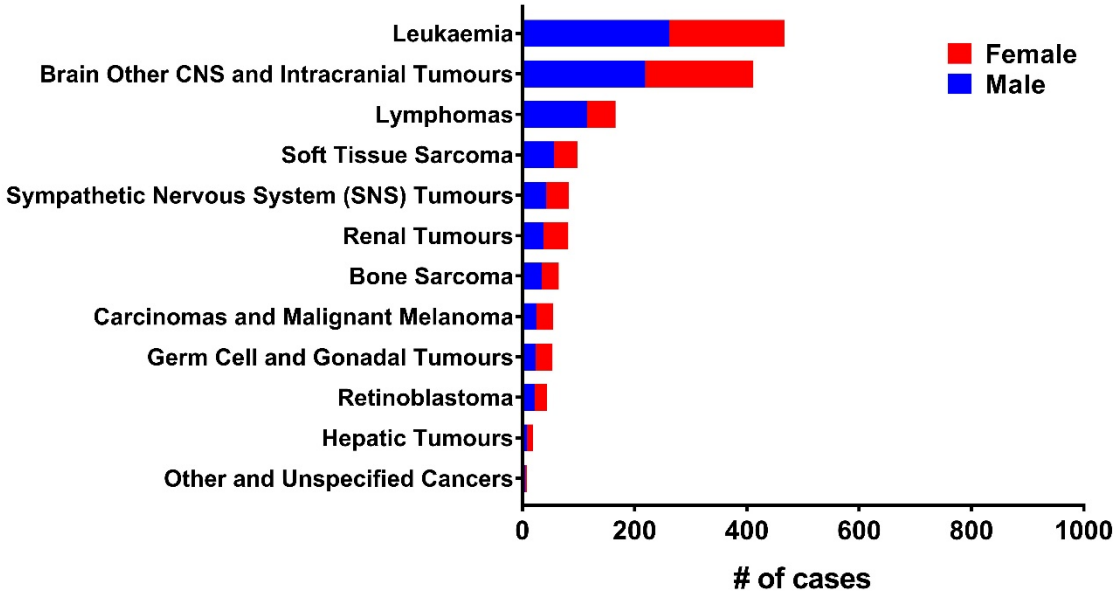

Figure 1.3 UK cancer incidence rates of paediatric cancers between 2006-2008

Incidence rates of paediatric cancers (children ages between 0-14) between 2006-2008. Cancer types are grouped into the 12 international Classification of Childhood Cancer (ICCC) categories. Sympathetic nervous system tumours include neuroblastoma, ganglioneuroma and pheochromocytoma. Based on a graphic created by Cancer Research UK, accessed Nov 2018 (https://www.cancerresearchuk.org/health-professional/cancer-statistics/childrens-cancers/incidence#heading-Three)

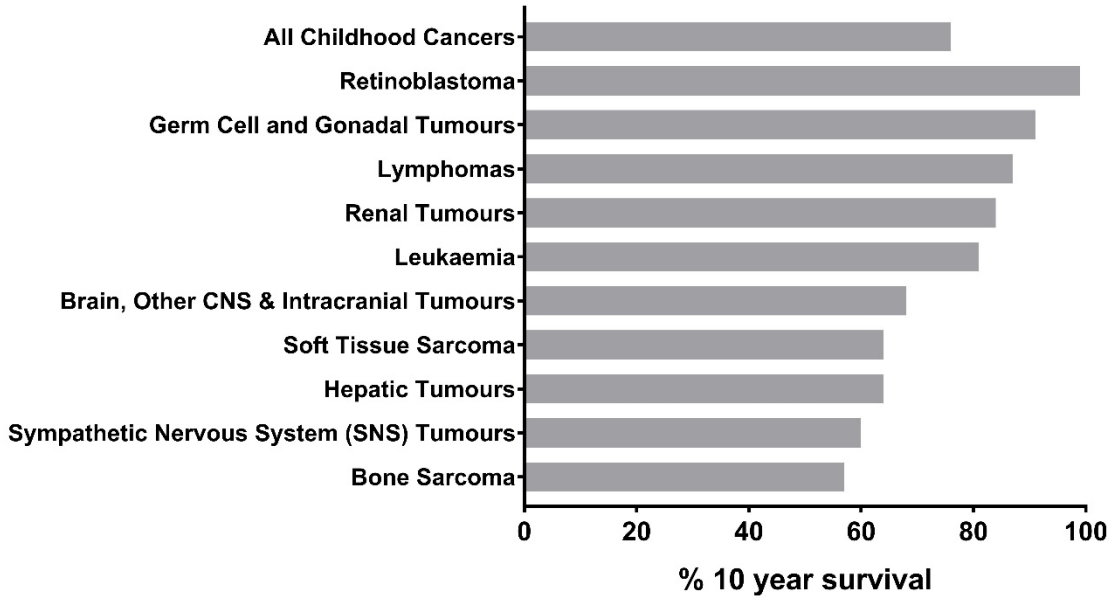

Figure 1.4 10 year survival rates for paediatric cancers 2001-2005

Percentage 10 year survival rates of paediatric cancers (children ages between 0-14) between 2001-2005. Cancer types are grouped into the 12 international Classification of Childhood Cancer (ICCC) categories. Based on a graphic created by Cancer Research UK, accessed Nov 2018 (https://www.cancerresearchuk.org/health-professional/cancer-statistics/childrens-cancers/survival#heading-Zero).

1.2 Neuroblastoma

1.2.1 Clinical overview

Neuroblastoma (NB) is a relatively rare childhood malignancy accounting for 15% of all paediatric cancer deaths but only 8% of new diagnosis [22]. It is a cancer of the sympathetic ganglion or adrenal medulla, forming from cells of neural crest origin [23,24] which have failed to differentiate [25]. In normal neural crest development in the embryo, neural crest cells migrate ventrally from the trunk along the neural tube to differentiate into sympathetic ganglia neurons, chromaffin cells of the adrenal medulla, Schwann cells and satellite cells in the peripheral nervous system [26,27]. These cells also give rise to cells of the craniofacial skeleton and melanocytes of the skin [28]. Due to its origins, the majority of NBs are diagnosed in the abdomen with adrenal medulla or lumbar sympathetic ganglion NBs accounting for 65% of diagnoses [29]. NB can also appear along any of the sympathetic ganglions within the pelvis, thorax and neck, however this is less common.

NB tumours can contain cells which resemble immature sympathetic neurons, schwann cells and stem-like cells [30], allowing for tumours to appear histologically heterogeneous [24]. As NB is a childhood disease, with tumour cells having similar protein expression patterns as embryonic neural crest cells, the development of the disease may be due to developing neuroblasts (from the neural crest) accumulating genetic/epigenetic alterations to form tumour stem like cells which then drive tumour formation [31].

NB is usually sporadic, but can occasionally (in < 2% of cases) be familial [32]. It is thought that mutations in two genes, PHOX2B and/or ALK, are thought to drive familial NB formation, both of which are involved in sympathoadrenal lineage development [29]. In sporadic cases, mutation of ALK gene is also seen in 6-10% of cases, and 3-4% of cases have an ALK amplification [33]. However, the most common genetic aberration associated with NB is amplification of MYCN gene. This occurs in 22% of tumours and is associated with more aggressive disease phenotypes [24,34,35]. MYCN normally functions to maintain pluripotency within neuroblast cells along with protecting their proliferative states and preventing differentiation until required [34-36]. Its role in NB development is demonstrated in the development of NBs in mice which have ectopic expression of MYCN under the control of a tyrosine hydroxylase promotor in neural crest derived cells [26,37], with the same outcome noted in a zebrafish model [38].

NB can also be characterised by expression of an oncofoetal differentiation antigen, GD2 [39,40]. GD2 is a T cell independent ganglioside carbohydrate antigen, with normal expression found on the cell surface of neuroblastic neuronal stem cells, mature neurons, pain fibres and melanocytes [40,41]. As this antigen is homogenously expressed across all NBs [42], it has become a therapeutic target in the

form of anti-GD2 antibody therapy, which has become a standard of care for high-risk NB patients, as will be discussed below.

1.2.2 Staging and outcomes

The clinical behaviour of NB is very heterogeneous, ranging from spontaneous regression to aggressive drug-resistant disease. An internationally agreed, risk classification system, combining clinical and biological characteristics, was therefore developed to predict survival and guide treatment [43,44]. The International NB Risk Group (INRG) used a database of over 8000 NB patients containing their clinical, radiographic, histological and biological data to develop the currently used staging and risk classification systems [43,44]. Firstly the INRG staging system (INRGSS) [43] (**Table 1.1**) aims to assess resectability of the tumours upon presentation. This is based on disease extent and presence of radiographic image defined risk factors [44,45]. From this the INRG pre-treatment classification schema was constructed which takes into account: INRGSS, age, histology, tumour differentiation, MYCN status, 11q LOH and ploidy [44,46] as shown in **Table 1.2**. This is used as an international standard to classify patients presenting with NB in order to accurately provide them with the current appropriate treatments.

Patients who present with low risk NB have good event free and overall survival, even with little or no therapy [46]. Patients with Intermediate risk disease also have good survival (90% event free survival – EFS) with surgical resection and/or chemotherapy [46,47]. However over 50% of patients present with high risk NB. Treatment for these children, as will be discussed in more detail, is an intense multi modal therapy programme, with many patients still relapsing and eventually succumbing to NB. Therefore the mortality associated with NB is mainly composed of patients dying of high risk disease either during treatment or due to relapse with treatment resistant disease.

Stage	Summary of staging
L1	Localised tumour not involving vital structures as defined by the list of image-defined risk factors and confined to one body compartment
L2	locoregional tumour with presence of one or more image defined risk factors
M	Distant metastatic disease
MS	Metastatic disease in children < 18 months - confined to skin, liver and/or bone marrow

Table 1.1 International NB Risk Group (INGR) staging system
This system is used to define NB stage at presentation and whether the tumours can be resected surgically. This staging classification is then further used as a factor for classifying risk group, as shown in table 1.2. *Adapted from Monclair, T., et al 2009* [43]

INGR stage	Age months	Histology category	Grade of tumour and differentiation	MYCN status	11q aberration	Ploidy	Risk group
L1/L2	ANY	Ganglioneuroma maturing or ganglioNB intermixed	ANY	ANY	ANY	ANY	A Very low
L1	ANY	ANY (except above)	ANY	Non-amplified	ANY	ANY	B Very low
				Amplified			K High
L2	< 18	Any (except above)	ANY	Non-amplified	No	ANY	D low
				Non-amplified	Yes		G Intermediate
L2	> 18	Ganglioneuroma nodular, NB	Differentiating	Non-amplified	No	ANY	E Low
			Differentiating	Non-amplified	Yes		H Intermediate
			Poorly differentiated/ no differentiated	Non-amplified			H Intermediate
				Amplified			N High
M	< 18	ANY	ANY	Non-amplified	ANY	Hyperdiploid	F Low
	< 12			Non-amplified		Diploid	J Intermediate
	12 to <18			Non-amplified		Diploid	J intermediate
	< 18			Amplified			O High
	>/= 18						P High
MS	< 18	ANY	ANY	Non-amplified	No	ANY	C Very low
				Non-amplified	Yes		Q High
				Amplified			R High

Table 1.2 INRG pretreatment classification schema
This scheme was designed to consistently assess mortality associated from NB, based on features of disease at presentation. This allows delivery of appropriate treatment according to risk group. This system depends on the factors: INRGSS, age, histology, tumour differentiation, MYCN status, 11q LOH and ploidy. *Adapted from Cohn, S.L., et al 2009* [44]

1.2.3 Current treatment strategies for high-risk disease

Treatment regimens for high risk disease are intensive, and consist of many different modes of therapies including chemotherapy, surgery, radiotherapy, to autologous stem cell transplants and immunotherapies. An example of standard treatment for high-risk NB patients is shown in **Figure 1.5**. Treatment is commenced with cycles of induction chemotherapy, which consists of a combination of agents including but not limited to doxorubicin, etoposide, cyclophosphamide and cisplatin, followed by surgical resection and radiotherapy [48]. This is followed by myeloablative chemotherapy with autologous stem cell rescue [48]. Following this, 13-cis-retinoic acid (13-cis-RA) is administered to drive any residual NB cells to differentiate into non-malignant cells [48]. Recently, additional immunotherapy with anti-GD2 antibody therapy together with interleukin-2 (IL-2) and granulocyte-macrophage colony-stimulating factor (GM-CSF) has been added, which resulted in a significant improvement in 2 year EFS from 48% in 13-cis-RA alone to 59% when this is combined with the above immunotherapies. Furthermore, overall survival (OS) was improved from 59% in the RA arm alone to 74% in the RA with immunotherapy arm [49]. Unfortunately, the administration of the anti-GD2 antibody is associated with quite high levels of toxicity, with more than 90% patients in the phase III trial experiencing an adverse event [49], with a significant number of grade 3+4

toxicities occurring in the patients receiving the antibody. Importantly, the most experienced toxicity was pain in 52% patients receiving the antibody compared to just 6% receiving 13-cis-RA alone [49]. Currently there are wide-scale trials in progress to assess whether interleukin (IL)-2 administration confers additional benefit to the anti-GD2 antibody, as the addition of this cytokine has been associated with some of the side effects caused by the therapy.

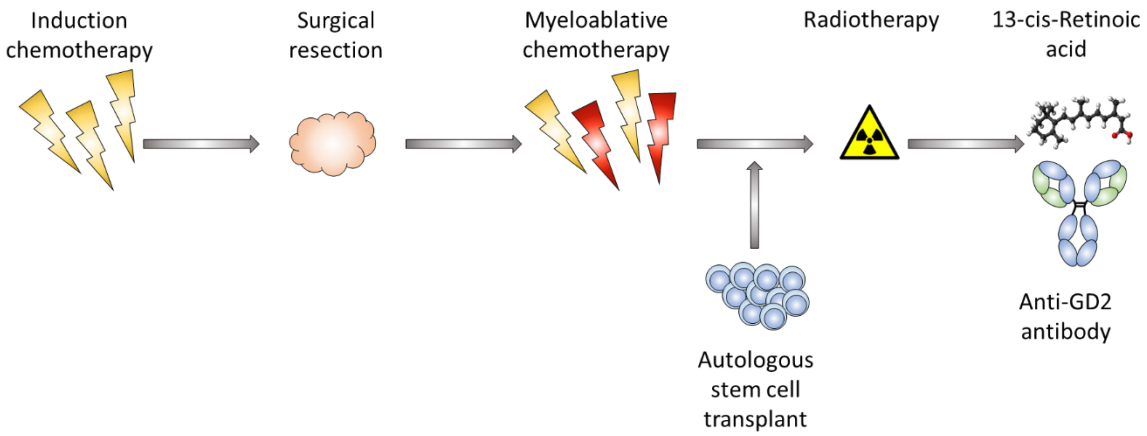

Figure 1.5 Example of current high-risk NB treatment programme (SIOPEN trial)

Most treatment strategies for high-risk NB patients involve intense multi-modal therapy, centring around chemotherapy and autologous stem cell transplants. An example of a current treatment pathway shown above is from the SIOPEN trial using the anti-GD2 antibody therapy which has proved to be quite efficacious. *Ladenstein et al., 2017*

Even with the intensive treatment described above, around 50% of patients will eventually relapse or develop refractory disease [50,51]. Most relapses present as metastatic drug resistant disease, in which the mutational landscape has been altered by the selective pressure of chemotherapy [46] and therefore the tumours are distinctly different from the original tumour at presentation. There is therefore a need to develop effective treatment strategies using approved therapeutics for NB therapy in order to tackle the problem of relapsed disease. This may be improved with the advent of rapid characterisation of the genomic landscape of biopsies from relapsed tumours to direct treatment in the right direction [46].

1.2.4 Can prognosis be improved?

Despite the intensive treatment regimen for patients presenting with high risk disease as described above, the current 5 year survival rate is only between 40-50% with around half of those patients going on to develop refractory disease or relapse (when treated without immunotherapy) [50,51]. With the addition of the anti-GD2 antibody, short term survival rates are high [49,52], however a high majority of patients still go on to relapse from the disease. Furthermore, this relatively high survival rate is from the start of immunotherapy, however, as not all patients respond well enough to

treatment prior to initiation of immunotherapy, this figure is a lot higher than if taken from diagnosis, which is demonstrated in **Figure 1.4** to be closer to ~60% (under SNS tumours). The intensive treatment regimen also comes with a risk of treatment related mortality, with around 3-5% patients dying from the treatment related complications [48]. Furthermore, as discussed, anti-GD2 antibody therapy is associated with high rates of adverse effects, including neuropathic pain, leading to cessation of the treatment early and therefore reduced efficacy. This toxicity limits the dosing of the antibody and therefore its full therapeutic potential may not be reached. Both the high treatment mortality rate related to high dose chemotherapy and stem cell transplant, and toxicities associated with overall treatment means there is little scope for further intensifications of current therapeutic strategies for high risk NB patients. The improvement of prognosis and treatment outcome for patients lies in refinement of the standard treatments already in place. A solution may be found using reduced and therefore more tolerable doses of chemotherapies, in combination with immunotherapies already proven to be efficacious in adult cancers but with low levels of associated toxicities. If this combination can be proven efficacious, this could provide a solution for increasing treatment completion rates, reducing treatment related mortality and hopefully decreasing the amount of disease relapse.

1.3 Immune system and cancer

The importance of the interplay between the immune system and tumour development has been recognised since the idea of immunosurvelliance was first put forward in the 1970s by Burnet [53,54]. So crucial is this relationship to understanding tumour progression, that the ability of the tumour cell to evade immune destruction was included as one of the essential 'Hallmarks of Cancer' by Hanahan and Weinberg, as discussed previously [1]. Understanding how the immune system interacts with the developing tumour is more imperative than ever with immunotherapies fast becoming an important and pivotal tool in the armoury of clinicians, mainly due to their observable potency and specificity for cancer cell removal. It is becoming increasingly clear that all arms of the immune system, both innate and adaptive, have a role to play within the tumour microenvironment, with both pro- and anti-tumourigenic effects. Therefore, when investigating cancer therapies it is important to consider the effect they will have on all immune cells within the host to make sure the balance is tipped in favour of tumour eradication.

1.3.1 Innate immune cell subsets

Cells of the innate immune system provide the first line of defence in the immune response, due to their generalised specificity and rapid activation that does not require priming unlike adaptive immune cells. These cells and pathways are ancient in terms of the evolution of the immune system

and are present in many organisms. They are primed to respond to evolutionary conserved patterns such as damage associated molecular patterns (DAMPs) and pathogen associated molecular patterns (PAMPs)[55]. Furthermore, they also act as the starting points for the development of a more potent and specific adaptive immune response, acting as antigen presenting cells and cytokine producers in order to activate and coordinate adaptive immune cells. Therefore cells of the innate immune system hold important roles in immune activation and have been shown to be particularly important orchestrators of the immune system in cancer, with both stimulation and repression of an anti-tumour response [56].

1.3.1.1 Myeloid cells

Cells of the myeloid lineage include macrophages, monocytes, neutrophils and dendritic cells (DCs), and act mainly as a quick initial effector response against pathogens and as antigen presenting cells (APCs).

Monocytes have long been considered precursors of macrophages and DCs and together they were thought to make up the mononuclear phagocyte system [57]. However this basic understanding has changed in recent years with monocytes very much an important effector cell in their own right with their own phagocytic and effector properties [58]. Monocytes are key effector cells in inflammation in pathogenic conditions [59], and can differentiate into macrophages under these conditions. All vertebrates have monocytes, which are defined as such by their location, phenotype, morphology and genetic signatures [60]. Humans have more than double the amount of monocytes circulating in the blood as mice, however both have considerable numbers of the cells in the spleen and liver ready to mobilise when needed [61,62]. Within mice the development of monocytes relies on the colony stimulating factor macrophage colony stimulating factor (M-CSF), which also determines their survival [63,64]. Human monocytes are divided into two subpopulations: $CD14^{low}$ CD16+, and CD14+ CD16+/- [65], and mouse monocytes consist of $LY6C^{hi}$ $CX3CR1^{mid}$ CCR2+ CD62L+ $CD43^{low}$ monocytes and $LY6C^{low}$ $CX3CR1^{hi}$ CCR2− CD62L− $CD43^{hi}$ monocytes [66-68]. As mentioned, when inflammation occurs monocytes a recruited to the site and once there can differentiate into mononuclear phagocyte population such as macrophages and DCs [59].

Macrophages are specialist in phagocytosing pathogens and cells, and are potent cytokine producers. Macrophages associated with tumour cells are known as tumour-associated macrophages (TAMs) and have been linked to a worse prognosis [69,70]. It appears that the tumour cells themselves may recruit macrophages to the microenvironment using a combination of factors including cytokines and chemokines [71,72]. Despite macrophages being able to induce a receptive environment for an immune response by secreting proinflammatory mediators, secretion of these factors (such as reactive oxygen/nitrogen species) during early tumour development actually

promote carcinogenesis via chronic inflammation [73]. Their ability to influence tumour progression involves promotion of angiogenesis and tumour invasion and metastasis, through a variety of secreted factors [74,75]. Within the tumour microenvironment, macrophages are seen to be polarised along a spectrum of phenotypes with extremes being referred to as either M1 or M2. Interferon gamma (IFNγ) and tumour necrosis factor alpha (TNFα) lead to stimulation of M1 polarisation, and IL-4 and IL-13 stimulation of M2 polarisation. The M1 phenotype is associated with promoting an anti-tumour response and tumour control due to their increased ability to secrete IL-12 and reduction in IL-10 production [76]. M2-like macrophages however secrete more IL-10 and therefore are associated with a protumourigenic role, suppressing the anti-tumour immune response [76]. Therefore, it is extremely important to take into account macrophage polarisation when investigating tumour immunology and developing new immunotherapeutics.

DCs are professional and proficient APCs and act as the most effective bridge between the innate and adaptive immune system. They are specialised cells, capable of uptaking antigenic components of dying tumour cells or pathogens which they can then present via MHC to T cells in order to direct an immune response against that particular antigen. Furthermore, as professional APCs, DCs are able to cross-present antigenic peptides to both MHC I and MHC II, leading to the most robust activation of both CD4+ and CD8+ T cells [77]. Cross-presentation of antigens is the process of an APC being capable of presenting extracellular derived antigens via MHC class I molecules, as demonstrated in **Figure 1.6** [78].

DCs are usually divided into two main subgroups: plasmacytoid (pDCs) and conventional (cDCs) [79], with pDCs specialising in type I interferon (IFN) production and cDCs specialising in efficient phagocytosis and cross presentation to CD8+ T cells [76,77]. Despite pDCs being able to prime T cell responses when appropriately activated [80], this DC subset may actually have a tolerogenic phenotype [81,82]. This is mediated by the immunosuppressive microenvironment surrounding tumours which can lead to improperly activated and matured pDCs [83,84]. CD8α+ DCs are one subtype of cDCs and has been found to be extremely proficient at cross-presentation [77] This ability may be due to an increase of expression of receptors which detect dying cells, such as CLEC9A [85,86], to efficiently prime immature cDC which can then go on to stimulate an anti-tumour immune response. Recently, it has been reported that CD103+ DCs are important cells within the tumour microenvironment that may be efficient in stimulating anti-tumour immune responses. Broz et al [87], demonstrated that after extensive immunophenotyping of murine tumour models a distinct population of CD103+ DCs which also expressed typical DC markers. However the CD103+ DCs, known as dendritic cell type 2 cells were demonstrated to have enhanced cross-presentation, increased ability to co-stimulate T cells and finally a higher expression of cytokines such as CCL5, which is involved in T cell interactions [87]. In one study, CD103+ DCs were found to be transporting

antigen to lymph nodes to prime anti-tumour CD8+ T cells, and were found to be important in response to anti-PD-L1 therapy in murine melanoma models [88].

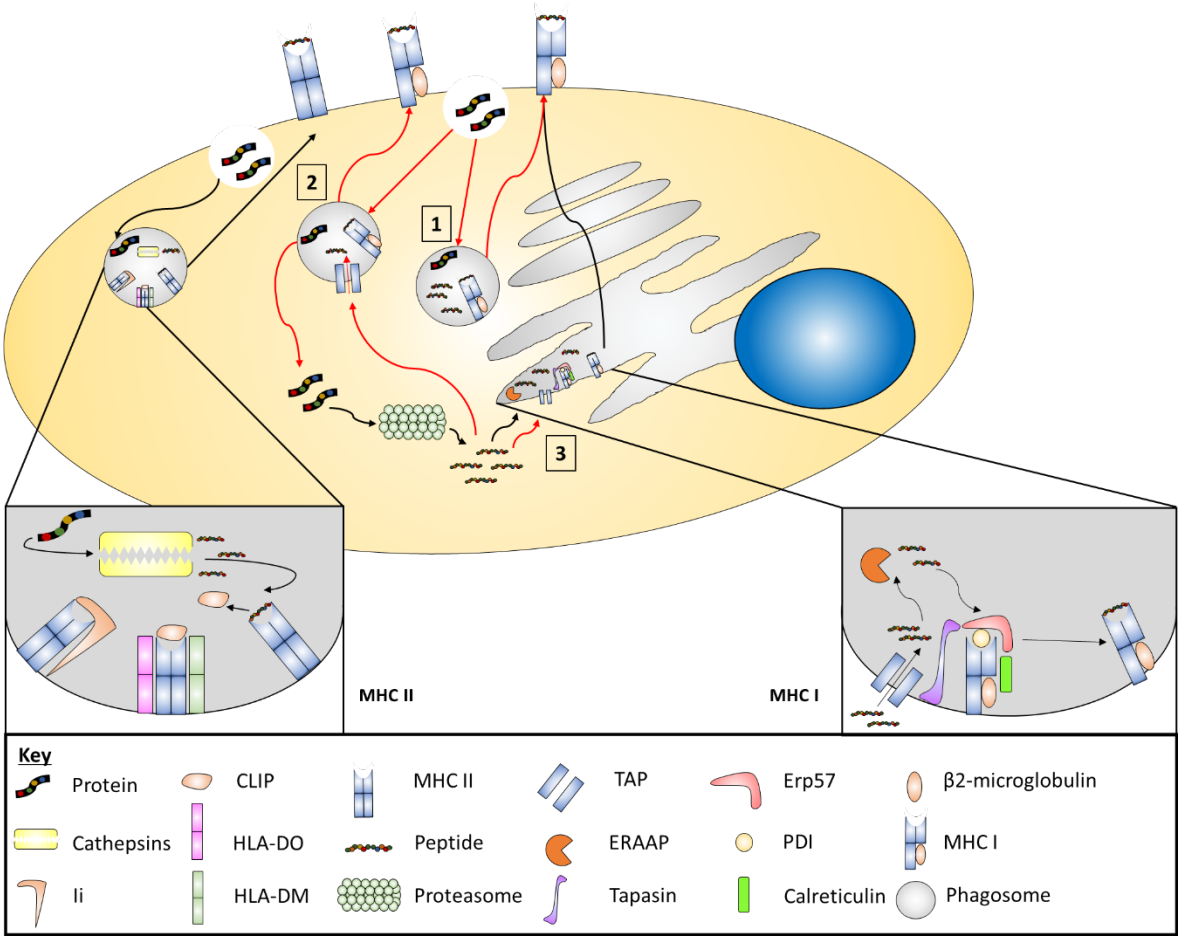

Figure 1.6 Mechanisms of antigen presentation by professional APCs

Antigen processing and presentation by APCs such as DCs requires different pathways in order to present via MHC class I or class II. Intracellular antigens are usually presented via MHC I, whereas extracellular antigens are presented by MHC II. For MHC I loading, intracellular proteins are processed into peptides by the proteasome. From here the peptides enter the endoplasmic reticulum via TAP, where they may undergo further processing via ERAAP. Within the ER MHC I is stabilised by chaperon proteins such as calreticulin, Erp57, PDI and tapasin. Once processed peptides associate with MHC I, the chaperone proteins disassociate from the complex and presentation of MHC I – peptide complex on the cell surface can be completed via transport through the Golgi network. For MHC II loading, extracellular proteins are phagocytosed, degraded in the endosomal pathway and then transported into the MHC class II compartment (MIIC). Here cathepsins digest the invariant chain (Ii) stabilising the MHC II molecule leaving CLIP in the peptide binding groove. CLIP is then exchanged for the peptide, which requires the chaperone protein HLA-DM or DO (B cells), and the MHC II – peptide complex can now be transported to the cell membrane for presentation. Via mechanisms of cross-presentation, extracellular antigens can be presented via MHC I. Cross presentation pathways include: **1)** Phagocytosis of extracellular antigens/proteins leads to their encapsulation into phagosomes, where the proteins can be degraded and immediately loaded onto MHC I molecules, known as the vacuolar pathway. **2)** Again phagocytosed proteins are encapsulated into phagosomes, but can be expelled into the cytoplasm, leading to proteasomal processing into peptides. From here the processed peptides can either be transported back into the phagosome and loaded directly onto MHC I, known as the cytosolic pathway with phagosomal loading. **3)** The peptides processed by the proteasome as described in pathway 2 could also be loaded onto MHC I after transport into the endoplasmic reticulum, with loading and presentation occurring as described above. This is known as the cytosolic pathway with ER loading. Red arrows = cross presentation pathways, Black arrows = MHC I or II peptide loading pathways. *Adapted from Joffre et al 2012.*

Neutrophils are a polymorphomuclear myeloid cell subset and have a major role during acute inflammation being the first cells to be recruited to sites of infection or inflammation[89-93]. These cells are generated in the bone marrow from precursor cells stimulated by granulocyte colony stimulating factor (G-CSF)[94]. Humans have considerably more neutrophils circulating than mice at 50-70% compared to 10-25% of circulating leukocytes respectively [95,96]. The most characteristic aspect of neutrophils are their segmented nucleus and cytoplasm full of granules and secretory vesicles filled with proinflammatory proteins [97,98]. In pathological conditions neutrophils are adept killers of pathogens using a variety of mechanisms to eliminate them. Firstly like other myeloid subsets, neutrophils are able to phagocytose pathogens and kill them intracellularly [97,98]. Another mechanism involves the generation of reactive oxygen species (ROS).This involves assembly and activation of NADPH oxidase, via subunits enclosed in numerous granules within the neutrophil. This functions as an electron transport chain to facilitate the reduction of O_2 to form superoxide ($\cdot O_2$-). Superoxide can then dismutate into ROS, including hydrogen peroxide and hydroxyl radicals [99]. Production of the ROS can lead to pathogen killing [97,98]. Finally, if a neutrophil becomes highly activated it can release a neutrophil extracellular trap (NET) [100]. These NETs are composed of DNA element where molecules such as histone proteins and enzymes are attached. These NETs catch pathogens and immobilise them and help subsequent phagocytosis and eventual destruction of the pathogen [101]. Interestingly it has been reported in many instances that neutrophils hold an important role with regulating how the immune system interacts with cancer. Neutrophils can express proteases such as matrix metalloprotease 9 (MMP9), which in turn activates VEGF to promote revascularisation [102]. Cancer cells have been shown to benefit from the proangiogenic functions of neutrophils to enhance their own growth [103]. Furthermore, neutrophils have long been known to be able to supress T cell proliferation and activity, possibly through IL-10 production [90,104]. In part this also may be due to secretion of arginase 1 [105], which neutrophils have a large store of, and therefore neutrophils could act as a granulocyte derived suppressor cell (GDSC), which supress antigen-specific T cell responses [106,107].

1.3.1.2 NK cells and NKT cells

Natural killer (NK) cells are an important innate immune effector cell subset which are able to efficiently kill tumour cells via innate recognition, and are therefore are quick to respond. NK cell infiltration within tumours is associated with a good prognosis [108,109], and they are important effector cells to reduce tumour growth in murine tumour models [110,111]. NK cells are lymphocytes arising from common lymphoid progenitor cells [112], along with B and T cells. They are characterised by their surface expression of CD56 and do not express CD3. Murine NKs however express CD49b

instead of CD56 but still lack CD3 expression [113]. The 'missing self' hypothesis describes one way NK cells are able to recognise targets [114]. In physiological conditions, NK cells are inhibited by the presence of MHC I expression on the surface of cells. When MHC I is downregulated, as tumour cells and virally infected cells are known to do, the inhibitory receptor is not stimulated and the NK cell can be activated by other receptors and kill the target cell [115]. Cellular stress and DNA damage, conditions common in tumour cells, can lead to NK cells activation by upregulation of MHC I chain related molecules A/B (MICA/B) and UL16-binding proteins 1-3 (ULBP1-3) expression which then activate the NKG2D receptor on NK cells leading to NK cell killing [116]. Cytokines such as IL-12, IL-18, IL-15 and type I interferons increase NK cell activation and tumour cell killing [117]. Mechanisms of tumour cell killing by NK cells includes release of cytotoxic granules, inducing apoptosis and secreting IFNγ [118].

Another subset of innate effector cells are natural killer T (NKT) cells. These cells express NK cell markers but also express CD3 and express an invariant T cell receptor (TCR) [119]. Invariant NKT cells (iNKT) are the main effector subset, expressing the invariant TCR which recognises glycolipid antigens presented on CD1d molecules [120]. Tumour derived GD3 has shown to be a ligand for iNKT cells [121], leading to activation of the iNKT and rapid cytokine production and cytotoxic activity [122]. Activated iNKT cells produce IL-2, IL-4 and IFNγ [123]. iNKT cells have been shown to be important in immunosurveillance and tumour control [124,125].

1.3.2 Adaptive immune cell subsets

The second line of immune system defence relies on cells of the adaptive immune system. This arm of the immune system can orchestrate an extremely specific directed response, however they require a longer period of time to prime themselves before becoming effective. Effector cells of the adaptive response are potent and critical for the elimination of virally-infected cells, and more importantly, tumour cells, as will be discussed below.

1.3.2.1 T cells

When considering tumour immunology T cells are often regarded as being the most important effector cell driving an anti-tumour immune response [126-128]. However, T cells consist of many different subsets, with most of them stimulating and carrying out an effective immune response. However, at least one subset is considered to be immunosuppressive and hinders a developing anti-tumour response. Therefore the presence of all these different subsets of T cells within tumour biopsies can determine either a positive or negative prognosis based on the prominent T cell subset and their relative activation states. Arguably there are two main subsets of T cells important in cancer immunology, which are subdivided by their expression of either CD8 or CD4 molecules along

with the αβ T cell receptor (TCR), with a further subset of more innate like T cell expressing the γδ TCR [129]. Both of the αβ T cell subsets are MHC restricted, therefore for the T cells to recognise antigen, antigens in the form of peptide needs to presented by either MHC class I molecules for CD8+ cells, or MHC class II molecules for CD4+ T cells [130]. After MHC-peptide engagement, TCR signal transduction occurs via CD3. This was demonstrated by T cell activation after anti-CD3 antibody application, with CD3 expression being vital for T cell function [131].

CD8+ T cells are regarded as the most potent effector cells of the adaptive immune response, due to their cytotoxic activities, and therefore are also known as cytotoxic T lymphocytes (CTL) and are vital to the immune response against viruses and cancer [132,133]. Their potency relies on development of a type I, pro inflammatory response, which also requires help from CD4+ T helper cells [133]. After pathogenic or tumour antigen presentation initiating TCR signalling, and activatory signalling into the T cell, CD8+ CTLs are able to produce cytotoxic molecules such as granzyme B and perforin which leads to virally infected or tumour cell lysis and death, via apoptosis. The importance of CTLs within the tumour microenvironment was noted in 1980s where tumour infiltrating lymphocytes (TILs) were identified in tumour biopsies and correlated with response to the adoptive T cell therapy [134,135]. Lack of T cells in immunodeficient mice was also correlated with higher incidence of cancer formation [136,137]. Furthermore, the CD8+ T cell associated proinflammatory cytokine IFNγ was found to be equally as important as CTL infiltration [138]. Presence of CD8+ T cells in the tumours of many cancers is associated with improved prognosis [139-142]. The presence of active effector CD8+ TILs is needed to effectively eliminate tumour cells. The priming of CD8+ T cells into effector cells occurs in the tumour draining lymph nodes via DC activation [143,144]. These cells are potently cytotoxic and express high levels of IFNγ, TNFα, granzymes and perforin. Potency of these cells to eradicate tumour cells has been demonstrated, as will be discussed later, by using these isolated TILs for adoptive cell therapy [134,145,146]. Due to their potency, these cells are usually very short lived under chronic stimulation, and therefore become anergic and eventually apoptotic [147]. Therefore in order to develop a long lived immune response to cancer another subtype of CD8+ cells needs to be stimulated, known as T memory cells. These cells form from T cells which have recognised antigen but have developed into a longer lived phenotype rather than potent effector cells [148,149]. There are two subsets of memory cells, central memory (CM) and effector memory (EM) [150]. CM have reduced potential to differentiate into effector cells but have high levels of proliferation and IL-2 production, whereas EM are more effector like, being able to rapidly differentiate into effector T cells [151].

T cells which express CD4 are also important immune cells with regards to developing an anti-tumour immune response, with their role mainly focussing on fine-tuning and regulating the CD8+ antigen specific responses [152,153]. CD4+ T helper (Th) cells are stimulated by DCs presenting tumour antigen via MHC II molecules within the draining lymph node. From here, the CD4+ cells migrate to

the tumour microenvironment and boost immune responses by the release of proinflammatory cytokines [152]. There are many CD4+ T cell subsets which are defined by transcription factor expression and cytokine profile among others factors. An example of a CD4+ subset are Th1 cells which are defined by their secretion of IFNγ and TNFα, two important proinflammatory cytokines [154]. Th2 cells however release a different pattern of cytokines including IL-4, IL-5 and IL-13 [154]. In terms of cancer prognosis, it has been reported that the presence of Th1 CD4+ cells within tumours is associated with good prognosis, whereas the opposite is seen with high Th2 infiltration [155].

However, we now know that not all CD4+ T cells are activatory in function and that some actually regulate and supress immune responses. These CD4+ T cells are known as T regulatory cells (Tregs) and are characterized by their expression of the transcription factor FoxP3 and their function in secreting IL-10 and tumour growth factor beta (TGFβ), two immunosuppressive cytokines [154]. This subset of CD4+ cells have been implicated as substantial regulators of an immunosuppressive tumour microenvironment, and have been reported as being the main subset of infiltrating CD4+ cells [156]. Recently the transcription factor BACH2 has been implicated as important for Treg immunosuppressive ability, along with Forkhead box P3 (FoxP3) [157]. Together with the immunosuppressive cytokine production mentioned above, Tregs can also supress effector T cells via cytotoxic T lymphocyte antigen 4 (CTLA-4) receptor signalling [158]. Their importance in the tumour microenvironment has been well noted, and depletion or disruption of these T cells has been shown to increase the anti-tumour immune response [159]. Furthermore, the efficacy of immune checkpoint antibody therapy may depend on the therapy's ability to deplete or switch off these suppressive cells, as will be discussed later.

1.3.2.2 B cells

B cells are the orchestrators of humoral immunity, Along with T cells, they drive the adaptive immune response to pathogens and tumour cells [160]. They mainly exert their effector function via the production of antibodies, which can bind and opsonise pathogens to aid their removal by other effector cells and mechanisms. Just like most other immune cells B cells have many different subsets which are defined depending on their anatomical location [161,162]. To produce antibodies and other effector functions B cells work via the B cell receptor (BCR). This receptor is specific for one target antigen as it is constructed from pairs of immunoglobulin heavy and immunoglobulin light chains [163]. These chains are membrane bound antibodies, and as such have a variable region which gives the receptor its specificity. When an antigen is bound, the receptor is able to signal through the coupling of a heterodimer of CD79A and CD79B molecules which mediate the signal transduction, due to their immunoreceptor tyrosine based activatory motifs (ITAM) [163,164]. The following signalling cascade leads to activation of pathways which increase proliferation and

survival of B cells [165]. If this is in response to a pathogenic antigen, B cells are activated in the germinal centres and are positively selected to differentiate into antibody-secreting plasma cells, with follicular CD4+ T cell help, based on their affinity to bind the target antigen [166,167]. B cells also require involvement of cytokines, complement derived factors and stimulation via TLR pathways to facilitate their activation into potent antibody producers. Follicular helper T cells promote activation of B cells via expression of CD40 ligand alongside production of cytokines [168]. Production of IL-4, IL-5 and IL-6 are key cytokines involved in T-cell dependent B cell activation, which promote the secretion of antibodies [169]. Regulation of B cell activation by the complement pathway is largely controlled by the expression of complement receptor CR2. This receptor acts as a co-receptor on naïve B cells and allows uptake of immune complexes during antigen-induced B cell activation [170]. Furthermore, C3d, a complement molecule, bound to CR2 on follicular DCs, or B cells themselves, can help antigen presentation to the BCR [171,172] Immature B cells can respond to LPS via TLR4 to induce fast antibody responses which do not rely on CD4+ T cell help [173,174]. Apart from antibody production B cells have many other functions including acting as antigen presenting cells for T cell responses. When the BCR has come into contact with antigen it internalises with the antigen, and can therefore be processed into peptide for presentation via MHC molecules to T cells. Furthermore, B cells also express co-stimulatory factors to mature T cells appropriately to lead to an effective T cell response, and can secrete proinflammatory cytokines such as IL-6 and IFNγ[175,176]. Despite expressing TLRs to enhance their presentation ability [175], B cells are not as professional an APC as DCs are, to T cells. B cells themselves can also function as effector cells in their own right, with some being able to produce proinflammatory cytokines during an immune response such as IFNγ, TNFα and IL-17, which again can effect T cell activation [175,177].

Since the 1970's it has become apparent that, like T cells, B cells also have a subset capable of performing regulatory and suppressive functions, named regulatory B cells (Breg) [178,179]. Under physiological conditions, Breg function is critical in supressing the immune system to prevent chronic inflammation and resultant tissue damage ensuing after an immune response [180]. Breg cells function by producing immunosuppressive cytokines such as IL-10, IL-35 [181] and TGFβ [182], with B-cell deficient mice developing chronic inflammation after experimental autoimmune encephalitis [183]. Furthermore, Breg cells, by secreting IL-10, can encourage T cells to develop into the immunosuppressive Treg phenotype, and are able to maintain this T cell skewing [184,185].They can also act upon DCs to supress a proinflammatory phenotype and therefore reduce T cell differentiation into Th17 and Th1 subsets [186,187]. Due to this suppressive role, Bregs are an important consideration in cancer immunology as they can influence the formation of an immunosuppressive environment. In a mammary carcinoma model with deficient B cells, inhibition of tumour growth was observed, with a reduction in the number of Treg cells [184].

1.3.3 Fc gamma receptors

All of the immune cell types above express a family of cell surface receptors known as Fc gamma receptors (FcγRs), except for T cells [188]. FcγRs allow binding and interaction with the Fc portion of IgG antibodies, leading to either an activation or suppression of effector functions depending on the FcγR receptor engaged. Myeloid cells described above express a wide selection of FcγRs which enables antibodies to regulate their effector functions via Fc engagement [189-191]. Humans express 6 versions of FcγRs: FcγRI, IIa, IIb, IIc, IIIa and IIIb, whereas mice express 4: FcγRI, IIb, III and IV [189,190]. However, these are not direct orthologs for each other with mouse FcγRIV being comparable to human FcγRIIIA, and mouse FcγRIII more closely related to human FcγRIIA [192]. For both mice and humans, the FcγRs are divided into both activatory and inhibitory receptors, based on their signalling effects after Fc engagement [188,193]. FcγRIIb found in both mice and humans is the only known inhibitory FcγR receptor to date, due to the presence of an immunoreceptor tyrosine based inhibitory motif (ITIM) in its intracellular signalling domain. The remaining receptors in both mice and humans are activatory, and (except GPI-anchored FcγRIIIb in humans) execute this function through ITAMs [189]. In both mice and humans, FcγRI or FcγRIV respectively, are the only high affinity receptors known [188], which bind IgG2a in mice and IgG1 or IgG3 in humans. The remaining receptors have a broad IgG specificity but have 100-1000 times lower affinity, which prevents binding of monomeric IgGs which are always present at high serum concentrations, preventing non-specific proinflammatory responses [188,189].

Differential expression patterns of these receptors can be found across all the immune cell types that express them, with innate immune cells being especially pervasive for FcγRs. In mice, DCs express FcγRI, IIb and III, monocytes and macrophages express all FcγRs, both activatory and inhibitory, with neutrophils mainly expressing FcγRIIb, III and IV [188]. NK cells, only express the activatory FcγRIII which helps their function in antibody dependent effector mechanisms. Furthermore, B cells of the adaptive immune system are known to only express the inhibitory FcγRIIb which helps in regulating signalling from the BCR [189].

1.3.4 Immune checkpoints

As discussed previously, it is essential to have appropriately activated tumour specific T cells in order to generate an anti-tumour immune response. This depends on the T cell being appropriately activated by the APC and maintenance of that activation to allow destruction of tumour cells. However, T cells intrinsically have regulatory mechanisms and circuits in order for them not to be inappropriately activated and cause an auto-immune response under normal physiological conditions. Although for the majority of the time effector T cell regulation is important to maintain

self-tolerance, cancer cells have exploited these mechanisms in order to prevent immune surveillance and avoid T cell destruction [1]. Therefore, it is important to understand immune checkpoints within the cancer setting to understand how the tumour and its microenvironment modulate an endogenous immune response, and how it can be targeted therapeutically.

The first immune checkpoint to be clinically targeted was the receptor CTLA-4, which is found to only be expressed on T cells. CTLA-4 functions to down-modulate the amplitude of T cell responses by inhibiting CD28 co-stimulation [194-196]. CD28 is the master T cell co-stimulator and amplifies TCR signalling after MHC/peptide/TCR complex formation [194]. Both CTLA-4 and CD28 share the same ligands, CD80 and CD86 [196], however CTLA-4 has higher affinity for these ligands and therefore outcompetes CD28 for ligation [197]. Furthermore, upon CTLA-4 engagement the receptor may endocytose the ligands reducing the availability for CD28 to engage [198]. This mechanism of controlling T cell responses occurs in tumour draining lymph node as the ligands are only expressed on APCs, and therefore function at the early stage of an immune response at the point of T cell activation. The signalling pathway of CTLA-4 inactivation of the T cell response appears to involve activation of SHP2 and PP2A which mitigate the activatory signals induced by the TCR and CD28 co-stimulation [195]. Unstimulated naïve T cells, and resting memory T cells, do not express CTLA-4 until they encounter their specific antigen and are activated allowing for appropriate co-stimulation via CD28. However, once activated CTLA-4 is rapidly mobilised from intracellular protein stores and expressed on the cell surface in order to switch off the T cell when the immune response is no longer required. Its role in maintaining peripheral immune tolerance has been demonstrated in *ctla-4* gene knockout mice which develop a lethal phenotype of immune hyperactivation [199,200]. CTLA-4 also has an important role in the function of Treg cells in maintaining their suppressive abilities [158,201]. This is due to *ctla-4* being a target gene of the FoxP3 transcription factor, leading to constitutive expression of CTLA-4 on Tregs [202,203].

Another extensively targeted checkpoint molecule is programmed death protein 1 (PD-1). PD-1 also modulates T cell activation [204], and is not expressed on naïve/resting memory T cells, as seen with CTLA-4. However, rather than being held in protein stores like CTLA-4, PD-1 needs to be transcriptionally activated before cell surface expression after TCR engagement. This leads to a delay after TCR engagement of around 6-12 hours before PD-1 can modulate the activated T cell [205]. PD-1 contains two inhibitory motifs within its cytoplasmic domain, an ITIM and an immunoreceptor tyrosine switch motif (ITSM). These both bind SHP2 and PD-1 activation can also activate PP2A to directly inhibit the TCR-mediated effector functions. Furthermore, PD-1 engagement decreases the time a T cell can survey an interacting cell for antigen by increasing migration into tissues to prevent the TCR from binding peptide/MHC complexes [205]. Recently, it has been suggested that inhibition of T cell responses through activation of the PD-1 pathway may be

due to its effects on CD28 co-stimulation [206]. Hui et al demonstrated, using a biochemical reconstitution system, that PD-1 favours CD28 suppression. It was found that after ligation by PD-L1, the PD-1 recruited Shp2 phosphatase dephosphorylated the CD28 co-stimulatory pathway, rather than TCR signalling [206]. However, some dephosphorylation of TCR components was noted when high PD-L1 levels were involved, which has also been previously reported as a mechanism of action of PD-1 [207]. Therefore, rather than prevent the activation of T cells in the first instance, the PD-1 pathway may inhibit the co-stimulation of antigen-specific T cells. The physiological role of PD-L1 expression is thought to limit nearby tissue damage during a T cell response to infection. However, tumour cells, which upregulate PD-L1 expression, are thought to have hijacked this pathway to supress anti-tumour T cell responses within the tumour microenvironment, as will be discussed later. Due to this localised ligand expression, murine knockouts of PD-1 are only associated with mild organ specific inflammation unlike the *CTLA-4* knockouts [208,209]. Although the two PD-1 ligands arose from a gene duplication event, their expression profiles and regulation differ [210,211]. PD-L1 is expressed on epithelial cells and some activated haematopoietic cells after IFNγ activation which is produced by activated T cells and NK cells. PD-L2 expression however, is regulated primarily by IL-4 and is mainly expressed on APCs such as DCs which have been activated and some macrophage subsets [212]. Expression of PD-1 ligands in the tumour microenvironment are due to two different mechanisms. Firstly, tumour cells may have genetic alterations, or activation of certain signalling pathways which then lead to the constitutive expression of PD-L1. These signalling pathways include AKT and STAT3 pathways, however determination whether these pathways lead to PD-L1 expression *in vivo* is currently under debate [213,214]. Another mechanism of PD-1 ligand expression is regulated the cytokine milieu expressed within the tumour microenvironment, as PD-L1 expression is induced on tumour cells after IFNγ exposure, with a link being seen between an increase in activated TIL infiltration and increasing PD-L1 expression [215,216]. Furthermore PD-1 expression is highly expressed on Treg cells, of which many reside within the tumour microenvironment. However rather than inhibiting the Treg cells upon ligand engagement, PD-1 receptor ligation may increase their proliferation [217].

1.3.5 Immune response to tumour cells

In the case of an anti-tumour response, CD8+ T cells are regarded as the main effectors cells [218,219] and therefore efficient priming of these cells is critical. The generation of functioning tumour specific T cells begins with activation and maturation of DCs which require two signals from the tumour cells themselves. Before a DC can process tumour antigen (TA) in order to display to T cells, it needs to engulf tumour cell debris to access the antigenic material. To initiate this an ‘eat me’ signal, such as ecto-calreticulin (ecto-CRT) signalling via SIRPα receptor, can be released or

displayed by dying tumour cells which signals to the DC to phagocytose the cellular material it is displayed on [220]. However this one signal is not enough to fully mature the DCs for efficient T cell priming. A second signal is needed in the form of a 'danger' signal, such as the release of DAMPs from dying tumour cells which interact with TLRs, on DCs [221]. The combination and timing of these two signals (as will be discussed in more detail later) is critical for efficiently maturing DCs so they are able to display the correct co-stimulatory receptors and produce the correct cytokines in order to induce efficient CD8+ effector cells, as shown in **Figure 1.7**.

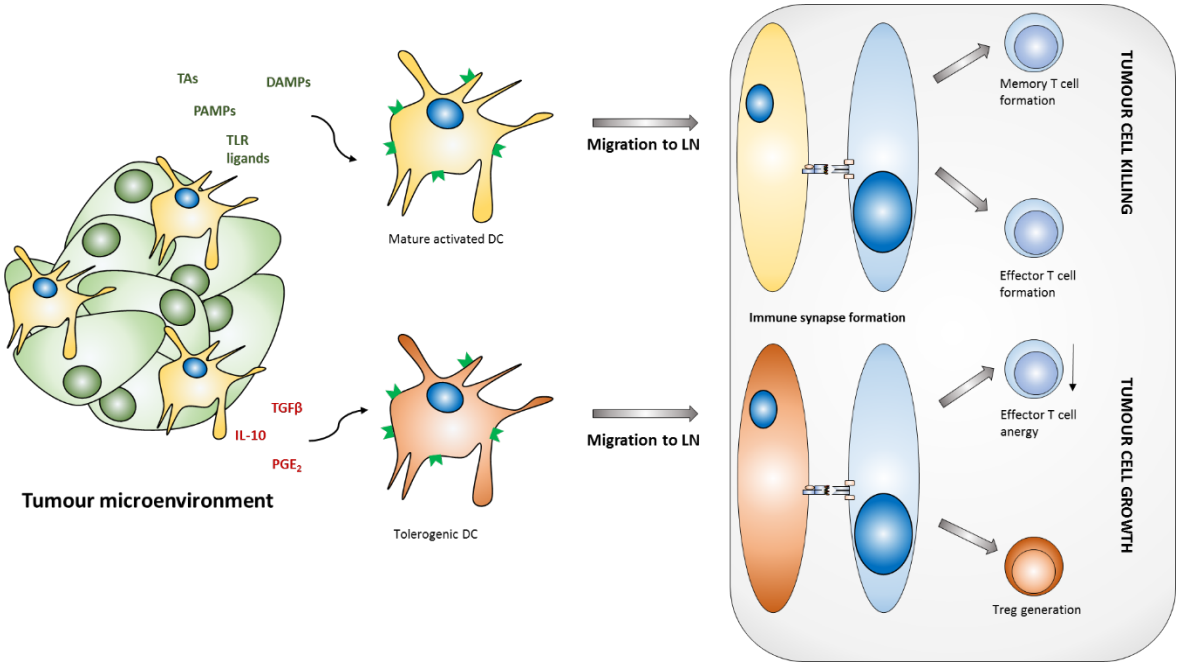

Figure 1.7 Generation of an anti-tumour immune response is dependent on DC activation

DCs are professional antigen presenting cells which are drivers of initiating an anti-tumour immune response by T cells. Firstly, an immature DCs migrates into the tumour microenvironment and encounters antigenic material. For DCs to be efficiently primed and matured, particular signals are needed, including DAMPs, PAMPs, TLR ligands and stimulatory cytokines. However the tumour microenvironment can be geared towards immune suppression, consisting of immunosuppressive cytokines and prostaglandins. If a DC encounters antigen under these suppressive conditions it can become tolerogenic. Once either primed or supressed after antigen uptake, the DCs migrate to the draining lymph node and here they either stimulate or supress an anti-tumour immune response, depending on how they were matured at the tumour site. Tolerogenic DCs lead to effector T cell anergy and Treg cell generation, whereas activated DCs lead to both memory and effector T cell generation.

Once the DCs are sufficiently matured, they are able to prime a naïve CD8+ T cell to be able to target and efficiently kill cells displaying the TA its TCR is specific for. In order to be primed, the naïve T cell needs to receive 3 signals from the matured DC [222,223]. Firstly, engagement of the TCR on the CD8+ T cell with the MHC I on the DC needs to occur [223]. The MHC molecule will be carrying a short peptide from a TA which the corresponding T cell's TCR can recognise and bind to. However, this signal alone is not enough to activate the T cell and if no other signals are received the T cell will

become anergic [224]. The binding of the MHC/peptide complex with the TCR creates an immunological synapse where other receptors and ligands translocate to provide the 2nd signal of co-stimulation. For this signal, receptor and ligand pairs on the matured DC and T cell interact to generate more intracellular signalling within the T cell and amplify the original MHC-TCR signal (see **Figure 1.8**) [222]. An example includes CD28-CD80/CD86 which is considered the archetype of co-stimulatory receptors [225]. Finally, it has recently been suggested that a 3rd signal is needed in the initial activation of naïve T cells, in the form of a stimulatory cytokine profile being produced from the appropriately matured DC [226]. If all these signals come into place, then the resultant primed CD8+ effector T cell population should be efficient at generating an anti-tumour response.

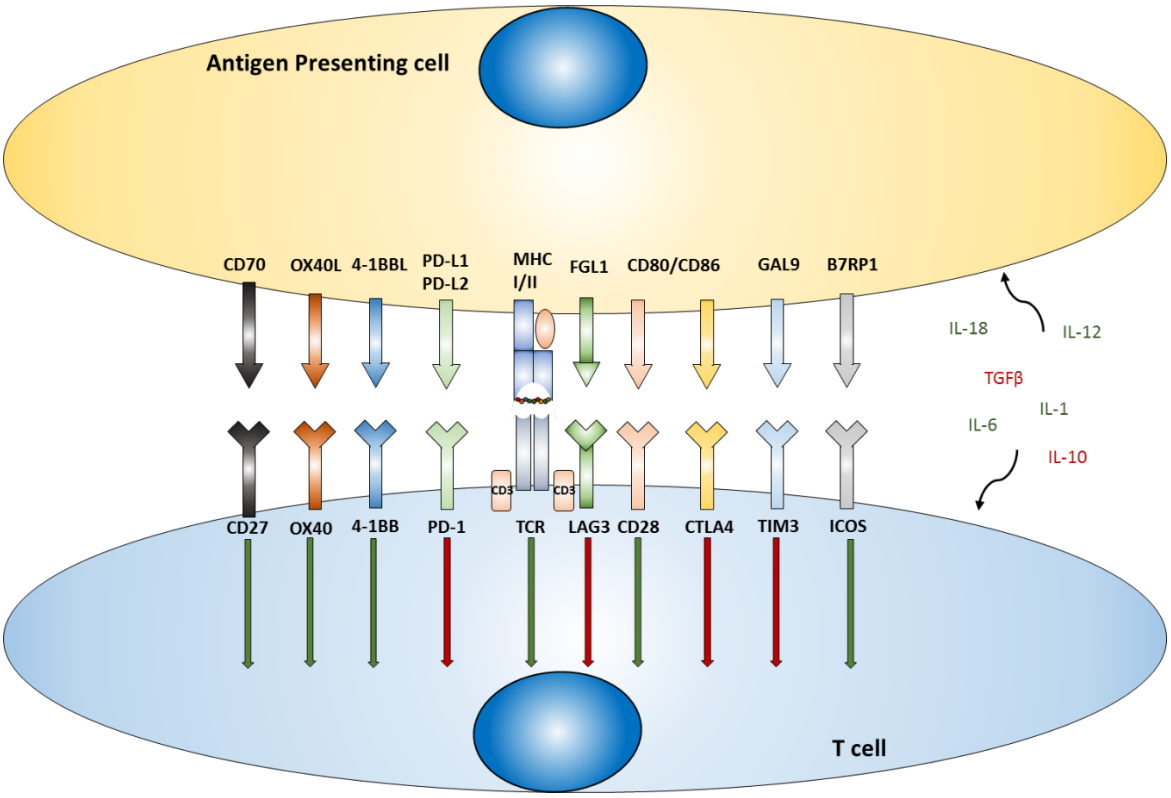

Figure 1.8 Immune synapse formation and immune checkpoints

When an APC presents antigen to its target T cell they interact and form an immunological synapse. This consists of MHC molecules presenting a peptide chain to the TCR to initiate T cell stimulation and proliferation. However a T cell will only be appropriately stimulated if the right balance between co-stimulatory and inhibitory molecules are also ligated at the same time. Furthermore, the correct cytokine milieu needs to be released from the APC, to fully mature and activate the T cell, to induce an appropriate immune response. Inhibitory receptors and cytokines are denoted by red, and activatory by green.

1.3.6 Immunoediting and the suppressive tumour microenvironment

Tumour cells, by nature, develop many mutations and have erroneous processing of proteins occurring within, which leads to expression of novel peptides in the form of neoantigens. These are only expressed by the tumours cells and therefore circulating T cells would not have been tolerised to them during thymic development. Furthermore, cell death, inflammation and stress responses occurring within the tumour microenvironment all lead to recruitment of immune cells and activation of an immune response. However, at different stages of tumour development, immune infiltrates can actually drive tumour growth and lead to cancer progression. This interplay of the immune system and tumour progression is known as cancer immunoediting [227], an idea which has been developed from the older concept of cancer immunosurveillance proposed by Burnet and Thomas [53]. Depending on the stage of tumour development, the immune system can either eliminate, shape or even promote tumour progression. These three stages are referred to as elimination, equilibrium and escape [228], and shape the outcome of tumour development. Experiments using transplantation of tumours grown in *rag2* deficient mice into immunocompetent mice have shown that these tumours are more immunogenic than tumours derived in immunocompetent hosts [229]. This suggests that T cell responses to tumour antigens sculpt the growing tumour, applying a selective pressure that the tumour cells need to develop methods to escape, such as altering antigen processing, in order to progress and grow [230,231]. Data has also shown that immunoediting may occur in patients who have received immunotherapy, showing that patient's tumours altered their expression of dominant antigens after immunotherapy [232]. Furthermore innate cells of the immune system are also involved in the immunoediting process, with NKs and macrophages both shown to be important effectors in the absence of adaptive cells [233].

The elimination phase of immunoediting has been extensively studied in mouse models with the use of immunodeficient mice showing that there is as higher incidence of tumour development in these mice compared with immunocompetent mice in carcinogen induced models [138,229,234]. These experiments showed that effector molecules such as IFNγ and perforin, alongside functioning lymphocytes were critical for tumour elimination at an early stage. Furthermore CD103+ DCs which are able to cross present were also required, and it has been demonstrated that some elimination mechanisms can rely on innate immune cells such as NKs and macrophages [235,236]. The equilibrium phase has been relatively difficult to study in murine models and therefore is as yet poorly understood. However data has shown there may be a role for Th1-like response and the delicate balance of cytokines IL-12 to promote elimination and IL-23 promoting tumour persistence [237].

Escape from immunoediting is the phase that allows for tumour progression. This phase is encompassed by the tumour creating a suppressive microenvironment which disarms infiltrating cytotoxic lymphocytes to prevent tumour cell destruction (**Figure 1.9**). Tumour cells can themselves disrupt immune recognition and facilitate their escape by many mechanisms, including downregulating antigen presentation by MHC I loss [238], losing expression of strongly activating antigens and increasing their resistance to death by upregulation anti-apoptotic molecules such as BCL-2 [239]. Furthermore, tumour cells and stromal cells within the tumour mass can create a microenvironment which actively supresses infiltrating T cells and can generate suppressive Tregs and innate immune cells which further promote tumour growth. They can utilise cytokines such as VEGF, TGFβ, prostaglandin E2 (PGE2) and IL-10 [240], alongside increasing expression of ligands for checkpoint molecules such as PD-L1 (**Figure 1.8** and **Figure 1.9**) and indoleamine 2,3-dioxygenase (IDO) [241-243]. These suppressive mechanisms can in turn create a negative feedback loop by generating tolerogenic DCs (**Figure 1.7**, as discussed previously) which leads to effector T cell anergy and generation of Treg cells [222]. These cells can then migrate back to the tumour site and continue to support the suppressive tumour microenvironment (**Figure 1.9**).

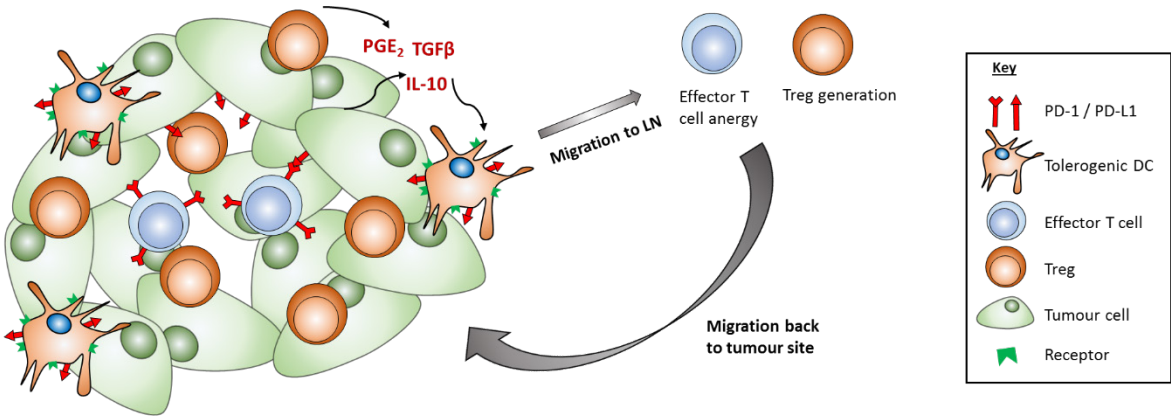

Figure 1.9 The suppressive tumour microenvironment network

Once tumours become established in equilibrium with the immune system, escape is needed in order to progress. This is achieved by numerous mechanisms, which includes the generation of a suppressive tumour microenvironment. Here tumour cells themselves or immune and stromal cells within the tumour mass are able to secrete immunosuppressive cytokines such as TGFβ, IL-10 and PGE2. These suppressive cytokines can lead to the development of tolerogenic DCs which can then migrate to a tumour draining lymph node. Here, tolerogenic DCs lead to insufficient activation of antigen-specific T cells, allowing the generation of Treg cells and anergy effector T cells. These Treg cells can then migrate back to the tumour site and continue suppression of infiltrating effector T cells, leading to a negative feedback loop. Furthermore tumour cells (and many other cells within the microenvironment) can express PD-L1 the ligand for PD-1, the checkpoint molecule on T cells. This allows for direct inhibition of effector T cells by tumour cells, again leading to immune suppression.

1.4 Chemotherapy in cancer therapy

1.4.1 Classical chemotherapy

Since the 1940s, chemotherapy has been the standard treatment for many cancers, despite the fact they can be associated with severe side effects [244,245]. Nevertheless, the heterogeneity between different cancers, and even between different patients with phenotypically similar cancers has led to the development of numerous classes of chemotherapies. Each class is defined by its specific pharmacological properties and what mechanism it uses to initiate cell death in cancer cells. Classes include but are not limited to, anthracyclines, platinum compounds and alkylating agents, each of which will be discussed in more detail below.

Anthracyclines are antibiotics which have been developed into anticancer treatments with a broad spectrum of use within many different solid and haematological cancers, both paediatric and adult [246,247]. Anthracyclines were first isolated from *Strepromyces peucetius* which also produces pigment explaining their colourful appearance [246,248]. Doxorubicin (DOX), is a member of this class of chemotherapy. DOX was approved in 1974 [247], as is still one of the most clinically used chemotherapeutic, even today [246]. However, considerable cardiotoxicity is associated with this agent, with around a 9% incidence rate, so its dose and therefore use is limited by its toxicity [247]. DOXs mechanism of action involves many effects including rapidly binding to DNA with high affinity in the nucleus of cells via intercalation between base pairs [249]. It acts by preventing topisomerase II from re-ligating the DNA and creating a cleavable complex [247,250]. Furthermore DOX can work through creation of DNA adducts and inhibiting DNA methyltransferases [247,251].

Another class of widely used chemotherapeutics are those of the platinum compounds class, used in many cancers, both adult and paediatric. The first platinum anticancer drug developed was cisplatin (CIS) discovered as a cytotoxic agent in the 1960's, with second generation carboplatin being invented to reduce toxicity, and finally third generation oxaliplatin (OXA) was developed to overcome drug resistance [252,253]. The main mechanism of action of cisplatin is DNA platination on purine bases [254], coupled with induction of cellular oxidative stress [255]. The DNA platination leads to cross linking of guanines leading to disruption of the DNA strand resulting in cytotoxicity [254]. However, cisplatin is associated with high toxicity and more importantly, many tumours develop resistance to the drug through repair of DNA lesions via nucleotide excision repair and by prevention of cisplatin entering the cells [255]. With a lower toxicity profile carboplatin is suitable for use in high dose regimes and has replaced cisplatin in combination therapies [256]. However, tumour cell resistance to this drug by the same mechanisms as cisplatin is still a major problem [257]. Finally,

oxaliplatin has significantly reduced side effects than the previous compounds [258], although its mechanism of action is still the same [252,259].

The final class of chemotherapy to be discussed here are the alkylating agents, the most widely used and successful of which is cyclophosphamide (CPM), used not only in many cancers but in conditioning regimens for transplants such as bone marrow [260,261]. CPM is a nitrogen mustard derivative which was first synthesised in 1958 in order to specifically target cancer cells [262,263]. The idea behind its specificity was that it was designed to be a prodrug which will only be metabolised into its active form within cancer cells [260,262], however after more research specificity for metabolism within tumour cells was not confirmed. CPM is still a prodrug and therefore needs to be metabolised within the body to become activated. Both enzymatic and chemical activation is needed, with the hepatic cytochrome P-450 enzyme starting the process. Further decomposition of the enzymatic products then occurs within the cells themselves forming the final DNA damaging metabolites, phosphoramide and acrolein [264]. CPM exerts is cytotoxic effects through the starting nitrogen mustard being converted to a cyclic cation under normal physiological conditions as discussed above. This cation then attaches on DNA guanine residues which release the nitrogen to allow the cation to then react with another guanine residue. This crosslinking leads to a halt in DNA replication by formation of both intra- and inter-strand DNA crosslinks [265]. Although its original design was supposed to be cancer cell specific, it does have significant off-target effects, as many highly proliferative cells, such as immune cells, are susceptible to CPM metabolites. Therefore, like most if not all chemotherapies, CPM does have associated toxicities, many of which are dose or duration dependent [260]. As mentioned CPM is used in conditioning therapies before transplants which is due to its myelodepletive effects, which are found to be high dose dependent [260]. Furthermore, the dose-limiting effect of this chemotherapy lies in its cardiotoxicity [266]. Other side effects include gonadal toxicities particularly in boys [267,268] and bladder toxicities including haemorrhagic cystitis which is caused by acrolein [260,269]. Importantly, CPM treatment itself can lead to cancer development due to its carcinogenic properties. Incidences of squamous cell carcinoma in the bladder, secondary acute leukaemia and skin cancer have all be noted [260]. However the risk of developing these secondary cancers from treatment increase with duration of CPM administration [270].

1.4.2 Chemotherapies used in the treatment of NB

As mentioned previously, the current treatment regimens for high-risk NB involve considerable amounts of chemotherapeutics, whether that be to reduce the tumour mass itself or to prime the bone marrow ready for a stem cell transplant. Therefore, it is important highlight what

chemotherapies are used, as the choice of chemotherapeutic could be critical if wanting to appropriately stimulate the immune response.

Induction chemotherapy is an important first step for high-risk NB therapy as discussed in **section 1.2.3**. Many different chemotherapeutic classes are regularly used for this step including anthracyclines, platinum compounds and alkylating agents as mentioned above [271]. It is usual for first-line induction chemotherapy to include more than one chemotherapy, with a combination revolving around DOX, CIS and CPM [44,48,272,273]. Furthermore, topisomerase inhibitors such as topotecan and irinotecan [274-277] and epipodophyllotoxins such as etoposide are also used in induction therapy [272,273]. Most of these chemotherapies are used in combination at high doses in order to reduce tumour size [271], however this does come with adverse side effects particularly myelosuppression which, when considering combinations with immunotherapies, may not be the best approach.

After surgical resection, patients usually receive chemotherapy prior to autologous stem cell transplant, in the form of myeloablative consolidation therapy. This high dose chemotherapy is designed to eradicate any remaining chemoresistant tumour cells, particularly residing in the bone marrow, and then replace the myeloablated cells with an autologous peripheral blood stem cell transplant [48,276,277]. Chemotherapy used in this step vary from trial to trial in dosages, timings and the drug combinations used, but commonly used regimens include high dose carboplatin, etoposide and melphalan (CEM) and high dose Busulfan /melphalan [277] [48] [276].

1.4.3 Apoptosis inducing vs immunogenic cell death inducing chemotherapy

As briefly mentioned, in order for an immune response to be generated against tumour cells, a specific set of signals are needed to appropriately prime the cells involved in the anti-tumour response. It has been proposed that for this to occur tumour cells need to die by an appropriate mechanism that will initiate the release of these signals, this has been termed immunogenic cell death (ICD) [220,278]. However, the consensus that most chemotherapies kill tumour cells via inducing apoptosis is contradictory to the idea that chemotherapies can lead to ICD. There has been a long held view that apoptosis is a physiological, programmed, immunologically silent method of cell death [279-281]. As millions of normal cells will be undergoing this process every day it is understandable to assume this idea [282,283]. Furthermore, the immunosuppressive ability of apoptosis is reflected by the fact that the process is associated with both inhibition of immunostimulatory cytokines and promotion of immunosuppressive cytokines [284,285]. However, it has recently been established that not all forms of apoptosis are immunologically silent and that some can actually elicit strong immune stimulation [278,286-289].

Apoptosis induction is one mechanism chemotherapies use to cause tumour cell death. Apoptosis, first described in 1970's [280] is a form of cell death that is described as being a controlled form of death that is actively coordinated by the cell itself in response to certain stimuli. This is important for many physiological conditions such as sculpting of tissue in embryonic development, replacement of the gut epithelium and shedding of the endometrium [290]. When apoptosis is initiated in cells, distinct morphological changes occur which are conserved across all cell types and many species [291,292]. Apoptosis can be triggered by both extrinsic (death receptor) or intrinsic (mitochondrial) pathways [281], which will eventually converge to a common pathway which involves the caspase cascade [293]. Hallmarks of apoptosis include, chromatin condensation and nuclear fragmentation, rounding of the cell, pyknosis and pseudopod retraction and initiation of apoptosis relies on caspase activation [279]. From the initiation to the final cellular fragmentation, the process usually takes several hours to complete [294].Throughout the process until the final moments, the plasma membrane remains intact, with phagocytic cells usually engulfing apoptotic cells before they become apoptotic bodies [279]. Any non-phagocytosed apoptotic bodies will degrade further in a necrotic fashion, which could activate an immune response [294]. In order to attract phagocytes, such as macrophages, proteins such as phosphatidylserine (PS) are expressed as 'eat me' signals on the surface of early apoptotic cells, and leads to phagocytosis without the release of proinflammatory signals and therefore an immune response is not initiated [281].

As mentioned previously, DCs need specific signalling events to occur in order to be properly activated and go on to efficiently prime tumour specific T cells. Contrary to previous proposals, there is more recent evidence to suggest that chemotherapy induced apoptosis can elicit this response. The immunogenicity of this response appears to be determined by the presentation of an 'eat me' signal through translocation of CRT to the cell surface after treatment [287]. CRT is usually present in the lumen of the endoplasmic reticulum of healthy cells as endo-CRT and is involved in calcium (Ca^{2+}) signalling and homeostasis [295,296]. Application of certain chemotherapies [287,297,298] but not others [287,298] leads to a rapid translocation of endo-CRT to the cell surface due to induction of certain cellular stressors (**Figure 1.10**) [220,299]. Endo-CRT is extracellularly expressed via movement through the Golgi apparatus and vesical transport system [299]. This translocation has been shown to only occur in ICD and before any other features of apoptosis are observed [287,298,300], such as chromatin condensation and fragmentation of the nucleus. Furthermore, it has been shown that cells lacking a nucleus are still able to express ecto-CRT [298], suggesting that ecto-CRT expression is independent of the nuclear machinery and DNA damage. The sum of all these mechanisms leads to ecto-CRT exposure which is believed to initiate phagocytosis ('eat me' signal) by DCs of the dying tumour cells (**Figure 1.10**) [298]. However, Obeid et al. [287] suggested that ecto-CRT induced phagocytosis alone may not be sufficient to efficiently prime an effective immune response. This is

due to the requirement of efficient antigen presentation and cross-priming by the DCs, which may be dictated by a second signal released at time of cell death.

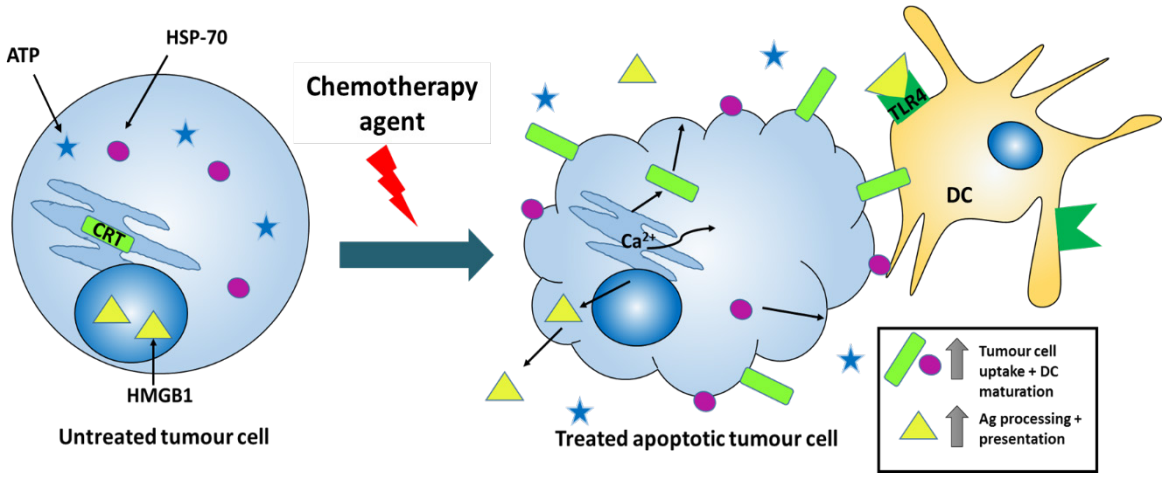

Figure 1.10 Chemotherapy driven ICD mechanisms in tumour cells

In physiological conditions, CRT, Hsp-70 and HMGB1 reside within the cell. However application of ICD inducing agents leads, to translocation of CRT and Hsp-70 to the cell surface and HMGB1 to be secreted. Danger signals released from the dying cell such as HMGB1 and ATP attract phagocytes to tumour site and increase antigen processing. Whereas 'eat me' signals displayed on the cell surface, such as ecto-CRT and HSP-70, increase uptake of tumour cell debris and DC maturation. From there these molecules augment DC function and lead to priming of an anti-tumour response.

A candidate for the second signal needed to induce an effective anti-tumour response has been pinpointed to a non-histone chromatin binding protein, high mobility group box 1 (HMGB1), and its interaction with an innate immune receptor; TLR4 [288,301]. The link between immunogenic cell death and TLR4 was first suggested after observing that TLR4 deficiency has a detrimental effect to chemotherapy treatment in *in vitro* and *in vivo* modelling. The deficient cells are unable to present antigen, due to reduced MHC I-peptide complexes on DC surface [221,301]. Furthermore, the immune response generated was abrogated with addition of small interfering (si)RNAs or antibodies to HMGB1 [301]. TLRs provide an essential link between the innate and the adaptive immune system by recognising pathogenic and, as in anti-tumour responses, endogenous molecules [302]. They are notably located on DCs (and other APCs) and signal via two pathways, MyD88 and TRIF, to enhance the cross-presentation of antigens and eventually lead to functional T cell activation via appropriate activation of DCs [302,303]. It is thought that this extra-cellular release of HMGB1, acts as the 'danger' signal in priming the DCs to appropriately generate an anti-tumour response, when coupled with the expression of ecto-CRT which acts as the 'eat me' signal. However, this may not be the end of the story with regards to ICD maturing DCs. It has been noted that the DCs are not fully primed with HMGB1 and CRT alone (or in combination), therefore it may be that other molecules released later

on in ICD (e.g. cytokines) equate to the last step needed to have fully functioning DCs ready to prime an effective anti-tumour response [288].

Extracellular release of ATP after application of chemotherapeutics has also been reported as an important marker of ICD [278,304-306]. It is proposed that ATP release is a result of chemotherapy effecting the autophagosome machinery [307,308] during the cell death process. ATP outside of the cell is known to attract myeloid cells such as macrophages, DCs and monocytes by binding to puragenic P2Y2 receptors on their cell surface [309]. The ATP can also activate DCs via activation of the nucleotide-binding oligomerization domain like receptor protein 3 (NLRP3) inflammasome leading to production of inflammatory cytokines IL-1b and IL-18 [310]. Oxaliplatin treatment in murine tumour models was shown to increase CD8+ priming and reduce tumour growth, however this effect was abrogated in IL-1R, NLRP3 or *Casp-1* knockout mice, supporting the importance of ICD and ATP release in these models [310]. However, contrary to this seemingly immunostimulatory effect, the breakdown on ATP into adenosine may actually impair immune responses [311,312]. Heat shock protein (Hsp)-70 and Hsp-90 have also been implicated as important markers of ICD [313,314]. When these molecules are expressed on the cell surface after chemotherapy induced cell death they are thought to stimulate the uptake of antigens from the dying cell by APCs such as DCs by acting as 'eat-me' signals. The receptor thought to be responsible for interaction with the HSPs and possibly with ecto-CRT, is CD91 which is also the main ER chaperone receptor expressed by both human and mouse myeloid cells [304,315,316]. Macrophages which lack this receptor show decreased phagocytic abilities hinting at its importance in stimulating antigen uptake [315,316]. However, it has been observed that these ER chaperone proteins and ecto-CRT do not actually require receptors to engage cell membranes due to their innate 'stickiness' [298,317].

To date most of the ICD investigations have been preclinical, focussing on chemotherapies in mouse models. However, in order to select chemotherapeutics based on their ICD potential in patients, clinical significance in humans needs to be determined. Ladoire et al 2015 [318], aimed to clarify whether ICD related markers could be effective biomarkers of prognosis in breast cancer patients who have previously undergone anthracycline based chemotherapy [318,319]. Here they noted that nucleic staining of HMGB1, an important molecule in ICD, is very heterogeneous between patient samples along with an autophagy-associated molecule L3CB. These two markers both hold key roles within the concept of ICD. Autophagy of the tumour cell is a prerequisite to inducing ICD after chemotherapy application as this leads to release of ATP into the local tumour microenvironment, which then recruits phagocytes to the area [320]. Tumour cells lacking key autophagy genes show no induction of ICD by anthracycline chemotherapy [307,320]. Furthermore, once the phagocytes, such as immature-DCs are recruited to the area they need to be activated into the right maturation status to activate an anti-tumour response. This can be achieved by the secretion of HMGB1 into the

tumour microenvironment, as consequence of ICD, which acts through the TLR receptor on DCs which encourages presentation of tumour associated antigens [87,221,301]. Patients with TLR4 loss of function alleles have been associated with an inferior response to chemotherapy [321], further highlighting the importance of this pathway. The heterogeneity of these molecules found in the breast cancer patients samples was quantified, and it was noted that >90% tumour cells had no L3CB expression, and >50% of tumour cells had no nuclear HMGB1 [318]. This suggests that these patients would have a poor response to anthracycline chemotherapy as ICD could not be induced in the majority of their tumour cells. Indeed, lack of either of these molecules were correlated with a reduction in overall and progression free survival, which was further reduced if the tumour cells were lacking staining for both molecules [318,319].

Investigations into whether the chemotherapies DOX and CIS, used in NB, can induce ICD on a NB cell line have been conducted [322]. Neuro2a, the cell line used in this study, is GD2-, unlike human NB cells which express this ganglioside which is used as an important therapeutic target [49]. The Neuro2a cells that were treated with doxorubicin and then co-cultured with CD11b+ spleen cells were able to induce the proliferation of CD8+ T cells (with CpG used as an adjuvant). Furthermore, they also noted increased IFNγ production, which was greater with doxorubicin compared to cisplatin treated cells. This suggests that doxorubicin does cause ICD to occur in Neuro2a cells. However, investigations into the induction of ICD related marker expression such as ecto-CRT, ATP, HMGB1 etc, was not analysed.

1.4.4 Effect of chemotherapy on immune cell subsets

As chemotherapeutic agents are given systemically and non-specifically target tumour cells, their administration can effect a variety of cell types including different cell subsets of the immune system both beneficially and detrimentally for an anti-tumour response. As mentioned, high doses of CPM are used for conditioning therapy before receiving a transplant, in order to supress the immune system [260]. Therefore, in order to select a chemotherapy that is most complementary to immunotherapy, it is imperative to know what effects they have on the immune system, if they are dose dependent.

DCs have already been extensively mentioned due to their role in bridging the innate and adaptive immune systems to lead to an effective anti-tumour response. As discussed, induction of ICD by chemotherapies can appropriately activate and prime DCs [287,301], however the DCs themselves can also be augmented by chemotherapy. Tanaka et al, conducted a screen to see the effects of 54 chemotherapies on different aspects of DC function including maturation and survival [323]. The effects from different chemotherapies included release of maturation signals by certain

topisomerase inhibitors, antimicrotubule agents and alkylating agents, which were coupled with minimal DC cell death [323]. However, these experiments were conducted *in vitro* so it is hard to extrapolate whether this could be the case *in vivo*. Induction of DC maturation and associated upregulation of antigen presentation, has also been demonstrated with both murine and human derived DCs and also *in vitro* and *in vivo* [324,325]. An interesting immune promoting effect of oxaliplatin is its ability to downregulate an immunosuppressive molecule, PD-L2, on DCs [326]. This prevents PD-L2 from supressing T cell activation when the cells form an immunological synapse in order send and receive signalling. Furthermore, CPM therapy may lead to an increase in numbers of particular DC subsets and subsequently promote their homing to the tumour microenvironment [327-329].

Another antigen presenting cell and important member of the innate immune armoury is the macrophage. These cells can also be augmented by chemotherapies via varying methods. Tumours are known to be infiltrated by TAMs [330], and therefore the phenotype of these cells along the M1 (stimulatory) to M2 (inhibitory) spectrum will be important with regards to the anti-tumour immune response [331,332]. The majority of TAMs are M2-like in phenotype and therefore are pro-tumourigenic and possibly immunosuppressive [330]. However, certain chemotherapies, such as CPM and DOX, can re-polarise these M2-like macrophages towards the more anti-tumourigenic M1 phenotype [333,334], or even cause direct cytotoxicity to these cells [335]. Contrastingly, chemotherapy induced TAM infiltration has been reported, and reduced the effectiveness of the chemotherapy in breast cancer patients [336].

The main effector cells of the innate system are NK cells which have the ability to directly target and kill tumour cells, and therefore are important in the early stages of tumour development. It has been reported that the immunomodulatory drug thalidomide, which is used in multiple myeloma treatment, can impact NK cell function in an immune-stimulatory fashion. Kawamata et al, suggested that thalidomide treatment in mice led to a substantial increase in an NK subset population, along with an increase in NK related cytokines (IFNγ, IL-12 and IL-18) and perforin [337]. However, studies involving patients have revealed mixed results when looking at NK cell function after chemotherapy treatment. For example, a study on breast cancer saw NK cell impairment after chemotherapy [338], whereas CPM given to end-stage patients in metronomic dosing showed an increase in NK cell responses [339]. Therefore, the type of chemotherapy, the timing of the treatment and the dosing are all factors that need to be considered to see whether NK cells will be impaired or stimulated.

As mentioned previously, T cells, and arguably more importantly CD8+ T cells, are the main player in the anti-tumour immune response, and therefore it is imperative to assess how chemotherapy effects their activation and function. The platinum compound cisplatin coupled with paclitaxel *in*

vivo (and in patients) has been shown to induce a potent tumour-specific CD8+ T cell response, which was mediated by secretion of two stimulatory cytokines, IL-2 and IFNγ [340]. In two models of carcinogen induced tumours, DOX was shown to augment the T cell infiltration and trafficking to the tumour site, after promoting proliferation of tumour specific T cells [341]. However, application of 5-FU along with CIS also demonstrated increased trafficking of both subsets of T cells into the tumour in *in vivo* models and patients [342,343]. It has been noted clinically that some tumours have a low number of tumour infiltrating lymphocytes [344,345], which may be due to poor immune cell trafficking to the tumour microenvironment. If chemotherapies can improve this trafficking it may lead to a reduction in tumour size, especially if combined with another immunostimulatory therapy. CD4+ T cells and the balance between stimulatory (Th1) and inhibitory (Th2) subtypes can also be augmented by chemotherapy. This was demonstrated by paclitaxel and also by CPM treatment, both of which showed a skewing towards Th1 cytokine production i.e IFNγ and IL-2 [346,347]. Doxorubicin and cisplatin have demonstrated their ability to increase survival of mice due to enhancement in an CD4+ T cell mediated anti-tumour response [348]. It may be that the immunogenicity of a particular chemotherapy may be based on how well they are able to stimulate CD8+ T cells and appropriate CD4+ subtypes, due to these cells being essential in generating a potent anti-tumour response.

Although B cells are an important part in the adaptive immune response for pathogens, they could be seen as less of an asset for tackling tumour progression. This is due to their main function being the production of antibodies which, although highly specific, may not be effective on their own against large tumour cells [349]. However, B cells also function as APCs and produce many supportive cytokines for T cells, therefore have an essential albeit indirect role in the anti-tumour immune response [350,351]. CPM has a debateable effect on B cells and may both impede humoral responses [352,353] and increase B cell numbers and antibody production [354,355] at low doses. Suppressive effects of CPM may be due to transient lymphodepletion, after which lymphocyte proliferation overshoots, possibly having a beneficial effect [346,356]. Wijayahadi et al, noted that combination (5-FU and CPM) therapy for breast cancer patients partnered with epirubicin caused a substantial loss of B cells, when compared to the combination therapy with doxorubicin [357]. However, the same study reported an increase in T cell an NK cell populations in the blood, suggesting that the B cells are particularly susceptible to epirubicin. Gemcitabine, a nucleoside analogue, has also been shown *in vivo* to reduce B cell numbers and function while simultaneously increasing T cell responses [358]. These results may suggest that B cells are more sensitive to anti-proliferative chemotherapies such as gemcitabine than other subsets of immune cells. On the other hand, 5-FU has been shown to possibly benefit B cell responses, as has been demonstrated with adjuvant chemotherapy in colon cancer patients [359]. As discussed before, many of the varying effects seen with different

chemotherapies may be dosage and time dependent, which demonstrates the importance of finding out what is the key dose and time point to administer these therapies to provide the most effective treatment.

Over the past few decades it has become clear that not all subsets of T cells have activatory properties, and some, known as Tregs, work to inhibit and supress other T cells in order to dampen down an immune response. In the 1980s it was noted that these suppressor cells are selectively targeted and show increased sensitivity to CPM therapy, which may be due to prolonged recovery of the Tregs after administration [356,360]. Tregs are also effected by other chemotherapies such as gemcitabine, which has been shown to delete Tregs within the tumour microenvironment in a pancreatic cancer model [361], and in turn increased the anti-tumour activity of infiltrating effector T cells. As Treg cells are more proliferative than other T cell subsets [362] this may explain the reason why they are more sensitive to gemcitabine which interrupts DNA replication. It has been shown that Treg percentages are decreased in peripheral blood of patients after gemcitabine treatment [362]. A taxane chemotherapy, paclitaxel, has also demonstrated selective inhibition of Treg cells [363], and temozolomide showed a reduction in number and function of Tregs when given metronomically [364]. It may be that the key to unlocking a potent anti-tumour response with chemotherapy is dependent on whether it can stop the function of these powerful suppressor cells. Low dose CPM has immune-modulatory properties by selectively targeting Treg cells and therefore lifting the 'brakes' off the dampened anti-tumour immune response [360,365,366]. Metronomic dosing of CPM involves the patient receiving CPM more frequently but at a lower dose than standard CPM dosing. In patients, it has been shown that this form of dosing specifically targets peripheral Treg cells, whereas patients on higher doses have depletion of all lymphocyte populations [339]. The depletion of the Treg cells leads to increases in cytotoxic activity of lymphocytes and NK cells and therefore a more potent anti-tumour response. Zhao et al, have suggested that the mechanism behind this effect may be due to Treg cells having lower levels of ATP production, which leaves them less able to clear CPM metabolites, which is dependent on glutathione synthesis [367]. Dimeloe et al, have also reported that Treg sensitivity to CPM may be due to their lack of expression of the ATP-binding cassette (ABC) transporter ABCB1 [368]. CPM is a known substrate of this transporter, and therefore the Tregs were found to have a reduced capacity to expel the drug and its metabolites. Furthermore Lutsiak et al, demonstrated that gene expression of both GITR and FoxP3 decreases on Tregs after CPM administration [365]. Both of these proteins are known to be involved in the suppressive activity of Treg cells [369,370], and therefore cyclophosphamide could also be dampening the suppressive activity of Tregs alongside depleting them.

Another subset of regulatory immune cell associated with cancer are myeloid derived suppressor cells (MDSCs), which function by many mechanisms including releasing reactive oxygen species

(ROS) and depleting L-arginine to hinder the function of tumour specific T cells [371,372]. 5-FU chemotherapy has been shown to lead to MDSC reduction coupled with an increase in T cell responses (noted by IFNγ release) in an *in vivo* model [373]. The increase in T cell responses, specifically tumour-specific, was likely caused by the depletion of the immunosuppressive cells i.e. the MDSCs. A different class of chemotherapy, cisplatin, showed a similar effect *in vivo*, however the number of DCs were increased in this scenario [374]. One particular drug, gemcitabine, may be particularly effective at eradicating MDSCs, and subsequently increasing T cell responses, with convincing results both *in vitro* and *in vivo* [373,375]. An interesting effect of re-polarisation of MDSCs to a phenotype more in line with M1 macrophages has been noted after treatment with docetaxel [376]. This not only releases the suppressive force of the MDSC on T cells, but also primes the tumour microenvironment to provide support for the anti-tumour response in the form of supportive cytokines released by the reprogrammed MDSCs to M1-like phenotypes. Effects of CPM therapy on MDSCs is undecided currently. Reports have shown data for both an immune-stimulating and immune-inhibitory effect on MDSCs, such as reporting that CPM induces their development [377], leads to their activation [378] and reduces their immune-suppression abilities [379].

1.5 Immunotherapy in cancer treatment

1.5.1 Monoclonal antibodies

Monoclonal antibodies (mAbs) as biological tools were first pioneered by work conducted by Kohler and Milstein in 1975, who developed the Nobel Prize winning hybridoma technique [380,381]. This involved the fusion of a myeloma cell line and antibody producing B cells in culture which led to the secretion of antibodies from a single clone of predetermined specificity [380]. The development of this technique revolutionised biological science, leading to diagnostic tools and invaluable applications for basic laboratory assays, such as immunohistochemistry (IHC)/immunofluorescence (IF), flow cytometry and enzyme-linked immunosorbent assay (ELISAs). As these mAbs were specific for a single antigen, they allowed for the identification and subsequent phenotyping of cells within blood and tissues, with molecules binding mAbs given CD numbers to identify them [382]. The hybridoma technique was also revolutionary for the development of targeted treatments for many disease, especially cancer, as it offered a way to continuously produce extremely specific therapeutics in unlimited amounts [383], something cancer treatment was lacking at the time.

Most antibody therapeutics currently used in cancer therapy are IgG isotypes, therefore understanding the structure of this molecule is important to understand its efficacy. Out of the 5 immunoglobulin classes, IgG is the most abundant in human serum, with four different subclasses: IgG1, IgG2, IgG3 and IgG4 [384,385]. These subclasses are 90% identical at the amino acid level, but

have unique effector mechanism initiation profiles, with different abilities of antigen binding, half-life and triggering of effector functions [384]. **Figure 1.11** represents the basic structure of an IgG1, showing the four polypeptide chains which make up the structure of all antibody classes. The 4 chains consist of two heavy (50 kilodaltons- kDa) chains and two light (25 kDa) chains [384]. These chains are linked by an interchain disulphide bond as shown on **Figure 1.11**. The heavy chains consist of 3 constant domains (CH1, CH2 and CH3), and one variable domain (VH), whereas the light chains consist of only 1 constant (CL) and 1 variable (VL) domain each. From this, the antibody molecule can be broken into two sections, as shown on **Figure 1.11**. Firstly, the Fab fragment can be formed by the association of the light chains and the VH and CH1 domains of the heavy chain. This domain contains the regions which bind the specific antigen via three complementary determining regions, found on the variable domains of the two chains [386,387]. The second fragment known as Fc (fragment crystalizable) is formed of the lower hinge region and the CH2 and CH3 domains of the heavy chains. Fc fragment is mainly responsible for half-life, mediated by FcRn receptor, and effector functions of the antibody, mediated by binding to FcγRs and complement molecules [384]. Between the CH2 and CH3 domains, glycosylation sites are located which alter the antibody's quaternary structure and mediates its docking to FcγR [388]. Deglycosylation at these sites leads to dissipation of FcγR binding [389].

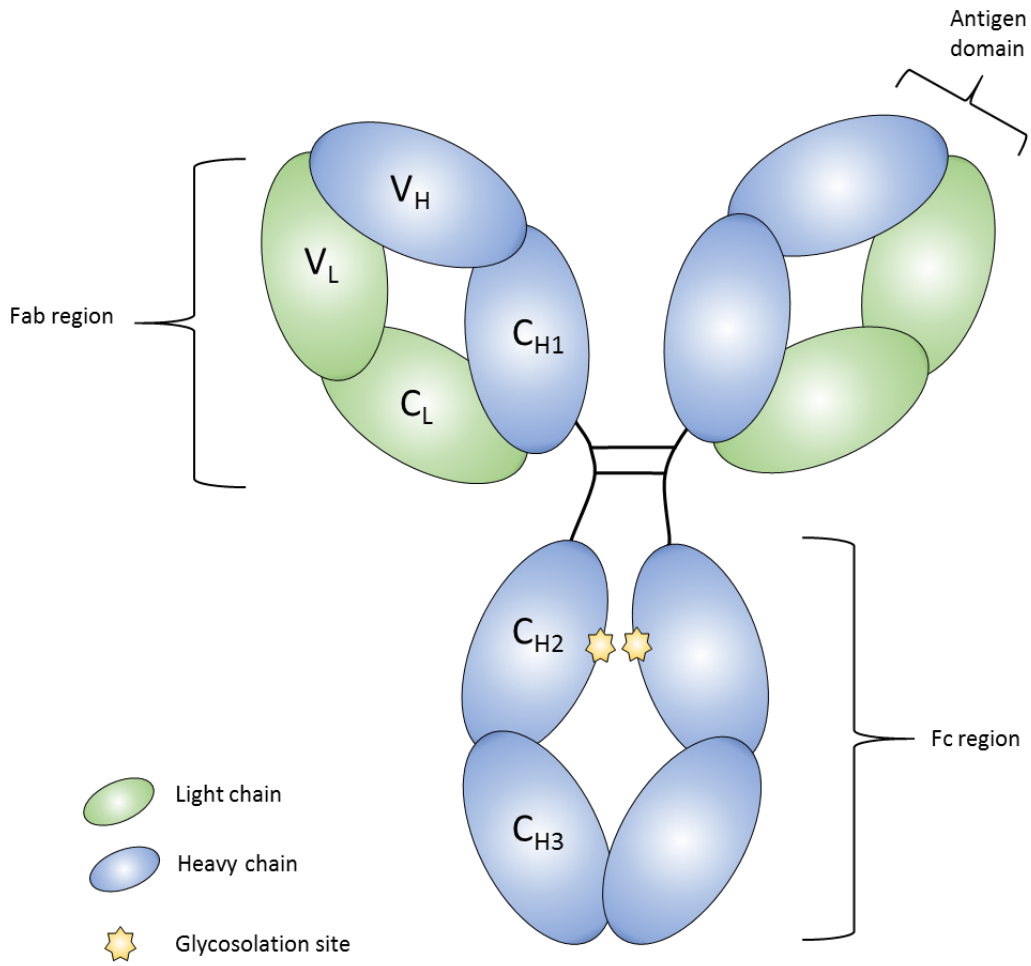

Figure 1.11 Basic structure of an IgG antibody molecule

Majority of monoclonal antibodies used in therapy for cancer are IgG molecules. The basic structure of an IgG molecule consists of 4 chains made up of a two pairs of a heavy and a light chain. The heavy chain contains 4 domains, two of which (CH2 and CH3) make up the Fc region of the antibody and interact with FcγRs. The CH2 domain of this region contains glycosylation sites which effect how the Fc portion interacts with its receptors. The remaining two regions of the heavy chain (CH1 and VH), together with the two regions of the light chain (VL and CL) form the Fab region, which binds antigens. The two variable domains of both chains (VL and VH) contain hypervariable complimentary determining regions which give each antibody its specificity for a particular antigen. The whole antibody structure is held together by disulphide bonds, some of which form a hinge region.

When developing therapeutic monoclonal antibodies, it is important to take into account the isotype of the IgG antibody in question. Different isotypes bind distinct FcγR with varying affinities, which in turn affects their effector function. Mice have 4 IgG isotypes: IgG1, IgG2a, IgG2b and IgG3, all of which bind with different affinities to the 4 different mouse FcγR receptors [390] (**Table 1.3**). In mice, FcγRI, FcγRIII and FcγRIV are all activatory receptors as they associate with the FcER1 gamma chain which contains an ITAM signalling motif, with FcγRII being inhibitory due to the presence of an ITIM [391]. As shown in **Table 1.3**, Mouse IgG2a is able to bind every FcγR however, it has the highest affinity for both FcγRI and FcγRIV, with a similar profile seen with IgG2b but with lower affinities [391,392]. Due to this high affinity for two activatory FcγR, IgG2a in mice is a good activator of

effector functions such as ADCC and ADCP. Mouse IgG1 on the other hand only binds to the low affinity activatory receptor FcγRIII and the inhibitory receptor FcγRII [393], which implies that mouse IgG1 antibodies have reduced efficacy for inducing effector functions. Therefore, the correct isotype choice is important when developing therapeutic antibodies. Depending on whether you want to active a strong effector immune response, such as with an antibody directly targeting immune cells or have minimal effector function with an antibody targeting immune effector cells, the correct isotype is key.

		IgG receptor			
		FcγRI	FcγRII	FcγRIII	FcγRIV
	Function	Activatory	Inhibitory	Activatory	Activatory
IgG Isotype	IgG1	-	++ $3x10^6$	++ $3x10^5$	-
	IgG2a	+++ $3x10^7$	++ $4x10^5$	++ $7x10^5$	+++ $3x10^7$
	IgG2b	++ $1x10^5$	++ $2x10^6$	++ $6x10^5$	+++ $2x10^7$
	IgG3	+	-	-	-

Table 1.3 Murine IgG isotypes and their binding affinity

Different mouse IgGs bind with different affinities to FcγRs. Affinities for bind are noted as – no binding, + low affinity, ++ average affinity and +++ high affinity. Quantified affinities are noted next to binding score. *Adapted from Bruhns et al., 2012 [391] and Bruhns and Jonsson et al., 2015 [390].*

Despite the promise seen in mAb therapy, little clinical benefit as a cancer treatment was seen in the early years after development [394,395]. This failure was more than likely due to early mAb therapeutics consisting of murine, not human, antibodies, and therefore in many instances, the patients receiving the murine antibody infusions developed immune responses in the form of antibodies against the foreign species mAb. This response is known as the development of human anti-mouse antibodies (HAMA), which lead to rapid clearance of the murine mAb, reducing its half-life in the blood and overall reducing its efficacy [396].

To overcome this hurdle and to release the full therapeutic potential of mAbs, modifications of the Fc regions of murine antibodies was undertaken to create new mouse-human chimeric mAbs, which when infused, behave as normal human IgG [397,398]. These chimeric mAbs, such as the anti-GD2 antibody, were less immunogenic leading to a longer half-life than murine mAbs and importantly, due to the human Fc region, interacted with the FcγR mediated effector cells to generate effective therapeutic responses [398]. Furthermore, mAbs are now being engineered or produced to be humanized (fully human structure except for CDRs), and even fully human, leading to better therapeutic activity, due to more physiological engagement of human FcγRs and better half-lives [399].

Along with these isotype engineering modifications described above, engineering of post-translational modifications of specific sites of the mAbs can also be conducted. One such modification of interest is changing the glycosylation of the Fc portion of the antibody (**Figure 1.11**). On the unmodified antibody, a carbohydrate moiety is attached post-translationally to this site, which regulates its ability to interact with Fc receptors efficiently [400]. This glycosylation can be prevented during antibody production itself or removed using enzymes after mAb production. Modifying glycosylation on mAbs is an important mechanism used to prevent or allow binding to FcγRs [389,401,402]. If a mAb is only required to block a specific target rather than have any subsequent effector function, removal of glycosylation may be beneficial to its efficacy, as it prevents binding to FcγRs and therefore blocks any downstream effector functions [389].

With the full potential of mAb therapy now beginning to be revealed, mAb therapy has become a staple in the clinicians tools for effective cancer therapy [403], particularly for B cell lymphomas, breast cancer [404,405], melanoma [406], Lung cancer [407] and NB [49], as shown in **Table 1.4**. As antibody engineering and modifications improve, more cancers could benefit from the remarkable effectiveness these molecules can impart to cancer treatment, and may begin to be combined with, or replace, traditional non-specific cancer therapies in the near future.

Generic name	*Target; isotype*	*Indication*	*FDA approval*	*EU approval*
Rituximab	CD20; Chimeric IgG1	NHL	1997	1998
Trastuzumab	Her2; humanised IgG1	Breast cancer	2000	1998
Ibritumomab tiuxetan	CD20; mIgG1	NHL	2004	2002
Cetuximab	EGFR; Chimeric IgG1	Colorectal cancer	2004	2004
Panitumumab	EGFR; hIgG2	Colorectal cancer	2007	2006
Ofatumumab	CD20; hIgG1	CLL	2009	2009
Pertuzumab	Her2; humanised IgG1	Breast Cancer	2013	2012
Obinutuzumab	CD20; Humanised IgG1; glycomod	CLL	2014	2013
Dinutuximab	GD2; chimeric IgG1	NB	2015	2015
Nectimumab	EGFR; hIgG1	NSCLC	2015	2015
Daratumumab	CD38; hIgG1	Multiple melanoma	2016	2015
Bevacizumab	VEGF; Humanised IgG1	Colorectal cancer	2005	2004
Ipilimumab	CTLA-4; hIgG1	Metastatic Melanoma	2011	2011
Ramucirumab	VEGFR2; hIgG1	Gastric cancer	2014	2014
Pembrolizumab	PD-1; Humanised IgG4	Melanoma	2015	2014
Blinatumomab	CD19-CD3; m-bispecific tandem scFv	Melanoma	2015	2014
Nivolumab	PD1; hIgG4	Melanoma; NSCLC	2015	2014
Elotuzumab	SLAMF7; humanised IgG1	Multiple myeloma	2016	2015
Olaratumab	PDGFRα; hIgG1	Soft tissue sarcoma	2016	2016
Atezolizumab	PD-L1; humanized IgG1	Bladder cancer	2017	2016
Avelumab	PD-L1; humanized IgG1	Merkel cell carcinoma	2017	2017
Durvalumab	PD-L1; hIgG1	Bladder cancer	In review	2017
Cemiplimab	PD-1; humanised IgG4	Cutaneous squamous cell carcinoma	In review	In review

Table 1.4 List of currently approved MAbs for cancer immunotherapy

From the first approved therapeutic of anti-CD20 antibody, many new targets for many cancers have appeared as suitable for mAb therapy as shown here. Multiple antibodies have been developed for the same target with advancement in understanding of antibody function, leading to modifications to antibody structures. Highlighted in light grey are all the current approved antibodies targeting checkpoint inhibitors. *Correct as of August 2018, adapted from http://www.antibodysociety.org/news/approved-antibodies*

1.5.1.1 Direct targeting - anti-GD2 antibody therapy

Monoclonal antibodies are fast becoming seen as powerful novel tools on the front line of treatment for many types of cancers, with many antibodies now approved for therapeutic used in clinic (see **Table 1.4**). These therapeutic antibodies can be divided into two classes based on their apparent therapeutic mechanism. Antibodies which exert their function on immune cells and therefore indirectly allow for tumour cell killing are known as immunomodulatory antibodies, as

discussed below. However, antibodies which target antigens expressed on tumour cells themselves are known as direct targeting antibodies. These direct targeting antibodies are seen as potential alternatives to classical cancer treatments due to their complete specificity for the antigen they are targeted to which is usually only expressed on the tumour cells in question. One example of a direct targeting antibody is the anti-GD2 antibody used in NB therapy as mentioned previously [52].

The currently approved anti-GD2 antibody for NB treatment is known as dinutuximab or ch14.18, and was engineered as a human-murine chimeric mAb which was clinically approved by the FDA in 2015 [52]. As mentioned previously this antibody is usually given after the current standard treatment for high-risk NB, and is combined with GM-CSF, IL-2 and 13-cis-RA [49,52]. The mechanism of action of ch14.18 involves directly binding to the tumour antigen GD2 on the surface of tumour cells and eliciting tumour cell destruction resulting in tumour regression. To do this, it is currently thought the antibody mainly employs two mechanisms : antibody dependent cellular cytotoxicity (ADCC) and complement dependent cytotoxicity (CDC) [408,409], however it has also been reported that it may function by antibody dependent cellular phagocytosis (ADCP) [29].

ADCC, CDC and ADCP are proposed mechanisms of action of direct targeting antibodies and are all initiated by the Fc portion of the monoclonal antibody in question, either by binding to the appropriate Fc receptor on effector cells or to complement initiator molecules as mentioned previously. ADCC is initiated by ch14.18 binding to GD2 on the tumour cell surface by its Fab and then binding an activatory FcγR via its Fc region on an NK cell [410]. FcγRIII which is expressed on human and murine NK cells is thought to be the important FcγR for this process to occur [411,412]. When this FcγR is engaged the NK cell is activated to release cytotoxic granules such as perforin and granzymes to cause target cell death by apoptosis. For ADCP, again ligation of FcγRs on effector cells by Fc portion of ch14.18 after GD2 Fab binding is required to initiate this mechanism. Here, at least in murine models, the effector cell is usually a macrophage which when activated by this FcγR engagement, engulfs and phagocytoses the target tumour cell [413]. This both destroys the tumour cell and could possibly lead to presentation of tumour antigens by the macrophages to other effector cells of the immune system, however this is not yet established for anti-GD2 therapy. The role of macrophages in this mechanism of ch14.18 in humans is as yet unclear. Finally, CDC is initiated by ch14.18 once the target cell has be opsonised via binding of high numbers of ch14.18 mAbs to multiple GD2 sites. Activation of CDC occurs when > 1 of the globular heads of the C1q molecules have bound to the Fc domain of the ch14.18 antibody. This initiates the cascade of complement molecules with many complement enzymes involved in the cleavage of more complement molecules which results in the formation of a membrane attack complex at the target cell's surface [414,415]. Once formed on the cell membrane the membrane attack complex leads to lysis of the tumour cell, and the remaining cleaved complement components act as potent

proinflammatory signals which recruit further immune cells such as phagocytes [416]. These recruited phagocytes can then remove the cell debris left by the lysed cells, and present the tumour antigens to effector cells of the adaptive immune system to generate a further anti-tumour response. The relative roles of these different mechanisms of actions in patients is unclear.

1.5.2 Monoclonal antibodies – immunomodulatory

Not only have mAbs been developed to directly target tumour cells, some have been engineered to target molecules of the immune system, with the aim of stimulating an anti-tumour immune response, or modulating the immune environment already present. This class of therapeutic mAbs are known as immunomodulatory antibodies, with many already being approved for clinical uses as shown in **Table 1.4**. Most of these mAbs function by targeting specific receptors or ligands involved with the generation and activation of an anti-tumour T cell response, and look to target the immune checkpoints as mentioned above (see **Figure 1.8**). Antibodies which target immune checkpoints have shown great promise in solid tumours such as metastatic melanoma [417,418], non-small cell lung cancer [419], bladder cancers [420] and head and neck cancers [212]. However, not all immunomodulatory antibodies target inhibitory mechanisms of T cells but can also target stimulatory mechanisms with the aim to agonise an antigen specific immune response, as will be discussed below.

1.5.2.1 Anti-CTLA-4 antibodies

Targeting immune checkpoints of T cells was first demonstrated to be a viable and efficacious therapy by the use of mAbs which target and block the receptor CTLA-4 [421]. Approval of an anti-CTLA-4 antibody, ipililmumab, was first achieved for use in metastatic melanoma in 2010 [422]. However, the road to clinical approval was delayed with observations that *CTLA-4* knockout mice developed lethal autoimmunity [199,200]. Due to this preclinical data, it was thought that infusion of the anti-CTLA-4 antibody may cause dramatic autoimmune toxicities. However, after demonstration that partial blocking of the receptor in preclinical models of immunogenic tumours still generated an impressive anti-tumour response without associated toxicities, the idea of using this as a clinical therapeutic was reignited [421]. Furthermore, from the study above it was noted that anti-CTLA-4 as a single agent therapy was only effective in stopping tumour growth in immunogenic tumours, with non-immunogenic tumours needing an extra boost of GM-CSF to show responses [423]. This inferred that cancers which are inherently immunogenic, such as melanomas, and have an endogenous immune response present, could see the greatest therapeutic benefit from CTLA-4 blockade. Initially two clinical anti-CTLA-4 mAbs were developed, ipilimumab and tremelimumab, with both showing an initial objective clinical responses of ~10% in patients [424-427]. However, in a

phase II and a randomised phase III trial tremelimumab was shown to not have efficacy in melanoma patients [425,428]. Currently, ipilimumab is seen as the front runner of the two anti-CTLA-4 antibodies, with Food and Drug Administration (FDA) approval achieved for melanoma. Although, it has only shown anti-tumour effects in a small proportion of patients with cancers other than melanoma, such as kidney, lung and prostate cancer [429]. Despite this, ongoing trials of both anti-CTLA-4 antibodies are continuing.

CTLA-4 blockade is currently considered to work via a few different mechanisms. Firstly, as there is an increased expression of CTLA-4 on CD4+ helper cells, blockade of CTLA-4 signalling is thought to release these cells from suppression in order for them to help tumour killing by CD8+ effector cells, increasing the endogenous anti-tumour response [212]. Furthermore, it was found that anti-CTLA-4 treatment induces the expression of activation markers on circulating T cells [430], therefore allowing the T cells to become more active. Anti-CTLA-4 blockade can also inactivate and supress Treg populations as the CTLA-4 receptor on these cells actually functions to increase their activity [158,201], and could even delete Tregs with high CTLA-4 expression [431]. All of these mechanisms lead to high levels of inflammation [426], and may be the reason anti-CTLA-4 therapy is associated with autoimmune related adverse events, as will be discussed below.

One of the major problems of anti-CTLA-4 therapy is the associated toxicity. This was a concern before clinical trials started, due to the lethal phenotypes of CTLA-4 knockout mice [199,200]. Adverse events seen in patients were given a new category of immune related adverse events (irAEs), and mainly consisted of autoimmune toxicities such as colitis observed in 25-30% of patients, which resulted in some fatalities [424-427]. Other irAEs included dermatitis, and hepatitis, with rapidly dividing tissues such as the skin and gut being the most effected [432]. However, having the irAEs was positively correlated with response to the treatment [433], and therefore showed that CTLA-4 blockade does 'release the brakes' off the immune system.

1.5.2.2 Anti-PD-1 antibodies

As discussed, above another promising immune checkpoint for therapy targeting in cancer is PD-1 and its ligands PD-L1 and PD-L2. PD-1 was identified as an interesting target for the development of immunotherapies, as its ligands are known to be upregulated in many human cancers [434], with solid tumours mainly overexpressing PD-L1, rather than PD-L2[435]. Furthermore, unlike CTLA-4, PD-1 (and PD-L1 and –L2) knockout mice did not have lethal autoimmune phenotypes, which suggested that in clinical practice, blockade of this pathway would have less side effects associated with its usage [208,209]. Preclinical mouse models also held promise for this therapy as a robust anti-tumour immune response and tumour regression was demonstrated [241,434,436]. Furthermore, after the

successes seen with anti-CTLA-4 therapy development of PD-1 pathway blocking antibodies was of particular clinical interest, with the hope of developing a more potent, less toxic immunotherapy.

The first human clinical trials were conducted in multiple cancer types including melanoma, kidney and colorectal cancers [437]. Tumour regression was observed in some patients, with a variable level of responses to the therapy being seen. In the follow up trial, notable objective responses were witnessed for multiple tumour types, which were shown to be durable over long term follow up [438,439]. Finally, after successful phase III trials for melanoma and NSCLC, nivolumab was approved for clinical use. Promise for PD-1 pathway blockade has also been shown also in renal cell carcinoma [440-442]. Within these trials a reduction in adverse events was witness compared to anti-CTLA-4, as expected from preclinical data [437]. It was also noted that level of PD-L1 expression on patients' tumour biopsies correlated with their response to the therapy [437], with patients who had little-to-no cell surface expression of PD-L1 not responding to the treatment [439]. However, CD8+ TIL location and PD-L1 expression by other immune cell subsets within the tumours may also infer response rate and outcome of targeting this pathway [441,443]. Due to the success of checkpoint inhibitor therapy, James Allison and Tasuku Honjo were recently awarded the Nobel Prize in medicine for their discovery of CTLA-4 and PD-1 receptors [444].

The ligands of PD-1, PD-L1 and PD-L2, are expressed by tumour cells and other infiltrating immune cells to engage PD-1 and therefore prevent TCR signalling at the point of effector-target cell contact. [242]. However, there could also be a role within the draining lymph node, as PD-1 has a role in early fate decisions of T cell differentiation after antigen presentation within lymph nodes [445]. It has been observed that tumour infiltrating T cells have increased expression of PD-1 receptor, which is believed to be due to chronic antigen stimulation leading to an exhausted T cell phenotype [446,447]. PD-1 blockade via mAb therapy aims to reverse this exhaustion, which has been shown to be possible in chronic viral infection models [448]. As mentioned previously, recent work has demonstrated that PD-1 inhibition of T cell function may work through blocking CD28 co-stimulation, rather than TCR signalling [206]. Further on from this Kamphorst et al, recently suggested that CD28 co-stimulation is required for efficacy of anti-PD-1 therapy in mouse tumour models [449]. They also demonstrated that in lung cancer patients who had been previously treated with anti-PD-1 therapy, the CD8 T cells which proliferated, expressed CD28. These data together suggests an interplay between PD-1 and CD28 signalling pathways, and a possible mechanism of action of anti-PD-1 therapy.

As discussed above, PD-1 blockade is believed to function mainly within the tumour microenvironment, whereas CTLA-4 blockade functions within the tumour draining lymph node [450]. These contrasting locations and mechanisms of actions suggest that combination of the two

therapies could have efficacy clinically. Consequently, a trial combining both PD-1 and CTLA-4 blockade was reported to have led to greater responses, than seen previously with monotherapy, when combining nivolumab and ipilimumab in melanoma [451]. However in this combination trial, due to the use of anti-CTLA-4 antibody, an increase in the number and intensity of irAEs was seen.

Despite the focus on how the blocking antibody works via modulating T cell activation T cells there may also be a role for its action upon myeloid cells within the tumour microenvironment. Successful blocking of PD-1/PD-L1 axis to promote an anti-tumour response may be attributable down to blocking the PD-L1 expressed on suppressive myeloid cells, and therefore preventing the interaction with PD-1 on T cells, preventing T cell suppression [441].

1.5.2.3 Anti-4-1BB antibodies

Another immunomodulatory antibody therapy currently under preclinical and clinical investigation is targeting the co-stimulatory molecule 4-1BB (also known as CD137 – see **Figure 1.8**). 4-1BB is a member of the tumour necrosis receptor (TNFR) superfamily, and was first identified as being expressed only on activated murine T cells [452]. 4-1BB acts as a co-stimulatory receptor for T cell responses as the cytoplasmic domain of 4-1BB contains four phosphorylation sites [453]. 4-1BB expression has also been reported on activated NK cells and some myeloid cell subsets [454], with its constitutive expression being found on Treg cells. 4-1BBL is the high affinity ligand for 4-1BB receptor and is expressed at low level on B cells, macrophages and DCs constitutively [455]. Due to 4-1BB being present on already activated cells, its main role focuses on modulating T cell responses rather than stimulating them, with ligation of the TCR required for function [456,457]. With activation of the 4-1BB receptor, both CD4+ and CD8+ T cell were found to increase proliferation and cytokine production, along with improved survival after activation [458].

Developing an agonistic antibody targeting the stimulation of this receptor to boost anti-tumour T cell responses is seen as an attractive prospect. Investigations have shown that administration of an anti-4-1BB antibody can lead to eradication of numerous tumours in murine models, with inherent immunogenicity of the tumour and tumour burden effecting outcome [459-463]. Several clinical trials have been conducted with the use of anti-4-1BB therapy for several solid tumours including melanoma [464], and its combination with direct targeting antibodies have proved efficacious in murine models [463,465-467].

1.5.3 Cellular based immunotherapies

Antibody treatment boosted the immunotherapy revolution for cancer treatment, with an explosion in newly developed therapies, all aimed at stimulating and maintaining an anti-tumour

immune response. Many of these new therapies involve targeting specific cells of the immune system to provoke an anti-tumour response, be that by vaccine stimulation or adoptive cellular immunotherapy.

Vaccines have been used for many years in order to prime and boost an immune response to pathogens such as viral infections, and are now beginning to be applied to cancer therapy [468]. An early proposal of cancer vaccination came in the form of development of vaccines for oncoviruses, such as human papilloma virus (HPV). Chronic infection with HPV can lead to cancer development, however vaccination against this virus can reduce this risk, and has led to the idea that vaccines could be developed to target tumours themselves [152,469,470]. Early clinical trials into cancer vaccines were not very successful [471], with a lack of understanding the role of immune tolerance to cancer antigens and the part DCs play. A consequence of an immunosuppressive tumour microenvironment, induction of immune tolerance to cancer antigens will occur, and therefore vaccination must be able to break this [469,472,473]. One way of breaking the tolerance is to appropriately target and stimulate DCs, so they can effectively prime the adaptive immune response [472,474]. Therefore, an ideal cancer vaccine will be able to trigger appropriate maturation of DCs to efficiently induce CD8+ tumour reactive T cells. However, the obstacle of a suppressive tumour microenvironment will still persist, therefore it is possible that stimulated tumour reactive T cells could be rendered inert once they reach the tumour, resulting in an unsuccessful anti-tumour response. It is more likely that vaccination strategies will be successful if they are used in combination with other therapies that can convert the microenvironment from suppressive to stimulatory.

A way that the immune tolerance barrier could be broken is by the use of adoptive cell transfer (ACT). This involves collecting effector T cells from the patient, culturing and stimulating them appropriately *ex vivo* and then re-infusing them back into the patients [475]. This *ex vivo* modulation was hoped to have lowered activation thresholds and expanded tumour-specific T cells, and has shown promise in clinical trials [476,477]. One method of ACT transfer is using TILs isolated from tumour biopsies of patients [475]. T cells from these biopsies were enriched for tumour reactivity but are usually anergised due to the immunosuppressive environment. Therefore, *ex vivo* activation of these TILs was required before reinfusion into patients. Early studies showed a 30% response rate in melanoma using this method, however actual persistence of the TILs within the patients was poor [134,135,478], and this was increased further once lymphodepleting chemotherapy was added to the regimen [145,146]. This approach is limited by the low presence of TILs in the first place, TILs reverting to supressed state in tumour microenvironment, labour intensive ex vivo manipulation and the fact that not all cancers come with readily available tumour specimens.

In order to overcome some of these problems, the idea of genetically engineering T cells to already possess tumour specificity was tested in the form of chimeric antigen receptor (CAR) T cell development [479]. CARs are engineered receptors which consist of a single-chain variable fragment (scFv) from an antibody, coupled with the intracellular signalling domains from the classical TCR, using the CD3ζ domain [475]. CAR receptors bypass the need for MHC-restricted antigen presentation, and can be engineered onto any of the patients T cell, negating the need for tumour-specific T cells. First generation CARs [479] contained only the CD3ζ chain signalling domain, which demonstrate promising by modest anti-tumour activity and expansion [480-482]. Second generation CAR T cells were developed having extra signalling domains from co-stimulatory receptors added in, including domains of CD28, OX40, 4-1BB etc [483-485]. This addition increased IL-2 production and tumour cell killing by the CAR T cells [483] showing promise in clinical trials [486]. Recently, third generation CARs have been developed which added a second co-stimulatory domain to see if this can increase the potency of the anti-tumour response even further [487,488].

1.5.4 Immunotherapy and immune modulation in NB

NB may be an effective target for immunotherapy, as the disease is proving receptive to direct targeting immunotherapy, in the form of anti-GD2 mAb therapy [49]. Interestingly, NB is known to have the highest rate of spontaneous regression among all cancers [489,490]. Despite this high rate, it has not been concluded what the exact mechanism is behind the regression. Proposals are focused on loss of telomerase activity, epigenetic alterations, neutrophin deprivation, and most importantly, an endogenous immune response [24,30,491]. It has been noted that regression of some cancers, including NB, appears to occur after an acute infection, where the immune system is activated and stimulated to eradicate the pathogen [30]. NB antigen specific TILs have been found present in tumour tissue, however these are rare [492]. Furthermore anti-neural antibodies have been discovered in some patients [492] which have previously been associated with a favourable outcome [493,494]. Interestingly, one immune mediated mechanism of spontaneous regression may be due to spontaneously regressing tumour cells expressing normal levels of human leukocyte antigen (HLA) class I [495], unlike most NB tumours which actively downregulate this molecule to avoid immune destruction [238,496]. Difficulty in determining why some NB tumours spontaneously regress, is due to the fact that the regression is usually only noticed during follow up of the patient, by which point all tumour tissue has disappeared. If tumour biopsies could be collected as tumours are regressing, this may allow for more insight into the mechanisms occurring here.

As previously mentioned, one of the treatments recommend for NB involves harnessing the anti-tumour immune response by combining an anti-GD2 mAb with two immune activating factors: GM-CSF and IL-2 [49]. This combination therapy works by recruiting the effector cells needed, via IL-2 and

GM-CSF, for the anti-GD2 antibody to function. Here, the anti-GD2 mAb binds to the tumour cell (opsonisation) and recruited NK cells kill the cells with ADCC, or possibly by recruiting macrophages for ADCP (**Figure 1.12**)[49,409,497]. Dinutuxumab (ch14.18) was the first immunotherapy shown to be clinically effective in paediatric cancers. Currently there are investigations being run into the use of bispecific antibodies targeting GD2 and CD3 in the hope of stimulating tumour infiltrating T cells against GD2+ tumour cells [498]. Neutrophils are also regarded as important effector cells within NB and its treatment. Previous data has demonstrated that treatment of NB with retinoic acid can lead to IL-8 production by the tumours cells, which in turn led to neutrophil recruitment [499]. This recruitment to the TME, which is enhanced by the administration of GM-CSF, is important for NB therapy as these cells can mediate ADCC after administration of anti-GD2 antibodies [500-502]. It has also been suggested that these cells are the most potent effector cell in neuroblastoma killing [503].

Unfortunately, autologous NB-specific T cells are very rare to find in patients, and have poor homing capabilities to tumour tissues [504]. Therefore, CAR T cells directed against GD2 are currently under investigation for high risk NB. As explained above, CAR T cells have the specificity of a Fab fragment of an antibody coupled with the signalling potency of a T cell as shown on **Figure 1.12** [480,505]. CARs have shown promise in adult cancers, however their response in solid tumour types is diminished compared to results from liquid tumours [506,507]. First generation GD2-CAR T cells were generated and tested in 2008 with two objective responses seen out of 8 patients [505], with long term follow up showing 2 complete responses out of 11 patients [508]. The first generation-CAR used in this trial only had TCRζ signalling domains attached to the scFV, with no additional costimulation, therefore the next generation of anti-GD2 CARs possessed additional CD28 and OX40 co-stimulatory domains [509]. In this trial however, no objective responses were seen in 11 patients, with no persistence of the CAR T cells at 6 weeks post treatment. The reduction in efficacy despite addition of co-stimulatory domains is thought to be due to tonic signalling and CAR T cell exhaustion due to clustering of the receptor [507]. Furthermore, the effect may have been due to the type of co-stimulatory domain included into the CAR signalling module, as when a 4-1BB domain was added, the T cell exhaustion was reduced [507]. This has led to a clinical trial being developed using these 4-1BB GD2-CAR T cells. With CAR T cells holding some promise in NB treatment, adoptive cytotherapy using NK and NKT cells is being considered [510].

Despite the promising and unprecedented results seen with the use of checkpoint inhibitory therapy seen in adult cancers, to date only one trial of checkpoint inhibitors within paediatric cancers has been reported [511], using ipilimumab. This was not a single disease study and involved many different forms of cancer including melanoma, sarcoma and NB, and included children and young adults from the ages of 2-21. Unfortunately, no objective anti-tumour immune responses were found, despite a comparable pharmacokinetic and toxicity profile as seen in adult cancers [511].

This lack of efficacy may be due to all patients being end-stage and therefore would have a considerable amounts of chemotherapy, radiotherapy etc. A study into PD-1 blockade in patients with paediatric histologies has not yet been fully reported, however, interim reports suggest there isn't any significant anti-tumour activity [512]. It may be that single-agent therapy in paediatric cancers is not enough to kick-start an anti-tumour immune response. Combinations with other therapies which make the paediatric tumour microenvironment more immunogenic, and therefore pervasive of checkpoint blockade, may be required for efficacy[20].

A reason for paediatric tumours not responding to single-agent immunotherapy may be due to the tumour cells themselves. Over the past few years, research has revealed that neoantigens, caused by nonsynonymous somatic mutations (NSSM) within tumour cells, may be the most immunogenic form of tumour associated antigen [18,19,513], with their expression being completely limited to tumour cells. Furthermore, response to checkpoint inhibitor therapy has been linked to the number of these mutations in tumours of patients, with higher response rates seen in patients with more mutations [514]. This becomes a problem in paediatric cancers, as on the whole the express very little neoantigens as most paediatric tumours only display mutations in a few key drivers of oncogenesis [17], such as MYCN amplification seen in NBs [515]. Having NSSM within paediatric tumours would greatly increase the levels of tumour specific antigens to be recognised by the immune system and targeted. An example demonstrating this idea are children with biallelic mismatch repair deficiency (bMMRD) who then develop cancers. The bMMRD inactivates DNA mismatch repair genes in the germline cells of these patients leading to a high incidence of cancers developing in childhood which, interestingly, have a high number of NSSMs [516,517]. Results using checkpoint blockade within these patients has shown an increase in anti-tumour responses leading to a planned clinical trial [516]. These data put forward the proposal that most paediatric cancers have a low mutational burden and therefore are inherently of diminished immunogenicity compared to adult cancers [17]. Development on new and more effective treatment regimens for cancers like NB should therefore be focussing on how to tip the immunogenicity balance in the favour of developing and effective anti-tumour response. Currently the only likely way this could be achieved in paediatric cancers is with finely tuned combinational therapy aimed at firstly increasing the immunogenicity of the cancer cells themselves, and secondly at stimulating the immune system to drive the anti-tumour immune response.

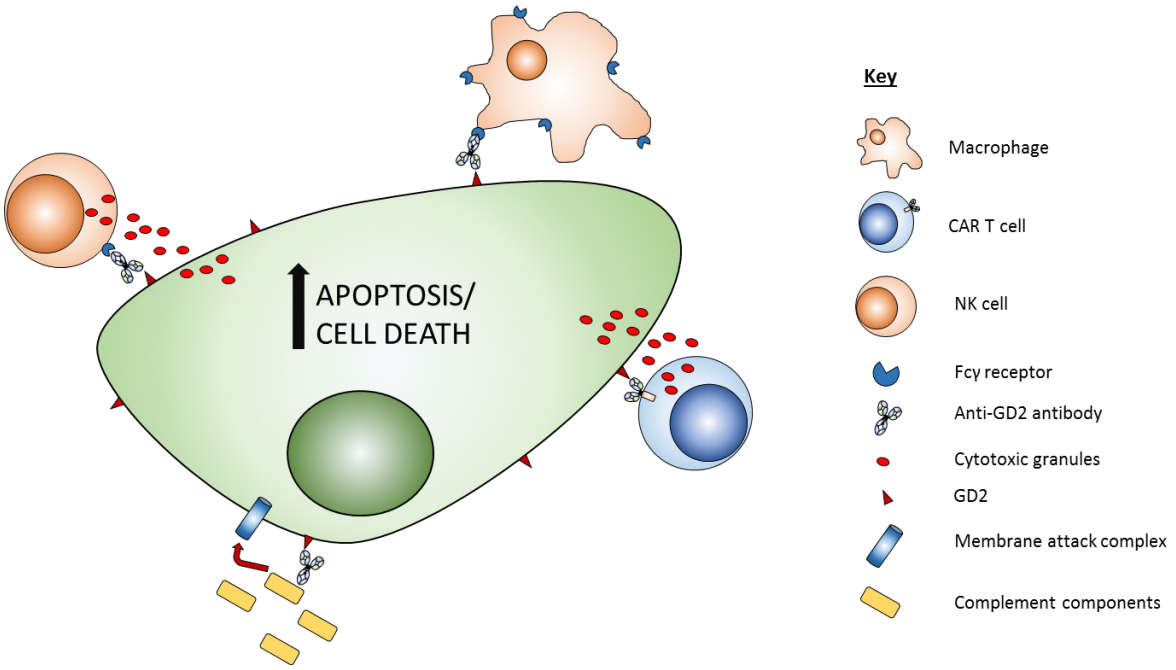

Figure 1.12 Immunotherapy of NB

Due to MHC downregulation, low mutational landscape, immature immune system, and high disease burden in high-risk NB patients, the tumour microenvironment is primed for dampening and preventing a proficient anti-tumour T cell response. However therapeutics can be introduced to manoeuvre around these immunosuppressive barriers. The advent of an antibody therapy targeting GD2 on NB cells has provided a potent treatment. This antibody can work with infiltrating immune cells to cause tumour cell death by ADCC, or granulocyte-mediated ADCC. This activates immune cells such as NKs cells via binding to FcγRs and causing the release of cytotoxic granules. Furthermore the antibody can bind to FcγR on monocytes or macrophages leading to antibody dependent cellular phagocytosis, allowing engulfment on NB cells. When the antibody is bound to GD2 on the NB cell surface it can also activate a complement cascade via engagement of complement component C1q. This allows for formation of a membrane attack complex on the NB cell surface and eventual lysis of the cell, along with release of complement components into circulation to attract phagocytes. Finally, polyclonal T cells from patients can be extracted and engineered with CAR-T cell receptors specific for GD2. These cells can then bind to GD2 on NB cell surface and become activated to produce cytotoxic granules leading to NB cell death.

1.5.5 Synergy of chemotherapy and immunotherapy

Chemotherapy which is able to induce ICD has potential to be combined with complementary immunotherapy, to promote the development of potent anti-tumour responses. Pfirschke et al 2016, looked at this possible synergy within a lung adenocarcinoma (LA) model, which has previously been described to be nonimmunogenic and a poor responder to immunotherapy, including anti-PD-1 therapy [518,519]. Chemotherapeutics used for lung adenocarcinoma treatment include CPM and OXA which have both demonstrated the ability to cause ICD in certain cancer models [520]. In this study, two murine LA models were used; a conditional genetic model expressing Kras and Trp53 (KP), and an orthotopic KP model. Arguably the genetic model is a more realistic representation of human LA as it has reduced T cell infiltrates and is shown to be resistant to chemotherapy and immunotherapy [519]. CPM+OXA were more effective at inducing ICD as a

combination than alone. It was observed that the CPM+OXA combination induced an immunogenic phenotype of KP cells, which resulted in CD8+ T cell infiltration into the tumour microenvironment, which was further correlated with a decrease in cancer progression. However, autochthonous tumours resist current chemotherapy and immunotherapy, even when they have a high neoantigen burden. This suggests that these tumours may be immunosuppressive and need a specific combination of immunogenic chemotherapy synergised with efficient checkpoint inhibition. This study demonstrated that these hard to treat tumours can be rendered sensitive to checkpoint therapy and an anti-tumour immune response can be generated if the right combination is used. The combination of CPM and OXA could generate an anti-tumour response, as demonstrated by the transplantation of CPM and OXA killed cells into mice inoculated with KP tumours, which lead to a decrease in tumour progression. This was due to the induction of an immunogenic phenotype by the chemotherapy combination, which was further shown to be entirely dependent on CD8+ T cells. When the same experiment was repeated in *rag2*$^{-/-}$ mice or in wild type mice with their CD8+ depleted, no tumour control was noted [519]. However other studies have suggested that in some models the reliance on CD8+ T cells is not as crucial as in this model [521]. Due to CD8+ infiltration, the ICD inducing chemotherapy was able to synergise with anti-PD-1 and anti-CTLA-4 therapy.

A more effective use of chemotherapy may be to increase its load at the tumour site to maximise the ICD inducing effect of these drugs. Some ideas include the use of nanoparticles [522], remodelling the tumour vasculature to improve perfusion [523] or using antibody dependent drug targeting [524]. This preclinical data is in line with clinical observation of the combinations of anti-CTLA-4 antibody therapy with paclitaxel and carboplatin in non-small cell lung cancer (NSCLC), which improved overall survival [525,526]. Furthermore, combination of anti-PD-1 therapy with carboplatin, may have resulted in great anti-tumour effectors than single therapies alone [527].

One such immunotherapy which looks promising in combination with chemotherapy is blockade of the IDO pathway. IDO is known to be upregulated on apoptotic cells [528], along with being expressed on immune cells, inflamed epithelial and fibroblast cells and some tumour cells [243]. Furthermore, IDO may be a key regulator for preventing autoimmune responses to self-antigens and has an important role in inducing peripheral tolerance of T cells to self-antigens [529]. IDO is an enzyme which converts tryptophan to kynurenine, which in turn activates the GCN2 kinase. This is notable, as activation of GCN2 increases the function of Tregs while also reducing effector function and proliferation of other T cell subsets [530,531]. Furthermore APCs such as DCs which express IDO can be programmed to be tolerogenic when presenting antigen to T cells, and therefore supress an immune response towards that particular antigen [532]. Activation of the IDO pathway determines whether antigen presentation is either immunogenic or suppressive. If mice are challenged with apoptotic tumour cells, IDO is upregulated and Tregs are induced [533]. This is an important point to

consider as many chemotherapies function by inducing apoptosis of tumour cells. Therefore, tumour cells may use the inhibitory IDO pathway to induce tolerance of antigen specific effector immune cells. This highlights the importance of choosing the right, ICD inducing chemotherapy to combine with the right immunotherapy. Using an appropriate checkpoint blocker may also render non-immunogenic chemotherapies more immunogenic. With this, the suppressive mechanisms utilised by tumour cells will be blocked, allowing for an anti-tumour response to released tumour antigen to occur. Thus, tumour cell death releases both tolerogenic and immunogenic signals but within a suppressive tumour microenvironment the tolerogenic signals tip the balance, preventing any ICD signals from inducing an anti-tumour response. Consequently, if the balance can be tipped in the favour of ICD by blocking a strong inhibitory pathway such as IDO, the anti-tumour response battle may be won.

Trials have already been conducted looking at combining immune stimulating treatments with chemotherapy [525,526,534]. Therefore, it can be hypothesised that the right chemotherapy, which has good immunostimulatory properties, may be efficiently partnered with current immune based treatments or novel therapies, to provide the most effective treatment for the patient. A current focus revolves around combining chemotherapy with checkpoint inhibitor mAbs [535-537]. Despite the fact that these antibodies have mainly been assessed in adult cancers, they may prove to be effective in NB. Reasoning for this is that checkpoint inhibitors have shown potent efficacy in melanoma, a skin cancer of which its cells are derived from the same linage as NB cells i.e. neural crest cells [23]. Therefore if an initial and primed immune response can be generated via inducing ICD with chemotherapy, combination with these antibodies may prove to be highly effective.

1.6 Hypothesis and aims

1.6.1 Hypothesis

The hypothesis tested in this project and thesis is that immunomodulatory monoclonal antibody therapy can be combined with immunogenic cyclophosphamide to generate a therapeutic anti-tumour response in syngeneic and spontaneous murine models of neuroblastoma.

1.6.2 Aims

1. To characterise the immune microenvironment of three different *in vivo* murine NB models to assess how comparable they are to human NB.
2. Establish if CPM can induce ICD in NB tumour cell lines *in vitro*
3. Investigate how CPM alters the immune microenvironment in NB models *in vivo*
4. Establish if CPM can be combined with anti-PD-1 antibody therapy *in vivo* to improve survival

Chapter 2: Materials and Methods

2.1 Animals

2.1.1 Ethics

All animals used were maintained by the Biomedical Research Facility at the University of Southampton in accordance with Home Office Regulations. All procedures carried out were approved by the local Animal Welfare and Ethics Review Board, and performed in accordance to the Animals (Scientific Procedures) Acts 1986 as set out in the Project Licences: RRF30/2964, PB24EEE31 and P81E129B7

2.1.2 AJ and C57BL/6 mice

Wild type inbred mice were bred by the Biomedical Research Facility at the University of Southampton. Either males or females were used at between 8 – 12 weeks.

2.1.3 TH-MYCN$^{+/-}$

TH-MYCN transgenic mice were first developed by Weiss et al [37], using the 129/svj.1 background. The colony was maintained by the Biomedical Research Facility at the University of Southampton. The mice are transgenic for the MYC-N gene controlled by a rat tyrosine hydroxylase (TH) promotor to be expressed in neuroectodermal tissue to mimic human neuroblastoma presentation. As homozygous mice develop the tumours at a very early age, heterozygous (het) mice are used to allow for full development of the immune system before tumour appearance.

2.1.3.1 Genotyping

Ear tip samples were obtained from mice once they were at least 5 weeks old to obtain a DNA sample. Tips were transferred to PCR tubes and 2.5µl of proteinase K (Thermo Scientific) and 100 µl of tail lysis buffer (50 mM Tris, 12.5 mM MgCl2 and 0.5 % Tween) was added to each tube. Tubes were then incubated in S1000 Thermocycler (BioRad) for 55^{o}C 18 hrs, 70^{o}C 1hr and 4^{o}C standing. Tubes were then transferred to -20^{o}C for at least 1 hr to inactivate the proteinase K. 1 µl of DNA from the digested tissue was added to new PCR tubes along with 1µl of DNA from a positive control mouse, and 1 µl of ultrapure (MilliQ) water for a negative control. A 24 µl of a prepared polymerase chain reaction (PCR) master mix was added to each tube (see **Table 2.1**) which included primers for the MYCN gene as below:

MYCN_RT_F1 CGACCACAAGGCCCTCAGTA

MYCN_RT_R1 CAGCCTTGGTGTTGGAGGAG

Strips were loaded into the S1000 Thermocycler and ran on the PCR settings described in **Table 2.2**. A 1 % agarose (Invitrogen) gel was made up with 5 µl of GelRed Nucleic Acid Gel Stain (Biotium) added before pouring into the mould. After PCR 5 µL of 6x Orange Loading Dye (Thermo Scientific) was added to each tube. 3 µL of O'Gene Ruler 1kb DNA Ladder (Fermentas) was loaded into the first well, followed by 30 µL of the PCR products. The gel was then ran at 167 volts for 45 mins. Gel was imaged in BioRad Gel Doc XR using Quantity One software.

Reagent	Company	Amount /tube
MilliQ H_2O	-	18 µL
GoTaq 5x Buffer	Promega	5.0 µL
dNTPs Mix 10mM	Promega	0.5 µL
TH-MYCN_RT_F1	Sigma Aldrich	0.1 µL
TH-MYCN_RT_R1	Sigma Aldrich	0.1 µL
GoTaq G2 DNA	Promega	0.3 µL

Table 2.1 Master mix for TH-MYCN genotyping PCR reaction

Temperature	Time	Cycles
92°C	2 minutes	
92°C	15 seconds	x30
66°C	15 seconds	
72°C	30 seconds	
4°C	Standing	

Table 2.2 PCR cycle for TH-MCYN genotyping

2.1.3.2 Tumour monitoring

All heterozygous mice were palpated twice weekly using two fingers to slide down the spine checking for abnormalities by trained animal technicians. Once tumour growth was noted, it was monitored closely for growth and once around 10 mm in diameter, animals were either given treatment or monitored until endpoint. Endpoint was decided by the technicians when the mice presented with symptoms alongside large tumour burden.

2.1.4 Vav-BCL-2 Transgenic mice

Vav-B cell lymphoma 2 (BCL-2) transgenic mice on C57BL/6 background were first developed by Ogilvy et al [538], and were kindly provided by Diego Gomez-Nicola, University of Southampton. These mice have constitutive expression of human BCL2 in all nucleated haematopoietic linage cells under the control of a vav promotor [538,539]. Female mice at no more than 12 weeks old were used, as germinal centre hyperplasia followed by follicular lymphoma like symptoms were seen at >10 months due to the anti-apoptotic side effects of the vav-BCL2 transgene [539].

2.2 Cell lines

2.2.1 NXS2

An adherent murine neuroblastoma cell line on an AJ background [540], expressing the neuroblastoma marker GD2, kindly provided by Professor Holger Lode, University of Greifswald, Germany. Cells were grown in 37^{o}C and 5 % CO_2 conditions using Dulbecco Modified Eagle Medium (DMEM) media (Gibco) supplemented with 10 % foetal calf serum (FCS - Sigma Aldrich) and 2 % glutamine and non-essential amino acids (GN - Gibco). Cells were split once 80 % confluent by a wash in phosphate buffered saline (PBS – Severn Biotech) and then removal from the flask via mechanical disassociation. Cells were spun at 450g for 5 minutes, and re-suspended in media for seeding of flasks. If cells were being used for injection into murine models, to reduce clumping cells were detached by incubating with 0.05 % Trypsin-EDTA for 5 minutes. Twice the amount of media was added to inhibit the trypsin enzyme, spun at 450g for 5 minutes, re-suspended in PBS and spun as previously.

2.2.2 9464D

An adherent murine neuroblastoma cell line derived from a spontaneous TH-MYCN tumours. These cells express GD2 and are reported to have low MHC class I expression [541,542]. These cells were kindly provided by Dr Rimas Orentas, NIH. Cells were grown in 37^{o}C and 5 % CO_2 conditions, using Roswell Park Memorial Institute medium (RPMI) 1640 media (Gibco) supplemented with 10 % FCS, 2 % GN and 0.36 % 2-mercaptoethanol (Sigma Aldrich). Cells were split once 80% confluent by washing in PBS and detachment from the flask by incubating with TripLE Express (Gibco) for 5-7 minutes. Twice the amount of media was added to inhibit the enzyme, spun at 450g for 5 minutes, re-suspended in media and seeded into flasks.

2.3 Antibodies

2.3.1 In house produced antibodies

Antibodies used throughout *in vivo* experiments and for flow cytometry were produced in house by the Antibody and Vaccine Group antibody production team. Details of the individual antibodies are listed in **Table 2.3**. Quality control of produced mAbs was conducted as follows. mAbs were initially screened and cells in positive wells were cloned twice and expanded in culture for IgG production. Antibodies were produced from hybridoma or CHOK1 cells and purified on Protein A with purity assessed by electrophoresis (Beckman EP system; Beckman Coulter) and lack of aggregation by SEC HPLC (all mAb less than 1%). All preparations were endotoxin low (< 10 EU endotoxin/mg) as determined using the Endosafe-PTS portable test system (Charles River Laboratories).

2.3.2 Commercially sourced antibodies

Primary, secondary and fluorophore conjugated antibodies used throughout flow cytometry, immunohistochemistry and immunofluorescence experiments were purchased from various commercial sources as detailed in **Table 2.4**.

Antigen	*Clone*	*Isotype*	*Reactivity*	*Fluorophore*	*Reference*
GD2	14G2a	Mouse IgG2a	Mouse	FITC	[543]
FcγRI	AT152	Fab_2	Mouse	FITC	[544]
FcγRIIb	AT130-2	Mouse IgG1 $N297A_2$	Mouse	FITC	[544]
FcγRIII	AT154	Fab_2	Mouse	FITC	[544]
FcγRIV	AT137	Fab_2	Mouse	FITC	[544]
PD-1	EW1.9	Rat IgG	Mouse	N/A	[463]
CTLA-4	UC10 F41011	Mouse IgG1	Mouse	N/A	
4-1BB	LOB 12.0	Mouse IgG1	Mouse	N/A	[545,546]
4-1BB	LOB 12.0	Mouse IgG2a	Mouse	N/A	[545,546]
Fc Block	2.4G2	Fab_2	Mouse	N/A	[547]

Table 2.3 In house produced monoclonal antibodies

Antigen	*Clone*	*Isotype*	*Reactivity*	*Conjugate*	*Supplier*	*Use*
CD11b	M1/70	R IgG2b, κ	M	PE	eBio	FC
F4/80	MCA497	R IgG2b	M	APC	BioRad	FC
Ly6C	RTK4174	R IgG2c, κ	M	PerCP-Cy5.5	eBio	FC
Ly6G	RB6-8C5	R IgG2b, κ	M	PE-Cy7	eBio	FC
CD11c	N418	ArH IgG	M	eFluor 450	eBio	FC
I-A/I-E	M5/114	R IgG2b, κ	M	V500	BD	FC
CD3e	500A2	SyrH IgG2	M	eFluor 450	BD	FC
CD49b	DX5	R IgM	M	PE	BD	FC
NKG2ACE	20d5	R IgG2a	M	PE	Novus	FC
CD45.2	104	M IgG2a	M	V450	BD	FC
CD45.2	104	M IgG2a	M	PE-Cy7	BD	FC
CD4	GK1.5	R IgG2b, k	M	eFluor 450	eBio	FC
CD4	RM4-5	R IgG2a	M	FITC	eBio	FC
CD8a	53-6.7	R IgG2a	M	PerCP-Cy5.5	eBio	FC
CD8a	53-6.7	R IgG2a	M	APC	eBio	FC
CD44	IM7	R IgG2b,	M	FITC	eBio	FC
CD44	IM7	R IgG2b, κ	M	PerCP-Cy5.5	Biolegend	FC
CD44	IM7	R IgG2b, κ	M	PE	BD	FC
CD62L	MEL-14	R IgG2a, κ	M	APC-Cy7	Biolegend	FC
CD62L	MEL-14	R IgG2a	M	PE-Cy7	BD	FC
Foxp3	FJK16s	R IgG2a	M	PE	eBio	FC
CTLA-4	UC10-4B9	ArH IgG	M	PerCP/Cy5.5	Biolegend	FC
PD-1	RMP1-30	R IgG2a, κ	M	APC	eBio	FC
PD-1	29F.1A12	R IgG2a, κ	M	PE/Cy7	Biolegend	FC
B220	RA3-6B2	R IgG2a, κ	M	PerCP-Cy5.5	Biolegend	FC
CD19	1D3	R IgG2a, κ	M	APC	eBio	FC
CD19	eBio1D3	R IgG2a, κ	M	PE-Cy7	eBio	FC
CRT	FMC75	M IgG1	M	PE	Abcam	FC
Hsp-70	ERP16892	Rb IgG	M	AlexaFluor 647	Abcam	FC
H-2Dd	34-2-12	M IgG2a	AJ	PE	Biolegend	FC
H-2Kk	36-7-5	M IgG2a	AJ	PE	Biolegend	FC
H-2kb/H-2Db	28-8-6	M IgG2a	129/svj.1; C57BL/6	PE	Biolegend	FC
4-1BB	17B5	SyrH IgG	M	APC	eBio	FC
4-1BB	17B5	SyrH IgG	M	PerCP-eFluor 710	eBio	FC
Ki67	16A8	R IgG2a, κ	M	FITC	Biolegend	FC
Ki67	16A8	R IgG2a, κ	M	PerCP-Cy5.5	Biolegend	FC
Ki67	16A8	R IgG2a, κ	M	PE-Cy7	Biolegend	FC
Tbet	4B10	M IgG1, κ	M	APC	Biolegend	FC
Tbet	4B10	M IgG1, κ	M	PerCP-Cy5.5	Biolegend	FC
EOMES	Dan11mag	R IgG2a, κ	M	AlexaFluor 488	eBio	FC
EOMES	Dan11mag	R IgG2a, κ	M	PE-Cy7	eBio	FC
KLRG1	2F1	SyrH IgG	M	APC	eBio	FC
Granzyme B	GB11	M IgG1, κ	M	FITC	Biolegend	FC
TIM3	RMT3-23	R IgG2a, κ	M	FITC	eBio	FC
LAG3	eBioC9B7W	R IgG1, κ	M	APC	eBio	FC

OX40	OX-86	R IgG1, κ	M	APC	eBio	FC
CD25	PC61	R IgG1, λ	M	APC	Biolegend	FC
CD107a	eBio1D4B	R IgG2a, κ	M	AlexaFluor 488	eBio	FC
IFNγ	XMG1.2	R IgG1, κ	M	FITC	eBio	FC
PD-L1	10F.9G2	R IgG2a, λ	M	PE	Biolegend	FC
BCL-2	6C8	Hamster	H	FITC	BD	FC
F4/80	Cl:A3-1	R IgG2b	M	N/A	Serotec	IHC
HMGB1	EPR3507	Rb IgG	M	N/A	Abcam	IHC/IF
BCL-2	7/Bcl-2	M IgG1	H/M	N/A	BD	WB
MCL-1	Y37	Rb IgG	M	N/A	Abcam	WB
Caspase 3	Asp175	Rb poly	M	N/A	Cell Sig	WB
Caspase 9	-	Rb poly	M	N/A	Cell Sig	WB
Alpha-tubulin	-	Rb poly	M	N/A	Cell Sig	WB
Beta-actin	8H10D10	M IgG2b	M	N/A	Cell Sig	WB
PARP	-	Rb poly	M	N/A	Cell Sig	WB

Table 2.4 Commercially sourced antibodies

M – mouse; **R** – Rat, **Rb** – Rabbit, **SyrH** – Syrian hamster, **ArmH** – Armenian hamster, **eBio** – eBioscience, **BD** – BD bioscience, **Cell Sig** – Cell Signalling, **FC** – flow cytometry, **IHC** – immunohistochemistry, **IF** – Immunofluorescence, **WB** – western blot, **poly** - polyclonal

2.4 Antibody modifications

2.4.1 Deglycosylation of EW1.9

Antibody concentration was first determined using a Nanodrop spectrophotometer, using molecular coefficient of 1.45. 0.05 units of PNGase F enzyme (Promega) were added per 1 µg of antibody and incubated overnight at 37 ^{o}C. The antibody and enzyme solution was then transferred to a 50 kDa molecular weight cut-off dialysis tube (Sigma Aldrich) and dialysed overnight in PBS to remove any excess enzyme. The antibody concentration was reassessed as before, using the Nanodrop spectrophotometer. Finally, antibody was sterile filtered using a syringe with 0.2µm filter (Whatman).

2.4.2 Sodium Dodecyl Sulphate Polyacrylamide Gel Electrophoresis (SDS-PAGE) analysis to confirm deglycosylation

2 µg of both wild type antibody and the PNGase treated antibody were first added x4 reducing Loading sample buffer, and made up to 16 µl with ultrapure water. The antibody mixes were then heated at 95^{o}C for 5 mins in heat block. A BOLT Bis-Tris 10% 10 well mini-gel (Thermo Fisher Scientific) was set up in a gel tank using 1X MOPS buffer (10X MOPS: 209.2 g 3-(N-mopholino) propanesulfonic acid (MOPS), 121.2 g TRIS, 20 g SDS, 6 g EDTA, 2 litres ultrapure H_2O; 1X MOPS: 100 ml 10X MOPS in 1 litre ultrapure H_2O). The antibody mixes were loaded into the wells of the

gel using a pipette in duplicate for each condition. Novex Sharpe pre-stained marker (ThermoFischer Scientific) was used as a guide for protein size. Gel was run at 200 volts for 40 minutes until the dye front had reached the bottom of the gel. The gel was then stained with Coomassie blue (Sigma Aldrich, 60mg/ml, in 10% acetic acid (v/v)) for 40 minutes and then destained with 10% ethanol/10% acetic acid (both v/v) until bands could be seen.

2.5 Syngeneic NXS2 mouse model of neuroblastoma

2.5.1 Subcutaneous model

Wild type AJ mice were injected subcutaneously with $2x10^6$ NXS2 cells, suspended in 100µl of PBS. Tumour growth was monitored using callipers, measuring the length and width of tumours in millimetres every 2 days. End point was considered to be reached once the product of the two measurements ≥ 250 or 400 mm^2, as detailed in figure legends of individual experiments.

2.6 Syngeneic 9464D mouse model of neuroblastoma

2.6.1 Subcutaneous (SC) model

Wild type C57BL/6 mice were injected subcutaneously with 9464D cell line doses assessed from $1x10^5$ to $5x10^6$ cells, as described within the individual experiments, diluted in 100 µl PBS. Tumour growth was monitored using callipers, measuring the length and width of tumours in millimetres. End point was considered to be reached once the product of the two measurements ≥ 250 or 400 mm^2, as detailed in figure legends of individual experiments.

2.7 Chemotherapy agents

2.7.1 *In vitro* use

As CPM is a pro-drug and therefore needs to be metabolically converted into its active form, mafosfamide (MAF), the active form of the drug, was used *in vitro* [548,549]. MAF powder (Santa Cruz) was first dissolved into a stock solution of 20 mg/ml in Dimethyl sulfoxide (DMSO – Sigma Aldrich Aldrich) and then further diluted for working concentrations. This was to ensure the highest concentration of DMSO in cell cultures was no more than 0.1 %, to prevent DMSO cytotoxicity. DOX powder (Sigma Aldrich) was dissolved into a stock solution of (5 mg/ml) in sterile H_2O and diluted further for working concentrations.

2.7.2 *In vivo* use

CPM crystals were weighed into a bijou and dissolved in sterile PBS to concentrations of 20, 40 and 150 mg/kg. The bijou was then vortexed for 5 mins to ensure all crystals have dissolved. Once prepared the drug was immediately administered to the mice via intraperitoneal injection within a class II hood, located in the cytotoxic room within the animal house. CPM administration and subsequent housing of mice in this room was utilised to avoid contamination of staff with the cytotoxic compound.

2.8 Assessment of the effect of chemotherapy and anti-PD-1 treatment on immune cell subsets and T cell markers

2.8.1 Tumour inoculation

Both the NXS2 and 9464D SC models were used. Tumours cells, at doses stated in **section 2.2.1** and **2.2.2** respectively, were administered to the mice SC and the resulting tumours were monitored for growth using callipers 3 times weekly.

2.8.2 Administration of Chemotherapy

Once tumours had reach as size of 8 x 8 mm, the mice were given a dose of CPM, as stated within the experiments, via intraperitoneal injection. CPM was prepared at point of use according to the weights of the mice and PBS was used as an excipient.

2.8.3 Administration of EW1-9 antibodies

3 days following CPM administration mice were administered IP with 250 µg of either EW1-9 (WT) or EW1-9 (DG) antibody diluted in sterile PBS. This was repeated at day 6 post CPM.

2.8.4 Tissue collection and processing

At a set time point after treatment initiation, as detailed in experiments, mice were culled, and tumours, spleens and lymph nodes were harvested. Both tumour and spleens were weighed and measured. Spleens and lymph nodes were mechanically disassociated using a scalpel and then passed through a 100 µm cell strainer. Mouse Tissue Disassociation Kit (Miltenyi Biotech) was used as per manufacturer's instructions to break up tumour tissues into single cell suspensions for flow cytometry analysis. Alternatively, tumours were incubated with Liberase TL (Roche) with DNAase for 15 mins at 37^{o}C, after which 15 ml of FCS containing RPMI was added to inhibit the enzyme.

Following either enzymatic disassociation protocol, tissue were passed through 100 µm cell strainer to further disassociate the remaining tumour tissue. Cells from all tissues were spun at 450g for 5 mins, re-suspended in PBS and spun again. Cells were re-suspended in PBS and counted using Coulter Counter (Beckman). Cells were then processed for immunophenotyping by flow cytometry analysis as detailed below (**Section 2.9**).

2.8.5 Serial blood sampling

For peripheral blood mononuclear cells (PBMCs) immunophenotyping 20 µl of blood was collected from mice at set time points as detailed in individual experiments, from before, during and after combination therapy. Mice were treated with CPM and anti-PD-1 therapy as detailed in **Section 2.8.2** and **2.8.3**. Blood was collected via serial sampling from the tail veins into an Eppendorf tube, then transferred to flow cytometry tubes. Antibodies used for flow cytometry staining were added directly into the whole blood, and staining and processing was carried out as below.

2.9 Flow cytometry

2.9.1 Live/dead staining

In certain experiments, as detailed, *ex vivo* tumour Cells were subjected to viability discrimination by the use of Live/Dead Fixable Aqua Dead Cell Stain kit (Invitrogen). Cells were suspended in PBS at $1x10^6$/ml, with 1 µL of fixable aqua being added for each 1 ml of cells. Cells were then incubated for 30 minutes at 4^{o}C in the dark. Cells were spun at 450g for 5 mins with 1 % BSA/PBS solution and finally re-suspended in PBS.

2.9.2 Direct staining

Antibodies were made into a master mix depending on the immune cell subset being analysed and aliquoted into flow cytometry tubes. 10 µl of 100 µg/ml Fc-Blocking antibody (2.4G2) was added to tubes. Cells were re-suspended in PBS to a concentration of $1x10^7$/ml and 100 µL was added to the tube, and incubated for 15 mins at room temperature (RT). Without washing, antibody master mixes were added into tubes and then incubated for 30 minutes in the dark at 4^{o}C. 1 ml 1X red cell lysis buffer (Bio Rad) was added, incubated for 5 mins at RT, and then centrifuged at 450g for 5 mins, waste poured off and re-suspended. 3 ml of FACS wash buffer (PBS, 1% bovine serum albumin (BSA) and 0.01% sodium azide – all Sigma-Aldrich) was added and the tubes were centrifuged as before. The waste was poured off and cells were kept in the dark at 4^{o}C until data collection on the flow cytometer as detailed below.

2.9.3 Intracellular staining

Cells being stained for intracellular markers were first cell surface stained as above, and washed in FACS wash buffer, at 450g for 5 mins. Afterwards, FoxP3 Staining Buffer set (eBioscience) was used. Fixation/permeabilisation solution was added the tubes and the cells were incubated overnight at 4^{o}C in the dark. Cells were then washed with 1X Permeabilisation Buffer and spun at 450g for 5 mins. Cells were re-suspended, intracellular antibody master mixes were added and incubated for 45 mins at 4^{o}C in the dark. Again, cells were washed with 1X Permeablisation Buffer as before and finally washed with FACS wash buffer at 450g for 5 mins. The waste was poured off and cells were kept in the dark at 4^{o}C until data collection on the flow cytometer as detailed below.

2.9.4 Flow cytometry analysis

All flow cytometry data from ex vivo experiments was collected on FACS Canto II (BD Biosciences). Cell culture flow cytometry data was collected either on FACS Canto II or FACS Calibre (BD Biosciences) as stated. In the multi-colour flow cytometry panels of ex vivo tissue 500,000 events were collected, whereas for *in vitro* cell based assays <100,000 events were collected. All fluorophores were compensated for using compensation software on FACS DIVA version 8 (BD Biosciences) at time of data collection. Single stained controls were also collected for manual compensation refinement at point of analysis on the FACS DIVA software. Data was analysed and gating was conducted using FACS DIVA or FCS express (DE Novo Software) software. Representative gating strategies used are detailed within the respective figures.

2.10 *In vitro* assessment of cell death

2.10.1 Induction of cell death

0.5x10^{6} NXS2 and 9464D cells were plated into a 96-well flat-bottomed plate and left to adhere for ~2 hrs. Cell death was induced with application of chemotherapy agent at concentrations as described in individual figure legends. For MAF, controls included untreated cells, 10 % DMSO positive controls, cells treated with the highest concentration of DMSO vehicle used (0.1 %), and blank media only wells, all in triplicate. For DOX, controls included untreated cells, 10 % DMSO positive controls, media containing 40 μM of DOX (for 24 hours) and blank media only wells, all in triplicate.

2.10.2 MTT assay

CellTiter 96 non-radioactive cell proliferation assay (Promega) was used to establish a cytostatic dose of each chemotherapy agent. The assay assesses how metabolically active cells are by their ability to convert the MTT dye into formazan crystals which are then solubilised [550]. Cells which are not metabolically active, due to cell cycle arrest or death, will not convert the dye into crystals. This is detected in the assay as a colour change. Assay was carried out in 96-well flat bottomed plates. Manufacturer's instructions were followed for MTT dye staining and solubilisation. In brief, 15 µl of MTT dye solution was added to wells and cells were incubated at 37^{o}C for 4 hrs to allow formazan crystal development. After which, 100 µl of solubilisation solution was added to break up the crystals and wells were thoroughly mixed to ensure uniform colour distribution. Absorbance was read at 530 nm (reference wavelength 700 nm) with Epoch plate reader after 1 hour and overnight incubation. A standard curve and appropriate cell seeding density was established for both NXS2 and NB95464D cell lines before conducting the assay with drug administration. For MAF, control wells with media only triplicates and then the reference wavelength readings at 700 nm were deducted to deduce the final values used for further analysis. For DOX, treated wells were blanked using the media + DOX wells to account for DOX's fluorescence, and the rest of the plate was blanked using the media only wells. Next, reference wavelength readings at 700 nm were deducted to deduce the final values for further analysis

2.11 Analysis of immunogenic cell death (ICD) marker expression *in vitro*

2.11.1 Induction of cell death

Cells were plated into a 96-well flat bottomed plate and left to adhere. Cell death was induced with application of chemotherapy agent at the stated dose for 24 hours. After which the cells were stained for immunogenic cell death markers.

2.11.2 Direct staining for ICD markers

After 24 hours the media was removed and 50 µl of TripLE express was added to cells to detach them. Once detached the cells were added to FACS tubes and washed with PBS. Antibodies detailed in **Table 2.4** for the ICD markers were added at the desired concentration. Staining continued as detailed in **Section 2.9.4** and then assessed by flow cytometry.

2.12 Development of a BCL-2 overexpressing 9464D line

2.12.1 Phoenix-eco cells

Phoenix-Eco cells were plated into 6 well plates to be cultured in DMEM supplemented with 10% FCS, 2mM glutamine, 1mM sodium pyruvate, 100U/ml streptomycin and 100µg/ml penicillin (all from Gibco). Cells were cultured at 37^{o}C at 10% CO_2, and maintained at a confluency of around 50%.

2.12.2 Transfection of Phoenix-Eco cells with GFP vector

Transfection of Phoenix-Eco cells was conducted using the Effectene transfection reagent (Qiagen). Either GFP vector, empty pMIH vector (EV) or human BCL-2 (hBCL-2) vector were used for transfection [551,552] (see appendix **Figure 7.1** and **Figure 7.2** for vector maps), with green fluorescent protein (GFP) transfection used as a positive control. Transfection was conducted as per manufacturer's instructions. Briefly, 0.4µg of plasmid was diluted in Buffer EC at a concentration of 0.1µg/ml. 3.2µl of Enhancer was added and incubated at RT for 5 mins. 10µl of Effectene Transfection Reagent was added to the mixture, and samples were incubated for 10 mins at RT to allow for complex formation. Medium was removed from Phoenix-Eco cells and cells were washed once in 3 ml of PBS. 1.6 ml of fresh media was added to the cells. 600µl of media was then added to the tube containing the transfection complexes, mixed and then added drop-wise onto the cells. Addition of 1:1000 5 nM chloroquine was used to improve transfection efficiency, as this enhances efficiency of DNA uptake via facilitating escape from endosomes via inhibition of endosomal acidification. Successful transfection of the Phoenix-Eco cells was checked under a fluorescence microscope (CKX41 inverted microscope equipped with a CCD colour camera connected to Cell B software was used (Olympus)) to see the presence of GFP+ cells.

2.12.3 Spin transduction of 9464D cells

Transfected Phoenix-Eco cells were incubated for 48hrs. Media from transfected cells was then removed and filtered through 0.2 µM filter to remove any floating cells. Polybrene (1:5000) was added to the viral supernatant to coat cells prior to transduction. 9464D cells were split and counted as detailed previously, and plated into 12 well plates. Viral supernatant was added on top of the cells and mixed. Plate was sealed with parafilm and then spun at 500g, 37^{o}C for 45 minutes. Cells were then placed into normal culture conditions in incubator. To check GFP transduction, GFP+ cell fluorescence was viewed under a fluorescence microscope around 48 hrs later.

2.12.4 Puromycin and hygromycin cell death curves

To select for GFP or hBCL-2 expression a kill curve using the appropriate selection antibiotics was conducted to establish the correct dosing of antibiotic to use. For GFP vector the selection antibiotic was puromycin (Sigma Aldrich), and for EV and hBCL-2 vector the selection antibiotic was hygromycin (Sigma Aldrich). Non-transduced 9464D cells were split as previously detailed in **section 2.2.2** and plated in a 96-well plate at $1x10^5$ cells per well in 100 µl of media. A stock of either puromycin (40µg/ml) or hygromycin (1mg/ml). This was then serially diluted 1:2 down the plate into 100 µl media. 100 µl of each dilution was then added to cells and a DMSO alone control was used. Cells were incubated for 24 hrs. Media from each well was placed into a FACS tube to collect floating cells and then detached cells from the plate were added. 1 ml PBS was added and spun at 450g for 5 minutes. Supernatant was removed and pellet re-suspended. Cell death was assessed by propridium iodide (PI) staining flow cytometry on FACS Calibre.

2.12.5 Analysis of human BCL-2 expression by intracellular flow cytometry

hBCL-2 transduced 9464D cells in hygromycin selection were harvested as detailed previously. Cells were spun at 450g for 5 mins and re-suspended in 5 ml PBS. Cells were counted and $1x10^6$ cells were stained per tube. 0.5% paraformaldehyde (PFA) was added to tubes for 15 mins. Tubes were spun as before and PFA removed, and tubes were washed twice in FACS wash (detailed in **Section 2.9.4**). As much supernatant as possible was removed. Anti-BCL-2 antibody or appropriate isotype was diluted in 0.5% saponin at 10 mg/ml and 100 µl was added into tubes. Cells were incubated at room temperature for 30 mins, and then washed twice in 0.05% saponin. Data was then collected on FACS Calibre.

2.13 Western blots

2.13.1 Harvesting cell lysates

Cells were collected from appropriate culture conditions using TrypLE express, and washed as detailed in **Section 2.2.2**. Cells were then counted and made up to a concentration of $10x10^6$/ml in PBS. 1 ml was transferred to Eppendorf and spun at 400g for 5 minutes. Supernatant was removed and cells were spun again, as before and any remaining supernatant was removed. 30 µl of RIPA buffer was added to each cell pellet and mixed thoroughly. Tubes were incubated on ice for 30 mins, and left at -20^{o}C overnight.

2.13.2 Bradford assay for assessing protein concentration

Cell lysates were spun at 5000g for 5 minutes. A standard curve using 2 mg/ml BSA was plated onto a Nunc MaxiSorp 96 well plates (ThermoFisher Scientific). 2 µl of lysate was added in duplicate and diluted with H_2O. Protein assay reagent (Biorad) was made up to a 1:5 dilution with H_2O and 200 µl was added to each well. Plates were read using an Epoch microplate reader (Biotek) at 570nm.

2.13.3 Sodium Dodecyl Sulphate Polyacrylamide Gel Electrophoresis (SDS-PAGE)

50ug of each cell lysate was added to an Eppendorf tube. 4X Laemmli sample buffer (Abcam) was added and the resulting mix was made up to 15 µl by adding MilliQ water. Solution was added to a heat block (95^oC) and left to boil for 5 minutes. Resulting samples were loaded into a BOLT Bis-Tris 10% mini gel (Invitrogen) alongside 5 µl of Novex Shape pre-stained marker (Invitrogen). Gel was run at 100 volts up to end of stacking gel and then 150 volts for the rest of the run.

2.13.4 Gel transfer to membrane

For transfer of gel onto membrane, iBlot 6-minute blotting system, using the iBlot Transfer stack (both Thermo Fischer) was utilised. Briefly, gel was removed from cassette and washed quickly in deionised water. iBlot Anode stack was assembled within the iBlot device, with the gel placed on the nitrocellulose membrane. iBlot Cathode stack was then placed on top, and using a roller, any air bubbles between the layers were removed to ensure efficient transfer of proteins. iBlot device was closed and transfer was run for 6-7 minutes at 23 volts.

2.13.5 Blocking and primary antibody incubation

Membrane was removed from iBlot device and placed in a dish. 1 drop of Ponzo 5 stain along with a ~5 mls of 1X TBS-T (10X TBS: 121.44g TRIS (0.5M), 175.32g NaCL (0.5M), 2 litres ultrapure H_2O, pH 7.4; 1X TBS-T: 100ml 10X TBS, 1ml Tween 20 (0.05%), 1 litre ultrapure H_2O) to dilute was added to check the gel had transfer correctly and no air bubbles were present. 3x 10 second and 3x 5 min washes were used to wash off Ponzo 5. Membrane was then blocked with non-fat milk protein (0.5 g in 10 ml TBS-T) for 10 mins. Primary antibody (as detailed in figure legends) was diluted to a 1:500 dilution in 5 ml of buffer (5% BSA+ TBS-T + azide). Membrane was washed with 3x 10 second and 3x 5 min washes in TBS-T, then rolled up and added to primary antibody tube. Tube was placed on a roller at 4^oC overnight.

2.13.6 Secondary antibody incubation and imaging

Membrane was washed with 3x 10 second and 3x 5 min washes in TBS-T. 2 µl of secondary antibody was added into diluted non-fat milk protein (10ml TBS-T, 0.5g milk powder). Membrane was added to tube and incubated for 1 hr at RT on a roller. Membrane was washed 3x 10 second and 3x 5 min washes in TBS-T. 1 ml of Immobilon Western Chemiluminescent HRP Substrate (Merck) was added over membrane and acetate was added over the top and incubated for 5 minutes. Bands were imaged on UVP BioSpectrum 810 Imaging System with VisionWorks LS software (both Analytik Jena). To strip off secondary antibody, membrane was washes with 3x 10 second and 3x 5 min washes in TBS-T to be able to add another primary antibody, secondary antibody and re-image.

2.14 Analysis of HMGB1 after CPM administration by IHC

2.14.1 Tumour collection

C57BL/6 mice were injected subcutaneously with 9464D cells as detailed previously. Once tumours had reached 10 x 10 mm, mice were injected with 40 mg/kg cyclophosphamide as detailed in **Section 2.8.2**. Mice were culled 3 days later and spleen and tumour tissue was collected. Half of each was either placed in optimal cutting temperature (OCT) compound and frozen in dry ice cooled isopentane, or fixed in 4% formalin and embedded in paraffin.

2.14.2 Cutting of slides and fixation

Samples frozen in OCT were first cut into 8 µm sections on a Microm HM560 cryostat and mounted on microscope slides (Superfrost Plus, Thermo Fisher Scientific). The slides were air-dried overnight and stored at -20^{o}C until use. Slides were defrosted in a sealed container at 37^{o}C for 30 mins and then fixed in 100% acetone for 10 mins.

2.14.3 Immunohistochemistry of OCT frozen sections

After fixation as detailed above, sections were washed in PBS-Tween to remove OCT. Endogenous peroxidases were inhibited using a peroxidase inhibitor (Pierce, Thermo Fischer Scientific) for 15 mins. Sections were then washed in PBS-Tween and then blocked for 30 mins at RT using the appropriate serum (at 2.5%) as indicated by species of origin of the primary antibody to be used. Without washing, primary antibodies (as detailed in figure legends) were added and incubated for 90 mins at RT in a humid chamber. After washing in PBS-Tween, sections were incubated for 45 mins at RT in a humid chamber in ImmPRESS anti-rat IgG (Vector Labs). Washes in PBS-Tween were conducted and then sections were incubated in Vector NovaRed-horse radish peroxidase (HRP –

Vector Labs) for ~10 mins until colour had developed. Sections were counterstained with Haematoxyclin for 1 min. to dehydrate the sections, slides were washed in an increasing alcohol concentration from 90-100%. Finally, sections were washed in Histoclear, air dried and coverslips mounted using Vectamount (Vector Labs) and left overnight to dry.

2.14.4 HMGB1 immunohistochemistry of formalin fixed paraffin embedded sections

Sections were first deparaffinised in Histoclear (3x7min) and then rehydrated through decreasing alcohol concentrations: 100%, 90%, 80%, 40%; for 2 mins. Sections were washed in H_2O, and EDTA (pH 9) antigen retrieval was carried out as follows. Buffer and slides were placed in a lidded tray and microwaved on medium for 20 mins. Buffer was topped up as required. Cold water was then ran over slides to cool, and slides were wiped to remove remaining water. Sections were washed x2 with PBS/Tween 0.05%, and then blocked with 2.5% horse serum. Rest of assay was carried out as detailed in **section 2.14.3**, using ImmPRESS™ HRP Anti-Rabbit IgG Polymer Detection Kit (Vector Labs).

2.14.5 HMGB1 immunofluorescence of 9464D cells

Coverslips were first coated with a drop of poly-L-lysine (PLL) solution for 5 mins in a Class II hood. PLL was then removes with a pipette and washed with a drop of sterile water. Water was then removed and coverslips were left to try within the hood. PLL coverslips were then placed in 6-well plates, and 20,000 9464D cells were seeded on top and left to adhere overnight. Media was then removed and coverslips were washed x2 in PBS, followed by fixation via 4% PFA for 15 minutes on ice. Coverslips were washed as before and then permabilised with 0.25% Triton X-100 in PBS for 10 minutes. Again coverslips were washed as before and then blocked with 2% BSA in PBS + 0.05% Tween for 30 minutes. Primary HMGB1 antibody was then added at 1:350 concentration for 1 hour at RT, followed by 2x PBS wash. Anti-rabbit AF488 secondary antibody was added at 1:1000 concentration for 1 hour at RT in the dark, and coverslips were then washed x3 with PBS. TOPRO-3 nuclear counterstain and incubated for 1 hour at RT, followed by x2 washes in PBS tween. Coverslips were mounted onto slides using Vectashield Hardset (Vector Labs), and then imaged using confocal microscopy as detailed below.

2.14.6 Imaging

To image stained sections, CKX41 inverted microscope equipped with a CCD colour camera connected to Cell B software was used (Olympus). Object lenses used: Plan Achromat 10 x 0.25 and 40 x 0.65; UPlanFLN 4 x 0.13 PhP (Olympus). Post-processing and merging of Immunofluorescence

images was conducted using Photoshop CS6 (Adobe). Laser scanning confocal microscopy was conducted using Leica TCS SP5 inverted microscope with environmental chamber (Leica), using oil x40 objectives.

2.15 Assessment of antibody half-life by ELISA

2.15.1 Blood sampling and serum collection

AJ and C57BL/6 mice were injected with either 100 µg or 500 µg dose of either EW1-9 wild type (WT) or EW1-9 deglycosylated (DG) antibody by i.p route. Mice were bled at time points detailed in figure legends. Serum was collected from blood samples by first incubating the blood at 4 ^{o}C for a few hours. Tubes were then spun at 5000g for 5 mins at 4 ^{o}C and resulting serum was collected and added into new tubes. These tubes were spun again as previously and serum was collected to make sure minimal red blood cell contamination. Serums were stored at -20 ^{o}C until analysed.

2.15.2 Enzyme linked immunosorbent assay (ELISA)

Nunc MaxiSorp ELISA plates (Thermo Fisher Scientific) were coated with goat anti-rat antibody at 25 µg/ml diluted in coating buffer (Na_2CO_3 15mM/L, $NaHCO_3$ 35mM). Plates were incubated first at 37^{o}C for 1 hr and then at 4 ^{o}C overnight. Coating antibody was discarded and 150 µl of 1% BSA-PBS was added to each well and incubated for 1 hr at 37 ^{o}C. Plate was washed 3x with PBS-Tween (0.05 %) using a Skanwasher 300 plate washer (Skatron). Standards at 100 µg/ml were prepared. Standards and samples was added at 2 µl in first well and then diluted 2 fold across the plate. Samples were incubated for 90 mins at 37 ^{o}C. Plate was washed as previously and 1:5000 sheep anti-rat HRP antibody was added and incubated at 37^{o}C for 90 mins. Substrate was prepared using a o-Phenylenediamine dihydrochloride (OPD) tablet (Sigma Aldrich) dissolved in 24.7 ml ELISA citrate (91mM Citric Acid Fisher Scientific), 25.5 ml ELISA phosphate (200mM Na_2HPO_4 ThermoFisher Scientific) and 50 ml distilled water. Plate was washed x5 in PBS-Tween (0.05 %) and blotted dry. 40 µl of peroxide was added to substrate mix and then added to each well. Plate was incubated in the dark at RT until sufficient colour had developed and reaction was stopped with 50 µl 2.5 M H_2SO_4. Plates were then read on an Epoch microplate reader (Biotek) at 450nm.

2.16 Assessment of anti-drug response by ELISA

2.16.1 Injection of antibodies

C57BL/6 mice were injected with either 2 weekly, 5 weekly shots or none of 150 µg EW1-9 (DG) antibody by IP route. Mice were bled at time points indicated in figure legends. Serum was collected from blood samples as detailed in **Section 2.15.1**.

2.16.2 Anti-drug response ELISA

Nunc MaxiSorp ELISA plates were coated with EW1-9(DG) antibody at 5 µg/ml diluted in coating buffer. Plates were incubated first at 37^{o}C for 1 hr and then at 4 ^{o}C overnight. Coating antibody was discarded and 150 µl of 1% BSA-PBS was added to each well and incubated for 1 hr at 37 ^{o}C. Plate was washed 3x with PBS-Tween (0.05 %) using a Skanwasher 300 plate washer. Standards at 100 µg/ml were prepared using Purified anti-rat IgG1 antibody (Biolegend). Standards and samples was added at 2 µl in first well and then diluted 2 fold across the plate. Samples were incubated for 90 mins at 37 ^{o}C. Plate was washed as previously and 1:5000 rat anti-mouse HRP antibody was added and incubated at 37^{o}C for 90 mins. The rest of the assay was completed as detailed in **Section 2.15.2**.

2.17 Combination treatment of cyclophosphamide and anti-PD-1 mAb in TH-MYCN transgenic mouse model

2.17.1 Tumour presentation

Heterozygous mice were palpated twice weekly by animal technicians and day of first tumour appearance was noted. As tumours were of varying sizes upon first palpation, a threshold tumour palpation size of ~ 10mm was implemented to ensure consistency between mice.

2.17.2 Administration of treatments

Once tumour sizes had reached the threshold level, mice were the administered treatment via intraperitoneal injection as detailed within the individual experiment.

2.17.3 Survival analysis

After treatment administration, mice were then monitored by palpation as before for tumour relapse and progression. A human end point was defined as when the mice first begin to deteriorate due to tumour size.

2.18 Statistical analysis

Microsoft Excel (Microsoft corporation) was used for preliminary analysis of data and generation of tables. All graphs and statistical analysis were conducted on GraphPad Prism software (GraphPad, version 7). Significance was assessed by either Mann-Whitney U test for comparing 2 groups, or Kruksalis-Wallis with Dunn's multiple comparisons for >2 groups, unless otherwise stated in figure legends. Significance was decided with P-values of <0.05, and noted within individual figures (<0.05 = *, <0.01 = **, <0.001 = ***, <0.0001 = ****).

Chapter 3: Immunophenotyping preclinical models of neuroblastoma

3.1 Chapter introduction

Despite intensive treatment strategies, the relapse rate for patients with high risk NB is still high. There is little room for further intensification, as current regimes are already associated with high treatment related mortality [49-52]. Refinement of treatments currently used for high-risk NB therapy, along with the implementation of immunotherapy may be ways of improving outcomes, and reducing treatment side effects. However, in order to develop effective immunotherapies for patients, appropriate pre-clinical murine models are required. These models should reflect the immune infiltrates found within human tumours, to allow accurate assessment of immunotherapies before their development into the clinic. Pre-clinical models are essential to the development of therapeutics for the clinic. They are essential for identifying biomarkers of response to treatments, understanding the mechanism of action of the therapeutics, ascertaining potential side effects and importantly investigating how they interact and respond in combination with other therapeutics. The need for accurate models is especially critical for rare paediatric tumours compared to relatively common adult cancers. There is usually a small patient cohort and therefore not all new therapies can be tested in clinical trials due to lack of patients. Furthermore, it becomes particularly important to have representative murine models when investigating immunotherapies, as this will enhance the likelihood of developing translatable therapies. The immune system of mice and humans, although comparable, have a number of important differences, including differences in FcγRs, different proportions of immune cell subsets, and different expression levels of particular receptors [95]. Therefore, for accurate assessment of immunotherapy based treatments in murine models, careful considerations of these factors need to be taken into account. Firstly, an immunocompetent murine model is required to preserve the complex interplay of an intact immune system, as will occur in humans. This limits the use of patient derived xenograft models, which use patient tissue inoculated into immunocompromised mice in order to best represent a human tumour microenvironment, minus the input of the immune system. Therefore, syngeneic murine derived models have been commonly employed to assess immunotherapy appropriately. However, these models may not accurately mirror the basic structure, microenvironment or immune infiltrate of human tumours. This is due, at least in part, to their origin as extensively passaged cell lines and that they are usually inoculated ectopically compared to tissues of origin of human tumours. However, the use of transgenic murine models, which spontaneously develop

tumours may be more comparable to human tumours, due to the similarity in their growth and anatomical location.

Taking into account the above considerations, and before assessing the efficacy of combination chemotherapy and immunotherapy within murine NB models, it was important to compare the infiltrating immune cells within the tumour microenvironments of the murine NB models at our disposal. To do this, three different murine models of NB were employed. NXS2 was the first syngeneic murine NB cell line developed and is known to express the ganglioside GD2, expressed on virtually all human NB, on the AJ mouse background. NXS2 was developed from a subline of the NX-31T28 hybrid cell line of C1300 NB cell line and dorsal root ganglion cells, and was originally intended for synapse function studies [540]. Throughout this chapter the TH-MYCN$^{+/-}$ spontaneous transgenic model was also used. The TH-MYCN$^{+/-}$ mouse was first developed in 1997, and involves the insertion of the MYCN gene under the control of a rat tyrosine hydroxalase promoter [37]. This limits expression of MYCN to cells of the neuroendocrine system, and allows for spontaneous development of NB within several months of birth. As discussed in **Section 1.2** MYCN amplification is found widely in high risk NB patients and leads to an aggressive disease phenotype, which translates into the mouse model [35,37,553]. As these tumours form mainly in the adrenal gland and sympathetic ganglions in the abdomen of mouse, this tumour model highly replicates the human disease in anatomical location[37]. Another murine cell line to be used is 9464D. This cell line was developed by passaging cells derived from spontaneous TH-MYCN$^{+/-}$ tumours from mice on C57BL/6 background, and therefore resembles a spontaneous tumour more so than the engineered NXS2 lines [37]. Furthermore, as this cell line was only recently developed, there has been little research characterising the tumour immune environment when it is used *in vivo*, and therefore work is needed to elucidate this.

Data presented in this chapter aimed to characterise the immune landscape within the three different murine models of NB. This included the subcutaneous models derived from the two cell lines NXS2 and 9464D, and the spontaneous tumours of the TH-MYCN$^{+/-}$ transgenic mice. This will highlight which of these models best represents human NB immunologically and aid in the selection of the most appropriate model to further investigate combination chemo-immunotherapy.

3.2 Results

3.2.1 Establishment of a 9464D sub-cutaneous model

The NXS2 cell line has been used extensively as a subcutaneous model within our laboratory, however the 9464D growth kinetics have not been well established. To this end, cultured 9464D cells were injected subcutaneously at 6 different dosages (ranging from $1x10^5$ to $5x10^6$ cells) in the left flank of male C57BL/6 mice and tumour growth being monitored, as shown in **Figure 3.1**.

Figure 3.1 A-G show that for most doses, the tumours were palpable at a similar time point, between 25-30 days after initial inoculation. However, for the highest dose they were palpable earlier (around 20 days) and for the lowest dose it was slightly later (around 35 days). Once the tumours were established the initial cell dosages seemed to affect how quickly the tumours reached their humane end point (>225 mm^2). As shown in **Figure 3.1 H**, at the highest dose of $5x10^6$ cells the mice quickly reached end point at around day 35 after initial inoculation, whereas the lowest dose of $1x10^5$ had not reached end point by day 70.

From the collated data shown in **Figure 3.1 G+H**, it was decided to use a dose of $5x10^5$ cells for future experiments as the tumours consistently became palpable around day 25 and were terminal around 15-20 days later, allowing time for interventions.

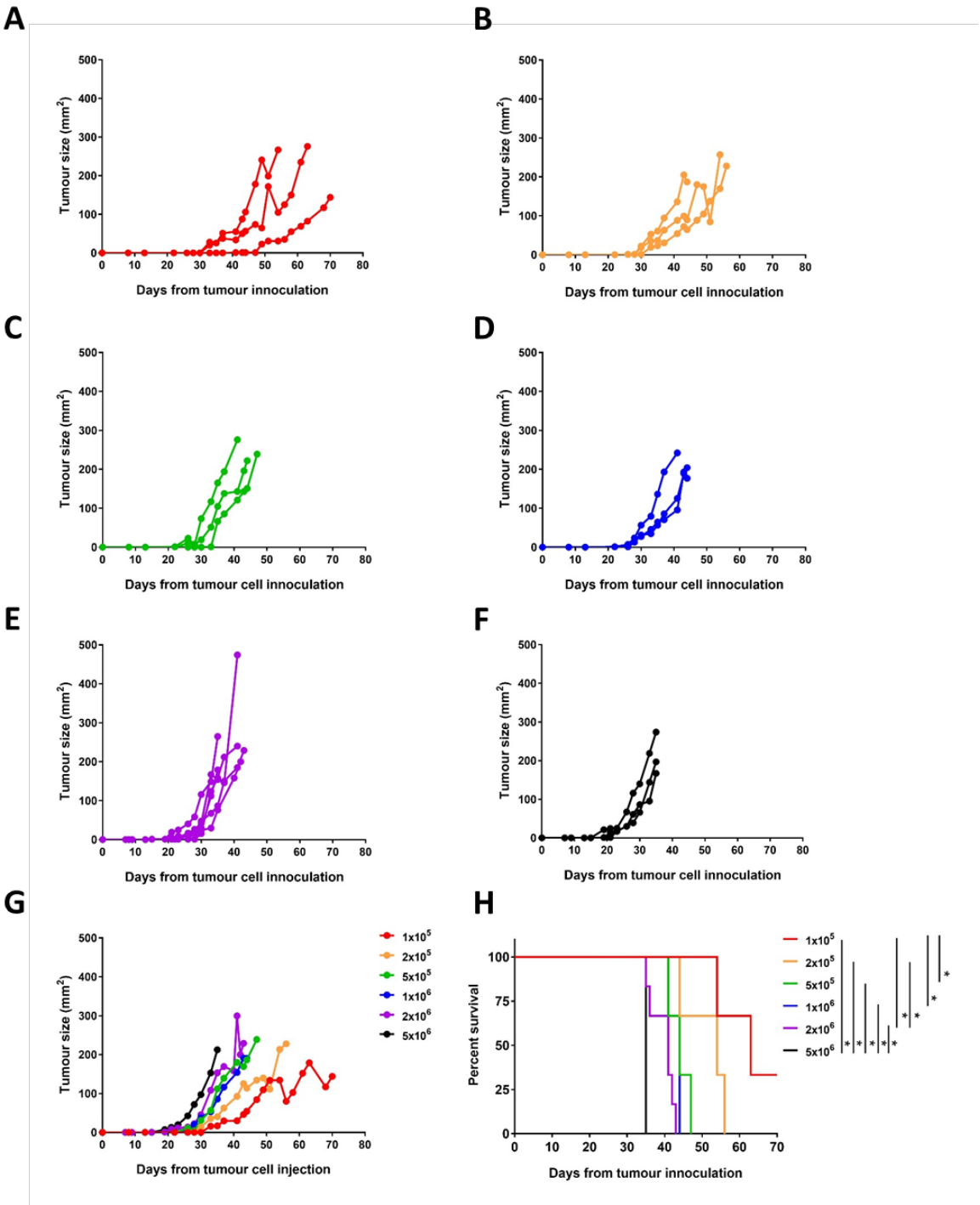

Figure 3.1 Tumour growth and survival of 9464D passaged tumours in C57BL/6 mice

A) C57BL/6 male mice were inoculated SC. in left Flank with doses of 9464D cells ranging from $1x10^5$ to $5x10^6$. Tumour growth was monitored three times a week and once palpable were measured with callipers, with sizes recorded in mm^2. Tumour growth was measured until end point at >200 mm^2 with final tumour size and time since inoculation recorded. Tumour growth is shown for individual mice inoculated with $1x10^5$, **B)** $2x10^5$, **C)** $5x10^5$, **D)** 1x106, **E)** $2x10^6$ and **F)** $5x10^6$. Average tumour growth for all mice is shown in **G)**, and overall survival to >225 mm^2 plotted in **H)**. n= 3 (A-D, F); n= 6 (E). Significance assessed by Log Rank test and denoted as: * = <0.05.

3.2.2 Comparison of the immune infiltrate within tumours of *in vivo* models of NB

As the models described in this chapter were disparate in their origins and growth patterns, it is imperative to compare the baseline immune composition both intratumourally and systemically before investigation into how this is altered with chemotherapy treatment. Furthermore, it was useful to establish which tumour model best represented the immune infiltrates within human tumours, in order to choose the most appropriate model within which to test possible therapies. Tumours and spleens were harvested from tumour bearing mice of the three models, tissue was disaggregated and flow cytometry was performed as detailed within the methods (see **Section 2.9**) to establish the immune architecture both systemically and within the tumour mass itself.

Firstly, **Figure 3.2** highlights the differences seen in the tumours macroscopically. Despite the fact that NXS2 and 9464D are both subcutaneous NB tumours, their appearance was very different. NXS2 (**Figure 3.2 A**) tumours are more vascularised when compared to 9464D (**Figure 3.2 B**). Macroscopic appearance of TH-MYCN$^{+/-}$ spontaneous tumours (**Figure 3.2 C**) differed to the subcutaneous tumours, however, this could be expected with the origins of growth being quite distinct. The tumours were highly vascularised, more so than the NXS2 model, and they appeared to be more lobular in appearance. Furthermore, indications into how the tumours in the TH-MYCN$^{+/-}$ mice formed are evident by the attachment of both kidneys, suggesting that the tumour arose from the adrenal glands, as is the case for many human NB tumours.

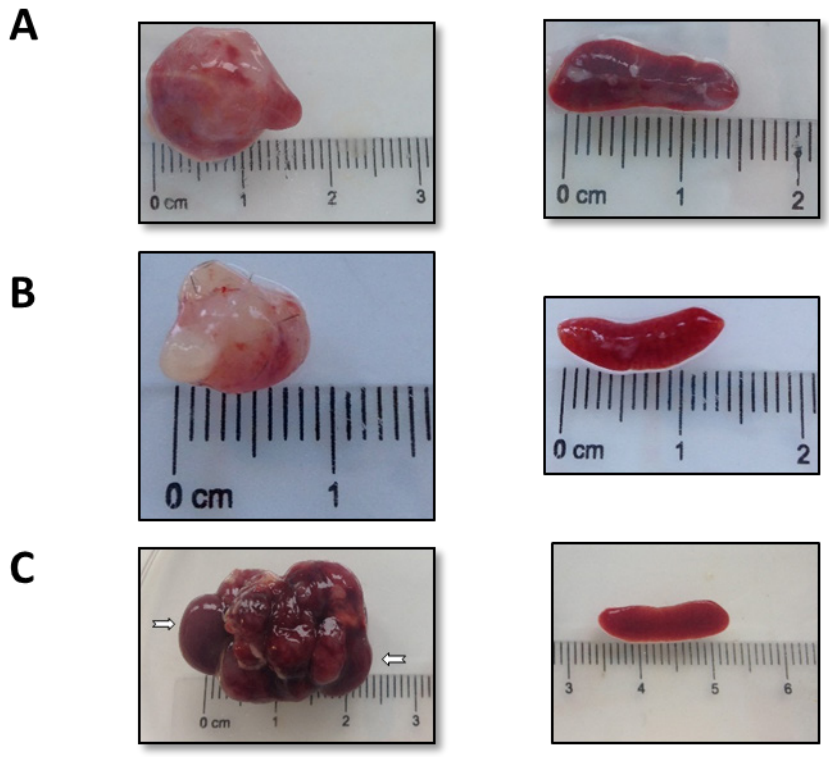

Figure 3.2 Macroscopic images of tumours and spleen from three different NB murine models

A) Comparison of the three different *in vivo* neuroblastoma models macroscopically, using representative images. NXS2 tumours and spleens which were injected subcutaneously and excised when tumours were around 8x8 mm. **B)** 9464D tumours and spleens as described in A. **C)** Spontaneous TH-MYCN$^{+/-}$ tumour and spleen which were excised at end point. Arrows denote location of kidneys.

3.2.2.1 Flow cytometry gating strategy for immunophenotyping of murine NB tumours

To analyse the immune infiltrates in the three tumour models, immunophenotyping was carried out using detailed multi-colour flow cytometry, as detailed previously (**Section 2.9**). Within this, myeloid and lymphocyte populations, and expression of GD2, MHC class I and FcγRs were investigated both in tumours and spleens of tumour bearing mice. **Figure 3.3 A** shows initial gating of forward scatter (FSC) and side (SSC), fixable aqua (live/dead) and singlet discrimination gating, which was used for all myeloid tumour and spleen populations. Gating for myeloid populations is shown in **Figure 3.3 B**. The three populations of myeloid cells investigated were defined as macrophages (F4/80^{hi}, CD11b^{mid}), monocytes (F4/80^{mid}, CD11b^{+} and Ly6C^{+}) and neutrophils (F4/80^{low}, CD11b^{+} Ly6G^{+}). FcγR expression on the three defined myeloid populations was investigated using the gating strategy defined in **Figure 3.3 C**. Finally, lymphocyte populations were also investigated. **Figure 3.4 A** shows FSC and SSC, live/dead, singlet discrimination and finally lymphocyte population gating. **Figure 3.4 B+C** shows how NK cells were gated as CD3^{-}, NKGACE+ and CD49b^{+}, and B cells as CD3^{-}, B220^{+} and CD19^{+}. For T cell subsets (**Figure 3.4 D)**, first CD3^{+} cells

were selected and then $CD8^+$ and $CD4^+$ T cells were discriminated. From this Treg cells were defined as being $FoxP3^+$ $CD4^+$ cells.

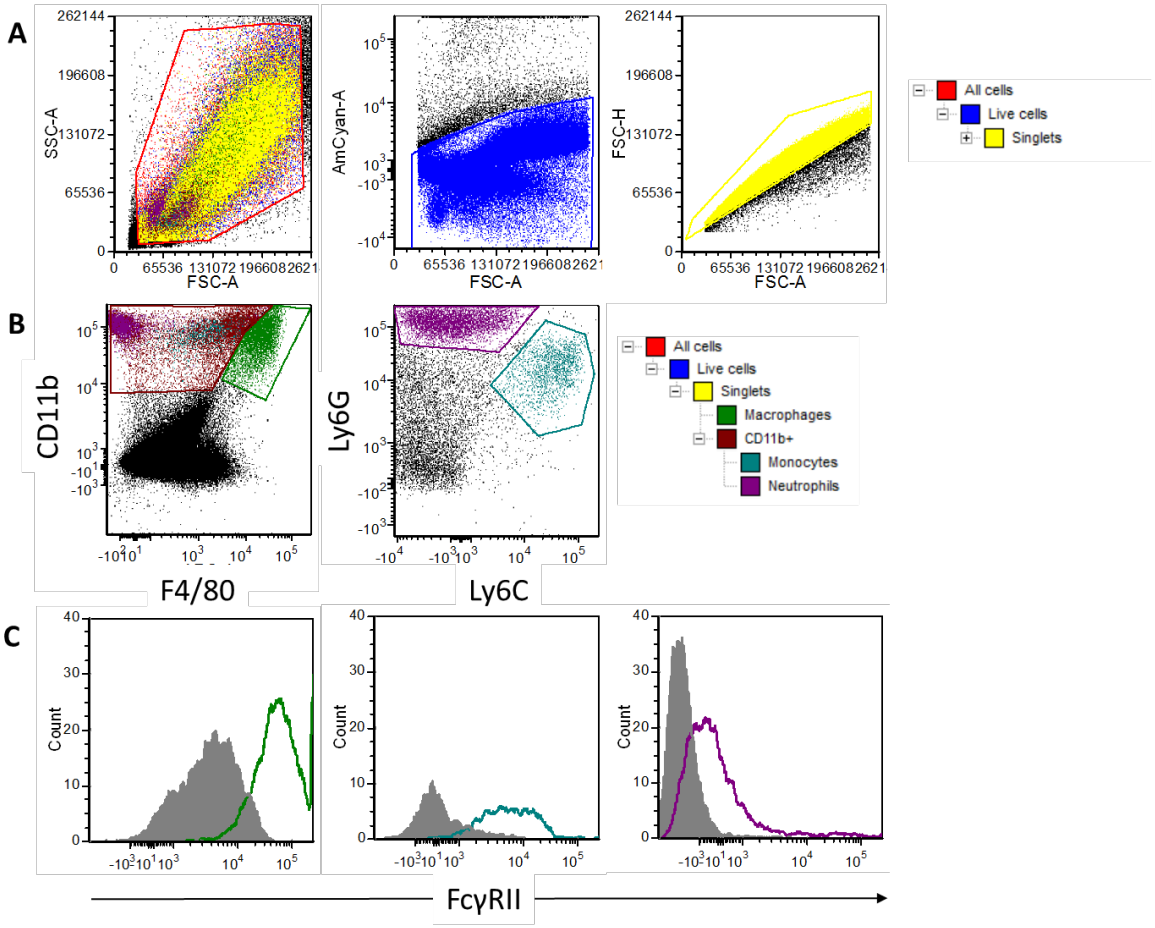

Figure 3.3 Examples of myeloid flow cytometry gaiting strategies for immunophenotyping tumours of murine neuroblastoma models

A) Data was collected on FACS Canto II. Debris removal gate on FCS and SSC plot live cell gating using fixable aqua (amcyan) and then singlet discrimination. **B)** Gating strategies are shown for macrophages and CD11b+ populations, with further gating on CD11b+ for neutrophils and monocytes. **C)** FcyR analysis the same gating was used as in **B**, with expression levels of FcyRs was assessed as MFI minus isotype control staining. Example histograms of FcyRII are shown. All gating strategies are shown using a representative tumour tissue sample, with spleen gating carried out in the same way minus live/dead discrimination.

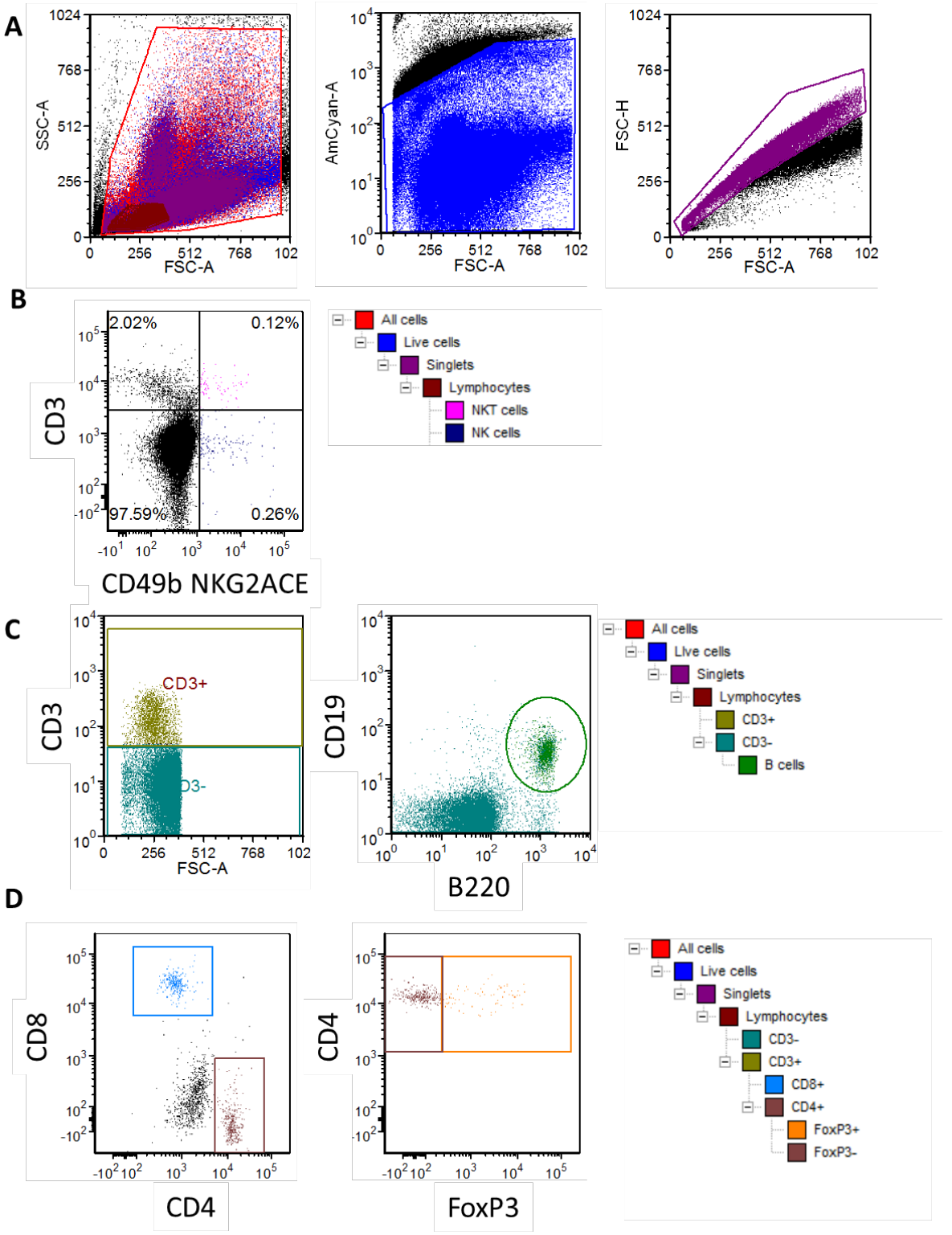

Figure 3.4 Examples of lymphocyte flow cytometry gaiting strategies for immunophenotyping tumours of murine neuroblastoma models

A) Data collected on FACS Canto II. Debris removal gate on FCS and SSC plot live cell gating using fixable aqua (amcyan), singlet discrimination and finally lymphocyte gating back on FCS SSC plot. **B)** Gating strategies are shown for NK and NKT cells. **C)** Gating of CD3+ and CD3- populations, followed by B cell population gating. **D)** CD4+, CD8+ and FoxP3+ gates are shown. All gating strategies are shown using a representative tumour tissue sample, with spleen gating carried out in the same way minus live/dead discrimination.

3.2.2.2 Immunophenotyping non-tumour bearing spleens of AJ, C57BL/6 and TH-MYCN$^{+/-}$ mice.

The three murine models of NB used in this chapter have differing strain backgrounds therefore, it was highly likely that splenic immune cell populations differ significantly at baseline. Therefore, in order to see tumour specific effects on spleen populations, immunophenotyping was performed on both non-tumour bearing (NTB) and tumour bearing (TB) mice of the relevant strains. For TH-MYCN$^{+/-}$ tumour model, non-tumour bearing TH-MYCN$^{+/-}$ mice were used rather than wild types in order to allow for any specific effects of the MYCN transgene.

In **Figure 3.5 A** no significant differences were seen between TB and NTB mice for NK cells in all three models. However for B cells, percentages have decreased in TB NXS2 mice and increased in TB 9464D spleens bearing tumours, compared to NTB mice. For all three models, percentage of CD3+ T cells was shown to be decreased in TB compared to NTB mice.

When looking at CD8+ and CD4+ T cell populations specifically as shown in **Figure 3.5 B**, TB mice of both SC strains showed a reduction in CD4+ T cells compared to NTB spleens, suggesting a tumour specific effect, which was found to be more variable for TH-MYCN mice. For splenic Treg cells (**Figure 3.5 C)**, TB NXS2 mice have increased Treg percentages, whereas TB mice from the other two models have similar levels compared to NTB mice of the same strain.

Finally when analysing myeloid populations in both TB and NTB mice few differences were noted. (**Figure 3.5 D**). However, in TH-MYCN TB mice there was a significant increase seen in neutrophils within the spleens when compared to NTB TH-MYCN mice.

These data demonstrate that systemic effects can be observed in mice bearing tumours in both spontaneous (TH-MYCN) and SC (NXS2 and 9464D) models. This may demonstrate changes in the systemic immune responses driven by the tumour mass itself.

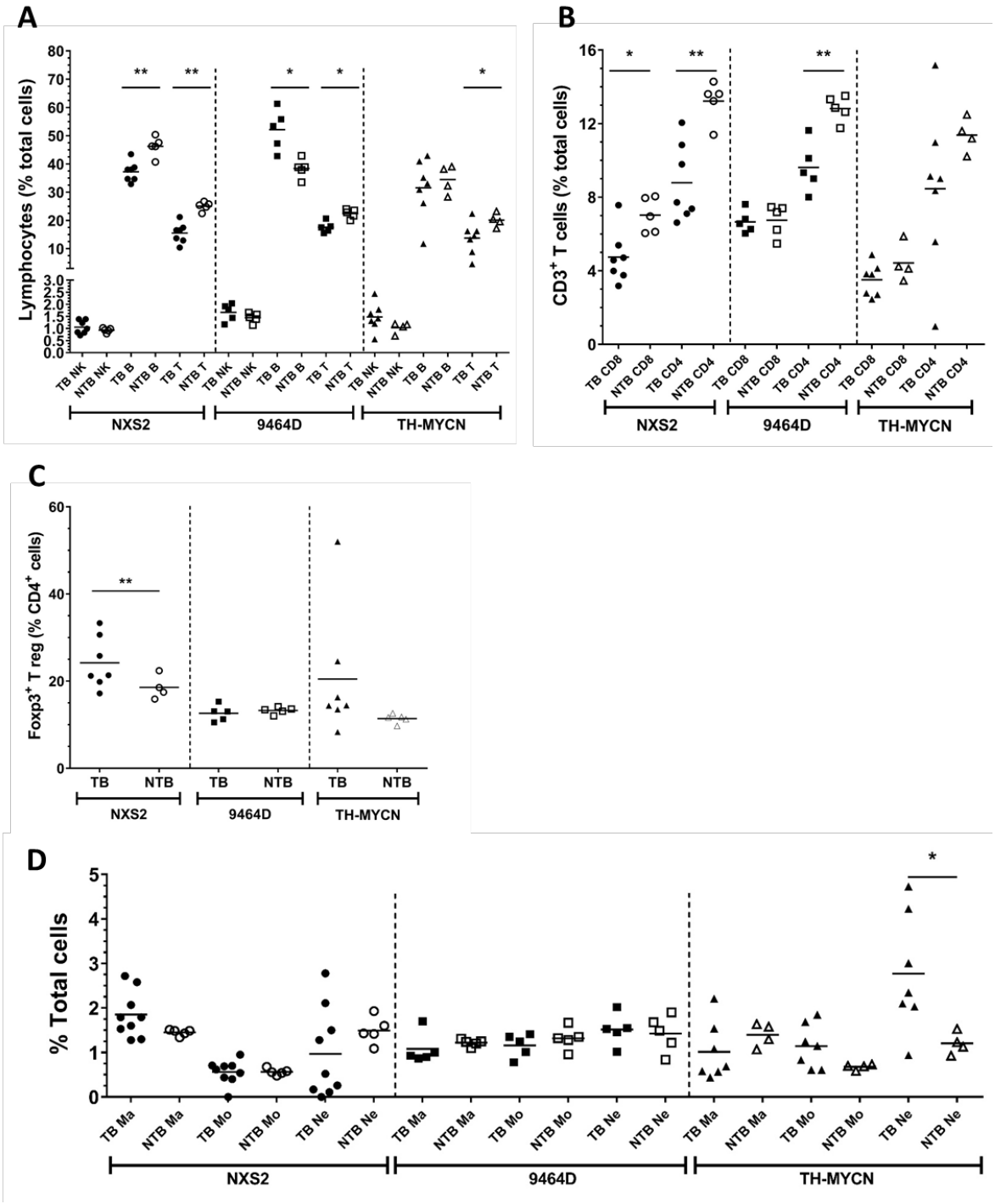

Figure 3.5 Immunophenotyping of spleens from tumour bearing and non-tumour bearing of the three murine neuroblastoma models.

A) AJ, C57BL/6 and TH-MYCN$^{+/-}$ mice, either non-tumour bearing (NTB) or tumour bearing (TB – NXS2, 9464D and spontaneous tumours respectively), were culled and spleens were harvested and stained for immunophenotyping by flow cytometry as detailed in **Section 2.9**. Gating was conducted as shown in **Figure 3.3** and **Figure 3.4**. Here, NK, B and T cells are shown. **B)** Proportion of CD8+ and CD4+ T cells. **C)** Proportion of Treg cells as a percentage of CD4+ T cells. **D)** Percentage of myeloid cells. Proportions of cells are shown as a percentage of total cells (singlets) unless otherwise stated. n= 9 (TB NXS2), 7 (TB TH-MYCN), 5 (NTB NXS2 and both 9464D) or 4 (NTB TH-MYCN). Significance calculated between NTB and TB of the same models per population using Mann-Whitney test. Significance denoted by: * = <0.05, ** = <0.01. Means are shown.

3.2.2.3 GD2 and MHC class I expression

Human NB is recognised to universally express high levels of the ganglioside GD2 [40]. GD2 is present on many cells of the nervous system, including neuroendocrine cells and nerve fibres. Expression of MHC class I has previously been shown to be downregulated by certain cancers, and may be an important mechanism of immune escape. In NB, levels of MHC class I are known to be downregulated in the human disease [40,238,495,496]. Therefore, it is important to establish if GD2 expression and MHC downregulation is replicated in different murine models. **Figure 3.6 A** demonstrates most cells in all 3 models express GD2. When staining with anti-GD2 antibody, the histograms have shifted to the right compared to isotype controls. **Figure 3.6 B** shows that the geoMFI of tumour cells expressing GD2 is relatively similar between NXS2 and TH-MYCN$^{+/-}$ tumours at around 60% of total cells. However, 9464D tumours have a lower geoMFI of GD2, compared to the other two models. To assess MHC class I expression on the tumour, cells were gated on GD2+ cells to establish the tumour component, and GD2- cells to highlight the 'non-tumour' cell population as shown in **Figure 3.6 A**. MHC class I expression, shown in **Figure 3.6 C+D**, is demonstrated to be more variable on GD2+ cells for NXS2 with some tumours having quite high expression at around 80%. However, the majority of tumours show MHC class I expression at a level between 20-40%. For 9464D and TH-MYCN$^{+/-}$ GD2+ cells, MHC class I expression is greatly reduced to < 5% when compared to NXS2 tumours, which was statistically significant. MHC class I expression is higher on GD2-cells (**Figure 3.6 A**), showing downregulation is restricted to GD2+ tumour cells. However, 9464D GD2- cells within the tumours have low expression of MHC class I, which could suggest that other non-tumour cells are also downregulating MHC class I, or not all tumour cells express GD2. Overall, 9464D and TH-MYCN$^{+/-}$ have a more comparable phenotype to the human tumours than the NXS2 model, due to the low levels of MHC class I expressed on the GD2+ tumour cells, as is seen in the human disease. However, 9464D tumours do have a lower expression of GD2+ within the tumour mass.

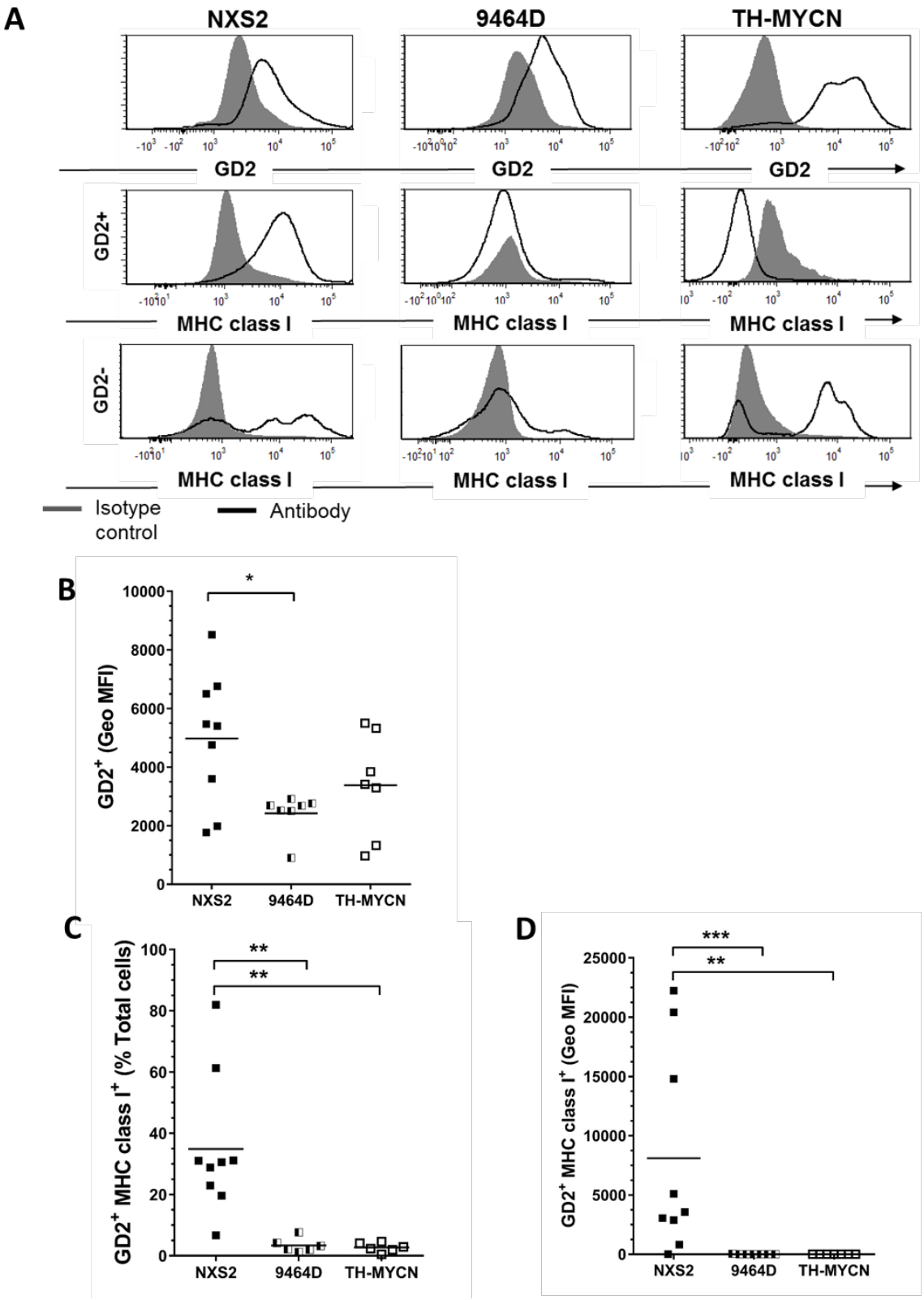

Figure 3.6 GD2 and MHC I expression on tumours NXS2 and TH-MYCN tumours ex vivo

A) SC models and TH-MYCN mice were established as previously detailed (**Sections 2.5, 2.6 and 2.17**). Once tumours had reached 8x8 mm the mice were culled and tissues were harvested for immunophenotyping by flow cytometry as detailed in **Section 2.9**, Gating was used as shown in **Figure 3.3 A**. Example histograms of GD2 gating and MHC I (grey = isotype; black line = GD2 antibody). **B)** Geo MFI of GD2 expression. **C)** % of GD2+ MHC I+ cells within the tumours. **D)** Geo MFI of MHC I expression. n= 9 (NXS2), n= 6 (9464D) and n= 7 (TH-MYCN$^{+/-}$). Significance calculated using Kruskal-Wallis with Dunn's multiple comparisons. Significance denoted by: * = <0.05, ** = <0.01, *** = <0.001. Means are shown.

3.2.2.4 Myeloid cells: neutrophils, monocytes and macrophages

Myeloid cells, which have been reported to be important modulators of the tumour microenvironment [76], were quantified within the tumours of the three models. Firstly, the expression of F4/80, a murine macrophage marker, was assessed by immunohistochemistry in frozen tumours of the three models in **Figure 3.7 A**. F4/80 expression in NXS2 tumours was very diffuse with macrophages spread throughout the tumour mass. Similarity was seen in 9464D tumours, however, there was notable staining around the edges of the tumour within the capsule. Finally, F4/80 expression in TH-MYCN$^{+/-}$ tumours was associated within the stromal septae of the tumour mass, and less so in the tumour islets.

More detailed immunophenotyping analysis was carried out by flow cytometry using the gating strategies shown in **Figure 3.3 B**. Within the tumour microenvironment (**Figure 3.7 B**), 9464D tumours were observed to have a significantly increased macrophage infiltration, at 4.2%, compared to both TH-MYCN$^{+/-}$ (0.52%) and NXS2 (2.3%). Furthermore, the NXS2 model has a higher number of TAMs compared to the TH-MYCN$^{+/-}$ tumours, with neutrophil infiltrates not being significantly different across the three different models. These data suggest that the two subcutaneous models, and particularly the 9464D model, contain a larger myeloid infiltrate compared to the TH-MYCN$^{+/-}$ tumours.

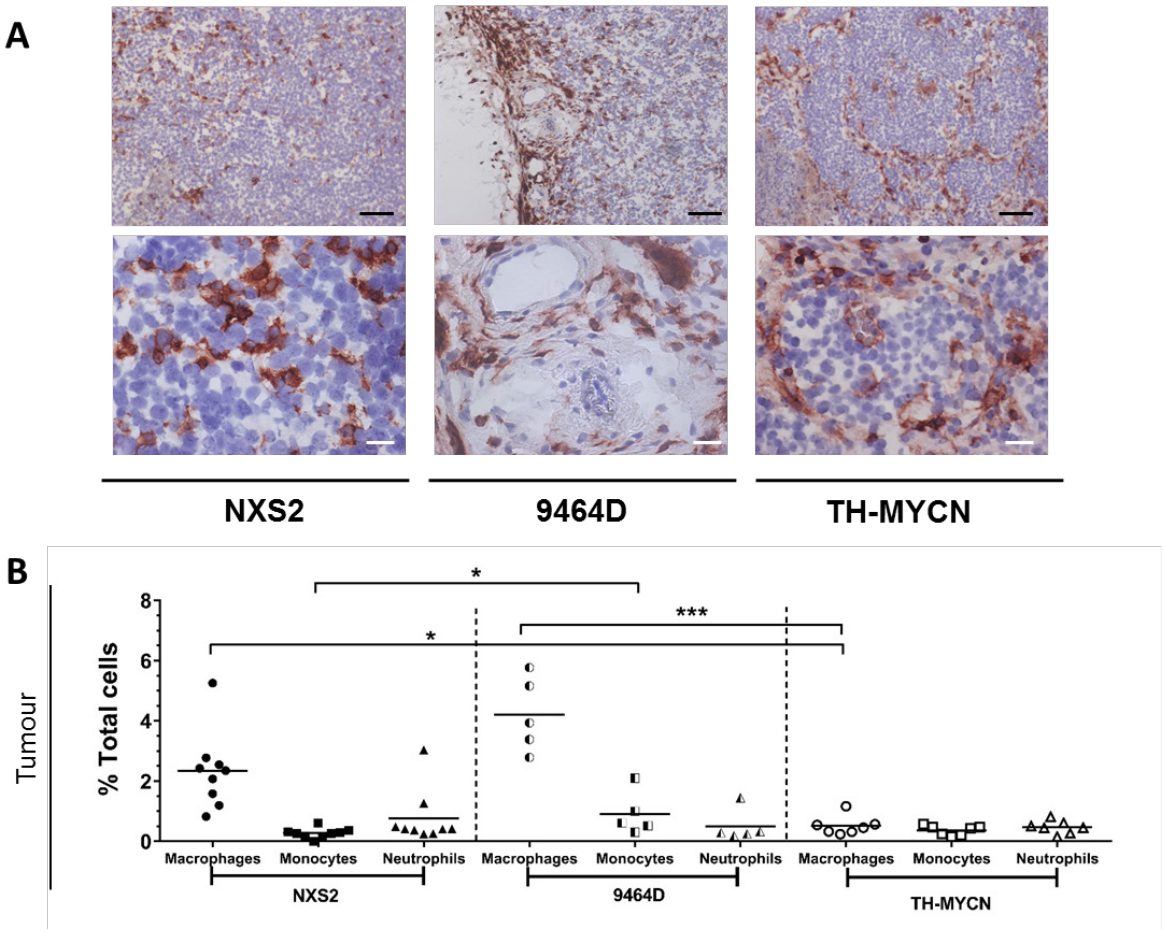

Figure 3.7 Myeloid populations within NXS2, 9464D and TH-MYCN NB tumours

A) SC models and TH-MYCN mice were established as previously detailed (**Sections 2.5, 2.6 and 2.17**). Once tumours had reached 8x8 mm the mice were culled and tissues were harvested for immunophenotyping by flow cytometry as detailed in **Section 2.9**, Gating was used as shown in **Figure 3.3**. Representative images of IHC staining for F4/80 in tumours. Top row shows x10 magnification and bottom row shows x40 magnification. **B)** Myeloid populations as a % of total cells (taken from singlet gate) within the tumours. n= 9 (NXS2), n= 5 (9464D) and n= 7 (TH-MYCN$^{+/-}$). Kruskal-Wallis with Dunn's multiple comparisons. Significance denoted by: * = <0.05, ** = <0.01, *** = <0.001. Means are shown.

3.2.2.5 Fc gamma receptors

Most cells of the immune system express FcγR on their surface, which bind to the Fc region of IgG antibodies which can lead to activation of different downstream pathways depending on the FcγR [189]. Myeloid cells in particular express these receptors, with the expression patterns being associated with activatory or suppressive phenotypes. Phenotypes can be assessed by looking at the expression levels of the individual receptors and then calculating an activatory to inhibitory receptor ratio (A:I ratio). To assess FcγR expression in the three models flow cytometry gating was utilised as detailed **Figure 3.3 C**.

TAMs of TH-MYCN$^{+/-}$ tumours (**Figure 3.8 A**), demonstrated a significant increase in expression of FcγRIV compared to NXS2 TAMs (MFIs of 12309 to 1942 respectively). Furthermore, expression of all FcγRs, except FcγRI, was significantly different in the 9464D TAMs to either NXS2 or TH-MYCN$^{+/-}$. Notably, expression of the inhibitory FcγRII was increased on 9464D TAMs (MFI= 29288) compared to both models (TH-MYCN= 10690; NXS2= 11534). Despite this, A:I ratio was similar between all three models. Tumour infiltrating monocytes demonstrated an increase of FcγRIII expression within NXS2 and 9464D tumours (**Figure 3.8 B**), with all other receptor expression remaining similar between the three models. TH-MYCN$^{+/-}$ monocytes were noted to have significantly reduced A:I ratio compared to the SC models. Neutrophils within the tumours were found to have highly variable FcγR expression (**Figure 3.8 C)**. Increased expression of FcγRII on 9464D (MFI= 23582) tumour neutrophils compared to both NXS2 (MFI= 2911) and TH-MYCN$^{+/-}$ (MFI= 7327) was noted. When compared to NXS2 tumours, both FcγRII and FcγRIII were significantly increased on 9464D neutrophils. Furthermore, FcγRI was increased upon TH-MYCN$^{-+/-}$ tumour neutrophils compared to NXS2 (MFIs= 2362 and 288.7 respectively). Overall, A:I ratios, were found to be similar levels and variable between the three models.

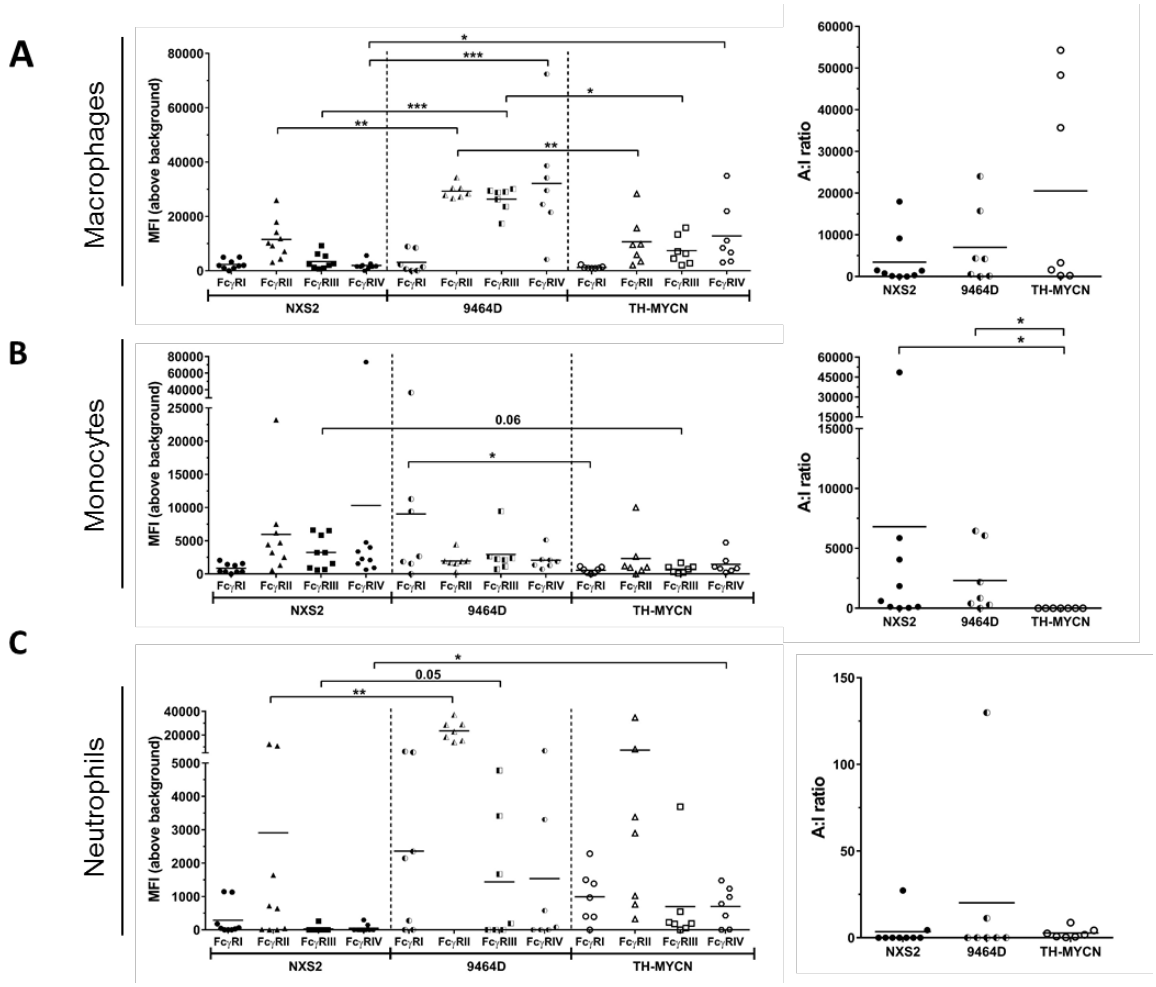

Figure 3.8 FcγR expression on 3 myeloid cell subsets within spleens and NXS2 and TH-MYCN tumours

A) SC models and TH-MYCN mice were established as previously detailed (**Sections 2.5, 2.6 and 2.17**). Once tumours had reached 8x8 mm the mice were culled and tissues were harvested for immunophenotyping by flow cytometry as detailed in section 2.9, Gating was used as shown in **Figure 3.3**. FcγR expression levels for tumours are shown for macrophages, **B)** monocytes and **C)** neutrophils. A:I ratios for each are shown on the right hand side. n= 9 (NXS2), n= 7 (TH-MYCN). Kruskal-Wallis with Dunn's multiple comparisons. Significance denoted by: * = <0.05, ** = <0.01, *** = <0.001. Means are shown.

3.2.2.6 NK cells + B cells

NK cells are potent innate effector cells and important in tumour immunosurveillance [76], therefore percentages were quantified for the NB models. Within tumours, NK cell percentage was relatively similar between all models (**Figure 3.9 A)**, representing a small percentage (<2%) of all cells within the tumours. B cells were quantified within tumours of the three models (**Figure 3.9 A**). TH-MYCN$^{+/-}$ tumours had a greater proportion of B cells at around 2% of total cells compared to NXS2 (<1%). 9464D tumours have similar levels of B cells to NXS2 tumours, with one outlier. Overall, TH-MYCN$^{+/-}$ tumours had an increase in B cell infiltration compared to the SC models.

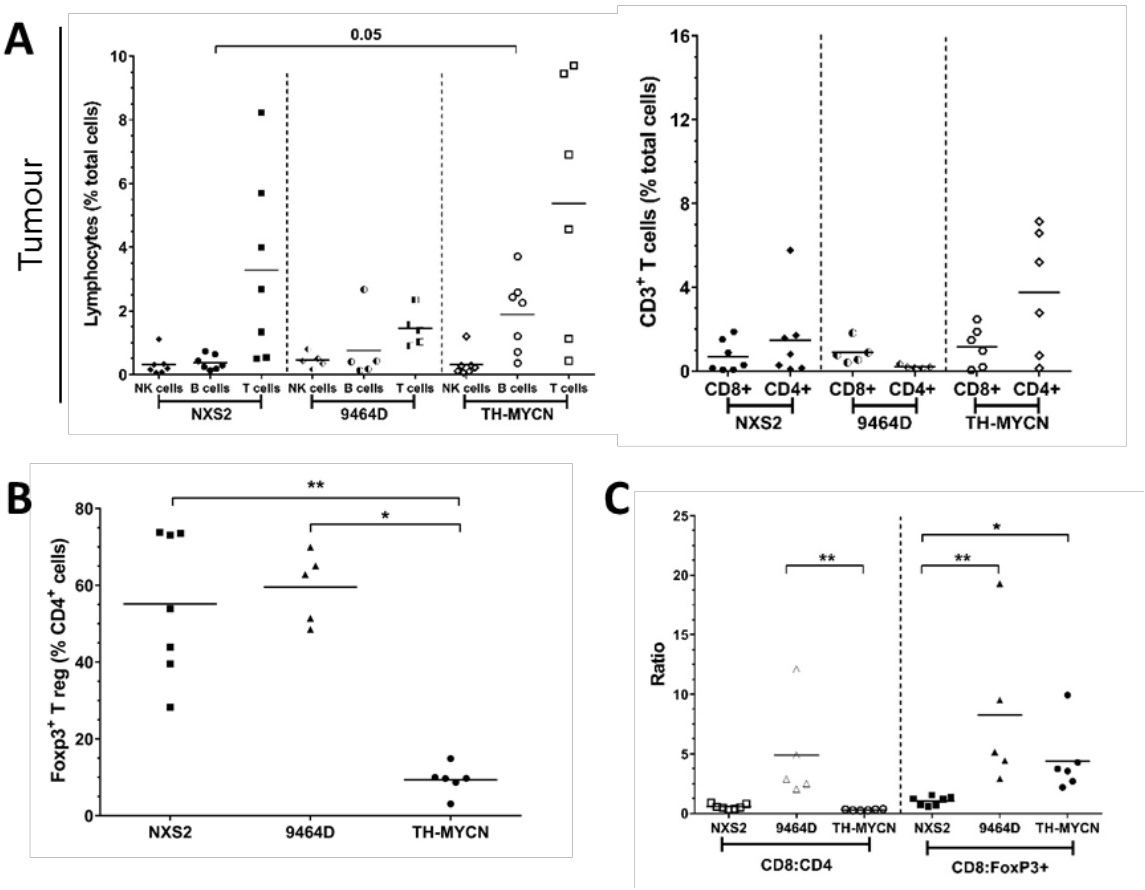

Figure 3.9 Lymphocyte populations within NXS2, NB9464 and TH-MYCN tumours and spleens

A) SC models and TH-MYCN mice were established as previously detailed (**Sections 2.5, 2.6 and 2.17**). Once tumours had reached 8x8 mm the mice were culled and tissues were harvested for immunophenotyping by flow cytometry as detailed in **Section 2.9**, Gating was used as shown in **Figure 3.4**. NK, B and T cells as a % of total cells (taken from singlet gate) within the tumours, with T cell subsets subdivided into CD8+ and CD4+ cells on the right hand side. **B)** Tregs defined by FoxP3 expression in tumours. **D)** CD8:CD4 ratio and CD8:FoxP3+ ratio for tumours. n= 7 (NXS2), n= 7 (TH-MYCN), n= 5 (9464D). Kruskal-Wallis with Dunn's multiple comparisons. Significance denoted by: * = <0.05, ** = <0.01. Means are shown.

3.2.2.7 T cell subsets

As T cells are known drivers of the anti-tumour immune response, the extent of their infiltration and distribution of subsets, was quantified within the three tumour models. Overall T cell infiltration was first quantified by assessing the percentage of CD3+ cells within tumours (**Figure 3.9 A**). A broad range of T cells within the tumours of both NXS2 (~0.5% - 8.5%) and TH-MYCN$^{+/-}$ (~ 0.5 – 10%) was seen. Whereas within the 9464D tumours, the proportion of CD3+ cells was lower (approximately 1.5% total lymphocytes) and less variable.

T cell subsets were then defined within tumour microenvironment (**Figure 3.9 A**). Very low levels of CD8+T cells were seen (<4% of total cells), with no significant variation across models. However, within the tumour it was clear that 9464D tumours have reduced CD4+ cell infiltration when compared to the other two models. TH-MYCN$^{+/-}$ tumours had the highest amount of CD4+ infiltration, but high variability was noted, ranging from ~8% to <1% of total cells.

Suppressive Treg cells, were also quantified (as percentage of CD4+ cells) tumours of the models, as demonstrated in **Figure 3.9 B.** Here, the SC models had considerably heightened Treg proportions compared to TH-MYCN$^{+/-}$ tumours. TH-MYCN$^{+/-}$ tumours have an average infiltration of ~10% whereas Tregs make up ~55% and ~60% of CD4+ cells within NXS2 and 9464D tumours respectively. This suggests that the SC tumours were a more suppressive environment when compared to the spontaneous tumour model.

A more comprehensive way of seeing how activated or supressed a T cell infiltrate is within the tumours is to utilise T cell ratios, as was quantified in **Figure 3.9 C**. Within tumours, 9464D had a significantly higher CD8:CD4 ratio than either of the other two models, at around 5. This suggests that the tumours had a substantially increased number of CD8+ cells infiltrating than CD4+ cells. NXS2 tumours had a higher ratio when compared to TH-MYCN$^{+/-}$. However, as their ratios are close to or lower than 1, its suggests that they have higher numbers of CD4+ cells infiltrating rather than CD8s. Ratio of CD8+ cells to FoxP3+ cells (i.e. the ratio of effector cells to suppressor cells) within the tumours was assessed. NXS2 had significantly lower CD8:FoxP3 ratio of 1.5 when compared to both TH-MYCN$^{+/-}$ and 9464D, suggesting a more suppressive environment. 9464D has the highest CD8:FoxP3 ratio of the three models with a ratio of around 8, with the TH-MYCN$^{+/-}$ tumours having a ratio within the middle of the three models. Having a higher CD8:FoxP3 ratio within the tumours suggests that 9464D has more activated, effector environment than the other two models.

Immunophenotyping data presented for all three models is summarised in **Table 3.1**.

	NXS2	9464D	TH-MYCN$^{+/-}$	Figure reference
Stain background	AJ	C57BL/6	129/SvJ	N/A
Location	Subcutaneous	Subcutanous	Spontaneous development in sympathetic tissue	N/A
Tumour development	Day 4-5	Day 25	8 - 26 weeks	N/A
Tumour penatrance	~100%	~100%	~70% (heterozygous mice)	N/A
Tumour measurement	Callipers	Callipers	Palpation/Ultrasound/CT	N/A
Days to end point (from palp/~1cm)	10-15 days	15-20 days	10-20 days	N/A
GD2 expression	High - variable	Low	Medium - variable	**Figure 3.6**
GD2+ MHC I+	Medium - Variable	Low/negative	Low/negative	**Figure 3.6**
Monocytes	Low	Medium	Low	**Figure 3.7**
Macrophages	High	High	Low	
Neutrophils	Low	Low	Low	
FcγRs (monocytes)	↑III	↑I	↓III	**Figure 3.8**
FcγRs (macrophages)	↓IV	↑II, III, IV	↑IV	
FcγRs (neutrophils)	↓I, III, IV	↑I, II, III	↑I, IV; ↕II	
NK cells	Low	Low	Low	**Figure 3.9**
B cells	Low	Low	High	
CD3+ cells	Variable	Medium	Variable	
CD4+ cells	Medium	Low	High	
CD8+ cells	Medium	Medium	Medium	
Treg cells	High	High	Low	
CD8/CD4	Low	High	Low	
CD8/Treg	Low	High	High	

Table 3.1 Summary table comparing immune infiltrates into tumours of the three murine models of NB

Tumour immunophenotyping data presented in this chapter is summarised. Percentage of immune cell infiltrates in tumours are denoted as low, medium or high compared with each of the models.

3.2.3 Establishment of transplant models of TH-MYCN$^{+/-}$ tumours

This chapter has demonstrated substantial variation in immune populations between the three murine models of NB we currently use in house. This disparity is most noticeable between the SC syngeneic models and the spontaneous transgenic TH-MYCN$^{+/-}$ model. In an effort to see whether location of tumours can affect their immune infiltrate, and whether one spontaneous tumour could be passaged into many recipients, a re-passage experiment was conducted using TH-MYCN$^{+/-}$ tumours. As demonstrated in **Figure 3.10 A**, a tumour bearing TH-MYCN$^{+/-}$ mouse was culled and tumour tissue was harvested. Tumour was disassociated into a single cell suspension as detailed in **Section 2.8.4**, with cells being repassaged into wild type 129/SvJ mice by injecting 1x10^{6} TH-MYCN$^{+/-}$ tumour cells either SC or IP.

Figure 3.10 B shows that tumour appearance for either SC or IP repassaged tumours was similar with all tumours appearing between 10-25 days. However, it is notable that over two experiments, only 2 mice successfully grew IP tumours out of 7 mice in total. Growth of SC passaged tumours was demonstrated in **Figure 3.10 C**, where variable tumour growth kinetics between the mice was observed. Finally, tumour and spleen weights of SC tumours recorded upon collection for immune population analysis, showed that tissues were of similar weights for immunophenotyping (**Figure 3.10 D**).

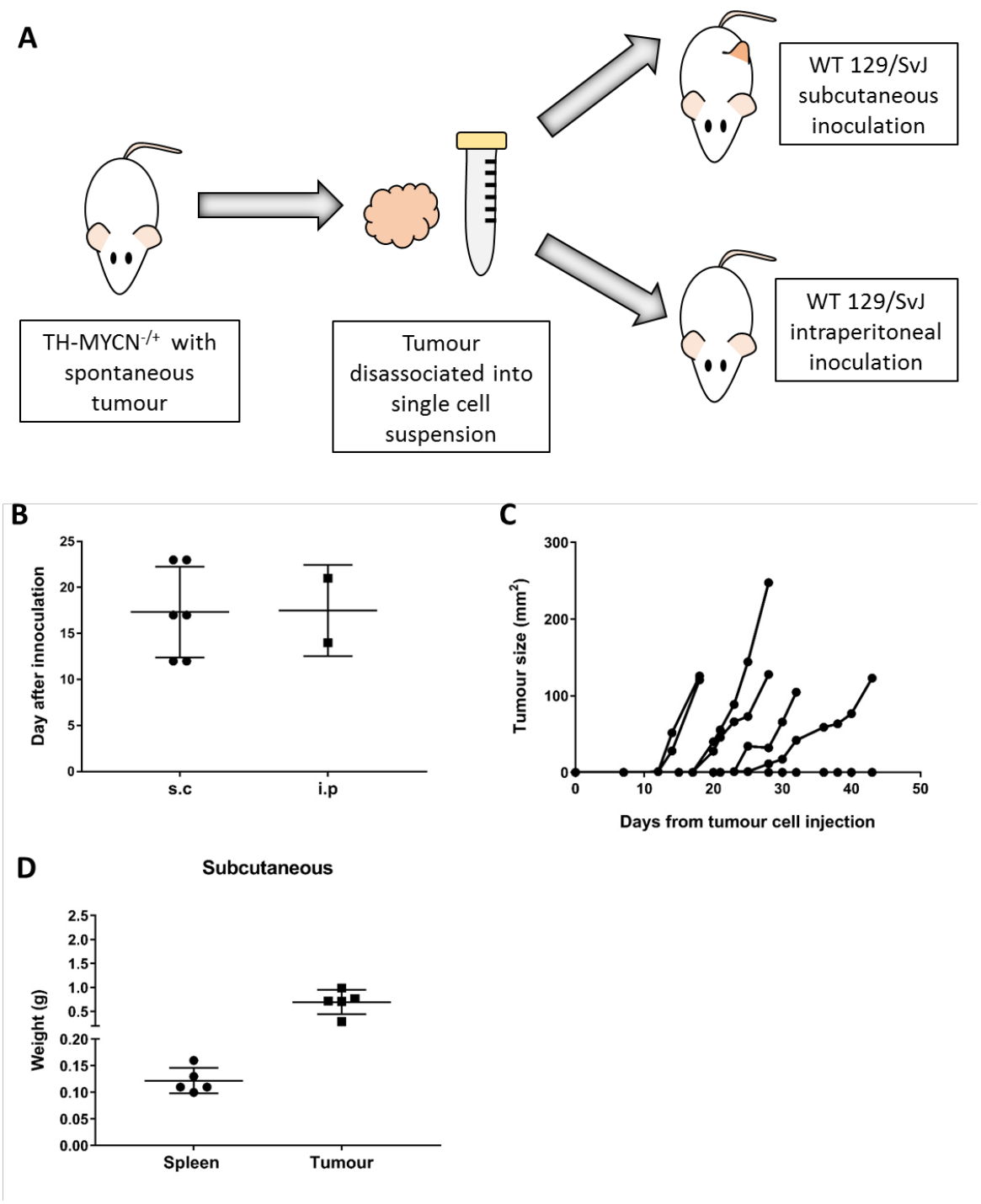

Figure 3.10 Tumour appearance and growth of tumours passaged from spontaneous TH-MYCN

A) Schematic of tumour passaging of TH-MYCN tumours into WT 129/SvJ mice. Tumour tissue is taken and disassociated as described in **Section 2.8.4**. Cells were then made into a single cell suspension and injected either SC or IP into recipient mice. SC growth was monitored by calliper measurements while IP tumour growth was measured by palpation. **B)** Date of appearance of passaged tumours after inoculation. **C)** Tumour growth monitoring of sub cutaneous passaged tumours. **D)** Weight of subcutaneous tumours and spleens at time of removal for immunophenotyping. Data is shown from two independent experiments, with n= 6 for subcutaneous tumours and n= 2 for intraperitoneal tumours. Mean and SD error bars are shown.

3.2.3.1 Myeloid infiltrates in sub cutaneous and IP passaged TH-MYCN$^{+/-}$ tumours compared to spontaneous TH-MYCN$^{+/-}$ tumours

Repassaging of abdominal spontaneous TH-MYCN$^{+/-}$ tumours into different ectopic locations may affect the immune infiltrate into the tumour microenvironment. To assess this, detailed immunophenotyping was performed of repassaged tumours and spleens from both SC and IP locations and compared to previous data collected from spontaneous TH-MYCN$^{+/-}$ tumours (as presented in **Figure 3.5** to **Figure 3.9**).

Firstly myeloid populations were analysed in **Figure 3.11 A**. A high percentage of splenic macrophages were present in both SC and IP passaged mice compared to spontaneous TH-MYCN$^{+/}$. Furthermore, SC tumours exhibited a significantly increased percentage of TAMs compared to spontaneous tumours. Levels of monocytes (**Figure 3.11 B**) and neutrophils (**Figure 3.11 C**) within both tumours and spleens were relatively similar for both repassaged and spontaneous tumours. However, there is an increase in neutrophils within spontaneous tumours compared to SC passaged tumours, but this is very variable.

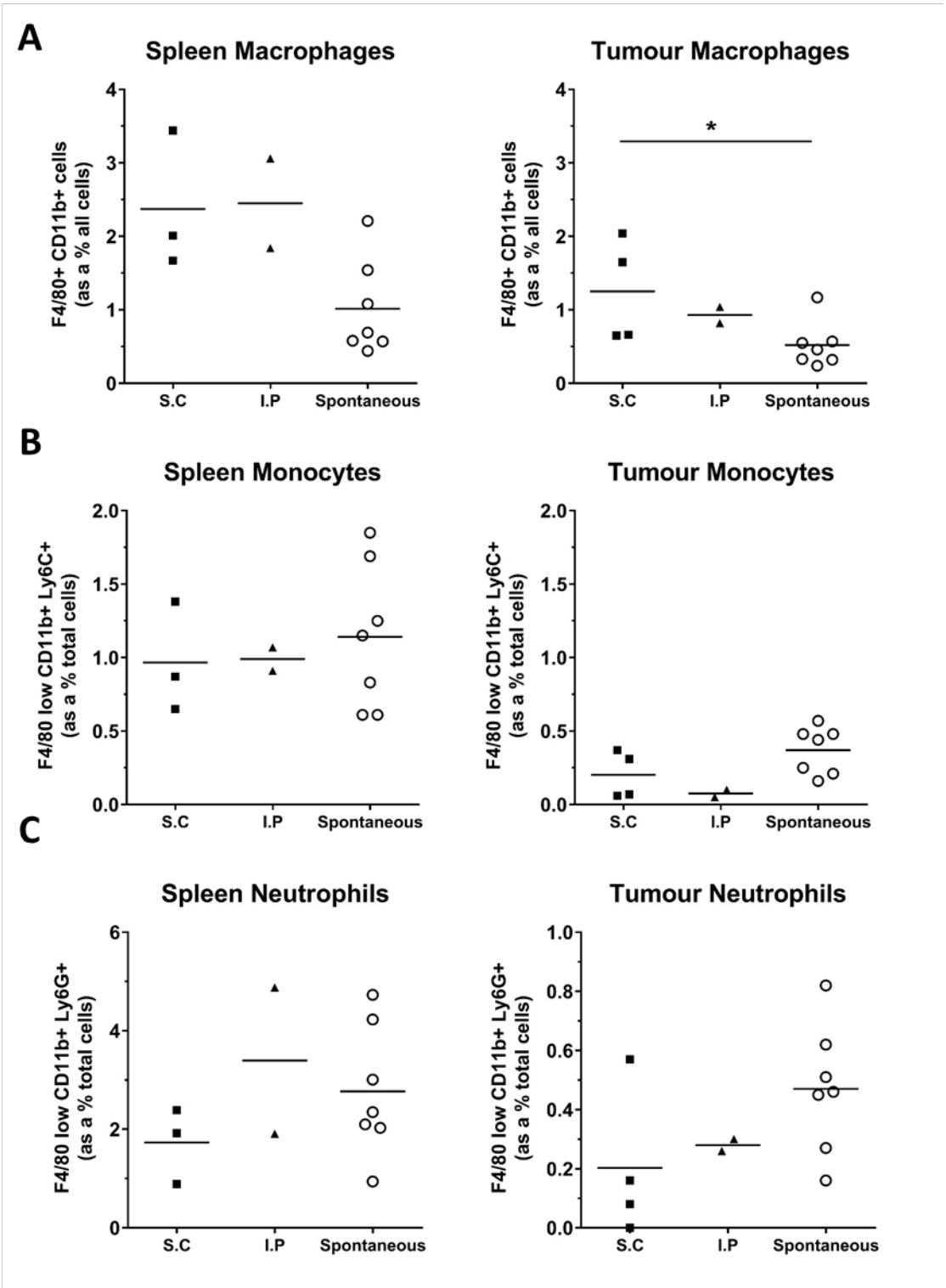

Figure 3.11 Analysis of tumour infiltrating and splenic myeloid populations of TH-MYCN sub cutaneous and intraperitoneal re-passaged tumours compared to spontaneous TH-MYCN tumours

A) SC and IP passaged mice were established as detailed in **Figure 3.10**. Once tumours had reached 10x10 mm the mice were culled and tissues were harvested for immunophenotyping by flow cytometry as detailed in **Section 2.9**, Gating was used as shown in **Figure 3.3**. Percentages of cells in both spleens and tumours are shown for macrophages, **B)** monocytes and **C)** neutrophils. Spontaneous data shown is taken from TH-MYCN data presented in **Figure 3.5** to **Figure 3.7**. Data is shown from two independent experiments, with n= 3-4 for subcutaneous tumours (SC) and n= 2 for intraperitoneal tumours (IP); n= 7 for TH-MYCN. Significance calculated using Mann-Whitney, with * = <0.05. Mean and SD error bars are shown.

3.2.3.2 NK and B cell infiltrates in TH-MYCN$^{+/-}$ passaged tumours compared to TH-MYCN$^{+/-}$ spontaneous tumours

Lymphocyte populations were also assessed in SC and IP passaged tumours. Notably, B cells were significantly higher in both SC and IP tumour bearing spleens compared to spontaneous tumour bearing mice as shown in **Figure 3.12 A**. This was reversed within the tumour microenvironment with a greater proportion of B cells found in spontaneous tumours compared to either passage location. Splenic and tumour NK cell populations were similar in all three models (**Figure 3.12 B**).

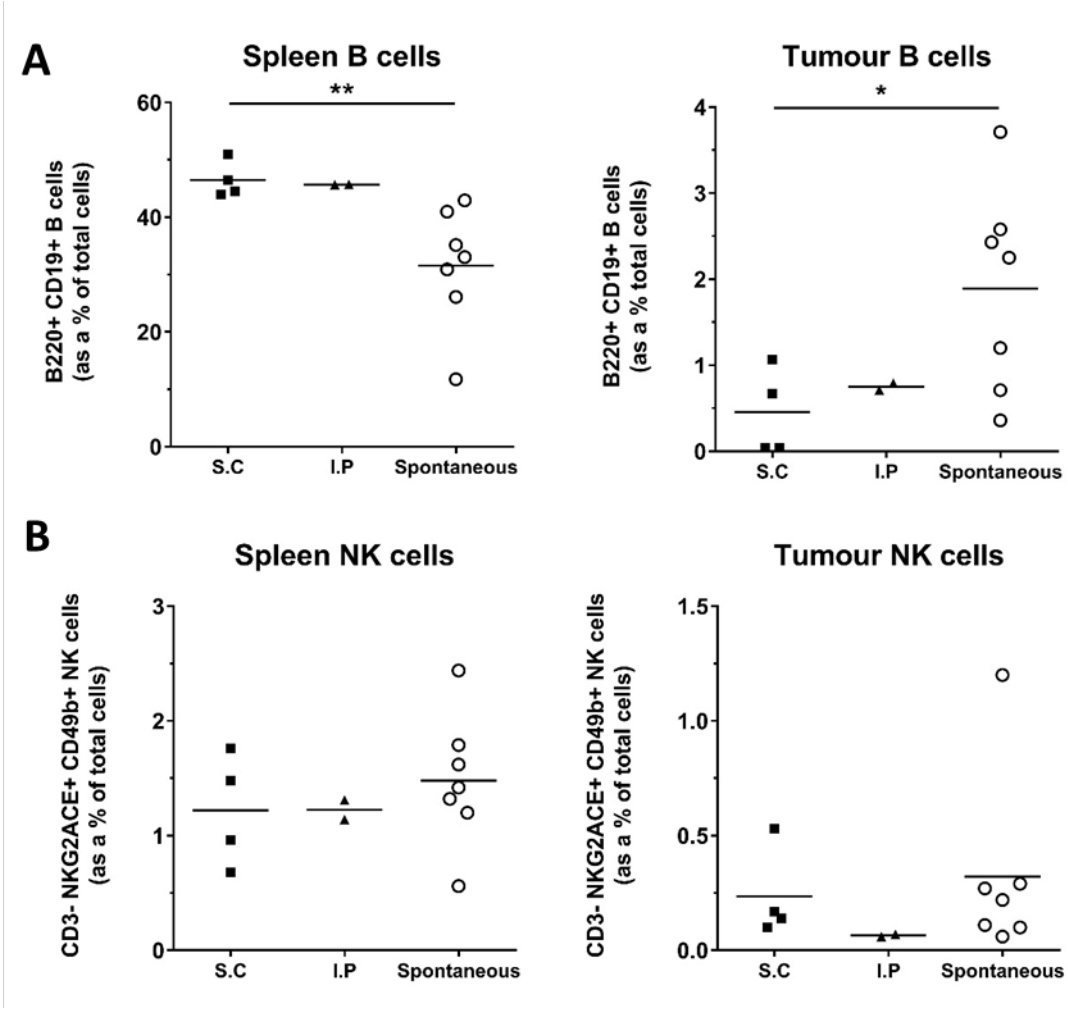

Figure 3.12 Analysis of tumour infiltrating and splenic NK and B cell populations of TH-MYCN sub cutaneous and intraperitoneal repassaged tumours compared to spontaneous TH-MYCN tumours

A) SC and IP passaged mice were established as detailed in **Figure 3.10**. Once tumours had reached 10x10 mm the mice were culled and tissues were harvested for immunophenotyping by flow cytometry as detailed in **Section 2.9**, Gating was used as shown in **Figure 3.4**. Percentages of cells in both spleens and tumours are shown for B cells and **B)** NK cells. Spontaneous data shown is taken from TH-MYCN data presented in **Figure 3.5** to **Figure 3.9**. Data is shown from two independent experiments, with n= 3-4 for subcutaneous tumours (SC) and n= 2 for intraperitoneal tumours (IP); n= 7 for TH-MYCN. Significance calculated using Mann-Whitney, with * = <0.05. Mean and SD error bars are shown.

3.2.3.3 Analysis of T cell subsets and ratios within TH-MYCN$^{+/-}$ subcutaneous and intraperitoneal passaged tumours compared to spontaneous TH-MYCN$^{+/-}$ tumours

Finally, the infiltration and distribution of T cells within the passaged tumour models and how they compare to the spontaneous tumours was assessed. Firstly, the total number of CD3+ cells within the spleens of both SC and IP tumour bearing mice was significantly higher than in spontaneous tumour bearing mice (**Figure 3.13 A**). However, within the tumour microenvironment, spontaneous tumours had significantly increased percentages of CD3+ cells compared to both forms of passage. When broken down into CD4+ (**Figure 3.13 B**) and CD8+ (**Figure 3.13 C**) cells, splenic percentages are similar in all tumour bearing mice. Conversely within the tumours, spontaneous mice had significantly increased CD4+ and CD8+ infiltration compared to passaged tumours. However, levels of the suppressive Treg cells are similar in both spleens and tumours of all models (**Figure 3.13 D**).

Finally, ratios of CD8:Treg (**Figure 3.14 A**) and CD8:CD4 (**Figure 3.14 B**) cells were analysed. Due to the increased percentage of CD8+ cells in spontaneous tumours, the CD8:Treg ratio was significantly higher in these tumours compared to both forms of passages. Splenic ratios remained similar between the three groups. Furthermore, **Figure 3.14 B** demonstrated that spontaneous tumours had a significantly higher CD8:CD4 ratio than either SC or IP passaged tumours, suggesting a greater number of effector CD8+ T cells present. Splenic CD8:Treg and CD8:CD4 ratios were similar between the three groups.

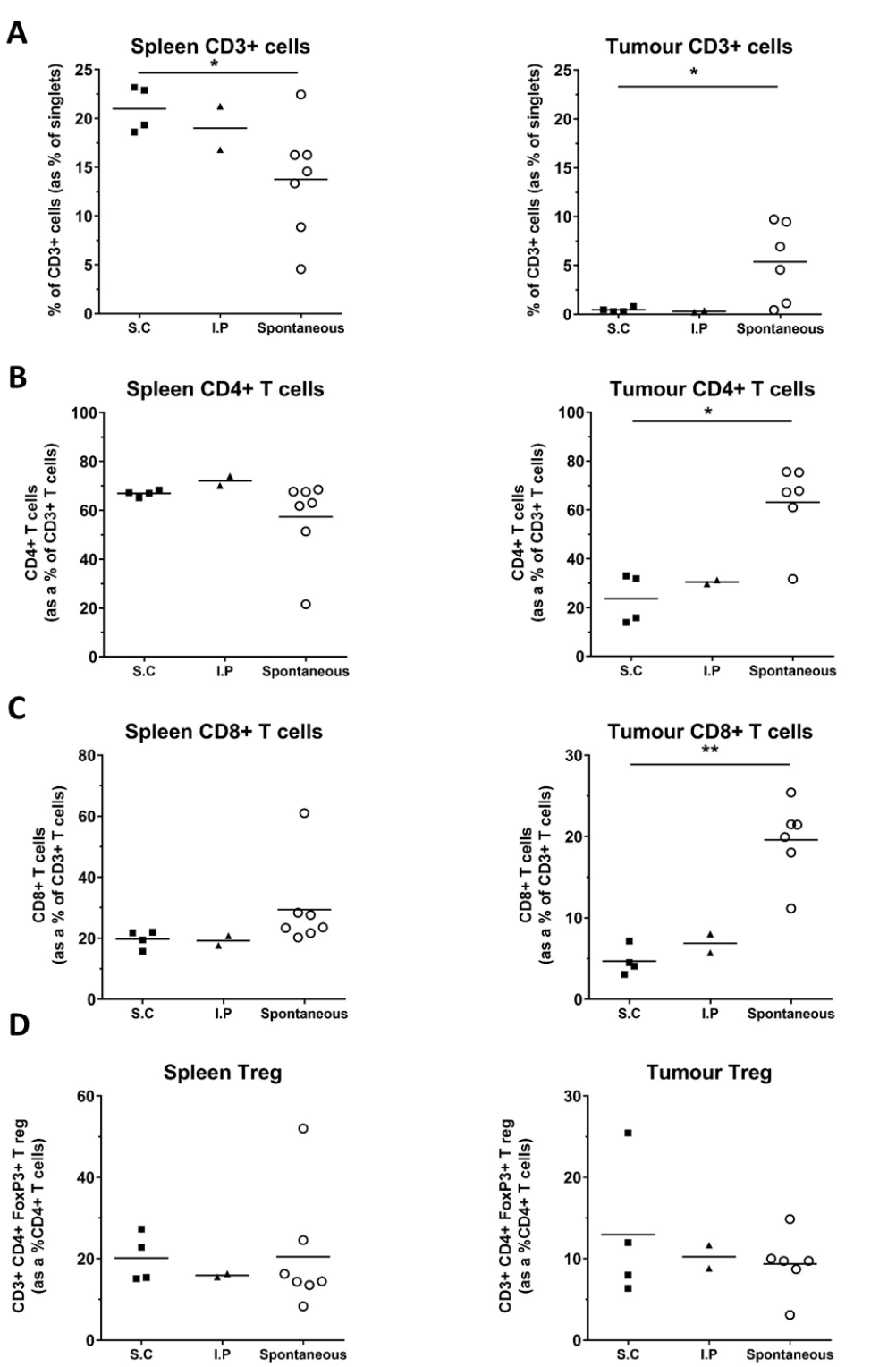

Figure 3.13 Analysis of tumour infiltrating and splenic T cell populations of TH-MYCN sub cutaneous and intraperitoneal repassaged tumours compared to spontaneous TH-MYCN tumours

A) SC and IP passaged mice were established as detailed in **Figure 3.10**. Once tumours had reached 10x10 mm the mice were culled and tissues were harvested for immunophenotyping by flow cytometry as detailed in **Section 2.9**, Gating was used as shown in **Figure 3.4**. Percentages of cells in both spleens and tumours are shown for CD3+ cells, **B)** CD4+ cells, **C)** CD8+ cells and **D)** FoxP3+. Spontaneous data shown is taken from TH-MYCN data presented in **Figure 3.5** to **Figure 3.9**. Data is shown from two independent experiments, with n= 3-4 for subcutaneous tumours (SC) and n= 2 for intraperitoneal tumours (IP); n= 7 for TH-MYCN. Significance calculated using Mann-Whitney, with * = <0.05. Mean and SD error bars are shown.

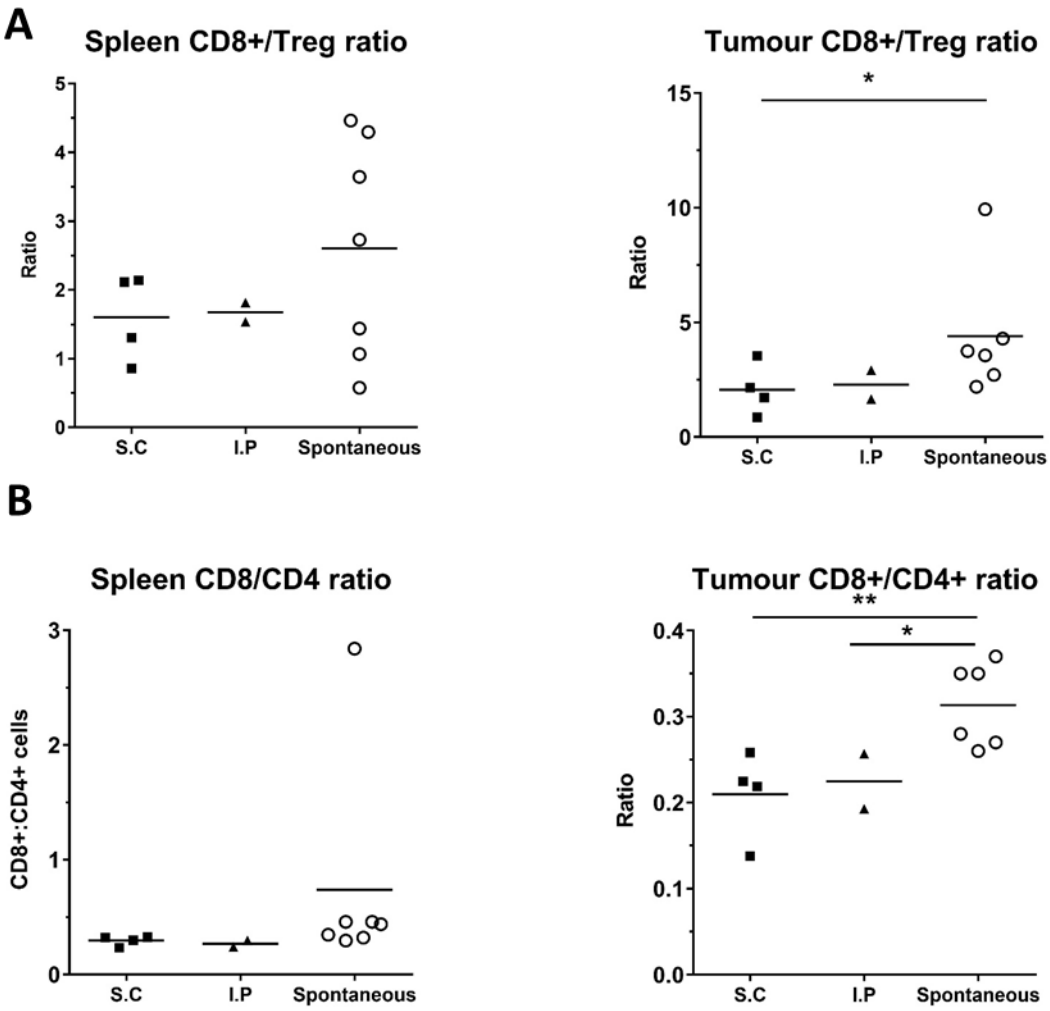

Figure 3.14 Analysis of tumour infiltrating and splenic T cell ratios of TH-MYCN sub cutaneous and intraperitoneal repassaged tumours compared to spontaneous TH-MYCN tumours

A) SC and IP passaged mice were established as detailed in **Figure 3.10**. Once tumours had reached 10x10 mm the mice were culled and tissues were harvested for immunophenotyping by flow cytometry as detailed in **Section 2.9**, Gating was used as shown in **Figure 3.4**. Percentages of cells in both spleens and tumours are shown for CD3+ cells, **B)** CD4+ cells, **C)** CD8+ cells and **D)** FoxP3+. Spontaneous data shown is taken from TH-MYCN data presented in **Figure 3.5** to **Figure 3.9**. Data is shown from two independent experiments, with n= 3-4 for subcutaneous tumours (SC) and n= 2 for intraperitoneal tumours (IP); n= 7 for TH-MYCN. Significance calculated using Mann-Whitney, with * = <0.05. Mean and SD error bars are shown.

3.3 Chapter discussion

In order to appropriately assess the efficacy of therapeutics that modulate the immune response to tumours, it is vital to have high quality *in vivo* models which recapitulate the immune infiltrate within human cancers to a high degree. This is especially true for paediatric cancers and NB, as these diseases tend to have small patient cohorts and therefore there is less scope for conducting large clinical trials. To that end, precise and relevant preclinical data needs to be extensive before new treatments or combinations are put forward into clinical trials. With three different murine NB tumour models to utilise in house, it is a logical step to define their immune infiltrates to see what model is both practical, and best represents the human disease *in vivo* to ensure we get translational results, as was shown in this chapter. Furthermore, these results can be used as a baseline to compare the effects chemotherapy has on infiltrates within these models. However, it is important to note that published data on the immune environment in human NB is sparse, which may be partly due to the lack of tumour samples. Reasons for this include only small diagnosis biopsies being taken, or tissue being removed after chemotherapy and surgery which is of poor quality due to being necrotic and calcified [554].

Splenic differences in immune cell populations between NTB and TB mice of the three models was assessed in **Figure 3.5**. The presence of tumour in the mice did lead to some systemic splenic changes. Notably, when compared to non-tumour bearing mice, all tumour bearing mice has a reduction in CD4+ cells within their spleens. Furthermore, TH-MYCN$^{+/-}$ mice had increased neutrophils, and finally, NXS2 tumour bearing mice had an increase in Tregs. This demonstrates that all the tumours, both spontaneous and subcutaneous, led to systemic changes in immune cell populations. These changes may be due to increased systemic inflammation due to secreted factors by tumour cells. The increase in two models, of neutrophils which can drive inflammation [92], and Tregs which are involved in inflammation regulation [555], provides evidence of this.

Human NB tumours are known to be GD2^{+} [40,42] and to downregulate MHC class I as a mechanism of immune escape [238,495,496,556,557]. Therefore their expression levels were assessed in **Figure 3.6** on the three murine NB models: NXS2, 9464D and TH-MYCN$^{+/-}$. Here, the TH-MYCN$^{+/-}$ model best replicated human NB as it had a fairly high GD2 expression combined with near complete loss of MHC class I, whereas the NXS2 tumours still maintained relatively high MHC class I and 9464D tumours had lower levels of GD2 expression. This loss of MHC class I in the TH-MYCN$^{+/-}$ model could suggest it is under more immune selective pressure than the NXS2 model, which may be due to the fact that the tumour grows spontaneously and is therefore subject to immune editing, whereas the NXS2 cells are grown in culture and therefore not subjected to immune selective pressure.

There is unfortunately very little data published on myeloid infiltrates in human NB. However, it has been previously reported that CD68+ and CD163+ tumour associated macrophages are present in human NB tumours [558-560]. Here the proportion, location and expression of FcγR expression on myeloid cells was analysed within the tumour microenvironments of the three murine tumour models using a combination of IHC and flow cytometry. Myeloid cells and their FcγR expression pattern can have important immune regulatory functions and direct impacts of mAb therapy within the tumour microenvironments [561]. **Figure 3.7** demonstrated the presence of F4/80+ macrophages within tumours from all three models. Furthermore, macrophages in the two subcutaneous models were diffusely distributed compared to the more stromal associated pattern seen in the spontaneous TH-MYCN$^{+/-}$ tumours (**Figure 3.7** A). Both of these distributions have been reported in human NB samples looking at CD68+ macrophages [560].

Importantly within the tumours, both of the subcutaneous models had a greater infiltration of macrophages when compared to the TH-MYCN$^{+/-}$ model. This may be due to the fact that these tumours are injected and grown ectopically under the skin, which could lead to increased inflammation at the tumour site. This could lead to an influx of inflammatory cells such as macrophages, compared to the spontaneous tumours which slowly develop over time, perhaps allowing for less inflammation. An increase in macrophages could cause an immunosuppressive environment if the macrophages are polarised to a suppressive phenotype, making these tumours more aggressive and harder to treat. One way of assessing their polarisation is looking at the pattern of FcγR expression. As discussed in **Section 1.3.3**, all but one of mouse FcγRs are activatory, with FcγRII being inhibitory. In the tumours, shown in **Figure 3.8**, FcγR expression varied greatly between the three models on the three subsets of myeloid cells. Notably, 9464D tumours had increased expression of the inhibitory receptor FcγRII on both macrophages and neutrophils compared to both TH-MYCN$^{+/-}$ and NXS2 tumours. Furthermore, an increased expression of FcγRIII and FcγRIV in 9464D was also seen on tumour infiltrating macrophages compared to the other models. This increase in expression of both activatory and inhibitory FcγRs on myeloid cells within 9464D tumours could suggest a more inflammatory tumour microenvironment compared to the other two models. Furthermore, TH-MYCN$^{+/-}$ macrophages have increased expression of both FcγRIII and FcγRIV compared to NXS2 tumours, whereas FcγRII is similar in both models. Although the inhibitory receptor levels is similar between the two models, the NXS2 macrophages have a decreased expression of two activatory markers, suggesting these macrophages may be polarised towards a suppressive phenotype, which may hinder treatment of these tumours. There is currently no data from human NB samples of myeloid FcγR expression, therefore it is challenging to assess how representative any of these tumour models are to human tumours with regards to FcγR expression.

TILs within the TH-MYCN$^{+/-}$ tumours have previously been assessed by Carlson *et al*, and to an extent for 9464D by Kroesen *et al* [542,562]. The only difference seen in the tumours between the three models was that TH-MYCN$^{+/-}$ tumours have a greater infiltration of B cells into the tumour microenvironment compared to NXS2 tumours as shown in **Figure 3.9 B**. These cells within the TH-MYCN$^{+/-}$ tumours may be acting as APCs to present tumour antigen to T cells to generate an anti-tumour immune response. It is hard to compare B cell infiltration in these mice models to human NB tumours as little data is available. However, in previous studies in human NB samples, B cells and NK cells have been reported as absent or rare within the tumour mass [504]. However another study, demonstrated a B cell gene signature in NB tumours, together with a with a macrophage signature, which was associated with poor prognosis [558].NK cells and B cells were demonstrated to be infiltrating tumour of both subcutaneous models at low levels, along with NK cells for TH-MYCN$^{+/-}$ tumours.

As discussed in **Section 1.3.2.1**, T cells are seen as the main effectors in an adaptive anti-tumour immune response, therefore it is vital to quantify their number, define what subsets are present and their respective activation states within the tumour microenvironment. Investigations into TILs in human NB are limited, despite CD3+ cell infiltration being seen as a positive prognostic factor for many years [563,564]. To date two, studies have investigated TIL populations within human NB thoroughly [565,566]. CD8+ and CD4+ T cells have been reported in NB tumour samples [565], along with the NB TME favouring the activation of TILs at the tumour site, rather than inducing Treg accumulation [566]. In one study, Coughlin et al, demonstrated with flow cytometry, low levels of CD3+ cell infiltration in human NB samples, at around < 5% of all cells [504]. In **Figure 3.9**, it was demonstrated that all three murine models have low CD3+ (as % of total cells) cell infiltrate, which for NXS2 and TH-MYCN$^{+/-}$ was highly variable. 9464D was found to have the lowest percentage of CD3+ cells at between 0.5 – 2.5%. Another study by Carlson et al, looked at 8 primary NB samples and found the presence of CD3+ T cells which varied considerably between samples, with a mean of 4.5% [566]. In the case of total T cell infiltrate, the murine models were comparable to human NB, when comparing to the data currently available.

Although overall T cell percentages within the three mice models were found to be similar, differences in subsets was noted, as shown in **Figure 3.9 B**. Firstly, within the tumours of all three models, CD8+ cells as a percentage of all cells in the tumour, were similar throughout. However, CD4+ percentages to appear to be lowest in the 9464D tumours compared to other models. This is highlighted when looking at CD8:CD4 ratio in **Figure 3.9 D**, which showed that the 9464D tumours have a strikingly increased ratio compared to both of the other models. This shows that these tumours have considerably more CD8+ cells than CD4+ cells infiltrating the tumours. This may explain why there was a long latency period between tumour cell injection and first becoming

palpable in this model. If the tumour has a large amount of infiltrating CD8+ it may take longer for the tumour cells to escape from a T cell response and be able to grow out. Furthermore, a CD4:CD8 ratio in human NB was previously reported as 0.82, which suggests there are more CD8+ cells than CD4+ cells infiltrating within the human tumours [566].

When looking at the suppressive Treg subset it is clear that the percentage of Tregs, as a proportion of CD4+ cells, is significantly increased within the tumours of both the subcutaneous models compared to the TH-MYCN$^{+/-}$ model. As with the myeloid infiltrate, this difference may be down to the environment being extremely inflammatory due to its ectopic location, leading to an increase in suppressive cells attempting to reduce the immune response to prevent collateral tissue damage. This response is needed physiologically, however it is a great hindrance to the anti-tumour immune response. Data has previously shown that human NB had a fairly substantial FoxP3+ cell infiltration of between 40-55% of CD4+ cells, however this was only a small cohort of 3 patients [566]. The amount of Tregs seen in NXS2 and 9464D is high at approximately 60% of CD4 cells compared to TH-MYCN$^{+/-}$, which have a Treg infiltrate of~10% CD4+ cells. Therefore, none of the murine models accurately represent the Treg infiltrate reported in human NB. This is important, as Tregs play an important role in controlling the immune response to tumours and many current immunotherapies target these cells to modulate the immune response. A tumour model which has more Tregs compared to human tumours, may not show the same response as would be seen in humans, as therapies targeting these suppressive cells may be more effective at generating immune responses in these models compared to in human NB. The high levels of Treg cells within NXS2 and 9464D tumours could suggest a more suppressive tumour microenvironment. One way to assess how suppressive is the tumour microenvironment is by looking at the effector to suppressor cells ratio in the form of CD8+ to Treg ratio as shown in **Figure 3.8 D**. Importantly, the NXS2 tumours have a dramatically decreased ratio compared to 9464D tumours, despite having similar Tregs as a percentage of CD4+ cells. The low ratio seen in the NXS2 model is due to low numbers of CD8+ cells infiltrating the tumours and high levels of Tregs meaning the ratio is in favour of a suppressive environment as it is <1. Although 9464D tumours also have high numbers of Tregs, they have considerably more CD8+ cells infiltrating meaning the effector ratio stays relatively high. This suggests that the NXS2 tumour microenvironment is more suppressive, and therefore, may not be a fair representation of human NB.

Although TH-MYCN$^{+/-}$ spontaneous tumours appear to have more comparable immune infiltrates to human NB than the two subcutaneous models, the spontaneity of tumour appearance means it is difficult to set up therapy experiments at the same time as can be achieved with syngeneic models. Therefore an effort to establish a passage model of TH-MYCN$^{+/-}$ tumours was attempted as described in **Figure 3.10**. Here, a spontaneous tumour taken from a TH-MYCN$^{+/-}$ mouse was

disassociated into a single cells suspension. This was then repassaged into wild type 129/SvJ mice either SC or IP and monitored for tumour appearance and growth. Although the SC passaged tumour grew relatively well, over the course of two independent experiments, only 2 out of 7 IP passaged tumours presented, suggesting the tumour cells are not supported to grow in this environment. However, previous data has demonstrated successful growth of the 9464D cell line when injected orthotopically into adrenal glands, suggesting NB cells can be passaged into this anatomical location [541]. Despite this, these two tumours along with the subcutaneous passaged tumours were excised and their immune infiltrates analysed by flow cytometry to compare with previously collected spontaneous TH-MYCN$^{+/-}$ tumour data. Analysis of myeloid populations in **Figure 3.11** showed a higher percentage of macrophages in SC tumours compared to spontaneous tumours, with monocytes and neutrophils being relatively similar between the three tumour types. As was seen with the two subcutaneous models NXS2 and 9464D, this increase in macrophages within tumour microenvironments may be due to the ectopic location of tumour growth which could leads to a more inflammatory tumour microenvironment, which could recruit more macrophages than in the spontaneously developing tumours. Big differences in tumour B cells was demonstrated in **Figure 3.12 A**, with higher percentages seen in spontaneous TH-MYCN$^{+/-}$ tumours. Again this difference was also see when comparing the subcutaneous NXS2 and 9464D models, which suggest the environment a tumour grows in influences its immune infiltrate. Furthermore, when analysing T cell infiltrates, the SC and IP passaged tumours have a reduced CD3+ infiltrate compared to spontaneous tumours, again mirroring the data seen when comparing subcutaneous 9464D tumours to TH-MYCN$^{+/-}$ tumours. Furthermore, percentages of CD8+ and CD4+ were higher in spontaneous tumours compared to SC passaged tumours, which was also shown when comparing TH-MYCN$^{+/-}$ tumours to 9464D tumours. Although, unlike the NXS2 and 9464D SC tumours, percentages of the suppressive cells Tregs was similar for all three models.

All the immunophenotyping data of passaged TH-MYCN$^{+/-}$ tumours suggests that by changing the environment in which the tumour cells are growing, i.e. moving from the abdominal cavity to a subcutaneous space, the immune infiltrate within the tumours is altered. Furthermore the differences seen between spontaneous TH-MYCN$^{+/-}$ tumours and passaged SC tumours are comparable to the differences seen between the two subcutaneous NXS2 and 9464D models, and the TH-MYCN$^{+/-}$ tumours demonstrated in this Chapter. Due to these changes in the immune infiltrates from spontaneous TH-MYCN$^{+/-}$ tumours once passaged SC, and the unreliability of tumour appearance with the IP passaged tumours, passaging of TH-MYCN$^{+/-}$ tumours does not appear to be an appropriate model for NB.

Overall, this chapter demonstrates the differences in immune infiltrates in different murine NB models, and how these infiltrates can be altered by changing the location of the tumour cells.

Differences between the models is summarised in **Table 3.1**. Importantly, when comparing the three established murine NB models to human NB lymphocyte infiltrates, the two subcutaneous models have a high Treg cell influx, which was higher than has been reported in humans [566]. Furthermore the NXS2 model has a poor CD8+/CD4+ effector T cell infiltrate, whereas the 9464D model has a high percentage of infiltrating CD8+ cells, which is more comparable to previous reports of human NB tumours [565,566]. The spontaneous TH-MYCN$^{+/-}$ model however, may be more representative of human disease, with high GD2 expression, smaller macrophage infiltrate with similar infiltration, comparable CD8+ and CD4+ TILs and importantly, a downregulation of MHC class I.

Chapter 4: Immunogenic cell death induction and immune cell modulation by cyclophosphamide

4.1 Chapter introduction

It is becoming increasingly clear that the use of immunomodulatory antibodies as single agents may not be sufficient to generate therapeutic immunity, and combinational therapies may be required. Importantly, work into whether these immunomodulatory antibodies can be combined with chemotherapy to produce synergy is in progress [519]. As discussed in section 1.3, it may be the choice of chemotherapy that determines if synergy can be achieved with immunotherapy. Some chemotherapy agents have been demonstrated to induce an apparently 'immunogenic' form of cell death contrasting with the general assertion that chemotherapy induces non-immunogenic apoptosis[278]. In this immunogenic form of death, important factors are ectopically expressed or released from the dying cells which promote a potent immune response. ICD related markers include the release HMGB1 and ATP which attract APCs, and ecto-calreticulin and Hsp-70 expression on the cell surface which act as 'eat me' signals to migrating phagocytes. These ICD factors lead to activation and maturation of APC in the tumour microenvironment, which can then migrate to the tumour draining lymph node to stimulate a potent adaptive T cell driven immune response. Therefore, it seems logical when investigating the effectiveness of immunomodulatory antibody therapy, to combine it with chemotherapies which induce ICD rather than agents which do not. With regards to current NB treatment, a few of the chemotherapeutic agents used include proposed ICD inducers, such as DOX and CPM. Therefore, investigations into whether these agents can synergise with immunomodulatory antibody therapy are imperative. Another important factor to take into account is that many chemotherapeutics are regarded as immunosuppressive, at doses used classically in cancer therapy, and indeed CPM is commonly used as an immunosuppressive agent in patients with autoimmune conditions [260,261]. NB patients currently receive relatively high doses of these agents, which may not create a supportive immune environment for immunotherapy to follow. However, low doses of chemotherapy can be beneficial to the anti-tumour response, with reduced levels of immune suppression when compared to higher doses [339,365]. Therefore detailed examination of how low doses of chemotherapy alter immune subsets within the tumour microenvironment still need to be conducted, to ensure that important effector subsets for immunomodulatory antibody therapy are not supressed.

The use of immunomodulatory antibody therapies in paediatric cancers is in its infancy, with comparatively few trails currently being conducted compared to adult cancers. However, it has

been demonstrated that monoagent therapy of monoclonal antibody therapy may not hold any success in paediatric patients and therefore combination treatments will be required. One strategy for this is to use the possible immunogenic effects of chemotherapy agents already used in NB and combine them with the immune boosting immunotherapy to enhance the efficacy of treatments. As discussed in **Section 1.5.4,** paediatric cancers may be good immunotherapy targets, and the early promise shown by CAR T cell therapy and monoclonal antibody therapy in NB adds weight to this idea. Extensive pre-clinical and clinical experience of immunotherapy in melanoma may shine some light as to whether this approach could be effective in neuroblastoma, as these cells are embryologically linked to NB cells, both developing from the neural crest [28]. In melanoma, therapeutic potential of anti-PD-1 and anti-CTLA-4 therapy has been witnessed [406,418,422] , holding hope for these therapies in NB. It is worth noting however, that the mutational burden seen in melanoma, which has been linked to an improved immunotherapy response [18], is considerably higher than in NB. Furthermore, there are relatively low levels of infiltrating T cells within NB tumours, and this coupled with low mutational burden has led to NB as being classified a relatively immunologically 'cold' tumour. Consequently, using immunotherapy as a monoagent may not be very effective. However, the addition of an adjuvant, such as immunogenic CPM, that can either boost the infiltration of T cells or increase the mutational burden may improve outcomes with immunotherapy.

This chapter investigates the immunogenic effects of CPM in murine models of neuroblastoma. Firstly, the ability of CPM to induce expression of ICD markers on two neuroblastoma murine cell lines *in vitro* were assessed. The *in vivo* effects on the immune infiltrates into the tumour microenvironment were then investigated. Finally, an apoptosis resistant BCL-2 overexpressing NB cell line was developed and apoptosis resistant BCL-2 overexpressing mouse line was used to explore the relative importance of tumour cell death versus immune cell death in the *in vivo* mechanisms of action.

4.2 Results

4.2.1 Establishing *in vitro* cytotoxic doses of mafosfamide and doxorubicin on NB murine cell lines

In order to establish whether chemotherapies used in neuroblastoma therapy can lead to the induction of ICD markers of murine NB cell lines, an appropriate cytotoxic dose needed to be determined. As the NXS2 and 9464D cell lines used in this chapter are both adherent, measuring cell death accurately becomes a challenge. Using the widely assay of Annexin V and PI staining would not be appropriate here, as methods used to detach the cells from flasks leads to expression of cell surface proteins, resulting in inaccurate Annexin V staining [567]. Therefore, a MTT assay was employed to infer cell death by measuring metabolic activity of the cells. This assay assesses how metabolically active cells are by their ability to convert the MTT dye into formazan crystals which are then solubilised [550]. Cells which are not metabolically active, due to cell cycle arrest or death, will not convert the dye into crystals. This is detected in the assay as a colour change.

4.2.1.1 Determining a standard curve and cell seeding density for NXS2 and 9464D cell lines with a MTT assay

Firstly, an appropriate seeding density for both NXS2 and 9464D needed to be determined. To achieve this cells were plated out at densities to form a standard curve ranging from $1x10^3$ to $2x10^5$ and a standard curve established (**Figure 4.1**). The curves produced established that a seeding density of $0.5x10^5$ per well would be most appropriate for use in further MTT assays as this value has a mean absorbance within the middle, most linear part, of the curve, which would permit more accurate measurements of cell number changes.

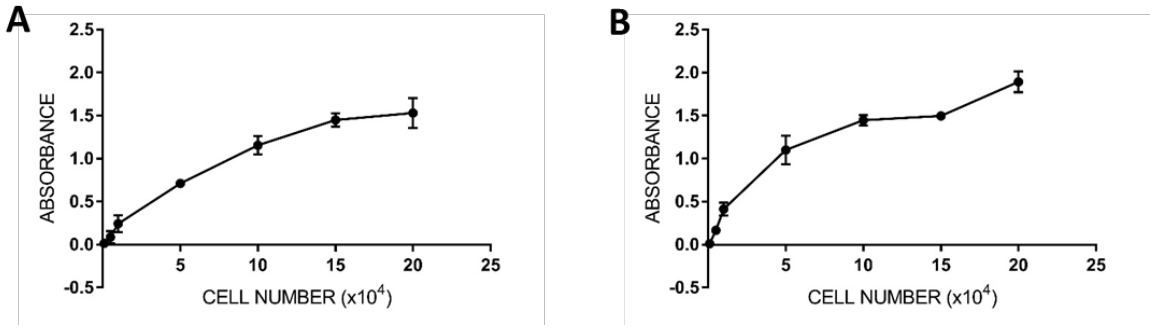

Figure 4.1 MTT standard curve optimisation with murine cell lines

A) Standard curve for NXS2 cell line plated at cell densities from 1×10^3 to 2×10^5. Cells were treated with MTT assay kit and absorbance measured. **B)** Standard curve established for 9464D as in A. Representative example of n=3. Mean and SD error bars are shown.

4.2.1.2 Assessing metabolic activity after chemotherapy application

The MTT assay and the standard curves established above (**Figure 4.1**) were used to establish the effect of different doses of chemotherapy on the metabolic activity of the respective cell lines, in order to identify the minimum cytotoxic dose.

As CPM is a pro-drug that requires metabolising in the liver to forms for *in vitro* experiments the metabolically active form of the drug, mafosfamide (MAF) was used [260]. Both cell lines were subjected to MAF treatment at a range of doses, based on the literature[519], to gauge their sensitivity. **Figure 4.2 A+B** show that 9464D is more resistant to MAF treatment when compared to NXS2. Whereas concentrations 33 µg/ml to 50 µg/ml completely supressed metabolic activity of the NSX2 cell line, these doses had little effect on 9464D cells. Therefore, the range of concentrations was increased and the assay repeated for 9464D which showed that these higher doses were able to halt metabolism within the cells (**Figure 4.2 C**).

The MTT assay was also employed to assess cytotoxicity of doxorubicin (DOX). As shown in **Figure 4.3**, at lower doses of DOX (2.5 µm) the 9464D cell lines appears slightly more resistant, with a smaller reduction in metabolic activity seen here than in the NXS2 cell line. At higher doses, the metabolic activity of both cells lines is reduced to zero.

From these data a cytotoxic dose for use in future experiments for MAF was decided to be 50 µg/ml for NXS2 and 75 µg/ml for 9464D. For doxorubicin, the dose was decided to be 40 µM for both of the cell lines. These specific doses were chosen as they induced either complete or near complete cessation in metabolic activity from which it can be inferred that most cells will either be dead or dying.

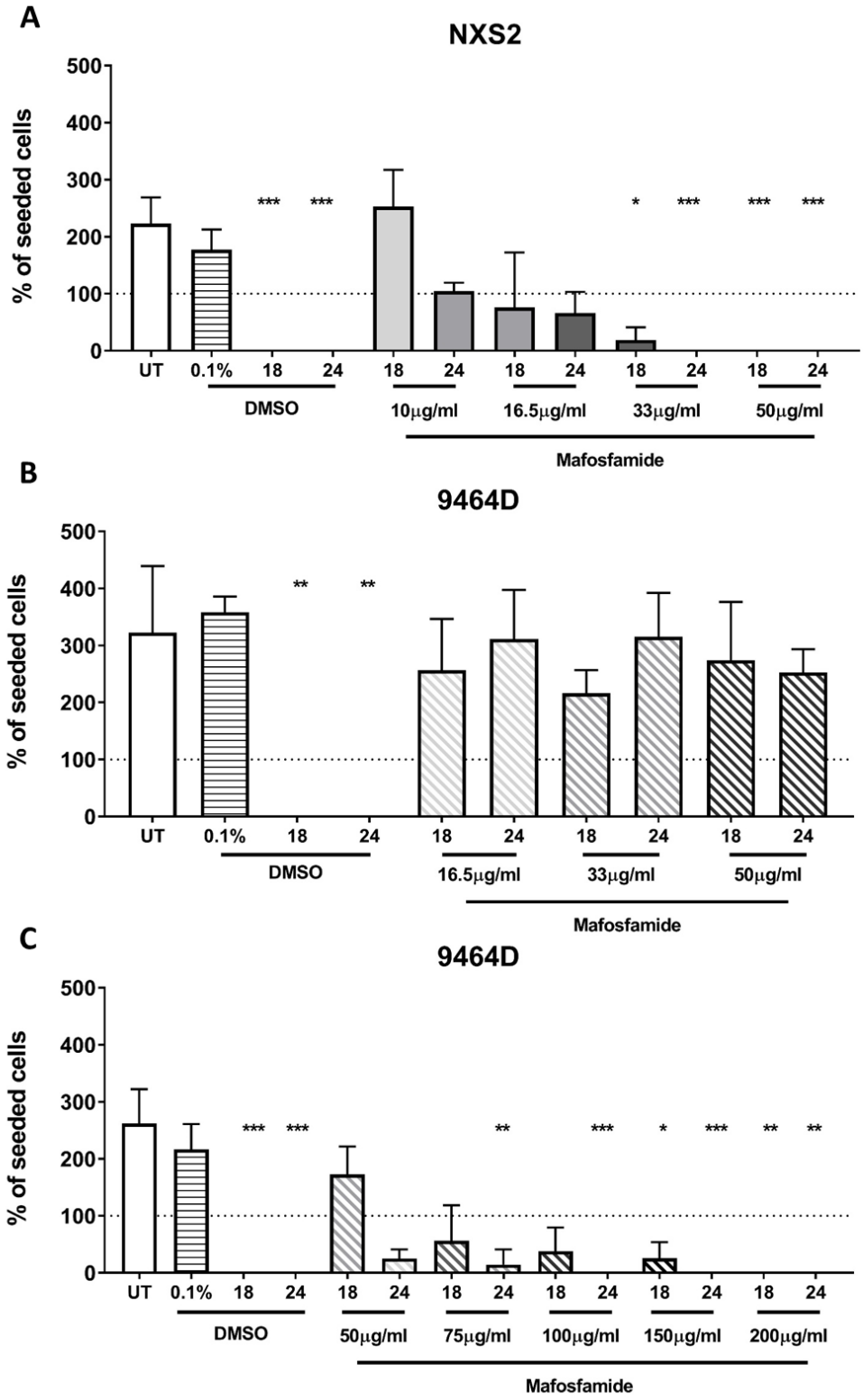

Figure 4.2 Percentage of seeded cells remaining after administration of mafosfamide

A) Cells were plated in a 96-well plate at a concentration of $5x10^4$ per well. MAF dosing was conducted as detailed in **Section 2.10.1**, with MTT assay being followed as detailed in **Section 2.10.2**. Cell numbers were calculated using a standard curve as set up in **Figure 4.1 C**. Percentage of seeded NXS2 cells remaining metabolically active after MAF administration are shown, with the same demonstrated in **B)** for 9464D cells. **C)** Higher MAF dosing using 9464D cells. n=3 (A+C), n=2(B). Significance calculated for each condition compared to untreated cells. Statistical analysis was conducted using Krusksal Wallis test with Dunn's multiple comparisons with all groups compared to UT group, and denoted as: *= <0.05. Means and SD error bars are shown

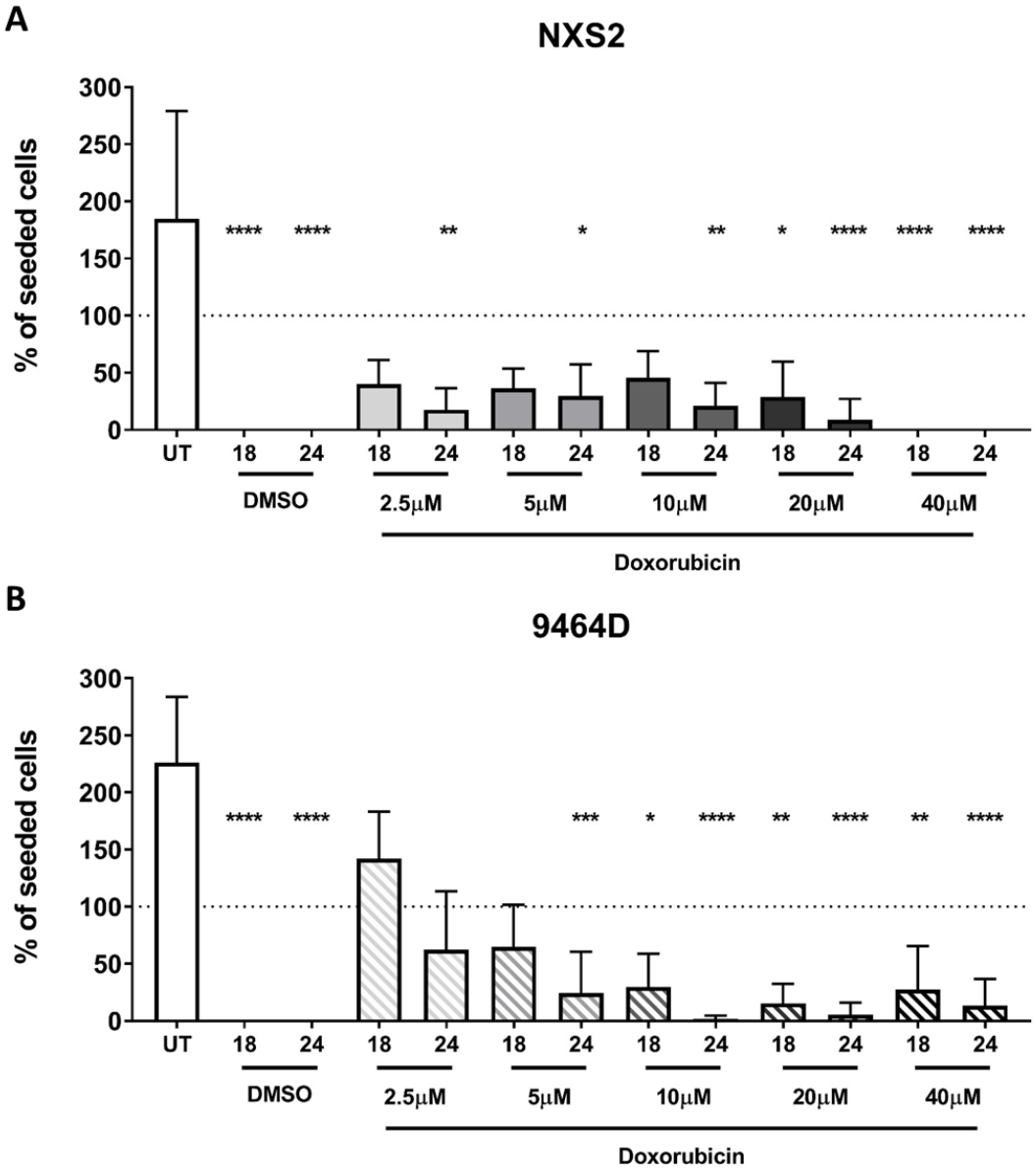

Figure 4.3 Percentage of seeded cells remaining after doxorubicin administration

A) Cells were plated in a 96-well plate at a concentration of $5x10^4$ per well. DOX dosing was conducted as detailed in **Section 2.10.1**, with MTT assay being followed as detailed in **Section 2.10.2**. Cell numbers were calculated using a standard curve as set up in **Figure 4.1 D**. Percentage of seeded NXS2 cells remaining metabolically active after DOX administration, is shown, with the same demonstrated in **B)** for 9464D cells. **C)** Higher MAF dosing using 9464D cells. n=3. Significance calculated for each condition compared to untreated cells. Statistical analysis was conducted using Krusksal Wallis test with Dunn's multiple comparisons with all groups compared to UT group, and denoted as: *= <0.05. Means and SD error bars are shown.

4.2.2 Induction of immunogenic cell death markers on NB cells after chemotherapy treatment *in vitro*

As discussed previously, some chemotherapeutics are now starting to be regarded as immunogenic due to their ability to cause expression of ICD markers and stimulate an anti-tumour immune response [278]. CPM and DOX are two such chemotherapy agents. However, most of the data reported to date has been in the context of the CT26 murine tumour model. Therefore, it was important to see whether these chemotherapies can have the same effect of inducing the expression of these markers on murine neuroblastoma cell lines *in vitro*.

4.2.2.1 Ecto-CRT and Hsp-70 expression on NB cell lines after cytotoxic drug application

Using the doses determined in **section 4.2.1**, both NXS2 and 9464D were plated and incubated with the chemotherapies for 24 hours before being harvested. Expression of two ICD-related makers, ecto-CRT and Hsp-70, were then assessed by flow cytometry, on treated and untreated cells. The geometric mean fluorescence intensity (geoMFI), reflective of expression of each marker, is shown in **Figure 4.4 A**. Exposure to either MAF or DOX resulted in an increase in the percentage of PI+ cells compared to untreated cells, for both cell lines, which was significant for DOX (**Figure 4.4 B**). This suggests that both MAF and DOX are leading to cell death in NXS2 and 9464D cells.

Figure 4.4 C demonstrates an increase in expression of ecto-CRT on each cell line after culture with either of the chemotherapies, compared to untreated dead cells. In the NXS2 cells, MAF seems to increase ecto-CRT more so than DOX, whereas in 9464D the increase seems to be of a similar range. For HSP-70 in **Figure 4.4 D**, a similar scenario is seen with both chemotherapies causing an increase, which is significant for DOX, in surface expression above untreated cells for both of the cell lines.

Overall, there seems to be an increase, in two important ICD markers upon application of two cytotoxic agents within two murine NB cell lines. However, it is worth noting that the increases for MAF and ecto-CRT are not statistically significant, potentially due to large variation between individual experiments.

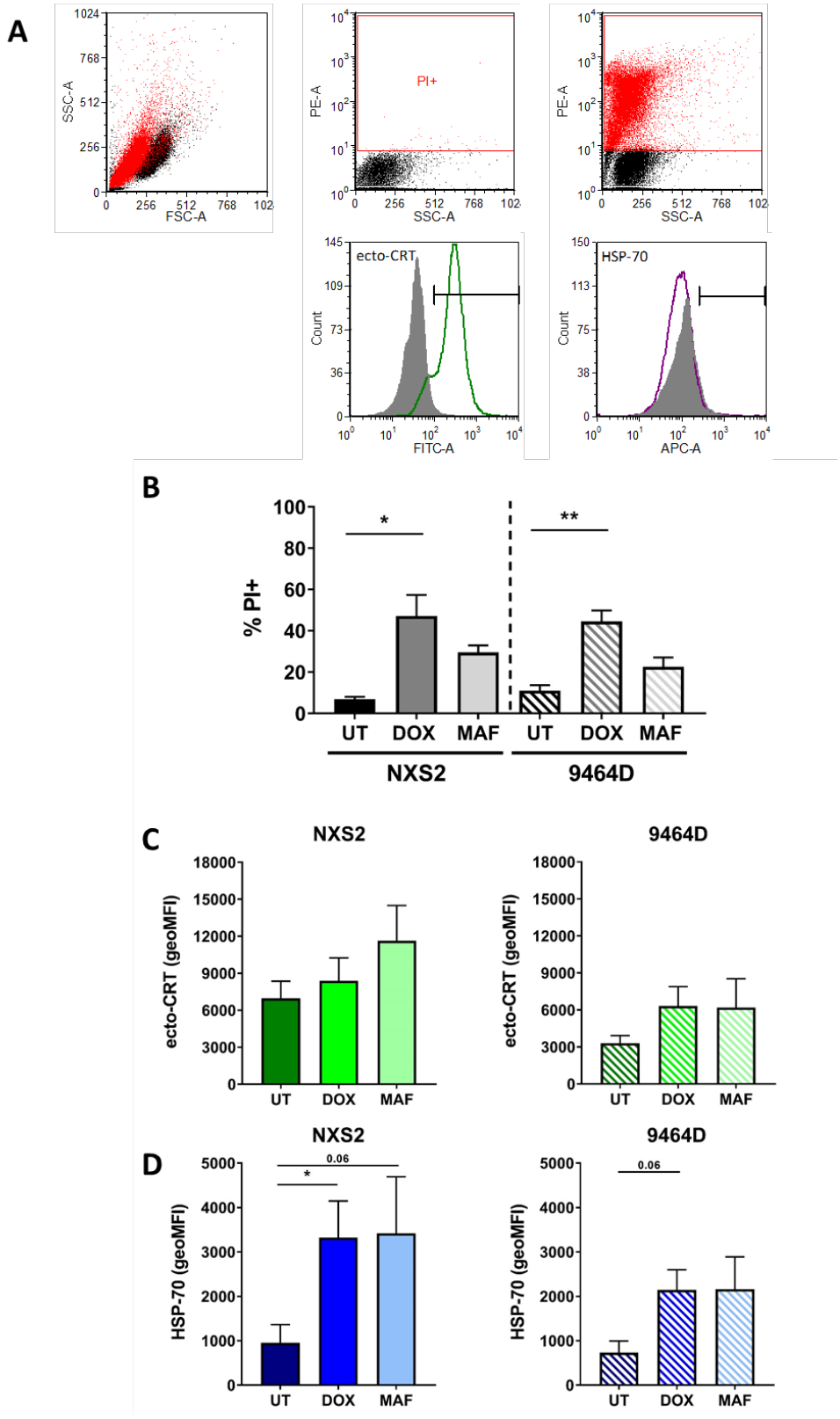

Figure 4.4 Expression of ecto-CRT and HSP-70 on NXS2 and 9464D cells after chemotherapy application

A) NXS2 and 9464D cells were plated in a 96-well plate at a concentration of $5x10^4$ per well, and assay was conducted as detailed in **Section 2.11**. Background isotype geoMFI was subtracted from the target geoMFI. Gating strategy used to calculate PI+ cells and geoMFI, showing a representative plot is shown. **B)** PI+ staining for both NXS2 and 9464D lines. **C)** ecto-CRT expression on NXS2 cells (left) and 9464D (right). **D)** HSP-70 expression for NXS2 (left) and 9464D (right) cells. n=6 (NXS2); n=5 (9464D). Significance calculated for each condition compared to untreated cells using Kruskal Wallis test with Dunn's multiple comparisons, and denoted as: *= <0.05. Means and SEM error bars are shown.

4.2.2.2 Expression of HMGB1 in 9464D cells *in vitro* after MAF treatment, and *ex vivo* after CPM

Another suggested ICD marker is HMGB1. This protein is established to be a 'danger signal' released from dying cells which can attract phagocytes such as macrophages, and other immune cells. As detailed in **Section 1.4.3**, this molecule has been implicated as a key mediator of ICD after chemotherapy application. To investigate whether HMGB1 expression or location changes after chemotherapy, immunofluorescence staining was used on non-treated and MAF treated 9464D cells. **Figure 4.5 A** demonstrates that in NT cells, HMGB1 levels are highest within the nucleus of cells with diffuse cytoplasmic staining also observed. Conversely, in MAF treated 9464D cells (**Figure 4.5 B**), HMGB1 is restricted to the nucleus, with little cytoplasmic staining seen. However, this may be due to changes in cell morphology caused by the MAF treatment, leading to reduction in cytoplasm area and a smaller nucleus. Despite this, the distribution and intensity of HMGB1 staining is very different between the NT and MAF treated cells, with the nuclear staining being more punctate and less intense in MAF treated cells

Expression of HMGB1 was also assessed ex vivo in FFPE sections from mice bearing 9464D SC tumours treated or not with CPM (**Figure 4.6**). Here, it was demonstrated that in NT tumours HMGB1 staining was strong and diffuse across the whole section, with nuclear staining also observed (**Figure 4.6 A**). Within the sections from CPM treated tumours (**Figure 4.6 B**) strong nuclear staining was seen, with reduced and diffuse cytoplasmic staining. These data corroborate the HMGB1 staining seen in the *in vitro* assay in **Figure 4.5**.

These results could be inferred to suggest that the HMGB1 has been secreted from the MAF treated cells, as has been reported to occur under cell stress and during ICD [221,318].

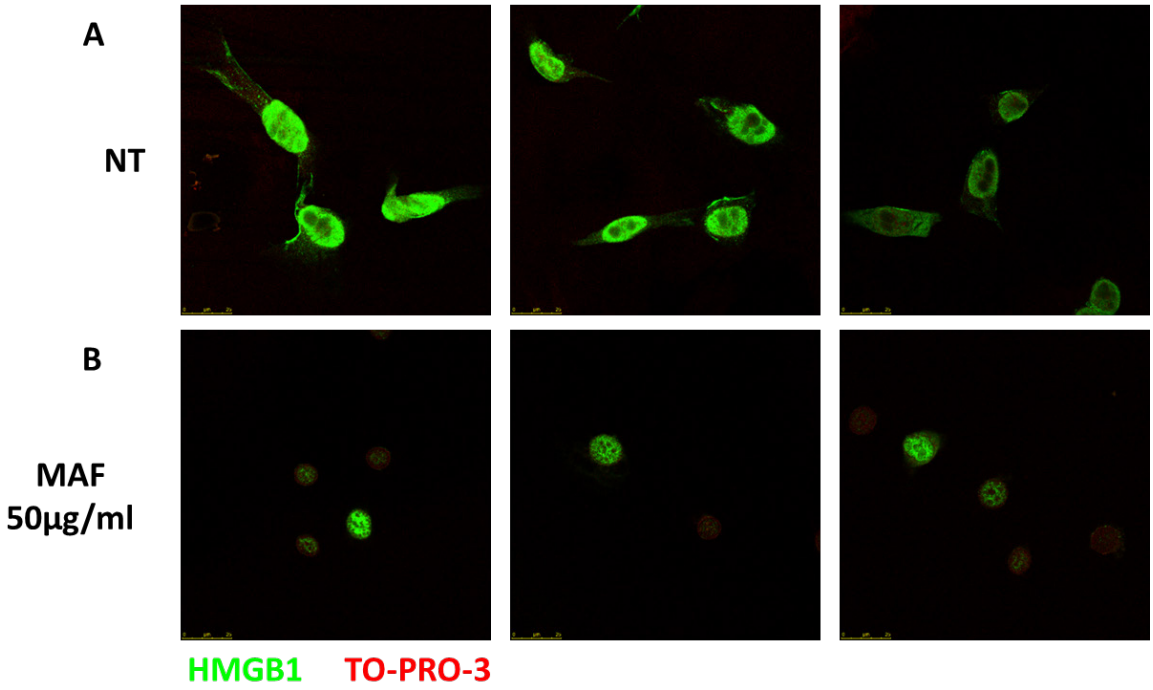

Figure 4.5 Expression of HMGB1 after MAF application in 9464D cells

A) 9464D cells were coated onto coverslips and treated with MAF at 50 ug/ml for 24 hrs and IF staining and confocal microscopy was conducted as described in **Section 2.14.5**. HMGB1 staining is shown on NT 9464D cells and **B)** MAF 9464D cells. 3 representative images are shown.

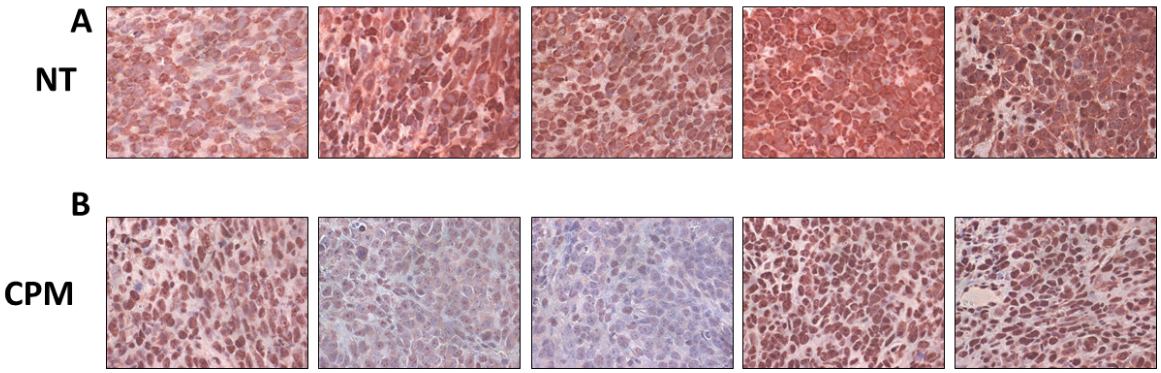

Figure 4.6 HMGB1 staining of FFPE 9464D tumours after CPM administration

A) $5x10^5$ 9464D cells were inoculated subcut into C57BL/6 females. Tumour growth was monitored and once reached 8x8 mm mice were either NT or **B)** given CPM 40 mg/kg. Tumours were harvested 3 days later to be FFPE as detailed in **Section 2.14.4**. A representative image is shown from 5 different tumours for each condition.

4.2.3 Immunophenotyping of NXS2 and 9464D tumours *ex vivo* after CPM administration

This chapter has so far demonstrated that MAF, a metabolite of CPM, is able to induce ecto-CRT and HSP-70 expression in murine NB cell lines and that differences in HMGB1 staining and location were also induced *in vitro* and *in vivo* by both MAF and CPM. These data support the potential direct ICD effects of CPM on tumour growth and therapy. However, CPM has been documented to have direct immunomodulatory effects upon immune cells infiltrating the tumour microenvironment [568]. Most notably, Treg specific depletion has been detailed both in preclinical models and in human disease [339,366].

Therefore, focus was shifted to investigate how CPM administration could modulate immune cells within the *in vivo* tumour microenvironment. To do this, as shown in **Figure 4.7**, NXS2 and 9464D subcutaneous tumour models were established. Once tumours reached a size of around 8x8 mm, CPM was administered at doses ranging from 20 to 150 mg/kg. After 72 hrs, tumour and spleen tissues were harvested, disaggregated and stained for immunophenotyping by flow cytometry. The gating strategies used to detect various populations are shown in (**Figure 3.3** and **Figure 3.4**).

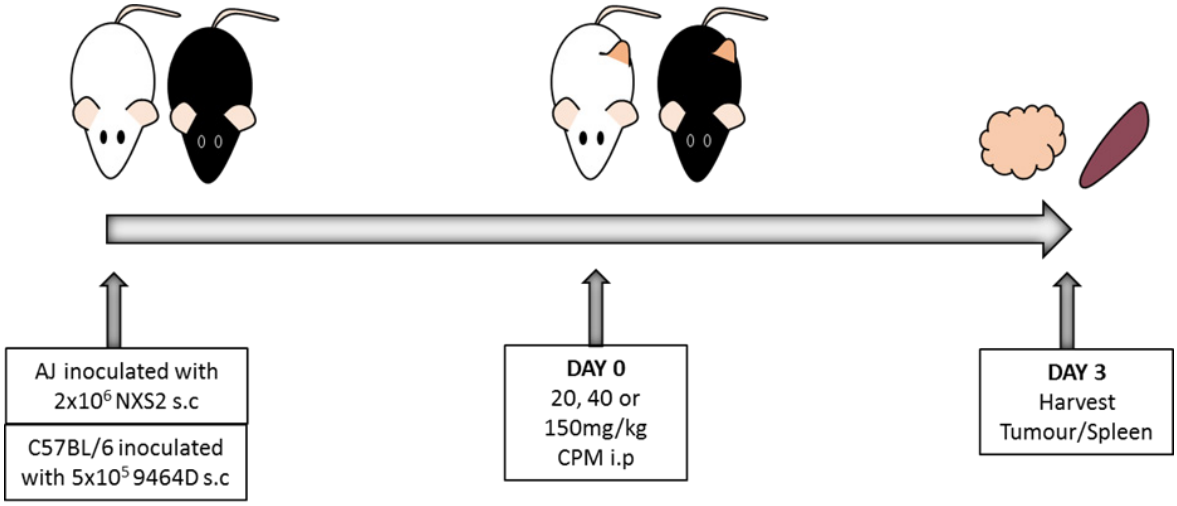

Figure 4.7 Experimental schematic of NXS2 and 9464D Immunophenotyping

Female AJ or C57BL/6 mice were injected SC with $2x10^6$ NXS2 or $5x10^5$ 9464D cell respectively as detailed in **Sections 2.5 and 2.6**. Tumour growth was monitored and once tumours had reached ~8x8 mm, mice were injected with either 20, 40 or 150 mg/kg CPM i.p. After 72 hrs tumours and spleens were harvested and processed for immunophenotyping by flow cytometry as detailed in **Section 2.9**.

4.2.3.1 Effects of CPM on myeloid infiltration in NXS2 and 9464D spleens and tumours

Spleen and tumour myeloid cell populations were investigated and results shown in **Figure 4.8** and **Figure 4.9** for NXS2 and 9464D respectively. Notably, for both NXS2 and 9464D, all doses of CPM led to an increase in the percentage of TAMs compared to non-treated mice and this increase was statistically significant at the 150mg/kg dose. This high dose also saw a significant increase in splenic macrophages. Percentages of monocytes and neutrophils were fairly consistent between the treatment groups, except for a significant increase in monocytes in spleens of mice treated with 40 mg/kg CPM.

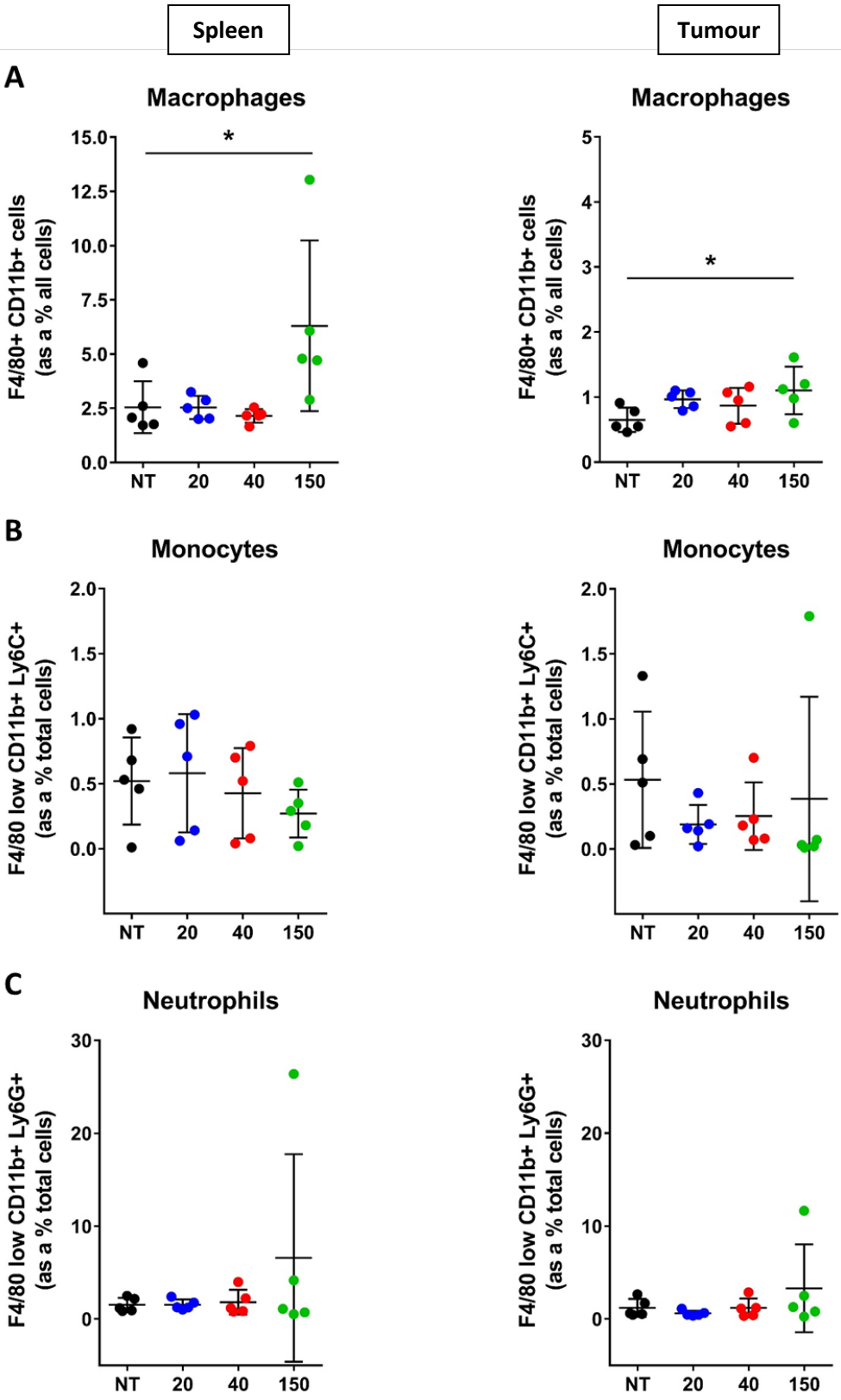

Figure 4.8 Effect of CPM administration on myeloid infiltrates in NXS2 tumours and spleens

A) NXS2 tumour bearing mice were treated with either 20, 40 or 150 mg/kg CPM and at Day 3 spleens and tumours were harvested as detailed in **Figure 4.7**, processed for flow cytometry for immunophenotyping as detailed in **Section 2.9**. Populations were defined as detailed in **Figure 3.3**. Macrophages as a percentage of total cells is shown, for spleen (left) and tumour (right). **B)** The same as in A for Monocytes, and **C)** Neutrophils. n= 5.Data pooled from two independent experiments Statistical analysis was conducted using Kruskal Wallis test with Dunn's multiple comparisons, and denoted as: *= <0.05. Means and SD error bars are shown.

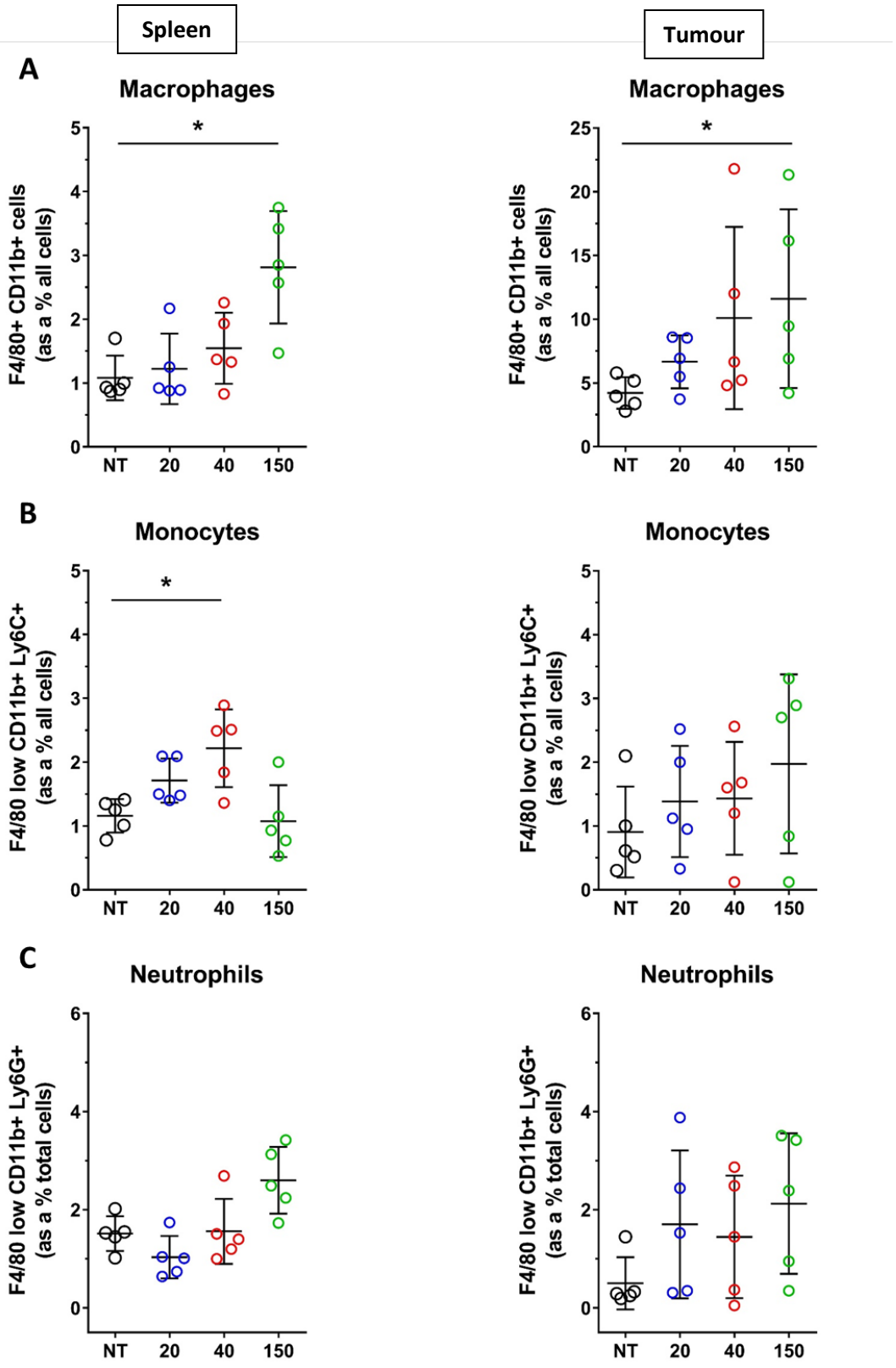

Figure 4.9 Effect of CPM administration on myeloid infiltrates in 9464D tumours and spleens

A) 9464D tumour bearing mice were treated with either 20, 40 or 150 mg/kg CPM and at Day 3 spleens and tumours were harvested as detailed in **Figure 4.7**, processed for flow cytometry for mmunophenotyping as detailed in **Section 2.9**. Populations were defined as detailed in **Figure 3.3**. Macrophages as a percentage of total cells is shown, for spleen (left) and tumour (right). **B)** The same as in A for Monocytes, and **C)** Neutrophils. n= 5. Statistical analysis was conducted using Krusksal Wallis test with Dunn's multiple comparisons, and denoted as: *= <0.05. Means and SD error bars are shown.

4.2.3.2 Effects of CPM on B cell, NK and NKT cell infiltration in NXS2 and 9464D tumours and spleens

Effects of CPM on non-T cell lymphocytes is demonstrated in **Figure 4.10** and **Figure 4.11**. Strikingly, B cells were shown to be particularly sensitive to CPM, with the higher dose resulting in a near complete depletion of B cells in both spleens and tumours of NXS2 tumour bearing AJ mice (**Figure 4.10 A**). A more modest reduction was seen in B cell numbers in 9464D tumour bearing C57BL/6 spleens (**Figure 4.11 A)**.

Figure 4.10 B+C demonstrates that the high 150 mg/kg CPM dose also resulted in an increase in both NK and NKT cells in spleens of NXS2 tumour bearing mice. This was significant for NKT cells and was also seen within spleens of 9464D tumour bearing mice, although this was not significant (**Figure 4.11 C**).

Aside from B cell reduction in the NXS2 model, little modulation seen of these cell types with any of the doses of CPM in tumours. Data was quite variable and there is low levels of infiltration of these cells into both tumour models in NT tumour conditions, which may explain this variability.

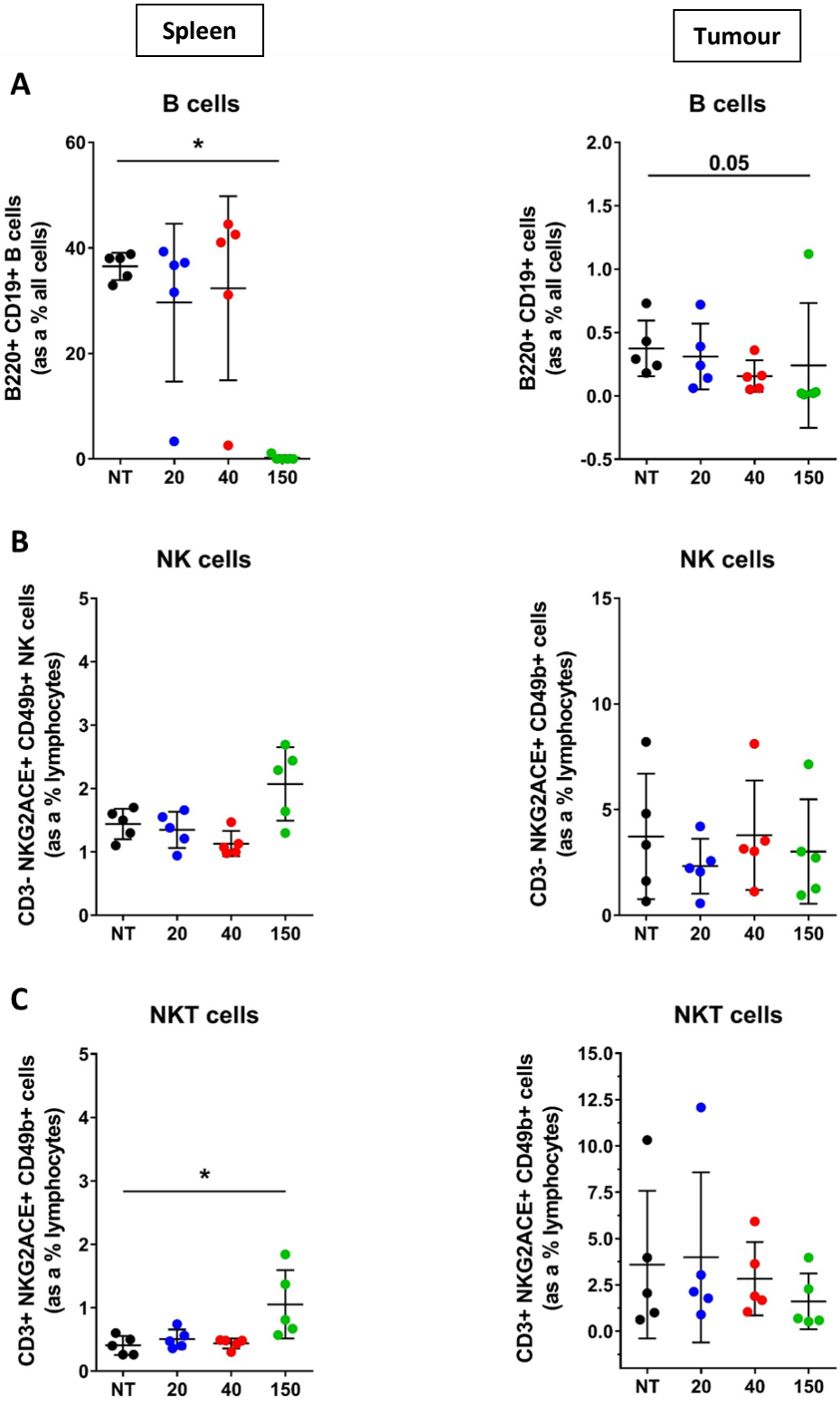

Figure 4.10 Effect of CPM administration on B, NK and NKT cell infiltrates in NXS2 tumours and spleens

A) NXS2 tumour bearing mice were treated with either 20, 40 or 150 mg/kg CPM and at Day 3 spleens and tumours were harvested as detailed in **Figure 4.7**, processed for flow cytometry for immunophenotyping as detailed in **Section 2.9**. Populations were defined as detailed in **Figure 3.4**. B cells as a percentage of total cells are shown, for spleen (left) and tumour (right). **B)** The same as in A for NK cells, and **C)** NKT cells. n= 5.Data pooled from two independent experiments Statistical analysis was conducted using Kruskal Wallis test with Dunn's multiple comparisons, and denoted as: *= <0.05. Means and SD error bars are shown.

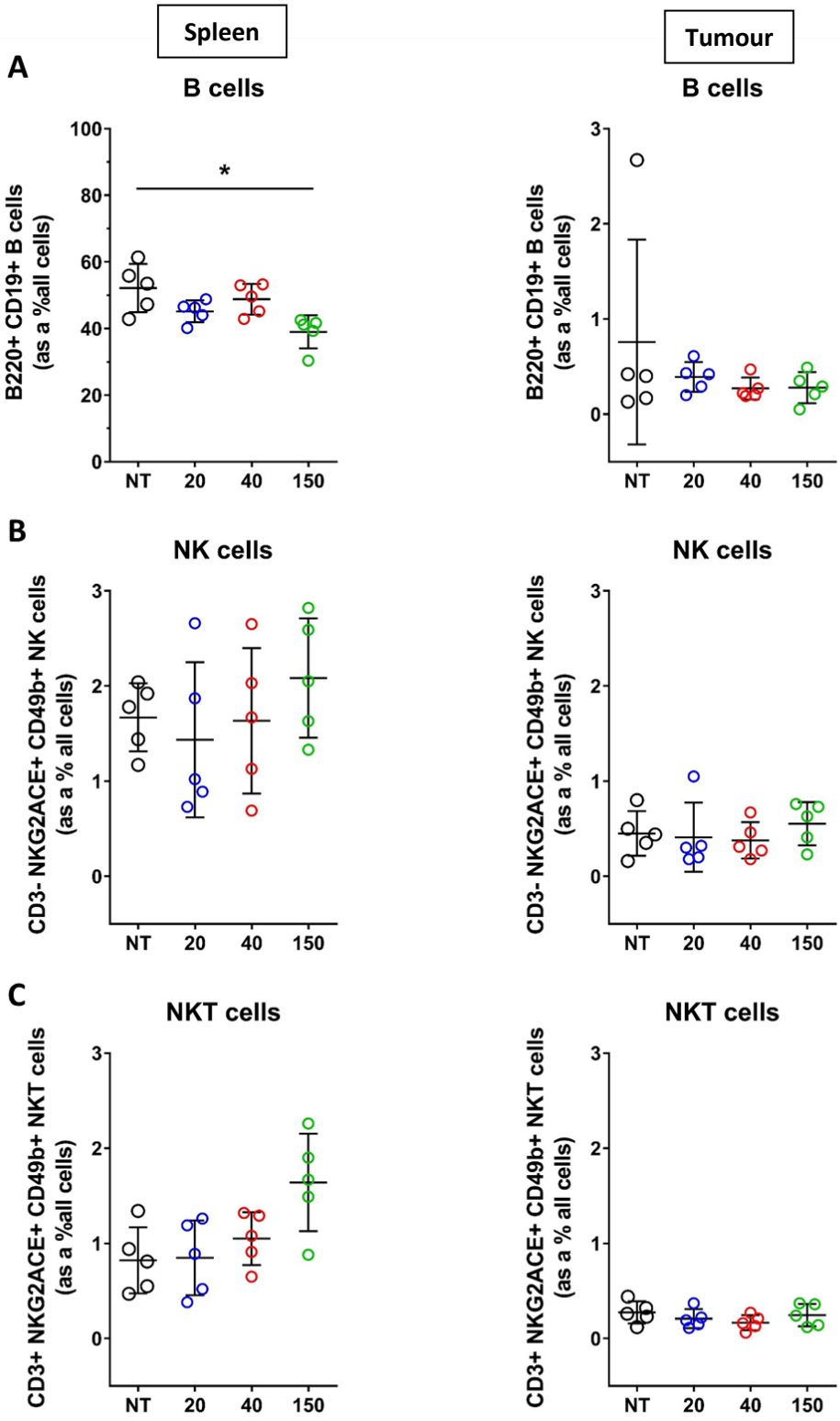

Figure 4.11 Effect of CPM administration on B, NK and NKT cell infiltrates in 9464D tumours and spleens

A) 9464D tumour bearing mice were treated with either 20, 40 or 150 mg/kg CPM and at Day 3 spleens and tumours were harvested as detailed in **Figure 4.7**, processed for flow cytometry for mmunophenotyping as detailed in **Section 2.9**. Populations were defined as detailed in **Figure 3.4**. B cells as a percentage of total cells are shown, for spleen (left) and tumour (right). **B)** The same as in A for NK cells, and **C)** NKT cells. n= 5. Statistical analysis was conducted using Kruksal Wallis test with Dunn's multiple comparisons, and denoted as: *= <0.05. Means and SD error bars are shown.

4.2.3.3 Effects of CPM on T cell infiltration in NXS2 and 9464D tumours and spleens

A substantial amount of previous research into CPM immune modulation has focused on T cells and specific subsets within them, as the balance between these cells is considered critical to the generation of an anti-tumour immune response. Consequently, modulation of these subsets was investigated here in NXS2 and 9464D NB models.

CPM resulted in a significant increase in the proportion of CD3+ cells in the spleens of both NXS2 (**Figure 4.12 A**) and 9464D tumour bearing mice (**Figure 4.13 A**). An inverse trend was seen in tumours, with a significant reduction in 9464D tumours treated with 40 mg/kg CPM. No significant changes were seen in CD8+ and CD4+ subsets, in either spleens or tumours of NXS2 mice, (**Figure 4.12 B+C)**. However, in the 9464D model after high dose CPM (**Figure 4.13 B+C**), CD4+ and CD8+ cells were observed to increase within tumours and decrease within spleens.

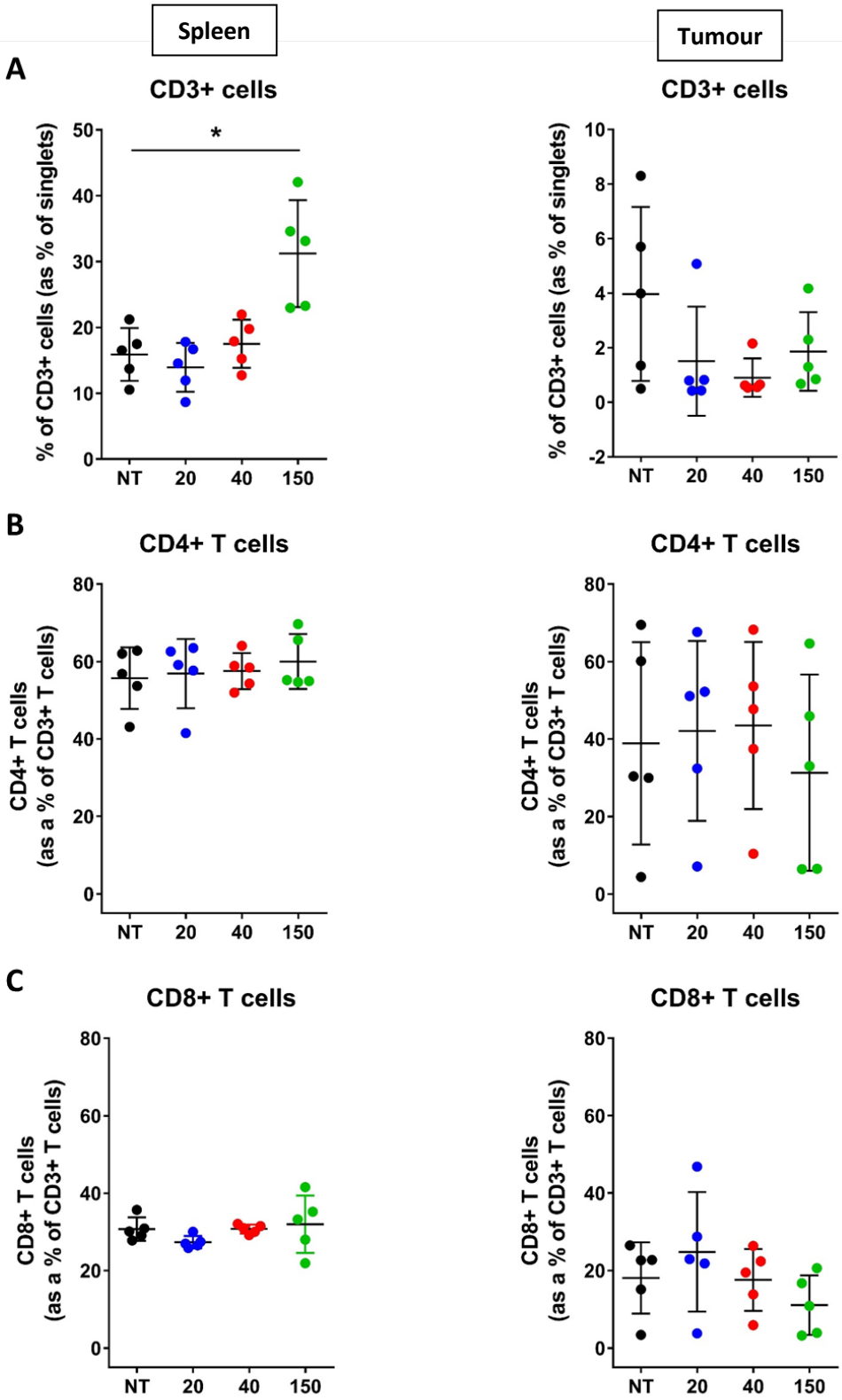

Figure 4.12 Effect of CPM administration on T cell infiltrates in NXS2 tumours and spleens

A) NXS2 tumour bearing mice were treated with either 20, 40 or 150 mg/kg CPM and at Day 3 spleens and tumours were harvested as detailed in **Figure 4.7**, processed for flow cytometry for mmunophenotyping as detailed in **Section 2.9**. Populations were defined as detailed in **Figure 3.4**. CD3+ cells as a percentage of total cells are shown, for spleen (left) and tumour (right). **B)** The same as in A for CD4+ cells as a percentage of CD3+, and **C)** CD8+ cells as a percentage of CD3+. n= 5.Data pooled from two independent experiments Statistical analysis was conducted using Krusksal Wallis test with Dunn's multiple comparisons, and denoted as: *= <0.05. Means and SD error bars are shown.

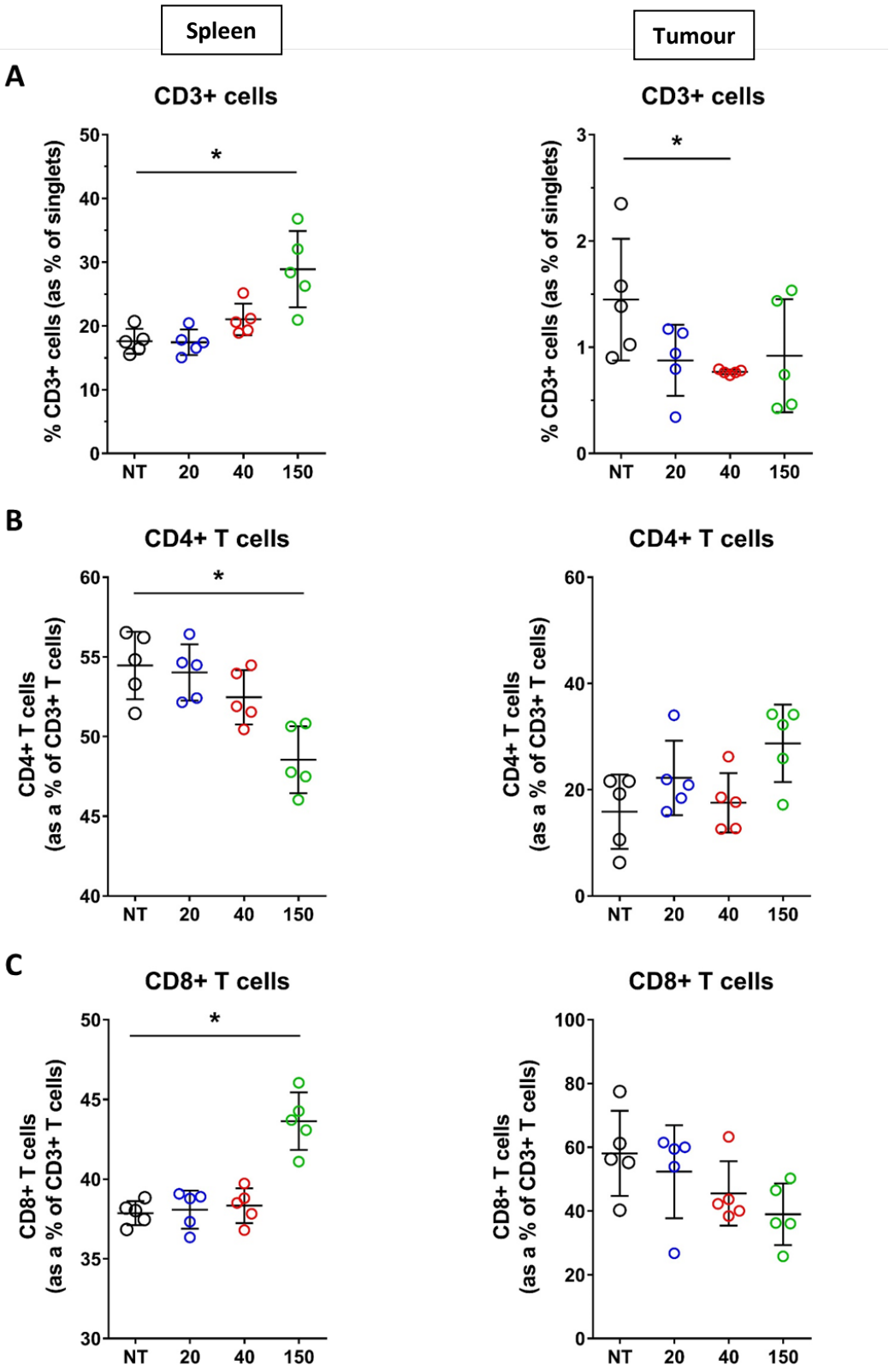

Figure 4.13 Effect of CPM administration on T cell infiltrates in 9464D tumours and spleens

A) 9464D tumour bearing mice were treated with either 20, 40 or 150 mg/kg CPM and at Day 3 spleens and tumours were harvested as detailed in **Figure 4.7**, processed for flow cytometry for mmunophenotyping as detailed in **Section 2.9**. Populations were defined as detailed in **Figure 3.4**. CD3+ cells as a percentage of total cells are shown, for spleen (left) and tumour (right). **B)** The same as in A for CD4+ cells as a percentage of CD3+, and **C)** CD8+ cells as a percentage of CD3+. n= 5. Statistical analysis was conducted using Krusksal Wallis test with Dunn's multiple comparisons, and denoted as: *= <0.05. Means and SD error bars are shown.

4.2.3.4 Effects of CPM on Treg infiltration and T cell ratios in NXS2 and 9464D tumours and spleens

Treg cells (defined as CD4+ FoxP3+) infiltrating in tumours were also assessed. Importantly, in NXS2 tumours almost half of Tregs were depleted with all CPM doses, which was significant in 40 and 150 mg/kg (**Figure 4.14 A**), and also demonstrated in 9464D at 40 mg/kg (**Figure 4.15 A**). Due to this depletion, an increase in both CD8:Treg and CD4+ FoxP3-:Treg ratio was observed in NXS2 tumours (**Figure 4.14 B+C)**. These ratios were more variable for 9464D and therefore no significant changes were seen (**Figure 4.15 B+C**).

Significant Treg depletion noted within the tumours of the two models was not demonstrated in the spleens of the mice (**Figure 4.12 A** and **Figure 4.13 A**). However 150mg/kg CPM increased the CD8:Treg and CD4:Treg ratio in both NXS2 and 9464D spleens.

Taking into account all the data presented in **section 4.2.3**, a low dose of 40 mg/kg CPM was used for future investigations into the immunomodulatory properties of this chemotherapy. This dose had minimal depletive effects on CD8 and CD4 T cells, while significantly depleting Treg cells.

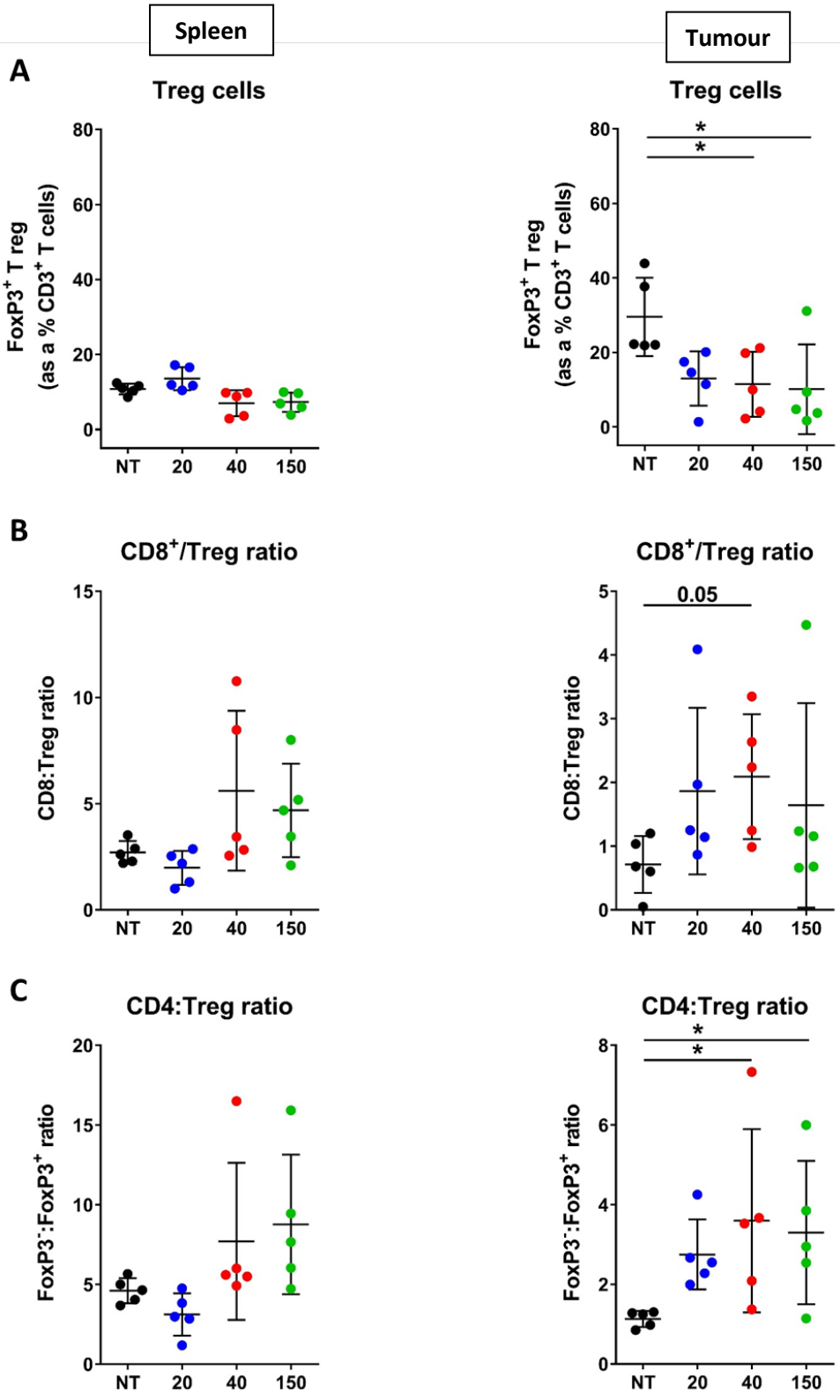

Figure 4.14 Effect of CPM administration on Treg cell infiltrates and T cell ratios in NXS2 tumours and spleens

A) NXS2 tumour bearing mice were treated with either 20, 40 or 150 mg/kg CPM and at Day 3 spleens and tumours were harvested as detailed in **Figure 4.7**, processed for flow cytometry for mmunophenotyping as detailed in **Section 2.9**. Populations were defined as detailed in **Figure 3.4**. Treg cells as a percentage of CD3+ cells are shown, for spleen (left) and tumour (right). **B)** CD8:Treg ratio, and **C)** CD4:Treg ratio. n= 5.Data pooled from two independent experiments Statistical analysis was conducted using Krusksal Wallis test with Dunn's multiple comparisons, and denoted as: *= <0.05. Means and SD error bars are shown.

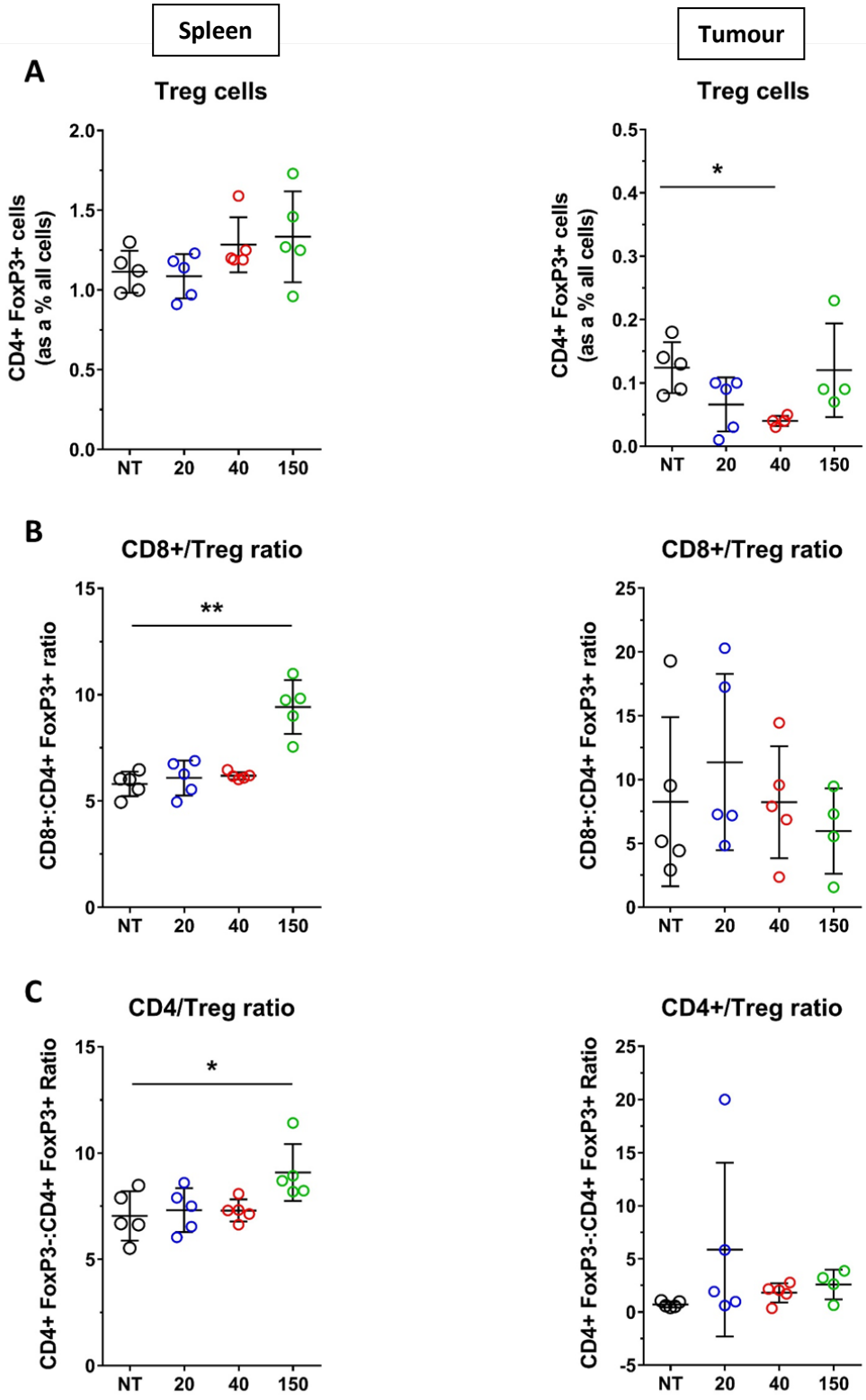

Figure 4.15 Effect of CPM administration on Treg cell infiltrates and T cell ratios in 9464D tumours and spleens

A) 9464D tumour bearing mice were treated with either 20, 40 or 150 mg/kg CPM and at Day 3 spleens and tumours were harvested as detailed in **Figure 4.7**, processed for flow cytometry for immunophenotyping as detailed in **Section 2.9**. Populations were defined as detailed in **Figure 3.4**. Treg cells as a percentage of CD3+ cells are shown, for spleen (left) and tumour (right). **B)** CD8:Treg ratio, and **C)** CD4:Treg ratio. n= 5. Statistical analysis was conducted using Kruskal Wallis test with Dunn's multiple comparisons, and denoted as: *= <0.05 and **= <0.01. Means and SD error bars are shown.

4.2.4 T cell subset modulation after CPM administration in non-tumour tissues

With depletion of Tregs observed only within the tumour microenvironment and not in spleens, further investigations were conducted into whether CPM specifically targeted tumour Tregs. Firstly, T cell populations within both tumour draining (dLN) and non-draining LNs (ndLNs) after CPM was analysed, using the gating strategy presented in **Figure 4.16**. dLNs were defined as the inguinal LNs, due to the location of the SC tumours, whereas ndLNs were defined as axillary LNs.

In both NXS2 (**Figure 4.17 A**) and 9464D (**Figure 4.17 B**), no modulation of CD8+ and CD4+ cells was observed. However, a significant increase in the percentages of both CD8+ and CD4+ T cells was observed in 9464D ndLNs. No depletion in Treg cells was seen in dLNs and ndLNs in both models.

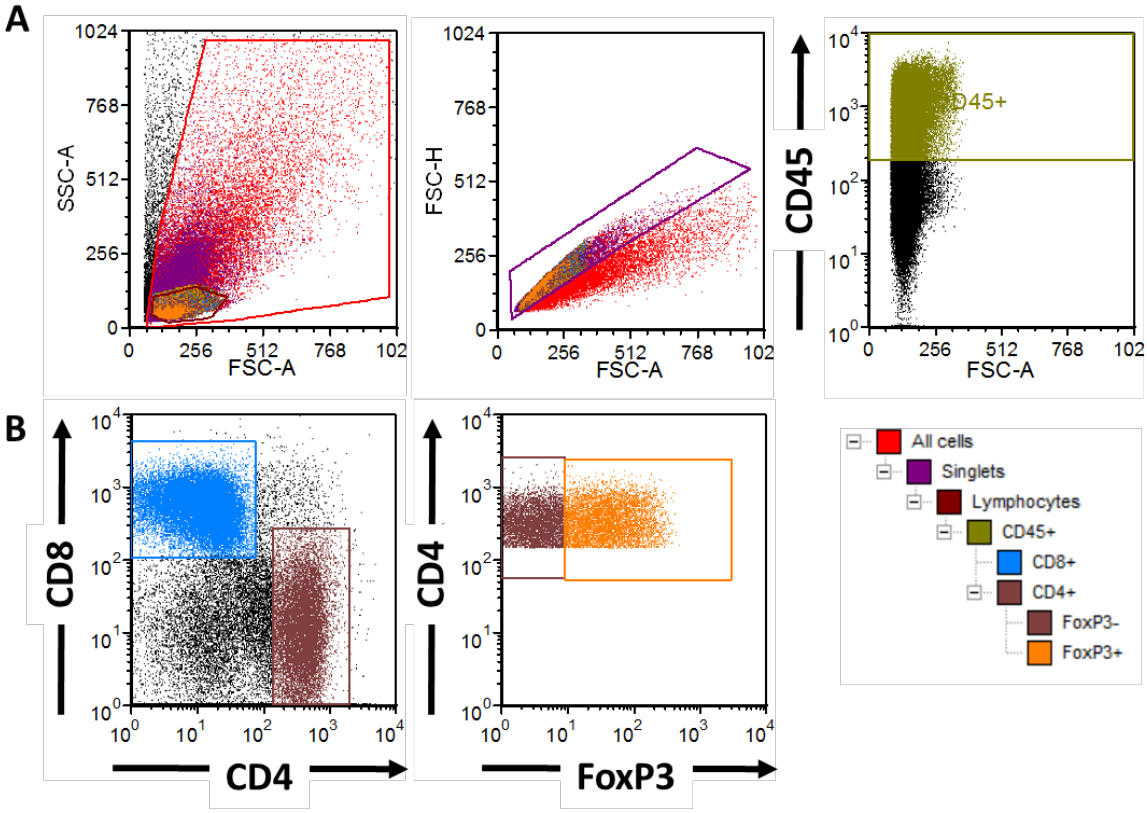

Figure 4.16 Flow cytometry gating for T cell populations on lymph nodes and PBMCs

A) Lymph nodes and PBMCs were collected from NXS2 or 9464D tumour bearing mice after CPM administration or NT and processed, and flow cytometry was conducted as detailed in **Section 2.9**. Debris removal, singlet discrimination, lymphocyte gating and finally gating of CD45+ cells is shown. **B)** Gating of CD8+ and CD4+ cells followed by further gating of FoxP3+ (Treg) cells. Population hierarchy is shown on the right.

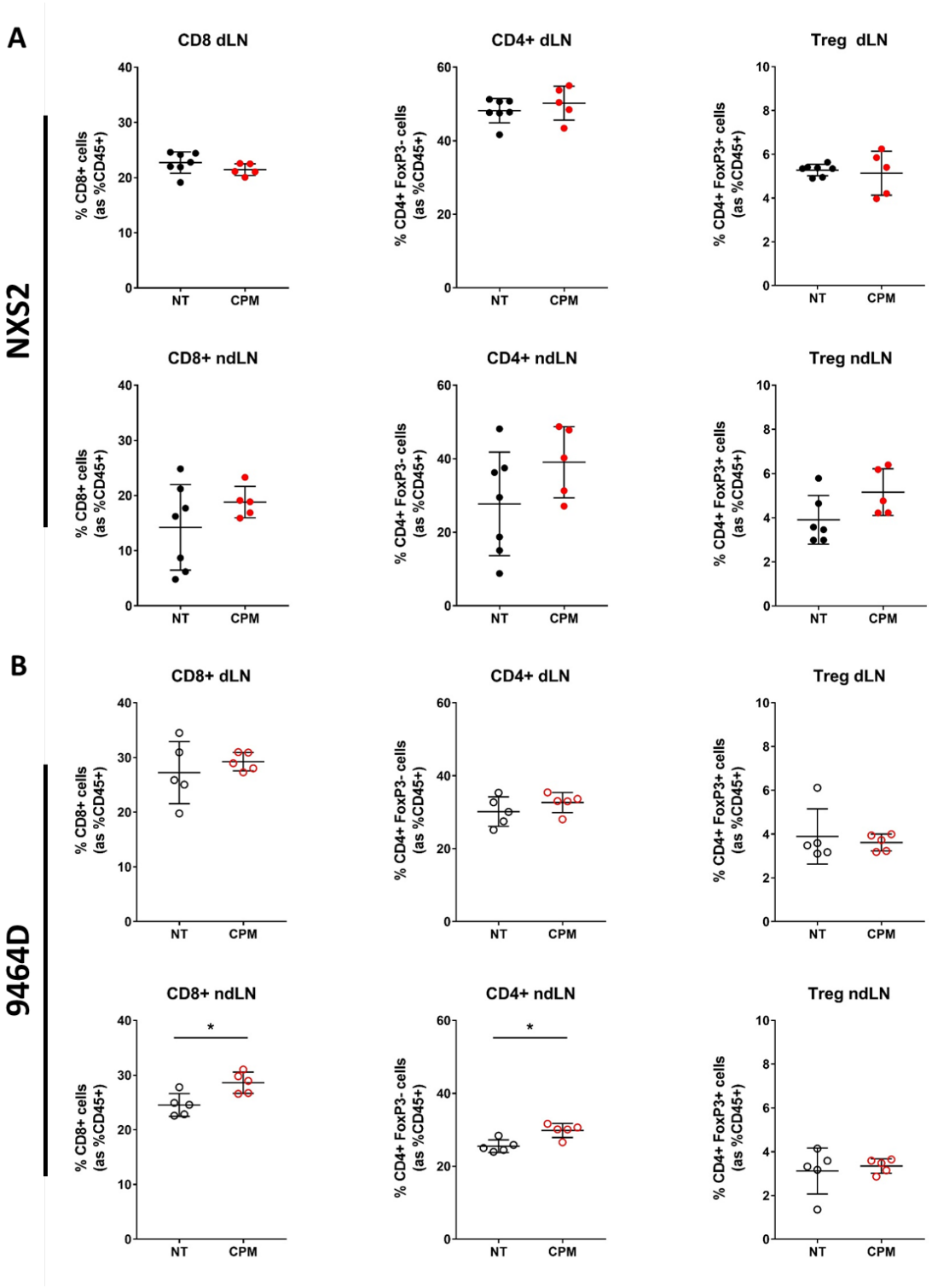

Figure 4.17 Effects of CPM administration on T cell subsets within LNs

A) NXS2 dLNS and ndLNs were processed for immunophenotyping using gating strategies defined in **Figure 4.16**, 72 hrs after 40mg/kg CPM administration. Percentages of CD8+, CD4+ and Treg cells are shown as a percentage of CD45+ cells, with dLNs show on top row, and ndLN on the bottom. Shame is shown in **B)** for 9464D. n= 7 (NT NXS2), n= 5 (CPM NXS2), n= 5 (9464D). Data pooled from two independent experiments. Significance was assessed by Mann-Whitney test and denoted as: * = <0.05.Mean and SD bars are shown.

Further analysis of Treg depletion was conducted in peripheral blood mononuclear cells (PBMCs), using the same gating described in **Figure 4.16**. Interestingly, in both NXS2 and 9464D models, CPM administration lead to a significant increase in both CD8+ and CD4+ cells as a percentage of CD45+ cells (**Figure 4.18 A** and **B** respectively). This could suggest a systemic immunomodulation effect of the CPM. Furthermore, as seen with other non-tumour tissues, no Treg depletion was observed in both NXS2 and 9464D PBMCs after CPM administration.

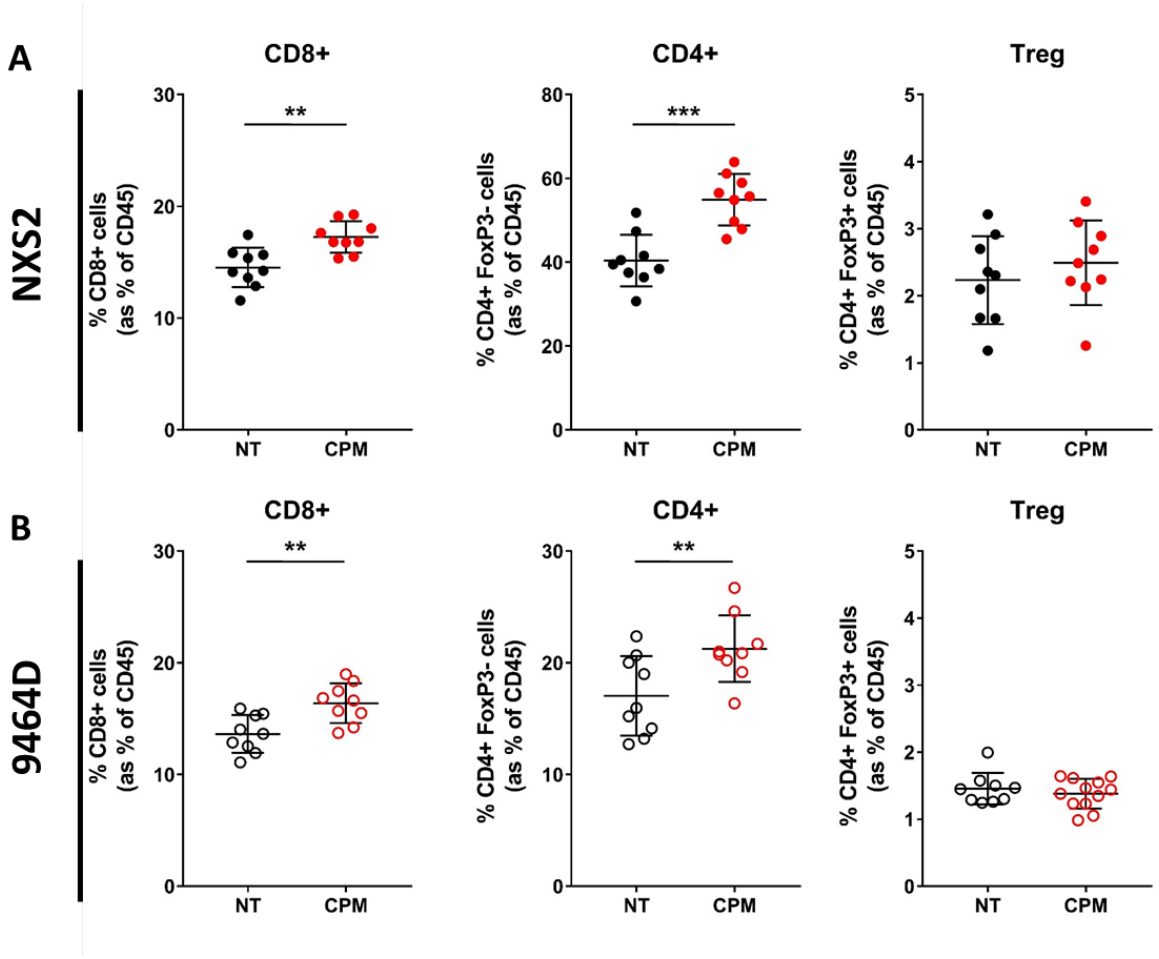

Figure 4.18 Effects of CPM administration on T cell subsets within PBMCs

A) NXS2 PBMCs were processed for immunophenotyping using gating strategies defined in **Figure 4.16**, 72 hrs after 40mg/kg CPM administration. Percentages of CD8+, CD4+ and Treg cells are shown as a percentage of CD45+ cells. Same is shown in **B)** for 9464D. n= 9 for both NXS2 and 9464D. Significance was assessed by Mann-Whitney test and denoted as: * = <0.05, ** = < 0.01, *** = < 0.001.Mean and SD bars are shown.

In summary, as demonstrated in **Figure 4.19**, low dose CPM administration of 40mg/kg led to a depletion of Tregs specifically within the tumour microenvironment of both NXS2 and 9464D tumours (fold change of ~-0.5). Analysis of PBMCs, dLN, ndLN and spleens in these models showed no Treg depletion, except a slight decrease in NXS2 spleens.

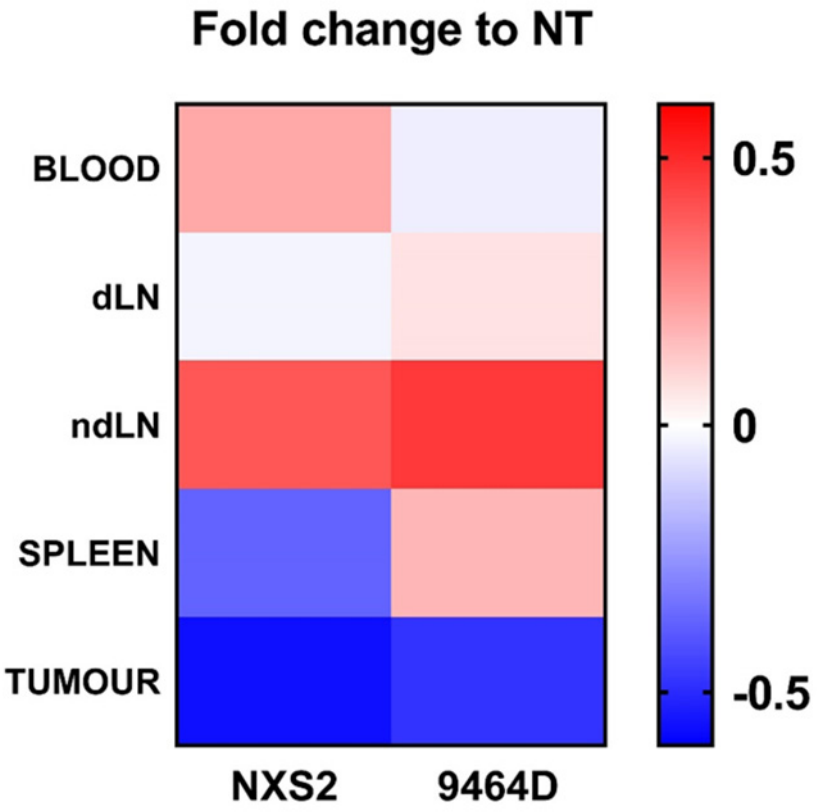

Figure 4.19 Heat map of Treg percentages in NXS2 and 9464D tissues after CPM administration

Heat map demonstrating fold change of CPM treated tissues over NT tissues for both NXS2 and 9464D tumours. Fold changes calculated for each individual CPM values using the mean of NT, implementing the formula: (CPM-NT)/NT. Fold change means for CPM are shown. Data is collated from figures: **Figure 4.14 A**, **Figure 4.15 A**, **Figure 4.17** and **Figure 4.18**.

4.2.5 Phenotyping of FcγRs on myeloid subsets in 9464D tumours

Modulation of myeloid cell percentages in tumours was assessed in **section 4.2.3**. Although no significant changes were seen when using the low dose of 40 mg/kg CPM, this may have been obscured by the variable data. Therefore, more in depth analysis of myeloid cell populations in 9464D tumours after 40 mg/kg CPM analysis was conducted, looking at Day 3 and Day 10 time points. Furthermore, assessment of how myeloid cell phenotypes change within the tumours after CPM was conducted by investigating modulation of FcγRs.

Contrary to what was observed in **Figure 4.9**, at Day 3 post CPM, a significant reduction in macrophages as a percentage of all cells was demonstrated in this experiment (**Figure 4.20 A**), which is no longer seen at Day 10 (**Figure 4.20 B**). Furthermore, at Day 10 a significant reduction in neutrophils, along with a slight increase in percentage of DCs was noted. The disparity between changes seen at Day 3 and Day 10 after CPM administration is summarised in **Figure 4.20 C**.

Phenotyping of the myeloid populations via detailed analysis of FcγR expression changes was conducted. For macrophages, a significant increase in expression of FcγRII was observed at Day 3 post CPM administration, however this was not maintained to Day 10 **Figure 4.21 A**. A significant reduction of FcγRIII expression was also seen at this later time point. Overall, macrophages were shown to have the highest expression of FcγRII compared to other myeloid cells. Monocytes (**Figure 4.21 B**) demonstrated a trend towards an increase of FcγRI expression at Day 3, although not significant. Both neutrophils and DCs (**Figure 4.21 C**+**D** respectively) demonstrated a significant upregulation of FcγRI and FcγRIII expression at Day 3 post CPM administration. For neutrophils, this was maintained at Day 10 for FcγRI, however for DCs, both FcγRI and FcγRIII were significantly downregulated at Day 10.

Using the FcγR data, A:I ratios were calculated and demonstrated in **Figure 4.22**. Although no significant modulation of individual FcγRs was seen on monocytes at Day 3 there was a significant increase in A:I ratio on these cells, which may be due to the increase in FcγRI. Furthermore, A:I ratio was increased at Day 3 on DCs significantly, but returns to NT levels by Day 10. The only significant alteration in A:I ratio at Day 10 after CPM was seen in macrophages, where a reduction was observed. This may be mainly driven by the downregulation of FcγRIII.

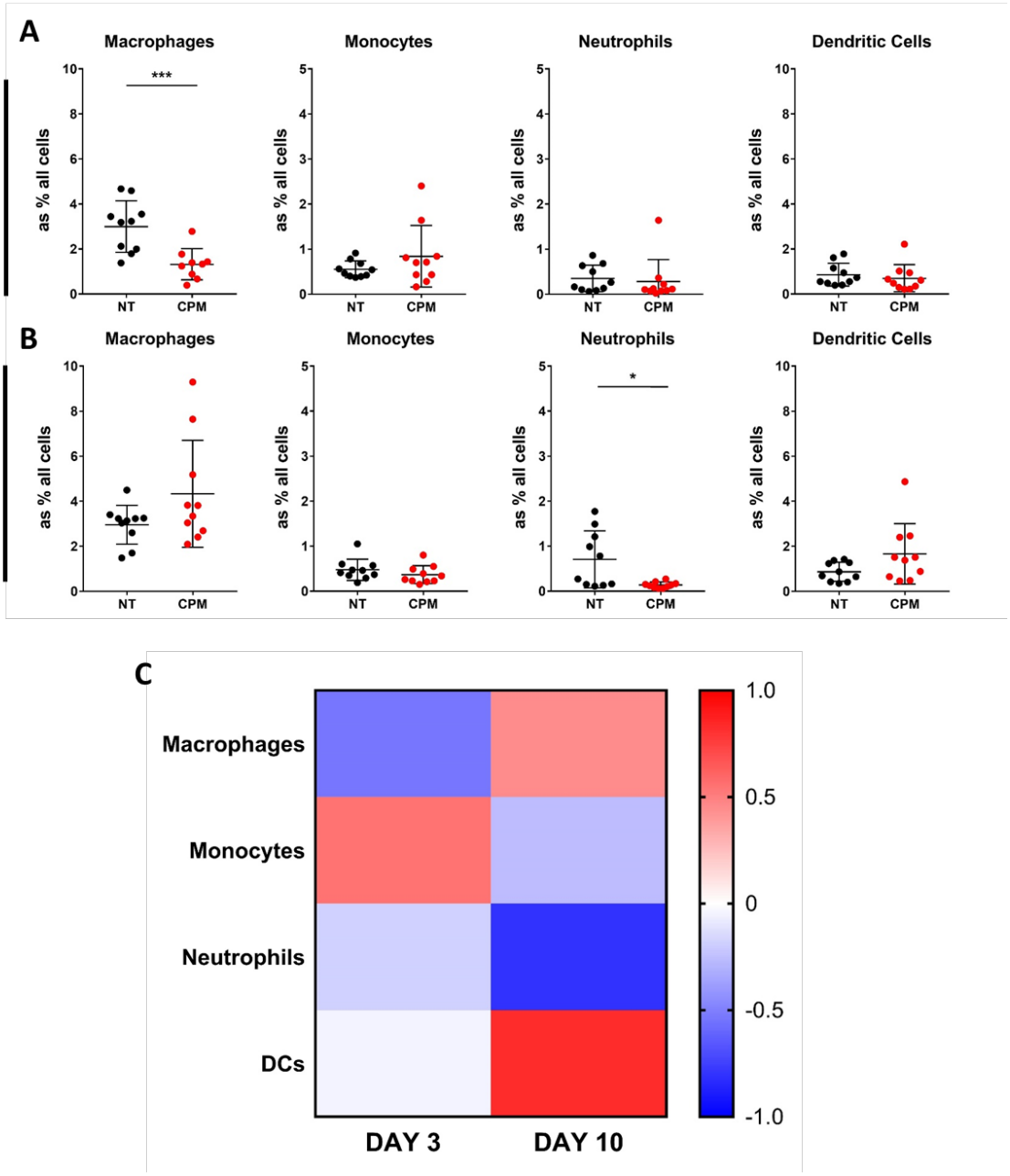

Figure 4.20 Percentages of myeloid cell subsets at Day 3 and Day 10 after CPM administration in 9464D tumours

A) 9464D tumours were treated with 40mg/kg CPM and at Day 3 were harvested, processed for flow cytometry for immunophenotyping as detailed in **Section 2.9**. Populations were defined as detailed in **Figure 3.4**. The same is shown in **B)** for Day 10. **C)** Heat map demonstrating fold change of CPM treated tumours over NT tumours for Day 3 and Day 10. Fold changes calculated for each individual CPM values using the mean of NT, implementing the formula: (CPM-NT)/NT. Fold change means for CPM are shown. n= 10 both Day 3 and Day 10. Data pooled from two independent experiments. Significance was assessed by Mann-Whitney test and denoted as: * = <0.05, ** = < 0.01, *** = < 0.001.Means and SD bars are shown.

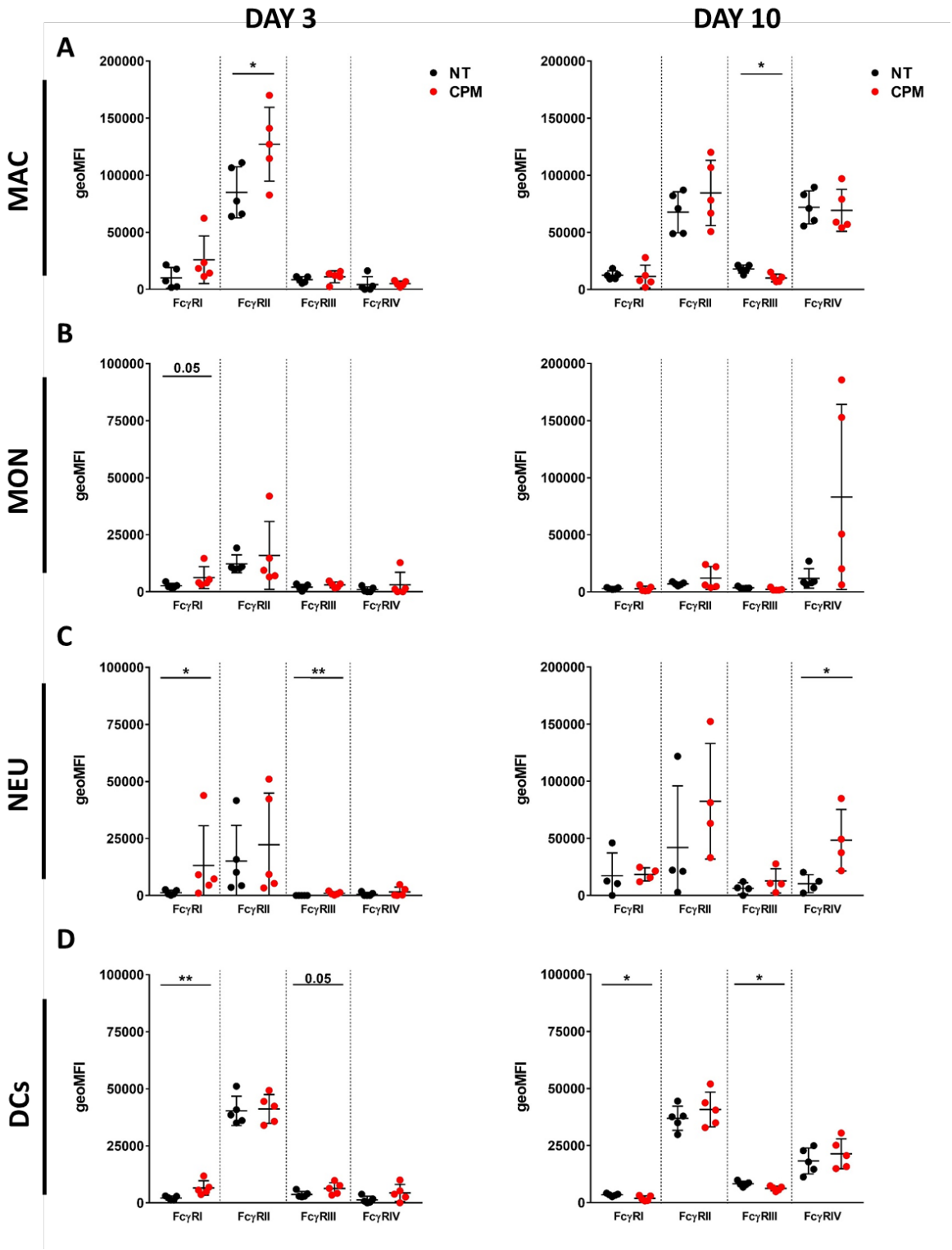

Figure 4.21 Modulation of FcγRs in 9464D tumours by CPM administration at Day 3 and Day 10

A) 9464D tumours were treated with 40mg/kg CPM and at Day 3 and Day 10 were harvested, processed for flow cytometry for immunophenotyping as detailed in immunophenotyping as detailed in **Section 2.9**. Populations were defined as detailed in **Figure 3.4**. FcγR expression (as geoMFI) is shown at Day 3 and Day 10 after CPM administration for macrophages. Same is shown in **B)** Monocytes, **C)** Neutrophils and **D)** DCs. n= 5 both Day 3 and Day 10. Significance was assessed by Mann-Whitney test and denoted as: * = <0.05, ** = < 0.01.Means and SD bars are shown.

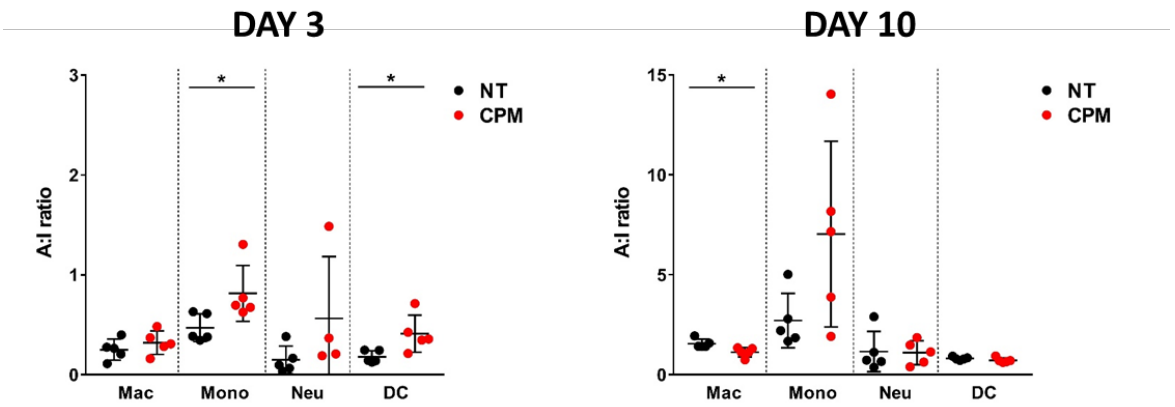

Figure 4.22 Modulation of AI ratios of FcγRs on myeloid populations at Day 3 and Day 10 after CPM administration

9464D tumours were treated with 40mg/kg CPM and at Day 3 and Day 10 were harvested, processed for flow cytometry for immunophenotyping as detailed in **Section 2.9**. Populations were defined as detailed in **Figure 3.4**. A:I ratios of FcγRs are shown at Day 3 (left) and Day 10 (right) after CPM administration for each myeloid population. A:I ratio was calculated as: (FcγRI+FcγRIII+FcγRIV)/FcγRII. n= 5 both Day 3 and Day 10. Significance was assessed by Mann-Whitney test and denoted as: * = <0.05, ** = < 0.01.Means and SD bars are shown.

4.2.6 Modulation of NXS2 TIL numbers and phenotypes at Day 3 post CPM administration

Previously in Immunophenotyping of NXS2 and 9464D tumours *ex vivo* after CPM administration **section 4.2.3**, TILs in NXS2 tumours were quantified and compared to those in tumour bearing mice treated with CPM. Here, quantification of these subsets was once again conducted along with more detailed analysis into the phenotypes of T cell subsets 72 hrs after both 20 and 40 mg/kg CPM. To do this, a panel of markers, ranging from proliferation to T cell function, were chosen including: Ki67, 4-1BB, PD-1, CTLA-4, Tbet and EOMES.

To achieve this, NXS2 tumours were treated with either 20 mg/kg or 40 mg/kg CPM at 8x8 mm, and harvested at Day 3 for immunophenotyping by flow cytometry. Gating of populations was conducted as detailed in **Figure 3.4**, and an example of marker gating is shown in **Figure 4.23**.

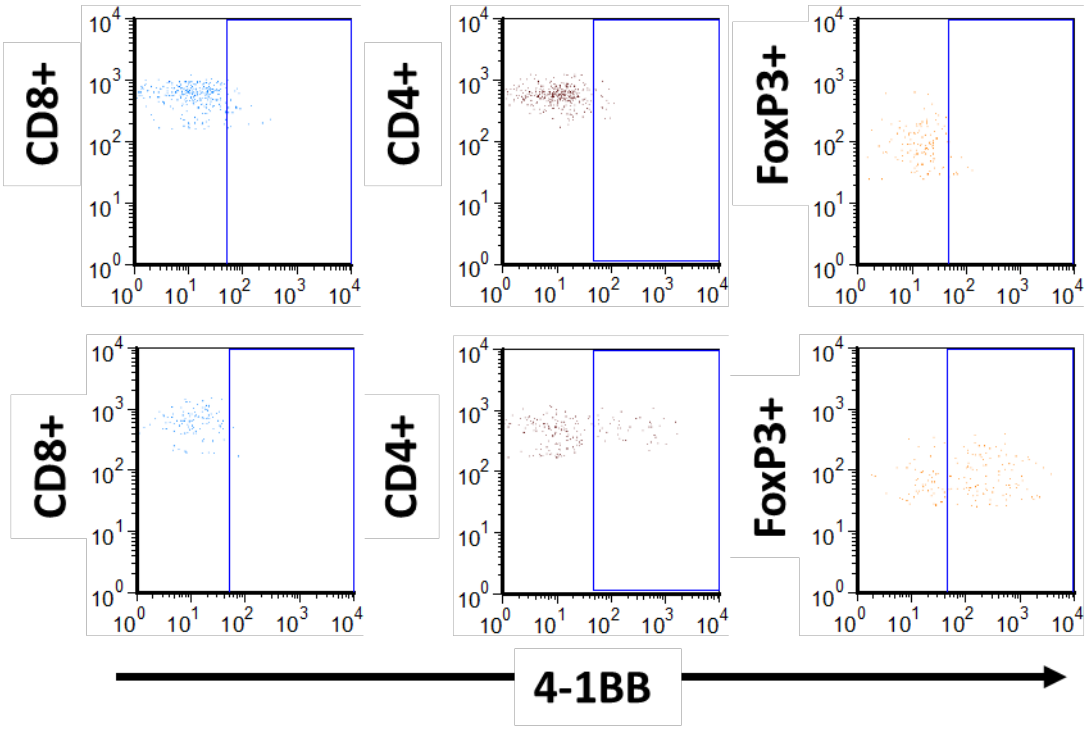

Figure 4.23 Gating and marker analysis examples for T cell subsets in tumours after CPM administration

Tumours were collected after CPM administration or NT and processed, and flow cytometry was conducted as detailed in **Section 2.9**. Gating of T cell subsets was completed as described in **Figure 3.4**. An example of marker staining for 4-1BB is shown with isotype on top and antibody staining on bottom.

4.2.6.1 Effect of CPM on T cell phenotypes in NXS2 tumours after 72 hrs

So far in this chapter, only analysis into how low dose CPM modulates immune cell percentages within the tumour microenvironment has been performed. However, it is plausible that CPM may be changing the phenotype of these T cell subsets rather than altering their number. To investigate this, a panel of markers were investigated using flow cytometry of CPM treated NXS2 tumours.

Alongside the T cell phenotype analysis, assessment of T cell percentages was conducted, to see if the Treg depletion demonstrated in **section 4.2.3** can be replicated. Here, as summarised in a fold change heat map in **Figure 4.24**, Treg depletion by 40 mg/kg CPM was observed, alongside an increase in CD8:Treg ratio. Individual plots are shown in Appendix **Figure 7.3**.

Highlighted in **Figure 4.25** are some selected changes seen with the phenotyping panel described above. Neither dose of CPM altered PD-1 expression compared to NT tumour TILs (**Figure 4.25 A**). However, it is worth noting however, that Treg cells have a much higher PD-1 expression level compared to both CD8 and CD4 cells. Expression levels of the proliferation marker Ki67 were observed to have diminished after CPM treatment, at both doses in CD4+ and Treg cells (**Figure 4.25 B**). Finally, EOMES a marker of T cell memory formation, was found to be reduced with both 20 and 40 mg/kg CPM compared to NT for all T cell subsets, as demonstrated in **Figure 4.25 C**.

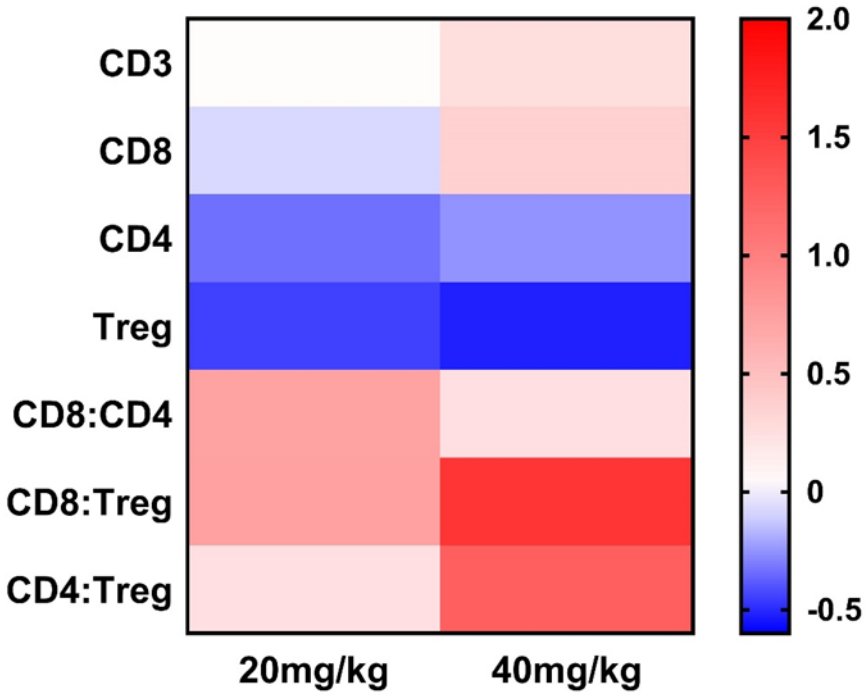

Figure 4.24 Heat map of T cell percentages and ratios in NXS2 tumours after CPM administration

Heat map demonstrating fold change of T cell percentages and ratios over NT tissues for both 20 and 40 mg/kg CPM in NXS2 tumours. Fold changes calculated for each individual CPM values using the mean of NT, implementing the formula: (CPM-NT)/NT. Fold change means for CPM are shown. Data is collated from **Figure 7.3**.

Summary of all panel markers tested is displayed in **Figure 4.26**. Overall, although some modulation over NT TILs was seen with both 20 mg/kg and 40 mg/kg CPM, the fold changes were not of high intensity as demonstrated in the heat map. Of note, a decrease in EOMES and Ki67 was prominent. Furthermore, a slight increase of CTLA-4 was noted on CD4+ and Treg cells, however this was minimal as expression of this marker was low at baseline on all cell types.

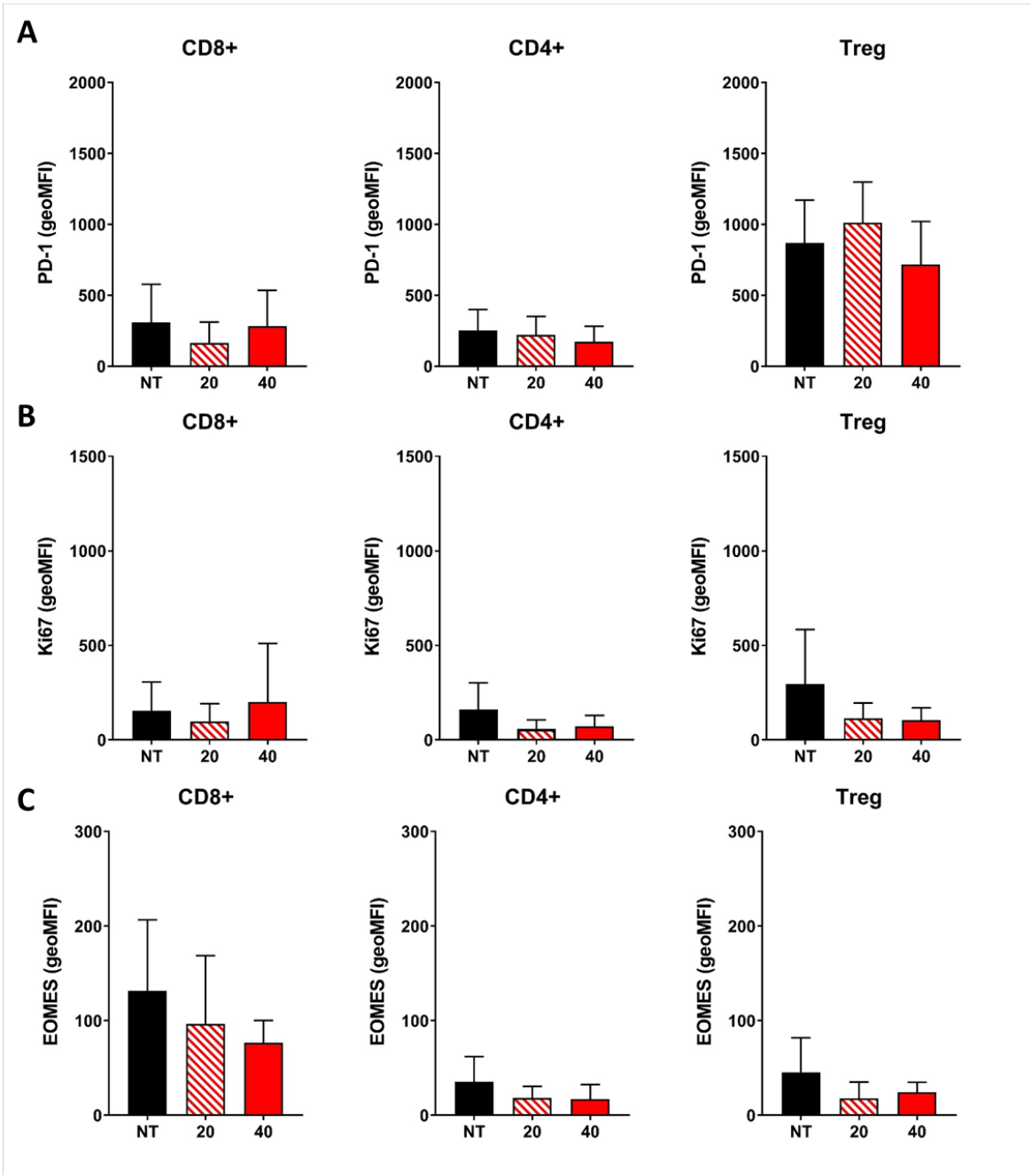

Figure 4.25 Modulation of a selection of markers on TILs in NXS2 tumours after CPM administration

A) NXS2 tumours were processed for immunophenotyping using gating strategies defined in **Figure 3.4** and **Figure 4.23**, 72 hrs after either 20 or 40 mg/kg CPM administration. Expression of PD-1 was quantified as geoMFI (minus isotype control) for CD8+, CD4+ and Treg subsets. The same is shown in **B)** for Ki67 and in **C)** for EOMES. n= 6 (NT), n= 8 (20 mg/kg) and n= 9 (40 mg/kg). Data pooled from two independent experiments. Statistical analysis was conducted using Krusksal Wallis test with Dunn's multiple comparisons. Mean and SD error bars are shown.

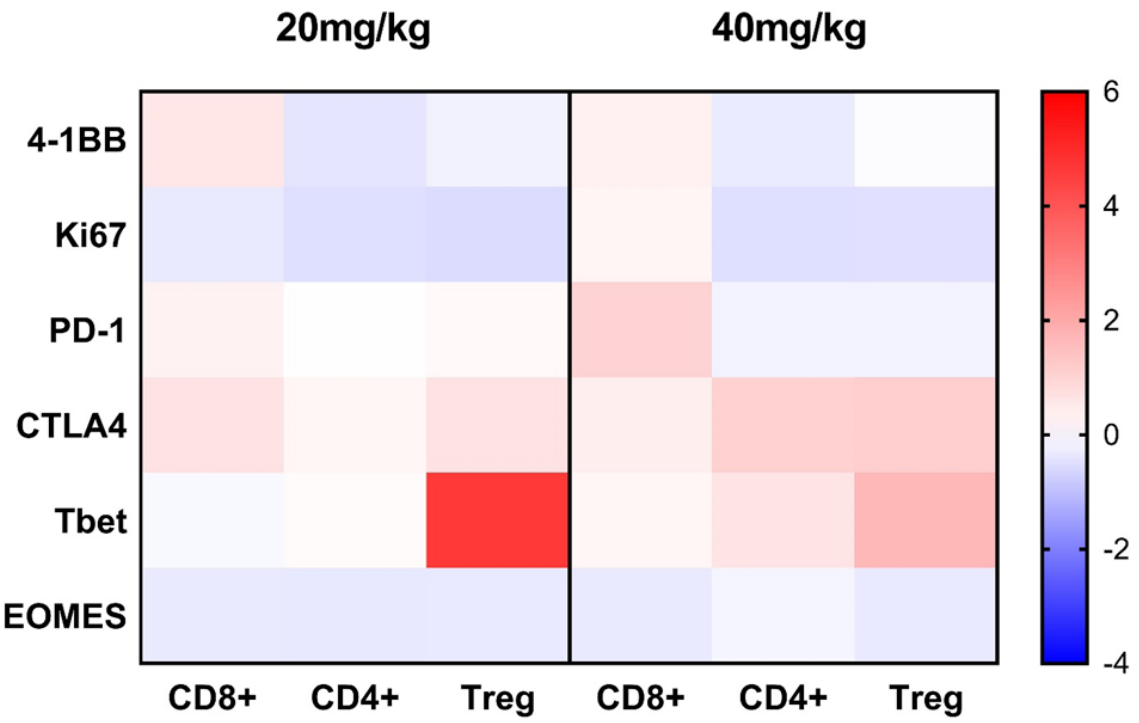

Figure 4.26 Heat map of modulation of markers on T cell subsets in NXS2 tumours after CPM administration.

Heat map demonstrating fold change of marker expression on T cell subsets over NT for both 20 and 40 mg/kg CPM in NXS2 tumours. Fold changes calculated for each individual CPM values using the mean of NT, implementing the formula: (CPM-NT)/NT. Fold change means for CPM are shown. Data is collated from **Figure 4.25** and data from the same experiments, not shown separately.

4.2.7 Modulation of T cells at Day 3 and Day 10 post CPM administration in 9464D tumours

In the previous section, a panel was utilised to investigate how CPM alters the phenotype of TILs in SC NXS2 tumours. However, significant notable changes in these markers appeared to be limited (**Figure 4.26**). Consequently, a more in-depth investigation into CPM modulatory potential on T cell phenotype was conducted utilising the 9464D SC tumour model. For this, a more detailed flow cytometry panel was designed, building from the data presented from the NXS2 model. As demonstrated in **Table 4.1**, a wide range of markers on 9464D infiltrating TILs were assessed, from proliferation, to function and memory. Furthermore, both short term (at Day 3) and long term effects (at Day 10) of CPM was assessed. Gating strategies used for T cell subsets are demonstrated in **Figure 4.27**, with an example of gating and marker analysis shown previously in **Figure 4.23**. Furthermore, double positive populations were analysed for some markers using the example gating shown in **Figure 4.28**.

Proliferation	Activation and Effector function	Memory and Lineage	Inhibitory receptors
Ki67	CD25 OX40 4-1BB CD107a Granzyme B IFNγ	CD62L CD44 Tbet EOMES	PD-1 LAG3 TIM3 KLRG1

Table 4.1 Immunophenotyping panel of T cell markers for flow cytometry of 9464D tumours at Day 3 and Day 10 post CPM administration

Each marker analysed in a phenotyping flow cytometry panel for T cells in 9464D tumours is shown. Marker expression will be assessed on the T cell subsets: CD8+, CD4+ and Treg cells, and quantified as percentage positive or as geoMFI, both minus isotype controls.

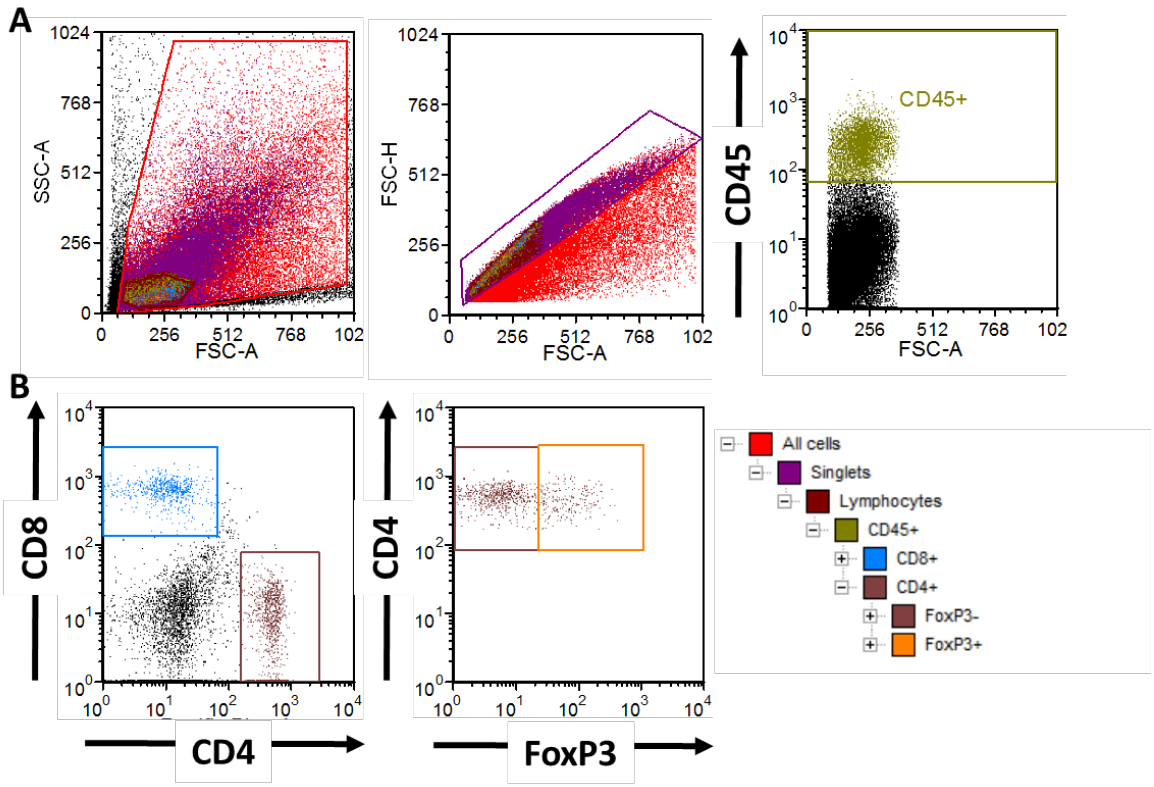

Figure 4.27 Gating strategies for T cell populations in tumours

A) Tumours were collected from 9464D tumour bearing mice after CPM administration or NT and processed and flow cytometry was conducted as detailed in **Section 2.9**. Debris removal, singlet discrimination, lymphocyte gating and finally gating of CD45+ cells is shown. **B)** Gating of CD8+ and CD4+ cells followed by further gating of FoxP3+ (Treg) cells. Population hierarchy is shown on the right.

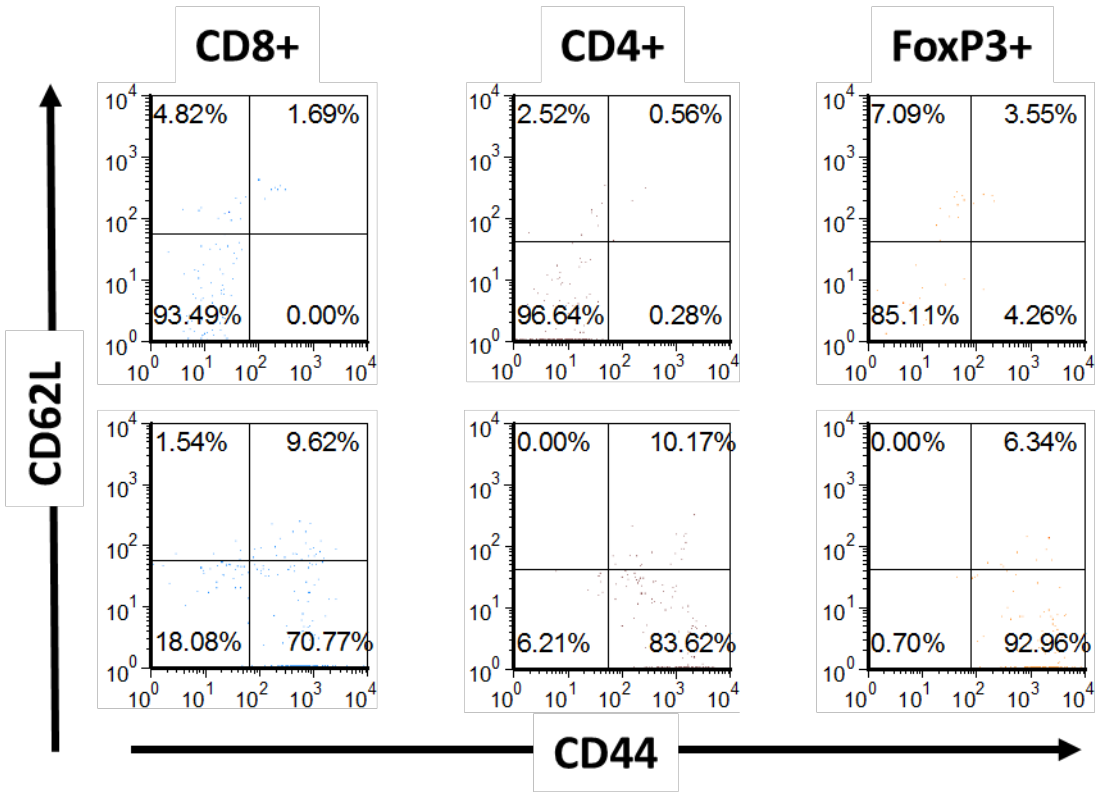

Figure 4.28 Gating for double positive marker analysis example for T cell subsets in tumours after CPM administration

Tumours were collected from 9464D tumour bearing mice after CPM administration or NT and processed and flow cytometry was conducted as detailed in **Section 2.9**. Gating of T cell subsets was completed as described in **Figure 4.26**. Analysis for double positive expression of markers using CD62L and CD44 as an example is shown. Isotypes are displayed on top, and antibodies on bottom.

4.2.7.1 Effect on T cell percentages at Day 3 and Day 10 post CPM administration

Before in-depth analysis of T cell subset phenotypes, quantification of total CD45+, CD8+, CD4+ and Treg cells was undertaken. At Day3 post 40 mg/kg CPM, no changes in T cell subsets or total CD45+ cells was observed except for a significant depletion of around half in Treg cells (**Figure 4.29 A**). This corroborates with the data presented previously in **Figure 4.13** and **Figure 4.15**. Interestingly, at Day 10 post CPM treatment, the initial depletion of Tregs seen at Day 3 is no longer observed.

When analysing T cell subset ratios, both CD8:Treg and CD4:Treg ratio in CPM treated tumours were significantly raised compared to NT at Day 3 (**Figure 4.29 B**), which was not seen previously (**Figure 4.15)**, due to the variability between tumours. However, at Day 10 the changes initially see with CPM are no longer significantly different to NT.

A summary of all T cell subset percentage changes are demonstrated in **Figure 4.30**. Here, the depletion of Tregs by 40 mg/kg CPM at Day 3 is clearly visualised, with a fold change of around -0.5

over NT tumours. Furthermore, the return to baseline at Day 10 for most of the changes seen at Day 3 are highlighted.

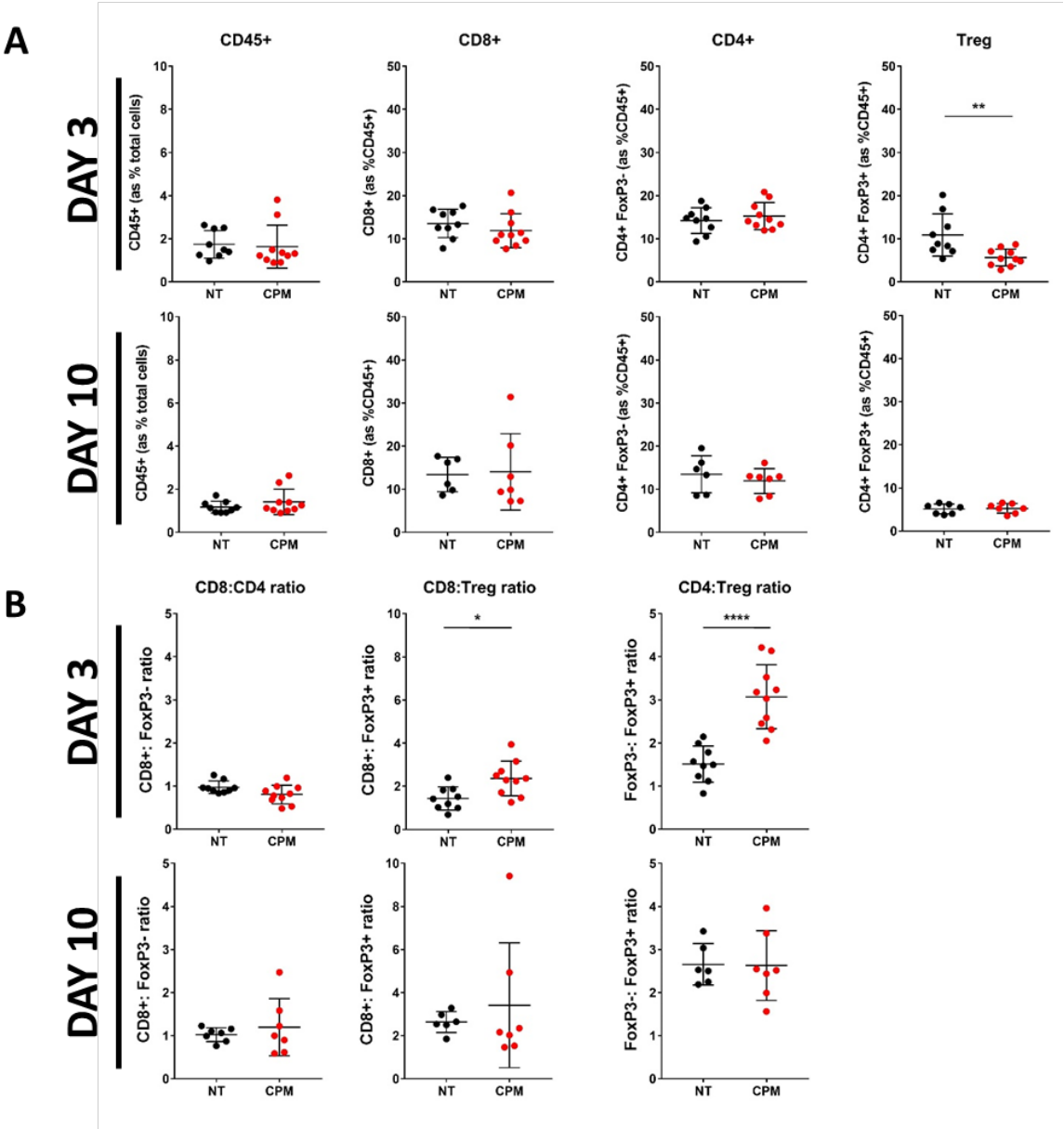

Figure 4.29 Modulation of T cell subset percentages and ratios Day 3 and Day 10 post CPM administrations

A) 9464D tumours around 8x8 mm were treated with 40 mg/kg CPM and at Day 3 and Day 10 were harvested, processed for flow cytometry for immunophenotyping as detailed in **Section 2.9**. Populations were defined as detailed in **Figure 4.27Figure 4.27**. T cell subsets as a percentage of CD45+ cells are shown for Day 3 and Day 10, with **B)** showing ratios between the subsets. n= 6-9 (NT) and n= 10 (40 mg/kg CPM). Data pooled from two independent experiments. Statistical analysis was conducted using Mann-Whitney test with significance defined as: *= <0.05, **= <0.01, ***= <0.001 and ****= <0.0001. Means and SD error bars are shown.

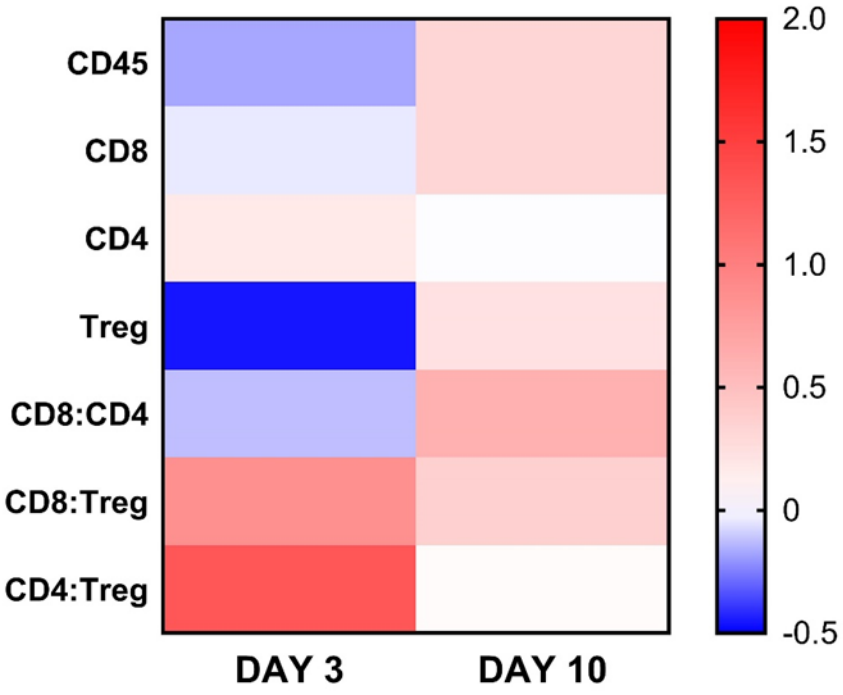

Figure 4.30 Heat map of T cell percentages and subset ratios in 9464D tumours at Day3 and Day 10 post CPM administration

Heat map demonstrating fold change of T cell percentages and ratios over NT for both Day 3 and Day 1 after 40 mg/kg CPM administration in 9464D tumours. Fold changes calculated for each individual CPM values using the mean of NT, implementing the formula: (CPM-NT)/NT. Fold change means for CPM are shown. Data is collated from **Figure 4.29**.

4.2.7.2 Effect on T cell memory populations at Day 3 and Day 10 post 40mg/kg CPM

Although percentages of CD8+ and CD4+ cells were not significantly altered by CPM at either Day 3 or Day 10, the memory phenotype of these cells may have been altered. To assess this, expression of two markers, CD62L and CD44, were used. Memory phenotypes were defined as: CD62L+ CD44- (naïve), CD62L- CD44+ (Effector memory – EM) and CD62L+ CD44+ (Central memory – CM). Analyses of these populations was conducted at both Day 3 and Day 10 post 40 mg/kg CPM administration.

There were no significant changes seen in any of the memory populations across all TILs at Day 3 post CPM (**Figure 4.31**). However, the data was quite variable between tumours, especially within the CPM treated tumours, and it may take longer than three days after CPM for changes in memory phenotypes to occur. This was demonstrated by a significant decrease in naïve CD8+ T cells, at Day 10 and a consequent slight increase in effector memory CD8+ T cells, although this was not significant (**Figure 4.32 A**). No other significant changes were seen in either CD4+ or Treg cell populations (**Figure 4.32 B+C**).

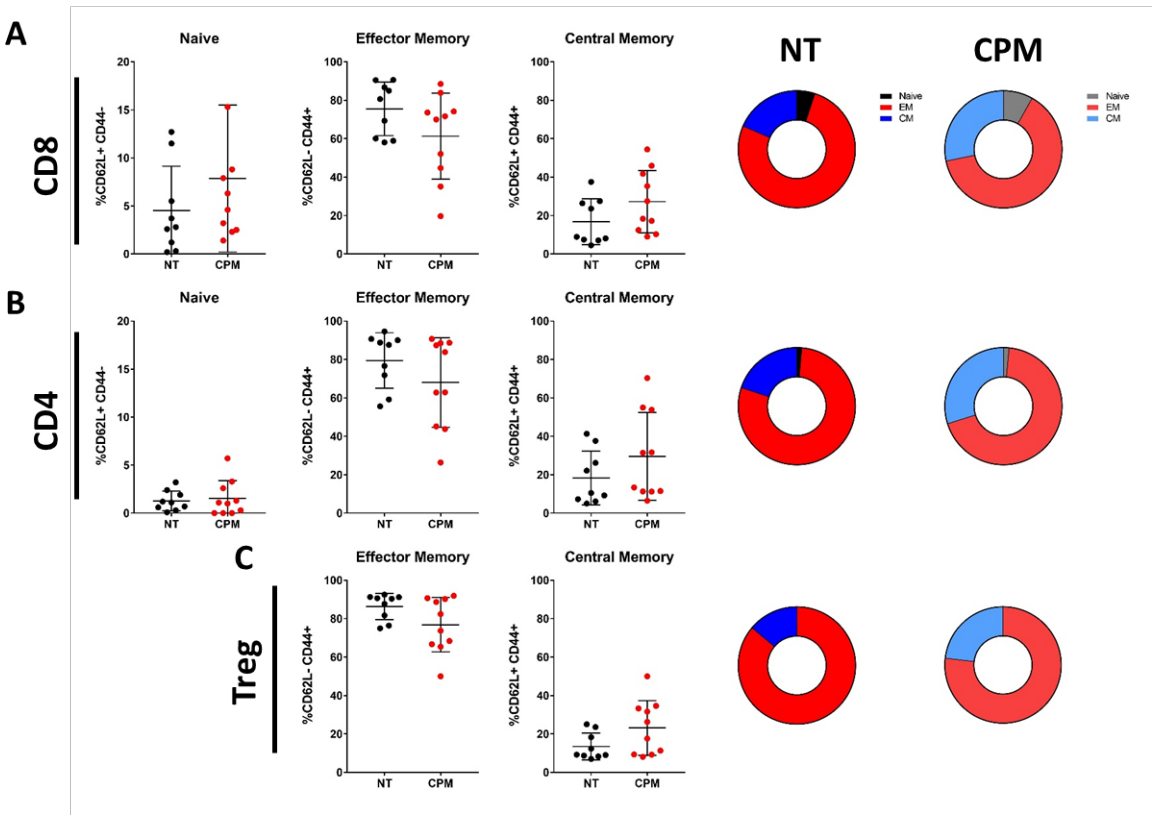

Figure 4.31 Effect of CPM on T cell memory populations at Day 3 post administration

A) 9464D tumours around 8x8 mm were treated with 40 mg/kg CPM and at Day 3 were harvested, processed for flow cytometry for immunophenotyping as detailed in **Section 2.9**. Populations were defined as detailed in **Figure 4.27**, with marker gating conducted as in **Figure 4.28Figure 4.27**. T cell memory populations as a percentage of CD8+ cells are shown. Memory population means are visualised as a pie chart on the right. **B)** As in A with CD4+ cells, and **C)** Treg cells. n= 9 (NT) and n= 10 (40 mg/kg CPM). Data pooled from two independent experiments. Statistical analysis was conducted using Mann-Whitney test. Means and SD error bars are shown. EM – effector memory, CM – central memory.

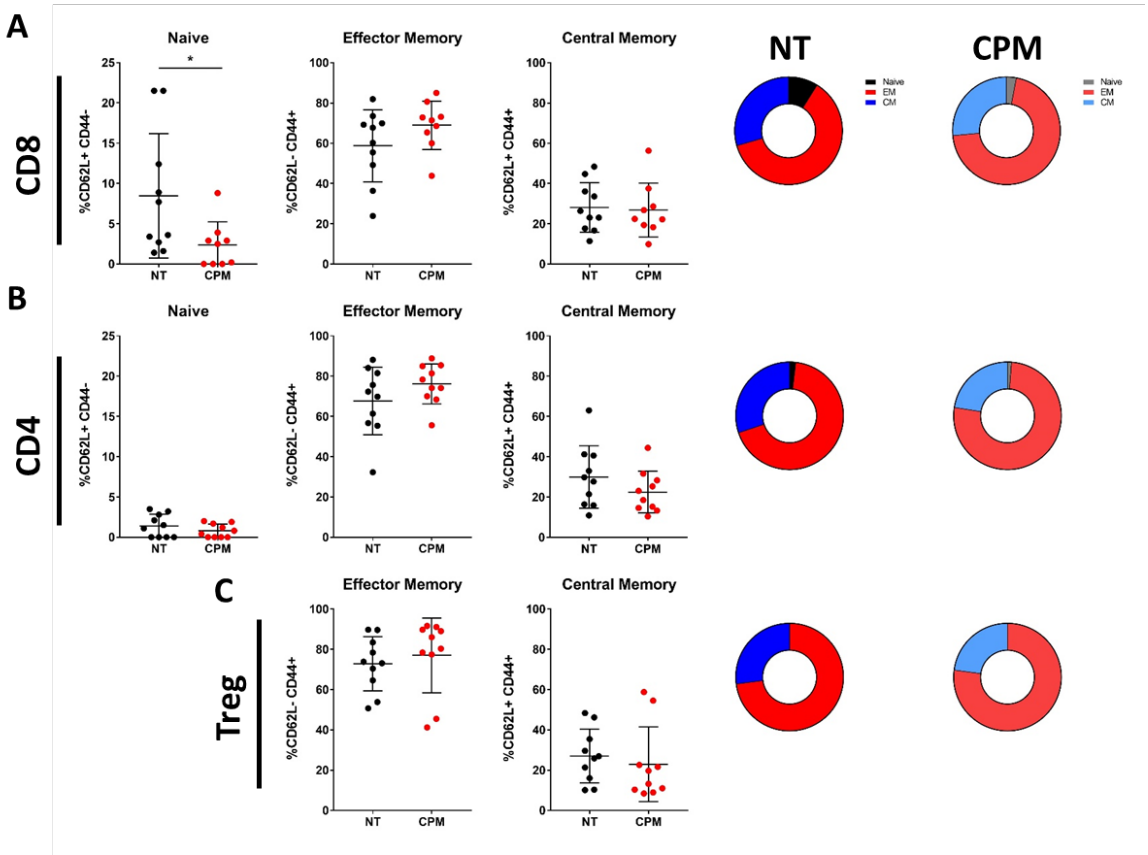

Figure 4.32 Effect of CPM on T cell memory populations at Day 10 post administration

A) 9464D tumours ~8x8 mm were treated with 40 mg/kg CPM and at Day 10 post treatment were harvested and processed for flow cytometry for immunophenotyping as detailed in **Section 2.9**. Populations were defined as detailed in **Figure 4.27**, with marker gating conducted as in **Figure 4.28Figure 4.27**. T cell memory populations as a percentage of CD8+ cells are shown. Memory population means are visualised as a pie chart on the right. **B)** As in A but with CD4+ cells, and **C)** Treg cells. n= 10. Data pooled from two independent experiments. Statistical analysis was conducted using Mann-Whitney test with significance defined as: *= <0.05. Means and SD error bars are shown. EM – effector memory, CM – central memory.

4.2.7.3 Modulation of T cell subset phenotype at Day 3 and Day 10 post 40mg/kg CPM

As demonstrated in **Table 4.1**, an extensive panel of T cell markers were investigated after CPM administration. Therefore, this section focused on highlighting important and significant changes in these markers on CD8+, CD4+ and Treg cells. Finally, a summary of changes in all the markers investigated is shown in **Figure 4.36**.

CD8 marker modulation at Day 3 and Day 10 post CPM was demonstrated in **Figure 4.33**. Interestingly, the only short-term changes seen at Day 3 were a significant increase in the functional markers IFNγ and CD107a (**Figure 4.33 A**). At Day 10, the increase in expression of IFNγ by CPM was still seen (**Figure 4.33 B**). Percentage of CD8+ T cells expressing 4-1BB, a co-stimulatory receptor,

was greater in CPM treated tumours. However, a significant upregulation of the inhibitory receptor TIM3, along with increased expression of EOMES a marker of exhaustion was also observed in tumours treated with CPM at Day 10.

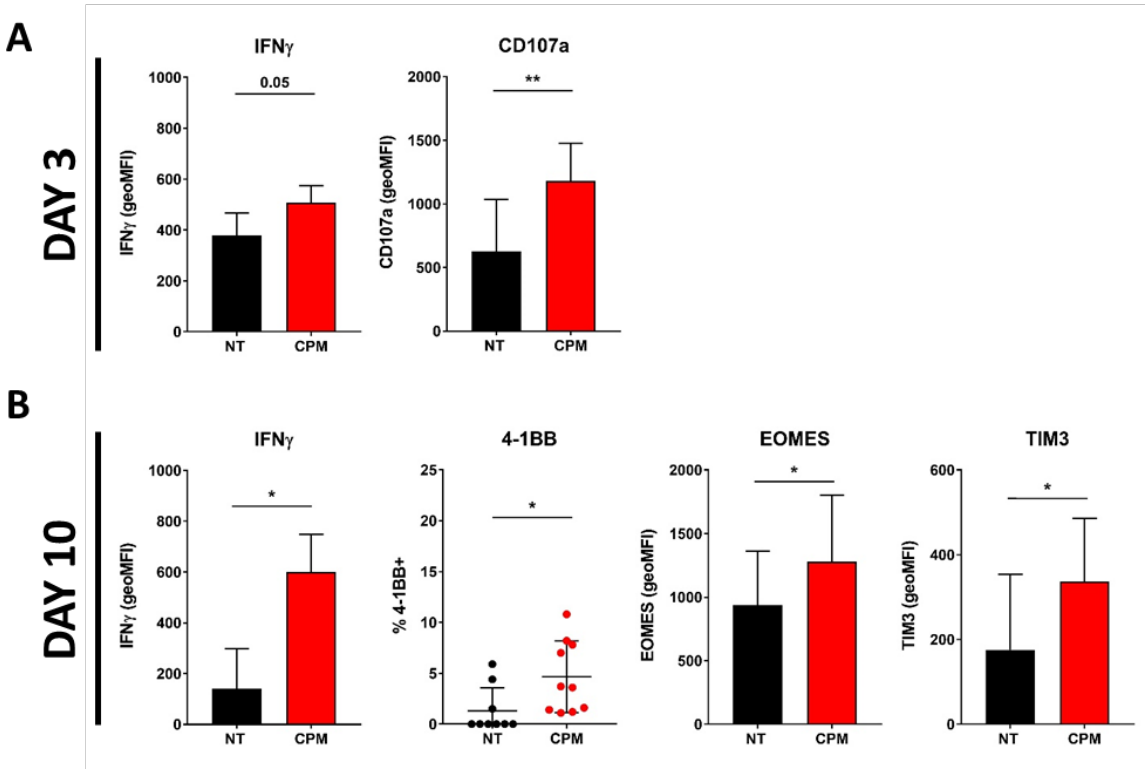

Figure 4.33 Modulation of CD8+ phenotype at Day 3 and Day 10 post 40mg/kg CPM

A) 9464D tumours around 8x8 mm were treated with 40 mg/kg CPM and at Day 3 and 10 were harvested, processed for flow cytometry for immunophenotyping as detailed in **Section 2.9**. Populations were defined as detailed in **Figure 4.27**, with marker gating conducted as in **Figure 4.23**. Significant effects of CPM on CD8+ markers at Day 3 and **B)** Day 10 are shown. n= 10. Data pooled from two independent experiments. Marker percentages are shown as scatter plots, with expression as geoMFIs (minus isotype) shown as bars. Statistical analysis was conducted using Mann-Whitney test with significance defined as: *= <0.05 and **= <0.01. Means and SD error bars are shown

Modulation of similar markers was observed in the CD4+ (FoxP3-) subset of T cells. As with CD8+ cells, a significant upregulation of IFNγ and CD107a expression was seen at Day 3 post CPM (**Figure 4.34 A**). A decrease in CD25 expression was also noted, along with an upregulation in EOMES, although expression of this marker is considerably lower than seen in CD8+ cells. At Day 10, the significant increase in IFNγ expression is still apparent, however EOMES is no longer different between NT and CPM treated tumours (**Figure 4.34 B**). Furthermore, a significant drop in the effector molecule Granzyme B is noted, along with a slight but significant increase in inhibitory receptor LAG3 expression.

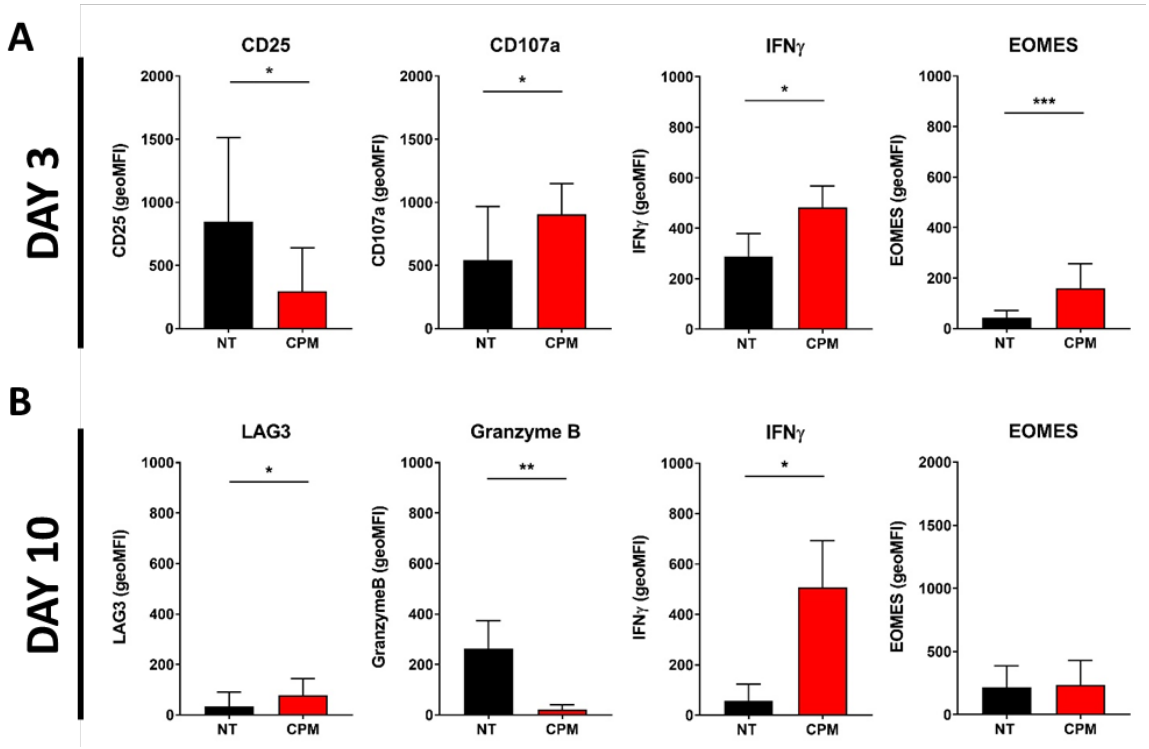

Figure 4.34 Modulation of CD4+ phenotype at Day 3 and Day 10 post 40mg/kg CPM

A) 9464D tumours around 8x8 mm were treated with 40 mg/kg CPM and at Day 3 and 10 were harvested, processed for flow cytometry for immunophenotyping as detailed in **Section 2.9**. Populations were defined as detailed in **Figure 4.27**, with marker gating conducted as in **Figure 4.23**. Significant effects of CPM on CD4+ markers at Day 3 and **B)** Day 10 are shown. n= 10. Data pooled from two independent experiments. Marker expression shown as geoMFIs (minus isotype) are shown. Statistical analysis was conducted using Mann-Whitney test with significance defined as: *= <0.05 and **= <0.01, ***= <0.001. SD error bars are shown

Finally investigation into how these markers were altered on Treg cells was conducted. As seen with both CD8+ and CD4+ T cells, Tregs also demonstrated a significant increase in CD107a expression at Day 3 post CPM (**Figure 4.35 A**). Furthermore, an upregulation of the proliferation marker Ki67 and inhibitory receptor TIM3 was also identified, alongside a strongly significant decrease in OX40 expression. Apart from the increased expression of TIM3, all of the changes in markers seen at Day 3 were not observed at the later time point of Day 10 (**Figure 4.35 B**). However, a higher percentage of Treg cells were shown to be both TIM3 and LAG3 positive at Day 10. CD25, which is constitutively expressed on Treg cells, was observed to be downregulated after CPM, whereas IFNγ expression was significantly increased. The decreased expression of CD25 may have been due to the highly expressing cells being depleted. Finally, an increase in percentage of Tregs expressing EOMES was demonstrated, however this was not significant.

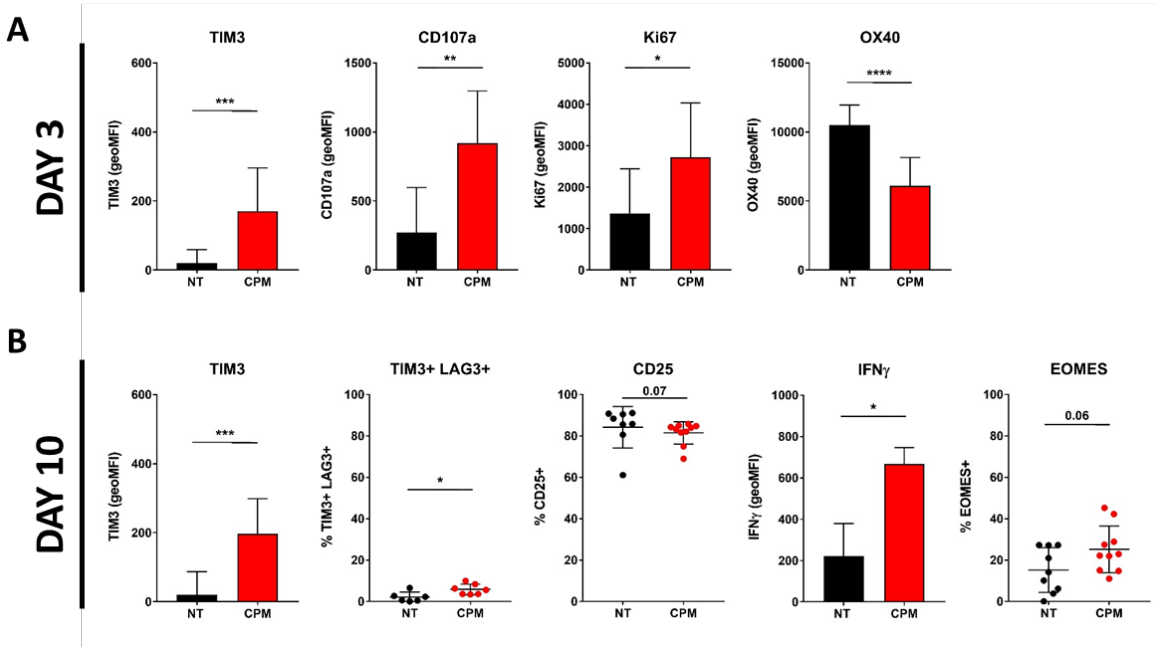

Figure 4.35 Modulation of Treg phenotype at Day 3 and Day 10 post 40mg/kg CPM

A) 9464D tumours around 8x8 mm were treated with 40 mg/kg CPM and at Day 3 and 10 were harvested, processed for flow cytometry for immunophenotyping as detailed in **Section 2.9**. Populations were defined as detailed in **Figure 4.27**, with marker gating conducted as in **Figure 4.23** and **Figure 4.28**. Significant effects of CPM on Treg markers at Day 3 and **B)** Day 10 are shown. n= 10. Data pooled from two independent experiments. Marker percentages are shown as scatter plots, with expression as geoMFIs (minus isotype) shown as bars. Statistical analysis was conducted using Mann-Whitney test with significance defined as: *= <0.05, **= <0.01, ***= <0.001 and ****= <0.0001. Means and SD error bars are shown.

The marker data presented in the previous section, along with all data collected from the phenotyping panel shown in **Table 4.1**, is summarised as a heat map presented in **Figure 4.36**. Overall, it appears most modulation of T cell markers induced by CPM administration occurred within a short time frame at Day 3, as the intensity of the modulation is reduced by Day 10. Furthermore, a consistent increase in effector molecules and markers such as IFNγ, CD107a and Granzyme B was seen across all three cell types at Day 3. Interestingly, the downregulation of two constitutively expressed activation markers on Tregs, OX40 and CD25, was observed. These data suggest that CPM at low doses (40 mg/kg) can modulate the expression of T cell subset functional markers, and possibly, in turn change their phenotype.

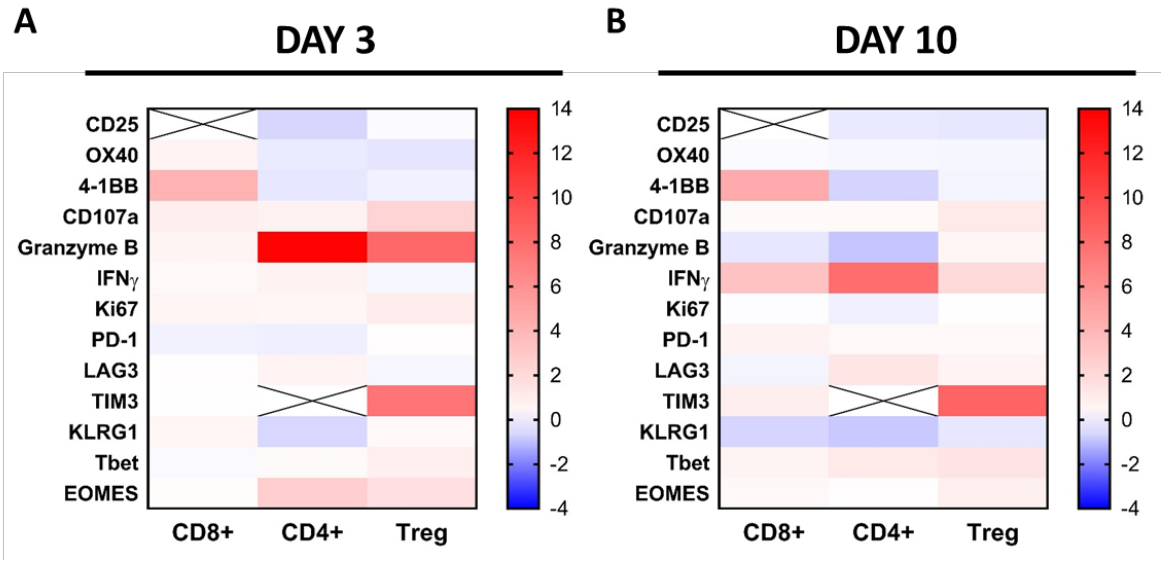

Figure 4.36 Heat map of modulation of markers on T cell subsets in 9464D tumours at Day 3 and Day 10 after CPM administration.

A) Heat map demonstrating fold change of marker expression (geoMFIs) on T cell subsets over NT after 40 mg/kg CPM in 9464D tumours. Fold changes calculated for each individual CPM values using the mean of NT, implementing the formula: (CPM-NT)/NT. Fold change means for CPM are shown for Day 3 and **B)** Day 10 post CPM administration. Data is collated from **Figure 4.33**, **Figure 4.34**, **Figure 4.35** and data from the same experiments, not shown separately. X – Low expression/not-detected.

4.2.8 Investigating the importance of ICD or Treg depletion in CPM induced immunomodulation

Work in this chapter has demonstrated that CPM can possibly induce the expression of ICD markers on NB cell lines, and lead to significant tumour specific Treg depletion. However, their relative contributions in determining the immunomodulatory activity of CPM has not yet been delineated. In an effort to investigate this, creation of a BCL-2 overexpressing 9464D cell line was conducted, alongside the use of a vav-BCL-2 transgenic C57BL/6 mouse model. CPM has previously been demonstrated to cause cell death by apoptosis induction [549], therefore over expression of the anti-apoptotic molecule BCL-2 should prevent cell death from occurring, and therefore stopping ICD, which is an immunogenic form of apoptosis [278]. Furthermore, the vav-BCL-2 mice overexpress BCL-2 in all haematopoietic cells that express the vav promotor, which includes Treg cells. Therefore if Treg cells have high expression of BCL-2, then CPM dependent depletion of these cells should be halted. Using both these models will allow for the assessment of their relative contributions to the immunomodulatory effects of CPM.

4.2.8.1 Transfection of phoenix-Eco cells and establishment of selection dose of puromycin and hygromycin in 9464D

To create an hBCL-2 over-expressing 9464D cell line, firstly viral producing phoenix-Eco cells were transfected with the DNA plasmid encoding either the hBCL-2 sequence as shown in Appendix **Figure 7.2**[551,552], or a pMIH empty vector (EV) control. As a further control, to assist in determining if the transfection and eventual transduction of 9464D cells of hBCL-2 was successful, phoenix-Eco cells were also transfected with a GFP expressing plasmid (Appendix **Figure 7.1**). Transfection of both plasmids was conducted as detailed in **Section 2.12**. After 48 hrs the GFP transfected phoenix-Eco cells were imaged under a fluorescent microscope as shown in **Figure 4.37**. It was observed that the cells were GFP positive, and therefore the transfection of the GFP and therefore likely the hBCL-2 was successful.

Before transduction of 9464D cells, appropriate dosing of selection antibiotics needed to be established. For the GFP- and hBCL-2 plasmids the selection antibiotics puromycin, and hygromycin were required respectively. Therefore cytotoxic curves were conducted for both antibiotics in 9464D cells (**Figure 4.38**). To ensure that only non-transduced 9464D cells will be depleted, a dose was required which caused only around 25% cell death. Example gating and PI+ staining for puromycin treatment of 9464D cells is shown in **Figure 4.38 A**, with resulting kill curve displayed in **Figure 4.38 B**. As demonstrated, a dose of 2.5 μg/ml was decided to be used for selection. For hygromycin (**Figure 4.38 C-D**), a dose of 50 μg/ml was selected for future selection.

After establishment of appropriate selection doses of both puromycin and hygromycin, 9464D cells were retrovirally transduced using the supernatant produced by transfected phoenix-Eco cells, as detailed in **Section 2.12.3**. 9464D cells were transduced with GFP (transduction control), Empty Vector or hBCL-2.

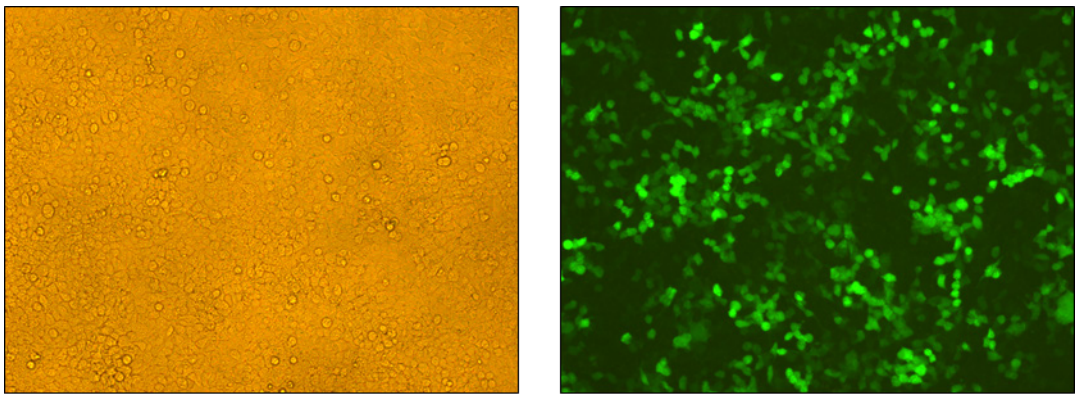

Figure 4.37 GFP expression of transfected Phoenix-Eco cells

Phoenix-Eco cells were transfected with GFP plasmid as described in **Section 2.12**. After 48 hrs cells were imaged on a fluorescent microscope. Phase contrast image of cells is shown on the left, with GFP fluorescence imaging shown on the right.

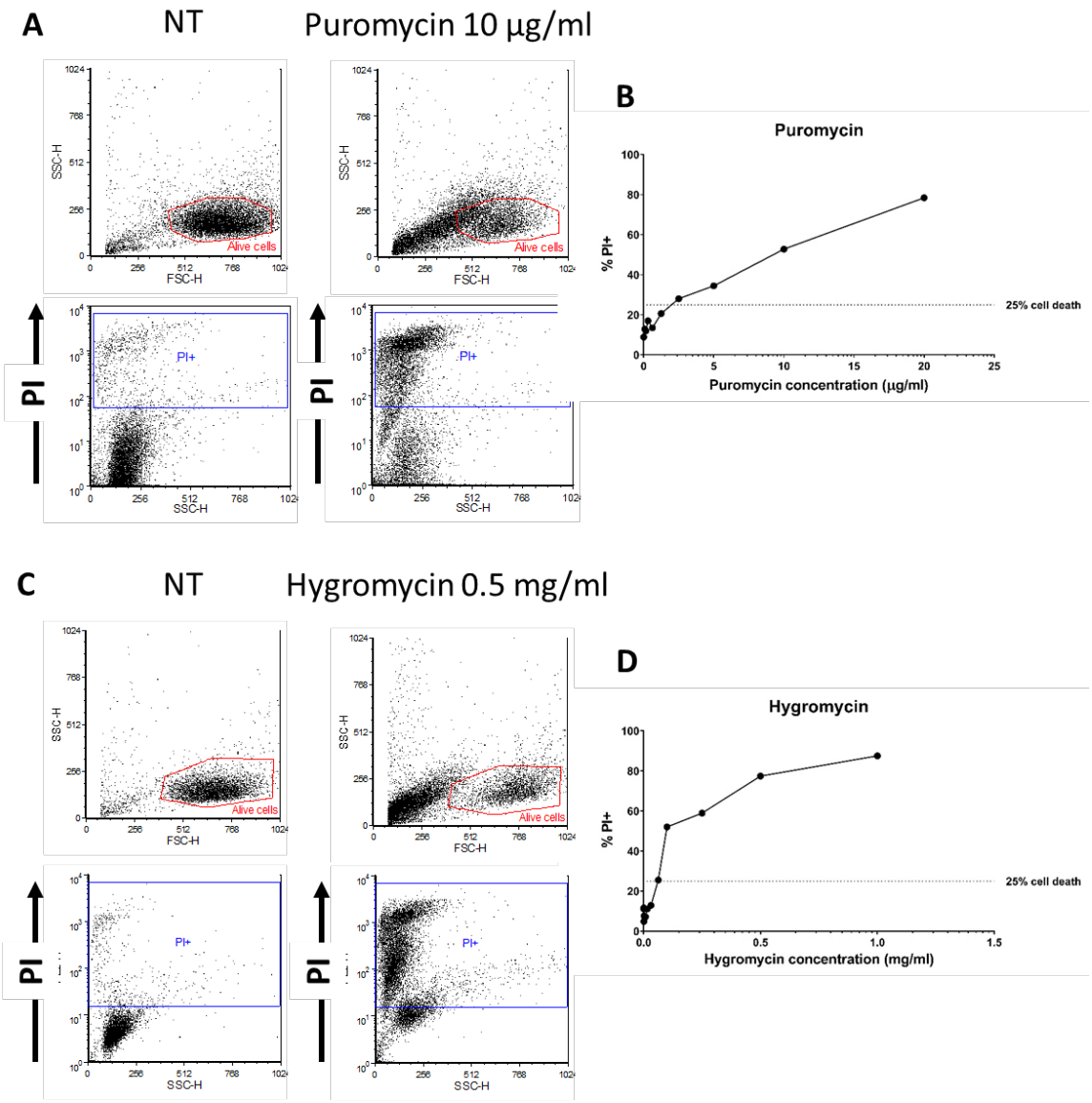

Figure 4.38 Development of puromycin and hygromycin kill curve for 9464D cells to determine appropriate selection dose

A) 9464D cells were treated with either puromycin or hygromycin, with subsequent cell death assessed by PI+ staining as detailed in **Section 2.12.4**. Example gating of NT and 10µg/ml puromycin treated 9464D cells is shown. **B)** Kill curve for titration of puromycin. **C)** Example gating of NT and 0.5mg/ml hygromycin treated 9464D cells. **D)** Kill curve for titration of hygromycin.

4.2.8.2 GFP expression of transduced 9464D cells after puromycin selection

After retroviral transduction of GFP, the selection antibiotic puromycin was added to culture as detailed in **Section 2.12**. Cells were cultured in puromycin selection for 10 days, at which point GFP transduction was assessed by both fluorescence microscopy and flow cytometry, as shown in **Figure 4.39**. It can be observed that at day 0, before selection was applied, GFP fluorescence was weak but present on both fluorescence microscopy (top panel) and flow cytometry (bottom panel - **Figure 4.39 A**). Furthermore, on flow cytometry, the cells which are GFP positive had variable GFP expression. After puromycin selection was applied for 10 days (**Figure 4.39 B**), there was a marked

increase in GFP fluorescence on microscopy (top panel) with most cells brightly expressing GFP protein. This was confirmed with flow cytometry (bottom panel) with most cells now highly expressing GFP protein. These data suggested the transduction for GFP was successful.

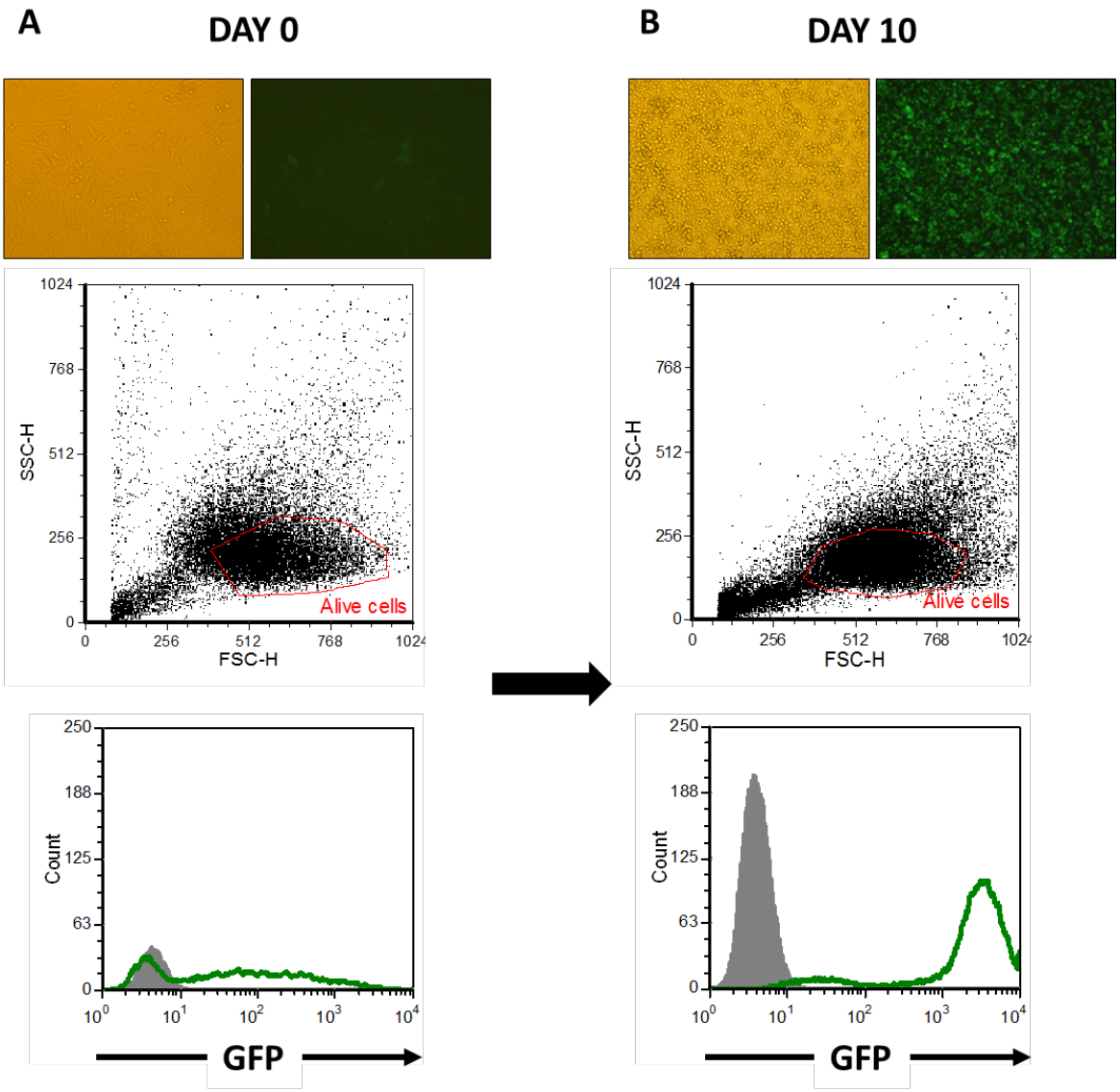

Figure 4.39 GFP expression of transduced 9464D cells after puromycin selection

A) 9464D cells were transduced with GFP as detailed in **Section 2.12**. GFP expression was assessed by fluorescence microscopy and flow cytometry as described in **Section 2.9**. GFP-transduced 9464D cells at day 0 before addition of selection puromycin is shown. Top panel: GFP expression assessed by fluorescence microscopy, bottom panel: GFP expression on flow cytometry. Same is shown in **B)** after 10 days of puromycin selection.

4.2.8.3 hBCL-2 expression in transduced 9464D cells after hygromycin selection

After transduction of EV and hBCL-2 into 9464D cells, hygromycin selection antibiotic was added to the culture to improve the purity of the transduced cells. After 7 days of growing in the selection antibiotic, expression of hBCL-2 was assessed in **Figure 4.40 A** by flow cytometry. 9464D cells and

9464D EV cells were demonstrated to have no expression of hBCL-2, whereas 9464D hBCL-2 cells were shown to have high hBCL-2 expression. When the histograms were overlaid in **Figure 4.40 B** the difference in hBCL-2 expression was clear with a large increase in geoMFI of hBCL-2 with 9464D hBCL-2 cells. The high level of hBCL-2 expression on hBCL-2 transduced cells was confirmed using western blotting shown in **Figure 4.40 C**. Here, expression of hBCL-2 was only seen in the 9464D hBCL-2 transduced cells, whereas mouse BCL-2 and another BCL-2 family member, MCL-1, had similar expression across all three cell lines.

Finally, morphology of all the cell lines transduced in this chapter was assessed by phase contrast imaging (**Figure 4.41**). Here, the 9464D EV, hBCL-2 and GFP lines created (**Figure 4.41 B-D**) were all shown to have similar morphology in culture conditions as the parental 9464D line (**Figure 4.41 A**), being large cells with long projections. This confirmed that transduction of the cells had not dramatically altered the overall morphology of the 9464D cells.

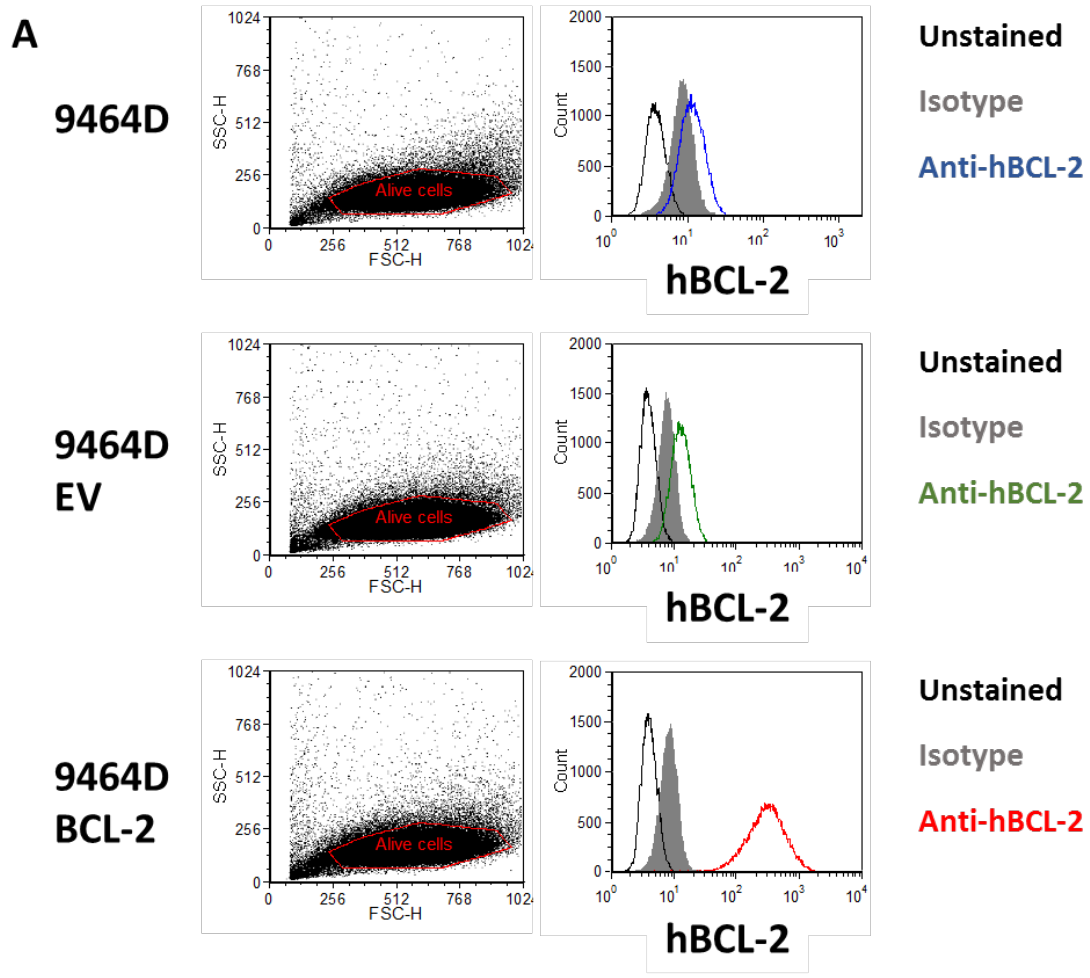

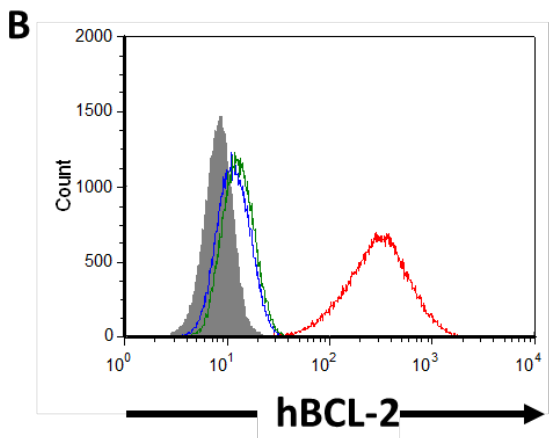

	geoMFI		
Cell line	Isotype	Anti-hBCL-2	**Minus isotype**
9464D	8.36	11.47	**3.11**
9464D EV	7.46	12.69	**5.23**
9464D BCL-2	8.21	280.97	**272.76**

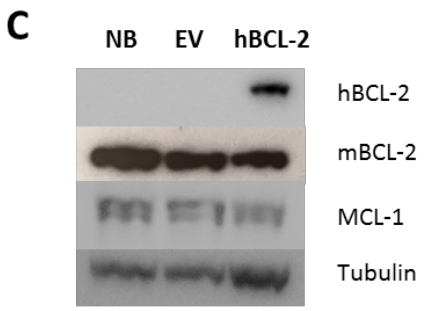

Figure 4.40 Expression of hBCL-2 in transduced 9464D cells after hygromycin selection

9464D cells were transduced with EV control or hBCL-2 as detailed in **Section 2.12**. Transduced cells were cultured with hygromycin selection. hBCL-2 expression was assessed by both flow cytometry and western blot, detailed in **Sections 2.12.5** and **2.13** respectively. **A)** Expression of hBCL-2 assessed by flow cytometry on (from top to bottom) 9464D, 9464D EV and 9464D BCL-2. **B)** Overlays of hBCL-2 expression on 9464D (blue), 9464D EV (green) and 9464D hBCL-2 (red). geoMFIs are shown in table. **C)** Western blot of 9464D, EV and hBCL-2 lines for hBCL-2, murine BCL-2 (mBCL-2) and MCL-1. Tubulin was used as loading control.

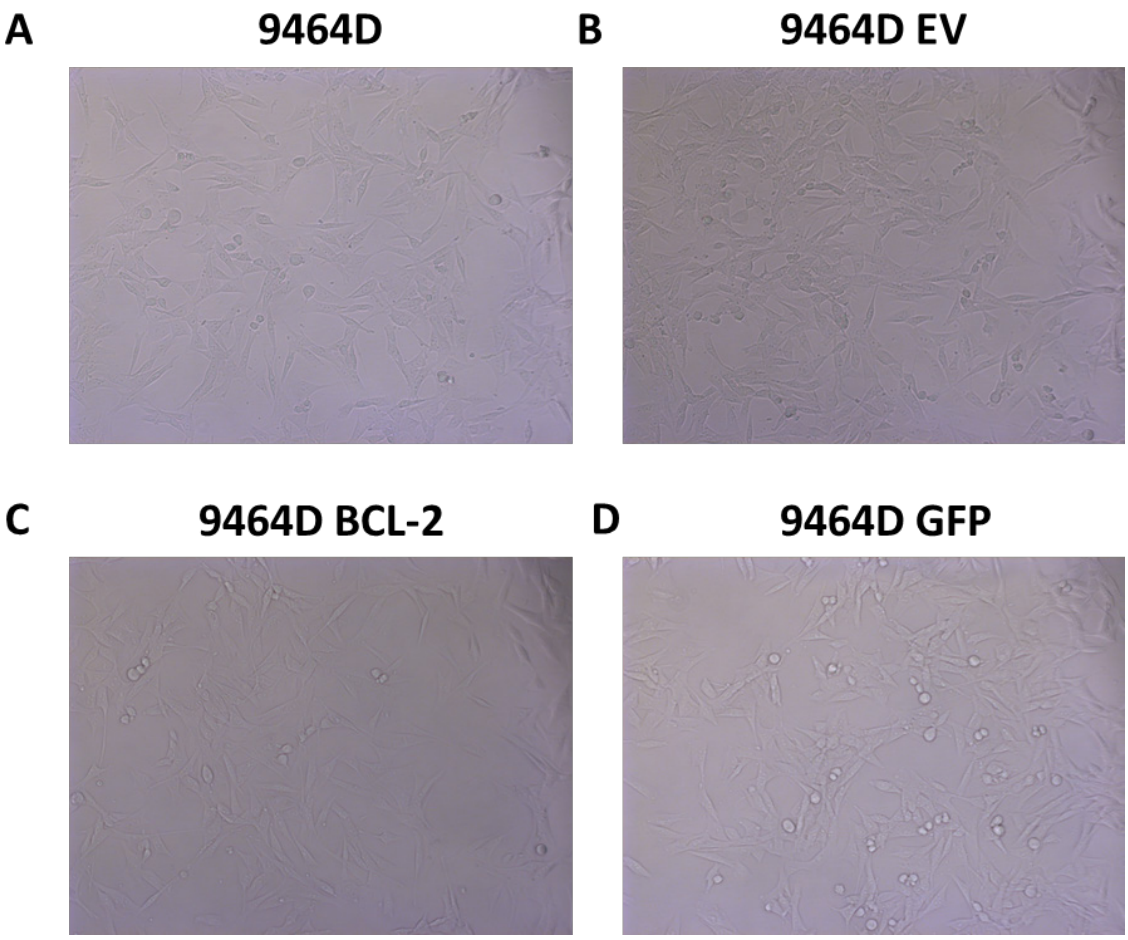

Figure 4.41 Morphology of transduced 9464D cell lines compared to 9464D parent line

Phase contrast imaging of **A)** parental 9464D cells line and transduced lines: **B)** EV, **C)** BCL-2 and **D)** GFP, all after selection.

4.2.9 Assessment of chemotherapy cytotoxicity on hBCL-2 transduced 9464D cell lines

After establishment of the hBCL-2 9464D cell line, it was imperative to check whether this overexpression of BCL-2 could lead to a diminished capacity of CPM to induce death. Firstly, an MTT assay was used to test whether metabolic activity of these cells changes when dosed with MAF along with other chemotherapies. **Figure 4.2** and **Figure 4.3** demonstrated previously that MAF and DOX lead to a decrease in cell proliferation in a dose dependent manor when these chemotherapies were applied to the parental 9464D cell line.

In **Figure 4.42** the three different cell lines were administered with MAF for 24 hrs, at which point an MTT assay was performed. **Figure 4.42 A** demonstrates that possibly some protection form MAF treatment seen in the hBCL-2 cell line, however data from the parental cell line was variable so it is difficult to assess. Alongside the MAF MTTs, the effect of DOX and etoposide was also assessed in **Figure 4.42 C+D** respectively. DOX was shown to be potent at reducing the proliferation of both the parent and EV cell lines, whereas some slight protection was seen in the hBCL-2 cell line.

Interestingly, all doses of etoposide did not seem to have an effect on any of the cells lines within the MTT assay.

Due to this variability in the MTT assay, which may in part be due to differences in cell confluence, date of previous passage and other culture dependent factors, it was decided to try looking at apoptosis more directly using western blotting for caspase activation. Firstly, as demonstrated in **Figure 4.43 A**, a time course experiment was conducted in parental 9464D to establish when would be most appropriate to look for apoptosis activation after MAF administration. Here, cleaved PARP expression was most prominent at 24 hrs post MAF administration compared to UT cells. Using this time point, investigation into expression of further apoptosis related proteins, as shown in **Figure 4.43 B**. For this, the parental cell line along with EV and hBCL-2 9464D cells were cultured with 50 ug/ml MAF for 24 hrs, after which lysates were collected and analysed for caspase activation. It was observed that a marked increase in cleaved PARP and cleaved Caspase-3 was seen in both parental 9464D and EV 9464D cells compared to the hBCL-2 overexpressing line. This suggests there is reduced apoptosis activity, at least in a pathway involving these proteins, in the hBCL-2 overexpressing cell line.

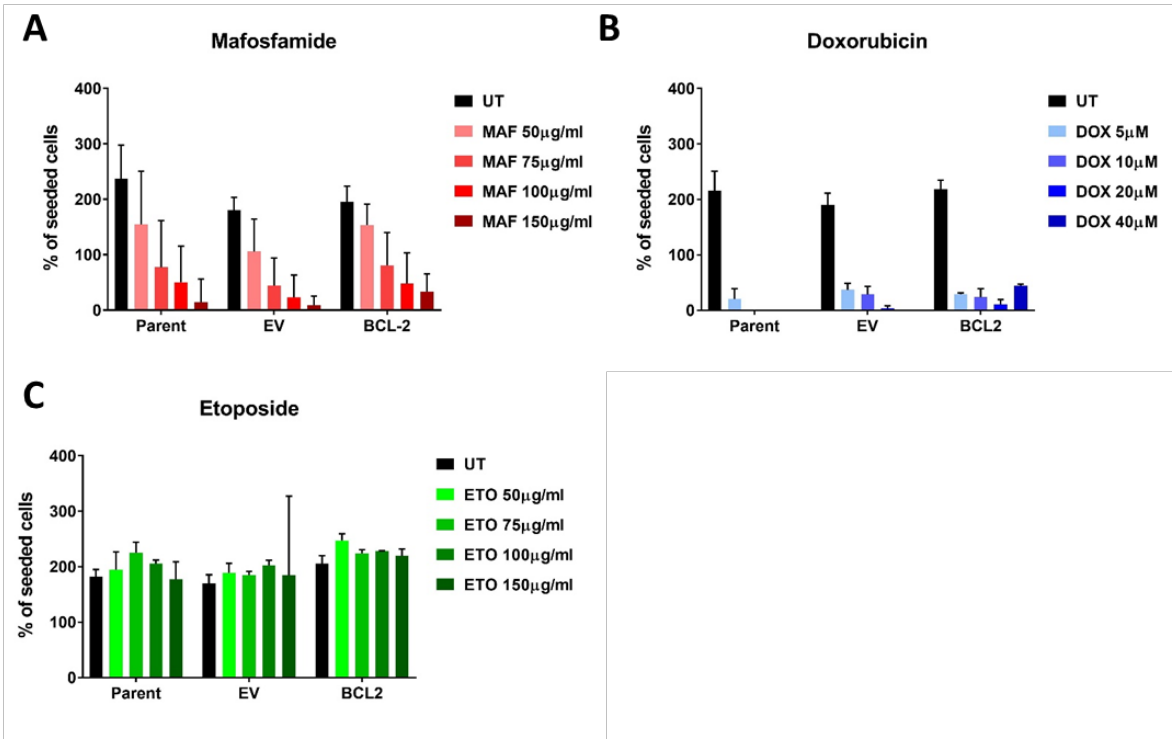

Figure 4.42 MTT assays after cytotoxic application using parental, EV and hBCL-2 9464D cell lines

A) Either parent, EV or hBCL-2 9464D Cells were plated in a 96-well plate at a concentration of $5x10^4$ per well. MAF dosing was conducted as detailed in **Section 2.10.1**, with MTT assay being followed as detailed in **Section 2.10.2**. Cell numbers were calculated using a standard curve as set up in **Figure 4.1**. Combined percentage of seeded cells remaining metabolically active after MAF administration is shown, for 3 independent experiments. **B)** Same MTT assay as above but using DOX, and **C)** etoposide. 3 independent experiments shown in **B**, with one experiment with technical repeats shown in **B + C**. Mean and SD error bars are shown.

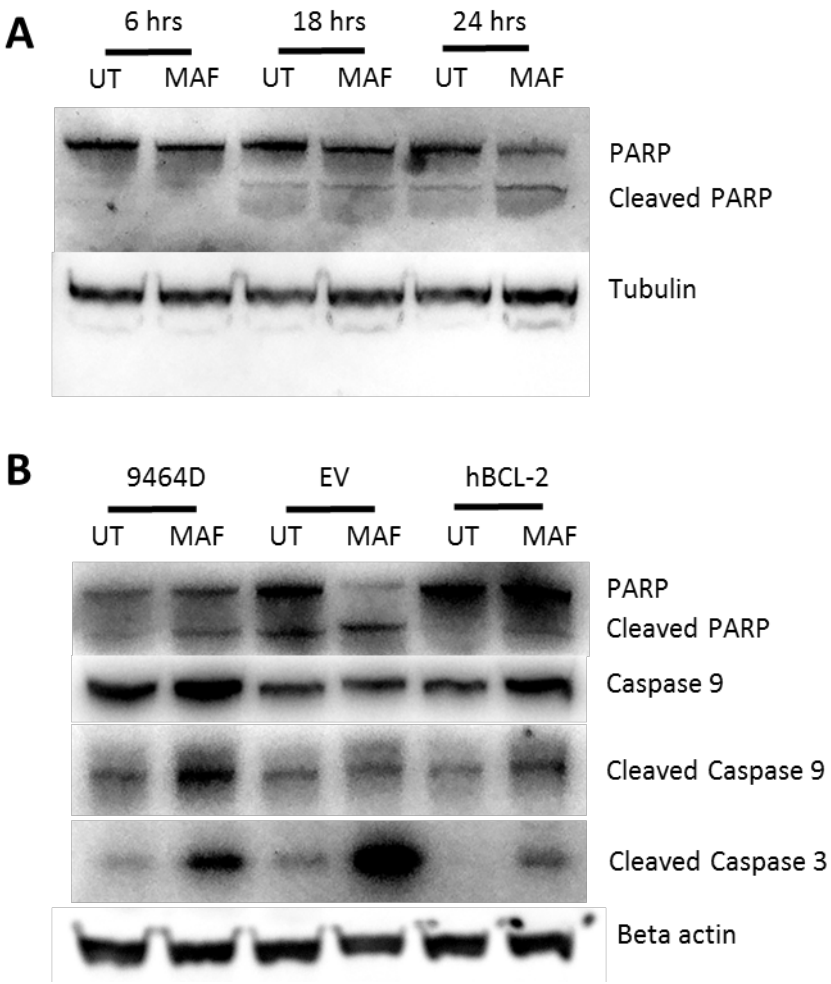

Figure 4.43 Western blot analysis of apoptosis activation after MAF treatment in 9464D cell lines

A) 5x10^6 9464D cells were plated into 6 well plates, and MAF was administered at set time points, and cell lysates were collected, with Western blots being conducted as detailed in **Section 2.13,** for PARP cleavage and tubulin loading control. **B)** Same process as conducted in A, with 9464D, EV and hBCL-2 cell lines. Western blot was carried out to identify: cleaved PARP, cleaved caspase 9, cleaved caspase 3 and beta actin loading control.

4.2.10 Assessment of growth of hBCL-2 9464D cell line *in vivo*

Having established *in vitro* that hBCL2 overexpression led to the reduction of caspase and apoptosis component activation it was next determined whether these cells would grow in immunocompetent mice. This would permit the assessment of cell death via BCL-2 in this tumour during chemotherapy. To this end, C57BL/6 mice were inoculated with the same dose of either 9464D, 9464D EV or 9464D BCL-2 cells and tumour growth was monitored, as shown in **Figure 4.44**. Attempts to grow the two transduced cell lines (EV and hBCL-2) were unsuccessful in three separate experiments (**Figure 4.44 A-C**) in female 8 -12 week old mice. In each experiment the un-transduced

parental 9464D cell line grew as expected, with 9464D EV and hBCL-2 tumours becoming palpable or slightly bigger until eventually regressing until no tumour was present. When immunophenotyping was performed on tumours from the EV and hBCL-2 cell lines, a higher percentage of infiltrating CD3+ cells driven by an increase in CD4+ cells was noted, alongside a significant increase in NK cells (Appendix **Figure 7.4**).

Due to the appearance and the regression of the transduced tumours, it was hypothesised that this may be due to an immune response against the retrovirally transduced cell lines. Therefore to test this, the three cell lines were inoculated SC into the left flanks of NOD/SCID immunocompromised mice and tumour growth was monitored as in **Figure 4.45**. Here, more rapid tumour growth was observed in hBCL-2 and to a lesser extent EV tumours compared to parental 9464D tumours (**Figure 4.45 A+B**). All mice inoculated with 9464D hBCL-2 had reached end point by day 40 (**Figure 4.45 C**) whereas 9464D tumours were still relatively small and therefore at 100% survival when the experiment was ended.

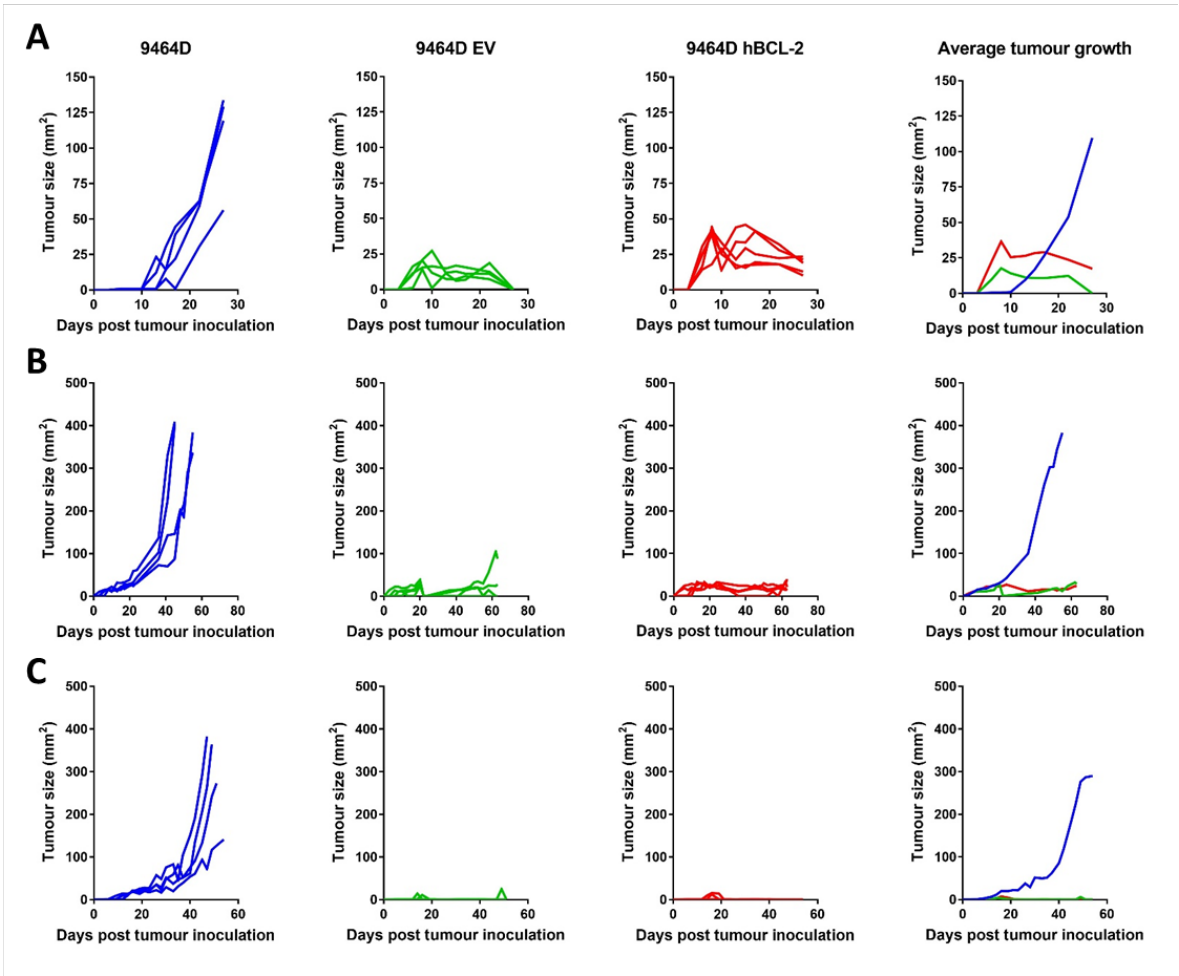

Figure 4.44 Tumour growth curves of hBCL-2 transduced 9464D cell line

A) C57BL/6 female mice were injected SC with $5x10^5$ cells of either 9464D, 9464D EV or 9464D hBCL-2 cells as detailed in **Section 2.6**. Tumour growth was monitored and mice were culled at set end points. Shown here is experiment one with **B)** experiment two and **C)** experiment 3. n= 4 mice per group.

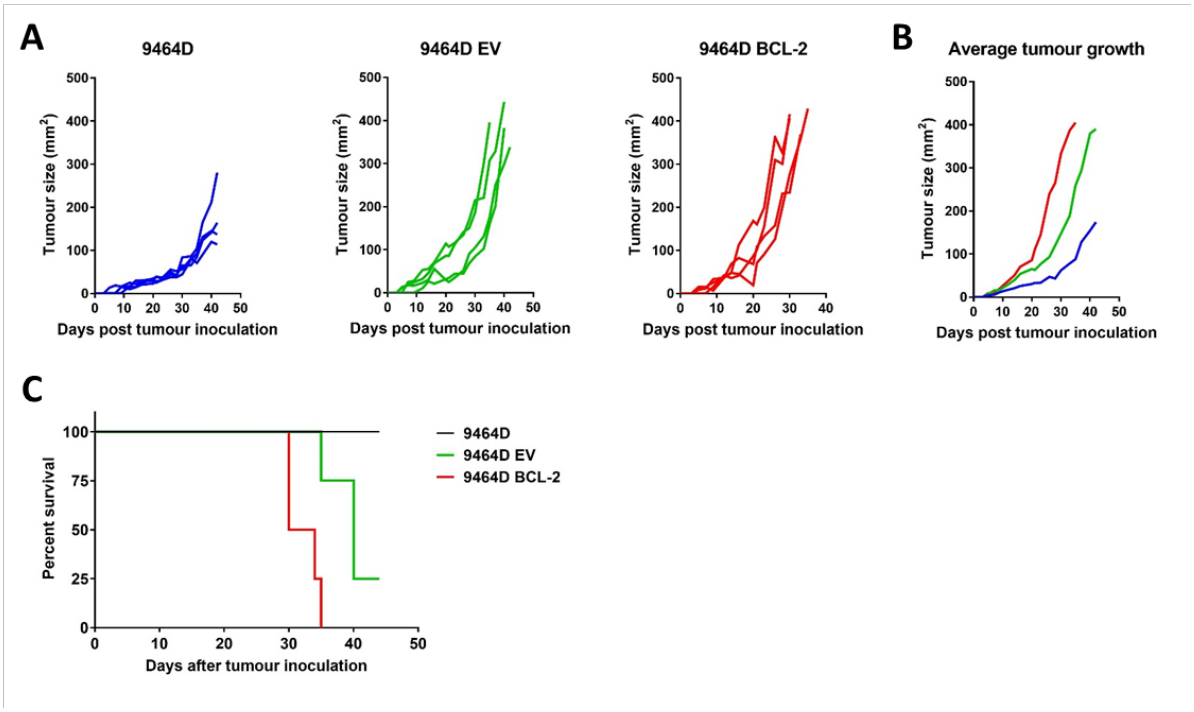

Figure 4.45 Tumour growth curves of hBCL-2 transduced 9464D cell line in NOD/SCID mice

A) NOD/SCID female mice were injected SC with $5x10^5$ cells of either 9464D, 9464D EV or 9464D hBCL-2 cells as detailed in **Section 2.6**. Tumour growth was monitored and mice were culled at set end points. **B)** Average tumour growth and **C)** Survival curve. n= 4 mice per group.

4.2.11 Modulation of T cell subsets of 9464D SC tumours in vav-BCL2 transgenic mice compared to C57BL/6 mice

So far, it has been observed that low dose CPM can lead to the tumour specific depletion of Treg cells, along with modulating T cell phenotypes. In an attempt to establish how this depletion is mediated, transgenic vav-BCL-2 mice, in which all lymphocytes overexpress hBCL-2 and hence are resistant to apoptosis, were utilised. As previously, vav-BCL-2 mice bearing 9464D tumours were dosed with 40 mg/kg CPM and tumours were harvested 72 hrs later for immunophenotyping. Immunophenotyping profiles of T cell subsets were compared with wt C57BL/6 9464D tumours. Here, significant Treg depletion was observed in C57BL/6 tumours treated with CPM (**Figure 4.46 A**), as demonstrated previously. Importantly, this Treg depletion was not seen in vav-BCL-2 mice treated with CPM. Furthermore, significant depletion of CD8+ cells was seen in C57BL/6 tumours, contrary to previous data. The levels of CD4+ and CD8+ cells were similar and unaltered in vav-BCL-2 9464D tumours treated with CPM (**Figure 4.46 B+C**).

Expression levels of PD-1, were assessed in TILs for both mouse strains, with or without CPM (**Figure 4.47**). Here similar levels of PD-1 expression were observed, with a decrease seen after CPM for CD4s and CD8s in both vav-BCL-2 and C57BL/6 tumours. A reduction in PD-1 expression on Tregs cells in both vav-BCL-2 tumours and C57BL/6 models (**Figure 4.47 A+B**).

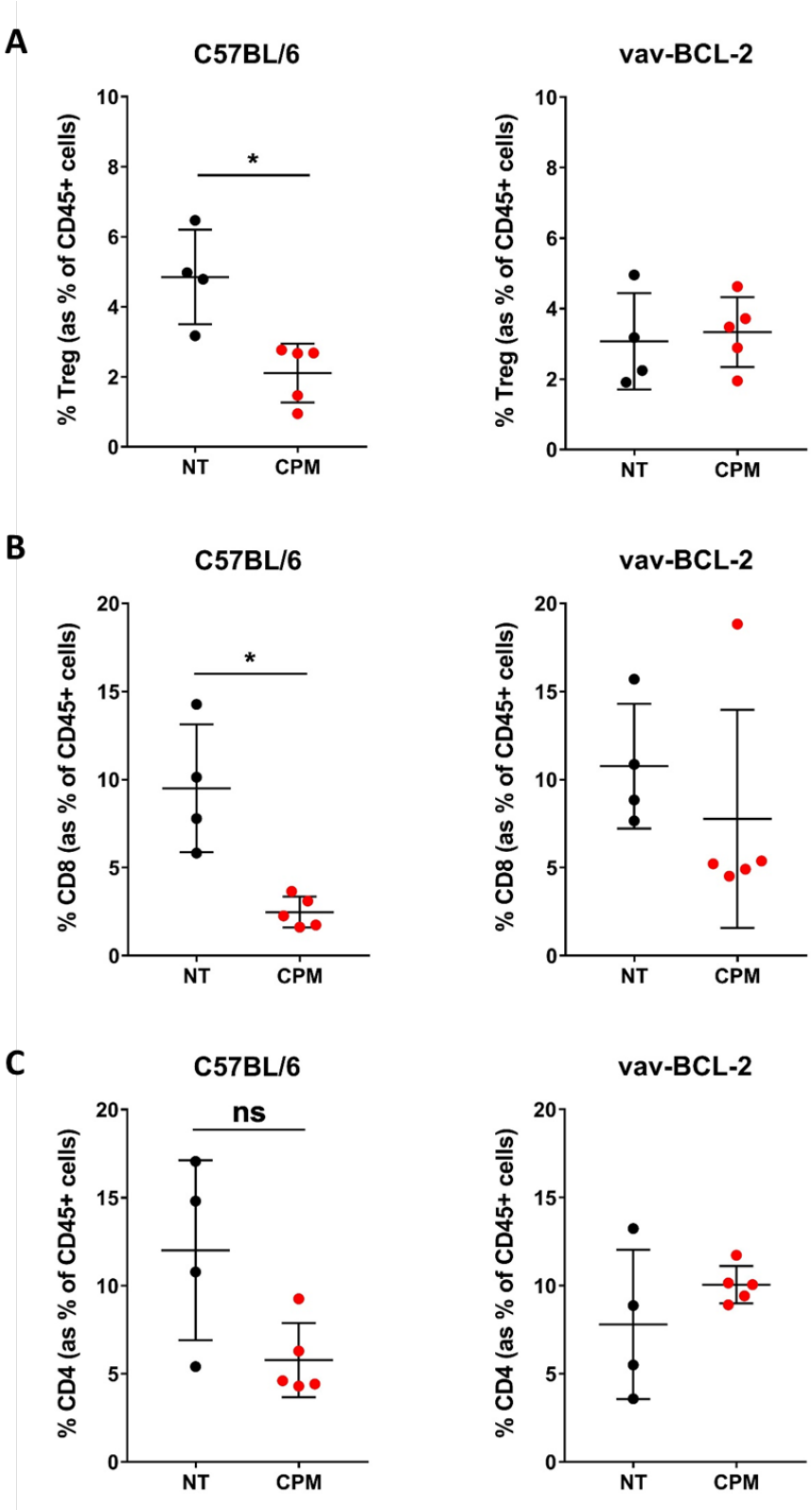

Figure 4.46 Effect of CPM administration on 9464D tumour TILs in both C57BL/6 and vav-BCL-2 mice

A) 9464D tumours in both C57BL/6 and vav-BCL-2 mice at around 8x8 mm were treated with 40 mg/kg CPM and at Day 3 were harvested, processed for flow cytometry for immunophenotyping as detailed in **Section 2.9**. Populations were defined as detailed in **Figure 4.23Figure 4.27**. Tregs as a percentage of CD45+ cells are shown. **B)** Same shown as in A but for CD8+ and **C)** CD4+.. n= 4 (NT) and n= 5 (40 mg/kg CPM). Statistical analysis was conducted using Mann-Whitney test with significance defined as: ns = not significant and *= <0.05. Means and SD error bars are shown.

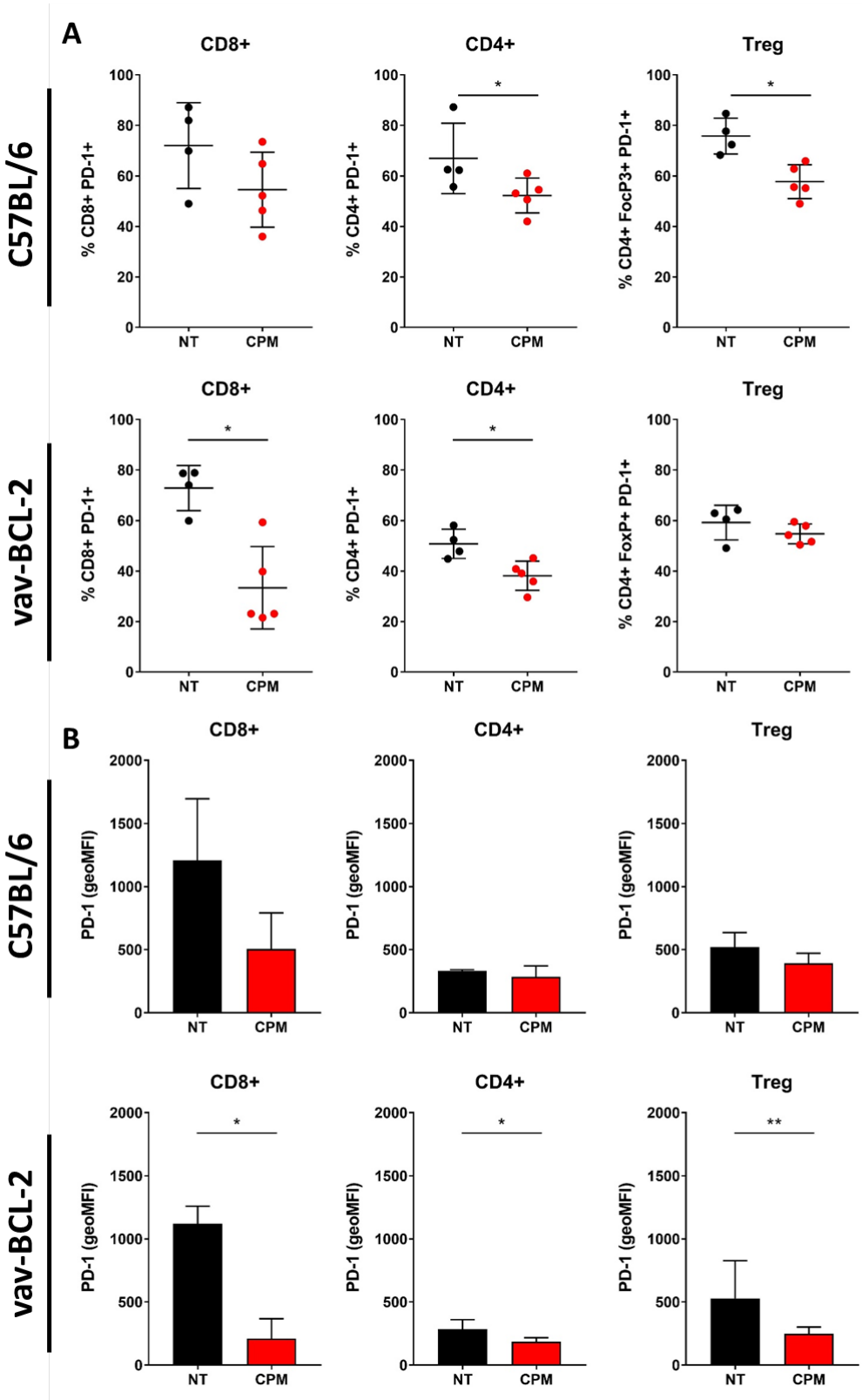

Figure 4.47 Modulation of PD-1 after CPM administration on 9464D tumour TILs in both C57BL/6 and vav-BCL-2 mice

A) 9464D tumours in both C57BL/6 and vav-BCL-2 mice at around 8x8 mm were treated with 40 mg/kg CPM and at Day 3 were harvested, processed for flow cytometry for immunophenotyping as detailed in **Section 2.9**. Populations were defined as detailed in **Figure 4.23**, with PD-1 analysis conducted as in **Figure 4.23Figure 4.27**. PD-1 expression as a percentage of CD8+, CD4+ and Treg cells is shown. **B)** Same as in A, but showing PD-1 expression as geoMFI (minus isotype). n= 4 (NT) and n= 5 (40 mg/kg CPM). Statistical analysis was conducted using Mann-Whitney test with significance defined as: *= <0.05 and **= <0.01. Means and SD error bars are shown.

4.3 Discussion

Treatment for high risk neuroblastoma includes the use of several different high dose chemotherapeutics, which are classically thought to be immunosuppressive and therefore not beneficial for combining with immunotherapies. However, recent research suggests that certain chemotherapies, including doxorubicin and CPM, can induced a form of immunogenic cell death (ICD) of tumour cells which has the potential to stimulate a potent anti-tumour immune response [278]. Furthermore, the use of low-dose, metronomic chemotherapy, particularly CPM, has been demonstrated to supress and deplete Treg cells while preserving and even stimulating other T cell subsets [339,365,569]. Although low dose chemotherapy and the induction of ICD has been studied extensively for adult cancers, research into how paediatric cancers respond is sparse. This chapter therefore focused on defining whether ICD can occur in murine neuroblastoma cells, and if CPM can have the same immunomodulatory properties within *in vivo* murine neuroblastoma models as previously reported for other cancers. Furthermore, attempts were made to determine whether ICD induction or direct immunomodulation was more important than the other.

ICD relies upon the expression of certain markers in a way that both attracts and stimulates the immune system to prime and anti-tumour immune response, as discussed previously (See **Section 1.4.3**). Expression of ICD markers, ecto-CRT and Hsp-70, both of which translocate to the cell surface after ICD inducer application [278], were investigated after MAF and DOX application. Firstly, an appropriate cytotoxic dose for each chemotherapy and each cell line was established as shown in **Figure 4.2** and **Figure 4.3**, using an MTT assay which measures metabolic activity of cells. Here, 9464D cells were slightly more resistant to MAF than the NXS2 cells, as higher doses were required to reduce metabolic activity to a minimum (**Figure 4.2**). From this a dose of 50 ug/ml (NXS2) or 75 ug/ml (9464D) of MAF, and 40uM of DOX were used in further *in vitro* analysis. Investigation into ecto-CRT and Hsp-70 expression by flow cytometry analysis was assessed (**Figure 4.4**). It was demonstrated that both cell lines were able to increase expression of both ecto-CRT and Hsp-70 after application of DOX or MAF. However, intra-assay variability was noted, and may suggest that the assay and subsequent expression of the markers was impacted by tissue culture specific conditions. Despite this, these data go some way to suggest that DOX and MAF can induce these ICD markers on these two cell lines, as has been reported in other tumour cell lines such as CT26 [297,298,301].

Expression of another ICD marker, HMGB1, was also assessed using 9464D cells both *in vitro* with MAF and in ex vivo tumours with CPM administration (**Figure 4.5** and **Figure 4.6**). Here, 9464D cells *in vitro* demonstrated aberrant HMGB1 expression compared to NT cells. Diffuse cytoplasmic and strong nuclear staining was observed in NT cells, and was not present in MAF treated cells were

only weak fluorescent staining of HMGB1 was demonstrated to be mainly nuclear. Furthermore, the nuclear staining was at lower intensity than seen in NT cells, and more punctate in its expression pattern. However, some of these changes in expression could be due to morphology of the cells related to induction of cell death processes. Ex vivo analysis using 9464D tumours which were treated with CPM, was conducted using IHC on FFPE sections. Here, in NT tumours, diffuse HMGB1 staining was seen across the whole tumour, however CPM treated tumours demonstrated strong nuclear staining, with reduced diffuse cytoplasmic staining. These data together suggest that HMGB1 expression patterns change after chemotherapy application. The reduction of cytoplasmic staining and reduced staining intensity of HMGB1 could suggest that the protein is being secreted by the cells in response to the chemotherapy. As nuclear staining is still present in CPM treated cells, both *in vitro* and *in vivo*, this could suggest that the expression alterations observed are due to the secretion of cytoplasmic HMGB1 rather than nuclear, and not due to differences in actual HMGB1 protein production. Together with the *in vitro* data suggesting increasing expression of ecto-CRT and Hsp-70, these data demonstrate modulation of ICD marker expression after CPM or MAF application. This infers an induction of an ICD response in these NB models, which could in turn, lead to the creation of an immunogenic environment after CPM treatment.

It has been previously reported that low doses of CPM can deplete Tregs while maintaining the numbers of other important T cell subsets in patients and in mice [329,339,346,366,568]. However it has not previously been investigated whether this effect is seen within the tumour microenvironment of NB models. For this the two SC models were employed, as they are more efficient to work with, compared to the spontaneous model, as large groups of mice can be set up at the same time point. For both models, tumour cells were injected subcutaneously into the corresponding mice and allowed to grow to 8x8 mm. At this point one of three doses of CPM were injected IP and 72 hrs later spleens and tumours were harvested to perform detailed immunophenotyping via flow cytometry.

Myeloid cells are an important arm of the innate immune system and have been well documented to play an important role within the tumour microenvironment, with both pro- and anti-tumour effects [14,15,87]. In CPM treated NXS2 tumours (**Figure 4.8**), it appeared that the high dose almost ablated monocytes in the tumours. However, the most significant finding of how myeloid cells respond to CPM was seen in macrophages. Macrophages, as discussed previously, can be both supportive and hindering to the anti-tumour immune response depending on their polarisation [76]. In the NXS2 model, both the lowest and the highest dose of CPM significantly increased macrophage infiltration into the tumour microenvironment. For the high does, this can somewhat be explained by the fact that this will cause widespread tumour cell death, with tumour shrinkage noted after just 3 days (data not shown). The large amounts of cell death, and therefore cell debris,

seen with this dose will attract macrophages into the tumour microenvironment to clear the debris caused by the apoptotic cells [281]. However, with the low dose, no widespread cell death will be seen as no tumour shrinkage was noted after 3 days (data not shown). Therefore, the infiltration of macrophages may be due to the low dose of CPM causing ICD of the tumour cells leading to release of markers such as ATP and HMGB1, which can attract the phagocytic cells to eat the dying tumour cells[311,570]. This increase in macrophages within the tumours was replicated in the 9464D model (**Figure 4.9**), although, no change was seen in 40 mg/kg. Furthermore, in 9464D tumours, an increase in neutrophils with CPM could be due to the creation of a proinflammatory environment, caused either by cell death or activated cells within the microenvironment which is leading to neutrophil recruitment [76]. In further experiments conducted in 9464D model (**Figure 4.20**), modulation of myeloid percentages were assessed at both Day 3 and Day 10 after 40 mg/kg CPM. Here, differing from what was seen previously, at Day 3 macrophages at 40 mg/kg were significantly depleted with CPM. Therefore, further investigation into unravelling how CPM effects numbers of tumour infiltrating myeloid cells needs to be conducted.

Although there is uncertainty between how CPM effects percentage of myeloid cells within tumours, an attempt was made to assess changes in myeloid cell phenotype after CPM administration (**Figure 4.21** and **Figure 4.22**). As discussed previously, CPM administration has been reported to repolarise TAMs into a more 'M1-like' anti-tumour phenotype [334]. Macrophages, were shown to have the highest expression of the inhibitory FcγRII at baseline compared to other myeloid cell types. This could suggest that these cells are more 'M2-like' and less activated in their phenotypes [571]. Furthermore, expression of FcγRII was significantly increased with CPM at Day 3, but not maintained to Day 10. This may have been due to CPM causing death of tumour cells and therefore release of cell debris and inflammation markers which could increase the expression of this receptor on the TAMs. Despite this alteration, there was no overall change in A:I ratio of macrophages in tumours, suggesting that CPM is not altering the overall phenotype. However, A:I ratio was significantly decreased at Day 10 with CPM, mainly driven by downregulation of FcγRIII. This could suggest that modulation of macrophage phenotype, with regards to FcγR expression, is not a fast process and may include changes in gene expression, therefore taking a longer period of time to occur. Contrary to macrophages, monocyte and DC A:I ratio at Day 3 had increased with CPM, suggesting these cells have become more activated, at least in regards to their FcγR expression. This was mainly driven, at least for DCs, by an increase in FcγRI and FcγRIII, however by Day 10 expression of these FcγRs was then decreased by CPM. For DCs there appears to be initial activation of these cells in the short term by CPM, followed by delayed downregulation of activatory FcγRs is at a longer time point. Overall, how CPM effects myeloid cell infiltrate is a complicated process with short term and long term effects, and cell specific alteration being disparate. If

activation of myeloid cells occurs short term after CPM and suggested here, it may be prudent to use more regular dosing of CPM in order to maintain this activated phenotype, such as dosing metronomically.

As discussed extensively in **Section 1.3.2.1**, T cells are the most important effector cell with regards to establishing and maintaining an anti-tumour immune response. It has been reported in many cancers that T cell infiltration into the tumour microenvironment positively correlates with good prognosis [139-142]. Furthermore, effective immunotherapeutics in the form of checkpoint inhibitors, specifically target these cells, and their apparent efficacy is down to activating a potent T cell response [432,472]. Therefore, quantifying these cells within the tumour microenvironment and how they are effected by CPM administration is vital, especially considering that CPM dose may dictate whether these cells are ablated or stimulated [569]. Furthermore, the T cell regulatory subset, Tregs, have been correlated with a worse prognosis in many cancers, and therefore establishing the ratio between promoting and suppressive T cell subsets is needed.

CD8+ T cells, the main effector cells of the anti-tumour immune response, were stable in tumours at lower doses of CPM for both models, with a decrease in CD8+ cells seen at the highest dose in both models. Importantly these data suggest that CD8+ T cells within the tumour microenvironment are not significantly reduced with the two lower doses of CPM, implying that using these doses in combination with immunotherapy may be beneficial, as it maintains effector cell numbers. For helper CD4+ cells, both models saw minimal changes in percentages within the spleens. In the tumours, CD4+ numbers has high variability within NXS2 tumours, therefore it was difficult to see any changes. This may be due to the highly vascularised tumours, which suggests high rates of angiogenesis and therefore poorly organised, immature and leaky vessels, which in turn can result in reduced T cell infiltration [572]. However, when quantification of NXS2 tumour was repeated for 20 and 40 mg/kg (**Figure 7.3** and **Figure 4.24**), reduced variability was observed, but still no significant changes were noted. In 9464D tumours, there was a significant increase with the highest dose of CPM, which could be due to the depletion in CD8+ cells, altering the percentages.

As previously mentioned it is important to see whether depletion of Treg percentages are observed with CPM, as this has been a reported as a documented effect in different tumour models and in patients [339,365,367,368]. In both models of NB, a depletion of tumour Tregs at all CPM doses was demonstrated, which was more significant in NXS2 tumours with nearly half of all Tregs depleted (**Figure 4.14** and **Figure 4.15**). Furthermore, depletion using the 40 mg/kg CPM was consistently seen in further phenotyping experiments (**Figure 7.3** and **Figure 4.29**). These data support the notion that CPM can selectively target Treg cells and deplete them, suggesting their sensitivity to CPM[339,365,366,568]. More importantly, this shows that this selective Treg depletion is maintained at

even the relatively low dose of 40 mg/kg CPM, suggesting that this could still be used effectively in immunotherapy combinations. Furthermore, it was demonstrated that the Treg depletion initiated by CPM at a low dose of 40 mg/kg was very tumour specific, with no depletion seen in spleens, dLN, ndLN and PBMCs of tumour bearing mice in both NXS2 and 9464D models (**Figure 4.19**). This tumour specific depletion may be due to Tregs within the tumour microenvironment being in a more activated state, which could render them more sensitive to CPM depletion using the low dose which is not high enough to effect less sensitive T cell subsets. Tregs in general are thought to be 'targeted' by CPM as they are at a highly proliferative state and express low levels of important CPM drug efflux transporters such as ABCB1 [368]. CPMs mechanism of action involves inducing DNA damage, therefore any cells that are proliferating readily, and consequently have their DNA exposed, are sensitive to CPM depletion [573]. Furthermore, as tumour microenvironments are generally highly hypoxic compared to normal tissues, there may be lower levels of ATP accessible to Tregs to enable them to proliferate and efficiently use the few efflux transports they have [367]. All of these factors collaborate to render tumour infiltrating Tregs sensitive to CPM depletion, which is significantly effective even at low doses. This is important as using the 40 mg/kg dose therapeutically will lead to Treg depletion, but will leave other immune cell populations, particularly effector CD8+ and CD4+ T cell, numbers intact.

Definition of whether a more stimulatory or suppressive T cell constituent within the tumour microenvironment can be inferred from looking at the ratios of the different subsets (**Figure 4.14** and **Figure 4.15**). Due to the Treg depletion mentioned above, the CD8:Treg ratio was increased in NXS2 tumours at 40 mg/kg CPM, however in 9464D this was highly variable, but when quantified in subsequent experiments, 9464D did demonstrate an increase in CD8:Treg ratio at 40mg/kg. The depletion of Tregs while CD8+ percentages remained relatively similar at this low dose, led to the increase in the ratio. This suggests that low dose CPM at 40 mg/kg creates a more anti-tumour immune environment, with the depletion of suppressive cells allowing for a release of effector CD8+ to mount any induced anti-tumour immune responses. The CD8:Treg ratio has been used clinically for prognosis estimation, with patients with higher CD8:Treg ratios in their tumour biopsies, having on the whole a better outcome [574,575]. Furthermore, when looking at the ratio between non-Treg CD4+:Treg in the NXS2 tumours, this was increased with all doses and importantly, this was significant at the low doses, which was replicated in the 9464D model in subsequent experiments (**Figure 4.29**) This highlights again the Treg specific CPM depletion, which must be due to mechanisms only applicable to Treg cells as non-FoxP3+ CD4+ T cell numbers remain untouched.

Overall, T cells within the tumour microenvironments of both models do not seem to be significantly altered at lower doses of chemotherapy, apart from significant depletion of tumour specific Tregs. This is promising for combining lower doses of chemotherapy with immunotherapy

as effector cells are still present and suppressive cells have been depleted, which could hopefully 'lift the breaks' and unleash an anti-tumour immune response. With similar results seen in both models after CPM administration it adds more substantial evidence of how CPM at different doses can modulate immune cells within NB tumours.

Although no modulation of tumour infiltrating CD8+ or CD4+ percentages was demonstrated, CPM may be altering the phenotypes of these cells instead. To assess this, the NXS2 model was utilised to design a flow cytometry panel to assess different aspects of T cell phenotype including: proliferation, activation and exhaustion. Overall in the NXS2 tumour infiltrating T cells, minimal modulation of all markers was observed, with no significant changes seen (**Figure 4.25** and **Figure 4.26**). However, there was a trend towards a decrease in EOMES and Ki67 expression on all T cell subsets after 40 mg/kg CPM, however the data for this model was again quite variable, which may be due to the inconsistent T cell infiltration, as discussed above.

Due to the variability in the NXS2 model, T cell phenotypes were assessed in greater depth utilising the 9464D model, in conjunction with a more comprehensive marker panel (**Table 4.1**). In this model, vast, significant modulation of a variety of markers on each T cell subset was noted and summarised in **Figure 4.36**. Furthermore, phenotypic changes were also analysed at a long term time point of Day 10 after CPM administration. In tumour infiltrating CD8+ T cells, CPM appeared to initially increase activation of these cells, as an upregulation of effector molecules, IFNγ and CD107a was observed. The elevation in CD107a suggests that degranulation of these effector T cell was initiated, and an increase in intracellular IFNγ within these cells denotes activation [138,234]. However, by Day 10 upregulation of exhaustion markers including EOMES and TIM3 on CD8+ T cells was observed, although IFNγ, along with co-stimulatory molecule 4-1BB, were also significantly upregulated. This could suggest that CPM initially leads to activation of effector CD8+ T cells, either directly or in-directly. However, this may have led to eventual exhaustion of activated T cells by Day 10. TIM3, like PD-1, is a checkpoint molecule which is known to be upregulated on exhausted T cells after chronic antigen stimulation [576]. EOMES, a T cell lineage marker, is also known to have increased expression on exhausted effector CD8+ T cells [577]. It was also observed that the only changes seen in T cell memory populations after CPM was a decrease in naïve CD8+ T cells at Day 10. CPM administration could have directly stimulated the CD8+ T cells, or have indirectly induced stimulation by causing cytotoxicity of tumour cells, possibly by ICD pathways, which would in turn lead to release of tumour antigens and initiate an anti-tumour immune response. Also, the Treg depletion observed with CPM may have lifted the suppression induced by these cells, releasing the effector T cells to become activated. Further investigation into the mechanisms behind this will need to be conducted, before this can be delineated fully.

CPM was also noted to initially lead to the increase in activation and possibly degranulation of CD4+ (non-Treg) cells at Day 3, with an elevation observed again in CD107a and IFNγ, suggesting that these cells may have some cytotoxic activity, alongside stimulating an effector immune response by IFNγ secretion [578,579]. However, concurrent downregulation of activation marker CD25 and upregulation of previously described EOMES was also noted at this time point. CD25 is the alpha-chain of the IL-2 receptor, which is known to be upregulated on T cells after activation, but is constitutively expressed on Tregs [370]. Therefore, these contradictory observations lead to inconclusive data as to whether CPM increases the activation or not of CD4+ T cells. By Day 10 in CD4+ T cells a reduction in intracellular granzyme B was noted, alongside an upregulation in IFNγ. The reduction in intracellular granzyme B could suggest that the chemotherapy may be having some toxic effects on these cells, leading to degranulation, rather than degranulation in response to an anti-tumour response. Furthermore, the continued elevation in IFNγ at Day 10 could suggest that these cells are activated and initiating a helper response by secretion of this molecule to boost effector T cell responses.

Interestingly, it was observed that the majority of modulation of T cell markers after CPM occurred on Treg cells. It is worth noting that at Day 3, as there was significant depletion of Treg cells, the phenotype on Tregs shown here was only representative of the remaining cells. Therefore, if CPM is specifically depleting a certain phenotype of Tregs, this would not be accounted for here. Importantly, there was a highly significant reduction in OX40 on Treg cells after CPM at Day 3. This T cell co-stimulatory marker is usually constitutively expressed on Tregs [580,581], suggesting a reduction in expression may be due to CPM either initiating its downregulation, or is leading to the depletion of activated Tregs which express the highest levels of OX40. Conversely to this however, significant upregulation of Ki67, CD107a and TIM3 was also observed. TIM3 expression is reported to be associated with enhanced suppressor function of Tregs [582]. Furthermore, transient expression of CD107a on Tregs has previously been reported, and suggested that these cells are capable of undergoing degranulation [583]. Here, using a model of lung infection, the degranulation of Treg cells was required for suppression of lung inflammation. Taking this into account, this could imply that CPM mediated depletion of Tregs leads to activation and proliferation of remaining Tregs, which may have greater suppressor activity including induction of degranulation, in order to account for the loss of Treg numbers. The possible increase in suppressor activity of Tregs after CPM was further implied at Day 10, with upregulation of double positive TIM3+ LAG3+ cells. LAG3 is another T cell checkpoint molecule, which has previously been shown to be associated with increased suppressor function of Tregs [584]. Despite this, it was also observed that CD25 was downregulated alongside an increase in EOMES and IFNγ. CD25 is known to be constitutively expressed on Treg cells [370], and therefore its downregulation may indicate a reduction in suppressive activity of these cells.

Furthermore, EOMES expression has been suggested to reduce the expression of FoxP3 in peripheral CD4+ cells [585], which again could imply suppressive function reduction, at this later time point.

Overall, CPM appears to be having a wide range of modulation on many different markers on different T cell subsets, which changes over time. For CD8+ cells, CPM is possibly leading to an increase in activation and generation of effector T cells in the short term. CPM's effect on CD4+ and Tregs however is more complicated, with suggestion of both an increase and decrease in activation. This is observed particularly for Tregs, where there could be both an upregulation of suppressive activity at Day 3, followed by a downregulation, mainly driven by EOMES upregulation. To test this idea, a suppression assay using purified intratumoural Tregs (after CPM administration) and CD8+ cells ex vivo would need to be conducted, to quantify changes in the suppressive capacity of these cells. However, in the NB models, there are low levels of T cell infiltration in total, and an even smaller proportion of Treg cells, therefore lots of tumour material would be required an pooled in order to acquire enough cells to perform this assay.

In order to assess the relative contributions of both ICD induction and Treg depletion towards CPM's immunomodulatory capacity, both a BCL-2 overexpressing 9464D cell line, and the vav-BCL-2 overexpressing mouse model were utilised. As ICD is thought to be a modulated pathway of apoptosis, a programmed version of cell death [278], overexpression of BCL-2 should prevent this from occurring. BCL-2 is a key component molecule of apoptosis and acts as an anti-apoptotic molecule, which promotes cell survival by inhibition Bax and Bak to prevent apoptosis [586]. Consequently, to assess whether overexpression of BCL-2 would prevent 9464D cells from undergoing apoptosis after MAF, cells were transduced with a vector containing hBCL-2, leading to an overexpression of this molecule (**Figure 4.37** to **Figure 4.41**). Using a MTT assay to assess cell death after MAF administration, no conclusive difference between the three cell lines could be observed due to intra-assay variability (**Figure 4.42**). However, as this assay quantifies metabolic activity and proliferation, it may be that the hBCL-2 cell lines are not dying, but the drug is still leading to a reduction of metabolic activity and therefore a decrease in proliferation. It has been previously reported that CPM requires apoptosis activation to cause cell death, but overexpression of BCL-2 in the 9L tumour cell line did not prevent the cytostatic effects caused by the drug [549]. To assess more directly whether apoptosis via the BCL-2 pathway is occurring in the 9464D cells after MAF administration, western blots were performed to analyse expression and cleavage of key caspase cascade apoptosis proteins (**Figure 4.43**). Here, at 24 hrs post MAF administration, cleavage of PARP and caspase 3 was demonstrated in both parent and EV cells. However, cleavage of these proteins was greatly reduced in the hBCL-2 cell line. These data together demonstrate that firstly, in 9464D cells MAF leads to initiation of apoptosis and is dependent, at least partly, on the BCL-2 protein.

Overexpression of the BCL-2 protein lead to a reduction in cleavage of apoptosis molecules suggesting that cell death is not initiated in these cells after MAF application.

After demonstration that the hBCL-2 overexpressing 9464D cells do not undergo apoptosis after MAF administration, it was decided to use these cells *in vivo* to assess whether ICD induction is an important pathway CPM uses to induce and anti-tumour immune response. To achieve this, attempts were made to grow the cells in immunocompetent syngeneic C57BL/6 mice (**Figure 4.44**). As demonstrated over three attempts, both EV and hBCL-2 cell lines either grew initially and then regressed, or failed to grow at all, whereas the parental cell line behaved as expected. Immunophenotyping of the tumours suggest CD4+ and NK cell immune involvement (Appendix **Figure 7.4**). These data suggest that, as these cell lines were transduced with viral vectors, this may have induced an immune response to the viral proteins, leading to cessation of growth and eventually clearance of tumours. This idea was further compounded when the cells lines were inoculated into immunocompromised NOD/SCID mice as demonstrated in **Figure 4.44**. Here, tumour appearance and growth was observed for all cells lines, suggesting that clearance of the two transduced cell lines is due to an adaptive immune response, as these mice like T and B cells. Furthermore, hBCL-2 cells were shown to have more rapid tumour growth compared to both EV and parental tumours. This observation could infer that as the cells have hBCl-2 overexpression, they are protected from death leading to increased tumour growth. Unfortunately, these cells were originally designed to be used in immune competent mice to quantify how much ICD contributes to anti-tumour activity of CPM. Therefore, as these cell cannot be grown in C57BL/6 using these viral vectors, new transductions with different vectors will be assessed.

Together with the hBCL-2 overexpressing cell line developed in this chapter, vav-BCL-2 mice were used to elucidate the contribution Treg depletion has on CPM induced immunomodulation. Vav-BCL-2 mice constitutively overexpress BCL-2 within all cells containing the vav promotor, and therefore all haematopoietic linage cells. Consequently, Tregs of these mice overexpress BCL-2 and will be more resistant to cell death via this pathway. To that end, vav-BCL-2 mice bearing 9464D tumours were administered with 40 mg/kg CPM and tumours were harvested for immunophenotyping as conducted throughout this chapter (**Figure 4.46**). Interestingly, it was demonstrated that in vav-BCL-2 mice, no significant Treg depletion was seen within the tumours, whereas wild type C57BL/6 mice with 9464D tumour analysed at the same time, showed significant tumour Treg depletion. These data suggest that CPM induced depletion of Treg cells is dependent on the BCL-2 pathway, as was also noted for the mechanism for 9464D tumour cell death *in vitro*. Furthermore, these mice will be utilised to investigate whether any therapeutic efficacy using CPM in wild type mice is abrogated in vav-BCL-2 mice. This will allow for elucidation into whether the depletion of tumour Treg cells is the driving factor determining therapeutic efficacy of CPM *in vivo*.

In summary, this chapter demonstrated numerous immunomodulatory properties of CPM both in *in vitro* and *in vivo* NB tumour models. Importantly, the induction of ICD marker expression after MAF or CPM administration, suggests that this chemotherapeutic can induce an immunogenic form of cell death in NB models, as was reported for other tumour models in the literature. Furthermore, the tumour specific Treg depletion and concurrent modulation of effector T cell activation seen with a low dose of CPM, demonstrated that *in vivo* modulation of tumour infiltrating immune cells can be induced with in NB models. However, using low dose CPM may not lead to any therapeutic efficacy alone, due to the chemotherapy not inducing enough direct death of tumour cells. Despite this, as this low dose can led to significant immunomodulation, CPM may combine effectively with other immunotherapies within the NB preclinical models investigated here.

Chapter 5: Combination of low dose CPM with anti-PD-1 antibody therapy increases survival in preclinical models of NB

5.1 Chapter introduction

The previous chapter demonstrated that 'low' doses of CPM, can deplete immunosuppressive tumour specific Tregs while maintaining, to an extent, effector T cell populations both in the tumours and spleens of two subcutaneous murine NB models. Detailed assessment of T cell populations showed modulation of activation after CPM administration. Furthermore, CPM *in vitro* was shown to increase the expression of ICD markers on both NXS2 and 9464D cell lines, and the modulation of HMGB1 expression both *in vitro* and *ex vivo*. These data together support the contention that low dose CPM given systemically may produce an immunogenic tumour microenvironment, paving the way for synergy with immunomodulatory immunotherapy. The rational for this comes from work in combining chemotherapy and checkpoint inhibitor therapy in adult cancers, which are currently undergoing clinical trials [525,526]. In this chapter, three different immunomodulatory antibodies: anti-4-1BB, anti-CTLA-4 and anti-PD-1 will be assessed. Expression levels of these receptors on TILs were previously assessed in chapter 4, showing high expression of high 4-1BB on Tregs, low expression of CTLA-4 and high PD-1 on TILs. As discussed in **Section 1.5.2**, both PD-1 and CTLA-4 blockade have shown promising therapeutic efficacy in adult cancers including melanoma and non-small cell lung cancer. However, there has been little research into the efficacy of these antibodies in paediatric cancers, including NB. These antibodies work by targeting and blocking checkpoint pathways between T cells and APCs or the microenvironment, which act to supress and regulate T cell function [432]. Anti-4-1BB therapy works differently, as rather than blocking a pathway, this antibody aims to agonise and stimulate the 4-1BB receptor to increase T cell activation. 4-1BB acts as a costimulatory T cell receptor which when activated, increases T cell proliferation and activation to an effector state to generate an anti-tumour response [456,457,587]. This antibody has not yet been approved for clinical use in humans, as promising preclinical data has failed to translate into humans. However, the reasons behind this is subject of ongoing work, and recent data has suggest this may be due to inadequate understanding of antibody and FcyR biology [461-464].

In this chapter, three different murine models of NB were used to study whether synergy can be achieved with CPM and immunotherapy involving the antibodies above. Firstly, the subcutaneous

NXS2 and 9464D models were used to assess the efficacy and mechanism of different antibody combinations with CPM administration. In the previous chapter, it was demonstrated that Tregs were significantly depleted and modulated in these models with sub-curative doses of CPM. Here, we hypothesise that the use of an antibody which then aids T cell stimulation, may synergise with low dose CPM to improve survival. Furthermore, as highlighted in **Section 4.2.7.1**, it was noted that initial Treg depletion by CPM was not sustained in the long term. In an effort to combat this, metronomic dosing strategies, in the form of weekly low doses, was also assessed. Chapter 3 defined the transgenic spontaneous TH-MYCN mouse model as a better immunological representation, of human NB tumours compared to the SC models. However, as previously discussed, this model has unpredictable tumour development, adding to the challenge of screening large amounts of therapy combinations. Hence, this model was only used to investigate the efficacy of the most promising chemotherapy-antibody combinations, elucidated in the subcutaneous NB murine models.

5.2 Results

5.2.1 Assessment of WT and DG EW1-9 antibody serum levels in AJ and C57BL/6 mice

Within this chapter an anti-PD-1 antibody (EW1-9) was utilised, in combination with CPM. As Fc function of an antibody can greatly impact its efficacy *in vivo*, deglycosylation using PNGase F of this region was conducted to see if this could increase survival in combination with CPM. As the main function of an anti-PD-1 antibody is to block the PD-1 receptor and not necessarily employ any effector functions to delete cells [389], Fc function may not be required. Therefore, the wild type (WT) EW1-9 antibody was deglycosylated (DG) to remove its Fc function as detailed in **Section 2.4**. This deglycosylation process could have affected the way the antibody is recycled *in vivo* and therefore may have had an impact on its half-life within the mice, and in turn its efficacy as a therapy. To check whether serum concentration levels had been altered by deglycosylation, C57BL/6 (**Figure 5.1 A**) mice were injected with either EW1-9(WT) or EW1-9(DG) at two different doses. Serial blood sampling and serum collection was performed and antibody concentration in serum was measured by ELISA.

Serum concentration of both EW1-9(WT) and EW1-9(DG) in C57BL/6 mice is shown in **Figure 5.1 B** respectively. Overall serum concentration decreased appeared to decrease similarly for both antibodies and at both concentrations, with antibody still present in the serum up to 14 days after injection. This was also assessed in the AJ mice, showing the same trend. (Appendix **Figure 7.5**)

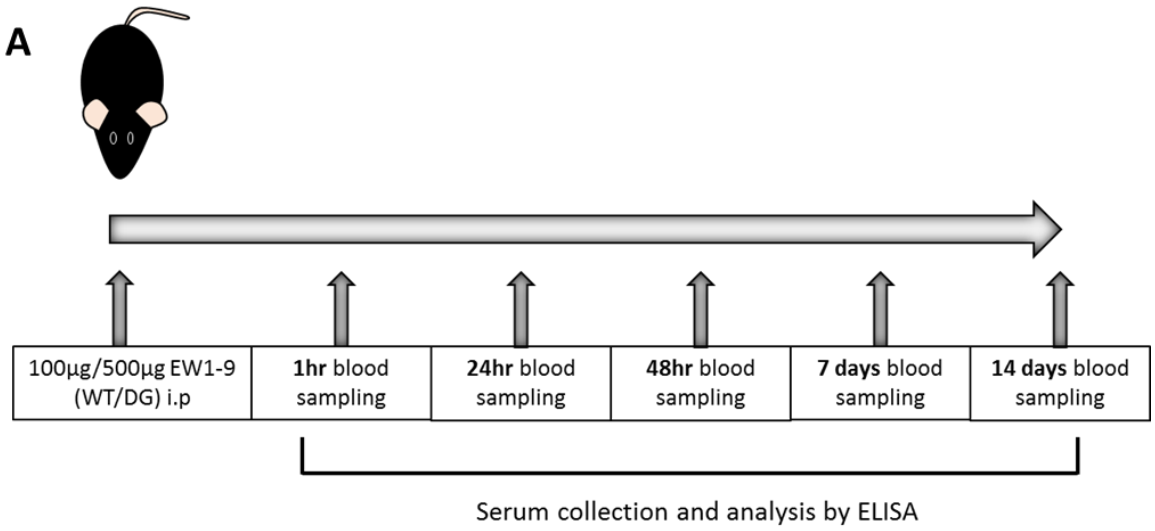

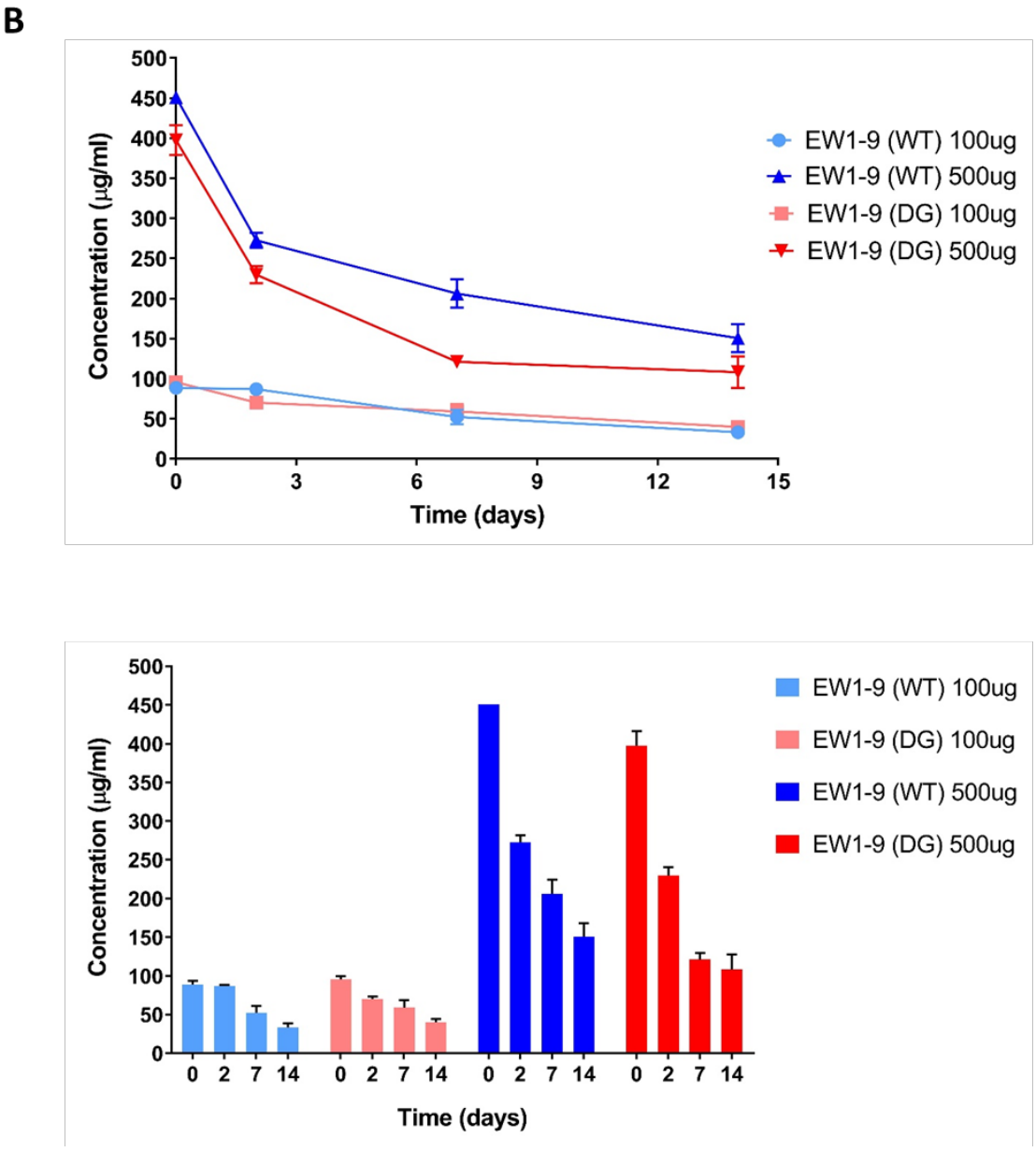

Figure 5.1 EW1-9(WT) and EW1-9(DG) antibody serum levels in C57BL/6 mice

A) Female C57BL/6 mice were dosed with either EW1-9(WT) or EW1-9(DG) at the doses stated by IP injections. Blood was collected at defined time points. From this serum was harvested and ELISA was performed as detailed in **Section 2.15**. **B) C**oncentration in ug/ml of EW1-9(WT) or (DG) remaining in the serum. n= 3 mice per group. Mean and SD error bars are shown.

5.2.2 Combining CPM with immunomodulatory antibody therapy

In order to assess whether it is possible to achieve synergy between chemotherapy and immunomodulatory antibody therapy, the NXS2 subcutaneous model was employed (see chapter 2). Here, mice were inoculated with NXS2 cells and then given their specified treatment once the tumours were established (~8x8 mm). The combination of CPM with three different types of immunomodulatory antibodies was measured by monitoring of tumour growth and survival. A dose of 40 mg/Kg of CPM was used in all experiments, as this dose led to significant depletion of Treg cells alongside activation of effector cells.

5.2.2.1 Anti-4-1BB therapy

Rather than blocking an inhibitory pathway, immune modulation can also be achieved by stimulating activatory pathways. An example of this is the use of anti 4-1BB antibody in order to stimulate effector T cells to mount an anti-tumour immune response. In chapter 4, it was demonstrated that tumour infiltrating Treg cells have higher levels of 4-1BB expression compared to CD8 and CD4 TILs (**Figure 4.36**). Investigations into whether stimulating this pathway can be combined with CPM to increase survival were performed, using the experimental schematic detailed in **Figure 5.2 A**. It has previously been demonstrated that the isotype of an antibody greatly impacts its function *in vivo* due to Fc receptor interactions [384,463,588]. To that end, two different isotypes, LOB12 mγ1 and LOB12 mγ2a, were tested to see if there were any differences in survival.

Figure 5.2 B-G show the individual tumour growth curves from tumour inoculation of non-treated, monotherapies and combination therapies with CPM and anti-4-1BB antibodies. Neither CPM combined with either LOB12 mγ1 or mγ2a showed any significant alteration in median survival (both 11 days) when compared to the monotherapies alone (CPM = 10 days, LOB12 mγ1 and mγ2a both 11 days). However, one mouse treated with CPM+LOB12 mγ1 survived considerably longer than the others to 28 days (**Figure 5.2 F and G**).

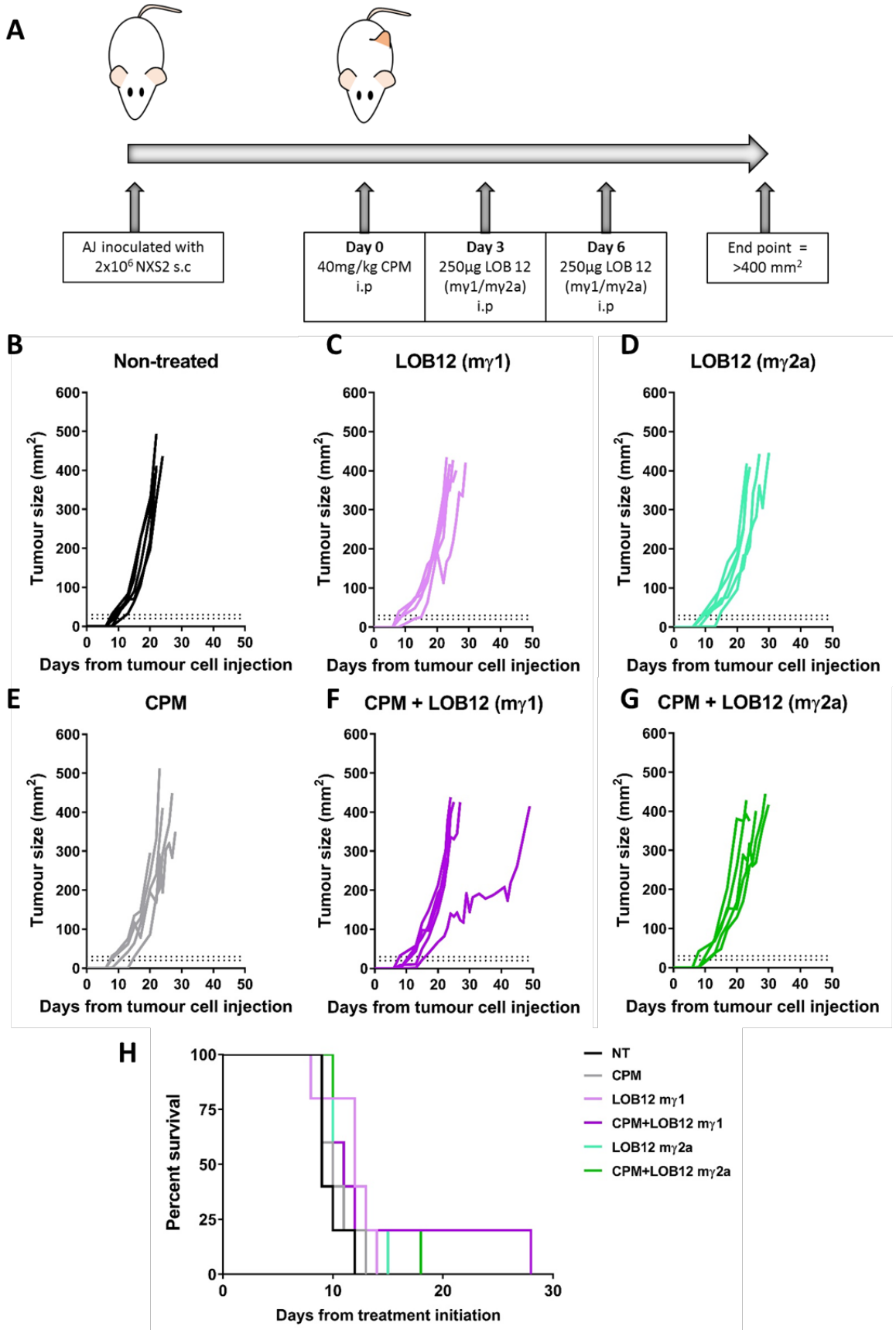

Figure 5.2 Tumour growth and survival of NXS2 tumour bearing mice after CPM and anti-4-1BB therapy

A) AJ female mice were inoculated s.c with $2x10^6$ NXS2 cells. Once tumours had reached 8x8 mm mice were treated with or without 40 mg/kg CPM alone or in combination with either LOB12 my1 or LOB12 my2a at 250ug per dose i.p. Tumour growth was monitored and survival was recorded when endpoint was reached at 400 mm^2. Individual growth curves are shown for each group: **B)** NT, **C)** LOB12 my1, **D)** LOB12 my2a alone, **E)** CPM alone, **F)** CPM+LOB12 my1 and **G)** CPM+LOB12 my2a. **H)** Survival to >400 mm^2 is shown in. n=5 mice per group.

5.2.2.2 Anti-CTLA-4 therapy

CTLA-4 was one of the first immune checkpoint molecules discovered and antibody therapies targeting this molecule are currently in the clinic for certain cancers. However in chapter 4 (**Figure 4.25**) it was demonstrated that CTLA-4 expression was minimal in TILs infiltrating NB tumours. Nevertheless, combination of an anti-CTLA-4 antibody with CPM was assessed in NXS2 tumour bearing mice. **Figure 5.3** shows how tumour growth and overall survival were effected by administration of a sub-curative dose of CPM alongside another immunomodulatory antibody anti-CTLA-4 (UC10), using the protocol detailed in **Figure 5.3 A**. When observing at the individual growth curves (**Figure 5.3 B-E**), no obvious slowing or decrease in growth of the NXS2 tumours was observed with either UC10 alone or in combination with CPM and there was no change in survival of the mice (**Figure 5.3 F)**, A median survival of CPM+UC10 treated mice (11 days) was seen when compared to CPM or UC10 monotherapy alone (10 days and 11 days respectively).

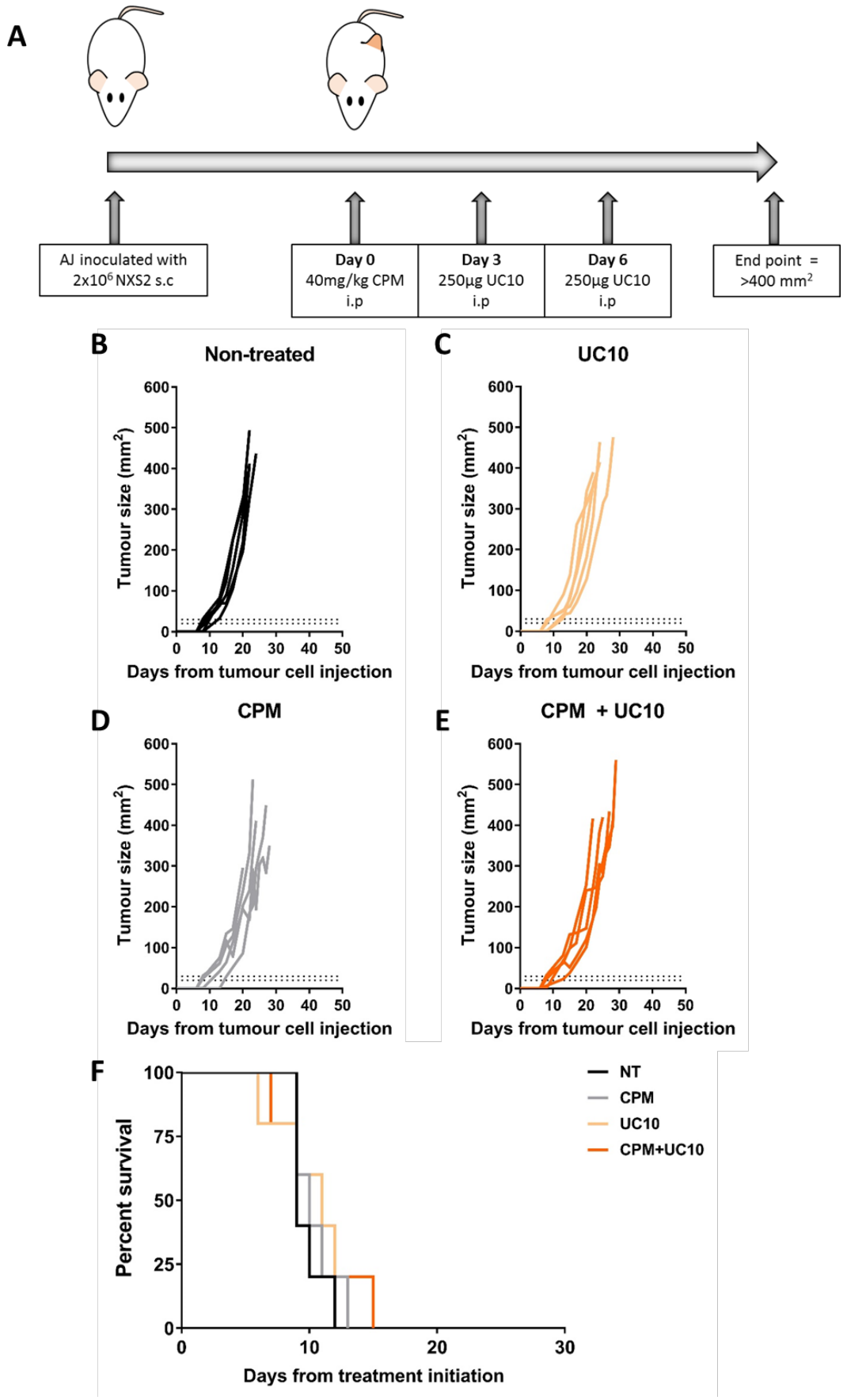

Figure 5.3 Tumour growth and survival of NXS2 tumour bearing mice after CPM and anti-CTLA-4 therapy

A) AJ female mice were inoculated s.c with 2x10^6 NXS2 cells. Once tumours had reached 8x8 mm mice were treated with or without 40 mg/kg CPM alone or in combination with UC10 at 250ug per dose i.p. Tumour growth was monitored and survival was recorded when endpoint was reached at 400 mm^2. Individual growth curves are shown for each group: **B)** NT, **C)** UC10, **D)** CPM, **E)** CPM+UC10, **F)** Survival to >400 mm^2. n=5 mice per group.

5.2.2.3 Anti-PD-1 therapy

As discussed previously, PD-1 is an important and clinically relevant immune checkpoint molecule, which is currently under investigation in clinical trials for NB. It is present on T cells and acts to regulate activation state in response to antigen. The previous chapter detailed how PD-1 expression on different T cell subsets can be altered by chemotherapy. Therefore, investigations into whether chemotherapy can be combined with an anti-PD-1 (EW1-9) antibody to induce therapeutic immunity was assessed (**Figure 5.4**). The effect of the deglycosylated antibody was compared against the efficacy of the WT EW1-9 in combination with CPM treatment, with the protocol detailed in **Figure 5.4 A**.

Figure 5.4 B-G shows the individual growth curves for all the treatment groups. From this it can be noted that the monotherapies of either antibody (**Figure 5.4 C+D**) alone did not slow tumour growth in any of the mice compared to NT or CPM alone (**Figure 5.4 B+E**). However in combination with CPM, EW1-9(WT) (**Figure 5.4 F**) showed some tumour growth arrest but EW1-9(DG) (**Figure 5.4 G**) showed a greater slowing of tumour growth compared to all other groups.

With regards to survival (**Figure 5.4 H**), neither EW1-9 (WT) or EW1-9 (DG) showed any improvement in survival (median 12 days and 10 days respectively) when compared to non-treated (9 days) or CPM alone (10 days) treated mice. Combination of EW1-9 (WT) with CPM did result in a significant improvement of median survival over NT and CPM to 13 days. However with CPM+EW1-9 (DG) the median survival of treated mice increased significantly to 16 days over NT, CPM and EW1-9 (DG) antibody alone.

In **Figure 5.5**, when combining the survival data of **Figure 5.4** and another independent experiment, there is a significant increase in survival of both CPM+EW1-9(WT) and CPM+EW1-9(DG) treated mice over NT and CPM treated groups. Furthermore, CPM+EW1-9(DG) also has an significant increase in survival over EW1-9(WT) or EW1-9(DG) antibody treatment groups alone, which is not seen with CPM+EW1-9(WT).

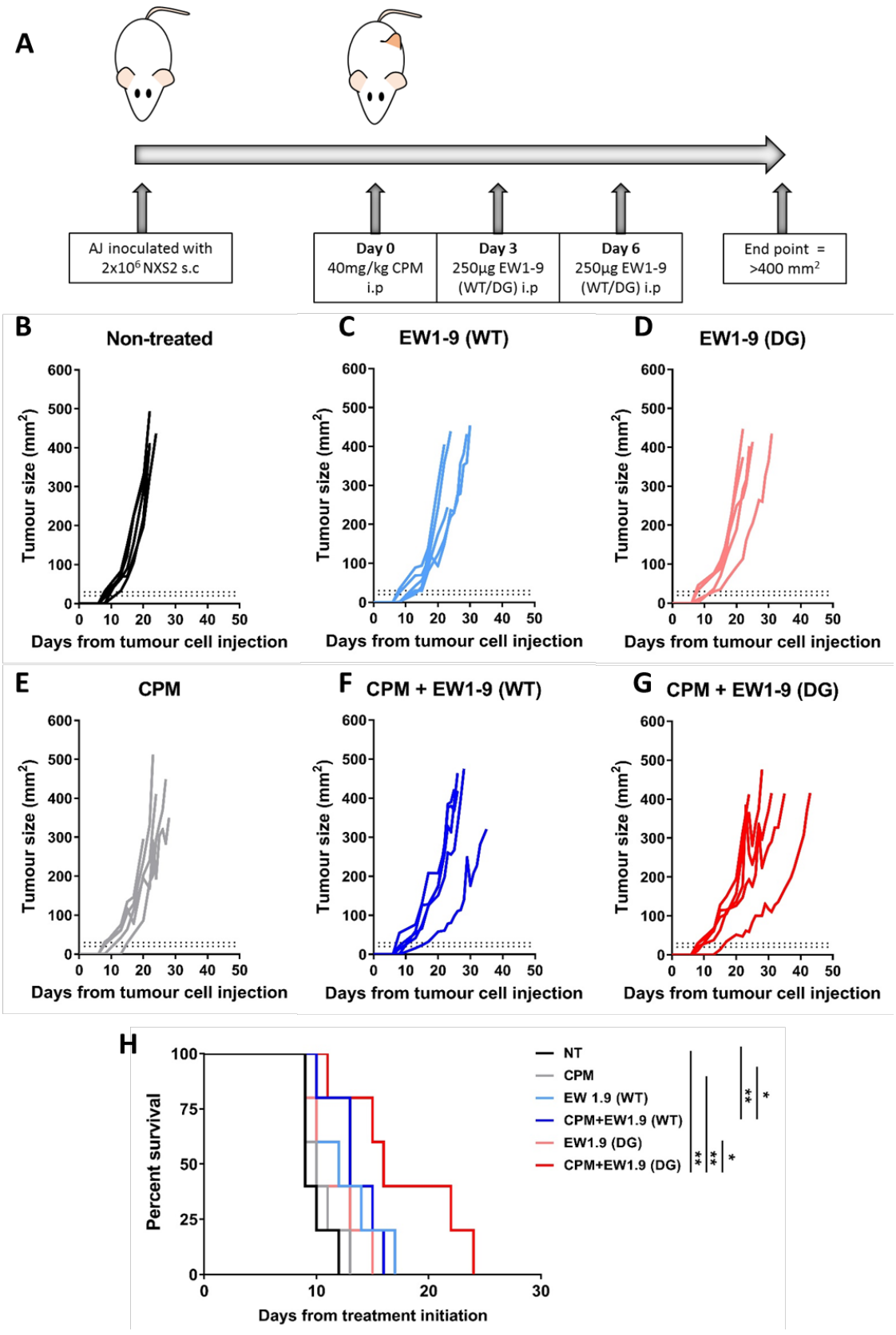

Figure 5.4 Representative example of tumour growth and survival of NXS2 tumour bearing mice after CPM and anti-PD-1 therapy

A) AJ female mice were inoculated s.c with 2x10^6 NXS2 cells. Once tumours had reached 8x8 mm, mice were treated with or without 40 mg/kg CPM alone or in combination with either EW1-9 (WT) or EW1-9 (DG) at 250ug per dose i.p. Tumour growth was monitored and survival was recorded when endpoint was reached at 400 mm^2. Individual growth curves are shown for each group: **B)** NT, **C)** EW1-9 (WT), **D)** EW1-2 (DG), **E)** CPM, **F)** CPM+EW1-9 (WT), **G)** CPM+EW1-9 (DG). **H)** Survival to >400 mm^2. n=5 mice per group. Significance assessed by Log Rank test, and denoted as: * = <0.05, ** = <0.01.

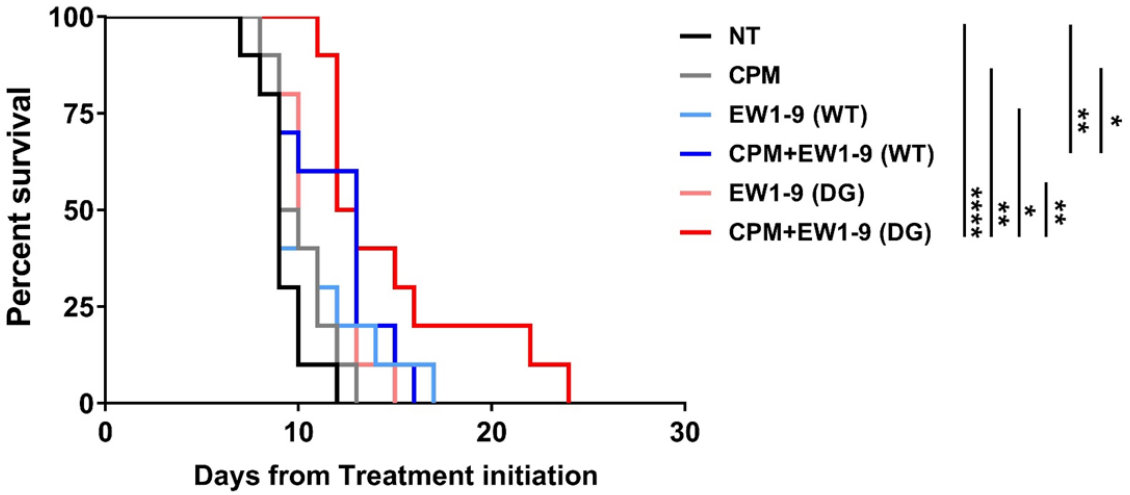

Figure 5.5 Combined data of survival of NXS2 tumour bearing mice after CPM and anti-PD-1 therapy

Survival of NXS2 tumour bearing AJ mice was combined from two experiments detailed in **Figure 5.4** and another independent experiment. n= 10 mice per group. Significance assessed by Log Rank test, and denoted as: * = <0.05, ** = <0.01, *** = < 0.001, **** = < 0.0001.

5.2.3 Combining CPM with anti-PD-1 antibody therapy in smaller NXS2 tumour bearing mice.

Tumour burden when treatment is first initiated could influence efficacy of immunotherapies. It has been suggested that immune infiltrates are different when comparing small and larger tumours, due to differences in vasculature and architecture of tumour [589]. Recently it has been discussed that tumour burden may have an influence on checkpoint therapy [590]. Previously, the combination therapy of CPM and anti-PD-1 therapy in NXS2 tumour bearing mice was initiated at a tumour start point of approximately 8x8 mm. To see if a smaller tumour start point would have an effect on combination treatment efficacy, in **Figure 5.6** a treatment initiation start point of 5x5 mm was used to implement the treatment protocol as described in **Figure 5.6 A**.

At the smaller tumour start point of 5x5 mm, tumour growth curves for all groups are shown in **Figure 5.6 B-G**. Here, as with tumour start point of 8x8 mm, a slowing of tumour growth was seen with both CPM+EW1-9 (WT) and CPM+EW1-9 (DG), when compared to NT, CPM or the antibody therapies alone. Although this slowing of tumour growth appears to be similar for both antibody combinations, when looking at survival in **Figure 5.6 H** only the combination therapy of CPM+EW1-9 (DG) was significantly different to all groups (apart from CPM+EW1-9 (WT)).

5.2.4 Combination of CPM and anti-PD-1 antibodies in 9464D subcutaneous tumour model

The combination of CPM+EW1-9(DG) was then investigated in the second subcutaneous model, 9464D. As described in Chapter 3, the immune infiltrates within the NXS2 and 9464D tumours differ and these differences may affect the therapeutic potential of combination CPM and anti-PD-1 antibodies.

The combination therapy of low dose CPM with either WT or DG anti-PD-1 (EW1-9) antibody therapy was assessed in 9464D tumour bearing mice. Treatment start point was initiated when tumours were 8x8 mm as detailed in **Figure 5.7 A**. Individual tumour growth curves are shown in **Figure 5.7 B-G**. When comparing the growth of NT 9464D tumours to NXS2 tumours (**Figure 5.2** to **Figure 5.6**) you can see that tumours start to grow exponentially at a later time point than in NXS2 tumours, and take longer to reach a terminal endpoint. The addition of CPM, WT or DG EW1-9 treatment did not have a significant effect on tumour growth rates (**Figure 5.7 B-C**). However, combination of CPM with either EW1-9(WT) or EW1-9(DG) resulted in slower tumour growth (**Figure 5.7 F+G**). As in the previously described NSX2 model, this effect was most apparent in the CPM+EW1-9(DG) combination group, where a significant increase in survival was seen **Figure 5.7 H** compared to control and all other treatment groups (median survival 53 days and 43 days respectively).

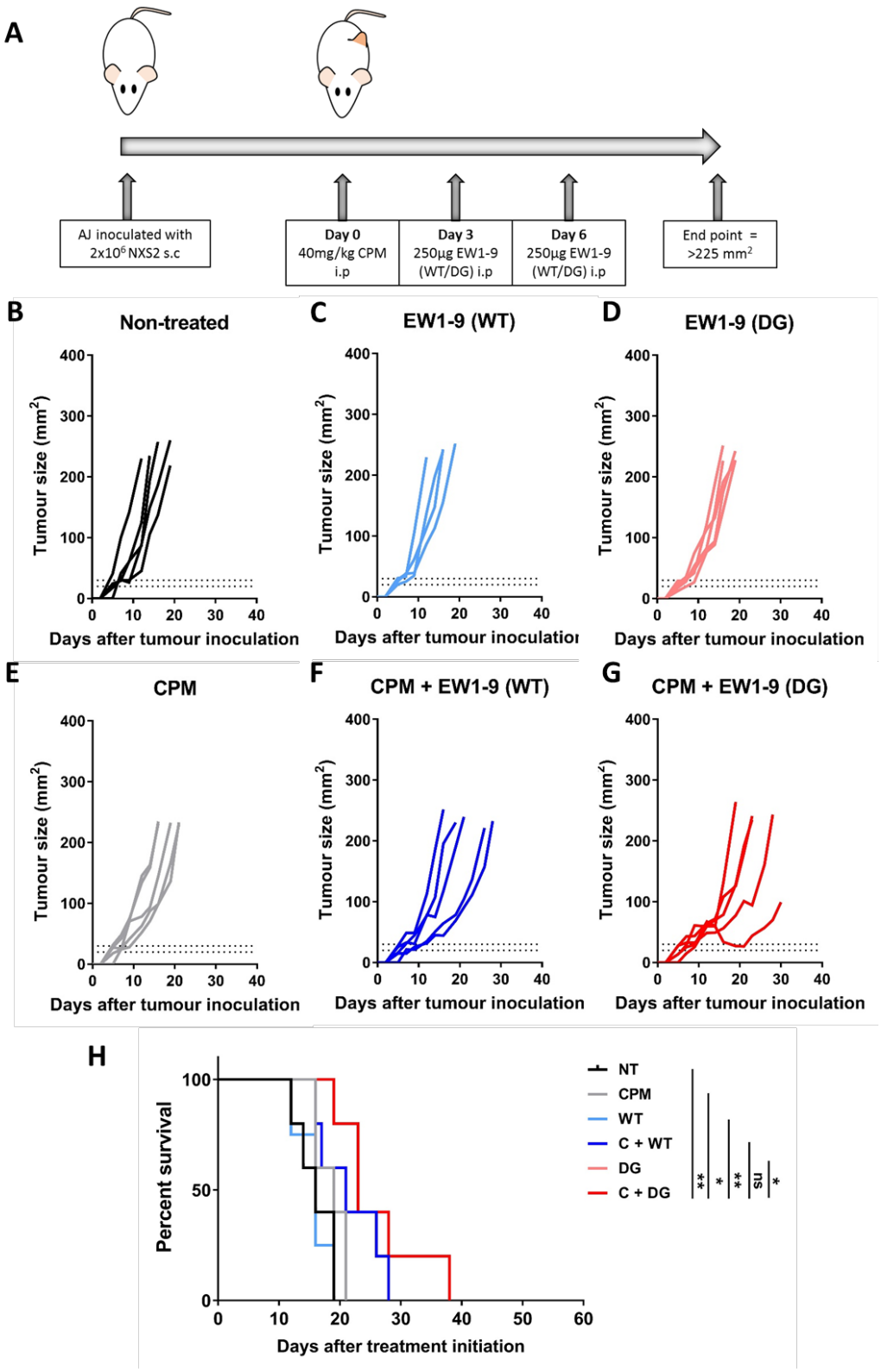

Figure 5.6 Tumour growth and survival of NXS2 tumour bearing mice after CPM and anti-PD-1 therapy at 5x5 mm start point

A) AJ female mice were inoculated s.c with 2x10^6 NXS2 cells. Once tumours had reached 5x5 mm, mice were treated with or without 40 mg/kg CPM alone or in combination with either EW1-9 (WT) or EW1-9 (DG) at 250ug per dose i.p. Tumour growth was monitored and survival was recorded when endpoint was reached at 225 mm^2. Individual growth curves are shown for each group: **B)** NT, **C)** EW1-9 (WT), **D)** EW1-2 (DG), **E)** CPM, **F)** CPM+EW1-9 (WT), **G)** CPM+EW1-9 (DG). **H)** Survival to >225 mm^2. n=5 mice per group. Significance assessed by Log Rank test and denoted as: ns = not significant, * = <0.05, ** = <0.01.

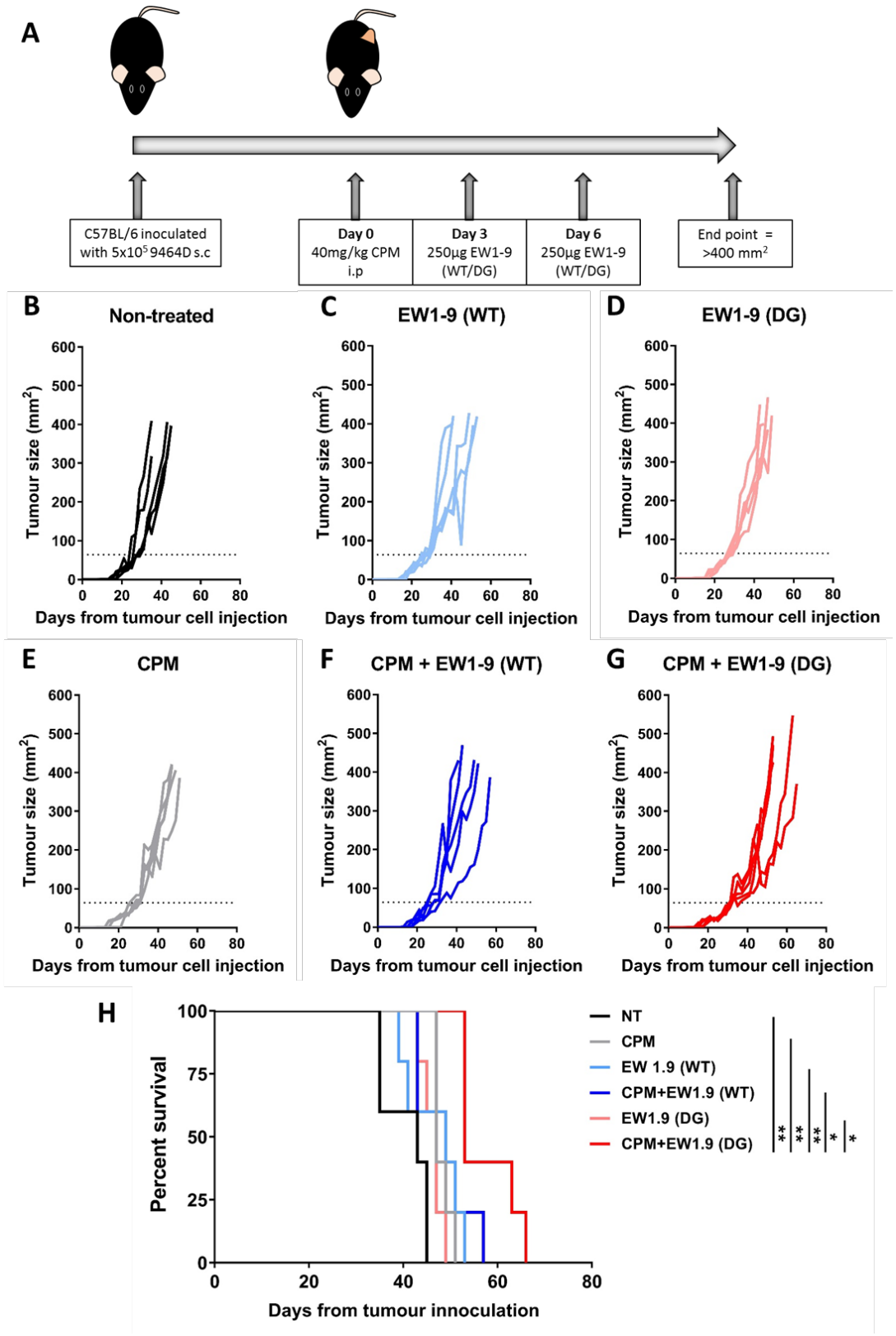

Figure 5.7 Tumour growth and survival of 9464D tumour bearing mice after CPM and anti-PD-1 therapy at 8x8 mm start point

A) C57BL/6 female mice were inoculated s.c with $5x10^5$ 9464D cells. Once tumours had reached 8x8 mm, mice were treated with or without 40 mg/kg CPM alone or in combination with either EW1-9 (WT) or EW1-9 (DG) at 250ug per dose i.p. Tumour growth was monitored and survival was recorded when endpoint was reached at 400 mm^2. Individual growth curves are shown for each group: **B)** NT, **C)** EW1-9 (WT), **D)** EW1-2 (DG), **E)** CPM, **F)** CPM+EW1-9 (WT), **G)** CPM+EW1-9 (DG). **H)** Survival to >400 mm^2. n=5 mice per group. Significance assessed by Log Rank test and denoted as: ns = not significant, * = <0.05, ** = <0.01.

5.2.4.1 Combining CPM and anti-PD-1 antibody therapy in 5x5 mm and palpable 9464D tumour bearing mice

Tumour size was assessed as to its effect on the efficacy of the CPM+EW1-9(DG) combination therapy, using start points were used of 5x5 mm and palpable, as shown in **Figure 5.8** to **Figure 5.11**.

Firstly, when looking at a treatment start point of 5x5 mm the treatment strategy was followed as detailed in **Figure 5.8 A**. Again as with the 8x8 mm start point, monotherapies alone did not have an effect on tumour growth as shown in **Figure 5.8 B-E**. However, the combination of CPM+EW1-9(DG) slowed tumour growth considerably initially, before eventual tumour escape and exponential growth (**Figure 5.8 G**). The combination of CPM+EW1-9(WT) was shown to be less effective in **Figure 5.8 F,** with only the CPM+EW1-9(DG) combination having a significant increase in survival (to a tumour size of >225 mm^2) over control mice, as shown in **Figure 5.8 H**. Here, median survival in CPM+EW1-9(DG) treated mice was 43 days compared to 37 in NT mice. When the survival data from **Figure 5.8** and a second independent experiment was combined, a significant increase in survival of 9464D tumour bearing mice was seen with the combination of CPM+EW1-9(DG) over NT and EW1-9(DG) alone treated mice (**Figure 5.9**). There was no significant increase in survival seen with the combination of CPM+EW1-9(WT).

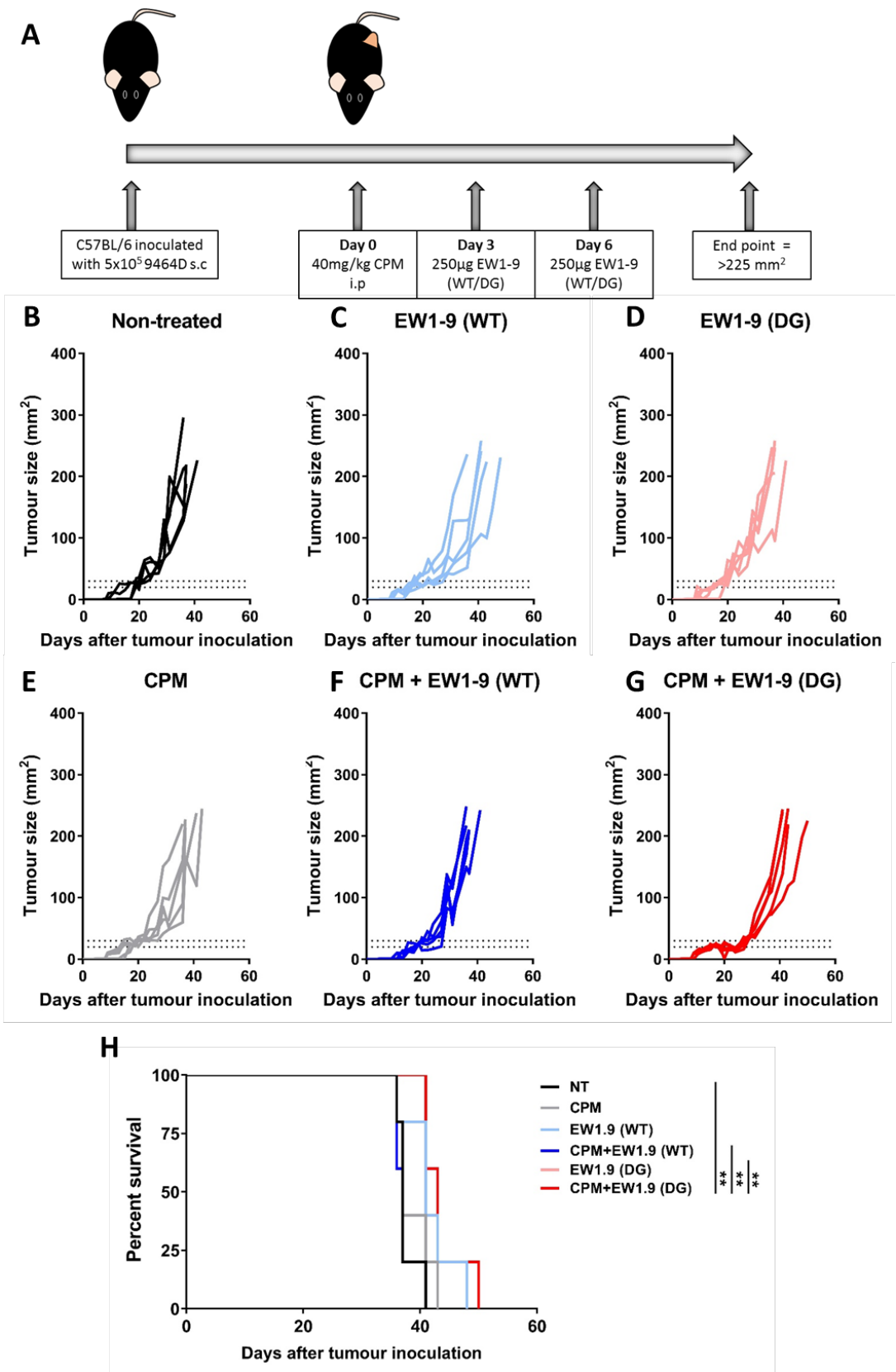

Figure 5.8 Representative example of tumour growth and survival of 9464D tumour bearing mice after CPM and anti-PD-1 therapy at 5x5 mm start point

A) C57BL/6 female mice were inoculated s.c with $5x10^5$ 9464D cells. Once tumours had reached 5x5 mm, mice were treated with or without 40 mg/kg CPM alone or in combination with either EW1-9 (WT) or EW1-9 (DG) at 250ug per dose i.p. Tumour growth was monitored and survival was recorded when endpoint was reached at 225 mm^2. Individual growth curves are shown for each group: **B)** NT, **C)** EW1-9 (WT), **D)** EW1-2 (DG), **E)** CPM, **F)** CPM+EW1-9 (WT), **G)** CPM+EW1-9 (DG). **H)** Survival to >225 mm^2. n=5 mice per group. Significance assessed by Log Rank test and denoted as: ** = <0.01.

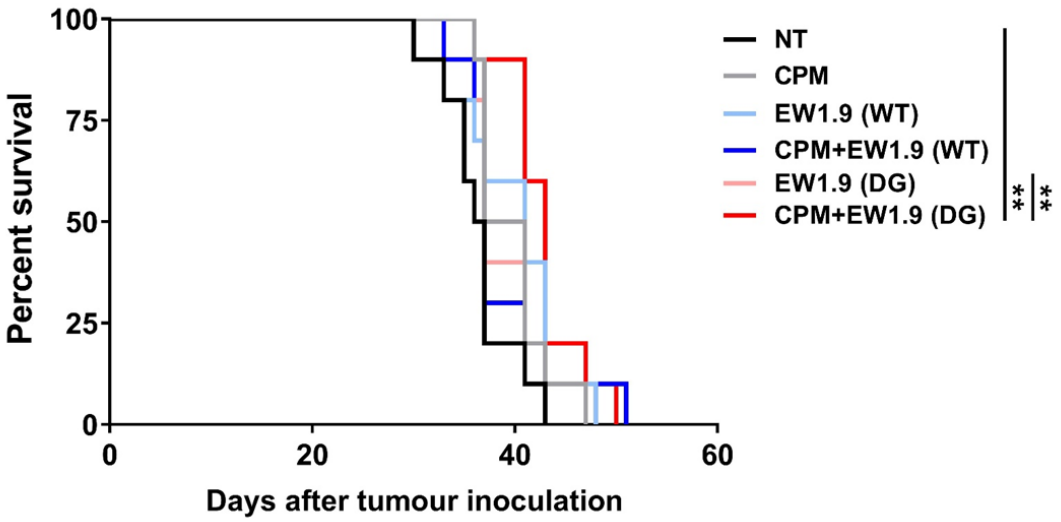

Figure 5.9 Combined data of survival of 9464D tumour bearing mice after CPM and anti-PD-1 therapy at 5x5 mm tumour start point

Survival of 9464D tumour bearing C57BL/6 mice was combined from two experiments detailed in **Figure 5.8** and a second independent experiment. n= 10 mice per group. Significance assessed by Log Rank test, and denoted as: * = <0.05, ** = <0.01.

As tumours in the 9464D model become palpable and then maintain a small tumour size for a long period before increasing dramatically, it was decided to test the combination therapy at an earlier time point, when the tumours first become palpable. **Figure 5.10 A** shows the treatment schedule followed. Again, as has been seen previously, monotherapies of CPM, EW1-9(WT) or EW1-9(DG) do not slow tumour growth of 9464D tumours compared to controls (**Figure 5.10 B-E**). When observing the combination therapies in **Figure 5.10 F+G**, it can be seen that only the combination of CPM+EW1-9(DG) had any appreciable effect on tumour growth. This slowing of tumour growth translated into a significantly increased survival (median survival 44 days) of CPM+EW1-9(DG) treated mice to both NT and CPM treated mice (both 36 days), as shown in **Figure 5.10 H**. An increase in survival of CPM+EW1-9(WT) treated mice over NT mice was also seen. When survival data from both **Figure 5.10** and a second independent experiment was combined, again CPM+EW1-9(DG) combination therapy was shown to significantly increase survival compared to NT mice and all other treatment groups (**Figure 5.11**).

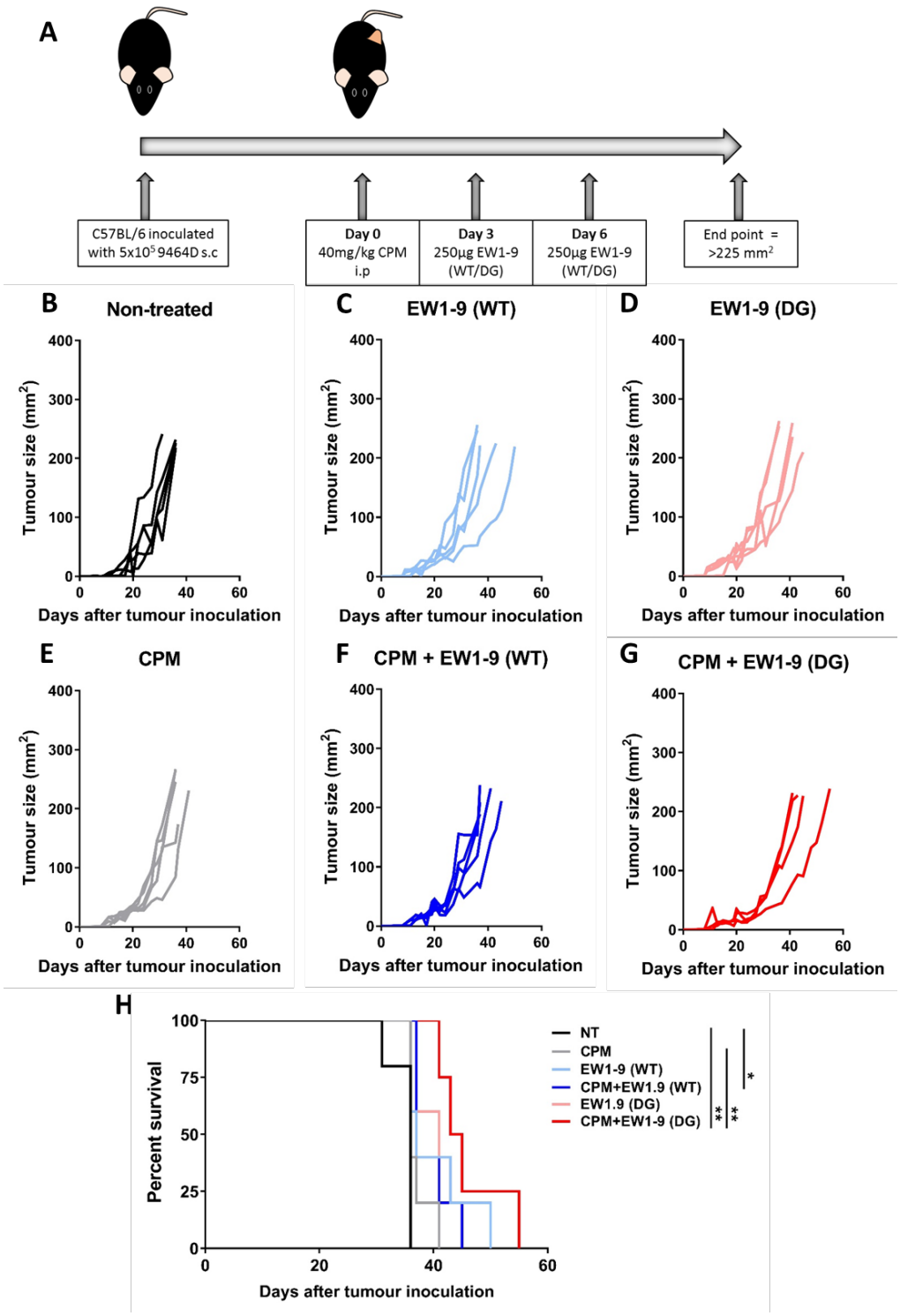

Figure 5.10 Representative example of tumour growth and survival of 9464D tumour bearing mice after CPM and anti-PD-1 therapy at palpable start point

A) C57BL/6 female mice were inoculated s.c with $5x10^5$ 9464D cells. Once tumours had reached palpable, mice were treated with or without 40 mg/kg CPM alone or in combination with either EW1-9 (WT) or EW1-9 (DG) at 250ug per dose i.p. Tumour growth was monitored and survival was recorded when endpoint was reached at 225 mm^2. Individual growth curves are shown for each group: **B)** NT, **C)** EW1-9 (WT), **D)** EW1-2 (DG), **E)** CPM, **F)** CPM+EW1-9 (WT), **G)** CPM+EW1-9 (DG). **H)** Survival to >225 mm^2. n=5 mice per group, n= 4 mice per group (CPM+EW1-9 (DG)). Significance assessed by Log Rank test, and denoted as: * = <0.05, ** = <0.01.

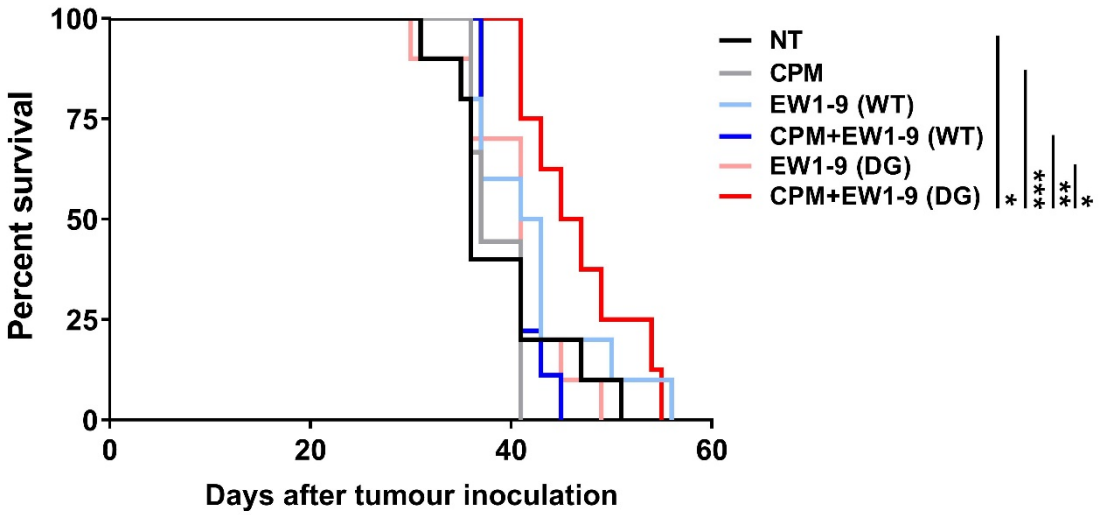

Figure 5.11 Combined data of survival of 9464D tumour bearing mice after CPM and anti-PD-1 therapy at palpable tumour start point

Survival of 9464D tumour bearing C57BL/6 mice was combined from two experiments detailed in **Figure 5.10** and second independent experiment. n= 10 (NT, EW1-9(WT) and EW1-9(DG)), n= 9 (CPM and CPM+EW1-9(WT)) and n= 8 (CPM+EW1-9(DG)) mice per group. Significance assessed by Log Rank test, and denoted as: * = <0.05, ** = <0.01, *** = <0.001.

5.2.5 Immunophenotyping of peripheral blood mononuclear cells of combination therapy treated mice

So far, it has been demonstrated that the combination of CPM+EW1-9(DG) significantly increases survival of mice in two different subcutaneous models of murine NB. Furthermore, the efficacy of this combination therapy was more effective than the combination of CPM+EW1-9(WT). Analysis of the immune cell populations in the blood of treated mice was conducted in order to better understand the mechanisms of action

Analysis of peripheral blood T cell subpopulations of NSX2 bearing mice treated with the CPM +/- anti-PD-1 mAb therapies was performed (**Figure 5.12**). Treatment was initiated once tumours were palpable, and blood sampling was conducted as described in **Figure 5.12 A.** Percentages of CD4+ FoxP3- cells (**Figure 5.12 B**) were significantly increased to 60% of CD3+ cells) in mice treated with CPM alone by day 6. This also coincided with an increase in CD8+ cells to ~20% (**Figure 5.12 C**). For all other treatment groups CD4+ and CD8+ levels remained at similar levels. When looking at Treg (FoxP3+) percentages in PBMCs in **Figure 5.12 D**, the combination therapy of CPM+EW1-9(DG) resulted in a significant increase of this population by day 6 after treatment initiation from ~3% to ~5.5%. A non-significant increase was seen following EW1-9(DG) alone and CPM+EW1-9(WT. **Figure 5.12 E** shows a significant decrease in the CD8+:Treg ratio in EW1-9(DG) alone and combination of CPM+EW1-9(DG), most likely due to the increase in Treg cells

As the combination of CPM+EW1-9(DG) was also shown to be effective in the 9464D model, T cell populations in PBMCs were also analysed using this model as detailed in **Figure 5.13 A,** using a later time point (Day 9) because of the slower growth kinetics of this model compared to NSX2. The increase in CD4+ FoxP3- cells with CPM seen in NXS2 model was not observed here, however both EW1-9(WT) and EW1-9(DG) treated mice saw a significant decrease in these cells (**Figure 5.13 B**). CD8+ cells were shown in this model to be significantly increase in CPM alone and both combination therapies in **Figure 5.13 C**, and a significant increase in Treg cells (**Figure 5.13 D**) was also seen in CPM+EW1-9(DG) treated mice from 1.5% to ~2.4%, as was also seen in the NXS2 model. Despite these changes, no significant alterations were seen in CD8+:Treg ratio.

PD-1 and Ki67 expression was also assessed, with no significant changes seen (Appendix **Figure 7.6** and **Figure 7.7**).

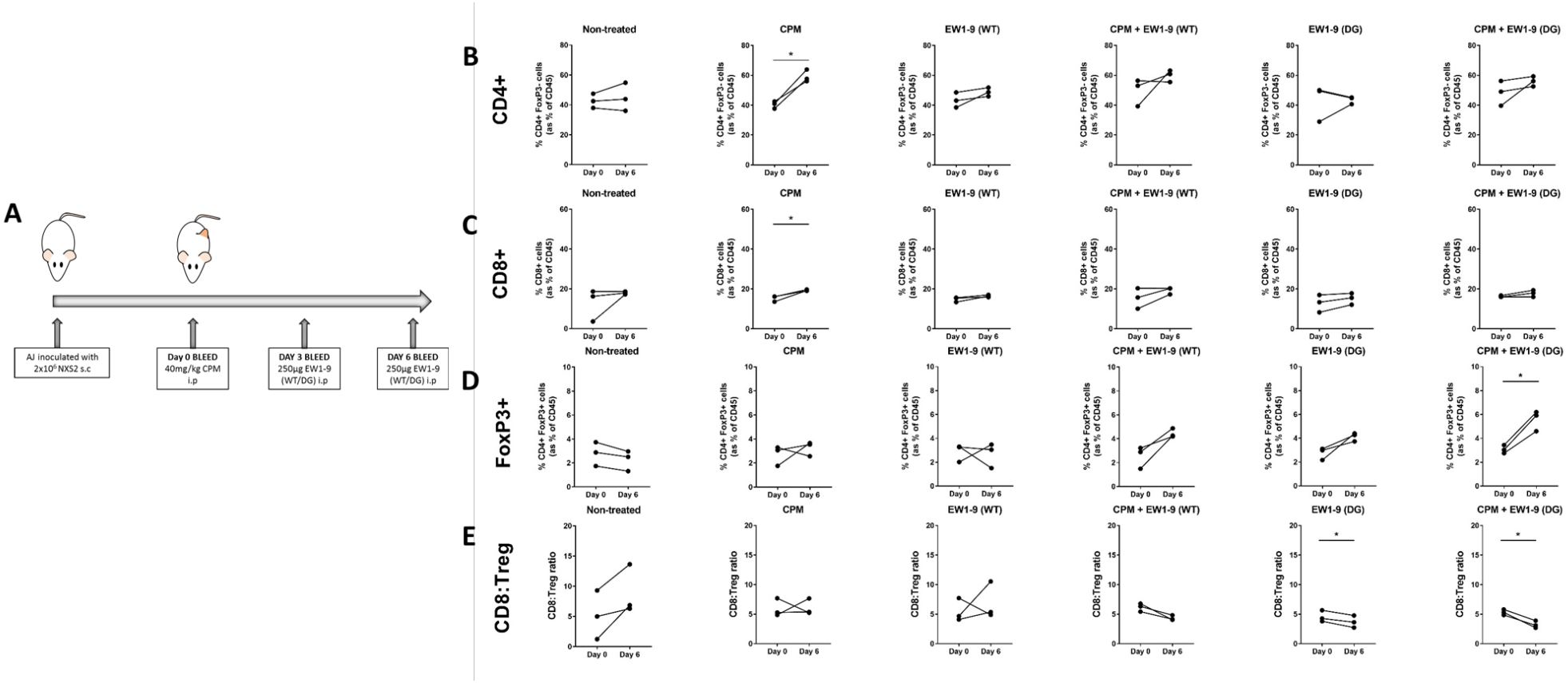

Figure 5.12 T cell percentages in blood of NXS2 tumour bearing mice after combination therapy

A) AJ female mice were inoculated s.c with $2x10^6$ NXS2 cells. Once tumours had reached 8x8 mm either EW1-9 (WT) or EW1-9 (DG) was given at 250ug per dose i.p, with or without 40mg/kg CPM 3 days earlier. Serial blood sampling was conducted at set time points, and flow cytometry was conducted for T cell populations. Gating strategy was used as shown previously (**Figure 4.16**). T cell populations are shown as: **B)** CD4+ FoxP3-, **C**) CD8+, **D)** CD4+ FoxP3+ and **E)** CD8:Treg ratio. n=3 mice per group. Significance assessed by paired t-test and denoted as: * = <0.05.

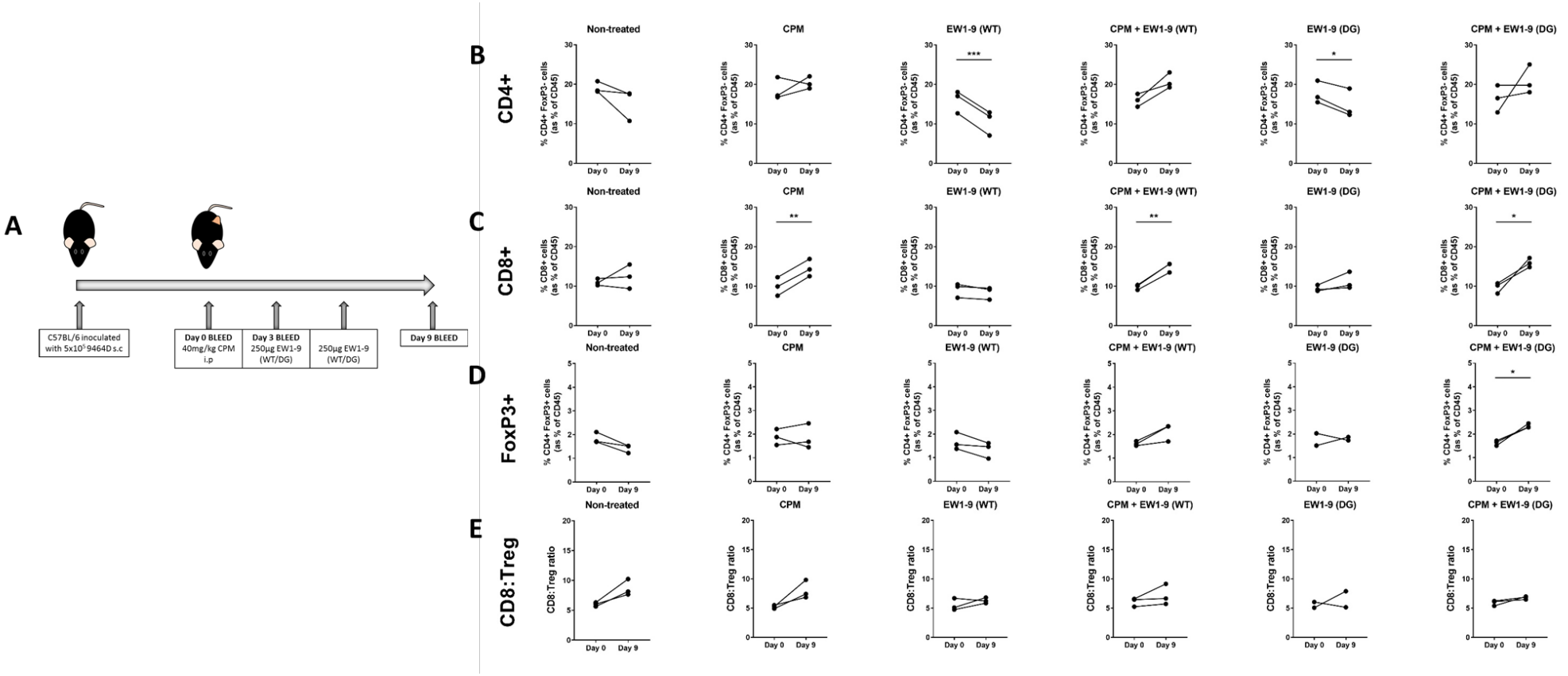

Figure 5.13 T cell percentages in blood of 9464D tumour bearing mice after combination therapy

A) C57BL/6 female mice were inoculated s.c with $5x10^5$ 9464D cells. Once tumours had reached 8x8 mm either EW1-9 (WT) or EW1-9 (DG) was given at 250ug per dose i.p, with or without 40mg/kg CPM 3 days earlier. Serial blood sampling was conducted at set time points, and flow cytometry was conducted for T cell populations. Gaiting strategy was used as shown previously (**Figure 4.16**). T cell populations are shown as: **B)** CD4+ FoxP3-, **C)** CD8+, **D)** CD4+ FoxP3+ and **E)** CD8:Treg ratio. n=3 mice per group. Significance assessed by paired t-test and denoted as: * = <0.05, ** = <0.01, *** = <0.001.

5.2.6 Analysis of GD2 and PD-L1 expression on NXS2 and 9464D tumours after combination therapy

To see how combination therapy effects immune cells within the tumour microenvironment, tumours were harvested from mice after therapy as detailed in **Figure 5.14 A** (NXS2) and **Figure 5.15 A** (9464D), disaggregated into a single cell suspension, and immunophenotyping was conducted using flow cytometry.

NB cells express the ganglioside GD2 on their cell surface, and have been shown in humans to express PD-L1 [591]. Analysis of expression of these markers was also assessed after combination therapy. As demonstrated in chapter 3, GD2 expression on NXS2 cells is higher than on 9464D cells (**Figure 3.6**), which was recapitulated here in **Figure 5.14 B** and **Figure 5.15 B**. In NXS2 tumours, application of treatment appears to have increased GD2 expression (both percentage and geoMFI), which was significant for EW1-9(WT) and EW1-9(DG) shown in **Figure 5.14 B**. However in 9464D tumours, GD2 expression was more variable, with a significant reduction in GD2 compared to NT (20.27%), with both EW1-9(WT) (8.9%) and CPM+EW1-9(WT) (9.5%) **Figure 5.15 B.** Furthermore, PD-L1 expression on 9464D cells was negligible on GD2+ cells (**Figure 5.15 C**), however in NXS2 tumours PD-L1 expression was detectable and found to be similar between treatment groups (**Figure 5.14 C**).

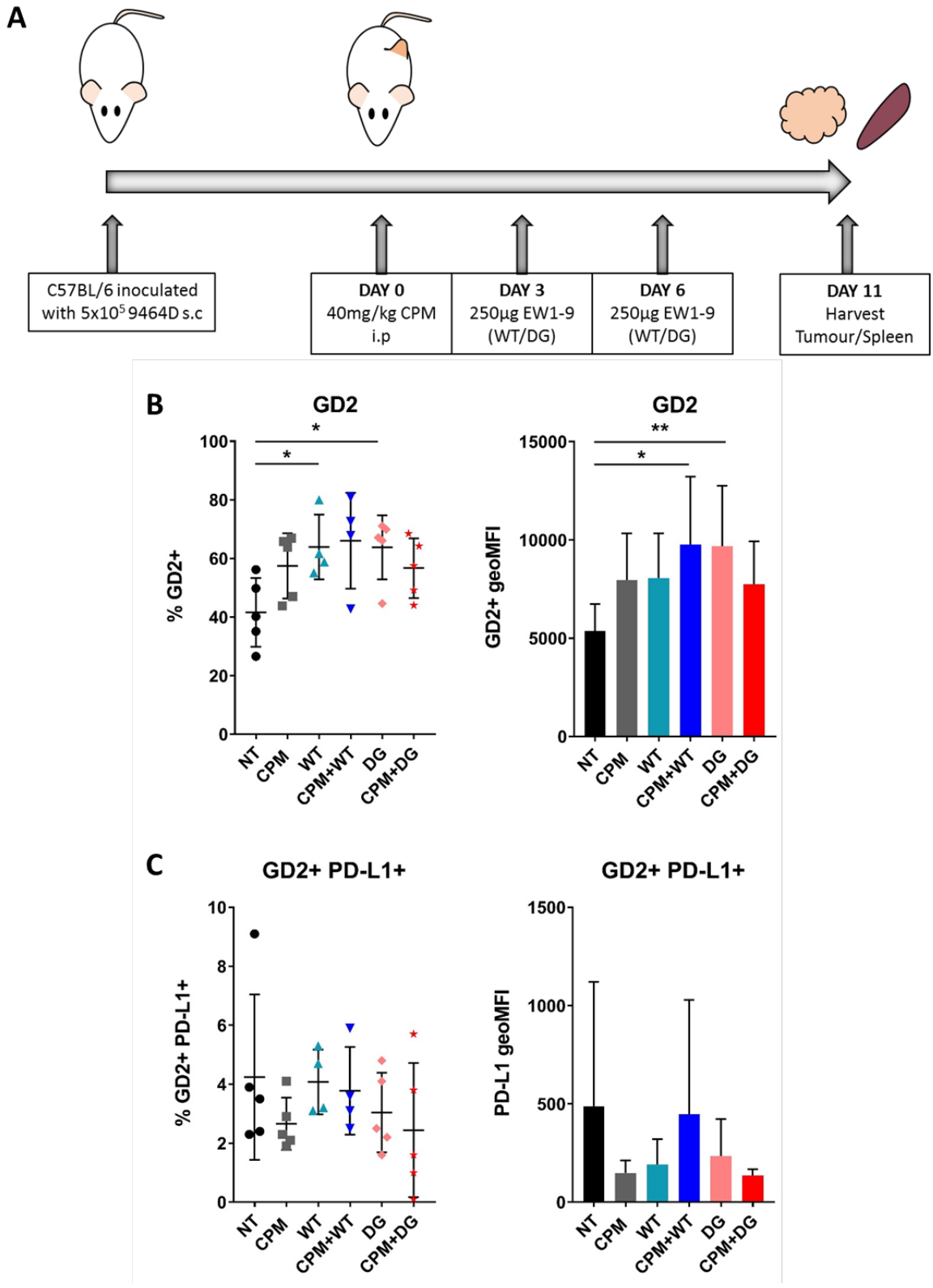

Figure 5.14 GD2 and PD-L1 expression on NXS2 tumours after combination therapy.

A) Schematic of experimental set up and treatment scheduling. AJ female mice were inoculated SC with $2x10^6$ NXS2 cells. Once tumours had reached 8x8 mm either EW1-9 (WT) or EW1-9 (DG) was given at 250ug per dose i.p, with or without 40mg/kg CPM 3 days earlier. Tissue was harvested for immunophenotyping by flow cytometry as detailed in **Section 2.9**. Debris removal, singlet discrimination and population gating were conducted as shown previously (**Figure 3.3**).**B)** Percentage and geoMFI of GD2+ cells. **C)** Percentage expression and geoMFI of PD-L1 expression on GD2+ cells. n=5 mice per group or 4 (EW1-9WT + CPM+EW1-9WT), combined from 2 independent experiments. Significance assessed by Mann-Whitney U test, and denoted as: * = <0.05, ** = <0.01. Mean and SD error bars are shown.

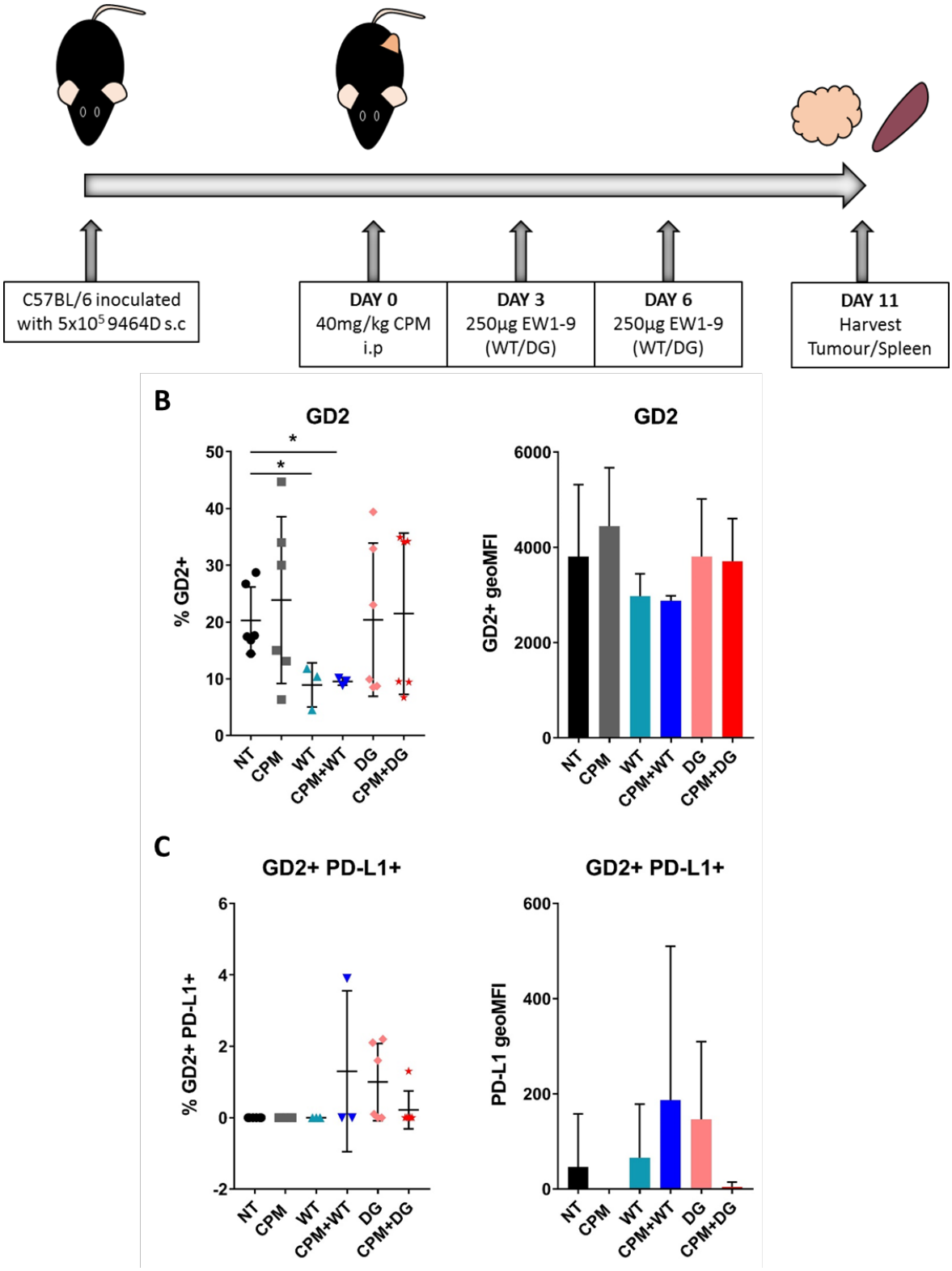

Figure 5.15 GD2 and PD-L1 expression on 9464D tumours after combination therapy.

A) Schematic of experimental set up and treatment scheduling. C57BL/6 female mice were inoculated SC with 5x10^5 9464D cells. Once tumours had reached 8x8 mm either EW1-9 (WT) or EW1-9 (DG) was given at 250ug per dose i.p, with or without 40mg/kg CPM 3 days earlier. Tissue was harvested for immunophenotyping by flow cytometry as detailed in **Section 2.9**. Debris removal, singlet discrimination and population gating were conducted as shown previously (**Figure 3.3**). **B)** Percentage and geoMFI of GD2+ cells. **B)** Percentage expression and geoMFI of PD-L1 expression on GD2+ cells**.** n=6 mice per group, n=3 for EW1-9WT and CPM+EW1-9(WT). Combined from 2 independent experiments. Significance assessed by Mann-Whitney U test, and denoted as: * = <0.05. Mean and SD error bars are shown.

5.2.6.1 Analysis of TIL populations in tumours of combination therapy treated NXS2 and 9464D tumour bearing mice

Moving on to lymphocyte populations within the tumours of NXS2 mice in **Figure 5.16 A**. CD4+ FoxP3- and CD8+ T cells were broadly similar across all treatment groups, with highly variable CD8+ cell infiltration. Importantly, the percentage of Treg cells were significantly increased from 5% in NT tumours, in mice treated with either EW1-9(DG) alone or CPM+EW1-9(DG) combination to ~9.9%. CPM+EW1-9(WT) treated mice also showed a slight increase in Treg percentages, but this wasn't significant. These alterations in Treg percentages led to a significant decrease in CD4:Treg ratio for EW1-9(DG) alone treated mice (**Figure 5.16 B**), although CD8+:Treg ratio was not significantly altered in any groups. Within 9464D, tumours CD4+ and Treg percentages were similar but variable across treatment groups, however there was an increase in CD8+ T cells (although not significant) in CPM+EW1-9(WT), CPM+EW1-9(DG) and EW1-9(DG) alone (**Figure 5.17 A**), which was not seen in NXS2 tumours. Due to this increase in CD8+ T cells there was a slight increase in CD8:Treg and CD8:CD4 ratio, particularly with CPM+EW1-9(DG) (**Figure 5.17 B**), however this was not significant. Furthermore, there was a small decrease in CD4:Treg ratio with most groups, as seen in NXS2 tumours also. Interestingly, we can see that with both NXS2 and 9464D models, the previous depletion of Tregs by CPM seen at day 3 (**Figure 4.29**) is not maintained at these later time points, with the Treg cell percentages returning to NT levels.

Along with cell percentages, PD-1 expression and proliferation using Ki67 of the TILs after combination therapy was assessed for both NXS2 (**Figure 5.18** and **Figure 5.20**) and 9464D (**Figure 5.19** and **Figure 5.21**). The anti-PD-1 mAb (RMPI-30) used to assess expression following EW1-9 therapy was shown to be non-competing by surface plasmon resonance (SPR) (data not shown). PD-1 expression on CD8+ cells was seen to be quite variable when looking at percentage expression, with a significant decrease in PD-1 percentage seen on both CD4+ and Tregs with all treatment groups including anti-PD-1 antibody (**Figure 5.18 A**). Furthermore, for all TIL cell types there is a decrease in seen in PD-1 expression by geoMFI seen with all antibody groups (**Figure 5.20 B**). In **Figure 5.19 A** it is clear that percentage CD4+ and Treg cells that express PD-1 is reduced on within EW1-9(DG) and CPM+EW1-9(DG) treated tumours. This decrease is not seen on CD8+ cells, which is similar to the NXS2 model. When looking at geoMFI of PD-1 expression (**Figure 5.19 B**), there is a significant reduction of PD-1 on CD8+ cells in tumours treated with all antibody containing treatment groups, along with a reduction seen on CD4+ and Treg cells. This again was also seen in NXS2 tumours. When analysing the proliferation marker, Ki67, in TILs in NXS2 tumours, no significant differences are seen compared to NT mice with most of the groups (**Figure 5.20 A+B**), as was also seen in 9464D tumours when looking at the percentage of Ki67 positive cells (**Figure 5.21 A**). CPM+EW1-9(WT) however does appear to have increased the proliferation of CD8+ and CD4+

FoxP3- cells, but this was not significant. Unlike NXS2 TILs, in 9464D TILs, Ki67 expression was reduced in all TILs, particularly in Tregs when looking at geoMFI expression (**Figure 5.21 B**).

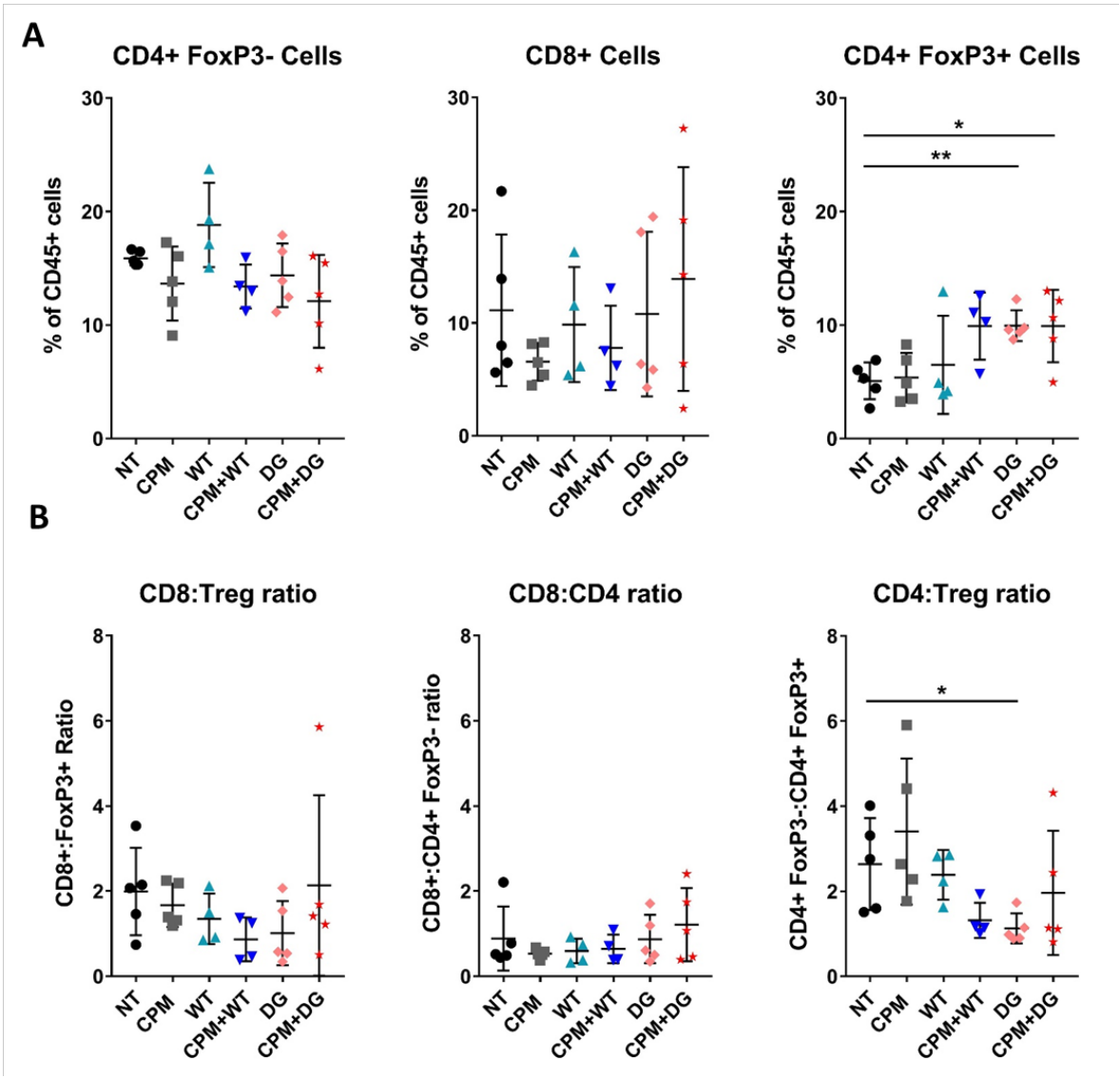

Figure 5.16 Immunophenotyping of tumour infiltrating lymphocytes after combination therapy in NXS2 tumour bearing mice

A) Experiment set up and treatment scheduling was followed as in **Figure 5.14 A.** Debris removal, singlet discrimination and population gating were conducted as shown previously (**Figure 4.27**). Percentages of tumour infiltrating T cells. **B)** Ratios of T cell subset percentages. n=5 mice per group or 4 (EW1-9WT + CPM+EW1-9WT), combined from 2 independent experiments. Significance assessed by Mann-Whitney U test, and denoted as: * = <0.05, ** = <0.01. Mean and SD error bars are shown.

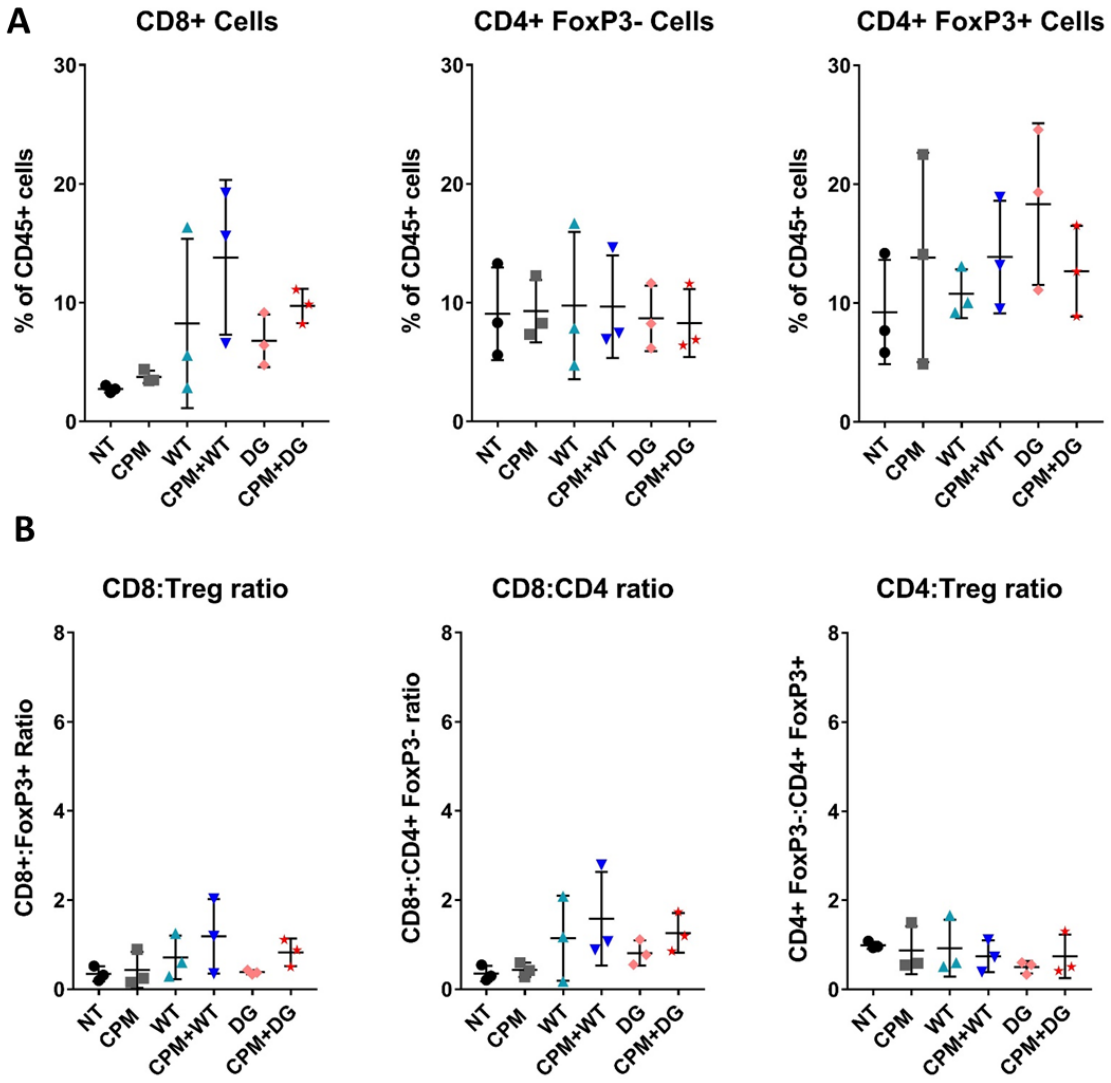

Figure 5.17 Immunophenotyping of tumour infiltrating lymphocytes after combination therapy in 9464D tumour bearing mice

A) Experiment set up and treatment scheduling was followed as in **Figure 5.15A.** Debris removal, singlet discrimination and population gating were conducted as shown previously (**Figure 4.27**). Percentages of tumour infiltrating T cells. **B)** Ratios of T cell subset percentages. n=3 mice per group. Significance assessed by Mann-Whitney U test. Mean and SD error bars are shown.

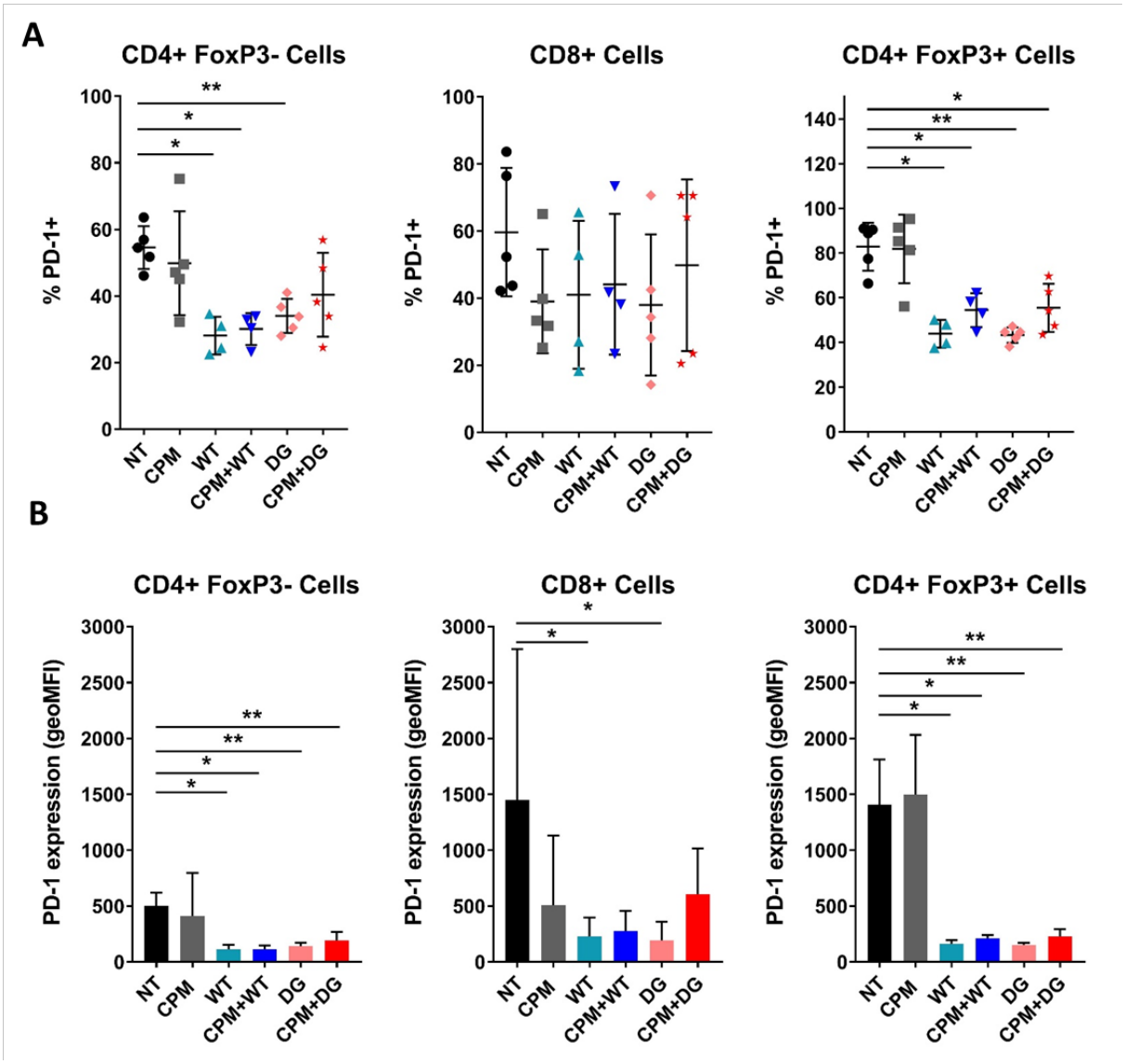

Figure 5.18 PD-1 expression on TILs after combination therapy in NXS2 tumour bearing mice

A) Experiment set up and treatment scheduling was followed as in **Figure 5.14 A**. Debris removal, singlet discrimination and population gating were conducted as shown previously (**Figure 4.27**). Percentages of PD-1 expression on TILs**, B)** geoMFIs. n=5 mice per group or 4 (EW1-9WT + CPM+EW1-9WT), combined from 2 independent experiments. Significance assessed by Mann-Whitney U test, and denoted as: * = <0.05, ** = <0.01. Mean and SD error bars are shown.

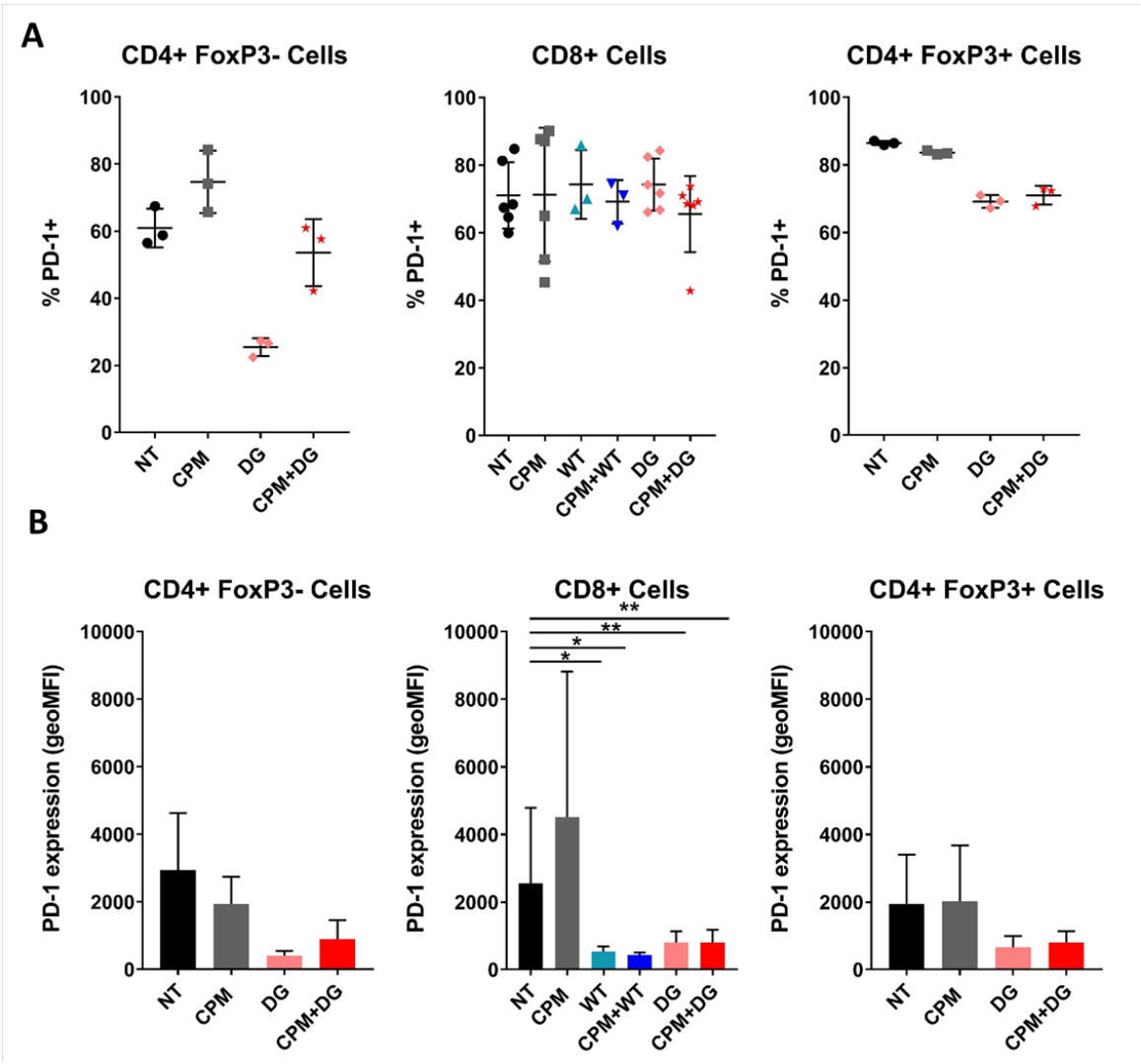

Figure 5.19 PD-1 expression on TILs after combination therapy in 9464D tumour bearing mice

A) Experiment set up and treatment scheduling was followed as in **Figure 5.15 A.** Debris removal, singlet discrimination and population gating were conducted as shown previously (**Figure 4.27**). Percentages of PD-1 expression on TILs. **B)** geoMFIs. n=3 mice per group or n=6 mice per group for CD8+ cells. Combined from 2 independent experiments. Significance assessed by Mann-Whitney U test, and denoted as: * = <0.05, ** = <0.01. Mean and SD error bars are shown.

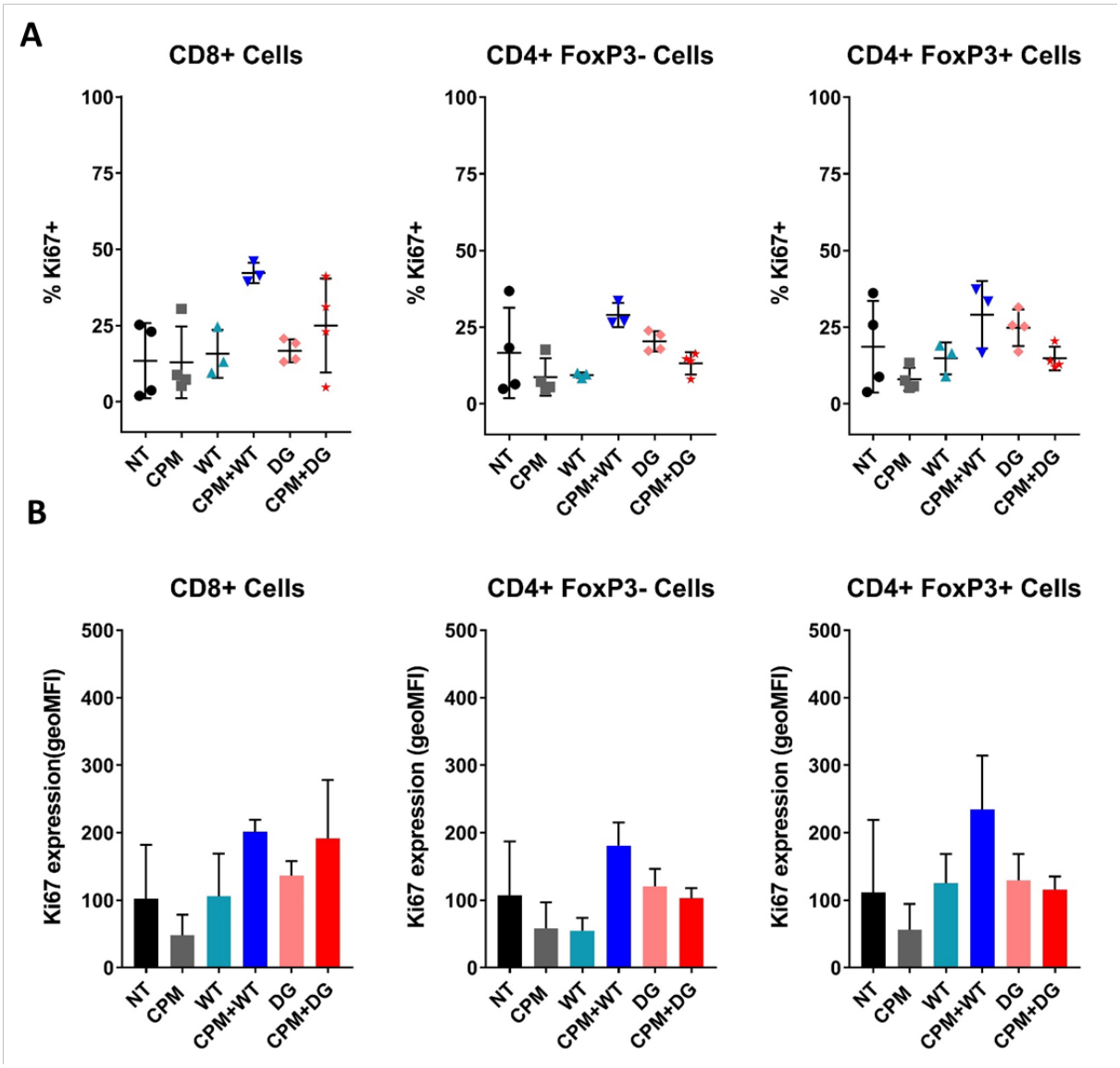

Figure 5.20 Ki67 expression on TILs after combination therapy in NXS2 tumour bearing mice

A) Experiment set up and treatment scheduling was followed as in **Figure 5.14 A**. Debris removal, singlet discrimination and population gating were conducted as shown previously (**Figure 4.27**). Percentages of Ki67 expression on TILs. **B)** geoMFIs. n=5 mice per group or 4 (EW1-9WT + CPM+EW1-9WT), combined from 2 independent experiments. Significance assessed by Mann-Whitney U test. Mean and SD error bars are shown.

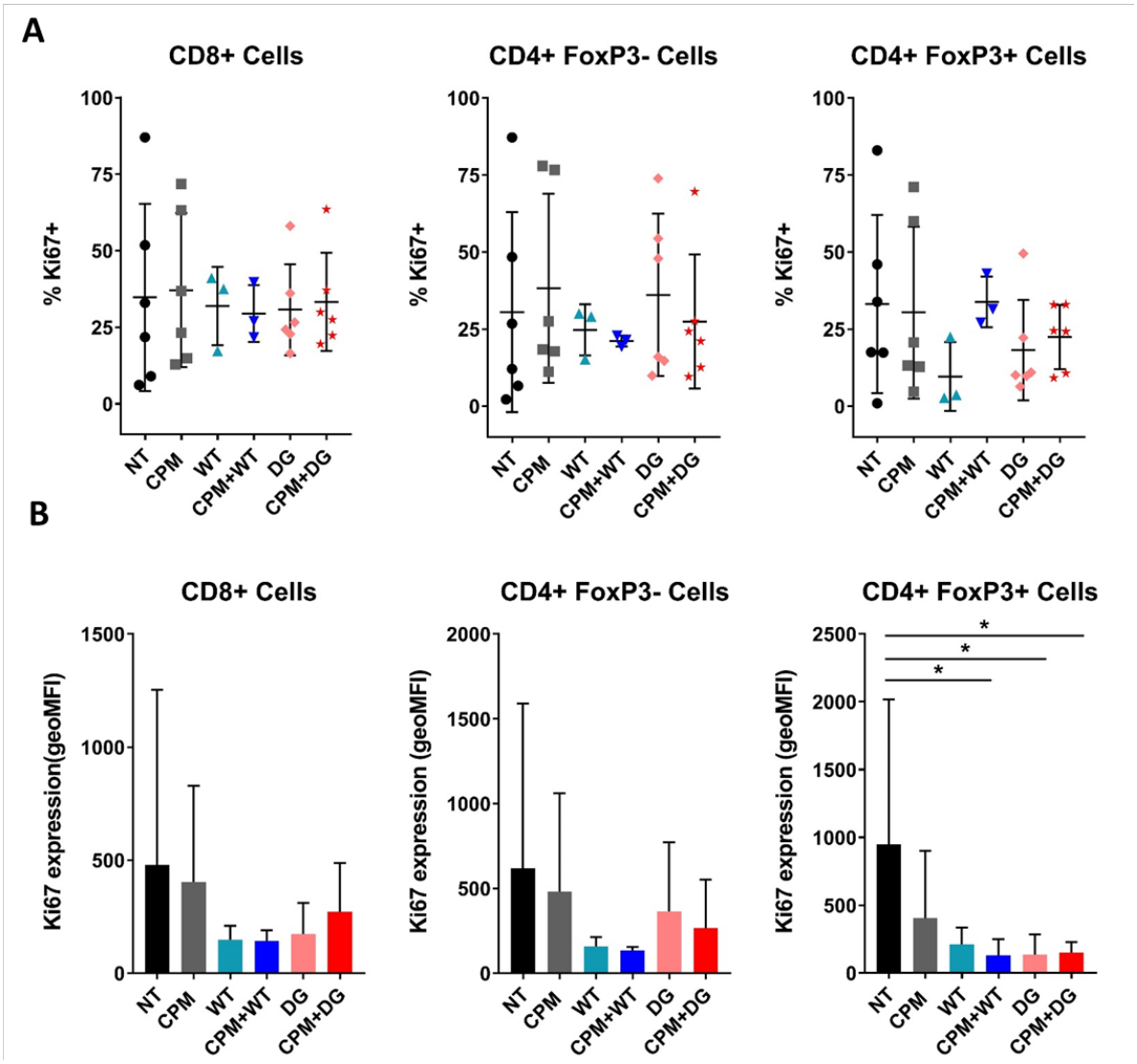

Figure 5.21 Ki67 expression on TILs after combination therapy in 9464D tumour bearing mice

A) Experiment set up and treatment scheduling was followed as in **Figure 5.15 A.** Debris removal, singlet discrimination and population gating were conducted as shown previously (**Figure 4.27**). Percentages of Ki67 expression on TILs**. B)** geoMFIs. n=6 mice per group, n=3 for EW1-9WT and CPM+EW1-9(WT). Combined from 2 independent experiments. Significance assessed by Mann-Whitney U test, and denoted as: * = <0.05. Mean and SD error bars are shown.

5.2.6.2 Memory populations in TILs of NXS2 and 9464D tumours after combination therapy

Looking at the memory status of TILs and how this changes with treatment is important, as this can suggest an initiation of an anti-tumour immune response. Memory proportions and ratios were analysed for both NXS2 (**Figure 5.22** and **Figure 5.24**) and 9464D (**Figure 5.23** and **Figure 5.25**) tumours after combination therapy. To do this proportions of naïve, EM and CM were used. Populations were defined as naïve: CD62L+ CD44-, EM: CD62L- CD44+ and CM: CD62L+ CD44+.

Firstly in NXS2 tumours, infiltrating CD4+ FoxP3- cells were shown to have decreased in naïve and CM proportions with both EW1-9(DG) and CPM+EW1-9(DG) treatment (**Figure 5.22 A**). This coincided with an increase in the relative proportion of EM cells from 62.2% in NT, to 76.9% and 81.2% respectively. This corresponded with an escalation in the EM:CM ratio in these two treatment groups on CD4+ cells (**Figure 5.24 A**). Within CD8+ T cell subset shown in **Figure 5.22 B**, CPM alone lead to a significant increase in the proportion of naïve cells with a subsequent decrease in the proportion EM cells, which resulted in a decrease in EM:naïve ratio and increase in CM:naïve ratio (**Figure 5.24 B**). The combination of CPM+EW1-9(DG) again led to an increase of EM cells and a relative reduction in CM cells, as seen in the CD4+ cells. These changes corresponded with an gain in both the EM:CM and EM:N ratios (**Figure 5.24 B**), which suggests an increase in EM cells are driving these changes. Within Tregs, levels of CM and EM cells were relatively similar between all treatment groups, along with a similar EM:CM ratio, with EW1-9(WT) treatment leading to an increase in CM cells (**Figure 5.22 C** and **Figure 5.24 C**).

In 9464D tumours (**Figure 5.23**), effects of combination therapy on T cell subsets were quite different to NXS2 tumours, particularly for CD8+ T cells. Firstly, in CD4+ T cells a reduction in naïve and a consequential increase in EM cells was seen in 9464D tumours treated with CPM, EW1-9(WT), EW1-9(DG) and CPM+EW1-9(DG), as shown in **Figure 5.23 A,** which is reflected in changes in memory ratios **(Figure 5.25 A)**. Furthermore, all antibody containing treatment groups led to a reduction in CM CD4+ cells. Importantly, the effects of CPM+EW1-9(DG) on CD4+ T cells by a drop in naïve and CM but increasing EM populations was also seen to an extent in NXS2 tumours. When looking at memory population ratios (**Figure 5.25 A**), there is an increase in EM:CM, EM:naïve and CM:naïve ratios with CPM+EW1-9(DG). The increase in EM:CM and EM:naïve ratios was also seen in NXS2 tumours. When looking at memory populations in CD8+ T cells, CPM+EW1-9(WT) treatment led to an increase in naïve and CM populations with a reduction in EM. Furthermore, CPM alone led to a slight drop in EM, which was seen in NXS2 tumours, and an expansion in CM populations. Overall, changes in CD8+ memory populations were variable. When looking at ratios (**Figure 5.25 B**) CPM and CPM+EW1-9(WT) treatments lead to a decrease in EM:naïve ratio, with most treatment groups leading to a reduction in EM:naïve ratios.

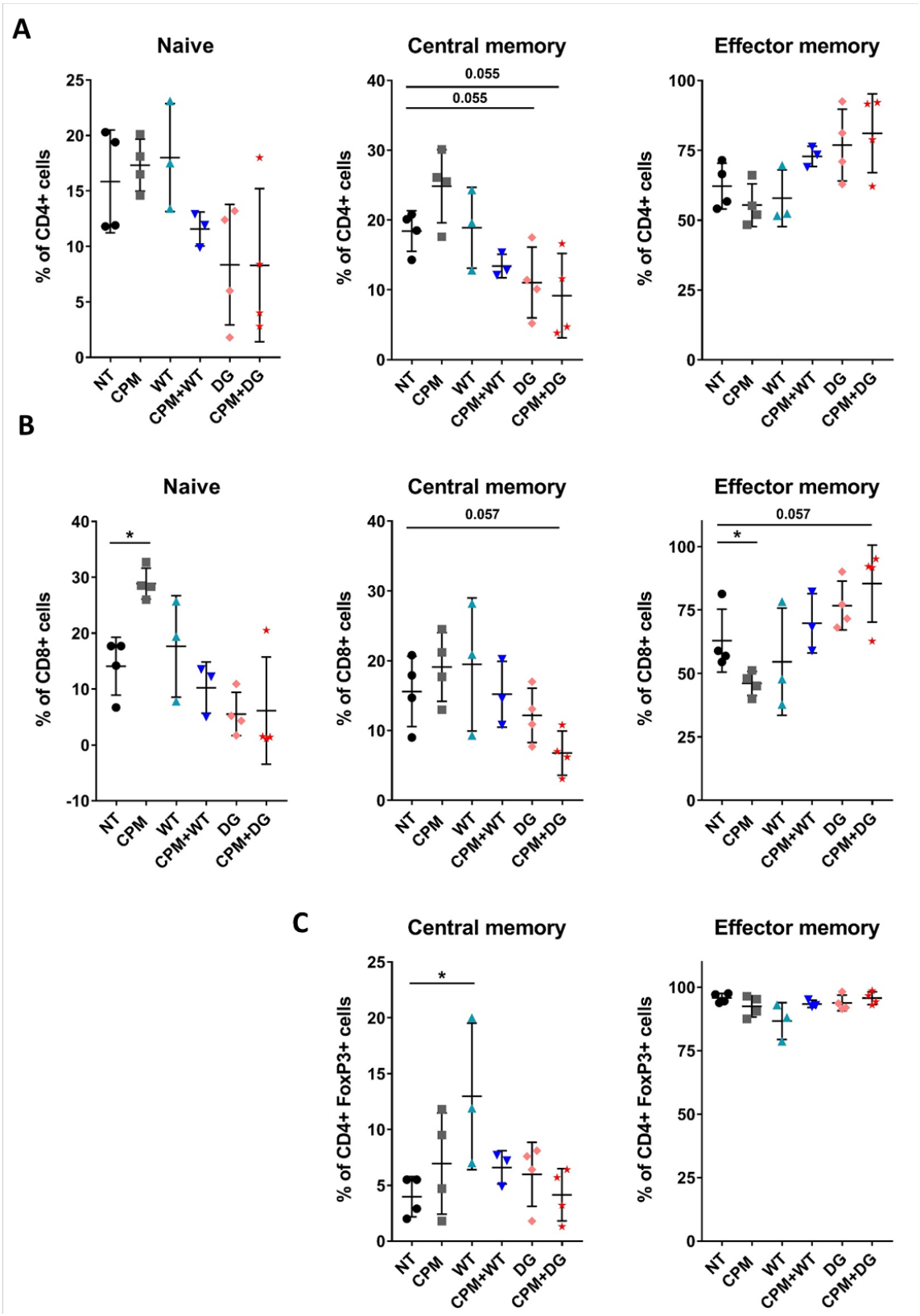

Figure 5.22 Memory populations of TILs in NXS2 tumours after combination therapy

Experiment set up and treatment scheduling was followed as in **Figure 5.14 A** Debris removal, singlet discrimination and population gating were conducted as shown previously (**Figure 4.27** and **Figure 4.28**).. Percentages of Naïve (CD62L+ CD44-), central memory (CD62L+ CD44+) and effector memory (CD62L- CD44+) cells are shown for: **A)** CD4+, **B)** CD8+ and **C)** Treg. n=5 mice per group or 4 (EW1-9WT + CPM+EW1-9WT), combined from 2 independent experiments. Significance assessed by Mann-Whitney U test, and denoted as: * = <0.05. Mean and SD error bars are shown.

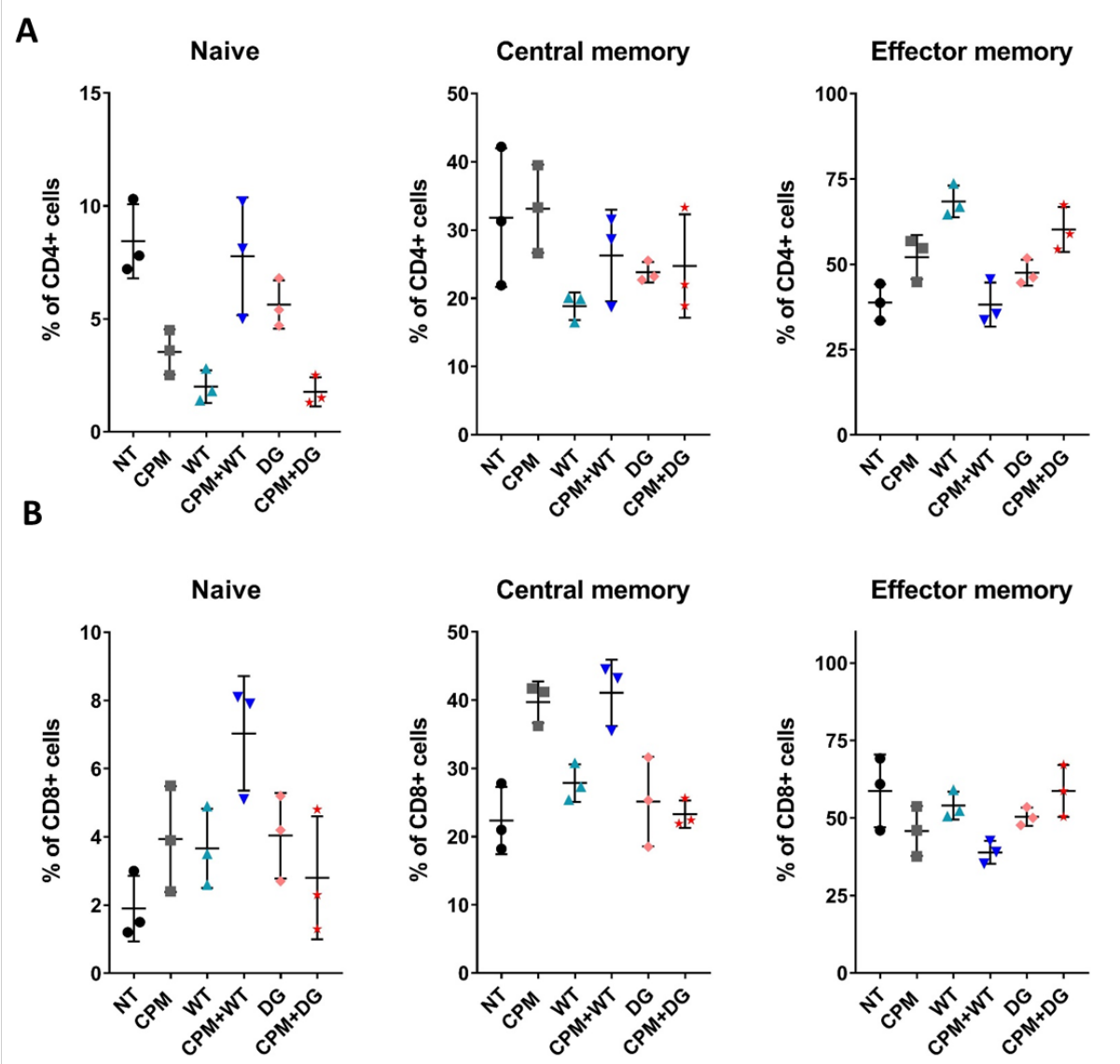

Figure 5.23 Memory populations of TILs in 9464D tumours after combination therapy

A) Experiment set up and treatment scheduling was followed as in **Figure 5.15 A.** Debris removal, singlet discrimination and population gating were conducted as shown previously (**Figure 4.27** and **Figure 4.28**). Percentages of Naïve (CD62L+ CD44-), central memory (CD62L+ CD44+) and effector memory (CD62L- CD44+) cells are shown for: CD4+ and **B)** CD8+. n=3 mice per group. Significance assessed by Mann-Whitney U test. Mean and SD error bars are shown.

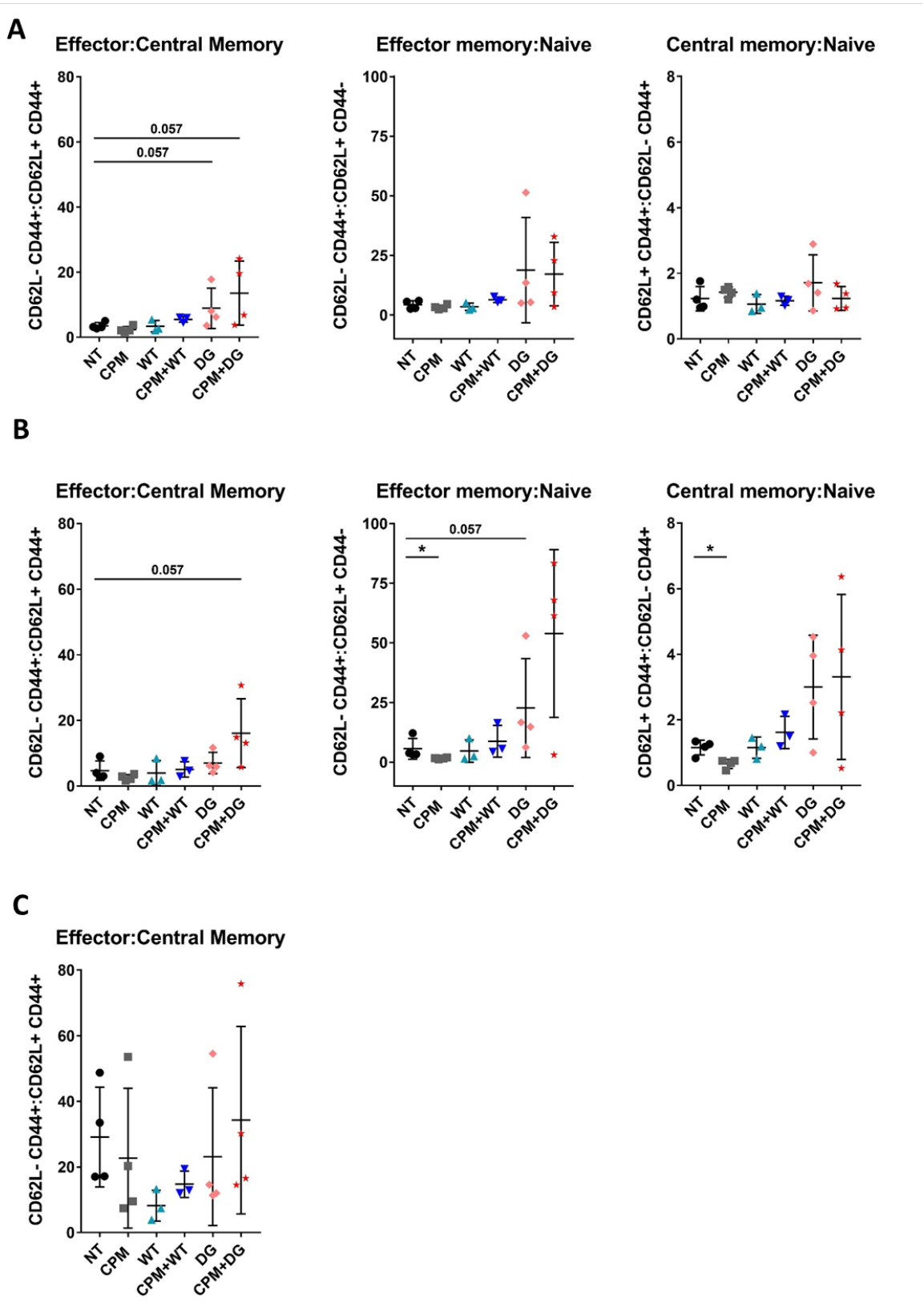

Figure 5.24 Memory population ratios of TILs in NXS2 tumours after combination therapy

A) Experiment set up and treatment scheduling was followed as in **Figure 5.14 A.** Debris removal, singlet discrimination and population gating were conducted as shown previously (**Figure 4.27** and **Figure 4.28**). Ratios of Effector:central memory, Effector:naïve and Central memory:naïve are shown for: CD4+, **B)** CD8+ and **C)** Treg. n=5 mice per group or 4 (EW1-9WT + CPM+EW1-9WT), combined from 2 independent experiments. Significance assessed by Mann-Whitney U test, and denoted as: * = <0.05. Mean and SD error bars are shown.

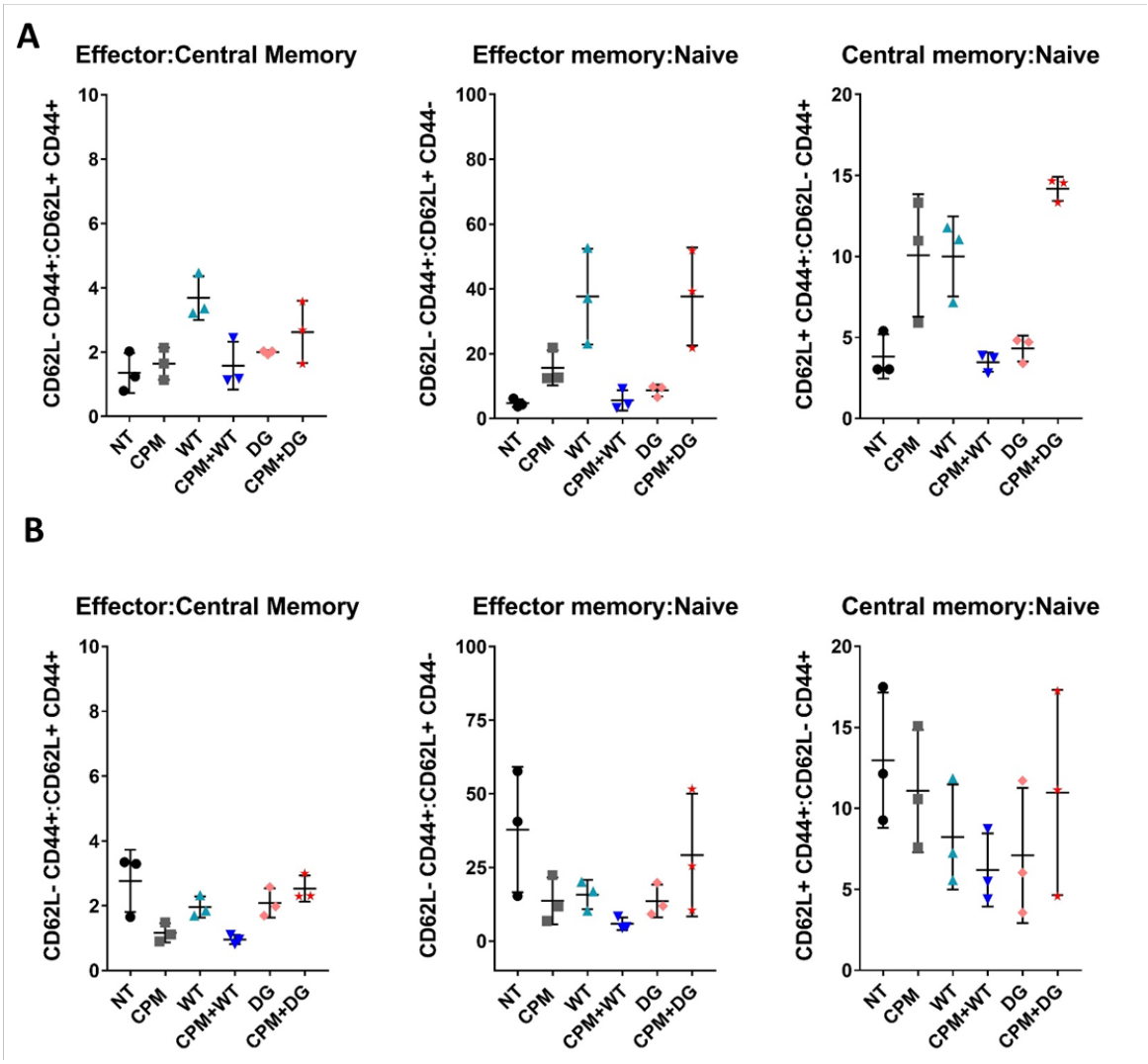

Figure 5.25 Memory population ratios of TILs in 9464D tumours after combination therapy

A) Experiment set up and treatment scheduling was followed as in **Figure 5.15 A.** Debris removal, singlet discrimination and population gating were conducted as shown previously (**Figure 4.27** and **Figure 4.28**). Ratios of Effector:central memory, Effector:naïve and Central memory:naïve are shown for: CD4+ and **B)** CD8+. n=3 mice per group. Significance assessed by Mann-Whitney U test. Mean and SD error bars are shown.

5.2.7 Tumour infiltrating myeloid percentages in tumours of NXS2 and 9464D combination therapy treated mice

Myeloid populations, including macrophages, monocytes and neutrophils were analysed. In the NXS2 model, neutrophil percentages remained relatively similar with all treatments as shown in **Figure 5.26 A**. However, both macrophages and monocytes were significantly increased in both CPM+EW1-9(WT) and CPM+EW1-9(DG) treatment groups. However in 9464D tumours (**Figure 5.27**), the only difference seen between macrophage percentages was seen with a slight increase in CPM+EW1-9(WT) compared to NT tumours. Monocyte and neutrophil percentages are similar between the groups. Expression of the ligand for PD-1, PD-L1, on myeloid cells was also assessed. In NXS2 tumours (**Figure 5.26 B+C**) No significant changes were seen with PD-L1 expression on myeloid cells. On monocytes (**Figure 5.26 C**), percentage expression of PD-L1 was similar for all groups, however geoMFI expression was decreased for both CPM alone and CPM+EW1-9(WT). 9464D tumour infiltrating macrophages show the opposite with an increase in PD-L1 expression in mice treated with EW1-9(DG) and CPM+EW1-9(DG), whereas monocytes have similar level of PD-L1 expression (**Figure 5.27 B+C**).

All data from **Figure 5.14** to **Figure 5.27** is summarised in **Table 5.1** (NXS2) and **Table 5.2** (9464D).

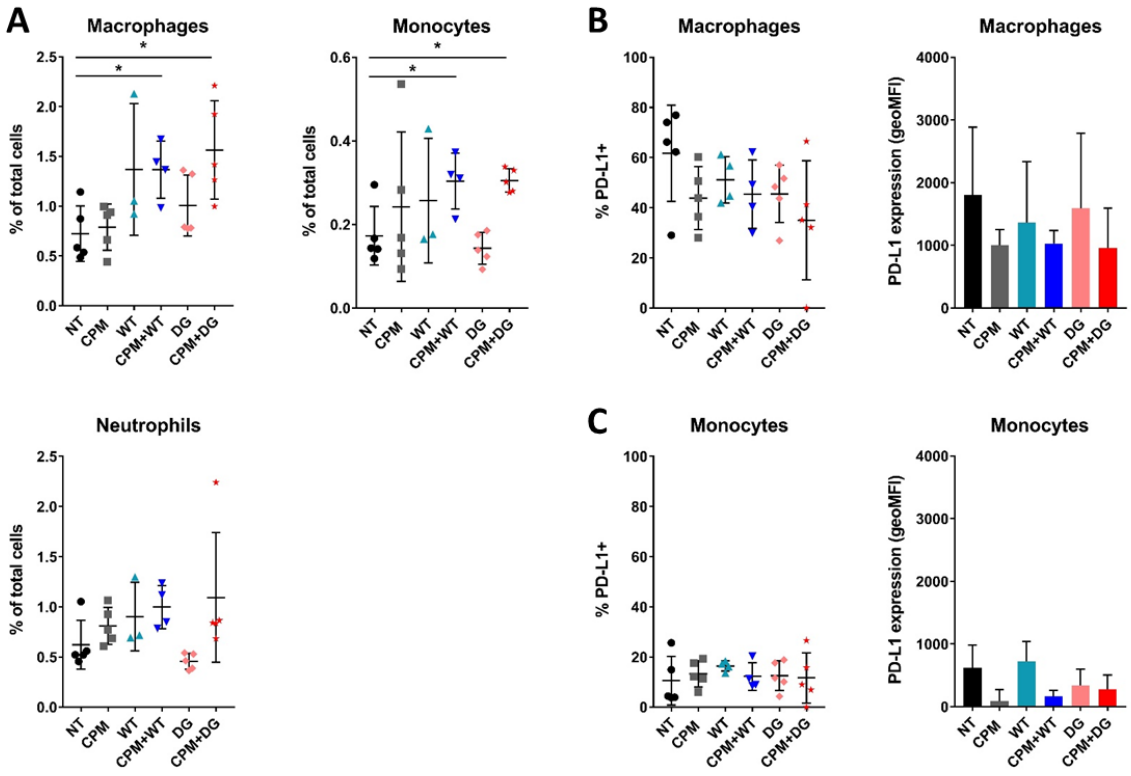

Figure 5.26 Immunophenotyping of tumour infiltrating myeloid cells after combination therapy in NXS2 tumour bearing mice.

A) Experiment set up and treatment scheduling was followed as in **Figure 5.14 A.** Debris removal, singlet discrimination and population gating were conducted as shown previously (**Figure 3.3**). Percentages of tumour infiltrating myeloid cells. **B)** Percentage expression and geoMFI of PD-L1 expression on macrophages and C**)** monocytes. n=5 mice per group or 3 (EW1-9WT) or 4 (CPM+EW1-9WT), combined from 2 independent experiments. Significance assessed by Mann-Whitney U test, and denoted as: * = <0.05. Mean and SD error bars are shown.

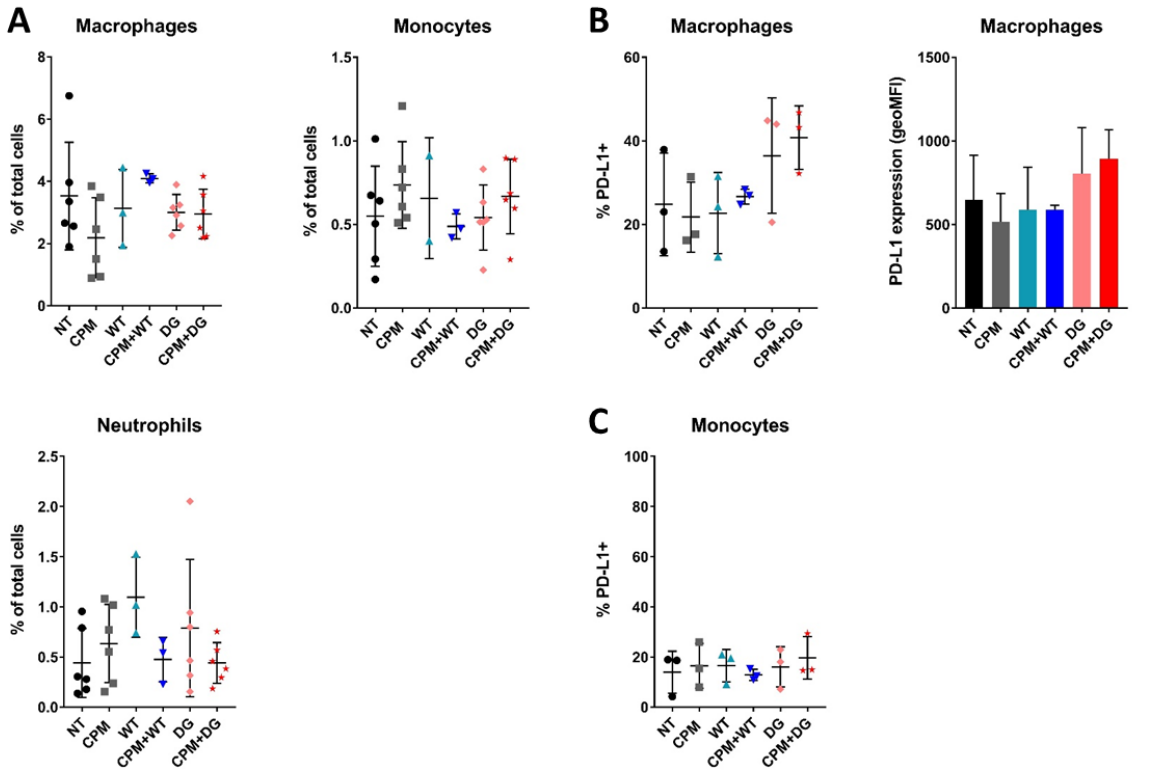

Figure 5.27 Immunophenotyping of tumour infiltrating myeloid cells after combination therapy in 9464D tumour bearing mice.

A) Experiment set up and treatment scheduling was followed as in **Figure 5.15 A.** Debris removal, singlet discrimination and population gating were conducted as shown previously (**Figure 3.3**). Percentages of tumour infiltrating myeloid cells. **B)** Percentage expression and geoMFI of PD-L1 expression on macrophages and **D)** monocytes. n=6 mice per group for cell numbers, n=3 for PD-L1 expression. n=3 for EW1-9WT and CPM+EW1-9(WT). Combined from 2 independent experiments. Significance assessed by Mann-Whitney U test. Mean and SD error bars are shown.

	NXS2	Percentage change to NT					
		CPM	EW1-9(WT)	CPM+EW1-9(WT)	EW1-9(DG)	CPM+EW1-9(DG)	Figure reference
	GD2 expression (%)	-		-		-	5.14
	GD2+ PD-L1+ (%)	-	-	-	-	-	
	CD4+ FoxP3-	-	-	-	-	-	5.16
	CD8+	-	-	-	-	-	
	CD4+ FoxP3+	-	-	-			
	CD8:Treg ratio	-	-	-	-	-	
	CD8:CD4 ratio	-	-	-	-	-	
	CD4:Treg ratio	-	-	-		-	
CD4+ FoxP3-	PD-1 expression (%)	-				-	5.18
	PD-1 expression (geoMFI)	-					
CD8+	PD-1 expression (%)	-	-	-	-	-	
	PD-1 expression (geoMFI)	-		-		-	
CD4+ FoxP3+	PD-1 expression (%)	-					
	PD-1 expression (geoMFI)	-					
CD4+ FoxP3-	Ki67 expression (%)	-	-	-	-	-	5.20
	Ki67 expression (geoMFI)	-	-	-	-	-	
CD8+	Ki67 expression (%)	-	-	-	-	-	
	Ki67 expression (geoMFI)	-	-	-	-	-	
CD4+ FoxP3+	Ki67 expression (%)	-	-	-	-	-	
	Ki67 expression (geoMFI)	-	-	-	-	-	
CD4+ FoxP3-	Naïve	-	-	-	-	-	5.22
	Central memory	-	-	-			
	Effector memory	-	-	-	-	-	
CD8+	Naïve		-	-	-	-	
	Central memory	-	-	-	-		
	Effector memory		-	-	-		
CD4+ FoxP3+	Central memory	-		-	-	-	
	Effector memory	-	-	-	-	-	
CD4+ FoxP3-	Effector:Central memory	-	-	-			5.24
	Effector:Naïve	-	-	-	-	-	
	Central memory:Naïve	-	-	-	-	-	
CD8+	Effector:Central memory	-	-	-	-		
	Effector:Naïve		-	-		-	
	Central memory:Naïve		-	-	-	-	
CD4 + FoxP 3+	Effector:Central memory	-	-	-	-	-	
	Macrophages	-	-		-		5.26
	Monocytes	-	-		-		
	Neutrophils	-	-	-	-	-	

Table 5.1 Summary of immunophenotyping data from combination therapy of NXS2 tumour bearing mice

Summary data from immunophenotyping of tumours from combination therapy treated NXS2 mice is demonstrated. Data is summarised using significant differences seen in the treatment groups compared to NT mice. Orange = decrease compared to NT mice, Green = increase compared to NT mice and - = no change.

	9464D	Percentage change to NT					Figure reference
		CPM	EW1-9(WT)	CPM+EW1-9(WT)	EW1-9(DG)	CPM+EW1-9(DG)	
	GD2 expression (%)	-			-	-	5.15
	GD2+ PD-L1+ (%)	-	-	-	-	-	
	CD4+ FoxP3-	-	-	-	-	-	5.17
	CD8+	-	-				
	CD4+ FoxP3+	-	-	-	-	-	
	CD8:Treg ratio	-	-	-	-	-	
	CD8:CD4 ratio	-	-	-	-		
	CD4:Treg ratio	-	-	-	-	-	
CD4+ FoxP3-	PD-1 expression (%)	-	X	X		-	5.19
	PD-1 expression (geoMFI	-	X	X	-	-	
CD8+	PD-1 expression (%)	-	-	-	-	-	
	PD-1 expression (geoMFI	-					
CD4+ FoxP3+	PD-1 expression (%)	-	X	X			
	PD-1 expression (geoMFI	-	X	X	-	-	
CD4+ FoxP3-	Ki67 expression (%)	-	-	-	-	-	5.21
	Ki67 expression (geoMFI)	-	-	-	-	-	
CD8+	Ki67 expression (%)	-	-	-	-	-	
	Ki67 expression (geoMFI)	-	-	-	-	-	
CD4+ FoxP3+	Ki67 expression (%)	-	-	-	-	-	
	Ki67 expression (geoMFI)	-	-				
CD4+ FoxP3-	Naïve			-	-		5.23
	Central memory	-	-		-	-	
	Effector memory			-	-		
CD8+	Naïve	-	-		-	-	
	Central memory		-		-	-	
	Effector memory	-	-		-	-	
CD4+ FoxP3+	Central memory	X	X	X	X	X	
	Effector memory	X	X	X	X	X	
CD4+ FoxP3-	Effector:Central memory	-	-		-	-	5.25
	Effector:Naïve		-		-		
	Central memory:Naïve				-		
CD8+	Effector:Central memory		-		-	-	
	Effector:Naïve	-	-		-	-	
	Central memory:Naïve	-	-	-	-	-	
CD4 + FoxP 3+	Effector:Central memory	X	X	X	X	X	
	Macrophages	-	-	-	-	-	5.27
	Monocytes	-	-	-	-	-	
	Neutrophils	-	-	-	-	-	

Table 5.2 Summary of immunophenotyping data from combination therapy of 9464D tumour bearing mice

Summary data from immunophenotyping of tumours from combination therapy treated 9464D mice is demonstrated. Due to low sample numbers, significant differences were not seen therefore data is summarised using whether an obvious difference is demonstrated and error bars do not overlap. Orange = decrease compared to NT mice, Green = increase compared to NT mice and - = no change. X = data not collected due to technical issues.

5.2.8 Metronomic dosing of CPM and anti-PD-1 antibody in 9464D tumour bearing mice

Data presented in chapter 4 demonstrated that low dose CPM at 40mg/kg was able to significantly specifically deplete tumour infiltrating Treg cells 72hrs after administration (**Figure 4.15**). However,

data also presented in chapter 4 and in this chapter showed that the depletion of Tregs is not maintained long after CPM administration, with Treg percentages returning to non-treated levels by 11 days after initial CPM (**Figure 4.29** and **Figure 5.16** and **Figure 5.17**). This chapter also demonstrated that the combination of CPM with anti-PD-1 antibody therapy was most potent when the antibody was DG. The mechanism behind this may involve modulation of T cell subsets within the tumours, specifically around the memory populations (**Figure 5.22** and **Figure 5.23**). With knowledge of all the above data, an experiment was conducted to see if using either CPM+/- anti-PD-1 antibody in a metronomic dosing strategy could further improve survival in the 9464D model.

As stated in the methods, the EW1-9 antibody is a rat IgG1 antibody, and therefore when injected into the mouse in repeated doses could lead to the production of anti-drug antibody response by the mouse due to species disparity. Therefore, if this was the case then using the antibody after this point would be counterproductive as the antibody would be rapidly cleared. To that end, ELISA analysis for anti-rat antibodies in serum samples of C57BL/6 mice when using the EW1-9(DG) antibody once a week for 5 weeks, was performed. This ELISA analysis suggested that no anti-rat antibodies were detected at any point after 5 weeks of weekly EW1-9(DG) antibody (data not shown). Suggesting metronomic dosing up to this point would still be viable, however this does not discount an anti-drug response developing at a time after 5 weeks.

Figure 5.28 A shows the treatment strategy used for metronomic dosing. Firstly, mice (except NT mice) were given the previously tested treatment schedule of 40mg/kg on day 0 followed by two doses of 250µg of EW1-9(DG) on day 3 and day 6. Mice that were then in the metronomic CPM arm (CPM (met) + EW1-9 DG) received 40mg/kg CPM on a weekly basis. Mice in the metronomic EW1-9(DG) arm (CPM+EW1-9 DG (met)) received 150µg EW1-9(DG) weekly and finally one group of mice received both CPM and EW1-9(DG) weekly (CPM (met)+EW1-9 DG (met)). When starting treatment at 5x5 mm start point as shown in **Figure 5.28 B-F,** the original therapy strategy used previously still slowed tumour growth down compared to NT mice. However the addition of CPM metronomicaly, either on its own or together with metronomic EW1-9(DG), led to a substantial delay before tumours started to grow exponentially. Metronomic EW1-9(DG) alone had a similar therapeutic efficacy as the standard treatment. When looking at overall survival of the mice, the combination of metronomic CPM and metronomic EW1-9(DG) was the most potent leading to a significant increase in median survival over NT mice from 49 to 62 days (**Figure 5.28 G**). The standard treatment alone and metronomic CPM alone also lead to an increase in survival. When combining the survival data with another independent experiment, as observed in **Figure 5.29**, metronomic dosing of both CPM and EW-19(DG) antibody in combination led to a significant improvement in median survival (72 days) compared to all other treatment groups, except metronomic EW1-9(DG).

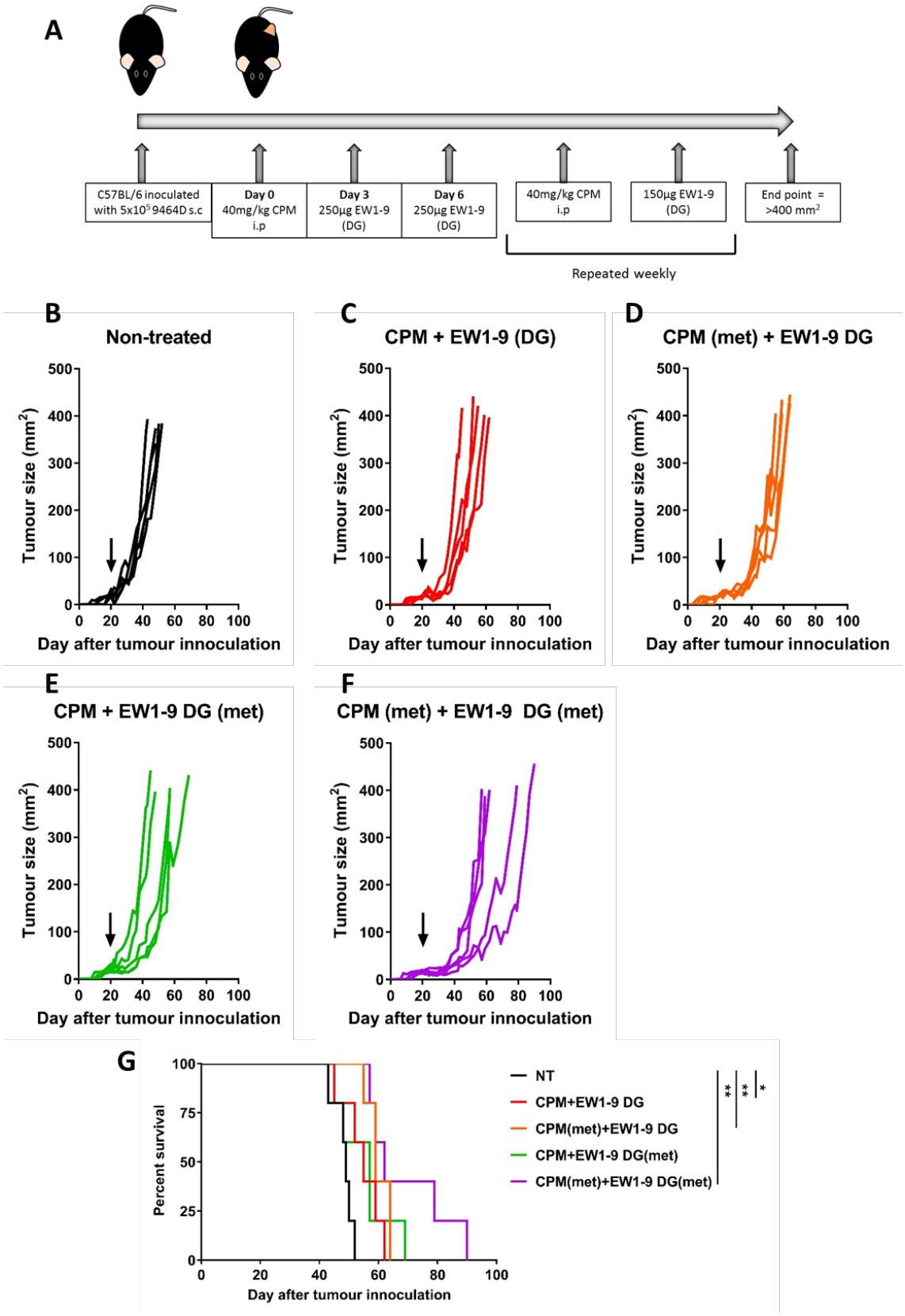

Figure 5.28 Representative example of tumour growth and survival of 9464D tumour bearing mice after metronomic CPM and anti-PD-1 therapy at 5x5 mm start point

A) C57BL/6 female mice were inoculated s.c with $5x10^5$ 9464D cells. Once tumours had reached 5x5 mm EW1-9 (DG) was given at 250ug per dose i.p, with or without 40mg/kg CPM 3 days earlier. This was either followed by weekly 40mg/kg CPM, 150ug EW1-9(DG) or both until end point at 400mm^2. Individual growth curves are shown for each group: **B)** NT, **C)** CPM+EW1-9DG, **D)** CPM(met)+EW1-9DG, **E)** CPM+EW1-9DG (met), **F)** CPM (met)+EW1-9DG (met), **G)** Survival to >400 mm^2. n=5 mice per group. Significance assessed by Log Rank test, and denoted as: * = <0.05, ** = <0.01.

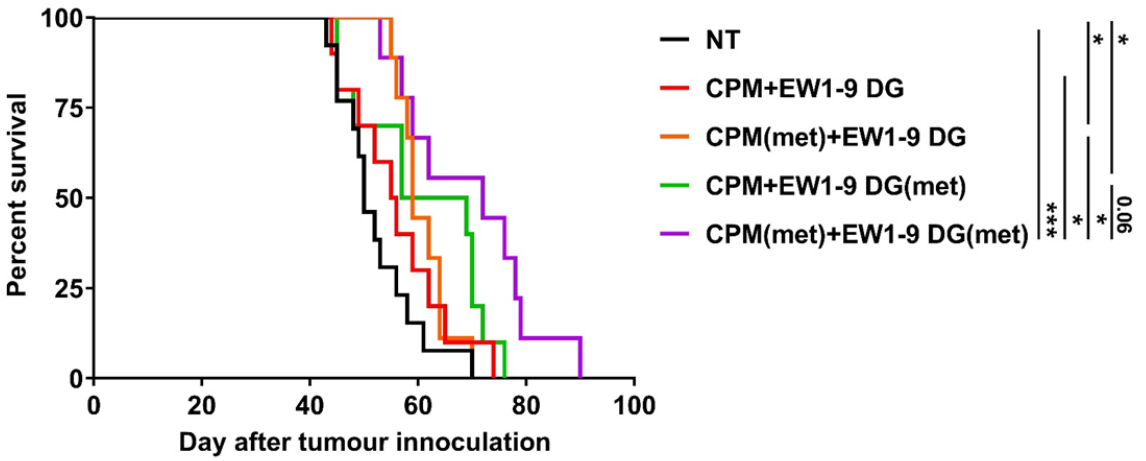

Figure 5.29 Combined data of survival of 9464D tumour bearing mice after CPM and anti-PD-1 therapy at 5x5 mm tumour start point

Survival of 9464D tumour bearing C57BL/6 mice was combined from two independent experiments detailed in **Figure 5.28** and second independent experiment. n= 13 (NT), n=10 (CPM+EW1-9 DG and CPM+EW1-9 DG(met)), n= 9 (CPM(met)+EW1-9 DG and CPM(met)+EW1-9 DG(met)) mice per group. Significance assessed by Log Rank test, and denoted as: * = <0.05, ** = <0.01, *** = <0.001.

5.2.8.1 Metronomic dosing in 9464D palpable tumour bearing mice

Data shown previously in **Figure 5.9** and **Figure 5.11**, demonstrated that greater median survival was achieved in the 9464D model using the combination of CPM+EW1-9(DG) in mice with smaller palpable tumours, compared to 5x5 mm tumours. Therefore, this combination therapy was tested using metronomic dosing commencing on palpable tumours, as demonstrated in **Figure 5.30 A**. Here, the combination of metronomic CPM and EW1-9(DG) showed a slowing of tumour growth (**Figure 5.30 F**) compared to NT mice (**Figure 5.30 B**). Metronomic CPM alone did demonstrate some tumour growth impedance (**Figure 5.30 D**), however this was more variable. Due to this slowing of tumour growth, CPM (met) + EW1-9 DG (met) treated mice demonstrated a significant improvement of median survival of 72 days, over NT (54.5 days), CPM+EW1-9 DG (53 days) and CPM+EW1-9 DG (met) (58 days - **Figure 5.30 H**).

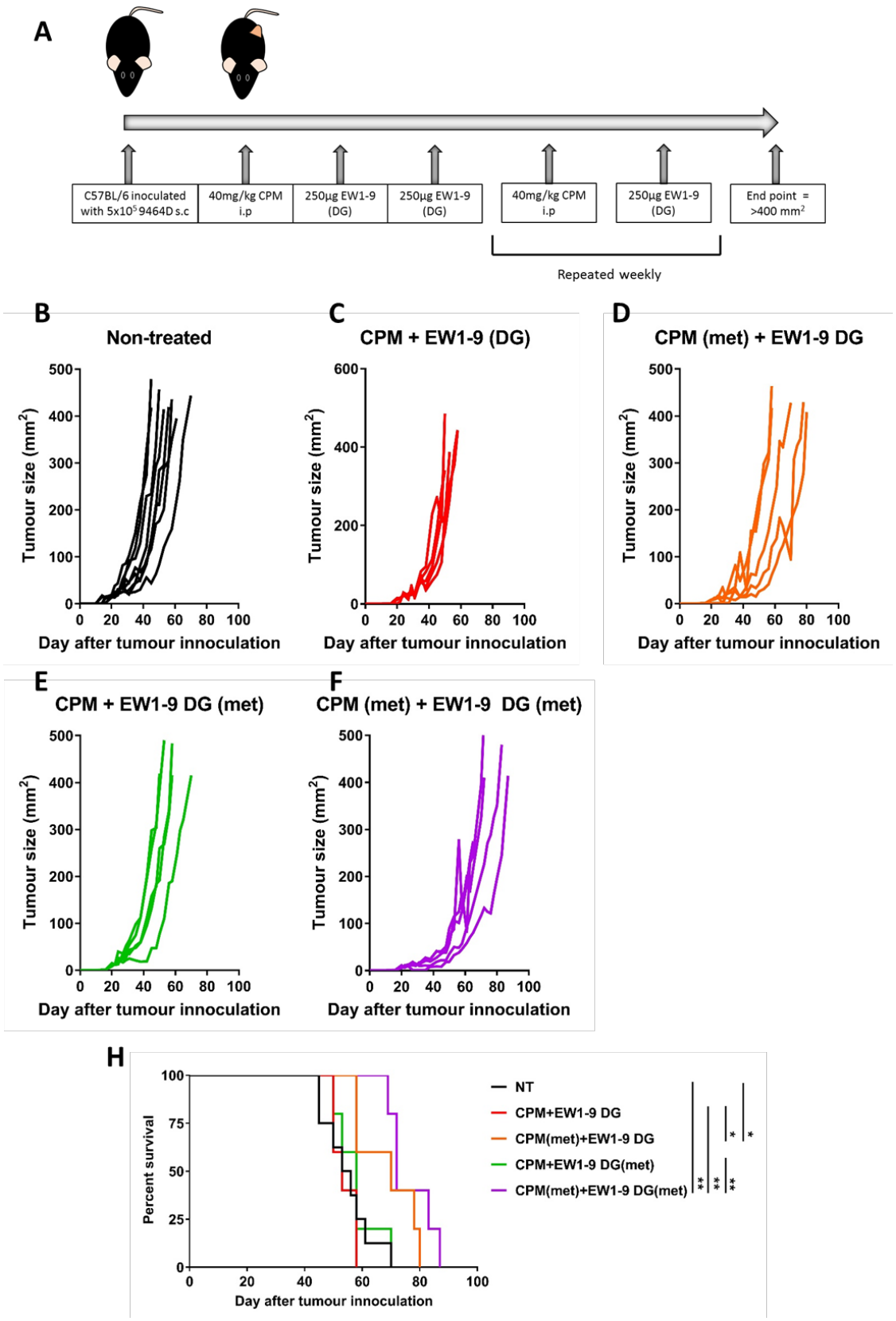

Figure 5.30 Tumour growth and survival of 9464D tumour bearing mice after metronomic CPM and anti-PD-1 therapy at palpable start point

A) C57BL/6 female mice were inoculated s.c with $5x10^5$ 9464D cells. Once tumours had become palpable mm EW1-9 (DG) was given at 250ug per dose i.p, with or without 40mg/kg CPM 3 days earlier. This was either followed by weekly 40mg/kg CPM, 150ug EW1-9(DG) or both until end point at 400mm^2. Individual growth curves are shown for each group: **B)** NT, **C)** CPM+EW1-9DG, **D)** CPM(met)+EW1-9DG, **E)** CPM+EW1-9DG (met), **F)** CPM (met)+EW1-9DG (met), **G)** Survival to >400 mm^2. n=5 or n= 8 (NT) mice per group. Significance assessed by Log Rank test, and denoted as: * = <0.05, ** = <0.01.

5.2.9 Assessment of CPM and anti-PD-1 antibody therapy in TH-MYCN spontaneous NB model

In chapter 3, the TH-MYCN transgenic spontaneous NB mouse models was demonstrated to be a better representation of the immune landscape of human NB tumours, compared to the SC models, NXS2 and 9464D. Consequently, this model was employed to investigate whether the synergy of CPM+EW1-9(DG) can also be achieved in this more translatable model. For this, TH-MYCN mice presenting with approximately 1cm tumours on palpation, were place into 1 of 6 treatment arms as demonstrated in **Figure 5.31 A**, and monitored for tumour representation. Firstly, it was observed in **Figure 5.31 B** that CPM alone in this model lead to a significant increase in median survival over NT mice (31 and 12.5 days respectively), however this benefit was improved significantly with combination of both CPM+EW1-9(DG) therapy (53 days). Furthermore, when metronomic dosing of both CPM and EW1-9(DG) was conducted for 100 days, all mice had no signs of tumour re-presentation by day 200. However, this was also seen to an extent in mice treated with just metronomic CPM, although survival of these mice has not yet been assessed up to 200 days. Together these data suggest that TH-MYCN tumours are inherently more sensitive to CPM than both SC models, but despite this, combination of CPM+ anti-PD-1 antibody did lead to the largest improvement in median survival.

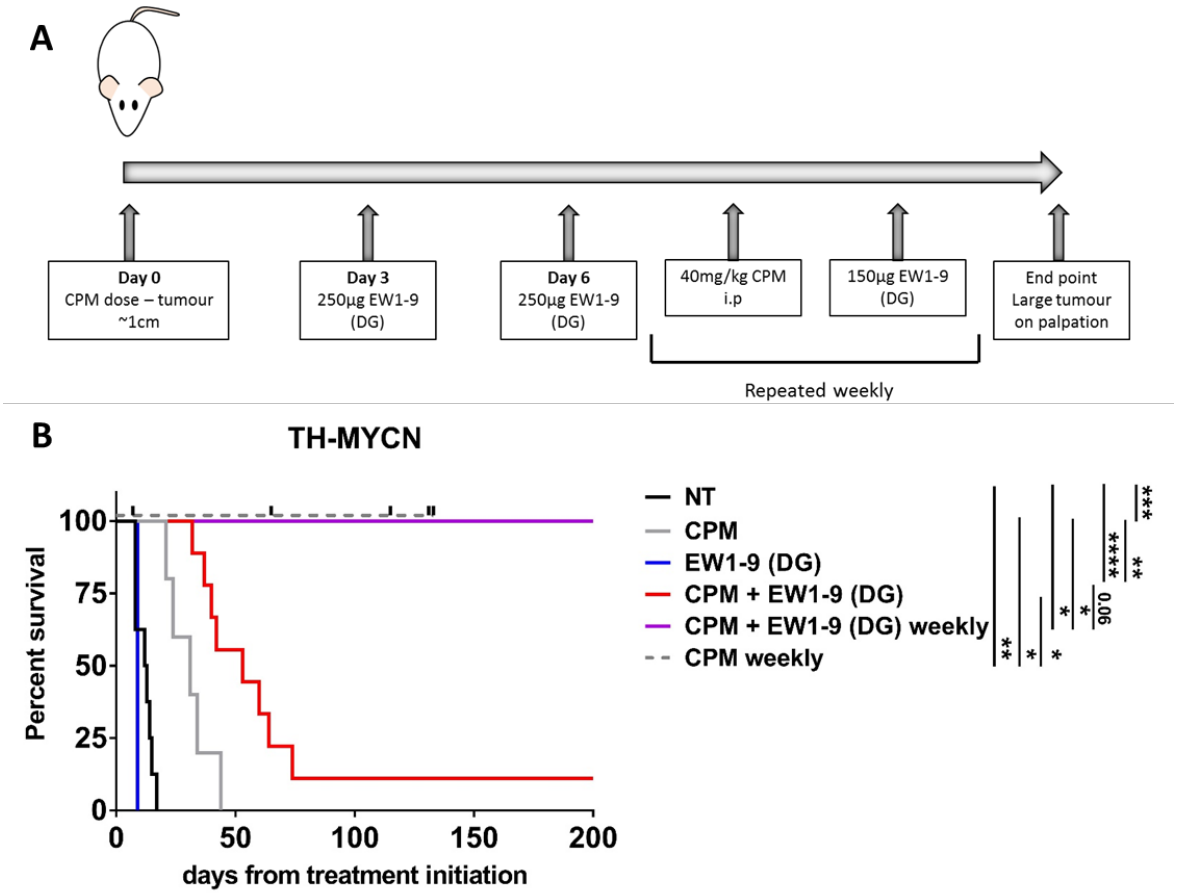

Figure 5.31 Survival of TH-MYCN mice treated with combination of CPM + EW1-9(DG) therapy

A) On palpation presentation of ~1cm tumour, TH-MYCN mice were allocated to therapy treatment groups as follows: NT, single dose CPM 40mg/kg, two doses of anti-PD-1 (EW1-9 DG), CPM+anti-PD-1, metronomic CPM and anti-PD-1 or metronomic CPM. Tumour recurrence was monitored and end point assessed as large tumour regrowth. **B)** Survival curve from treatment initiation of TH-MYCN treatment groups as in A. Black ticks denote positions of CPM weekly treated mice free from tumour. n= 8 (NT and CPM+EW1-9 (DG)), n=5 (CPM), n=1 (EW1-9(DG), n=2 (CPM + EW1-9 (DG) weekly) and n=5 (CPM weekly). Significance assessed by Log Rank test, and denoted as: * = <0.05, ** = <0.01, *** = <0.001 and **** = <0.0001.

5.3 Discussion

Immunotherapy is fast becoming a potent weapon in the oncologist's arsenal against many different cancers, however, its potential has not yet begun to be realised in paediatric cancers. As discussed in chapter 1 paediatric cancers and particularly neuroblastoma could be interesting targets for immunotherapy, with an anti-GD2 antibody already part of standard treatment for high-risk neuroblastoma [52]. In adult cancers the immunomodulatory antibody therapy revolution was initiated with the use of monoclonal antibodies targeting checkpoint inhibitor molecules on the surface of activated T cells. These have had a dramatic impact on cancer treatment with striking objective responses seen in cancers such as melanoma and NSCLC [406,437]. However, these therapies do not work for everyone as single agents, and it is fast becoming clear that to harness their full potential, they will need to be used in combination with other immunotherapies or current standard treatments for cancers. With treatment for high risk NB consisting of an intensive multimodal regime with little scope for further intensification, new treatment strategies need to be designed which incorporate and synergise with these treatments to improve survival. Chemotherapy is a large part of the treatment regime and as the previous chapter discussed, can have immunomodulatory effects of its own. Therefore, this chapter aimed to elucidate whether immunomodulatory antibody therapies could be combined with a commonly used chemotherapeutics in neuroblastoma to increase survival in the three different murine models.

Using the NXS2 subcutaneous model, investigations into whether three different immunomodulatory antibodies could be combined with CPM to improve survival was conducted, as shown in **section 5.2.2**. In this study, mAbs which blocked the immune checkpoints CTLA-4 and PD-1 were investigated along with mAbs which agonise the co-stimulatory receptor 4-1BB. Anti-CTLA-4 therapy was the first checkpoint blocker antibody to be approved, followed swiftly by anti-PD-1 antibody, and both have shown potency in the clinical setting, as discussed in chapter 1 [432]. Anti-4-1BB antibodies on the other hand are yet to be approved for clinical use but have shown promise in preclinical settings, being able to enhance an endogenous anti-tumour T cell response [463,464].

Combination of 4-1BB antibodies with CPM was first assessed in **Figure 5.2**. It has previously been demonstrated that NXS2 tumours grow fairly rapidly, with end point being reached around day 23, therefore if any therapy is seen with any of the treatments it will have to act within a fairly short time frame. 4-1BB was targeted with two different isotypes of agonistic antibody. Here, no increase in median survival was seen over the single agents. Anti-4-1BB works to agonise co-stimulation in T cells within the tumour to boost an anti-tumour immune response as discussed in chapter 1. However as discussed in chapter 4, the NXS2 tumour model has very little T cell and, importantly,

CD8+ infiltration into the TME, as they were shown to have a low CD8+:Treg ratio. Therefore, anti-4-1BB may not be having any benefit in combination as there are few T cells present for the antibody to activate. The lack of T cells may be due to the poor and disorganised vasculature found in this model, therefore this type of antibody may have greater benefit in a more maturely vascularised, more T cell rich tumour [572]. 4-1BB expression levels were assessed in chapter 4 after application of CPM, demonstrating low expression of 4-1BB on CD8+ T cells within the tumour microenvironment. As 4-1BB is an activation marker, this could suggest that these CD8+ T cells are not activated. As expression levels of 4-1BB are low, this could explain the anti-4-1BB antibody's lack of efficacy.

Unfortunately, with anti-CTLA-4 antibody treatment, no difference in survival was seen between the combination of CPM and anti-CTLA-4 and either of the single agent arms (**Figure 5.3**). As demonstrated in the previous chapter CPM was shown to deplete Treg cells within the tumour microenvironment. This is an important consideration as one of the mechanisms of anti-CTLA-4 therapy may be to bind to CTLA-4 on Tregs and deplete them [592,593]. Therefore, if Tregs in the tumour have already been depleted by the CPM, further depletion by an antibody may not increase survival over chemotherapy alone. Furthermore, as discussed in chapter 1, the ligands for CTLA-4 are only present on APCs, and therefore blocking this checkpoint receptor only stops the action of suppression mediated by APC contact in the immune synapse. As will be discussed shortly, the tumour microenvironment, including tumour cells themselves, can express ligands for other checkpoint receptors and therefore, anti-CTLA-4 therapy may not be enough to overcome suppression mediated by these other receptors as there will be substantially more cells expressing ligands for these than just the APCs for the CTLA-4 receptor.

Although no therapeutic benefit was seen with anti-CTLA-4 therapy, combination between CPM and anti-PD-1 showed greater promise (**Figure 5.4**). Although in the NXS2 subcutaneous tumour model, no improvement over the single agent therapies was seen with the combination of the wild type anti-PD-1 and CPM. However, when anti-PD-1 was deglycosylated (EW1-9 DG), an increase in median survival was seen, and a slowing of tumour growth was also noted. As mentioned previously, deglycosylation of an antibody removes its Fc function and prevents it from interacting with Fc receptors on innate immune cells [389]. As PD-1 treatment is mainly targeting CD8+ effector cells, having no Fc function prevents bound antibody from initiating depletion of that cell by innate immune effectors. Anti PD-1 therapy may have greater efficacy than the other checkpoint inhibitor in this combination setting as use of this antibody blocks a pathway that is not just regulated by APCs and Tregs as discussed above. This is because the ligands for PD-1: PD-L1 and PD-L2, are expressed on many cell types including APCs, tumour cells and other cells within the tumour microenvironment [210,211,436], allowing these cells to also regulate the T cell response. With Tregs

depleted by the use of CPM, the anti-PD-1 therapy could work by blocking these other regulators, and allows for activated CD8+ cells. This combination therapy was also assessed in the 9464D tumour model (**Figure 5.7**), where a significant improvement in survival was also observed. These data together suggest that, at least in the NB models, combination of anti-PD-1 antibodies with low dose cyclophosphamide is a promising treatment strategy.

In the NXS2 and 9464D models assessed above, combination treatment was started at a fairly large tumour burden start point of 8x8 mm. Therefore, to establish whether tumour size can impact efficacy of the combination treatment, NXS2 and 9464D mice bearing 5x5 mm tumours were utilised (**Figure 5.6** and **Figure 5.9** respectively). Here, it was demonstrated for both models that combination of CPM and EW1-9(DG) led to the most significant increase in survival compared to the other treatment arms, as was seen with an 8x8 mm start point. For NXS2 the smaller tumour start point appeared to slightly increase the efficacy of CPM+EW1-9(DG) compared to the larger start point. Furthermore, in the 9464D model, a tumour start point of palpable was also investigated. As demonstrated previously, 9464D tumours become palpable and stay at this small tumour size for an extended period of time before tumour growth accelerates. Therefore, assessment of starting treatment within the 'lag' phase of growth was conducted to see if combination therapy efficacy could be increased (**Figure 5.11**). Despite this smaller treatment start point, efficacy of the combination of CPM+EW1-9(DG) was relatively similar to the larger treatment start points of 5x5 and 8x8 mm. This demonstrated that in these particular tumour models, tumour size at start point was not a determining factor of treatment efficacy. It has been reported that tumour burden can be a predictive factor for outcome after immunotherapy[590]. It is worth noting however, that patients in NB would most likely be receiving this combination treatment after surgical removal of the large tumour mass most patients present with (**Section 1.2.3**). Therefore, it may be more representative to use a small tumour start point in these models, as most NB patients would only begin treatment with residual disease.

In an attempt to understand the immunological mechanism behind why combination of low dose CPM and anti-PD-1 immunotherapy led to an increase in survival in NB tumour bearing mice, immunophenotyping of mice after therapy was conducted, in both NXS2 and 9464D after treatment administration. Firstly, PBMCs were assessed for modulation of T cell subset populations. Here, PBMCs for both models saw a significant increase in circulating Treg cells after treatment with CPM+EW1-9(DG), which in the NXS2 model lead to a significant decrease in CD8:Treg ratio. Although an increase in circulating Tregs in the treatment group which showed significant increases in survival appears contradictory, it could suggest that systemic activation of T cells has occurred, possibly driven by increase inflammation at the tumour site due to increased tumour cell death.

This systemic activation may have stimulated the increase in Tregs to compensate for effector T cell activation, in order to dampen down the immune response.

Although analysing systemic effects of treatment is important, it is imperative to assess how combination therapy is effecting immune infiltrates at the tumour site. Firstly, it was observed that 9464D GD2+ tumour cells had low to negligible expression of PD-L1 on their cell surface, which was notably lower than seen on NXS2 GD2+ cells. This may suggest that 9464D cells are under less immunological pressure and have not required the upregulation of PD-L1 to combat an endogenous immune response. Furthermore, tumours cells have been reported to increase their expression of PD-L1 after exposure to IFNγ release [594], therefore this low level of PD-L1 may suggest there are few immune cells within the TME, such as cytotoxic T cells, activated and secreting this immunostimulatory cytokine. None of the treatment arms in both models appeared to significantly affect PD-L1 expression.

TILs are considered the drivers of an anti-tumour immune response, and therefore quantification of their percentages, PD-1 expression, proliferation and memory were assessed after combination therapy (**Figure 5.16** to **Figure 5.25**). Notably, CPM in combination with both EW1-9(WT) and EW1-9(DG) along with EW1-9(DG) alone, resulted in an increase in tumour infiltrating CD8+ T cells in the 9464D model. Furthermore, an increase in CD8:Treg and CD8:CD4 ratio, particularly in the CPM+EW1-9(DG) group was observed. This could explain why this combination treatment resulted in a significant increase in survival in this model, as the therapy led to an increase in CD8+ cells within the TME. The increase in CD8:Treg ratio means there are more effector cells compared to suppressive cells within the TME, which could suggest the activation of an anti-tumour immune response. Interestingly, in both NXS2 and 9464D no depletion of tumour infiltrating Tregs was noted, with any of the CPM containing treatment arms, as has been noted throughout at Day 3 after CPM. However, immunophenotyping for this experiment wasn't conducted until after treatment had been completed, more than 9 days after initial CPM administration. As noted in chapter 4, no Treg depletion is seen at Day 10 after CPM. Together these data suggest that the CPM mediated Treg depletion is a transient effect, after which Treg cells proliferate and return to non-treated tumour levels.

Importantly, significant downregulation of PD-1 expression was noted on TILs in all anti-PD-1 treated groups, with either the EW1-9(WT) or EW1-9(DG) antibody. As mentioned briefly, SPR data has demonstrated that the flow cytometry PD-1 detection antibody clone does not compete for binding with the therapeutic anti-PD-1 clone. This suggests that the downregulation of PD-1 is not due to the therapeutic antibody blocking access to the flow cytometry antibody, but due to physical downregulation of expression of the receptor. It is possible that as the therapeutic anti-PD-1

antibody binds its target, the receptor is then internalised, leading to downregulation, as has been described for an anti-CD20 antibody rituximab [595]. If this is true, then it will be imperative to ensure that adequate levels of anti-PD-1 antibody are maintained throughout therapy, as receptor internalisation may lead to enhanced clearance of bound antibody. However, for the antibodies used here, serum levels are still present at detectable levels at 14 days post administration, as demonstrated in **Figure 5.1**. Moving on to proliferation, using analysis of Ki67 expression, minimal changes were observed for all treatment arms for the TIL subsets. However in the 9464D model, significant downregulation of Ki67 was observed in CPM+EW1-9(DG), EW1-9(DG) alone and CPM+EW1-9(WT), specifically on Tregs. Therefore, although no depletion of Tregs is seen at this time point, the combination therapies are leading to a reduction of Treg proliferation within the tumour microenvironment. This may in part be mediated by the downregulation of PD-1 see in these therapies, as it has previously been reported that PD-1 expression is required for Treg activity, and possibly survival [217].

Finally, assessment of memory population modulation of TIL subsets was conducted to see if combination therapy effected their proportions within the TME. In both NXS2 and 9464D models, an increase in the percentage of EM CD4+ cells was observed with both EW1-9(DG) alone, and particularly with the combination of CPM+EW1-9(DG). This increase in EM cells led to an elevation of EM:CM and EM:N ratios, demonstrating that a greater number of CD4+ cells within the TME are of the effector phenotype. This could suggest that the combination of CPM+EW1-9(DG) is leading to either activation of naïve CD4+ T cells already within the TME, or recruiting effector CD4+ T cells from other lymphoid sites. In either scenario, it demonstrates that the efficacy of this combination therapy may be due to stimulating an immune response at the tumour site, which has led to an increase in effector CD4+ cells which can provide T cell help to the effector CD8+ cells within the TME. Furthermore within the NXS2 model, an increase in EM percentage of CD8+ T cell was also observed in this combination therapy, again demonstrating the possibility of an induction of an anti-tumour immune response.

When observing the myeloid component of NXS2 and 9464D tumours after combination therapy, few significant changes were reported (**Figure 5.26** and **Figure 5.27**). Within the NXS2 model, an increase in both tumour infiltrating macrophages and monocytes was seen in both CPM+EW1-9(WT) and CPM+EW1-9(DG), which was not observed in 9464D tumours. This could suggest in the NXS2 model that the combination treatments are leading to increased tumour cell death and or inflammation of the tumour site, resulting is a recruitment of macrophages and monocytes. This recruitment may be due to the release of ICD markers into the TME, however this would need to be quantifiably assessed, possibly by conducting ELISAs of tumour lysates to see if there is an increase in markers such as ATP or HMGB1. Furthermore, expression levels of PD-L1 was also

assessed on myeloid cells, as high levels of this ligand on these cells, which can also function as APCs, can lead to activation of T cells [596]. In NXS2 tumour infiltrating myeloid cells, no real changes of PD-L1 expression was reported in any of the therapy arms, however in 9464D a slight (but not significant) increase in expression on macrophages in EW1-9(DG) and CPM+EW1-9(DG) groups was noted. This increase may be due to an induction of an anti-tumour immune response leading to the increased release of IFNγ into the tumour microenvironment, which can induce the expression of PD-L1 on the cell surface [594]. However, these changes are small and more repeats of the phenotyping would need to be conducted before determining this, alongside quantification of IFNγ within the TME.

It was noted in chapter 4, that the short term immunomodulatory effects of low-dose CPM, were not maintained out to longer time points after administration. These effects included alteration of myeloid cell phenotypes, increased activation of CD8+ effector cells, and most prominently a tumour specific depletion of Treg cells. Therefore, in an effort to maintain the short term immunostimulatory effects, combination therapy of low dose CPM with EW1-9(DG) antibody was performed using a metronomic dosing strategy. Metronomic dosing is regularly used in patients and involves using low doses of chemotherapy given repeatedly over a number of weeks, rather than large doses given over a short period of time. These dosing strategies are mainly utilised to limit side effects from the chemotherapy, however reports have demonstrated that this form of dosing may lead to favourable immunomodulatory effects [339,379,597]. When using the metronomic strategy in the 9464D model, at both 5x5 mm and palpable start points, a significant increase in survival was seen in mice receiving both CPM and EW1-9(DG) on a weekly basis (**Figure 5.29** and **Figure 5.30**). Importantly, a significant increase in survival was observed over the single dosing strategy originally used in previous experiments. This increase in survival outcomes may be due to the metronomic dosing of CPM continuously depleting Treg cells within the tumour microenvironment, alongside continuous release of ICD markers. As demonstrated previously, Treg cells increased their proliferation and returned to levels seen in NT mice after 10 days of 1 shot of CPM, therefore weekly dosing of CPM may be preventing this rebound. Weekly dosing of the EW1-9(DG) antibody will also ensure that serum levels of the antibody are maintained, and as demonstrated previously administration of the antibody led to a downregulation of PD-1 on the surface of effector cells. Downregulation of the checkpoint molecule combined with the continued depletion of suppressive Treg cells, and release of tumour antigens and ICD molecules could all work together to create a more immunostimulatory TME, leading to improved survival within this preclinical model of NB.

The data presented in this chapter together with chapter 4, has so far demonstrated that combination of CPM with anti-PD-1 antibody (EW1-9 DG) therapy combine to deplete Treg cells,

block the PD-1 pathway to boost T cell activation, and importantly, increase survival in SC murine models of NB. However, as discussed in chapter 3, the SC models tested here may not be the most translational models available for investigating immunotherapy based treatments pre-clinically for human NB. The TH-MYCN spontaneous model was previously described and immunophenotyped in chapter 3, and was demonstrated to be the most similar to human NB out of the three murine models. As this chapter defined the combination of CPM with anti-PD-1 antibody therapy as the most effective at improving survival in both NXS2 and 9464D models, this combination was then assessed in the TH-MYCN model. Due to the spontaneity of tumour appearance, mice were randomised into treatment groups upon tumour presentation. Here, significant efficacy of CPM+EW1-9(DG) antibody was shown in the spontaneous TH-MYCN mouse model (**Figure 5.31**), as was seen with the two SC models. It is worth noting however, that treatment with CPM alone lead to a significant improvement in survival compared to NT mice. This suggests that these spontaneous tumours are more sensitive to CPM that the SC tumours. TH-MYCN tumours are more vascularised and grow within the abdomen microenvironment, which as the CPM is given IP, may lead to more of the drug reaching the tumour. Furthermore, when CPM + EW1-9(DG) were given metronomicaly, 100% survival was achieved out to 200 days. However, this appeared to mainly driven by CPM rather that the antibody therapy, as mice just receiving CPM metronomicaly also appeared to survive, although mice in this treatment group had not all been assessed out to day 200 at this point. Lower doses of metronomic CPM are currently being assessed to see if a suboptimal dose can be reached in order to establish if the combination with anti-PD-1 is having an effect.

Overall, this chapter assessed the efficacy of low dose CPM in combination with anti-PD-1 therapy in three distinct preclinical mouse models of NB. It was consistently shown using three separate *in vivo* models of NB on three different genetic backgrounds that combination of CPM with EW1-9(DG) antibody therapy led to the most effective increase in survival. This may have been driven by activation of a T cell response, due to an increase in effector CD4+ cell numbers, increase in infiltrating CD8+ cells leading to an elevation of CD8:Treg ratio and finally a downregulation on all TILs of the PD-1 receptor. It was also demonstrated that metronomic, weekly, dosing of both CPM and EW1-9(DG) resulted in improved efficacy of the combination therapy, which was most likely driven by the continual depletion of tumour infiltrating Treg cells. Furthermore, significant efficacy of this combination therapy was achieved in a transgenic spontaneous mouse model of NB, demonstrating the potency of the therapy.

Chapter 6: Discussion and Future Work

6.1 Discussion

Chemotherapy has been the standard treatment for many cancers for over 50 years, yet it is only recently that the mechanisms behind why some chemotherapeutics are more successful than others are being resolved. One of the factors that may contribute to this is the emerging realisation that certain chemotherapies may actually modulate the immune infiltrates in tumours, either in suppressive or activatory ways. Such immunomodulatory effects may be dependent on dosing and must be better understood in order to rationally combine chemotherapy with immunotherapeutics such as immunomodulatory antibody therapy. As stated in **Section 1.5.5**, multiple chemo-immunotherapy trials are currently being conducted in adult cancers, and in many instances the clinical experience is growing faster than the pre-clinical research and understanding of the mechanisms of action underpinning them. Although the immunotherapy revolution has proven successful in some adult cancers, to date, comparatively few trials exist in paediatric cancers, such as NB. In the few paediatric trials of checkpoint blockade antibodies undertaken to date, there has been very little evidence of efficacy, suggesting that this class of therapeutics will not be of clinical benefit as single agents in most children [20]. This may in part be a reflection of the fact that paediatric tumours, particularly NB, have a lower mutational burden than responsive adult cancers which has been suggested to be a prognostic marker for response to immunomodulatory antibody therapy [18]. However, use of an anti-GD2 direct targeting antibody in NB has shown clinical benefit, and demonstrates that, at least transiently, induction of passive immunity against the tumour can be induced. With this in mind, this work aimed to elucidate the immunomodulatory effects of low dose CPM, and test whether combination with immunomodulatory antibody therapy could enhance responses within preclinical models of NB.

Pre-clinical assessment of cancer immunotherapeutics relies largely on the use of various immunocompetent murine cancer models These include a range of histological subtypes, various background strains and growth within different tissue compartments; subcutaneous, orthotopic injection, or the use of spontaneous transgenic murine models for example. Beyond fundamental strain differences the different anatomical locations of these tumours, and the way in which they are generated can lead to disparity between models, particularly within tumour immune infiltrates. It is important to elucidate what models most accurately reflect human NB, in order to ensure research on possible treatments is conducted in a translatable environment. Therefore in the first part of this project (detailed in Chapter 3), three different models of murine NB were characterised, with a focus on comparing their tumour immune infiltrates, to see how representative of human

NB they were. Two passaged SC cell line models, NXS2 and 9464D were compared to a spontaneous transgenic TH-MYCN mouse model. The main findings demonstrated that great disparity existed between infiltrating immune cells within the three models, with most differences being noted between the two SC models and the spontaneous tumour model. Both NXS2 and 9464D had increased macrophage and Treg cell infiltration within their tumours, suggesting a more suppressive environment is created during the rapid generation of a SC tumour, compared to the perhaps slower more physiologically representative growth of a spontaneous tumour. Overall, the spontaneous TH-MYCN model, which had relatively high GD2 expression and low MHC class I expression, as reported in human NB tumours, also appeared to be the most accurate representation of human NB, immunologically. Moreover, similar levels of T cell infiltrates were noted, with consistent CD3+ infiltrating cells. However, it is worth noting that this model, due to its spontaneity and < 100% tumour penetrance, is not the most practical of the three models, with tumours appearing at any time between 8 and 26 weeks. Consequently, a large colony is required to achieve sufficient tumour numbers to allow for screening of multiple combinational therapies. In an effort to improve this, spontaneous TH-MYCN tumours were passaged into non-tumour bearing mice to see if the immunophenotype of the spontaneous tumours was maintained despite anatomical location being changed. In both SC and IP passage locations the immune infiltrates were shown to be disparate from spontaneous TH-MYCN tumours, suggesting that changing the anatomical location of a tumour has an influence on the immune cells which infiltrate the resulting tumour mass. This demonstrates that it is important to consider the anatomical location of tumours and their immune infiltrates, when testing immunotherapeutics in these models to ensure the most appropriate translation into human patients. Despite the TH-MYCN model being the most comparative to human NB its limitations, detailed above, mean that the favoured model to use routinely in basic research would be the 9464D SC model. The tumour growth pattern of this model is slower compared to the NXS2 SC model, shows downregulation of MHC I (as seen in human NB) and has more comparable immune infiltrates than NXS2. Furthermore, this model can also been grown orthotopically, in the adrenal glands, which again is more translatable to the human disease [541]. Finally, this model is on a C57BL/6 background and therefore offers unique opportunities to dissect the underlying mechanisms of therapy, due to the wide availability of genetically modified strains on this background, particularly in relation to immunology research. Overall, the aim would be to use the 9464D model to test a wide range of different combination therapies and perform basic research into mechanisms, and then utilise the TH-MYCN model to test selected treatments in the most translational model.

Building on the model characterisation, chapter 4 focused on profiling the immunomodulatory effects of CPM in, *in vitro* and *in vivo* neuroblastoma models. CPM has previously been

demonstrated to induce ICD marker expression, and specifically deplete Treg cells in both preclinical models and patients [339,366,368,568]. Additionally, CPM is already used within NB treatment regimens and therefore any new combinational therapies including it will likely be readily translatable to human NB. These factors suggested that CPM would be a good candidate to first analyse its immunomodulatory capacity and then assess whether synergy can be achieved with antibody immunotherapy. Firstly, increased expression of ecto-CRT and Hsp-70, alongside changes in HMGB1 expression was demonstrated in both cell lines and treated tumours with either CPM or its active metabolite MAF. These data suggested that CPM could lead to increased expression and ectopic secretion of known ICD markers, which has not previously been demonstrated in NB models. Most of the previous murine ICD research has been focused on the CT26 model, which is a relatively immunologically hot tumour compared to the NB models, due to its increased T cell infiltrates, leading to sensitivity to immunotherapy [598]. Induction of ICD of NB cells by CPM could lead to creating a more immunogenic TME, resulting in the generation or 'boosting' of an anti-tumour immune response. To assess whether immune cell subsets are modulated (either in number or phenotype) by low dose (40 mg/kg) CPM; detailed immunophenotyping was conducted in both NXS2 and 9464D models. In the myeloid subset, although percentage changes were not noted, alteration of FcyR expression, and therefore possibly phenotype, was observed. Here, induction of activatory receptors on DCs was noted after CPM, whereas macrophages demonstrated an increase in the inhibitory FcyRII. These data highlight the cell specific effects of CPM, leading to the activation of some, whereas inducing suppressive phenotypes in others. Furthermore, tumour specific Treg depletion in both models was demonstrated, which was robust and reproducible. Treg depletion sensitivity to CPM is known [366,368], however this has not previously been shown in a NB setting. Tumour Treg depletion led to an increase in the CD8:Treg ratio, which is routinely used as a prognostic marker for patients undergoing immunotherapy [574,575]. A higher CD8:Treg ratio demonstrates more effector T cells are present within the tumour mass compared to suppressive cells, which could be exploited by using a concurrent checkpoint blockade immunotherapy to further boost the effector T cells. Despite percentages of effector and helper T cell remaining similar after CPM treatment, demonstrable modulation of their phenotypes was observed in all three T cell subsets. Short term effects induced a more activated CD8 phenotype with increased expression of IFNy, while Tregs appeared to have an increased suppressor phenotype denoted by increase in TIM3 expression amongst other markers. However by later time points, the suppressive activity of Tregs may have decreased as an increase in EOMES expression was noted. These data demonstrated that CPM is capable of modulating immune cells within the tumour microenvironment, and is able to do so at a relatively low dose of 40 mg/kg. In order to determine whether Treg depletion or induction of tumour ICD were more important in mediating CPM immunomodulatory activity, an apoptotic resistant BCL-2 overexpressing 9464D cell line was

developed together with the use of vav-BCL-2 transgenic mice. The BCL-2 overexpressing 9464D cell line demonstrated *in vitro* that CPM, at least in part, uses a BCL-2 dependent form of cell death in these cell lines. However, the cell lines did not lead to development of sustained tumours when implanted into immune competent mice, which was likely due to the viral vector increasing immunogenicity of both the BCL-2 and EV lines, resulting in tumour clearance. Therefore, this cell line needs to be recreated using less immunogenic viral vectors in order to study ICD role in CPM immunomodulation. Using the vav-BCL-2 mice bearing wild-type 9464D tumours, it was observed that depletion of Tregs no longer occurred post-CPM, demonstrating again that CPM initiates cell death through a BCL-2 sensitive pathway. These mice will be utilised for future experiments as discussed below.

As CPM had been established as potentially capable of 'boosting' endogenous anti-tumour immune responses, investigation into its efficacy as a combination therapy with immunomodulatory antibodies were next assessed (Chapter 5), using the three previously defined murine models. Furthermore, as most of the modulation by CPM was demonstrated at Day 3, antibody therapy was initiated at this point, where Treg cells were significantly depleted and effector cells were deemed most likely to be efficiently activated. Preliminary investigations using the NXS2 model, determined that anti-PD-1 antibodies in combination in CPM were the most effective. Combination of these antibodies with CPM led to a significant increase in survival, whereas both anti-CTLA-4 and anti-4-1BB in combination with CPM did not. After analysis of anti-PD-1 therapy in combination with CPM, using both NXS2 and 9464D models and a range of tumour size starting points, the use of an FcγR null-engaging deglycosylated version of anti-PD-1 antibody (EW1-9 DG) consistently led to the most significant increase in survival within both models. Investigation into the mechanism behind why the combination of CPM + EW1-9(DG) was conducted using detailed immunophenotyping of tumours after therapy. Here, it was observed that this combination led to an increase in both CD8+ T cells and CD8:Treg ratio, which could explain why greater tumour control was seen in this therapy. Furthermore, all groups treated with either WT or DG EW1-9 antibody demonstrated a significant downregulation of PD-1 on all TILs. This suggests that after antibody binding, the PD-1 receptor is internalised. PD-1 downregulation has been variously demonstrated to be particularly important on CD8+ T cells, by 'lifting the brakes' and promoting activation, and on Tregs by decreasing suppressive activity[447]. Finally, it is worth noting that disparity within the immunophenotyping was observed between the two models of NB assessed. However, as previously discussed, the 9464D model is more representative of human NB, and therefore more data from this model is more likely to be translatable. This suggests that it would be prudent to whenever possible analyse the mechanisms of potential immunotherapies in more than one murine model, in order to avoid biasing results that could be in fact only specific in one particular scenario.

Throughout chapters 4 and 5, it was consistently noted that CPM mediated Treg depletion, alongside other positive modulatory effects, were transient, and were not observed at day 10 post administration. Therefore, in an attempt to overcome this, metronomic dosing of both CPM and anti-PD-1 (DG) was tested using the 9464D model. Here, it was consistently observed that weekly dosing of both CPM and the antibody led to an increase in survival compared to both non-treated mice, and importantly, over the single dosing treatment strategy used in previous experiments. The mechanism of action likely relied on the continuous depletion of Treg cells by the CPM, and maintenance of high serum levels of the anti-PD-1 antibody to block and downregulate the PD-1 receptor, both of which require further detailed investigation.

Given the practical issues in using the spontaneous TH-MYCN model for the mechanistic studies detailed above, SC models were used throughout chapters 4 and 5 to overcome this. After extensive investigation into CPM with anti-PD-1(DG) therapy, it was determined to test this combination within the context of the TH-MYCN model. Notably, here the same results were observed as seen in the 9464D and NXS2 models, with the combination of CPM and EW1-9(DG) antibody significantly improving survival over NT and the monotherapies. Additionally, metronomic dosing of either CPM alone or in combination with the antibody lead to 100% survival. It was also noted however, that the TH-MYCN had increased sensitivity to CPM therapy, with significantly increased survival been noted as a monotherapy. This may be due to the anatomical location of the tumours which grow within the abdomen, and are also highly vascularised, both of which could lead to increased accumulation of the IP injected CPM within the tumour mass. Despite this, efficacy of the combination therapy was demonstrated in the most translational murine model of NB.

Overall, this work demonstrated that the combination of CPM with anti-PD-1 antibody therapy could lead to significantly increased survival and slowing of tumour growth in three distinct pre-clinical models of NB. The proposed mechanism of action behind the combination activity is demonstrated in **Figure 6.1**. Here, it is postulated that initial treatment with CPM leads to a depletion of intratumoral Treg cells by a BCL-2 sensitive cell death pathway, which leads to an increase in the CD8:Treg ratio, alongside the release of ICD molecules and tumour antigens upon tumour cell death. The ICD molecules together with other DAMPs and TLR ligands leads to activation of DCs within the TME, which in turn can either migrate to the tumour dLN, or remain at the TME, to activate and prime effector CD8+ T cells. Administration of and Fc inert anti-PD-1 antibody can then both block the effects of PD-1 suppression induced by PD-L1 on cells within the TME, and downregulates the expression of the PD-1 receptor, most likely due to internalisation after binding. Blocking this pathway without FcγR engagement allows for effector T cells to remain active and induce an anti-tumour immune response without their deletion. Furthermore, the

downregulation of PD-1 and modulatory effects of CPM on Tregs could lead to a decrease in suppressive activity of these cells.

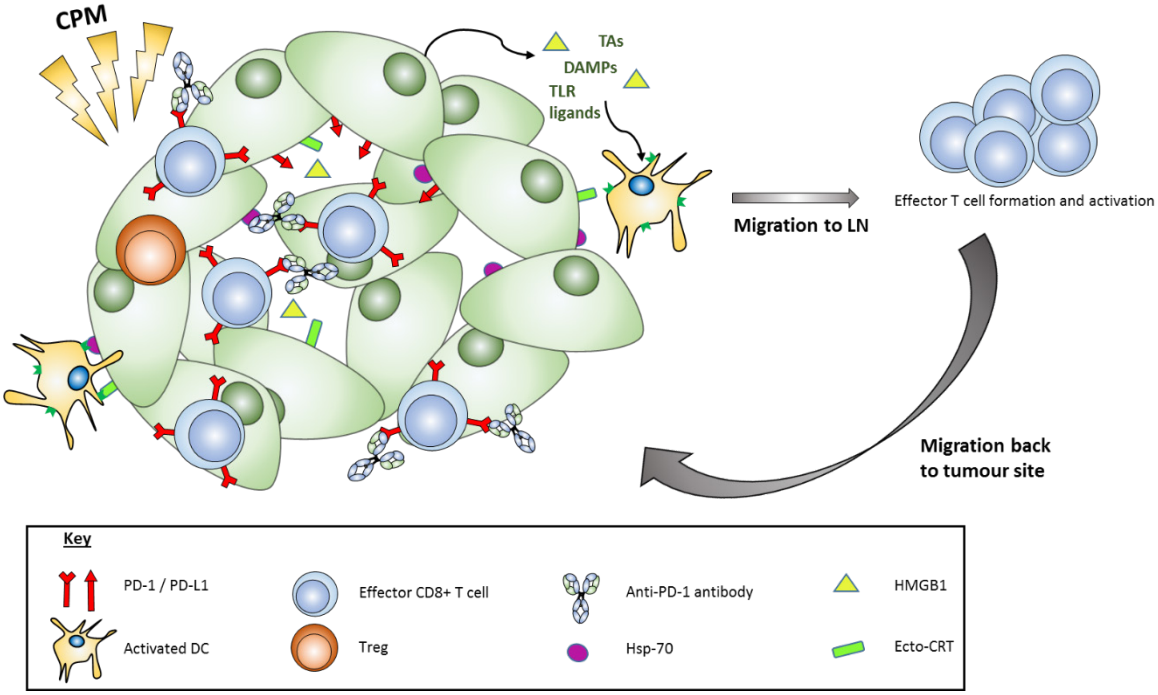

Figure 6.1 Summary of proposed mechanism of action of CPM and anti-PD-1 antibody therapy in NB models

Demonstration of the proposed mechanism of action of combination of CPM and anti-PD1 (DG) antibody therapy, within preclinical models of NB. CPM leads to depletion of Treg cells and modulation of their suppressive activity, alongside inducing ICD in NB tumour cells. This leads to activation of DCs which then prime and activate effector CD8+ T cells. Anti-PD-1 antibody blocks activation of the suppressive PD-1 pathway on CD8+ T cells and leads to the receptors downregulation. Together the therapies allow for generation of an anti-tumour immune response.

6.2 Future work

The work presented here in this thesis has generated a proposed mechanism of action for the combination of CPM and anti-PD-1 in NB therapy. Additional work is required to further elucidate certain aspects mediating these combination effects and to understand others in more detail. Firstly, formally determining whether CPM leads directly to ICD in NB cells is required, especially with regards to expression of markers *in vivo*. One way to achieve this would be to use ELISAs of tumour lysates after treatment *in vivo* with CPM, to look for increased levels of secreted ATP and HMGB1. Also, the use of immunohistochemistry and immunofluorescence could be employed to investigate whether ecto-CRT and Hsp-70 are expressed on the cytoplasm of tumour cells in ex vivo tumour samples after CPM treatment, as so far this has only been assessed *in vitro*. Secondly, establishing whether CPM is directly or indirectly increasing the activation of CD8+ T cells within the tumours would be beneficial. It may be that CPM is directly activating DCs and leading to the release of a range of molecules alongside tumour antigens, all of which could result in a mature activated DC. These DCs could then stimulate the activation of T cells within the TME or within the tumour dLN, therefore these pathways need to be elucidated. Notably, it was observed that anti-PD-1 antibody treatment led to downregulation of the PD-1 receptor, which could be due to internalisation of the receptor after antibody binding. However, this requires further validating and could be investigated by using fluorescence confocal time-lapse microscopy, to see if the receptor internalisation is responsible for the downregulation.

Currently, it is not defined whether it is the induction of ICD in the tumour cells or the depletion and modulation of Tregs that is the driving factor behind CPM's immunomodulatory activity. The development of the BCL-2 overexpressing 9464D cell line together with the use of vav-BCL-2 transgenic mice were used to try and delineate this. However, as discussed previously, the retroviral transduction of the 9464D cells resulted in increased immunogenicity of the cells, leading to tumour clearance. Therefore, generation of a BCL-2 overexpressing cell line will need to be developed again using a different viral vector. However, it was demonstrated that CPM did not induce Treg depletion in tumour bearing vav-BCL-2 transgenic mice. Therefore, further work with this model will focus on using this model in combination therapy survival experiments parallel to age and sex matched wild type C57BL/6 mice. If Treg depletion is the driving factor behind the improved survival of CPM+anti-PD-1 therapy, then this efficacy should be reduced or even eradicated in the vav-BCL-2 mice. Furthermore, one group could receive the combination therapy together with a BCL-2 inhibitor venetoclax, to see if deactivation of the BCL-2 then re-sensitises these mice to combination therapy.

Although detailed immunophenotyping of T cells after CPM was conducted throughout this work, it was limited in its scope as it was by necessity focused on a relatively small number of markers.

Therefore, greater understanding of how CPM modulates these immune cells needs to be generated. One way this could be achieved is by the use of RNAseq of CPM treated tumours, possibly with the combination of single cell analysis. This would allow in depth investigation into how CPM changes the gene expression within specific cell subsets, with particular focus on T cells. There may be some limitation using this technique however, as the CPM will lead to cell death which may reduce the final quality of the samples, and therefore the overall quality of the resulting RNAseq data. Furthermore, it would be prudent to conduct detailed immunophenotyping after combination therapy using the TH-MYCN mouse model, to see if similar patterns are seen as observed in the two SC models. However, as previously mentioned, this is harder to conduct in this model. Maintenance of large stock numbers would however be expensive and wasteful of wild type litter mates. Finally, the use of metronomic CPM and anti-PD-1 therapy was based on the hypothesis, informed by single dosing experiments that continued administration of CPM would maintain depletion of Tregs, whilst weekly dosing of anti-PD-1 antibody would keep serum levels high. In order to determine this definitively, further immunophenotyping of metronomic treated mice at set time points throughout therapy would be required. This would demonstrate whether Tregs are continuously depleted, or if after a certain number of CPM doses the remaining Treg populations become resistant to this depletion. This could potentially explain the eventual tumour escape, as shown in the survival experiments.

Throughout this work there has been continued focus on the importance of using the most translatable murine models to human disease to ensure the results presented are an accurate reflection of what may occur in patients. As discussed, of the models utilised here, the transgenic spontaneous TH-MYCN model was demonstrated to be the most translatable of the three, however it is not a perfect preclinical model. All work was conducted using murine models and anti-mouse antibodies, and, although very similar, murine and human immune systems do have substantial differences which could reduce the translatability of all murine models. Therefore, the use of humanised mice in conjunction with either human NB cell lines, or more appropriately, patient derived xerographs (PDXs) may ensure the most accurate representation of human disease. In brief, these are severely immunocompromised mice which have then been reconstituted with human haematopoietic stem cells, leading to the development of a human immune system [599], and allows assessment of immunotherapeutics in a highly translational model. Furthermore, these models still maintain the benefits of using a murine system, such as quick breeding times and ability to set up many mice at once to have large treatment group numbers. These models would allow for assessment of combination therapy with CPM and anti-human anti-PD-1 antibodies, such as nivolumab which are already approved for use in clinic, which again might increase the translatability of this work towards human NB. However, a specific issue for use of these models in

NB, would be acquiring enough tissue to be able to set up PDX models. This is due to the rarity of the disease, resulting in few opportunities to collect tissue for PDX generation. Furthermore, tissue samples would either consist of pre-treatment biopsies, or post-surgery tissue samples. Ideally, pre-treatment biopsies would be the most appropriate sample, as the patients at this point are treatment naïve, however these will be very small samples and therefore there would most likely not be enough cells to set up many PDX mice. Although post-surgery tissue samples will be considerably bigger, these patients would have undergone induction chemotherapy in order to shrink the tumour size ready for surgery, and this could therefore could alter the tumour microenvironment before engraftment into humanised mice. Despite these limitation, humanised mice may be the most appropriate preclinical murine model to use to ensure any treatments assessed are the most translatable to patients.

Chapter 7: Appendix

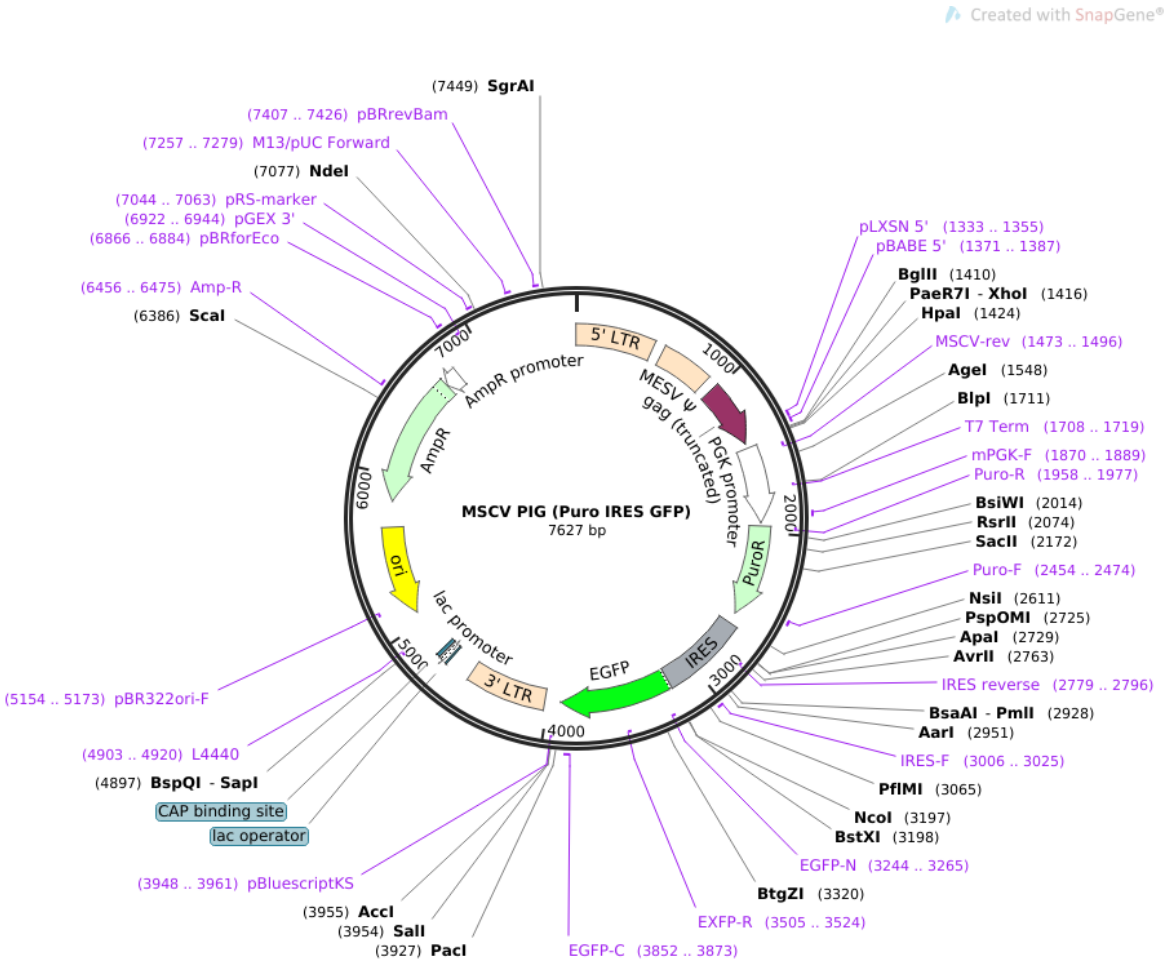

Figure 7.1 MSCV PIG GFP vector map for GFP transduction

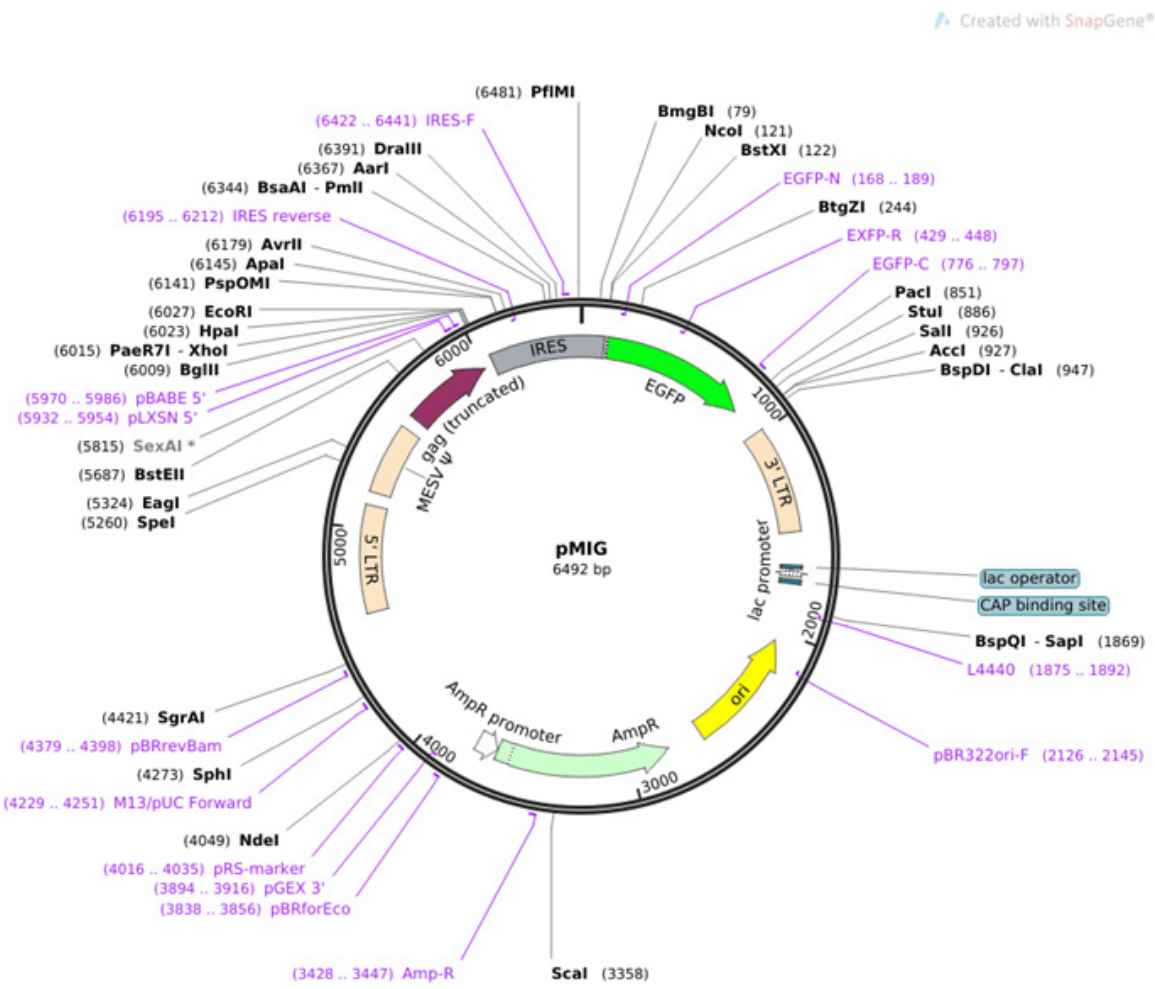

Figure 7.2 pMIG vector map for BCL-2 transduction

For pMIH vector, EGFP is replaced by hygromycin resistance gene.

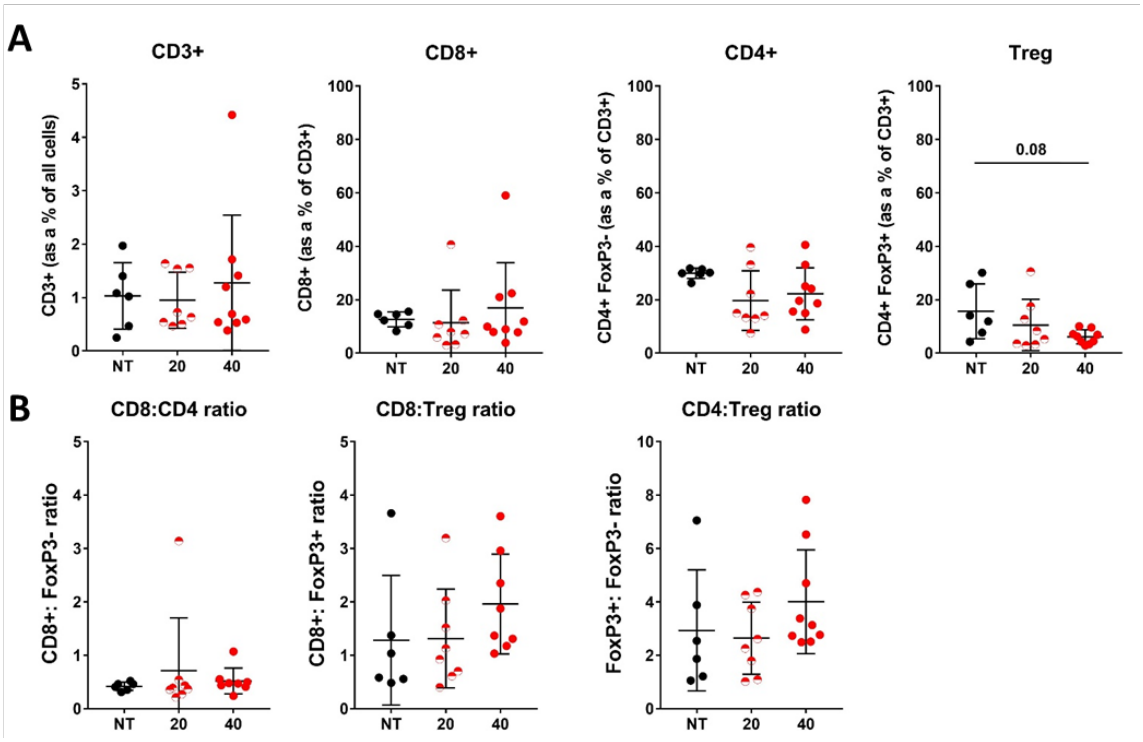

Figure 7.3 Modulation of T cell percentages in NXS2 tumours after CPM administration

A) NSX2 tumours around 8x8 mm were treated with either 20 or 40 mg/kg CPM and at Day 3 were harvested, processed for flow cytometry for immunophenotyping as detailed in **Section 2.9**. Populations were defined as detailed in **Figure 4.23**. T cell subsets as a percentage of CD3+ cells is shown, with **B)** showing ratios between the subsets. n= 6 (NT), n= 8 (20 mg/kg) and n= 9 (40 mg/kg). Data pooled from two independent experiments. Statistical analysis was conducted using Krusksal Wallis test with Dunn's multiple comparisons. Means and SD error bars are shown.

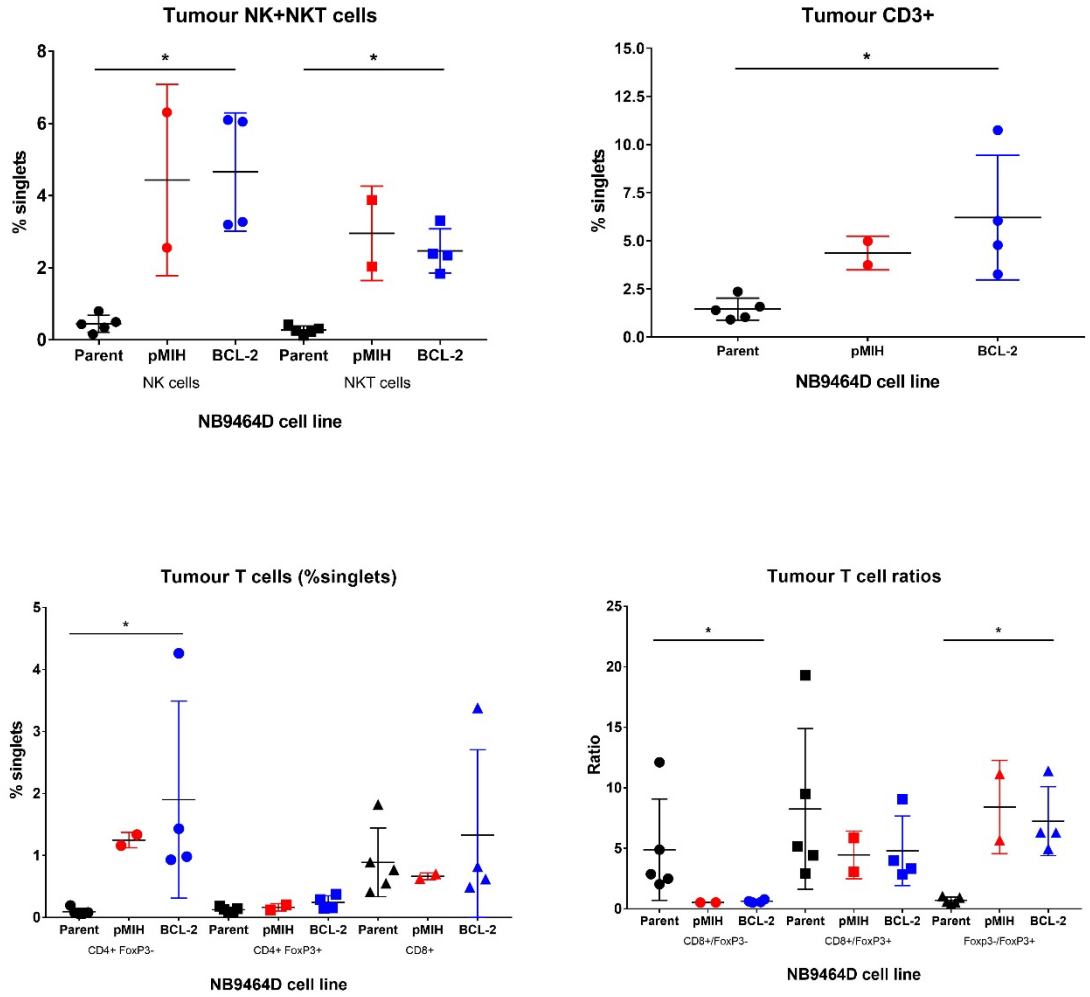

Figure 7.4 Immunophenotyping of tumours from BCL-2 transduced 9464D cell lines

9464D cell lines (either Empty vector (pMIH) or BCL-2) were inoculated into C57BL/6 mice as detailed in **Section 2.6**. Flow cytometry and tissue processing was conducted as described in **Section 2.9,** with gating used as shown in **Figure 3.4.**.Parent data is shown from a previous experiment detailed in **Figure 3.13** and **Figure 3.14** for comparison. Percentages of NK, NKT, CD3, CD4, Treg and CD8 cells are all shown as a percent of singlets. Ratios between T cell subsets are demonstrated in the bottom right. n= 5 (previous parent data), n= 4 (BCL-2) and n= 2 (pMIH). Statistical analysis was conducted using Mann-Whitney U test, with significance denoted as * = <0.05. Means and SD error bars are shown.

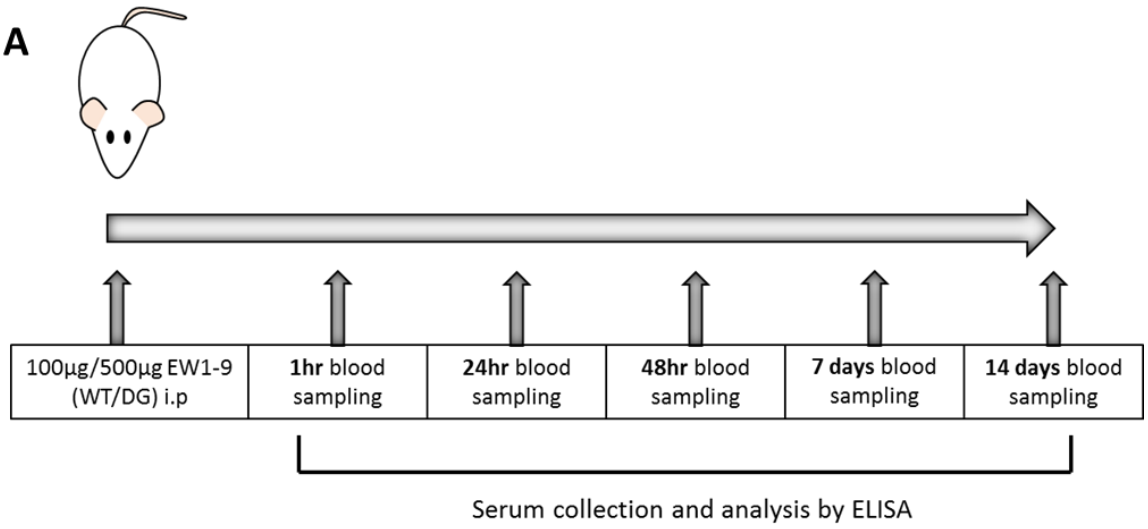

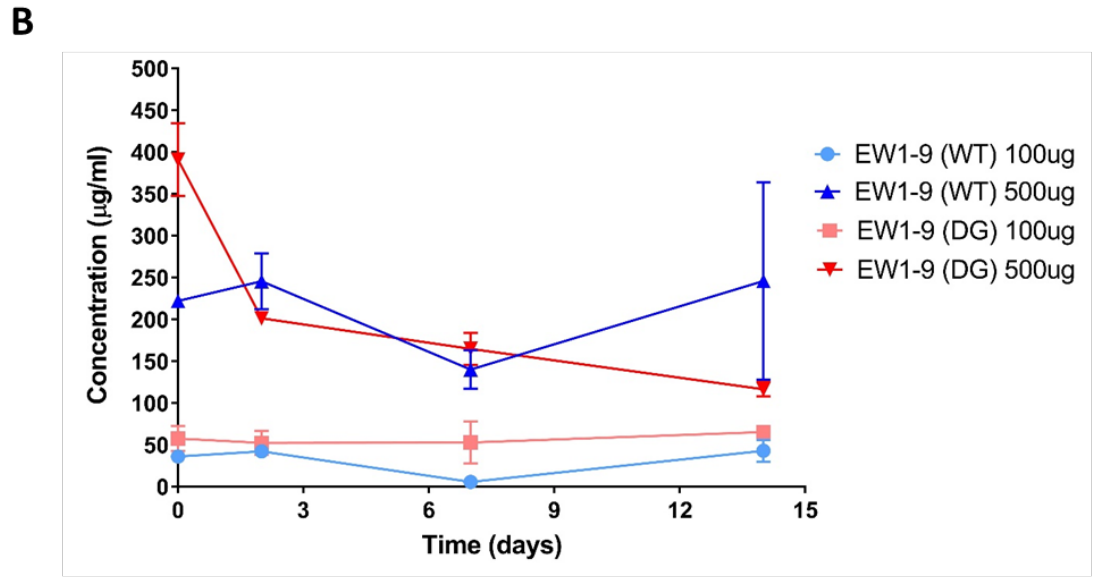

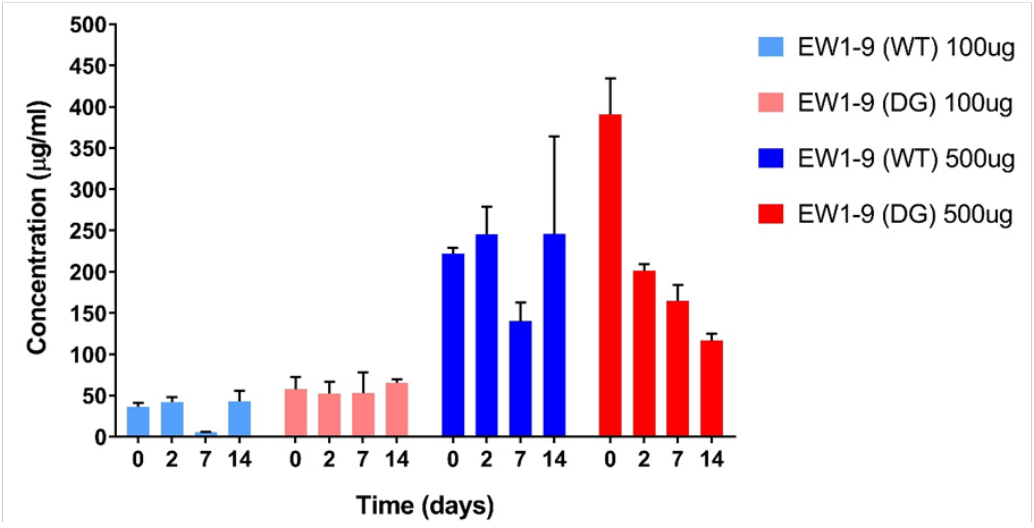

Figure 7.5 EW1-9(WT) and EW1-9(DG) antibody serum concentrations over time in AJ mice

A) Female AJ mice were dosed with either EW1-9(WT) or EW1-9(DG) at the doses stated by i.p injections. Blood was collected at defined time points. From this serum was harvested and ELISA was performed as detailed in methods. **B+C** show concentration in in ug/ml of EW1-9(WT) or (DG) remaining in the serum. n= 3 mice per group. Mean and SD error bars are shown.

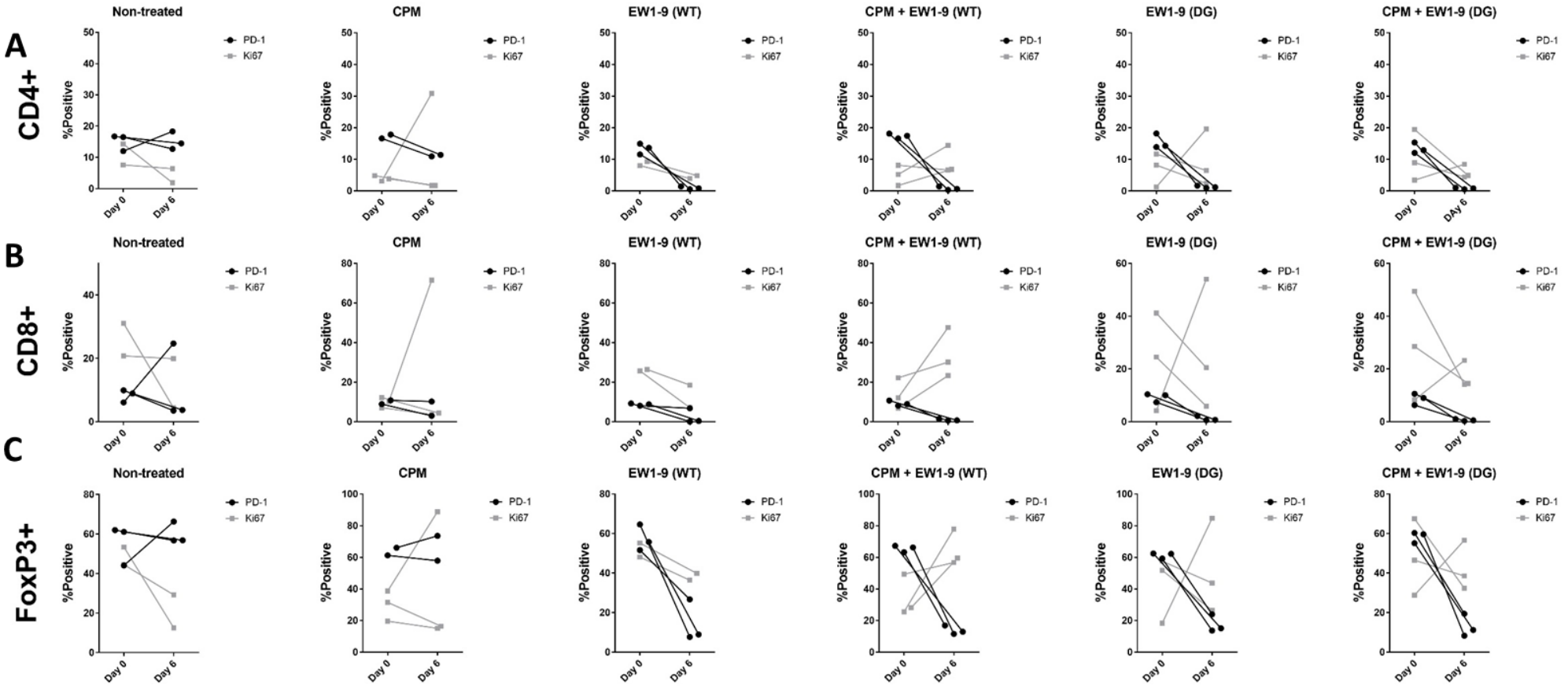

Figure 7.6 T cell PD-1 and Ki67 expression in blood of NXS2 tumour bearing mice after combination therapy

Mice and treatment was conducted as detailed in **Figure 5.12 A**. Gaiting strategy was used as shown previously (**Figure 4.16** and **Figure 4.23**). Percentage expression of PD-1 and Ki67 is shown on T cell subsets as follows: **A)** CD4+ FoxP3-, **B)** CD8+ and **C)** CD4+ FoxP3+. n=3 mice per group.

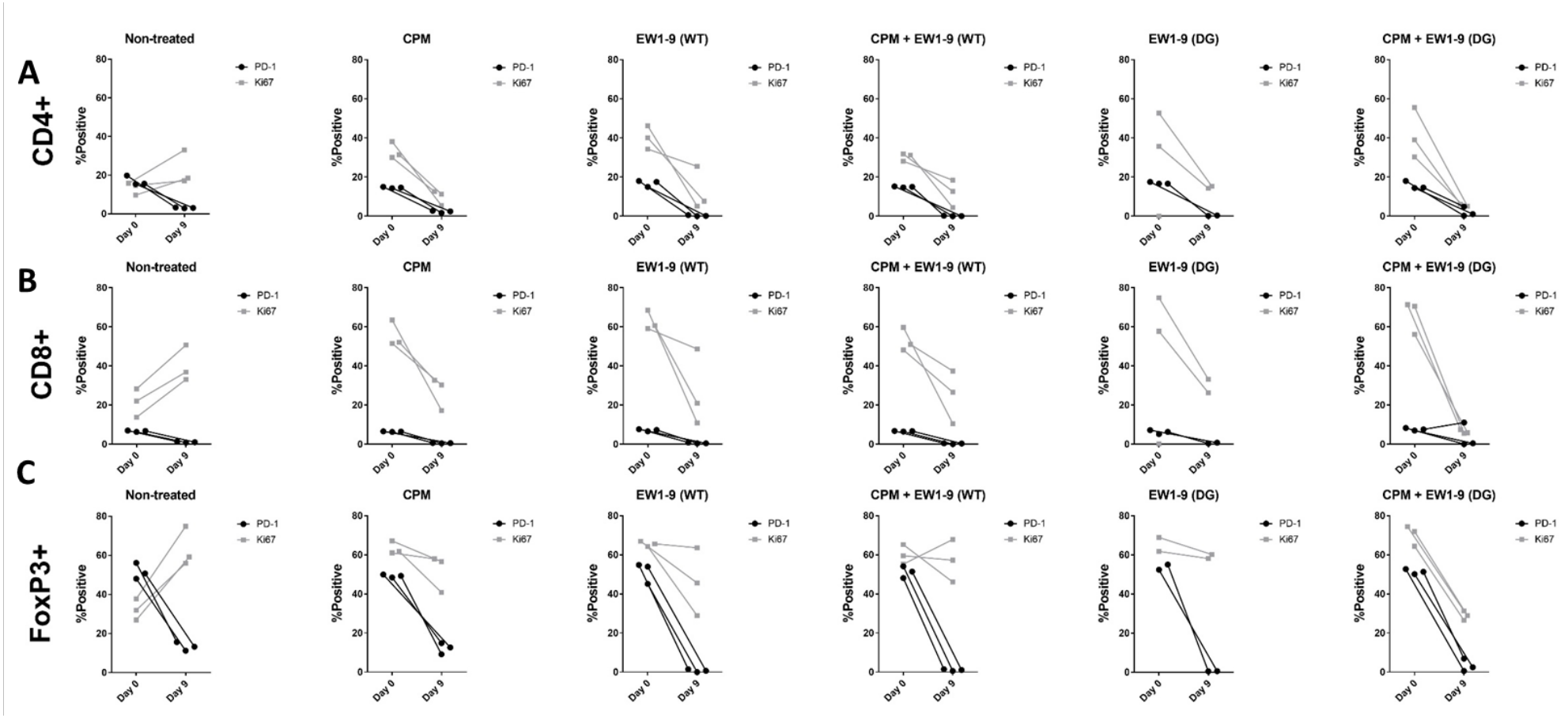

Figure 7.7 T cell PD-1 and Ki67 expression in blood of 9464D tumour bearing mice after combination therapy

Mice and treatment was conducted as detailed in **Figure 5.12 A**. Gaiting strategy was used as shown previously (**Figure 4.16** and **Figure 4.23**). Percentage expression of PD-1 and Ki67 is shown on T cell subsets as follows: **A)** CD4+ FoxP3-, **B)** CD8+ and **C)** CD4+ FoxP3+. n=3 mice per group.

Chapter 8: References

1 Hanahan, D. & Weinberg, R. A. Hallmarks of cancer: the next generation. *Cell* **144**, 646-674, doi:10.1016/j.cell.2011.02.013 (2011).

2 Hanahan, D. & Weinberg, R. A. The hallmarks of cancer. *Cell* **100**, 57-70 (2000).

3 Lemmon, M. A. & Schlessinger, J. Cell signaling by receptor tyrosine kinases. *Cell* **141**, 1117-1134, doi:10.1016/j.cell.2010.06.011 (2010).

4 Witsch, E., Sela, M. & Yarden, Y. Roles for growth factors in cancer progression. *Physiology (Bethesda, Md.)* **25**, 85-101, doi:10.1152/physiol.00045.2009 (2010).

5 Hynes, N. E. & MacDonald, G. ErbB receptors and signaling pathways in cancer. *Current opinion in cell biology* **21**, 177-184, doi:10.1016/j.ceb.2008.12.010 (2009).

6 Adams, J. M. & Cory, S. The Bcl-2 apoptotic switch in cancer development and therapy. *Oncogene* **26**, 1324-1337, doi:10.1038/sj.onc.1210220 (2007).

7 Junttila, M. R. & Evan, G. I. p53--a Jack of all trades but master of none. *Nat Rev Cancer* **9**, 821-829, doi:10.1038/nrc2728 (2009).

8 Hanahan, D. & Folkman, J. Patterns and emerging mechanisms of the angiogenic switch during tumorigenesis. *Cell* **86**, 353-364 (1996).

9 Berx, G. & van Roy, F. Involvement of members of the cadherin superfamily in cancer. *Cold Spring Harbor perspectives in biology* **1**, a003129, doi:10.1101/cshperspect.a003129 (2009).

10 Cavallaro, U. & Christofori, G. Cell adhesion and signalling by cadherins and Ig-CAMs in cancer. *Nat Rev Cancer* **4**, 118-132, doi:10.1038/nrc1276 (2004).

11 Berdasco, M. & Esteller, M. Aberrant epigenetic landscape in cancer: how cellular identity goes awry. *Developmental cell* **19**, 698-711, doi:10.1016/j.devcel.2010.10.005 (2010).

12 Dvorak, H. F. Tumors: wounds that do not heal. Similarities between tumor stroma generation and wound healing. *N Engl J Med* **315**, 1650-1659, doi:10.1056/nejm198612253152606 (1986).

13 Vajdic, C. M. & van Leeuwen, M. T. Cancer incidence and risk factors after solid organ transplantation. *International journal of cancer. Journal international du cancer* **125**, 1747-1754, doi:10.1002/ijc.24439 (2009).

14 Munn, D. H. & Bronte, V. Immune suppressive mechanisms in the tumor microenvironment. *Curr Opin Immunol* **39**, 1-6, doi:10.1016/j.coi.2015.10.009 (2016).

15 Lindau, D., Gielen, P., Kroesen, M., Wesseling, P. & Adema, G. J. The immunosuppressive tumour network: myeloid-derived suppressor cells, regulatory T cells and natural killer T cells. *Immunology* **138**, 105-115, doi:10.1111/imm.12036 (2013).

16 Warburg, O. On respiratory impairment in cancer cells. *Science* **124**, 269-270 (1956).

17 Alexandrov, L. B. *et al.* Signatures of mutational processes in human cancer. *Nature* **500**, 415-421, doi:10.1038/nature12477 (2013).

18 McGranahan, N. *et al.* Clonal neoantigens elicit T cell immunoreactivity and sensitivity to immune checkpoint blockade. *Science* **351**, 1463-1469, doi:10.1126/science.aaf1490 (2016).

19 Schumacher, T. N. & Schreiber, R. D. Neoantigens in cancer immunotherapy. *Science* **348**, 69-74, doi:10.1126/science.aaa4971 (2015).

20 Anderson, J. Unleashing the immune response against childhood solid cancers. *Pediatric Blood & Cancer* **64**, e26548, doi:doi:10.1002/pbc.26548 (2017).

21 Simon, A. K., Hollander, G. A. & McMichael, A. Evolution of the immune system in humans from infancy to old age. *Proceedings. Biological sciences* **282**, 20143085-20143085, doi:10.1098/rspb.2014.3085 (2015).

22 National Cancer, I. & Program, S. *Cancer incidence and survival among children and adolescents: United States SEER Program, 1975-1995*. (National Cancer Institute, 1999).

23 Maris, J. M., Hogarty, M. D., Bagatell, R. & Cohn, S. L. Neuroblastoma. *Lancet* **369**, 2106-2120, doi:10.1016/s0140-6736(07)60983-0 (2007).

24 Brodeur, G. M. Neuroblastoma: biological insights into a clinical enigma. *Nat Rev Cancer* **3**, 203-216, doi:10.1038/nrc1014 (2003).

25 Saito, D., Takase, Y., Murai, H. & Takahashi, Y. The dorsal aorta initiates a molecular cascade that instructs sympatho-adrenal specification. *Science* **336**, 1578-1581, doi:10.1126/science.1222369 (2012).

26 Anderson, D. J., Carnahan, J. F., Michelsohn, A. & Patterson, P. H. Antibody markers identify a common progenitor to sympathetic neurons and chromaffin cells in vivo and reveal the timing of commitment to neuronal differentiation in the sympathoadrenal lineage. *The Journal of neuroscience : the official journal of the Society for Neuroscience* **11**, 3507-3519 (1991).

27 Anderson, D. J. & Axel, R. A bipotential neuroendocrine precursor whose choice of cell fate is determined by NGF and glucocorticoids. *Cell* **47**, 1079-1090 (1986).

28 Noisa, P. & Raivio, T. Neural crest cells: from developmental biology to clinical interventions. *Birth defects research. Part C, Embryo today : reviews* **102**, 263-274, doi:10.1002/bdrc.21074 (2014).

29 Cheung, N. K. & Dyer, M. A. Neuroblastoma: developmental biology, cancer genomics and immunotherapy. *Nat Rev Cancer* **13**, 397-411, doi:10.1038/nrc3526 (2013).

30 Ratner, N., Brodeur, G. M., Dale, R. C. & Schor, N. F. The “neuro” of neuroblastoma: Neuroblastoma as a neurodevelopmental disorder. *Annals of Neurology* **80**, 13-23, doi:10.1002/ana.24659 (2016).

31 Wylie, L. A., Hardwick, L. J., Papkovskaia, T. D., Thiele, C. J. & Philpott, A. Ascl1 phospho-status regulates neuronal differentiation in a Xenopus developmental model of neuroblastoma. *Disease models & mechanisms* **8**, 429-441, doi:10.1242/dmm.018630 (2015).

32 Maris, J. M. *et al.* Evidence for a hereditary neuroblastoma predisposition locus at chromosome 16p12-13. *Cancer Res* **62**, 6651-6658 (2002).

33 Pages, P. M. *et al.* Bilateral adrenal neuroblastoma. *Pediatr Blood Cancer* **52**, 196-202, doi:10.1002/pbc.21765 (2009).

34 Ruiz-Pérez, M. V., Henley, A. B. & Arsenian-Henriksson, M. The MYCN Protein in Health and Disease. *Genes* **8**, 113 (2017).

35 Huang, M. & Weiss, W. A. Neuroblastoma and MYCN. *Cold Spring Harbor perspectives in medicine* **3**, a014415, doi:10.1101/cshperspect.a014415 (2013).

36 Grimmer, M. R. & Weiss, W. A. Childhood tumors of the nervous system as disorders of normal development. *Current opinion in pediatrics* **18**, 634-638, doi:10.1097/MOP.0b013e32801080fe (2006).

37 Weiss, W. A., Aldape, K., Mohapatra, G., Feuerstein, B. G. & Bishop, J. M. Targeted expression of MYCN causes neuroblastoma in transgenic mice. *The EMBO Journal* **16**, 2985-2995, doi:10.1093/emboj/16.11.2985 (1997).

38 Zhu, S. *et al.* Activated ALK collaborates with MYCN in neuroblastoma pathogenesis. *Cancer Cell* **21**, 362-373, doi:10.1016/j.ccr.2012.02.010 (2012).

39 Shochat, S. J., Abt, A. B. & Schengrund, C. L. VCN-releasable sialic acid and gangliosides in human neuroblastomas. *Journal of pediatric surgery* **12**, 413-418 (1977).

40 Schulz, G. *et al.* Detection of ganglioside GD2 in tumor tissues and sera of neuroblastoma patients. *Cancer Res* **44**, 5914-5920 (1984).

41 Yanagisawa, M., Yoshimura, S. & Yu, R. K. Expression of GD2 and GD3 gangliosides in human embryonic neural stem cells. *ASN neuro* **3**, doi:10.1042/an20110006 (2011).

42 Kramer, K. *et al.* Disialoganglioside G(D2) loss following monoclonal antibody therapy is rare in neuroblastoma. *Clinical cancer research : an official journal of the American Association for Cancer Research* **4**, 2135-2139 (1998).

43 Monclair, T. *et al.* The International Neuroblastoma Risk Group (INRG) staging system: an INRG Task Force report. *J Clin Oncol* **27**, 298-303, doi:10.1200/jco.2008.16.6876 (2009).

44 Cohn, S. L. *et al.* The International Neuroblastoma Risk Group (INRG) classification system: an INRG Task Force report. *J Clin Oncol* **27**, 289-297, doi:10.1200/jco.2008.16.6785 (2009).

45 Owens, C. & Irwin, M. Neuroblastoma: the impact of biology and cooperation leading to personalized treatments. *Critical reviews in clinical laboratory sciences* **49**, 85-115, doi:10.3109/10408363.2012.683483 (2012).

46 Louis, C. U. & Shohet, J. M. Neuroblastoma: molecular pathogenesis and therapy. *Annual review of medicine* **66**, 49-63, doi:10.1146/annurev-med-011514-023121 (2015).

47 Park, J. R. *et al.* Children's Oncology Group's 2013 blueprint for research: neuroblastoma. *Pediatr Blood Cancer* **60**, 985-993, doi:10.1002/pbc.24433 (2013).

48 Matthay, K. K. *et al.* Long-Term Results for Children With High-Risk Neuroblastoma Treated on a Randomized Trial of Myeloablative Therapy Followed by 13-cis-Retinoic Acid: A Children's Oncology Group Study. *Journal of Clinical Oncology* **27**, 1007-1013, doi:10.1200/jco.2007.13.8925 (2009).

49 Yu, A. L. *et al.* Anti-GD2 Antibody with GM-CSF, Interleukin-2, and Isotretinoin for Neuroblastoma. *New England Journal of Medicine* **363**, 1324-1334, doi:doi:10.1056/NEJMoa0911123 (2010).

50 Schrey, D., Vaidya, S. J., Levine, D., Pearson, A. D. & Moreno, L. Additional Therapies to Improve Metastatic Response to Induction Therapy in Children With High-risk

Neuroblastoma. *Journal of pediatric hematology/oncology* **37**, e150-153, doi:10.1097/mph.0000000000000308 (2015).

51 Pinto, N. R. *et al.* Advances in Risk Classification and Treatment Strategies for Neuroblastoma. *J Clin Oncol* **33**, 3008-3017, doi:10.1200/jco.2014.59.4648 (2015).

52 Ploessl, C., Pan, A., Maples, K. T. & Lowe, D. K. Dinutuximab: An Anti-GD2 Monoclonal Antibody for High-Risk Neuroblastoma. *The Annals of pharmacotherapy*, doi:10.1177/1060028016632013 (2016).

53 Burnet, F. M. The concept of immunological surveillance. *Progress in experimental tumor research* **13**, 1-27 (1970).

54 Dunn, G. P., Old, L. J. & Schreiber, R. D. The three Es of cancer immunoediting. *Annual review of immunology* **22**, 329-360, doi:10.1146/annurev.immunol.22.012703.104803 (2004).

55 Tang, D., Kang, R., Coyne, C. B., Zeh, H. J. & Lotze, M. T. PAMPs and DAMPs: signal 0s that spur autophagy and immunity. *Immunol Rev* **249**, 158-175, doi:10.1111/j.1600-065X.2012.01146.x (2012).

56 Liu, Y. & Zeng, G. Cancer and innate immune system interactions: translational potentials for cancer immunotherapy. *Journal of immunotherapy (Hagerstown, Md. : 1997)* **35**, 299-308, doi:10.1097/CJI.0b013e3182518e83 (2012).

57 van Furth, R. & Cohn, Z. A. The origin and kinetics of mononuclear phagocytes. *J Exp Med* **128**, 415-435 (1968).

58 Guilliams, M. *et al.* Dendritic cells, monocytes and macrophages: a unified nomenclature based on ontogeny. *Nat Rev Immunol* **14**, 571-578, doi:10.1038/nri3712

http://www.nature.com/nri/journal/v14/n8/abs/nri3712.html#supplementary-information (2014).

59 Ginhoux, F. & Jung, S. Monocytes and macrophages: developmental pathways and tissue homeostasis. *Nat Rev Immunol* **14**, 392-404, doi:10.1038/nri3671 (2014).

60 Ingersoll, M. A. *et al.* Comparison of gene expression profiles between human and mouse monocyte subsets. *Blood* **115**, e10-19, doi:10.1182/blood-2009-07-235028 (2010).

61 van Furth, R. & Sluiter, W. Distribution of blood monocytes between a marginating and a circulating pool. *J Exp Med* **163**, 474-479 (1986).

62 Swirski, F. K. *et al.* Identification of splenic reservoir monocytes and their deployment to inflammatory sites. *Science* **325**, 612-616, doi:10.1126/science.1175202 (2009).

63 Dai, X. M. *et al.* Targeted disruption of the mouse colony-stimulating factor 1 receptor gene results in osteopetrosis, mononuclear phagocyte deficiency, increased primitive progenitor cell frequencies, and reproductive defects. *Blood* **99**, 111-120 (2002).

64 Cecchini, M. G. *et al.* Role of colony stimulating factor-1 in the establishment and regulation of tissue macrophages during postnatal development of the mouse. *Development (Cambridge, England)* **120**, 1357-1372 (1994).

65 Ziegler-Heitbrock, L. & Hofer, T. P. Toward a refined definition of monocyte subsets. *Front Immunol* **4**, 23, doi:10.3389/fimmu.2013.00023 (2013).

66 Jakubzick, C. *et al.* Minimal differentiation of classical monocytes as they survey steady-state tissues and transport antigen to lymph nodes. *Immunity* **39**, 599-610, doi:10.1016/j.immuni.2013.08.007 (2013).

67 Palframan, R. T. *et al.* Inflammatory chemokine transport and presentation in HEV: a remote control mechanism for monocyte recruitment to lymph nodes in inflamed tissues. *J Exp Med* **194**, 1361-1373 (2001).

68 Geissmann, F., Jung, S. & Littman, D. R. Blood monocytes consist of two principal subsets with distinct migratory properties. *Immunity* **19**, 71-82 (2003).

69 Bingle, L., Brown, N. J. & Lewis, C. E. The role of tumour-associated macrophages in tumour progression: implications for new anticancer therapies. *The Journal of pathology* **196**, 254-265, doi:10.1002/path.1027 (2002).

70 Chen, J. J. *et al.* Tumor-associated macrophages: the double-edged sword in cancer progression. *J Clin Oncol* **23**, 953-964, doi:10.1200/jco.2005.12.172 (2005).

71 Chitu, V. & Stanley, E. R. Colony-stimulating factor-1 in immunity and inflammation. *Curr Opin Immunol* **18**, 39-48, doi:10.1016/j.coi.2005.11.006 (2006).

72 Mantovani, A. *et al.* The chemokine system in cancer biology and therapy. *Cytokine & growth factor reviews* **21**, 27-39, doi:10.1016/j.cytogfr.2009.11.007 (2010).

73 Mantovani, A., Allavena, P., Sica, A. & Balkwill, F. Cancer-related inflammation. *Nature* **454**, 436-444, doi:10.1038/nature07205 (2008).

74 Kessenbrock, K., Plaks, V. & Werb, Z. Matrix metalloproteinases: regulators of the tumor microenvironment. *Cell* **141**, 52-67, doi:10.1016/j.cell.2010.03.015 (2010).

75 Lin, E. Y. *et al.* Macrophages regulate the angiogenic switch in a mouse model of breast cancer. *Cancer Res* **66**, 11238-11246, doi:10.1158/0008-5472.can-06-1278 (2006).

76 Woo, S. R., Corrales, L. & Gajewski, T. F. Innate immune recognition of cancer. *Annual review of immunology* **33**, 445-474, doi:10.1146/annurev-immunol-032414-112043 (2015).

77 den Haan, J. M., Lehar, S. M. & Bevan, M. J. CD8(+) but not CD8(-) dendritic cells cross-prime cytotoxic T cells in vivo. *J Exp Med* **192**, 1685-1696 (2000).

78 Joffre, O. P., Segura, E., Savina, A. & Amigorena, S. Cross-presentation by dendritic cells. *Nature Reviews Immunology* **12**, 557, doi:10.1038/nri3254 (2012).

79 Villadangos, J. A. & Schnorrer, P. Intrinsic and cooperative antigen-presenting functions of dendritic-cell subsets in vivo. *Nat Rev Immunol* **7**, 543-555, doi:10.1038/nri2103 (2007).

80 Liu, C. *et al.* Plasmacytoid dendritic cells induce NK cell-dependent, tumor antigen-specific T cell cross-priming and tumor regression in mice. *J Clin Invest* **118**, 1165-1175, doi:10.1172/jci33583 (2008).

81 Labidi-Galy, S. I. *et al.* Plasmacytoid dendritic cells infiltrating ovarian cancer are associated with poor prognosis. *Oncoimmunology* **1**, 380-382, doi:10.4161/onci.18801 (2012).

82 Wei, S. *et al.* Plasmacytoid dendritic cells induce CD8+ regulatory T cells in human ovarian carcinoma. *Cancer Res* **65**, 5020-5026, doi:10.1158/0008-5472.can-04-4043 (2005).

83 Demoulin, S., Herfs, M., Delvenne, P. & Hubert, P. Tumor microenvironment converts plasmacytoid dendritic cells into immunosuppressive/tolerogenic cells: insight into the molecular mechanisms. *Journal of leukocyte biology* **93**, 343-352, doi:10.1189/jlb.0812397 (2013).

84 Sisirak, V. *et al.* Impaired IFN-alpha production by plasmacytoid dendritic cells favors regulatory T-cell expansion that may contribute to breast cancer progression. *Cancer Res* **72**, 5188-5197, doi:10.1158/0008-5472.can-11-3468 (2012).

85 Ahrens, S. *et al.* F-actin is an evolutionarily conserved damage-associated molecular pattern recognized by DNGR-1, a receptor for dead cells. *Immunity* **36**, 635-645, doi:10.1016/j.immuni.2012.03.008 (2012).

86 Sancho, D. *et al.* Identification of a dendritic cell receptor that couples sensing of necrosis to immunity. *Nature* **458**, 899-903, doi:10.1038/nature07750 (2009).

87 Broz, M. L. *et al.* Dissecting the tumor myeloid compartment reveals rare activating antigen-presenting cells critical for T cell immunity. *Cancer Cell* **26**, 638-652, doi:10.1016/j.ccell.2014.09.007 (2014).

88 Salmon, H. *et al.* Expansion and Activation of CD103+ Dendritic Cell Progenitors at the Tumor Site Enhances Tumor Responses to Therapeutic PD-L1 and BRAF Inhibition. *Immunity* **44**, 924-938, doi:https://doi.org/10.1016/j.immuni.2016.03.012 (2016).

89 Phillipson, M. & Kubes, P. The neutrophil in vascular inflammation. *Nat Med* **17**, 1381-1390, doi:10.1038/nm.2514 (2011).

90 Mantovani, A., Cassatella, M. A., Costantini, C. & Jaillon, S. Neutrophils in the activation and regulation of innate and adaptive immunity. *Nat Rev Immunol* **11**, 519-531, doi:10.1038/nri3024 (2011).

91 Ley, K., Laudanna, C., Cybulsky, M. I. & Nourshargh, S. Getting to the site of inflammation: the leukocyte adhesion cascade updated. *Nat Rev Immunol* **7**, 678-689, doi:10.1038/nri2156 (2007).

92 Kolaczkowska, E. & Kubes, P. Neutrophil recruitment and function in health and inflammation. *Nat Rev Immunol* **13**, 159-175, doi:10.1038/nri3399 (2013).

93 Amulic, B., Cazalet, C., Hayes, G. L., Metzler, K. D. & Zychlinsky, A. Neutrophil function: from mechanisms to disease. *Annual review of immunology* **30**, 459-489, doi:10.1146/annurev-immunol-020711-074942 (2012).

94 Lieschke, G. *et al.* Mice lacking granulocyte colony-stimulating factor have chronic neutropenia, granulocyte and macrophage progenitor cell deficiency, and impaired neutrophil mobilization. *Blood* **84**, 1737-1746 (1994).

95 Mestas, J. & Hughes, C. C. Of mice and not men: differences between mouse and human immunology. *Journal of immunology (Baltimore, Md. : 1950)* **172**, 2731-2738 (2004).

96 Doeing, D. C., Borowicz, J. L. & Crockett, E. T. Gender dimorphism in differential peripheral blood leukocyte counts in mice using cardiac, tail, foot, and saphenous vein puncture methods. *BMC clinical pathology* **3**, 3, doi:10.1186/1472-6890-3-3 (2003).

97 Hager, M., Cowland, J. B. & Borregaard, N. Neutrophil granules in health and disease. *Journal of internal medicine* **268**, 25-34, doi:10.1111/j.1365-2796.2010.02237.x (2010).

98 Borregaard, N. Neutrophils, from marrow to microbes. *Immunity* **33**, 657-670, doi:10.1016/j.immuni.2010.11.011 (2010).

99 Mayadas, T. N., Cullere, X. & Lowell, C. A. The multifaceted functions of neutrophils. *Annual review of pathology* **9**, 181-218, doi:10.1146/annurev-pathol-020712-164023 (2014).

100 Brinkmann, V. *et al.* Neutrophil extracellular traps kill bacteria. *Science* **303**, 1532-1535, doi:10.1126/science.1092385 (2004).

101 Papayannopoulos, V. & Zychlinsky, A. NETs: a new strategy for using old weapons. *Trends in immunology* **30**, 513-521, doi:10.1016/j.it.2009.07.011 (2009).

102 Christoffersson, G. *et al.* VEGF-A recruits a proangiogenic MMP-9-delivering neutrophil subset that induces angiogenesis in transplanted hypoxic tissue. *Blood* **120**, 4653-4662, doi:10.1182/blood-2012-04-421040 (2012).

103 Jablonska, J., Leschner, S., Westphal, K., Lienenklaus, S. & Weiss, S. Neutrophils responsive to endogenous IFN-beta regulate tumor angiogenesis and growth in a mouse tumor model. *J Clin Invest* **120**, 1151-1164, doi:10.1172/jci37223 (2010).

104 Pillay, J. *et al.* A subset of neutrophils in human systemic inflammation inhibits T cell responses through Mac-1. *J Clin Invest* **122**, 327-336, doi:10.1172/jci57990 (2012).

105 Galli, S. J., Borregaard, N. & Wynn, T. A. Phenotypic and functional plasticity of cells of innate immunity: macrophages, mast cells and neutrophils. *Nat Immunol* **12**, 1035-1044, doi:10.1038/ni.2109 (2011).

106 Ochando, J. C. & Chen, S. H. Myeloid-derived suppressor cells in transplantation and cancer. *Immunol Res* **54**, 275-285, doi:10.1007/s12026-012-8335-1 (2012).

107 Gabrilovich, D. I. & Nagaraj, S. Myeloid-derived suppressor cells as regulators of the immune system. *Nat Rev Immunol* **9**, 162-174, doi:10.1038/nri2506 (2009).

108 Ishigami, S. *et al.* Prognostic value of intratumoral natural killer cells in gastric carcinoma. *Cancer* **88**, 577-583 (2000).

109 Villegas, F. R. *et al.* Prognostic significance of tumor infiltrating natural killer cells subset CD57 in patients with squamous cell lung cancer. *Lung cancer (Amsterdam, Netherlands)* **35**, 23-28 (2002).

110 Guerra, N. *et al.* NKG2D-deficient mice are defective in tumor surveillance in models of spontaneous malignancy. *Immunity* **28**, 571-580, doi:10.1016/j.immuni.2008.02.016 (2008).

111 Smyth, M. J. *et al.* NKG2D function protects the host from tumor initiation. *J Exp Med* **202**, 583-588, doi:10.1084/jem.20050994 (2005).

112 Di Santo, J. P. Natural killer cell developmental pathways: a question of balance. *Annual review of immunology* **24**, 257-286, doi:10.1146/annurev.immunol.24.021605.090700 (2006).

113 Inngjerdingen, M., Kveberg, L., Naper, C. & Vaage, J. T. Natural killer cell subsets in man and rodents. *Tissue antigens* **78**, 81-88, doi:10.1111/j.1399-0039.2011.01714.x (2011).

114 Ljunggren, H. G. & Karre, K. In search of the 'missing self': MHC molecules and NK cell recognition. *Immunology today* **11**, 237-244 (1990).

115 Vivier, E., Ugolini, S., Blaise, D., Chabannon, C. & Brossay, L. Targeting natural killer cells and natural killer T cells in cancer. *Nat Rev Immunol* **12**, 239-252, doi:10.1038/nri3174 (2012).

116 Liu, X. V., Ho, S. S., Tan, J. J., Kamran, N. & Gasser, S. Ras activation induces expression of Raet1 family NK receptor ligands. *Journal of immunology (Baltimore, Md. : 1950)* **189**, 1826-1834, doi:10.4049/jimmunol.1200965 (2012).

117 Waldhauer, I. & Steinle, A. NK cells and cancer immunosurveillance. *Oncogene* **27**, 5932-5943, doi:10.1038/onc.2008.267 (2008).

118 Cheng, M., Chen, Y., Xiao, W., Sun, R. & Tian, Z. NK cell-based immunotherapy for malignant diseases. *Cellular & molecular immunology* **10**, 230-252, doi:10.1038/cmi.2013.10 (2013).

119 Lantz, O. & Bendelac, A. An invariant T cell receptor alpha chain is used by a unique subset of major histocompatibility complex class I-specific CD4+ and CD4-8- T cells in mice and humans. *J Exp Med* **180**, 1097-1106 (1994).

120 Bendelac, A. *et al.* CD1 recognition by mouse NK1+ T lymphocytes. *Science* **268**, 863-865 (1995).

121 Wu, D. Y., Segal, N. H., Sidobre, S., Kronenberg, M. & Chapman, P. B. Cross-presentation of disialoganglioside GD3 to natural killer T cells. *J Exp Med* **198**, 173-181, doi:10.1084/jem.20030446 (2003).

122 Matsuda, J. L., Mallevaey, T., Scott-Browne, J. & Gapin, L. CD1d-restricted iNKT cells, the 'Swiss-Army knife' of the immune system. *Curr Opin Immunol* **20**, 358-368, doi:10.1016/j.coi.2008.03.018 (2008).

123 Van Kaer, L., Parekh, V. V. & Wu, L. Invariant natural killer T cells: bridging innate and adaptive immunity. *Cell and tissue research* **343**, 43-55, doi:10.1007/s00441-010-1023-3 (2011).

124 Crowe, N. Y., Smyth, M. J. & Godfrey, D. I. A critical role for natural killer T cells in immunosurveillance of methylcholanthrene-induced sarcomas. *J Exp Med* **196**, 119-127 (2002).

125 Smyth, M. J. *et al.* Differential tumor surveillance by natural killer (NK) and NKT cells. *J Exp Med* **191**, 661-668 (2000).

126 Medler, T. R., Cotechini, T. & Coussens, L. M. Immune response to cancer therapy: mounting an effective antitumor response and mechanisms of resistance. *Trends Cancer* **1**, 66-75, doi:10.1016/j.trecan.2015.07.008 (2015).

127 Mina, M. *et al.* Tumor-infiltrating T lymphocytes improve clinical outcome of therapy-resistant neuroblastoma. *Oncoimmunology* **4**, e1019981, doi:10.1080/2162402x.2015.1019981 (2015).

128 Gajewski, T. F., Schreiber, H. & Fu, Y. X. Innate and adaptive immune cells in the tumor microenvironment. *Nat Immunol* **14**, 1014-1022, doi:10.1038/ni.2703 (2013).

129 Haskins, K. *et al.* The major histocompatibility complex-restricted antigen receptor on T cells. I. Isolation with a monoclonal antibody. *J Exp Med* **157**, 1149-1169 (1983).

130 Zinkernagel, R. M. & Doherty, P. C. Immunological surveillance against altered self components by sensitised T lymphocytes in lymphocytes choriomeningitis. *Nature* **251**, 547-548 (1974).

131 Weiss, A. & Stobo, J. D. Requirement for the coexpression of T3 and the T cell antigen receptor on a malignant human T cell line. *J Exp Med* **160**, 1284-1299 (1984).

132 Pardoll, D. M. Immunology beats cancer: a blueprint for successful translation. *Nat Immunol* **13**, 1129-1132, doi:10.1038/ni.2392 (2012).

133 Smyth, M. J., Dunn, G. P. & Schreiber, R. D. Cancer immunosurveillance and immunoediting: the roles of immunity in suppressing tumor development and shaping tumor immunogenicity. *Advances in immunology* **90**, 1-50, doi:10.1016/s0065-2776(06)90001-7 (2006).

134 Rosenberg, S. A. *et al.* Use of tumor-infiltrating lymphocytes and interleukin-2 in the immunotherapy of patients with metastatic melanoma. A preliminary report. *N Engl J Med* **319**, 1676-1680, doi:10.1056/nejm198812223192527 (1988).

135 Rosenberg, S. A., Spiess, P. & Lafreniere, R. A NEW APPROACH TO THE ADOPTIVE IMMUNOTHERAPY OF CANCER WITH TUMOR-INFILTRATING LYMPHOCYTES. *Science* **233**, 1318-1321, doi:10.1126/science.3489291 (1986).

136 Engel, A. M. *et al.* Methylcholanthrene-induced sarcomas in nude mice have short induction times and relatively low levels of surface MHC class I expression. *APMIS : acta pathologica, microbiologica, et immunologica Scandinavica* **104**, 629-639 (1996).

137 Engel, A. M., Svane, I. M., Rygaard, J. & Werdelin, O. MCA sarcomas induced in scid mice are more immunogenic than MCA sarcomas induced in congenic, immunocompetent mice. *Scand J Immunol* **45**, 463-470 (1997).

138 Shankaran, V. *et al.* IFNgamma and lymphocytes prevent primary tumour development and shape tumour immunogenicity. *Nature* **410**, 1107-1111, doi:10.1038/35074122 (2001).

139 Djenidi, F. *et al.* CD8+CD103+ tumor-infiltrating lymphocytes are tumor-specific tissue-resident memory T cells and a prognostic factor for survival in lung cancer patients. *Journal of immunology (Baltimore, Md. : 1950)* **194**, 3475-3486, doi:10.4049/jimmunol.1402711 (2015).

140 Galon, J. *et al.* Type, density, and location of immune cells within human colorectal tumors predict clinical outcome. *Science* **313**, 1960-1964, doi:10.1126/science.1129139 (2006).

141 Kmiecik, J. *et al.* Elevated CD3+ and CD8+ tumor-infiltrating immune cells correlate with prolonged survival in glioblastoma patients despite integrated immunosuppressive mechanisms in the tumor microenvironment and at the systemic level. *Journal of neuroimmunology* **264**, 71-83, doi:10.1016/j.jneuroim.2013.08.013 (2013).

142 Mahmoud, S. M. *et al.* Tumor-infiltrating CD8+ lymphocytes predict clinical outcome in breast cancer. *J Clin Oncol* **29**, 1949-1955, doi:10.1200/jco.2010.30.5037 (2011).

143 Thompson, E. D., Enriquez, H. L., Fu, Y. X. & Engelhard, V. H. Tumor masses support naive T cell infiltration, activation, and differentiation into effectors. *J Exp Med* **207**, 1791-1804, doi:10.1084/jem.20092454 (2010).

144 Marzo, A. L. *et al.* Tumor antigens are constitutively presented in the draining lymph nodes. *Journal of immunology (Baltimore, Md. : 1950)* **162**, 5838-5845 (1999).

145 Dudley, M. E. *et al.* Cancer regression and autoimmunity in patients after clonal repopulation with antitumor lymphocytes. *Science* **298**, 850-854, doi:10.1126/science.1076514 (2002).

146 Dudley, M. E. *et al.* Adoptive cell therapy for patients with metastatic melanoma: evaluation of intensive myeloablative chemoradiation preparative regimens. *J Clin Oncol* **26**, 5233-5239, doi:10.1200/jco.2008.16.5449 (2008).

147 Williams, M. A. & Bevan, M. J. Effector and memory CTL differentiation. *Annual review of immunology* **25**, 171-192, doi:10.1146/annurev.immunol.25.022106.141548 (2007).

148 Kaech, S. M., Hemby, S., Kersh, E. & Ahmed, R. Molecular and functional profiling of memory CD8 T cell differentiation. *Cell* **111**, 837-851 (2002).

149 Masopust, D. & Picker, L. J. Hidden memories: frontline memory T cells and early pathogen interception. *Journal of immunology (Baltimore, Md. : 1950)* **188**, 5811-5817, doi:10.4049/jimmunol.1102695 (2012).

150 Sallusto, F., Lenig, D., Forster, R., Lipp, M. & Lanzavecchia, A. Two subsets of memory T lymphocytes with distinct homing potentials and effector functions. *Nature* **401**, 708-712, doi:10.1038/44385 (1999).

151 Sallusto, F., Geginat, J. & Lanzavecchia, A. Central memory and effector memory T cell subsets: function, generation, and maintenance. *Annual review of immunology* **22**, 745-763, doi:10.1146/annurev.immunol.22.012703.104702 (2004).

152 Pardoll, D. M. & Topalian, S. L. The role of CD4+ T cell responses in antitumor immunity. *Curr Opin Immunol* **10**, 588-594 (1998).

153 Topalian, S. L. MHC class II restricted tumor antigens and the role of CD4+ T cells in cancer immunotherapy. *Curr Opin Immunol* **6**, 741-745 (1994).

154 Zhu, J., Yamane, H. & Paul, W. E. Differentiation of effector CD4 T cell populations (*). *Annual review of immunology* **28**, 445-489, doi:10.1146/annurev-immunol-030409-101212 (2010).

155 Fridman, W. H., Pages, F., Sautes-Fridman, C. & Galon, J. The immune contexture in human tumours: impact on clinical outcome. *Nat Rev Cancer* **12**, 298-306, doi:10.1038/nrc3245 (2012).

156 Nishikawa, H. & Sakaguchi, S. Regulatory T cells in cancer immunotherapy. *Curr Opin Immunol* **27**, 1-7, doi:10.1016/j.coi.2013.12.005 (2014).

157 Roychoudhuri, R. *et al.* BACH2 represses effector programs to stabilize T(reg)-mediated immune homeostasis. *Nature* **498**, 506-510, doi:10.1038/nature12199 (2013).

158 Peggs, K. S. Blockade of CTLA-4 on both effector and regulatory T cell compartments contributes to the antitumor activity of anti-CTLA-4 antibodies. *J Exp Med* **206** (2009).

159 Quezada, S. A. *et al.* Limited tumor infiltration by activated T effector cells restricts the therapeutic activity of regulatory T cell depletion against established melanoma. *J Exp Med* **205**, 2125-2138, doi:10.1084/jem.20080099 (2008).

160 Cooper, M. D. The early history of B cells. *Nat Rev Immunol* **15**, 191-197, doi:10.1038/nri3801 (2015).

161 Montecino-Rodriguez, E. & Dorshkind, K. B-1 B cell development in the fetus and adult. *Immunity* **36**, 13-21, doi:10.1016/j.immuni.2011.11.017 (2012).

162 Pillai, S. & Cariappa, A. The follicular versus marginal zone B lymphocyte cell fate decision. *Nat Rev Immunol* **9**, 767-777, doi:10.1038/nri2656 (2009).

163 Clark, M. R., Tanaka, A., Powers, S. E. & Veselits, M. Receptors, subcellular compartments and the regulation of peripheral B cell responses: the illuminating state of anergy. *Mol Immunol* **48**, 1281-1286, doi:10.1016/j.molimm.2010.10.024 (2011).

164 Reth, M. Antigen receptor tail clue. *Nature* **338**, 383-384, doi:10.1038/338383b0 (1989).

165 Dal Porto, J. M. *et al.* B cell antigen receptor signaling 101. *Mol Immunol* **41**, 599-613, doi:10.1016/j.molimm.2004.04.008 (2004).

166 Shaffer, A. L., 3rd, Young, R. M. & Staudt, L. M. Pathogenesis of human B cell lymphomas. *Annual review of immunology* **30**, 565-610, doi:10.1146/annurev-immunol-020711-075027 (2012).

167 Victora, G. D. & Nussenzweig, M. C. Germinal centers. *Annual review of immunology* **30**, 429-457, doi:10.1146/annurev-immunol-020711-075032 (2012).

168 Coffey, F., Alabyev, B. & Manser, T. Initial clonal expansion of germinal center B cells takes place at the perimeter of follicles. *Immunity* **30**, 599-609, doi:10.1016/j.immuni.2009.01.011 (2009).

169 Mosmann, T. R., Cherwinski, H., Bond, M. W., Giedlin, M. A. & Coffman, R. L. Two types of murine helper T cell clone. I. Definition according to profiles of lymphokine activities and secreted proteins. *Journal of immunology (Baltimore, Md. : 1950)* **136**, 2348-2357 (1986).

170 Phan, T. G., Grigorova, I., Okada, T. & Cyster, J. G. Subcapsular encounter and complement-dependent transport of immune complexes by lymph node B cells. *Nat Immunol* **8**, 992-1000, doi:10.1038/ni1494 (2007).

171 Cherukuri, A., Cheng, P. C. & Pierce, S. K. The Role of the CD19/CD21 Complex in B Cell Processing and Presentation of Complement-Tagged Antigens. *The Journal of Immunology* **167**, 163-172, doi:10.4049/jimmunol.167.1.163 (2001).

172 Fang, Y., Xu, C., Fu, Y. X., Holers, V. M. & Molina, H. Expression of complement receptors 1 and 2 on follicular dendritic cells is necessary for the generation of a strong antigen-specific IgG response. *Journal of immunology (Baltimore, Md. : 1950)* **160**, 5273-5279 (1998).

173 LeBien, T. W. & Tedder, T. F. B lymphocytes: how they develop and function. *Blood* **112**, 1570-1580, doi:10.1182/blood-2008-02-078071 (2008).

174 Coutinho, A. & Moller, G. Thymus-independent B-cell induction and paralysis. *Advances in immunology* **21**, 113-236 (1975).

175 Barr, T. A., Brown, S., Mastroeni, P. & Gray, D. TLR and B cell receptor signals to B cells differentially program primary and memory Th1 responses to Salmonella enterica. *Journal of immunology (Baltimore, Md. : 1950)* **185**, 2783-2789, doi:10.4049/jimmunol.1001431 (2010).

176 Lund, F. E. *et al.* B cells are required for generation of protective effector and memory CD4 cells in response to Pneumocystis lung infection. *Journal of immunology (Baltimore, Md. : 1950)* **176**, 6147-6154 (2006).

177 Lund, F. E. & Randall, T. D. Effector and regulatory B cells: modulators of CD4+ T cell immunity. *Nat Rev Immunol* **10**, 236-247, doi:10.1038/nri2729 (2010).

178 Rosser, E. C. & Mauri, C. Regulatory B cells: origin, phenotype, and function. *Immunity* **42**, 607-612, doi:10.1016/j.immuni.2015.04.005 (2015).

179 Mauri, C. & Bosma, A. Immune regulatory function of B cells. *Annual review of immunology* **30**, 221-241, doi:10.1146/annurev-immunol-020711-074934 (2012).

180 Nathan, C. & Ding, A. Nonresolving inflammation. *Cell* **140**, 871-882, doi:10.1016/j.cell.2010.02.029 (2010).

181 Wang, R. X. *et al.* Interleukin-35 induces regulatory B cells that suppress autoimmune disease. *Nat Med* **20**, 633-641, doi:10.1038/nm.3554 (2014).

182 Parekh, V. V. *et al.* B cells activated by lipopolysaccharide, but not by anti-Ig and anti-CD40 antibody, induce anergy in CD8+ T cells: role of TGF-beta 1. *Journal of immunology (Baltimore, Md. : 1950)* **170**, 5897-5911 (2003).

183 Wolf, S. D., Dittel, B. N., Hardardottir, F. & Janeway, C. A., Jr. Experimental autoimmune encephalomyelitis induction in genetically B cell-deficient mice. *J Exp Med* **184**, 2271-2278 (1996).

184 Tadmor, T., Zhang, Y., Cho, H. M., Podack, E. R. & Rosenblatt, J. D. The absence of B lymphocytes reduces the number and function of T-regulatory cells and enhances the anti-tumor response in a murine tumor model. *Cancer immunology, immunotherapy : CII* **60**, 609-619, doi:10.1007/s00262-011-0972-z (2011).

185 Carter, N. A. *et al.* Mice lacking endogenous IL-10-producing regulatory B cells develop exacerbated disease and present with an increased frequency of Th1/Th17 but a decrease in regulatory T cells. *Journal of immunology (Baltimore, Md. : 1950)* **186**, 5569-5579, doi:10.4049/jimmunol.1100284 (2011).

186 Matsumoto, M. *et al.* Interleukin-10-producing plasmablasts exert regulatory function in autoimmune inflammation. *Immunity* **41**, 1040-1051, doi:10.1016/j.immuni.2014.10.016 (2014).

187 Sun, C. M., Deriaud, E., Leclerc, C. & Lo-Man, R. Upon TLR9 signaling, CD5+ B cells control the IL-12-dependent Th1-priming capacity of neonatal DCs. *Immunity* **22**, 467-477, doi:10.1016/j.immuni.2005.02.008 (2005).

188 Ravetch, J. V. in *Fundamental Immunology* (ed W. E. Paul) 685-700 (Lippincott-Raven, 2003).

189 Nimmerjahn, F. & Ravetch, J. V. Fc[gamma] receptors as regulators of immune responses. *Nat Rev Immunol* **8**, 34-47 (2008).

190 Guilliams, M., Bruhns, P., Saeys, Y., Hammad, H. & Lambrecht, B. N. The function of Fcgamma receptors in dendritic cells and macrophages. *Nat Rev Immunol* **14**, 94-108, doi:10.1038/nri3582 (2014).

191 Ravetch, J. V. & Lanier, L. L. Immune inhibitory receptors. *Science* **290**, 84-89 (2000).

192 Nimmerjahn, F. & Ravetch, J. V. Fcgamma receptors: old friends and new family members. *Immunity* **24**, 19-28, doi:10.1016/j.immuni.2005.11.010 (2006).

193 Hulett, M. D. & Hogarth, P. M. Molecular basis of Fc receptor function. *Advances in immunology* **57**, 1-127 (1994).

194 Schwartz, R. H. Costimulation of T lymphocytes: the role of CD28, CTLA-4, and B7/BB1 in interleukin-2 production and immunotherapy. *Cell* **71**, 1065-1068 (1992).

195 Rudd, C. E., Taylor, A. & Schneider, H. CD28 and CTLA-4 coreceptor expression and signal transduction. *Immunol Rev* **229** (2009).

196 Lenschow, D. J., Walunas, T. L. & Bluestone, J. A. CD28/B7 system of T cell costimulation. *Annual review of immunology* **14**, 233-258, doi:10.1146/annurev.immunol.14.1.233 (1996).

197 Linsley, P. S. *et al.* Human B7-1 (CD80) and B7-2 (CD86) bind with similar avidities but distinct kinetics to CD28 and CTLA-4 receptors. *Immunity* **1**, 793-801 (1994).

198 Qureshi, O. S. Trans-endocytosis of CD80 and CD86: a molecular basis for the cell-extrinsic function of CTLA-4. *Science* **332** (2011).

199 Tivol, E. A. Loss of CTLA-4 leads to massive lymphoproliferation and fatal multiorgan tissue destruction, revealing a critical negative regulatory role of CTLA-4. *Immunity* **3** (1995).

200 Waterhouse, P. Lymphoproliferative disorders with early lethality in mice deficient in Ctla-4. *Science* **270** (1995).

201 Wing, K. CTLA-4 control over Foxp3+ regulatory T cell function. *Science* **322** (2008).

202 Hill, J. A. *et al.* Foxp3 transcription-factor-dependent and -independent regulation of the regulatory T cell transcriptional signature. *Immunity* **27**, 786-800, doi:10.1016/j.immuni.2007.09.010 (2007).

203 Gavin, M. A. *et al.* Foxp3-dependent programme of regulatory T-cell differentiation. *Nature* **445**, 771-775, doi:10.1038/nature05543 (2007).

204 Parry, R. V. CTLA-4 and PD-1 receptors inhibit T-cell activation by distinct mechanisms. *Mol Cell Biol* **25** (2005).

205 Honda, T. *et al.* Tuning of Antigen Sensitivity by T Cell Receptor-Dependent Negative Feedback Controls T Cell Effector Function in Inflamed Tissues. *Immunity* **40**, 235-247, doi:http://dx.doi.org/10.1016/j.immuni.2013.11.017 (2014).

206 Hui, E. *et al.* T cell costimulatory receptor CD28 is a primary target for PD-1-mediated inhibition. *Science* **355**, 1428-1433, doi:10.1126/science.aaf1292 (2017).

207 Yokosuka, T. Programmed cell death 1 forms negative costimulatory microclusters that directly inhibit T cell receptor signaling by recruiting phosphatase SHP2. *J Exp Med* **209** (2012).

208 Nishimura, H. *et al.* Autoimmune dilated cardiomyopathy in PD-1 receptor-deficient mice. *Science* **291**, 319-322, doi:10.1126/science.291.5502.319 (2001).

209 Nishimura, H. Development of lupus-like autoimmune diseases by disruption of the PD-1 gene encoding an ITIM motif-carrying immunoreceptor. *Immunity* **11** (1999).

210 Latchman, Y. *et al.* PD-L2 is a second ligand for PD-1 and inhibits T cell activation. *Nat Immunol* **2**, 261-268, doi:10.1038/85330 (2001).

211 Dong, H., Zhu, G., Tamada, K. & Chen, L. B7-H1, a third member of the B7 family, co-stimulates T-cell proliferation and interleukin-10 secretion. *Nat Med* **5**, 1365-1369, doi:10.1038/70932 (1999).

212 Topalian, Suzanne L., Drake, Charles G. & Pardoll, Drew M. Immune Checkpoint Blockade: A Common Denominator Approach to Cancer Therapy. *Cancer Cell* **27**, 450-461, doi:http://dx.doi.org/10.1016/j.ccell.2015.03.001 (2015).

213 Parsa, A. T. *et al.* Loss of tumor suppressor PTEN function increases B7-H1 expression and immunoresistance in glioma. *Nat Med* **13**, 84-88, doi:10.1038/nm1517 (2007).

214 Marzec, M. *et al.* Oncogenic kinase NPM/ALK induces through STAT3 expression of immunosuppressive protein CD274 (PD-L1, B7-H1). *Proc Natl Acad Sci U S A* **105**, 20852-20857, doi:10.1073/pnas.0810958105 (2008).

215 Taube, J. M. *et al.* Colocalization of inflammatory response with B7-h1 expression in human melanocytic lesions supports an adaptive resistance mechanism of immune escape. *Science translational medicine* **4**, 127ra137, doi:10.1126/scitranslmed.3003689 (2012).

216 Spranger, S. *et al.* Up-regulation of PD-L1, IDO, and T(regs) in the melanoma tumor microenvironment is driven by CD8(+) T cells. *Science translational medicine* **5**, 200ra116, doi:10.1126/scitranslmed.3006504 (2013).

217 Francisco, L. M. *et al.* PD-L1 regulates the development, maintenance, and function of induced regulatory T cells. *J Exp Med* **206**, 3015-3029, doi:10.1084/jem.20090847 (2009).

218 Boon, T., Coulie, P. G., Van den Eynde, B. J. & van der Bruggen, P. in *Annual review of immunology* Vol. 24 *Annual Review of Immunology* 175-208 (2006).

219 Frey, A. B. & Monu, N. Signaling defects in anti-tumor T cells. *Immunological Reviews* **222**, 192-205, doi:10.1111/j.1600-065X.2008.00606.x (2008).

220 Zitvogel, L. *et al.* Immunogenic Tumor Cell Death for Optimal Anticancer Therapy: The Calreticulin Exposure Pathway. *Clinical Cancer Research* **16**, 3100-3104, doi:10.1158/1078-0432.ccr-09-2891 (2010).

221 Apetoh, L. *et al.* The interaction between HMGB1 and TLR4 dictates the outcome of anticancer chemotherapy and radiotherapy. *Immunological Reviews* **220**, 47-59, doi:10.1111/j.1600-065X.2007.00573.x (2007).

222 Bakdash, G., Sittig, S. P., van Dijk, T., Figdor, C. G. & de Vries, L. J. M. The nature of activatory and tolerogenic dendritic cell-derived signal II. *Frontiers in Immunology* **4**, doi:10.3389/fimmu.2013.00053 (2013).

223 Szamel, M. & Resch, K. T-CELL ANTIGEN RECEPTOR-INDUCED SIGNAL-TRANSDUCTION PATHWAYS - ACTIVATION AND FUNCTION OF PROTEIN KINASES-C IN T-LYMPHOCYTES. *European Journal of Biochemistry* **228**, 1-15 (1995).

224 Skov, S., Bregenholt, S. & Claesson, M. H. MHC class I ligation of human T cells activates the ZAP70 and p56(lck) tyrosine kinases, leads to an alternative phenotype of the TCR/CD3 zeta-chain, and induces apoptosis. *Journal of Immunology* **158**, 3189-3196 (1997).

225 Krogsgaard, M., Huppa, J. B., Purbhoo, M. A. & Davis, M. A. Linking molecular and cellular events in T-cell activation and synapse formation. *Seminars in Immunology* **15**, 307-315, doi:10.1016/j.smim.2003.09.002 (2003).

226 Curtsinger, J. M. & Mescher, M. F. Inflammatory cytokines as a third signal for T cell activation. *Current Opinion in Immunology* **22**, 333-340, doi:http://dx.doi.org/10.1016/j.coi.2010.02.013 (2010).

227 Dunn, G. P., Koebel, C. M. & Schreiber, R. D. Interferons, immunity and cancer immunoediting. *Nature Reviews Immunology* **6**, 836, doi:10.1038/nri1961 (2006).

228 Mittal, D., Gubin, M. M., Schreiber, R. D. & Smyth, M. J. New insights into cancer immunoediting and its three component phases—elimination, equilibrium and escape. *Current Opinion in Immunology* **27**, 16-25, doi:https://doi.org/10.1016/j.coi.2014.01.004 (2014).

229 Schreiber, R. D., Old, L. J. & Smyth, M. J. Cancer Immunoediting: Integrating Immunity's Roles in Cancer Suppression and Promotion. *Science* **331**, 1565-1570, doi:10.1126/science.1203486 (2011).

230 Matsushita, H. *et al.* Cancer exome analysis reveals a T-cell-dependent mechanism of cancer immunoediting. *Nature* **482**, 400-U149, doi:10.1038/nature10755 (2012).

231 DuPage, M., Mazumdar, C., Schmidt, L. M., Cheung, A. F. & Jacks, T. Expression of tumour-specific antigens underlies cancer immunoediting. *Nature* **482**, 405, doi:10.1038/nature10803

https://www.nature.com/articles/nature10803#supplementary-information (2012).

232 von Boehmer, L. *et al.* NY-ESO-1–specific immunological pressure and escape in a patient with metastatic melanoma. *Cancer Immunity Archive* **13** (2013).

233 O'Sullivan, T. *et al.* Cancer immunoediting by the innate immune system in the absence of adaptive immunity. *The Journal of Experimental Medicine* **209**, 1869-1882, doi:10.1084/jem.20112738 (2012).

234 Kaplan, D. H. *et al.* Demonstration of an interferon gamma-dependent tumor surveillance system in immunocompetent mice. *Proc Natl Acad Sci U S A* **95**, 7556-7561 (1998).

235 Iannello, A., Thompson, T. W., Ardolino, M., Lowe, S. W. & Raulet, D. H. p53-dependent chemokine production by senescent tumor cells supports NKG2D-dependent tumor elimination by natural killer cells. *The Journal of Experimental Medicine* **210**, 2057-2069, doi:10.1084/jem.20130783 (2013).

236 Willingham, S. B. *et al.* The CD47-signal regulatory protein alpha (SIRPa) interaction is a therapeutic target for human solid tumors. *Proceedings of the National Academy of Sciences* **109**, 6662-6667, doi:10.1073/pnas.1121623109 (2012).

237 Teng, M. W. L. *et al.* Opposing Roles for IL-23 and IL-12 in Maintaining Occult Cancer in an Equilibrium State. *Cancer Research* **72**, 3987-3996, doi:10.1158/0008-5472.can-12-1337 (2012).

238 Raffaghello, L. *et al.* Multiple defects of the antigen-processing machinery components in human neuroblastoma: immunotherapeutic implications. *Oncogene* **24**, 4634-4644, doi:10.1038/sj.onc.1208594 (2005).

239 Placzek, W. J. *et al.* A survey of the anti-apoptotic Bcl-2 subfamily expression in cancer types provides a platform to predict the efficacy of Bcl-2 antagonists in cancer therapy. *Cell Death &Amp; Disease* **1**, e40, doi:10.1038/cddis.2010.18

https://www.nature.com/articles/cddis201018#supplementary-information (2010).

240 Bouzin, C., Brouet, A., De Vriese, J., Dewever, J. & Feron, O. Effects of vascular endothelial growth factor on the lymphocyte-endothelium interactions: identification of caveolin-1

and nitric oxide as control points of endothelial cell anergy. *Journal of immunology (Baltimore, Md. : 1950)* **178**, 1505-1511 (2007).

241 Blank, C. *et al.* PD-L1/B7H-1 inhibits the effector phase of tumor rejection by T cell receptor (TCR) transgenic CD8+ T cells. *Cancer Res* **64**, 1140-1145 (2004).

242 Keir, M. E., Butte, M. J., Freeman, G. J. & Sharpe, A. H. PD-1 and its ligands in tolerance and immunity. *Annual review of immunology* **26**, 677-704, doi:10.1146/annurev.immunol.26.021607.090331 (2008).

243 Munn, D. H. & Mellor, A. L. IDO in the Tumor Microenvironment: Inflammation, Counter-Regulation, and Tolerance. *Trends in immunology* **37**, 193-207, doi:10.1016/j.it.2016.01.002 (2016).

244 Carelle, N. *et al.* Changing patient perceptions of the side effects of cancer chemotherapy. *Cancer* **95**, 155-163, doi:10.1002/cncr.10630 (2002).

245 Ramirez, L. Y. *et al.* Potential Chemotherapy Side Effects: What Do Oncologists Tell Parents? *Pediatric Blood & Cancer* **52**, 497-502, doi:10.1002/pbc.21835 (2009).

246 Weiss, R. B. The anthracyclines: will we ever find a better doxorubicin? *Semin Oncol* **19**, 670-686 (1992).

247 Cutts, S. M., Nudelman, A., Rephaeli, A. & Phillips, D. R. The Power and Potential of Doxorubicin-DNA Adducts. *IUBMB Life* **57**, 73-81, doi:10.1080/15216540500079093 (2005).

248 Arcamone, F. *Doxorubicin: anticancer antibiotics*. (Elsevier, 2012).

249 Phillips, D. R., Greif, P. C. & Boston, R. C. Daunomycin-DNA dissociation kinetics. *Molecular pharmacology* **33**, 225-230 (1988).

250 Larsen, A. K., Escargueil, A. E. & Skladanowski, A. Catalytic topoisomerase II inhibitors in cancer therapy. *Pharmacology & therapeutics* **99**, 167-181 (2003).

251 Yokochi, T. & Robertson, K. D. Doxorubicin inhibits DNMT1, resulting in conditional apoptosis. *Molecular pharmacology* **66**, 1415-1420, doi:10.1124/mol.104.002634 (2004).

252 Dilruba, S. & Kalayda, G. V. Platinum-based drugs: past, present and future. *Cancer Chemotherapy and Pharmacology* **77**, 1103-1124, doi:10.1007/s00280-016-2976-z (2016).

253 Stordal, B., Pavlakis, N. & Davey, R. Oxaliplatin for the treatment of cisplatin-resistant cancer: A systematic review. *Cancer treatment reviews* **33**, 347-357, doi:10.1016/j.ctrv.2007.01.009 (2007).

254 Takahara, P. M., Rosenzweig, A. C., Frederick, C. A. & Lippard, S. J. Crystal structure of double-stranded DNA containing the major adduct of the anticancer drug cisplatin. *Nature* **377**, 649-652, doi:10.1038/377649a0 (1995).

255 Galluzzi, L. *et al.* Molecular mechanisms of cisplatin resistance. *Oncogene* **31**, 1869-1883, doi:10.1038/onc.2011.384 (2012).

256 Ozols, R. F. *et al.* Phase III trial of carboplatin and paclitaxel compared with cisplatin and paclitaxel in patients with optimally resected stage III ovarian cancer: a Gynecologic Oncology Group study. *J Clin Oncol* **21**, 3194-3200, doi:10.1200/jco.2003.02.153 (2003).

257 Stewart, D. J. Mechanisms of resistance to cisplatin and carboplatin. *Critical reviews in oncology/hematology* **63**, 12-31, doi:10.1016/j.critrevonc.2007.02.001 (2007).

258 Wheate, N. J., Walker, S., Craig, G. E. & Oun, R. The status of platinum anticancer drugs in the clinic and in clinical trials. *Dalton transactions (Cambridge, England : 2003)* **39**, 8113-8127, doi:10.1039/c0dt00292e (2010).

259 Di Francesco, A. M., Ruggiero, A. & Riccardi, R. Cellular and molecular aspects of drugs of the future: oxaliplatin. *Cellular and molecular life sciences : CMLS* **59**, 1914-1927 (2002).

260 Emadi, A., Jones, R. J. & Brodsky, R. A. Cyclophosphamide and cancer: golden anniversary. *Nature Reviews Clinical Oncology* **6**, 638-647, doi:10.1038/nrclinonc.2009.146 (2009).

261 Santos, G. W. *et al.* The use of cyclophosphamide for clinical marrow transplantation. *Transplantation proceedings* **4**, 559-564 (1972).

262 Friedman, O. M. & Seligman, A. M. Preparation of N-Phosphorylated Derivatives of Bis-β-chloroethylamine1a. *Journal of the American Chemical Society* **76**, 655-658, doi:10.1021/ja01632a006 (1954).

263 Arnold, H., Bourseaux, F. & Brock, N. Chemotherapeutic action of a cyclic nitrogen mustard phosphamide ester (B 518-ASTA) in experimental tumours of the rat. *Nature* **181**, 931 (1958).

264 Boddy, A. V. & Yule, S. M. Metabolism and pharmacokinetics of oxazaphosphorines. *Clinical pharmacokinetics* **38**, 291-304, doi:10.2165/00003088-200038040-00001 (2000).

265 Dong, Q. *et al.* A structural basis for a phosphoramide mustard-induced DNA interstrand cross-link at 5'-d(GAC). *Proc Natl Acad Sci U S A* **92**, 12170-12174 (1995).

266 Ayash, L. J. *et al.* Cyclophosphamide pharmacokinetics: correlation with cardiac toxicity and tumor response. *J Clin Oncol* **10**, 995-1000, doi:10.1200/jco.1992.10.6.995 (1992).

267 Watson, A. R., Rance, C. P. & Bain, J. Long term effects of cyclophosphamide on testicular function. *British medical journal (Clinical research ed.)* **291**, 1457-1460 (1985).

268 Boumpas, D. T. *et al.* Risk for sustained amenorrhea in patients with systemic lupus erythematosus receiving intermittent pulse cyclophosphamide therapy. *Annals of internal medicine* **119**, 366-369 (1993).

269 Stillwell, T. J. & Benson, R. C., Jr. Cyclophosphamide-induced hemorrhagic cystitis. A review of 100 patients. *Cancer* **61**, 451-457 (1988).

270 Levine, E. G. & Bloomfield, C. D. Leukemias and myelodysplastic syndromes secondary to drug, radiation, and environmental exposure. *Semin Oncol* **19**, 47-84 (1992).

271 Hara, J. Development of treatment strategies for advanced neuroblastoma. *International journal of clinical oncology* **17**, 196-203, doi:10.1007/s10147-012-0417-5 (2012).

272 Russo, C., Cohn, S. L., Petruzzi, M. J. & de Alarcon, P. A. Long-term neurologic outcome in children with opsoclonus-myoclonus associated with neuroblastoma: a report from the Pediatric Oncology Group. *Medical and pediatric oncology* **28**, 284-288 (1997).

273 Halperin, E. C. & Cox, E. B. Radiation therapy in the management of neuroblastoma: the Duke University Medical Center experience 1967-1984. *Int J Radiat Oncol Biol Phys* **12**, 1829-1837 (1986).

274 Park, J. R. *et al.* Pilot induction regimen incorporating pharmacokinetically guided topotecan for treatment of newly diagnosed high-risk neuroblastoma: a Children's Oncology Group study. *J Clin Oncol* **29**, 4351-4357, doi:10.1200/jco.2010.34.3293 (2011).

276

275 London, W. B. *et al.* Phase II randomized comparison of topotecan plus cyclophosphamide versus topotecan alone in children with recurrent or refractory neuroblastoma: a Children's Oncology Group study. *J Clin Oncol* **28**, 3808-3815, doi:10.1200/jco.2009.27.5016 (2010).

276 Ladenstein, R. *et al.* Busulfan and melphalan versus carboplatin, etoposide, and melphalan as high-dose chemotherapy for high-risk neuroblastoma (HR-NBL1/SIOPEN): an international, randomised, multi-arm, open-label, phase 3 trial. *The Lancet. Oncology* **18**, 500-514, doi:10.1016/s1470-2045(17)30070-0 (2017).

277 Berthold, F. *et al.* Myeloablative megatherapy with autologous stem-cell rescue versus oral maintenance chemotherapy as consolidation treatment in patients with high-risk neuroblastoma: a randomised controlled trial. *The Lancet. Oncology* **6**, 649-658, doi:10.1016/s1470-2045(05)70291-6 (2005).

278 Galluzzi, L., Buque, A., Kepp, O., Zitvogel, L. & Kroemer, G. Immunogenic cell death in cancer and infectious disease. *Nat Rev Immunol*, doi:10.1038/nri.2016.107 (2016).

279 Kroemer, G. *et al.* Classification of cell death: recommendations of the Nomenclature Committee on Cell Death 2009. *Cell Death and Differentiation* **16**, 3-11, doi:10.1038/cdd.2008.150 (2009).

280 Kerr, J. F. R., Wyllie, A. H. & Currie, A. R. APOPTOSIS - BASIC BIOLOGICAL PHENOMENON WITH WIDE-RANGING IMPLICATIONS IN TISSUE KINETICS. *British Journal of Cancer* **26**, 239-&, doi:10.1038/bjc.1972.33 (1972).

281 Hengartner, M. O. Apoptosis: Corralling the corpses. *Cell* **104**, 325-328, doi:10.1016/s0092-8674(01)00219-7 (2001).

282 Lauber, K., Blumenthal, S. G., Waibel, M. & Wesselborg, S. Clearance of apoptotic cells: Getting rid of the corpses. *Molecular Cell* **14**, 277-287, doi:10.1016/s1097-2765(04)00237-0 (2004).

283 Savill, J. & Fadok, V. Corpse clearance defines the meaning of cell death. *Nature* **407**, 784-788, doi:10.1038/35037722 (2000).

284 Kim, S. J., Elkon, K. B. & Ma, X. J. Transcriptional suppression of interleukin-12 gene expression following phagocytosis of apoptotic cells. *Immunity* **21**, 643-653, doi:10.1016/j.immuni.2004.09.009 (2004).

285 Hoffmann, P. R. *et al.* Interaction between phosphatidylserine and the phosphatidylserine receptor inhibits immune responses in vivo. *Journal of Immunology* **174**, 1393-1404 (2005).

286 Green, D. R., Ferguson, T., Zitvogel, L. & Kroemer, G. Immunogenic and tolerogenic cell death. *Nature Reviews Immunology* **9**, 353-363, doi:10.1038/nri2545 (2009).

287 Obeid, M. *et al.* Ecto-calreticulin in immunogenic chemotherapy. *Immunological Reviews* **220**, 22-34, doi:10.1111/j.1600-065X.2007.00567.x (2007).

288 Zitvogel, L., Apetoh, L., Ghiringhelli, F. & Kroemer, G. Immunological aspects of cancer chemotherapy. *Nat Rev Immunol* **8**, 59-73 (2008).

289 Galluzzi, L., Buque, A., Kepp, O., Zitvogel, L. & Kroemer, G. Immunological Effects of Conventional Chemotherapy and Targeted Anticancer Agents. *Cancer Cell* **28**, 690-714, doi:10.1016/j.ccell.2015.10.012 (2015).

290 Wong, R. S. Apoptosis in cancer: from pathogenesis to treatment. *Journal of experimental & clinical cancer research : CR* **30**, 87, doi:10.1186/1756-9966-30-87 (2011).

291 Saraste, A. & Pulkki, K. Morphologic and biochemical hallmarks of apoptosis. *Cardiovascular research* **45**, 528-537 (2000).

292 Hacker, G. The morphology of apoptosis. *Cell and tissue research* **301**, 5-17 (2000).

293 Ghobrial, I. M., Witzig, T. E. & Adjei, A. A. Targeting apoptosis pathways in cancer therapy. *CA: a cancer journal for clinicians* **55**, 178-194 (2005).

294 Ziegler, U. & Groscurth, P. Morphological features of cell death. *News in physiological sciences : an international journal of physiology produced jointly by the International Union of Physiological Sciences and the American Physiological Society* **19**, 124-128 (2004).

295 Gelebart, P., Opas, M. & Michalak, M. Calreticulin, a Ca2+-binding chaperone of the endoplasmic reticulum. *International Journal of Biochemistry & Cell Biology* **37**, 260-266, doi:10.1016/j.biocel.2004.02.030 (2005).

296 Williams, D. B. Beyond lectins: the calnexin/calreticulin chaperone system of the endoplasmic reticulum. *Journal of Cell Science* **119**, 615-623, doi:10.1242/jcs.02856 (2006).

297 Casares, N. *et al.* Caspase-dependent immunogenicity of doxorubicin-induced tumor cell death. *Journal of Experimental Medicine* **202**, 1691-1701, doi:10.1084/jem.20050915 (2005).

298 Obeid, M. *et al.* Calreticulin exposure dictates the immunogenicity of cancer cell death. *Nature Medicine* **13**, 54-61, doi:10.1038/nm1523 (2007).

299 Panaretakis, T. *et al.* Mechanisms of pre-apoptotic calreticulin exposure in immunogenic cell death. *Embo Journal* **28**, 578-590, doi:10.1038/emboj.2009.1 (2009).

300 Obeid, M. *et al.* Calreticulin exposure is required for the immunogenicity of gamma-irradiation and UVC light-induced apoptosis. *Cell Death and Differentiation* **14**, 1848-1850, doi:10.1038/sj.cdd.4402201 (2007).

301 Apetoh, L. *et al.* Toll-like receptor 4-dependent contribution of the immune system to anticancer chemotherapy and radiotherapy. *Nature Medicine* **13**, 1050-1059, doi:10.1038/nm1622 (2007).

302 Medzhitov, R. & Janeway, C. A. Innate immunity: The virtues of a nonclonal system of recognition. *Cell* **91**, 295-298, doi:10.1016/s0092-8674(00)80412-2 (1997).

303 Jung, S. *et al.* In vivo depletion of CD11c(+) dendritic cells abrogates priming of CD8(+) T cells by exogenous cell-associated antigens. *Immunity* **17**, 211-220, doi:10.1016/s1074-7613(02)00365-5 (2002).

304 Garg, A. D. *et al.* A novel pathway combining calreticulin exposure and ATP secretion in immunogenic cancer cell death. *Embo j* **31**, 1062-1079, doi:10.1038/emboj.2011.497 (2012).

305 Bezu, L. *et al.* Combinatorial strategies for the induction of immunogenic cell death. *Front Immunol* **6**, 187, doi:10.3389/fimmu.2015.00187 (2015).

306 Martins, I. *et al.* Chemotherapy induces ATP release from tumor cells. *Cell Cycle* **8**, 3723-3728, doi:10.4161/cc.8.22.10026 (2009).

278

307 Michaud, M. *et al.* An autophagy-dependent anticancer immune response determines the efficacy of melanoma chemotherapy. *Oncoimmunology* **3**, e944047, doi:10.4161/21624011.2014.944047 (2014).

308 Martins, I. *et al.* Premortem autophagy determines the immunogenicity of chemotherapy-induced cancer cell death. *Autophagy* **8**, 413-415, doi:10.4161/auto.19009 (2012).

309 Elliott, M. R. *et al.* Nucleotides released by apoptotic cells act as a find-me signal to promote phagocytic clearance. *Nature* **461**, 282-286, doi:10.1038/nature08296 (2009).

310 Ghiringhelli, F. *et al.* Activation of the NLRP3 inflammasome in dendritic cells induces IL-1beta-dependent adaptive immunity against tumors. *Nat Med* **15**, 1170-1178, doi:10.1038/nm.2028 (2009).

311 Krysko, D. V. *et al.* Immunogenic cell death and DAMPs in cancer therapy. *Nat Rev Cancer* **12**, 860-875, doi:10.1038/nrc3380 (2012).

312 Stagg, J. *et al.* CD73-deficient mice are resistant to carcinogenesis. *Cancer Res* **72**, 2190-2196, doi:10.1158/0008-5472.can-12-0420 (2012).

313 Fucikova, J. *et al.* High hydrostatic pressure induces immunogenic cell death in human tumor cells. *International journal of cancer. Journal international du cancer* **135**, 1165-1177, doi:10.1002/ijc.28766 (2014).

314 Fucikova, J. *et al.* Human tumor cells killed by anthracyclines induce a tumor-specific immune response. *Cancer Res* **71**, 4821-4833, doi:10.1158/0008-5472.can-11-0950 (2011).

315 Basu, S., Binder, R. J., Ramalingam, T. & Srivastava, P. K. CD91 is a common receptor for heat shock proteins gp96, hsp90, hsp70, and calreticulin. *Immunity* **14**, 303-313 (2001).

316 Gardai, S. J. *et al.* Cell-surface calreticulin initiates clearance of viable or apoptotic cells through trans-activation of LRP on the phagocyte. *Cell* **123**, 321-334, doi:10.1016/j.cell.2005.08.032 (2005).

317 Garg, A. D. *et al.* Resistance to anticancer vaccination effect is controlled by a cancer cell-autonomous phenotype that disrupts immunogenic phagocytic removal. *Oncotarget* **6**, 26841-26860, doi:10.18632/oncotarget.4754 (2015).

318 Ladoire, S. *et al.* Combined evaluation of LC3B puncta and HMGB1 expression predicts residual risk of relapse after adjuvant chemotherapy in breast cancer. *Autophagy* **11**, 1878-1890, doi:10.1080/15548627.2015.1082022 (2015).

319 Ladoire, S., Enot, D., Andre, F., Zitvogel, L. & Kroemer, G. Immunogenic cell death-related biomarkers: Impact on the survival of breast cancer patients after adjuvant chemotherapy. *Oncoimmunology* **5**, e1082706, doi:10.1080/2162402x.2015.1082706 (2016).

320 Rao, S. *et al.* A dual role for autophagy in a murine model of lung cancer. *Nature communications* **5**, 3056, doi:10.1038/ncomms4056 (2014).

321 Zitvogel, L., Galluzzi, L., Smyth, M. J. & Kroemer, G. Mechanism of action of conventional and targeted anticancer therapies: reinstating immunosurveillance. *Immunity* **39**, 74-88, doi:10.1016/j.immuni.2013.06.014 (2013).

322 Inoue, S., Setoyama, Y. & Odaka, A. Doxorubicin treatment induces tumor cell death followed by immunomodulation in a murine neuroblastoma model. *Experimental and Therapeutic Medicine* **7**, 703-708, doi:10.3892/etm.2014.1489 (2014).

323 Tanaka, H., Matsushima, H., Mizumoto, N. & Takashima, A. Classification of Chemotherapeutic Agents Based on Their Differential In vitro Effects on Dendritic Cells. *Cancer Research* **69**, 6978-6986, doi:10.1158/0008-5472.can-09-1101 (2009).

324 Shurin, G. V., Tourkova, I. L., Kaneno, R. & Shurin, M. R. Chemotherapeutic Agents in Noncytotoxic Concentrations Increase Antigen Presentation by Dendritic Cells via an IL-12-Dependent Mechanism. *Journal of Immunology* **183**, 137-144, doi:10.4049/jimmunol.0900734 (2009).

325 Kaneno, R., Shurin, G. V., Tourkova, I. L. & Shurin, M. R. Chemomodulation of human dendritic cell function by antineoplastic agents in low noncytotoxic concentrations. *Journal of Translational Medicine* **7**, doi:10.1186/1479-5876-7-58 (2009).

326 Lesterhuis, W. J. *et al.* Platinum-based drugs disrupt STAT6-mediated suppression of immune responses against cancer in humans and mice. *Journal of Clinical Investigation* **121**, 3100-3108, doi:10.1172/jci43656 (2011).

327 Bracci, L., Schiavoni, G., Sistigu, A. & Belardelli, F. Immune-based mechanisms of cytotoxic chemotherapy: implications for the design of novel and rationale-based combined treatments against cancer. *Cell Death and Differentiation* **21**, 15-25, doi:10.1038/cdd.2013.67 (2014).

328 Nakahara, T. *et al.* Cyclophosphamide enhances immunity by modulating the balance of dendritic cell subsets in lymphoid organs. *Blood* **115**, 4384-4392, doi:10.1182/blood-2009-11-251231 (2010).

329 Schiavoni, G. *et al.* Cyclophosphamide Synergizes with Type I Interferons through Systemic Dendritic Cell Reactivation and Induction of Immunogenic Tumor Apoptosis. *Cancer Research* **71**, 768-778, doi:10.1158/0008-5472.can-10-2788 (2011).

330 Heusinkveld, M. & van der Burg, S. H. Identification and manipulation of tumor associated macrophages in human cancers. *Journal of Translational Medicine* **9**, doi:10.1186/1479-5876-9-216 (2011).

331 Murray, Peter J. *et al.* Macrophage Activation and Polarization: Nomenclature and Experimental Guidelines. *Immunity* **41**, 14-20, doi:http://dx.doi.org/10.1016/j.immuni.2014.06.008 (2014).

332 Mills, C. D., Kincaid, K., Alt, J. M., Heilman, M. J. & Hill, A. M. M-1/M-2 macrophages and the Th1/Th2 paradigm. *Journal of Immunology* **164**, 6166-6173 (2000).

333 Bryniarski, K., Szczepanik, M., Ptak, M., Zemelka, M. & Ptak, W. Influence of cyclophosphamide and its metabolic products on the activity of peritoneal macrophages in mice. *Pharmacological Reports* **61**, 550-557 (2009).

334 Buhtoiarov, I. N. *et al.* Anti-tumour synergy of cytotoxic chemotherapy and anti-CD40 plus CpG-ODN immunotherapy through repolarization of tumour-associated macrophages. *Immunology* **132**, 226-239, doi:10.1111/j.1365-2567.2010.03357.x (2011).

335 Park, S. *et al.* Tumor suppression via paclitaxel-loaded drug carriers that target inflammation marker upregulated in tumor vasculature and macrophages. *Biomaterials* **34**, 598-605, doi:10.1016/j.biomaterials.2012.10.004 (2013).

280

336 Shree, T. *et al.* Macrophages and cathepsin proteases blunt chemotherapeutic response in breast cancer. *Genes & Development* **25**, 2465-2479, doi:10.1101/gad.180331.111 (2011).

337 Kawamata, A. *et al.* Thalidomide suppresses melanoma growth by activating natural killer cells in mice. *Oncology Reports* **16**, 1231-1236 (2006).

338 Brenner, B. G. & Margolese, R. G. THE RELATIONSHIP OF CHEMOTHERAPEUTIC AND ENDOCRINE INTERVENTION ON NATURAL-KILLER-CELL ACTIVITY IN HUMAN BREAST-CANCER. *Cancer* **68**, 482-488, doi:10.1002/1097-0142(19910801)68:3<482::aid-cncr2820680306>3.0.co;2-9 (1991).

339 Ghiringhelli, F. *et al.* Metronomic cyclophosphamide regimen selectively depletes CD4(+) CD25(+) regulatory T cells and restores T and NK effector functions in end stage cancer patients. *Cancer Immunology Immunotherapy* **56**, 641-648, doi:10.1007/s00262-006-0225-8 (2007).

340 Chang, C.-L. *et al.* Dose-Dense Chemotherapy Improves Mechanisms of Antitumor Immune Response. *Cancer Research* **73**, 119-127, doi:10.1158/0008-5472.can-12-2225 (2013).

341 Mattarollo, S. R. *et al.* Pivotal Role of Innate and Adaptive Immunity in Anthracycline Chemotherapy of Established Tumors. *Cancer Research* **71**, 4809-4820, doi:10.1158/0008-5472.can-11-0753 (2011).

342 Predina, J. D. *et al.* Neoadjuvant in situ gene-mediated cytotoxic immunotherapy improves postoperative outcomes in novel syngeneic esophageal carcinoma models. *Cancer Gene Therapy* **18**, 871-883, doi:10.1038/cgt.2011.56 (2011).

343 Tsuchikawa, T. *et al.* The Immunological Impact of Neoadjuvant Chemotherapy on the Tumor Microenvironment of Esophageal Squamous Cell Carcinoma. *Annals of Surgical Oncology* **19**, 1713-1719, doi:10.1245/s10434-011-1906-x (2012).

344 Bienkowski, M. & Preusser, M. Prognostic role of tumour-infiltrating inflammatory cells in brain tumours: literature review. *Current Opinion in Neurology* **28**, 647-658 (2015).

345 Mei, Z. *et al.* Tumour-infiltrating inflammation and prognosis in colorectal cancer: systematic review and meta-analysis. *British Journal of Cancer* **110**, 1595-1605, doi:10.1038/bjc.2014.46 (2014).

346 Bracci, L. *et al.* Cyclophosphamide enhances the antitumor efficacy of adoptively transferred immune cells through the induction of cytokine expression, B-cell and T-cell homeostatic proliferation, and specific tumor infiltration. *Clinical Cancer Research* **13**, 644-653, doi:10.1158/1078-0432.ccr-06-1209 (2007).

347 Zhang, L. *et al.* Differential impairment of regulatory T cells rather than effector T cells by paclitaxel-based chemotherapy. *Clinical Immunology* **129**, 219-229, doi:10.1016/j.clim.2008.07.013 (2008).

348 Kim, J.-E. *et al.* Cancer Cells Containing Nanoscale Chemotherapeutic Drugs Generate Antiovarian Cancer-specific CD4(+) T Cells in Peritoneal Space. *Journal of Immunotherapy* **35**, 1-13, doi:10.1097/CJI.0b013e3182328569 (2012).

349 Zhang, Y., Morgan, R., Podack, E. R. & Rosenblatt, J. B cell regulation of anti-tumor immune response. *Immunol Res* **57**, 115-124, doi:10.1007/s12026-013-8472-1 (2013).

350 Candolfi, M. *et al.* B Cells Are Critical to T-cell-Mediated Antitumor Immunity Induced by a Combined Immune-Stimulatory/Conditionally Cytotoxic Therapy for Glioblastoma. *Neoplasia (New York, N.Y.)* **13**, 947-960 (2011).

351 Rodríguez-Pinto, D. B cells as antigen presenting cells. *Cellular Immunology* **238**, 67-75, doi:http://dx.doi.org/10.1016/j.cellimm.2006.02.005 (2005).

352 Otterness, I. G. & Chang, Y. H. COMPARATIVE-STUDY OF CYCLOPHOSPHAMIDE, 6-MERCAPTOPURINE, AZATHIOPURINE AND METHOTREXATE - RELATIVE EFFECTS ON HUMORAL AND CELLULAR IMMUNE-RESPONSE IN MOUSE. *Clinical and Experimental Immunology* **26**, 346-354 (1976).

353 Smith, S. R., Terminelli, C., Kipilman, C. T. & Smith, Y. COMPARATIVE EFFECTS OF AZATHIOPRINE, CYCLOPHOSPHAMIDE AND FRENTIZOLE ON CELLULAR-IMMUNITY IN MICE. *Journal of Immunopharmacology* **3**, 133-170 (1981).

354 Berd, D., Maguire, H. C. & Mastrangelo, M. J. POTENTIATION OF HUMAN CELL-MEDIATED AND HUMORAL IMMUNITY BY LOW-DOSE CYCLOPHOSPHAMIDE. *Cancer Research* **44**, 5439-5443 (1984).

355 Liu, P., Jaffar, J., Hellstrom, I. & Hellstrom, K. E. Administration of Cyclophosphamide Changes the Immune Profile of Tumor-bearing Mice. *Journal of Immunotherapy* **33**, 53-59 (2010).

356 Moschella, F. *et al.* Unraveling Cancer Chemoimmunotherapy Mechanisms by Gene and Protein Expression Profiling of Responses to Cyclophosphamide. *Cancer Research* **71**, 3528-3539, doi:10.1158/0008-5472.can-10-4523 (2011).

357 Wijayahadi, N., Haron, M. R., Stanslas, J. & Yusuf, Z. Changes in cellular immunity during chemotherapy for primary breast cancer with anthracycline regimens. *Journal of Chemotherapy* **19**, 716-723 (2007).

358 Nowak, A. K., Robinson, B. W. S. & Lake, R. A. Gemcitabine exerts a selective effect on the humoral immune response: Implications for combination chemo-immunotherapy. *Cancer Research* **62**, 2353-2358 (2002).

359 Shebzukhov, Y. V. *et al.* Humoral immune response to thymidylate synthase in colon cancer patients after 5-FU chemotherapy. *Immunology letters* **100**, 88-93, doi:10.1016/j.imlet.2005.06.011 (2005).

360 North, R. J. CYCLOPHOSPHAMIDE-FACILITATED ADOPTIVE IMMUNOTHERAPY OF AN ESTABLISHED TUMOR DEPENDS ON ELIMINATION OF TUMOR-INDUCED SUPPRESSOR T-CELLS. *Journal of Experimental Medicine* **155**, 1063-1074, doi:10.1084/jem.155.4.1063 (1982).

361 Shevchenko, I. *et al.* Low-dose gemcitabine depletes regulatory T cells and improves survival in the orthotopic Panc02 model of pancreatic cancer. *International Journal of Cancer* **133**, 98-107, doi:10.1002/ijc.27990 (2013).

362 Rettig, L. *et al.* Gemcitabine depletes regulatory T-cells in human and mice and enhances triggering of vaccine-specific cytotoxic T-cells. *International Journal of Cancer* **129**, 832-838, doi:10.1002/ijc.25756 (2011).

363 Zhu, Y., Liu, N., Xiong, S. D., Zheng, Y. J. & Chu, Y. W. CD4(+)Foxp3(+) Regulatory T-cell Impairment by Paclitaxel is Independent of Toll-like Receptor 4. *Scandinavian Journal of Immunology* **73**, 301-308, doi:10.1111/j.1365-3083.2011.02514.x (2011).

282

364 Banissi, C., Ghiringhelli, F., Chen, L. & Carpentier, A. F. Treg depletion with a low-dose metronomic temozolomide regimen in a rat glioma model. *Cancer Immunology Immunotherapy* **58**, 1627-1634, doi:10.1007/s00262-009-0671-1 (2009).

365 Lutsiak, M. E. C. *et al.* Inhibition of CD4(+)25(+) T regulatory cell function implicated in enhanced immune response by low-dose cyclophosphamide. *Blood* **105**, 2862-2868, doi:10.1182/blood-2004-06-2410 (2005).

366 Ghiringhelli, F. *et al.* CD4(+)CD25(+) regulatory T cells suppress tumor immunity but are sensitive to cyclophosphamide which allows immunotherapy of established tumors to be curative. *European Journal of Immunology* **34**, 336-344, doi:10.1002/eji.200324181 (2004).

367 Zhao, J. *et al.* Selective Depletion of CD4(+)CD25(+)Foxp3(+) Regulatory T Cells by Low-Dose Cyclophosphamide Is Explained by Reduced Intracellular ATP Levels. *Cancer Research* **70**, 4850-4858, doi:10.1158/0008-5472.can-10-0283 (2010).

368 Dimeloe, S. *et al.* Human regulatory T cells lack the cyclophosphamide-extruding transporter ABCB1 and are more susceptible to cyclophosphamide-induced apoptosis. *Eur J Immunol* **44**, 3614-3620, doi:10.1002/eji.201444879 (2014).

369 Shimizu, J., Yamazaki, S., Takahashi, T., Ishida, Y. & Sakaguchi, S. Stimulation of CD25(+)CD4(+) regulatory T cells through GITR breaks immunological self-tolerance. *Nat Immunol* **3**, 135-142, doi:10.1038/ni759 (2002).

370 Fontenot, J. D., Gavin, M. A. & Rudensky, A. Y. Foxp3 programs the development and function of CD4+CD25+ regulatory T cells. *Nature Immunology* **4**, 330, doi:10.1038/ni904

https://www.nature.com/articles/ni904#supplementary-information (2003).

371 Rodriguez, P. C. *et al.* Arginase I-Producing Myeloid-Derived Suppressor Cells in Renal Cell Carcinoma Are a Subpopulation of Activated Granulocytes. *Cancer Research* **69**, 1553-1560, doi:10.1158/0008-5472.can-08-1921 (2009).

372 Rodriguez, P. C. *et al.* Arginase I in myeloid suppressor cells is induced by COX-2 in lung carcinoma. *Journal of Experimental Medicine* **202**, 931-939, doi:10.1084/jem.20050715 (2005).

373 Vincent, J. *et al.* 5-Fluorouracil Selectively Kills Tumor-Associated Myeloid-Derived Suppressor Cells Resulting in Enhanced T Cell-Dependent Antitumor Immunity. *Cancer Research* **70**, 3052-3061, doi:10.1158/0008-5472.can-09-3690 (2010).

374 Chen, J. *et al.* Preconditioning Chemotherapy with Cisplatin Enhances the Antitumor Activity of Cytokine-Induced Killer Cells in a Murine Melanoma Model. *Cancer Biotherapy and Radiopharmaceuticals* **27**, 210-220, doi:10.1089/cbr.2011.1116 (2012).

375 Mundy-Bosse, B. L. *et al.* Myeloid-Derived Suppressor Cell Inhibition of the IFN Response in Tumor-Bearing Mice. *Cancer Research* **71**, 5101-5110, doi:10.1158/0008-5472.can-10-2670 (2011).

376 Kodumudi, K. N. *et al.* A Novel Chemoimmunomodulating Property of Docetaxel: Suppression of Myeloid-Derived Suppressor Cells in Tumor Bearers. *Clinical Cancer Research* **16**, 4583-4594, doi:10.1158/1078-0432.ccr-10-0733 (2010).

377 Nikcevich, D. A. *et al.* STIMULATION OF SUPPRESSOR CELLS IN THE BONE-MARROW AND SPLEENS OF HIGH-DOSE CYCLOPHOSPHAMIDE-TREATED C57BI/6 MICE. *Cellular Immunology* **109**, 349-359, doi:10.1016/0008-8749(87)90318-2 (1987).

378 Sevko, A. *et al.* Cyclophosphamide promotes chronic inflammation-dependent immunosuppression and prevents antitumor response in melanoma. *The Journal of investigative dermatology* **133**, 1610-1619, doi:10.1038/jid.2012.444 (2013).

379 Tongu, M. *et al.* Metronomic chemotherapy with low-dose cyclophosphamide plus gemcitabine can induce anti-tumor T cell immunity in vivo. *Cancer Immunology Immunotherapy* **62**, 383-391, doi:10.1007/s00262-012-1343-0 (2013).

380 Kohler, G. & Milstein, C. Continuous cultures of fused cells secreting antibody of predefined specificity. *Nature* **256**, 495-497 (1975).

381 Köhler, G. & Milstein, C. Derivation of specific antibody-producing tissue culture and tumor lines by cell fusion. *European Journal of Immunology* **6**, 511-519, doi:10.1002/eji.1830060713 (1976).

382 Bernard, A. & Boumsell, L. The clusters of differentiation (CD) defined by the First International Workshop on Human Leucocyte Differentiation Antigens. *Human immunology* **11**, 1-10 (1984).

383 Weiner, G. J. Building better monoclonal antibody-based therapeutics. *Nat Rev Cancer* **15**, 361-370, doi:10.1038/nrc3930 (2015).

384 Vidarsson, G., Dekkers, G. & Rispens, T. IgG subclasses and allotypes: from structure to effector functions. *Front Immunol* **5**, 520, doi:10.3389/fimmu.2014.00520 (2014).

385 Schur, P. H. IgG subclasses. A historical perspective. *Monographs in allergy* **23**, 1-11 (1988).

386 Wu, T. T., Johnson, G. & Kabat, E. A. Length distribution of CDRH3 in antibodies. *Proteins* **16**, 1-7, doi:10.1002/prot.340160102 (1993).

387 Kabat, E. A., Wu, T. T. & Bilofsky, H. Variable region genes for the immunoglobulin framework are assembled from small segments of DNA--a hypothesis. *Proc Natl Acad Sci U S A* **75**, 2429-2433 (1978).

388 Wuhrer, M. *et al.* Regulated glycosylation patterns of IgG during alloimmune responses against human platelet antigens. *Journal of proteome research* **8**, 450-456, doi:10.1021/pr800651j (2009).

389 Dahan, R. *et al.* FcgammaRs Modulate the Anti-tumor Activity of Antibodies Targeting the PD-1/PD-L1 Axis. *Cancer Cell* **28**, 285-295, doi:10.1016/j.ccell.2015.08.004 (2015).

390 Bruhns, P. & Jonsson, F. Mouse and human FcR effector functions. *Immunol Rev* **268**, 25-51, doi:10.1111/imr.12350 (2015).

391 Bruhns, P. Properties of mouse and human IgG receptors and their contribution to disease models. *Blood* **119**, 5640-5649, doi:10.1182/blood-2012-01-380121 (2012).

392 Mancardi, D. A. *et al.* FcgammaRIV is a mouse IgE receptor that resembles macrophage FcepsilonRI in humans and promotes IgE-induced lung inflammation. *J Clin Invest* **118**, 3738-3750, doi:10.1172/jci36452 (2008).

393 Daeron, M. Fc receptor biology. *Annual review of immunology* **15**, 203-234, doi:10.1146/annurev.immunol.15.1.203 (1997).

394 Meeker, T. C. *et al.* A clinical trial of anti-idiotype therapy for B cell malignancy. *Blood* **65**, 1349-1363 (1985).

284

395 Vaickus, L. & Foon, K. A. Overview of monoclonal antibodies in the diagnosis and therapy of cancer. *Cancer investigation* **9**, 195-209 (1991).

396 Tjandra, J. J., Ramadi, L. & McKenzie, I. F. Development of human anti-murine antibody (HAMA) response in patients. *Immunology and cell biology* **68 (Pt 6)**, 367-376, doi:10.1038/icb.1990.50 (1990).

397 LoBuglio, A. F. *et al.* Mouse/human chimeric monoclonal antibody in man: kinetics and immune response. *Proc Natl Acad Sci U S A* **86**, 4220-4224 (1989).

398 Maloney, D. G. *et al.* IDEC-C2B8 (Rituximab) anti-CD20 monoclonal antibody therapy in patients with relapsed low-grade non-Hodgkin's lymphoma. *Blood* **90**, 2188-2195 (1997).

399 Nelson, A. L., Dhimolea, E. & Reichert, J. M. Development trends for human monoclonal antibody therapeutics. *Nat Rev Drug Discov* **9**, 767-774 (2010).

400 Jefferis, R. Recombinant antibody therapeutics: the impact of glycosylation on mechanisms of action. *Trends in Pharmacological Sciences* **30**, 356-362, doi:http://doi.org/10.1016/j.tips.2009.04.007 (2009).

401 Dalle, S. *et al.* Preclinical studies on the mechanism of action and the anti-lymphoma activity of the novel anti-CD20 antibody GA101. *Mol Cancer Ther* **10**, 178-185, doi:10.1158/1535-7163.mct-10-0385 (2011).

402 Mossner, E. *et al.* Increasing the efficacy of CD20 antibody therapy through the engineering of a new type II anti-CD20 antibody with enhanced direct and immune effector cell-mediated B-cell cytotoxicity. *Blood* **115**, 4393-4402, doi:10.1182/blood-2009-06-225979 (2010).

403 Scott, A. M., Wolchok, J. D. & Old, L. J. Antibody therapy of cancer. *Nat Rev Cancer* **12**, 278-287, doi:10.1038/nrc3236 (2012).

404 Glennie, M. J., French, R. R., Cragg, M. S. & Taylor, R. P. Mechanisms of killing by anti-CD20 monoclonal antibodies. *Mol Immunol* **44**, 3823-3837, doi:10.1016/j.molimm.2007.06.151 (2007).

405 Weiner, G. J. Rituximab: mechanism of action. *Seminars in hematology* **47**, 115-123, doi:10.1053/j.seminhematol.2010.01.011 (2010).

406 Hodi, F. S. Improved survival with ipilimumab in patients with metastatic melanoma. *N Engl J Med* **363** (2010).

407 Rolfo, C. *et al.* Immunotherapy in NSCLC: A Promising and Revolutionary Weapon. *Advances in experimental medicine and biology* **995**, 97-125, doi:10.1007/978-3-319-53156-4_5 (2017).

408 Modak, S. & Cheung, N. K. Disialoganglioside directed immunotherapy of neuroblastoma. *Cancer investigation* **25**, 67-77, doi:10.1080/07357900601130763 (2007).

409 Mueller, B. M., Romerdahl, C. A., Gillies, S. D. & Reisfeld, R. A. ENHANCEMENT OF ANTIBODY-DEPENDENT CYTOTOXICITY WITH A CHIMERIC ANTI-GD2 ANTIBODY. *Journal of Immunology* **144**, 1382-1386 (1990).

410 Weiner, G. J. Monoclonal antibody mechanisms of action in cancer. *Immunol Res* **39**, 271-278 (2007).

411 Bowles, J. A. & Weiner, G. J. CD16 polymorphisms and NK activation induced by monoclonal antibody-coated target cells. *Journal of Immunological Methods* **304**, 88-99, doi:http://doi.org/10.1016/j.jim.2005.06.018 (2005).

412 Cartron, G. *et al.* Therapeutic activity of humanized anti-CD20 monoclonal antibody and polymorphism in IgG Fc receptor FcgammaRIIIa gene. *Blood* **99**, 754-758 (2002).

413 Gul, N. & van Egmond, M. Antibody-Dependent Phagocytosis of Tumor Cells by Macrophages: A Potent Effector Mechanism of Monoclonal Antibody Therapy of Cancer. *Cancer Res* **75**, 5008-5013, doi:10.1158/0008-5472.can-15-1330 (2015).

414 Cheung, I. Y., Hsu, K. & Cheung, N. K. Activation of peripheral-blood granulocytes is strongly correlated with patient outcome after immunotherapy with anti-GD2 monoclonal antibody and granulocyte-macrophage colony-stimulating factor. *J Clin Oncol* **30**, 426-432, doi:10.1200/jco.2011.37.6236 (2012).

415 Tarek, N. *et al.* Unlicensed NK cells target neuroblastoma following anti-GD2 antibody treatment. *J Clin Invest* **122**, 3260-3270, doi:10.1172/jci62749 (2012).

416 Melis, J. P. M. *et al.* Complement in therapy and disease: Regulating the complement system with antibody-based therapeutics. *Molecular Immunology* **67**, 117-130, doi:http://doi.org/10.1016/j.molimm.2015.01.028 (2015).

417 Robert, C. *et al.* Pembrolizumab versus Ipilimumab in Advanced Melanoma. *N Engl J Med* **372**, 2521-2532, doi:10.1056/NEJMoa1503093 (2015).

418 Postow, M. A. *et al.* Nivolumab and ipilimumab versus ipilimumab in untreated melanoma. *N Engl J Med* **372**, 2006-2017, doi:10.1056/NEJMoa1414428 (2015).

419 Brahmer, J. Nivolumab versus Docetaxel in Advanced Squamous-Cell Non-Small-Cell Lung Cancer. *N Engl J Med* **373** (2015).

420 Powles, T. *et al.* MPDL3280A (anti-PD-L1) treatment leads to clinical activity in metastatic bladder cancer. *Nature* **515**, 558-562, doi:10.1038/nature13904 (2014).

421 Leach, D. R., Krummel, M. F. & Allison, J. P. Enhancement of antitumor immunity by CTLA-4 blockade. *Science* **271**, 1734-1736 (1996).

422 Hodi, F. S. *et al.* Biologic activity of cytotoxic T lymphocyte-associated antigen 4 antibody blockade in previously vaccinated metastatic melanoma and ovarian carcinoma patients. *Proc Natl Acad Sci U S A* **100**, 4712-4717, doi:10.1073/pnas.0830997100 (2003).

423 van Elsas, A., Hurwitz, A. A. & Allison, J. P. Combination immunotherapy of B16 melanoma using anti-cytotoxic T lymphocyte-associated antigen 4 (CTLA-4) and granulocyte/macrophage colony-stimulating factor (GM-CSF)-producing vaccines induces rejection of subcutaneous and metastatic tumors accompanied by autoimmune depigmentation. *J Exp Med* **190**, 355-366 (1999).

424 Ribas, A. *et al.* Antitumor activity in melanoma and anti-self responses in a phase I trial with the anti-cytotoxic T lymphocyte-associated antigen 4 monoclonal antibody CP-675,206. *J Clin Oncol* **23**, 8968-8977, doi:10.1200/jco.2005.01.109 (2005).

425 Ribas, A. Clinical development of the anti-CTLA-4 antibody tremelimumab. *Semin Oncol* **37**, 450-454, doi:10.1053/j.seminoncol.2010.09.010 (2010).

426 Phan, G. Q. *et al.* Cancer regression and autoimmunity induced by cytotoxic T lymphocyte-associated antigen 4 blockade in patients with metastatic melanoma. *Proc Natl Acad Sci U S A* **100**, 8372-8377, doi:10.1073/pnas.1533209100 (2003).

427 Beck, K. E. *et al.* Enterocolitis in patients with cancer after antibody blockade of cytotoxic T-lymphocyte-associated antigen 4. *J Clin Oncol* **24**, 2283-2289, doi:10.1200/jco.2005.04.5716 (2006).

428 Ribas, A. *et al.* Phase III randomized clinical trial comparing tremelimumab with standard-of-care chemotherapy in patients with advanced melanoma. *J Clin Oncol* **31**, 616-622, doi:10.1200/jco.2012.44.6112 (2013).

429 Weber, J. S. Current perspectives on immunotherapy. *Semin Oncol* **41 Suppl 5**, S14-29, doi:10.1053/j.seminoncol.2014.09.003 (2014).

430 Maker, A. V., Attia, P. & Rosenberg, S. A. Analysis of the cellular mechanism of antitumor responses and autoimmunity in patients treated with CTLA-4 blockade. *Journal of immunology (Baltimore, Md. : 1950)* **175**, 7746-7754 (2005).

431 Selby, M. J. *et al.* Anti-CTLA-4 antibodies of IgG2a isotype enhance antitumor activity through reduction of intratumoral regulatory T cells. *Cancer Immunol Res* **1**, 32-42, doi:10.1158/2326-6066.cir-13-0013 (2013).

432 Pardoll, D. M. The blockade of immune checkpoints in cancer immunotherapy. *Nat Rev Cancer* **12**, 252-264 (2012).

433 Wolchok, J. D. *et al.* Guidelines for the evaluation of immune therapy activity in solid tumors: immune-related response criteria. *Clinical cancer research : an official journal of the American Association for Cancer Research* **15**, 7412-7420, doi:10.1158/1078-0432.ccr-09-1624 (2009).

434 Dong, H. Tumor-associated B7-H1 promotes T-cell apoptosis: a potential mechanism of immune evasion. *Nat Med* **8** (2002).

435 Ansell, S. M. *et al.* PD-1 blockade with nivolumab in relapsed or refractory Hodgkin's lymphoma. *N Engl J Med* **372**, 311-319, doi:10.1056/NEJMoa1411087 (2015).

436 Iwai, Y. *et al.* Involvement of PD-L1 on tumor cells in the escape from host immune system and tumor immunotherapy by PD-L1 blockade. *Proc Natl Acad Sci U S A* **99**, 12293-12297, doi:10.1073/pnas.192461099 (2002).

437 Brahmer, J. R. *et al.* Phase I study of single-agent anti-programmed death-1 (MDX-1106) in refractory solid tumors: safety, clinical activity, pharmacodynamics, and immunologic correlates. *J Clin Oncol* **28**, 3167-3175, doi:10.1200/jco.2009.26.7609 (2010).

438 Topalian, S. L. *et al.* Survival, durable tumor remission, and long-term safety in patients with advanced melanoma receiving nivolumab. *J Clin Oncol* **32**, 1020-1030, doi:10.1200/jco.2013.53.0105 (2014).

439 Topalian, S. L. *et al.* Safety, activity, and immune correlates of anti-PD-1 antibody in cancer. *N Engl J Med* **366**, 2443-2454, doi:10.1056/NEJMoa1200690 (2012).

440 Brahmer, J. R. *et al.* Safety and activity of anti-PD-L1 antibody in patients with advanced cancer. *N Engl J Med* **366**, 2455-2465, doi:10.1056/NEJMoa1200694 (2012).

441 Herbst, R. S. *et al.* Predictive correlates of response to the anti-PD-L1 antibody MPDL3280A in cancer patients. *Nature* **515**, 563-567, doi:10.1038/nature14011 (2014).

442 Motzer, R. J. *et al.* Nivolumab for Metastatic Renal Cell Carcinoma: Results of a Randomized Phase II Trial. *J Clin Oncol* **33**, 1430-1437, doi:10.1200/jco.2014.59.0703 (2015).

443 Tumeh, P. C. *et al.* PD-1 blockade induces responses by inhibiting adaptive immune resistance. *Nature* **515**, 568-571, doi:10.1038/nature13954 (2014).

444 Wolchok, J. Putting the Immunologic Brakes on Cancer. *Cell* **175**, 1452-1454, doi:10.1016/j.cell.2018.11.006 (2018).

445 Goldberg, M. V. *et al.* Role of PD-1 and its ligand, B7-H1, in early fate decisions of CD8 T cells. *Blood* **110**, 186-192, doi:10.1182/blood-2006-12-062422 (2007).

446 Sfanos, K. S. *et al.* Human prostate-infiltrating CD8+ T lymphocytes are oligoclonal and PD-1+. *The Prostate* **69**, 1694-1703, doi:10.1002/pros.21020 (2009).

447 Ahmadzadeh, M. *et al.* Tumor antigen-specific CD8 T cells infiltrating the tumor express high levels of PD-1 and are functionally impaired. *Blood* **114**, 1537-1544, doi:10.1182/blood-2008-12-195792 (2009).

448 Barber, D. L. Restoring function in exhausted CD8 T cells during chronic viral infection. *Nature* **439** (2006).

449 Kamphorst, A. O. *et al.* Rescue of exhausted CD8 T cells by PD-1-targeted therapies is CD28-dependent. *Science* **355**, 1423-1427, doi:10.1126/science.aaf0683 (2017).

450 Buchbinder, E. I. & Desai, A. CTLA-4 and PD-1 Pathways: Similarities, Differences, and Implications of Their Inhibition. *American journal of clinical oncology* **39**, 98-106, doi:10.1097/coc.0000000000000239 (2016).

451 Wolchok, J. D. *et al.* Nivolumab plus ipilimumab in advanced melanoma. *N Engl J Med* **369**, 122-133, doi:10.1056/NEJMoa1302369 (2013).

452 Kwon, B. S. & Weissman, S. M. cDNA sequences of two inducible T-cell genes. *Proc Natl Acad Sci U S A* **86**, 1963-1967 (1989).

453 Pollok, K. E. *et al.* Inducible T cell antigen 4-1BB. Analysis of expression and function. *Journal of immunology (Baltimore, Md. : 1950)* **150**, 771-781 (1993).

454 Vinay, D. S. & Kwon, B. S. 4-1BB signaling beyond T cells. *Cellular & molecular immunology* **8**, 281-284, doi:10.1038/cmi.2010.82 (2011).

455 Pollok, K. E. *et al.* 4-1BB T-cell antigen binds to mature B cells and macrophages, and costimulates anti-mu-primed splenic B cells. *Eur J Immunol* **24**, 367-374, doi:10.1002/eji.1830240215 (1994).

456 Shuford, W. W. *et al.* 4-1BB costimulatory signals preferentially induce CD8+ T cell proliferation and lead to the amplification in vivo of cytotoxic T cell responses. *J Exp Med* **186**, 47-55 (1997).

457 Cannons, J. L. *et al.* 4-1BB ligand induces cell division, sustains survival, and enhances effector function of CD4 and CD8 T cells with similar efficacy. *Journal of immunology (Baltimore, Md. : 1950)* **167**, 1313-1324 (2001).

458 Chu, N. R., DeBenedette, M. A., Stiernholm, B. J., Barber, B. H. & Watts, T. H. Role of IL-12 and 4-1BB ligand in cytokine production by CD28+ and CD28- T cells. *Journal of immunology (Baltimore, Md. : 1950)* **158**, 3081-3089 (1997).

459 Taraban, V. Y. *et al.* Expression and costimulatory effects of the TNF receptor superfamily members CD134 (OX40) and CD137 (4-1BB), and their role in the generation of anti-tumor immune responses. *Eur J Immunol* **32**, 3617-3627, doi:10.1002/1521-4141(200212)32:12<3617::aid-immu3617>3.0.co;2-m (2002).

460 Miller, R. E. *et al.* 4-1BB-specific monoclonal antibody promotes the generation of tumor-specific immune responses by direct activation of CD8 T cells in a CD40-dependent manner. *Journal of immunology (Baltimore, Md. : 1950)* **169**, 1792-1800 (2002).

461 Melero, I. *et al.* Monoclonal antibodies against the 4-1BB T-cell activation molecule eradicate established tumors. *Nat Med* **3**, 682-685 (1997).

462 Murillo, O. *et al.* Therapeutic antitumor efficacy of anti-CD137 agonistic monoclonal antibody in mouse models of myeloma. *Clinical cancer research : an official journal of the American Association for Cancer Research* **14**, 6895-6906, doi:10.1158/1078-0432.ccr-08-0285 (2008).

463 Buchan, S. L. *et al.* Antibodies to Costimulatory Receptor 4-1BB Enhance Anti-tumor Immunity via T Regulatory Cell Depletion and Promotion of CD8 T Cell Effector Function. *Immunity* **49**, 958-970.e957, doi:10.1016/j.immuni.2018.09.014 (2018).

464 Melero, I., Hervas-Stubbs, S., Glennie, M., Pardoll, D. M. & Chen, L. Immunostimulatory monoclonal antibodies for cancer therapy. *Nat Rev Cancer* **7**, 95-106, doi:10.1038/nrc2051 (2007).

465 Kohrt, H. E. *et al.* Stimulation of natural killer cells with a CD137-specific antibody enhances trastuzumab efficacy in xenotransplant models of breast cancer. *J Clin Invest* **122**, 1066-1075, doi:10.1172/jci61226 (2012).

466 Kohrt, H. E. *et al.* CD137 stimulation enhances the antilymphoma activity of anti-CD20 antibodies. *Blood* **117**, 2423-2432, doi:10.1182/blood-2010-08-301945 (2011).

467 Kohrt, H. E. *et al.* Targeting CD137 enhances the efficacy of cetuximab. *J Clin Invest* **124**, 2668-2682, doi:10.1172/jci73014 (2014).

468 Thomas, S. & Prendergast, G. C. Cancer Vaccines: A Brief Overview. *Methods in molecular biology (Clifton, N.J.)* **1403**, 755-761, doi:10.1007/978-1-4939-3387-7_43 (2016).

469 Mellman, I., Coukos, G. & Dranoff, G. Cancer immunotherapy comes of age. *Nature* **480**, 480-489, doi:10.1038/nature10673 (2011).

470 Yaddanapudi, K., Mitchell, R. A. & Eaton, J. W. Cancer vaccines: Looking to the future. *Oncoimmunology* **2**, e23403, doi:10.4161/onci.23403 (2013).

471 Rosenberg, S. A., Yang, J. C. & Restifo, N. P. Cancer immunotherapy: moving beyond current vaccines. *Nat Med* **10**, 909-915, doi:10.1038/nm1100 (2004).

472 Topalian, S. L., Weiner, G. J. & Pardoll, D. M. Cancer immunotherapy comes of age. *J Clin Oncol* **29**, 4828-4836, doi:10.1200/jco.2011.38.0899 (2011).

473 Palucka, K. & Banchereau, J. Dendritic-cell-based therapeutic cancer vaccines. *Immunity* **39**, 38-48, doi:10.1016/j.immuni.2013.07.004 (2013).

474 Palucka, K. & Banchereau, J. Cancer immunotherapy via dendritic cells. *Nat Rev Cancer* **12**, 265-277, doi:10.1038/nrc3258 (2012).

475 Ruella, M. & Kalos, M. Adoptive immunotherapy for cancer. *Immunological Reviews* **257**, 14-38, doi:10.1111/imr.12136 (2014).

476 Rapoport, A. P. *et al.* Combination immunotherapy using adoptive T-cell transfer and tumor antigen vaccination on the basis of hTERT and survivin after ASCT for myeloma. *Blood* **117**, 788-797, doi:10.1182/blood-2010-08-299396 (2011).

477 Rapoport, A. P. *et al.* Restoration of immunity in lymphopenic individuals with cancer by vaccination and adoptive T-cell transfer. *Nat Med* **11**, 1230-1237, doi:10.1038/nm1310 (2005).

478 Rosenberg, S. A. *et al.* Treatment of patients with metastatic melanoma with autologous tumor-infiltrating lymphocytes and interleukin 2. *Journal of the National Cancer Institute* **86**, 1159-1166 (1994).

479 Gross, G., Waks, T. & Eshhar, Z. Expression of immunoglobulin-T-cell receptor chimeric molecules as functional receptors with antibody-type specificity. *Proc Natl Acad Sci U S A* **86**, 10024-10028 (1989).

480 Park, J. R. *et al.* Adoptive transfer of chimeric antigen receptor re-directed cytolytic T lymphocyte clones in patients with neuroblastoma. *Mol Ther* **15**, 825-833, doi:10.1038/sj.mt.6300104 (2007).

481 Till, B. G. *et al.* Adoptive immunotherapy for indolent non-Hodgkin lymphoma and mantle cell lymphoma using genetically modified autologous CD20-specific T cells. *Blood* **112**, 2261-2271, doi:10.1182/blood-2007-12-128843 (2008).

482 Kershaw, M. H. *et al.* A phase I study on adoptive immunotherapy using gene-modified T cells for ovarian cancer. *Clinical cancer research : an official journal of the American Association for Cancer Research* **12**, 6106-6115, doi:10.1158/1078-0432.ccr-06-1183 (2006).

483 Maher, J., Brentjens, R. J., Gunset, G., Riviere, I. & Sadelain, M. Human T-lymphocyte cytotoxicity and proliferation directed by a single chimeric TCRzeta /CD28 receptor. *Nature biotechnology* **20**, 70-75, doi:10.1038/nbt0102-70 (2002).

484 Hombach, A. A., Heiders, J., Foppe, M., Chmielewski, M. & Abken, H. OX40 costimulation by a chimeric antigen receptor abrogates CD28 and IL-2 induced IL-10 secretion by redirected CD4(+) T cells. *Oncoimmunology* **1**, 458-466 (2012).

485 Song, D. G. *et al.* In vivo persistence, tumor localization, and antitumor activity of CAR-engineered T cells is enhanced by costimulatory signaling through CD137 (4-1BB). *Cancer Res* **71**, 4617-4627, doi:10.1158/0008-5472.can-11-0422 (2011).

486 Gill, S. & Kalos, M. T cell-based gene therapy of cancer. *Translational research : the journal of laboratory and clinical medicine* **161**, 365-379, doi:10.1016/j.trsl.2012.11.002 (2013).

487 Till, B. G. *et al.* CD20-specific adoptive immunotherapy for lymphoma using a chimeric antigen receptor with both CD28 and 4-1BB domains: pilot clinical trial results. *Blood* **119**, 3940-3950, doi:10.1182/blood-2011-10-387969 (2012).

488 Zhong, X. S., Matsushita, M., Plotkin, J., Riviere, I. & Sadelain, M. Chimeric antigen receptors combining 4-1BB and CD28 signaling domains augment PI3kinase/AKT/Bcl-XL activation and CD8+ T cell-mediated tumor eradication. *Mol Ther* **18**, 413-420, doi:10.1038/mt.2009.210 (2010).

489 Papac, R. J. Spontaneous regression of cancer: possible mechanisms. *In vivo (Athens, Greece)* **12**, 571-578 (1998).

290

490 Challis, G. B. & Stam, H. J. The spontaneous regression of cancer. A review of cases from 1900 to 1987. *Acta oncologica (Stockholm, Sweden)* **29**, 545-550 (1990).

491 Brodeur, G. M. & Bagatell, R. Mechanisms of neuroblastoma regression. *Nature reviews. Clinical oncology* **11**, 704-713, doi:10.1038/nrclinonc.2014.168 (2014).

492 Kataoka, Y., Matsumura, T., Yamamoto, S., Sugimoto, T. & Sawada, T. Distinct cytotoxicity against neuroblastoma cells of peripheral blood and tumor-infiltrating lymphocytes from patients with neuroblastoma. *Cancer Lett* **73**, 11-21 (1993).

493 Rudnick, E. *et al.* Opsoclonus-myoclonus-ataxia syndrome in neuroblastoma: clinical outcome and antineuronal antibodies-a report from the Children's Cancer Group Study. *Medical and pediatric oncology* **36**, 612-622, doi:10.1002/mpo.1138 (2001).

494 Pranzatelli, M. R. *et al.* B- and T-cell markers in opsoclonus-myoclonus syndrome: immunophenotyping of CSF lymphocytes. *Neurology* **62**, 1526-1532 (2004).

495 Squire, R., Fowler, C. L., Brooks, S. P., Rich, G. A. & Cooney, D. R. The relationship of class I MHC antigen expression to stage IV-S disease and survival in neuroblastoma. *Journal of pediatric surgery* **25**, 381-386 (1990).

496 Raffaghello, L. *et al.* Mechanisms of immune evasion of human neuroblastoma. *Cancer Lett* **228**, 155-161, doi:10.1016/j.canlet.2004.11.064 (2005).

497 Choi, B. *et al.* Phase I trial of combined treatment with ch14.18 and R24 monoclonal antibodies and interleukin-2 for patients with melanoma or sarcoma. *Cancer Immunology Immunotherapy* **55**, 761-774, doi:10.1007/s00262-005-0069-7 (2006).

498 Yankelevich, M. *et al.* Anti-CD3 x anti-GD2 bispecific antibody redirects T-cell cytolytic activity to neuroblastoma targets. *Pediatr Blood Cancer* **59**, 1198-1205, doi:10.1002/pbc.24237 (2012).

499 Yang, K. D., Cheng, S. N., Wu, N. C. & Shaio, M. F. Induction of interleukin-8 expression in neuroblastoma cells by retinoic acid: implication of leukocyte chemotaxis and activation. *Pediatric research* **34**, 720-724, doi:10.1203/00006450-199312000-00005 (1993).

500 Metelitsa, L. S. *et al.* Antidisialoganglioside/granulocyte macrophage–colony-stimulating factor fusion protein facilitates neutrophil antibody-dependent cellular cytotoxicity and depends on FcγRII (CD32) and Mac-1 (CD11b/CD18) for enhanced effector cell adhesion and azurophil granule exocytosis. *Blood* **99**, 4166-4173, doi:10.1182/blood.V99.11.4166 (2002).

501 Kushner, B. H. & Cheung, N. K. Absolute requirement of CD11/CD18 adhesion molecules, FcRII and the phosphatidylinositol-linked FcRIII for monoclonal antibody-mediated neutrophil antihuman tumor cytotoxicity. *Blood* **79**, 1484-1490 (1992).

502 Di Carlo, E. *et al.* The intriguing role of polymorphonuclear neutrophils in antitumor reactions. *Blood* **97**, 339-345 (2001).

503 Kushner, B. H. & Cheung, N.-K. V. Clinically Effective Monoclonal Antibody 3F8 Mediates Nonoxidative Lysis of Human Neuroectodermal Tumor Cells by Polymorphonuclear Leukocytes. *Cancer Research* **51**, 4865-4870 (1991).

504 Coughlin, C. M. *et al.* Immunosurveillance and survivin-specific T-cell immunity in children with high-risk neuroblastoma. *J Clin Oncol* **24**, 5725-5734, doi:10.1200/jco.2005.05.3314 (2006).

505 Pule, M. A. *et al.* Virus-specific T cells engineered to coexpress tumor-specific receptors: persistence and antitumor activity in individuals with neuroblastoma. *Nature Medicine* **14**, 1264-1270, doi:10.1038/nm.1882 (2008).

506 Caruana, I. *et al.* Heparanase promotes tumor infiltration and antitumor activity of CAR-redirected T lymphocytes. *Nat Med* **21**, 524-529, doi:10.1038/nm.3833 (2015).

507 Long, A. H. *et al.* 4-1BB costimulation ameliorates T cell exhaustion induced by tonic signaling of chimeric antigen receptors. *Nat Med* **21**, 581-590, doi:10.1038/nm.3838 (2015).

508 Louis, C. U. *et al.* Antitumor activity and long-term fate of chimeric antigen receptor-positive T cells in patients with neuroblastoma. *Blood* **118**, 6050-6056, doi:10.1182/blood-2011-05-354449 (2011).

509 Heczey A., L. C. U., Savoldo B., Dakhova O., Grilley B.J., Gee A., Dotti GP., Heslop H.E., Rooney C.M., Brenner M.K. in *Advances in Neuroblastoma Research Congress* (2016).

510 Cho, D. *et al.* Cytotoxicity of activated natural killer cells against pediatric solid tumors. *Clinical cancer research : an official journal of the American Association for Cancer Research* **16**, 3901-3909, doi:10.1158/1078-0432.ccr-10-0735 (2010).

511 Merchant, M. S. *et al.* Phase I Clinical Trial of Ipilimumab in Pediatric Patients with Advanced Solid Tumors. *Clinical cancer research : an official journal of the American Association for Cancer Research* **22**, 1364-1370, doi:10.1158/1078-0432.ccr-15-0491 (2016).

512 Burgess, M., Crowley., J Reinke, D., Reidel, R., George, S., Movva, S., Van Tine, B.A., Davis, L.E., Schuetze, S., Hu, J., et al. in *American Society of Clinical Oncology* (2015).

513 Rizvi, N. A. Cancer immunology. Mutational landscape determines sensitivity to PD-1 blockade in non-small cell lung cancer. *Science* **348** (2015).

514 Le, D. T. PD-1 Blockade in Tumors with Mismatch-Repair Deficiency. *N Engl J Med* **372** (2015).

515 Schwab, M. *et al.* AMPLIFIED DNA WITH LIMITED HOMOLOGY TO MYC CELLULAR ONCOGENE IS SHARED BY HUMAN NEURO-BLASTOMA CELL-LINES AND A NEURO-BLASTOMA TUMOR. *Nature* **305**, 245-248, doi:10.1038/305245a0 (1983).

516 Bouffet, E. *et al.* Immune Checkpoint Inhibition for Hypermutant Glioblastoma Multiforme Resulting From Germline Biallelic Mismatch Repair Deficiency. *J Clin Oncol* **34**, 2206-2211, doi:10.1200/jco.2016.66.6552 (2016).

517 Shlien, A. *et al.* Combined hereditary and somatic mutations of replication error repair genes result in rapid onset of ultra-hypermutated cancers. *Nature genetics* **47**, 257-262, doi:10.1038/ng.3202 (2015).

518 Torre, L. A. *et al.* Global cancer statistics, 2012. *CA: a cancer journal for clinicians* **65**, 87-108, doi:10.3322/caac.21262 (2015).

519 Pfirschke, C. *et al.* Immunogenic Chemotherapy Sensitizes Tumors to Checkpoint Blockade Therapy. *Immunity* **44**, 343-354, doi:10.1016/j.immuni.2015.11.024.

520 Vacchelli, E. *et al.* Trial watch Chemotherapy with immunogenic cell death inducers. *Oncoimmunology* **1**, 179-188, doi:10.4161/onci.1.2.19026 (2012).

292

521 Ciampricotti, M., Hau, C. S., Doornebal, C. W., Jonkers, J. & de Visser, K. E. Chemotherapy response of spontaneous mammary tumors is independent of the adaptive immune system. *Nat Med* **18**, 344-346; author reply 346, doi:10.1038/nm.2652 (2012).

522 Peer, D. *et al.* Nanocarriers as an emerging platform for cancer therapy. *Nature nanotechnology* **2**, 751-760, doi:10.1038/nnano.2007.387 (2007).

523 Chauhan, V. P. *et al.* Normalization of tumour blood vessels improves the delivery of nanomedicines in a size-dependent manner. *Nature nanotechnology* **7**, 383-388, doi:10.1038/nnano.2012.45 (2012).

524 Thomas, A., Teicher, B. A. & Hassan, R. Antibody-drug conjugates for cancer therapy. *The Lancet. Oncology* **17**, e254-262, doi:10.1016/s1470-2045(16)30030-4 (2016).

525 Reck, M. *et al.* Ipilimumab in combination with paclitaxel and carboplatin as first-line therapy in extensive-disease-small-cell lung cancer: results from a randomized, double-blind, multicenter phase 2 trial. *Annals of oncology : official journal of the European Society for Medical Oncology / ESMO* **24**, 75-83, doi:10.1093/annonc/mds213 (2013).

526 Lynch, T. J. *et al.* Ipilimumab in combination with paclitaxel and carboplatin as first-line treatment in stage IIIB/IV non-small-cell lung cancer: results from a randomized, double-blind, multicenter phase II study. *J Clin Oncol* **30**, 2046-2054, doi:10.1200/jco.2011.38.4032 (2012).

527 Langer, C. J. *et al.* Carboplatin and pemetrexed with or without pembrolizumab for advanced, non-squamous non-small-cell lung cancer: a randomised, phase 2 cohort of the open-label KEYNOTE-021 study. *The Lancet. Oncology* **17**, 1497-1508, doi:10.1016/s1470-2045(16)30498-3 (2016).

528 Ravishankar, B. *et al.* Tolerance to apoptotic cells is regulated by indoleamine 2,3-dioxygenase. *Proc Natl Acad Sci U S A* **109**, 3909-3914, doi:10.1073/pnas.1117736109 (2012).

529 Mellor, A. L. *et al.* Cutting edge: induced indoleamine 2,3 dioxygenase expression in dendritic cell subsets suppresses T cell clonal expansion. *Journal of immunology (Baltimore, Md. : 1950)* **171**, 1652-1655 (2003).

530 Munn, D. H. *et al.* GCN2 kinase in T cells mediates proliferative arrest and anergy induction in response to indoleamine 2,3-dioxygenase. *Immunity* **22**, 633-642, doi:10.1016/j.immuni.2005.03.013 (2005).

531 Mezrich, J. D. *et al.* An interaction between kynurenine and the aryl hydrocarbon receptor can generate regulatory T cells. *Journal of immunology (Baltimore, Md. : 1950)* **185**, 3190-3198, doi:10.4049/jimmunol.0903670 (2010).

532 Ravishankar, B. *et al.* The amino acid sensor GCN2 inhibits inflammatory responses to apoptotic cells promoting tolerance and suppressing systemic autoimmunity. *Proc Natl Acad Sci U S A* **112**, 10774-10779, doi:10.1073/pnas.1504276112 (2015).

533 Sharma, M. D. *et al.* The PTEN pathway in Tregs is a critical driver of the suppressive tumor microenvironment. *Science advances* **1**, e1500845, doi:10.1126/sciadv.1500845 (2015).

534 Fernandez, M. C., Krailo, M. D., Gerbing, R. R. & Matthay, K. K. A phase I dose escalation of combination chemotherapy with granulocyte-macrophage-colony stimulating factor in patients with neuroblastoma. *Cancer* **88**, 2838-2844, doi:10.1002/1097-0142(20000615)88:12<2838::aid-cncr25>3.0.co;2-9 (2000).

535 Das, R. *et al.* Combination Therapy with Anti-CTLA-4 and Anti-PD-1 Leads to Distinct Immunologic Changes In Vivo. *Journal of Immunology* **194**, 950-959, doi:10.4049/jimmunol.1401686 (2015).

536 Meng, X., Huang, Z., Teng, F., Xing, L. & Yu, J. Predictive biomarkers in PD-1/PD-L1 checkpoint blockade immunotherapy. *Cancer treatment reviews*, doi:10.1016/j.ctrv.2015.11.001 (2015).

537 Sledzinska, A., Menger, L., Bergerhoff, K., Peggs, K. S. & Quezada, S. A. Negative immune checkpoints on T lymphocytes and their relevance to cancer immunotherapy. *Molecular oncology*, doi:10.1016/j.molonc.2015.10.008 (2015).

538 Ogilvy, S. *et al.* Constitutive Bcl-2 expression throughout the hematopoietic compartment affects multiple lineages and enhances progenitor cell survival. *Proc Natl Acad Sci U S A* **96**, 14943-14948 (1999).

539 Egle, A., Harris, A. W., Bath, M. L., O'Reilly, L. & Cory, S. VavP-Bcl2 transgenic mice develop follicular lymphoma preceded by germinal center hyperplasia. *Blood* **103**, 2276-2283, doi:10.1182/blood-2003-07-2469 (2004).

540 Lode, H. N. *et al.* Targeted interleukin-2 therapy for spontaneous neuroblastoma metastases to bone marrow. *Journal of the National Cancer Institute* **89**, 1586-1594 (1997).

541 Kroesen, M. *et al.* Intra-adrenal murine TH-MYCN neuroblastoma tumors grow more aggressive and exhibit a distinct tumor microenvironment relative to their subcutaneous equivalents. *Cancer Immunology, Immunotherapy* **64**, 563-572, doi:10.1007/s00262-015-1663-y (2015).

542 Kroesen, M. *et al.* A transplantable TH-MYCN transgenic tumor model in C57Bl/6 mice for preclinical immunological studies in neuroblastoma. *International journal of cancer. Journal international du cancer* **134**, 1335-1345, doi:10.1002/ijc.28463 (2014).

543 Mujoo, K. *et al.* Functional properties and effect on growth suppression of human neuroblastoma tumors by isotype switch variants of monoclonal antiganglioside GD2 antibody 14.18. *Cancer Res* **49**, 2857-2861 (1989).

544 Tutt, A. L. *et al.* Development and Characterization of Monoclonal Antibodies Specific for Mouse and Human Fcγ Receptors. *The Journal of Immunology* **195**, 5503-5516, doi:10.4049/jimmunol.1402988 (2015).

545 White, A. L. *et al.* Conformation of the human immunoglobulin G2 hinge imparts superagonistic properties to immunostimulatory anticancer antibodies. *Cancer Cell* **27**, 138-148, doi:10.1016/j.ccell.2014.11.001 (2015).

546 White, A. L. *et al.* Interaction with FcgammaRIIB is critical for the agonistic activity of anti-CD40 monoclonal antibody. *Journal of immunology (Baltimore, Md. : 1950)* **187**, 1754-1763, doi:10.4049/jimmunol.1101135 (2011).

547 Daëron, M., Néauport-Sautès, C., Blank, U. & Fridman, W. H. 2.4G2, a monoclonal antibody to macrophage Fcγ receptors, reacts with murine T cell Fcγ receptors and IgG-binding factors. *European Journal of Immunology* **16**, 1545-1550, doi:doi:10.1002/eji.1830161213 (1986).

548 Moore, M. J. Clinical pharmacokinetics of cyclophosphamide. *Clinical pharmacokinetics* **20**, 194-208, doi:10.2165/00003088-199120030-00002 (1991).

549 Schwartz, P. S. & Waxman, D. J. Cyclophosphamide induces caspase 9-dependent apoptosis in 9L tumor cells. *Molecular pharmacology* **60**, 1268-1279 (2001).

550 Cory, A. H., Owen, T. C., Barltrop, J. A. & Cory, J. G. USE OF AN AQUEOUS SOLUBLE TETRAZOLIUM FORMAZAN ASSAY FOR CELL-GROWTH ASSAYS IN CULTURE. *Cancer Communications* **3**, 207-212 (1991).

551 Huang, D. C. S. *et al.* Activation of Fas by FasL induces apoptosis by a mechanism that cannot be blocked by Bcl-2 or Bcl-x_L. *Proceedings of the National Academy of Sciences* **96**, 14871-14876, doi:10.1073/pnas.96.26.14871 (1999).

552 Strasser, A., Harris, A. W., Huang, D. C., Krammer, P. H. & Cory, S. Bcl-2 and Fas/APO-1 regulate distinct pathways to lymphocyte apoptosis. *Embo j* **14**, 6136-6147 (1995).

553 Moore, H. C. *et al.* Histological profile of tumours from MYCN transgenic mice. *Journal of Clinical Pathology* **61**, 1098-1103, doi:10.1136/jcp.2007.054627 (2008).

554 Pistoia, V. *et al.* Immunosuppressive microenvironment in neuroblastoma. *Frontiers in oncology* **3**, 167, doi:10.3389/fonc.2013.00167 (2013).

555 Lei, H., Schmidt-Bleek, K., Dienelt, A., Reinke, P. & Volk, H. D. Regulatory T cell-mediated anti-inflammatory effects promote successful tissue repair in both indirect and direct manners. *Frontiers in pharmacology* **6**, 184, doi:10.3389/fphar.2015.00184 (2015).

556 Wölfl, M. *et al.* Expression of MHC class I, MHC class II, and cancer germline antigens in neuroblastoma. *Cancer Immunology, Immunotherapy* **54**, 400-406, doi:10.1007/s00262-004-0603-z (2005).

557 Main, E. K., Lampson, L. A., Hart, M. K., Kornbluth, J. & Wilson, D. B. Human neuroblastoma cell lines are susceptible to lysis by natural killer cells but not by cytotoxic T lymphocytes. *Journal of immunology (Baltimore, Md. : 1950)* **135**, 242-246 (1985).

558 Song, L. *et al.* Valpha24-invariant NKT cells mediate antitumor activity via killing of tumor-associated macrophages. *J Clin Invest* **119**, 1524-1536, doi:10.1172/jci37869 (2009).

559 Asgharzadeh, S. *et al.* Clinical significance of tumor-associated inflammatory cells in metastatic neuroblastoma. *J Clin Oncol* **30**, 3525-3532, doi:10.1200/jco.2011.40.9169 (2012).

560 Apps, J. R. *et al.* The immune environment of paediatric solid malignancies: evidence from an immunohistochemical study of clinical cases. *Fetal and pediatric pathology* **32**, 298-307, doi:10.3109/15513815.2012.754527 (2013).

561 Dahal, L. N., Roghanian, A., Beers, S. A. & Cragg, M. S. FcγR requirements leading to successful immunotherapy. *Immunological Reviews* **268**, 104-122, doi:doi:10.1111/imr.12342 (2015).

562 Carlson, L. M. *et al.* Low-dose aspirin delays an inflammatory tumor progression in vivo in a transgenic mouse model of neuroblastoma. *Carcinogenesis* **34**, 1081-1088, doi:10.1093/carcin/bgt009 (2013).

563 Lauder, I. & Aherne, W. The significance of lymphocytic infiltration in neuroblastoma. *Br J Cancer* **26**, 321-330 (1972).

564 Martin, R. F. & Beckwith, J. B. Lymphoid infiltrates in neuroblastomas: their occurrence and prognostic significance. *Journal of pediatric surgery* **3**, 161-164 (1968).

565 Facchetti, P. *et al.* Functional and molecular characterization of tumour-infiltrating lymphocytes and clones thereof from a major-histocompatibility-complex-negative human tumour: neuroblastoma. *Cancer immunology, immunotherapy : CII* **42**, 170-178 (1996).

566 Carlson, L. M. *et al.* The microenvironment of human neuroblastoma supports the activation of tumor-associated T lymphocytes. *Oncoimmunology* **2**, e23618, doi:10.4161/onci.23618 (2013).

567 Bundscherer, A. *et al.* Cell harvesting method influences results of apoptosis analysis by annexin V staining. *Anticancer research* **33**, 3201-3204 (2013).

568 Ahlmann, M. & Hempel, G. The effect of cyclophosphamide on the immune system: implications for clinical cancer therapy. *Cancer Chemotherapy and Pharmacology* **78**, 661-671, doi:10.1007/s00280-016-3152-1 (2016).

569 Madondo, M. T., Quinn, M. & Plebanski, M. Low dose cyclophosphamide: Mechanisms of T cell modulation. *Cancer treatment reviews* **42**, 3-9, doi:10.1016/j.ctrv.2015.11.005 (2016).

570 Son, M. *et al.* C1q and HMGB1 reciprocally regulate human macrophage polarization. *Blood*, doi:10.1182/blood-2016-05-719757 (2016).

571 Tridandapani, S. *et al.* Regulated expression and inhibitory function of Fcgamma RIIb in human monocytic cells. *J Biol Chem* **277**, 5082-5089, doi:10.1074/jbc.M110277200 (2002).

572 Lanitis, E., Irving, M. & Coukos, G. Targeting the tumor vasculature to enhance T cell activity. *Current Opinion in Immunology* **33**, 55-63, doi:10.1016/j.coi.2015.01.011 (2015).

573 Tanaka, A. & Sakaguchi, S. Regulatory T cells in cancer immunotherapy. *Cell Research* **27**, 109, doi:10.1038/cr.2016.151 (2016).

574 Baras, A. S. *et al.* The ratio of CD8 to Treg tumor-infiltrating lymphocytes is associated with response to cisplatin-based neoadjuvant chemotherapy in patients with muscle invasive urothelial carcinoma of the bladder. *Oncoimmunology* **5**, e1134412, doi:10.1080/2162402x.2015.1134412 (2016).

575 Sato, E. *et al.* Intraepithelial CD8+ tumor-infiltrating lymphocytes and a high CD8+/regulatory T cell ratio are associated with favorable prognosis in ovarian cancer. *Proc Natl Acad Sci U S A* **102**, 18538-18543, doi:10.1073/pnas.0509182102 (2005).

576 Gravelle, P. *et al.* Impaired functional responses in follicular lymphoma CD8(+)TIM-3(+) T lymphocytes following TCR engagement. *Oncoimmunology* **5**, e1224044, doi:10.1080/2162402x.2016.1224044 (2016).

577 Buggert, M. *et al.* T-bet and Eomes are differentially linked to the exhausted phenotype of CD8+ T cells in HIV infection. *PLoS Pathog* **10**, e1004251, doi:10.1371/journal.ppat.1004251 (2014).

578 Schoenborn, J. R. & Wilson, C. B. Regulation of interferon-gamma during innate and adaptive immune responses. *Advances in immunology* **96**, 41-101, doi:10.1016/s0065-2776(07)96002-2 (2007).

579 Zhou, L., Chong, M. M. & Littman, D. R. Plasticity of CD4+ T cell lineage differentiation. *Immunity* **30**, 646-655, doi:10.1016/j.immuni.2009.05.001 (2009).

580 Buchan, S. L., Rogel, A. & Al-Shamkhani, A. The immunobiology of CD27 and OX40 and their potential as targets for cancer immunotherapy. *Blood* **131**, 39-48, doi:10.1182/blood-2017-07-741025 (2018).

581 Willoughby, J., Griffiths, J., Tews, I. & Cragg, M. S. OX40: Structure and function - What questions remain? *Mol Immunol* **83**, 13-22, doi:10.1016/j.molimm.2017.01.006 (2017).

582 Gautron, A. S., Dominguez-Villar, M., de Marcken, M. & Hafler, D. A. Enhanced suppressor function of TIM-3+ FoxP3+ regulatory T cells. *Eur J Immunol* **44**, 2703-2711, doi:10.1002/eji.201344392 (2014).

583 Loebbermann, J. *et al.* Regulatory T cells expressing granzyme B play a critical role in controlling lung inflammation during acute viral infection. *Mucosal immunology* **5**, 161-172, doi:10.1038/mi.2011.62 (2012).

584 Anderson, A. C., Joller, N. & Kuchroo, V. K. Lag-3, Tim-3, and TIGIT: Co-inhibitory Receptors with Specialized Functions in Immune Regulation. *Immunity* **44**, 989-1004, doi:10.1016/j.immuni.2016.05.001 (2016).

585 Lupar, E. *et al.* Eomesodermin Expression in CD4⁺ T Cells Restricts Peripheral Foxp3 Induction. *The Journal of Immunology* **195**, 4742-4752, doi:10.4049/jimmunol.1501159 (2015).

586 Reed, J. C. Bcl-2 on the brink of breakthroughs in cancer treatment. *Cell Death And Differentiation* **25**, 3, doi:10.1038/cdd.2017.188 (2017).

587 Lee, H. W. *et al.* 4-1BB promotes the survival of CD8+ T lymphocytes by increasing expression of Bcl-xL and Bfl-1. *Journal of immunology (Baltimore, Md. : 1950)* **169**, 4882-4888 (2002).

588 Yu, X. *et al.* Complex Interplay between Epitope Specificity and Isotype Dictates the Biological Activity of Anti-human CD40 Antibodies. *Cancer Cell* **33**, 664-675.e664, doi:10.1016/j.ccell.2018.02.009 (2018).

589 Ji, H. *et al.* Ratio of Immune Response to Tumor Burden Predicts Survival Via Regulating Functions of Lymphocytes and Monocytes in Diffuse Large B-Cell Lymphoma. *Cellular physiology and biochemistry : international journal of experimental cellular physiology, biochemistry, and pharmacology* **45**, 951-961, doi:10.1159/000487288 (2018).

590 Huang, A. C. *et al.* T-cell invigoration to tumour burden ratio associated with anti-PD-1 response. *Nature* **545**, 60-65, doi:10.1038/nature22079 (2017).

591 Nallasamy, P. *et al.* PD-L1, inflammation, non-coding RNAs, and neuroblastoma: Immuno-oncology perspective. *Seminars in cancer biology* **52**, 53-65, doi:10.1016/j.semcancer.2017.11.009 (2018).

592 Bulliard, Y. *et al.* Activating Fc gamma receptors contribute to the antitumor activities of immunoregulatory receptor-targeting antibodies. *J Exp Med* **210**, 1685-1693, doi:10.1084/jem.20130573 (2013).

593 Simpson, T. R. *et al.* Fc-dependent depletion of tumor-infiltrating regulatory T cells co-defines the efficacy of anti-CTLA-4 therapy against melanoma. *J Exp Med* **210**, 1695-1710, doi:10.1084/jem.20130579 (2013).

594 Mandai, M. *et al.* Dual Faces of IFNγ in Cancer Progression: A Role of PD-L1 Induction in the Determination of Pro- and Antitumor Immunity. *Clinical Cancer Research* **22**, 2329-2334, doi:10.1158/1078-0432.ccr-16-0224 (2016).

595 Tipton, T. R. *et al.* Antigenic modulation limits the effector cell mechanisms employed by type I anti-CD20 monoclonal antibodies. *Blood* **125**, 1901-1909, doi:10.1182/blood-2014-07-588376 (2015).

596 Goto, T. *et al.* PD-L1 on Antigen-Presenting Cells Facilitate the Induction of Antigen-Specific Cytotoxic T Lymphocytes. *Blood* **126**, 1021-1021 (2015).

597 Wu, J. & Waxman, D. J. Metronomic cyclophosphamide schedule-dependence of innate immune cell recruitment and tumor regression in an implanted glioma model. *Cancer Lett* **353**, 272-280, doi:10.1016/j.canlet.2014.07.033 (2014).

598 Lechner, M. G. *et al.* Immunogenicity of murine solid tumor models as a defining feature of in vivo behavior and response to immunotherapy. *Journal of immunotherapy (Hagerstown, Md. : 1997)* **36**, 477-489, doi:10.1097/01.cji.0000436722.46675.4a (2013).

599 Zhao, Y. *et al.* Development of a new patient-derived xenograft humanised mouse model to study human-specific tumour microenvironment and immunotherapy. *Gut* **67**, 1845-1854, doi:10.1136/gutjnl-2017-315201 (2018).